

2008-12-09

The Evolution of the Carbonate Shelf Margins and Fill of the Antler Foreland Basin by Prograding Mississippian Carbonates, Northern U.S. Rockies

Matthew Robert Buoniconti

University of Miami, mbuoniconti@gmail.com

Follow this and additional works at: https://scholarlyrepository.miami.edu/oa_dissertations

Recommended Citation

Buoniconti, Matthew Robert, "The Evolution of the Carbonate Shelf Margins and Fill of the Antler Foreland Basin by Prograding Mississippian Carbonates, Northern U.S. Rockies" (2008). *Open Access Dissertations*. 330.
https://scholarlyrepository.miami.edu/oa_dissertations/330

This Open access is brought to you for free and open access by the Electronic Theses and Dissertations at Scholarly Repository. It has been accepted for inclusion in Open Access Dissertations by an authorized administrator of Scholarly Repository. For more information, please contact repository.library@miami.edu.

UNIVERSITY OF MIAMI

THE EVOLUTION OF THE CARBONATE SHELF MARGINS AND FILL OF
THE ANTLER FORELAND BASIN BY PROGRADING MISSISSIPPIAN
CARBONATES, NORTHERN U.S. ROCKIES

By

Matthew Robert Buoniconti

A DISSERTATION

Submitted to the Faculty
of the University of Miami
in partial fulfillment of the requirements for
the degree of Doctor of Philosophy

Coral Gables, Florida

December 2008

©2008
Matthew R. Buoniconti
All Rights Reserved

UNIVERSITY OF MIAMI

A dissertation submitted in partial fulfillment of
the requirements for the degree of
Doctor of Philosophy

THE EVOLUTION OF THE CARBONATE SHELF MARGINS AND FILL OF
THE ANTLER FORELAND BASIN BY PROGRADING MISSISSIPPIAN
CARBONATES, NORTHERN U.S. ROCKIES

Matthew Robert Buoniconti

Approved:

Gregor P. Eberli, Ph.D.
Professor of Marine Geology
and Geophysics

Terri A. Scandura, Ph.D.
Dean of the Graduate School

Christopher G.A. Harrison, Ph.D.
Professor of Marine Geology
and Geophysics

Harold R. Wanless, Ph.D.
Professor of Geology

Langhorne B. Smith, Ph.D.
New York State Museum

BUONICONTI, MATTHEW
The Evolution of the Carbonate
Shelf Margins and Fill of the
Antler Foreland Basin by
Prograding Mississippian
Carbonates, Northern U.S. Rockies

(Ph.D., Marine Geology and Geophysics)
(December 2008)

Abstract of a dissertation at the University of Miami

Dissertation supervised by Professor Gregor P. Eberli
Number of pages in text. (436)

The aims of this study are to extend the established high-resolution sequence stratigraphic framework of the Madison Formation of Wyoming and southern central Montana to the correlative and genetically-related Mississippian carbonate ramp, ramp margin, and basin strata of the central Montana trough and Antler foreland basin in order to examine and discriminate the controls on depositional processes and the resulting stratigraphic architecture through space and time in tectonically-active settings. An outcrop-based, high-resolution sequence stratigraphic study of two ramp-to-basin transects, one in central Montana and the other in southwestern Montana and east-central Idaho, is conducted in order to examine these deposits across two coeval margins with differing subsidence, hydrodynamic, and physiographic configurations and histories.

Independent measurements of system response to global and local forcings allows disentanglement of primary controls on deposition and allows us to gain understanding of the roles and interplay of these controls, in particular eustasy and tectonics, on the system's architectural development. Conversely, insight into the geodynamic evolution of western North America, glacioeustatic changes, and variations in global climate and oceanographic systems during the greenhouse-to-icehouse transition is gained.

A series of high-resolution sequence stratigraphic cross-sections and time-slices are produced incorporating outcrop measured sections and measured sections previously collected by members of the Comparative Sedimentology Laboratory in a series of transects across the Madison ramp system. A new chronostratigraphic framework for Madison carbonates is developed by using Lower Carboniferous $\delta^{13}\text{C}$ isotope excursions as isochronous tie points between ramp-top, margin, and basinal sections. These $\delta^{13}\text{C}$ excursion events have been documented to be time-invariant globally due to global changes in ocean chemistry. The results of the study include resolution and discrimination of sequential foreland basin subsidence, carbonate sediment production and progradation, subsidence and uplift of foreland basin structures along a carbonate shelf edge, diachronous subsidence of discrete depocenters, and eustasy.

ACKNOWLEDGEMENTS

This dissertation may be the culmination of my work on Mississippian carbonates over the past several years, but it is obvious that this work did not occur in a vacuum. I'd first like to thank my committee, whose members, Drs. Gregor Eberli, Hal Wanless, Chris Harrison, and Taury Smith, devoted extensive time reading and commenting on the numerous drafts of this document. I thank you gentlemen for helping round this work into its final form. Instruction and mentoring, although a critical component of what is contained herein, would have been rendered a bit moot if I was unable to feed myself over the past few years. I'd like to thank the industrial associates of the Comparative Sedimentology Laboratory for supporting this work financially as well as AAPG Grants-in-Aid program and the Tobacco Root Geological Society for backing this work.

As enriching and invigorating as this work has been, I'm pleased to say that it was not the only thing occurring in my life over the early years of the new millennium. I'd like to thank my wife Margaret for being there for me even though you've been 3000 miles away for the past few years. Your patience and understanding through this process may have made you crazy, but it's allowed me to hang on to a shred my sanity. For that and everything else, I give my greatest thanks. Thanks also to my parents Bob and Candis and my sister Lisa. You guys have made life, in many ways, a real breeze, especially over the last six months of this work. Thanks for supporting me and my work. I owe a great many thanks to a few others who supported me by literally putting a roof over my head for long stretches over the past two years. Thanks to Nick and Carol Peters and to Odessa Bowen for doing this. You have no clue how much this gesture meant to me. I'd finally

like to thank my friends, too many to be named. Thanks for being there and making life in Miami an amazing time!

I've managed to hint and somewhat enumerate the contribution that others have made to this work, but I'd like to name names now and give out thanks to those who gave their time to me out in the field. I know it was a tough assignment to be out in Montana and Idaho in the summer, but you all stepped up and lugged samples, whacked bush, and helped me change tires. Thanks to Guido Bracco Gartner, Dave Katz, Jason Kislak, Brad Rosenheim, David Shoore, Guillermina Sagasti, Ralf Weger, and Kathleen Willis as well as Margaret and Nick, who deserve additional mention for serving me in this capacity as well. Thanks also to the landowners in Montana who allowed access on or through their land and occasionally pulled me out of the mud. I appreciate it! I'm sure that I have left out people who have contributed to my life over the past six years, so here's to you. I'm trying to protect the innocent here, but seriously you all have helped me weave a tapestry of memories which won't soon fade. Thank you!

TABLE OF CONTENTS

LIST OF FIGURES	ix
LIST OF APPENDICES	xii
CHAPTER 1. GEOLOGIC SETTING AND REGIONAL FRAMEWORK	1
1.1 Summary	1
1.2 Introduction	2
1.3 Why Study the Madison?	4
1.4 Discussion	5
<i>1.4.1 Deconvolution of Relative Sea-Level Controls on Architecture Development</i>	5
<i>1.4.2 Tectonic Framework for Accommodation Development in a Foreland Setting</i>	6
<i>1.4.3 Foreland Basin and Geodynamic Evolution</i>	7
1.5 Previous Work	9
<i>1.5.1 Geologic Setting</i>	9
1.5.1.1 Litho- and Biostratigraphy	9
1.5.1.2 Sequence Stratigraphy	10
1.5.1.3 Regional Tectonics and Geodynamics	11
CHAPTER 2. FACIES DESCRIPTION AND DEPOSITIONAL ENVIRONMENTS	31
2.1 Overview	31
2.2 Methods	31
2.3 Basin Depozone	32
<i>2.3.1 Cherty Peloid/Skeletal Calcisiltite Facies</i>	32
<i>2.3.2 Bedded Chert Facies</i>	33
<i>2.3.3 Argillite/Shale Facies</i>	34
<i>2.3.4 Polymict Breccia Facies</i>	35
2.4 Outer Ramp Depozone	35
<i>2.4.1 Limestone/Argillite Couplets Facies</i>	36
2.5 Mid-ramp Depozone	37
<i>2.5.1 Graded Peloidal/Skeletal Packstone-Grainstone Facies</i>	38
<i>2.5.2 Oolitic Packstone-Grainstone Facies</i>	39
<i>2.5.3 Skeletal Packstone-Grainstone Facies</i>	39
<i>2.5.4 Massive Crinoidal/Skeletal Facies</i>	40
<i>2.5.5 Bioturbated Wackeston-Packstone Facies</i>	41
2.6 Inner Ramp Depozone	42
<i>2.6.1 Shoalwater/Barrier Facies Association</i>	43
2.6.1.1 Cross-Bedded Ooid Packstone-Grainstone Facies	43
2.6.1.2 Cross-Bedded Skeletal Packstone-Grainstone Shoal Facies	44

2.6.2 <i>Lagoonal Facies Association</i>	45
2.6.2.1 Peloidal/Micropeloidal Wackestone-Grainstone Facies	45
2.6.2.2 Bioturbated Peloidal Wackestone-Packstone Facies	46
2.6.2.3 Pellet/Restricted Fauna Mudstone-Wackestone Facies	47
2.6.3 <i>Peritidal Facies Association</i>	48
2.6.3.1 Pisoid Packstone-Grainstone Facies	48
2.6.3.2 Algal Laminite Facies	49
2.6.3.3 Mudclast Conglomerate Facies	49
2.6.3.4 Red Shale/Siltstone Facies	50
2.6.4 <i>Evaporite Solution Collapse Breccia Facies</i>	50

CHAPTER 3. SEQUENCE STRATIGRAPHY AND FACIES ORGANIZATION

3.1 Overview	65
3.2 Genetic Units	67
3.2.1 <i>Slope-to-Basin Cycles</i>	67
3.2.2 <i>Outer Ramp Cycles</i>	68
3.2.3 <i>Middle Ramp-to-Foreshoal Cycles</i>	69
3.2.4 <i>Restricted Subtidal Cycles</i>	70
3.2.5 <i>Peritidal Cycles</i>	71
3.3 Sequence Stratigraphy	71
3.3.1 <i>3rd-Order Sequence Evolution</i>	73
3.3.1.1 Lodgepole Sequence 1	73
3.3.1.1.1 Transgressive Systems Tract	74
3.3.1.1.2 Highstand Systems Tract	75
3.3.1.2 Lodgepole Sequence 2	76
3.3.1.2.1 Lowstand Systems Tract	76
3.3.1.2.2 Transgressive Systems Tract	76
3.3.1.2.3 Highstand Systems Tract	77
3.3.1.3 Lodgepole Sequence 3	78
3.3.1.3.1 Lowstand Systems Tract	78
3.3.1.3.2 Transgressive Systems Tract	79
3.3.1.3.3 Highstand Systems Tract	80
3.3.1.4 Mission Canyon Sequence 1	81
3.3.1.4.1 Lowstand Systems Tract	82
3.3.1.4.2 Transgressive Systems Tract	82
3.3.1.4.3 Highstand Systems Tract	83
3.3.1.5 Mission Canyon Sequence 2	84
3.3.1.5.1 Transgressive Systems Tract	84
3.3.1.5.2 Highstand Systems Tract	86
3.3.1.6 Mission Canyon Sequence 3	87
3.3.1.6.1 Transgressive Systems Tract	87
3.3.1.6.2 Highstand Systems Tract	88
3.3.1.7 Mission Canyon Sequence 4	90
3.3.1.7.1 Transgressive Systems Tract	90

3.3.1.7.2 Highstand Systems Tract	92
3.3.1.8 Scott Peak Sequence 1	93
3.3.1.8.1 Transgressive Systems Tract	93
3.3.1.8.2 Highstand Systems Tract	95
3.3.1.9 Scott Peak Sequence 2	96
3.3.1.9.1 Transgressive Systems Tract	96
3.3.1.9.2 Highstand Systems Tract	97
3.3.1.10 Scott Peak Sequence 3	99
3.3.1.10.1 Transgressive Systems Tract	99
3.3.1.10.2 Highstand Systems Tract	101
3.3.1.11 Scott Peak Sequence 4	102
3.3.1.11.1 Transgressive Systems Tract	102
3.3.1.11.2 Highstand Systems Tract	104
3.3.1.12 Scott Peak Sequence 5	105
3.3.1.12.1 Transgressive Systems Tract	106
3.3.1.12.2 Highstand Systems Tract	107
3.3.1.13 Scott Peak Sequence 6	108
3.3.1.13.1 Transgressive Systems Tract	109
3.3.1.13.2 Highstand Systems Tract	110
3.3.1.14 Scott Peak Sequence 7	111
3.3.1.14.1 Transgressive Systems Tract	112
3.3.1.14.2 Highstand Systems Tract	113
3.3.1.15 Post-Scott Peak Deposition	114
3.4 Discussion	115
3.4.1 <i>Accommodation, Basin Evolution, and Carbonate Sedimentation: A Comparison of the Central Montana Trough and the Proximal Antler Foreland Basin</i>	115
3.4.2 <i>System Requirements for Progradation of Carbonate Sand Belts into the Antler Foreland Basin</i>	120
 CHAPTER 4. RECONCILING ANTLER FORELAND BASIN DEVELOPMENT WITH THE MADISON DEPOSITIONAL RECORD: A DYNAMIC FRAMEWORK FOR ACCOMMODATION EVOLUTION	194
4.1 Overview	194
4.2 Geological Background	195
4.2.1 <i>The Antler Orogeny</i>	195
4.2.2 <i>Elastic Response to Loading</i>	197
4.2.3 <i>Paleogeography</i>	198
4.2.4 <i>Regional Antler foreland sedimentary architecture</i>	199
4.2.5 <i>Madison sequence architecture</i>	199
4.3 Methodology	200
4.3.1 <i>Approach</i>	200
4.3.2 <i>Flexure of an elastic plate</i>	202
4.3.3 <i>Time-dependent flexure of a viscoelastic plate</i>	204
4.3.4 <i>Conformable mapping of sequences on modeled</i>	206

<i>flexural profiles</i>	207
4.4 Modeling Results	207
4.4.1 <i>Elastic model</i>	207
4.4.2 <i>Viscous stress relaxation</i>	208
4.4.3 <i>Conformable mapping</i>	209
4.5 Discussion	211
4.5.1 <i>Introduction to previous modeling</i>	211
4.5.1.1 <i>Antler foreland basin evolution and accommodation development</i>	212
4.5.2 <i>Stratigraphic architecture and facies motifs</i>	213
4.5.3 <i>Regional carbonate stratigraphic architecture and lithospheric strength</i>	215
4.5.4 <i>Mechanics of decreasing lithospheric effective elastic thicknesses</i>	216
4.6 Conclusions	217
REFERENCES	231
APPENDICES	244

LIST OF FIGURES

Figure 1.1: Flexure and carbonate ramp development	14
Figure 1.2: Carbonate ramp development in active convergence	15
Figure 1.3: Subsidence model for central Montana trough	16
Figure 1.4: Mississippian paleogeographic map	17
Figure 1.5: Mississippian chronostratigraphic chart	18
Figure 1.6: Early Kinderhookian facies map	19
Figure 1.7: Latest Kinderhookian facies map	20
Figure 1.8: Early Meramecian facies map	21
Figure 1.9: Latest early Meramecian facies map	22
Figure 1.10: Latest Meramecian facies map	23
Figure 1.11: Conceptual models of the Antler orogeny	24
Figure 1.12: Regional Mississippian stratigraphic cross section	25
Figure 1.13: Foreland basin depozones	26
Figure 1.14: Surfaced regional Mississippian isopach map	27
Figure 1.15: Mississippian isopach with Antler cross-section location	28
Figure 1.16: Mississippian isopach with central Montana cross-section	29
Figure 1.17: Outcrop section location map	30
Figure 2.1: Cross-sectional carbonate ramp profile	51
Figure 2.2: Mississippian chronostratigraphic chart	52
Figure 2.3: Basin depozone facies	53
Figure 2.4: Limestone-argillite couplet facies	55
Figure 2.5: Mid-ramp depozone facies	56
Figure 2.6: Inner ramp facies – shoalwater/barrier facies	58
Figure 2.7: Inner ramp facies – lagoonal facies	60
Figure 2.8: Inner ramp facies – tidal flat facies	62
Figure 2.9: Evaporite solution collapse breccia	64
Figure 3.1: Allochem symbols legend	124
Figure 3.2: Lithology legend	125
Figure 3.3: 4 th and 5 th order basinal cycles	126
Figure 3.4: 4 th and 5 th order outer ramp cycles	127
Figure 3.5: 4 th and 5 th order middle-to-inner ramp cycles	128
Figure 3.6: 5 th order intertidal-to-subtidal cycle	129
Figure 3.7: 5 th order subtidal-to-intertidal cycle	130
Figure 3.8: Mississippian chronostratigraphic chart	131
Figure 3.9: Study location map with outcrop section locations	132
Figure 3.10: Mississippian paleogeographic map	133
Figure 3.11: Stratigraphic cross-section, sequence LP1, central Montana	134
Figure 3.12: Carbon isotope cross-section, sequence LP1, central Montana	135
Figure 3.13: Stratigraphic cross-section, sequence LP1, SW Montana	136
Figure 3.14: Carbon isotope cross-section, sequence LP1, SW Montana	137
Figure 3.15: Outcrop photograph of section Ashbough Canyon	138
Figure 3.16: Graphic sedimentary log, sequence LP1, 16 Mile Creek	139

Figure 3.17: Stratigraphic cross-section, sequence LP2, central Montana	140
Figure 3.18: Carbon isotope cross-section, sequence LP2, central Montana	141
Figure 3.19: Graphic sedimentary log, sequence LP2, Livingston	142
Figure 3.20: Stratigraphic cross-section, sequence LP2, SW Montana	143
Figure 3.21: Carbon isotope cross-section, sequence LP2, SW Montana	144
Figure 3.22: Stratigraphic cross-section, sequence LP3, central Montana	145
Figure 3.23: Carbon isotope cross-section, sequence LP3, central Montana	146
Figure 3.24: Stratigraphic cross-section, sequence LP3, SW Montana	147
Figure 3.25: Carbon isotope cross-section, sequence LP3, SW Montana	148
Figure 3.26: Sedimentary log, sequences LP2 and LP3, Bell-McKenzie	149
Figure 3.27: Graphic sedimentary log, sequence LP3, 16 Mile Creek	150
Figure 3.28: Graphic sedimentary log, sequence LP3, Livingston	151
Figure 3.29: Stratigraphic cross-section, sequence MC1, central Montana	152
Figure 3.30: Graphic sedimentary log, sequence MC1, Sacagawea Peak	153
Figure 3.31: Stratigraphic cross-section, sequence MC1, SW Montana	154
Figure 3.32: Graphic sedimentary log, sequence MC1, Livingston	155
Figure 3.33: Outcrop photograph from sequence MC2, Monarch	156
Figure 3.34: Graphic sedimentary log, sequence MC2, Sacagawea Peak	157
Figure 3.35: Stratigraphic cross-section, sequence MC2, central Montana	158
Figure 3.36: Stratigraphic cross-section, sequence MC2, SW Montana	159
Figure 3.37: Graphic sedimentary log, sequence MC2, Bell-McKenzie	160
Figure 3.38: Graphic sedimentary log, sequence MC3, Bell-McKenzie	161
Figure 3.39: Stratigraphic cross-section, sequence MC3, central Montana	162
Figure 3.40: Stratigraphic cross-section, sequence MC3, SW Montana	163
Figure 3.41: Graphic sedimentary log, sequence MC3, Livingston	164
Figure 3.42: Stratigraphic cross-section, sequence MC4, SW Montana	165
Figure 3.43: Graphic sedimentary log, sequence MC4, Bell-McKenzie	166
Figure 3.44: Graphic sedimentary log, sequence MC4, Sacagawea Peak	167
Figure 3.45: Stratigraphic cross-section, sequence MC4, central Montana	168
Figure 3.46: Stratigraphic cross-section, sequence SP1	169
Figure 3.47: Graphic sedimentary log, sequence SP1, Bell-McKenzie	170
Figure 3.48: Graphic sedimentary log, sequence SP1, Copper Mountain	171
Figure 3.49: Graphic sedimentary log, sequence SP2, Bell-McKenzie	172
Figure 3.50: Stratigraphic cross-section, sequence SP2	173
Figure 3.51: Graphic sedimentary log, sequence SP2, Copper Mountain	174
Figure 3.52: Stratigraphic cross-section, sequence SP3	175
Figure 3.53: Graphic sedimentary log, sequence SP3, Bell-McKenzie	176
Figure 3.54: Graphic sedimentary log, sequence SP3, Copper Mountain	177
Figure 3.55: Stratigraphic cross-section, sequence SP4	178
Figure 3.56: Graphic sedimentary log, sequence SP4, Copper Mountain	179
Figure 3.57: Outcrop photograph, sequence SP4, Copper Mountain	180
Figure 3.58: Stratigraphic cross-section, sequence SP5	181
Figure 3.59: Graphic sedimentary log, sequence SP5, East Canyon	182
Figure 3.60: Stratigraphic cross-section, sequence SP6	183
Figure 3.61: Graphic sedimentary log, sequence SP6, East Canyon	184
Figure 3.62: Stratigraphic cross-section, sequence SP7	185

Figure 3.63: Graphic sedimentary log, sequence SP7, East Canyon	186
Figure 3.64: Outcrop photograph, Scott Peak and South Creek Fms	187
Figure 3.65: Map of Mississippian regional paleotectonic elements	188
Figure 3.66: Mississippian isopach with Antler cross-section location	189
Figure 3.67: Mississippian isopach with central Montana cross-section	190
Figure 3.68: Sequence stratigraphic cross-section, SW Montana and Idaho	191
Figure 3.69: Sequence stratigraphic cross-section, central Montana	192
Figure 3.70: Sequence stratigraphic cross-section, central Montana	193
Figure 4.1: Tectonostratigraphic boundary chart, Great Basin, USA	220
Figure 4.2: Flexural profile of a retroarc foreland basin	221
Figure 4.3: Mississippian paleogeographic map of the western USA	222
Figure 4.4: Mississippian regional formation-scale stratigraphic cross-section	223
Figure 4.5: Viscoelastic material response to stress in time	224
Figure 4.6: Viscoelastic relaxation of a semi-infinite broken plate	225
Figure 4.7: Sequence stratigraphic cross-section, Madison Gp, SW MT	226
Figure 4.8: Conformable mapping of stratigraphic sequences	227
Figure 4.9: Lower and middle Mississippian regional tectonic element map	228
Figure 4.10: Precambrian basement map, western USA	229
Figure 4.11: Cross-sectional profiles of flexed lithosphere	230

LIST OF APPENDICES

APPENDIX 1

Appendix 1.1: Lithology legend for graphic sedimentary logs	244
Appendix 1.2: Allochem symbol legend for sedimentary logs	245
Appendix 1.3: Sedimentary structure symbol legend for graphic logs	246

APPENDIX 2

Appendix 2.1: Section Livingston	247
Appendix 2.2: Section Livingston, continued	248
Appendix 2.3: Section Livingston, continued	249
Appendix 2.4: Section Livingston, continued	250
Appendix 2.5: Section Livingston, continued	251
Appendix 2.6: Section Livingston, continued	252
Appendix 2.7: Section Livingston, continued	253
Appendix 2.8: Section Livingston, continued	254
Appendix 2.9: Section Livingston, continued	255
Appendix 2.10: Section Livingston, continued	256
Appendix 2.11: Section Livingston, continued	257

APPENDIX 3

Appendix 3.1: Section Sacagawea Peak	258
Appendix 3.2: Section Sacagawea Peak, continued	259
Appendix 3.3: Section Sacagawea Peak, continued	260
Appendix 3.4: Section Sacagawea Peak, continued	261
Appendix 3.5: Section Sacagawea Peak, continued	262
Appendix 3.6: Section Sacagawea Peak, continued	263
Appendix 3.7: Section Sacagawea Peak, continued	264
Appendix 3.8: Section Sacagawea Peak, continued	265
Appendix 3.9: Section Sacagawea Peak, continued	266
Appendix 3.10: Section Sacagawea Peak, continued	267
Appendix 3.11: Section Sacagawea Peak, continued	268
Appendix 3.12: Section Sacagawea Peak, continued	269

APPENDIX 4

Appendix 4.1: Section 16 Mile Creek	270
Appendix 4.2: Section 16 Mile Creek, continued	271
Appendix 4.3: Section 16 Mile Creek, continued	272
Appendix 4.4: Section 16 Mile Creek, continued	273
Appendix 4.5: Section 16 Mile Creek, continued	274
Appendix 4.6: Section 16 Mile Creek, continued	275
Appendix 4.7: Section 16 Mile Creek, continued	276
Appendix 4.8: Section 16 Mile Creek, continued	277
Appendix 4.9: Section 16 Mile Creek, continued	278
Appendix 4.10: Section 16 Mile Creek, continued	279
Appendix 4.11: Section 16 Mile Creek, continued	280

Appendix 4.12: Section 16 Mile Creek, continued	281
Appendix 4.13: Section 16 Mile Creek, continued	282
Appendix 4.14: Section 16 Mile Creek, continued	283
Appendix 4.15: Section 16 Mile Creek, continued	284

APPENDIX 5

Appendix 5.1: Section Monarch	285
Appendix 5.2: Section Monarch, continued	286
Appendix 5.3: Section Monarch, continued	287
Appendix 5.4: Section Monarch, continued	288
Appendix 5.5: Section Monarch, continued	289
Appendix 5.6: Section Monarch, continued	290
Appendix 5.7: Section Monarch, continued	291
Appendix 5.8: Section Monarch, continued	292
Appendix 5.9: Section Monarch, continued	293
Appendix 5.10: Section Monarch, continued	294
Appendix 5.11: Section Monarch, continued	295
Appendix 5.12: Section Monarch, continued	296

APPENDIX 6

Appendix 6.1: Section Baldy Mountain	297
Appendix 6.2: Section Baldy Mountain, continued	298
Appendix 6.3: Section Baldy Mountain, continued	299
Appendix 6.4: Section Baldy Mountain, continued	300
Appendix 6.5: Section Baldy Mountain, continued	301
Appendix 6.6: Section Baldy Mountain, continued	302
Appendix 6.7: Section Baldy Mountain, continued	303
Appendix 6.8: Section Baldy Mountain, continued	304
Appendix 6.9: Section Baldy Mountain, continued	305
Appendix 6.10: Section Baldy Mountain, continued	306
Appendix 6.11: Section Baldy Mountain, continued	307
Appendix 6.12: Section Baldy Mountain, continued	308
Appendix 6.13: Section Baldy Mountain, continued	309
Appendix 6.14: Section Baldy Mountain, continued	310
Appendix 6.15: Section Baldy Mountain, continued	311

APPENDIX 7

Appendix 7.1: Section Ashbough Canyon	312
Appendix 7.2: Section Ashbough Canyon, continued	313
Appendix 7.3: Section Ashbough Canyon, continued	314
Appendix 7.4: Section Ashbough Canyon, continued	315
Appendix 7.5: Section Ashbough Canyon, continued	316
Appendix 7.6: Section Ashbough Canyon, continued	317
Appendix 7.7: Section Ashbough Canyon, continued	318
Appendix 7.8: Section Ashbough Canyon, continued	319
Appendix 7.9: Section Ashbough Canyon, continued	320

APPENDIX 8

Appendix 8.1: Section Bell-McKenzie Canyons	321
Appendix 8.2: Section Bell-McKenzie Canyons, continued	322
Appendix 8.3: Section Bell-McKenzie Canyons, continued	323
Appendix 8.4: Section Bell-McKenzie Canyons, continued	324
Appendix 8.5: Section Bell-McKenzie Canyons, continued	325
Appendix 8.6: Section Bell-McKenzie Canyons, continued	326
Appendix 8.7: Section Bell-McKenzie Canyons, continued	327
Appendix 8.8: Section Bell-McKenzie Canyons, continued	328
Appendix 8.9: Section Bell-McKenzie Canyons, continued	329
Appendix 8.10: Section Bell-McKenzie Canyons, continued	330
Appendix 8.11: Section Bell-McKenzie Canyons, continued	331
Appendix 8.12: Section Bell-McKenzie Canyons, continued	332
Appendix 8.13: Section Bell-McKenzie Canyons, continued	333
Appendix 8.14: Section Bell-McKenzie Canyons, continued	334
Appendix 8.15: Section Bell-McKenzie Canyons, continued	335
Appendix 8.16: Section Bell-McKenzie Canyons, continued	336
Appendix 8.17: Section Bell-McKenzie Canyons, continued	337
Appendix 8.18: Section Bell-McKenzie Canyons, continued	338
Appendix 8.19: Section Bell-McKenzie Canyons, continued	339
Appendix 8.20: Section Bell-McKenzie Canyons, continued	340
Appendix 8.21: Section Bell-McKenzie Canyons, continued	341
Appendix 8.22: Section Bell-McKenzie Canyons, continued	342
Appendix 8.23: Section Bell-McKenzie Canyons, continued	343
Appendix 8.24: Section Bell-McKenzie Canyons, continued	344
Appendix 8.25: Section Bell-McKenzie Canyons, continued	345
Appendix 8.26: Section Bell-McKenzie Canyons, continued	346
Appendix 8.27: Section Bell-McKenzie Canyons, continued	347
Appendix 8.28: Section Bell-McKenzie Canyons, continued	348
Appendix 8.29: Section Bell-McKenzie Canyons, continued	349
Appendix 8.30: Section Bell-McKenzie Canyons, continued	350
Appendix 8.31: Section Bell-McKenzie Canyons, continued	351
Appendix 8.32: Section Bell-McKenzie Canyons, continued	352

APPENDIX 9

Appendix 9.1: Section Copper Mountain	353
Appendix 9.2: Section Copper Mountain, continued	354
Appendix 9.3: Section Copper Mountain, continued	355
Appendix 9.4: Section Copper Mountain, continued	356
Appendix 9.5: Section Copper Mountain, continued	357
Appendix 9.6: Section Copper Mountain, continued	358
Appendix 9.7: Section Copper Mountain, continued	359
Appendix 9.8: Section Copper Mountain, continued	360
Appendix 9.9: Section Copper Mountain, continued	361
Appendix 9.10: Section Copper Mountain, continued	362

Appendix 9.11: Section Copper Mountain, continued	363
Appendix 9.12: Section Copper Mountain, continued	364
Appendix 9.13: Section Copper Mountain, continued	365
Appendix 9.14: Section Copper Mountain, continued	366
Appendix 9.15: Section Copper Mountain, continued	367
Appendix 9.16: Section Copper Mountain, continued	368
Appendix 9.17: Section Copper Mountain, continued	369
Appendix 9.18: Section Copper Mountain, continued	370
Appendix 9.19: Section Copper Mountain, continued	371
Appendix 9.20: Section Copper Mountain, continued	372
Appendix 9.21: Section Copper Mountain, continued	373
Appendix 9.22: Section Copper Mountain, continued	374
Appendix 9.23: Section Copper Mountain, continued	375
Appendix 9.24: Section Copper Mountain, continued	376
Appendix 9.25: Section Copper Mountain, continued	377
Appendix 9.26: Section Copper Mountain, continued	378
Appendix 9.27: Section Copper Mountain, continued	379
Appendix 9.28: Section Copper Mountain, continued	380
Appendix 9.29: Section Copper Mountain, continued	381

APPENDIX 10

Appendix 10.1: Section East Canyon	382
Appendix 10.2: Section East Canyon, continued	383
Appendix 10.3: Section East Canyon, continued	384
Appendix 10.4: Section East Canyon, continued	385
Appendix 10.5: Section East Canyon, continued	386
Appendix 10.6: Section East Canyon, continued	387
Appendix 10.7: Section East Canyon, continued	388
Appendix 10.8: Section East Canyon, continued	389
Appendix 10.9: Section East Canyon, continued	390
Appendix 10.10: Section East Canyon, continued	391
Appendix 10.11: Section East Canyon, continued	392
Appendix 10.12: Section East Canyon, continued	393
Appendix 10.13: Section East Canyon, continued	394
Appendix 10.14: Section East Canyon, continued	395
Appendix 10.15: Section East Canyon, continued	396
Appendix 10.16: Section East Canyon, continued	397
Appendix 10.17: Section East Canyon, continued	398
Appendix 10.18: Section East Canyon, continued	399
Appendix 10.19: Section East Canyon, continued	400
Appendix 10.20: Section East Canyon, continued	401
Appendix 10.21: Section East Canyon, continued	402
Appendix 10.22: Section East Canyon, continued	403
Appendix 10.23: Section East Canyon, continued	404
Appendix 10.24: Section East Canyon, continued	405
Appendix 10.25: Section East Canyon, continued	406

APPENDIX 11

Appendix 11.1: Section Upper Pahsimeroi	407
Appendix 11.2: Section Upper Pahsimeroi, continued	408
Appendix 11.3: Section Upper Pahsimeroi, continued	409
Appendix 11.4: Section Upper Pahsimeroi, continued	410
Appendix 11.5: Section Upper Pahsimeroi, continued	411
Appendix 11.6: Section Upper Pahsimeroi, continued	412
Appendix 11.7: Section Upper Pahsimeroi, continued	413
Appendix 11.8: Section Upper Pahsimeroi, continued	414
Appendix 11.9: Section Upper Pahsimeroi, continued	415
Appendix 11.10: Section Upper Pahsimeroi, continued	416
Appendix 11.11: Section Upper Pahsimeroi, continued	417
Appendix 11.12: Section Upper Pahsimeroi, continued	418
Appendix 11.13: Section Upper Pahsimeroi, continued	419
Appendix 11.14: Section Upper Pahsimeroi, continued	420
Appendix 11.15: Section Upper Pahsimeroi, continued	421
Appendix 11.16: Section Upper Pahsimeroi, continued	422
Appendix 11.17: Section Upper Pahsimeroi, continued	423

APPENDIX 12

Appendix 12.1: Section Antelope Creek	424
Appendix 12.2: Section Antelope Creek, continued	425
Appendix 12.3: Section Antelope Creek, continued	426
Appendix 12.4: Section Antelope Creek, continued	427
Appendix 12.5: Section Antelope Creek, continued	428
Appendix 12.6: Section Antelope Creek, continued	429
Appendix 12.7: Section Antelope Creek, continued	430
Appendix 12.8: Section Antelope Creek, continued	431
Appendix 12.9: Section Antelope Creek, continued	432
Appendix 12.10: Section Antelope Creek, continued	433
Appendix 12.11: Section Antelope Creek, continued	434
Appendix 12.12: Section Antelope Creek, continued	435
Appendix 12.13: Section Antelope Creek, continued	436

CHAPTER 1. GEOLOGIC SETTING AND REGIONAL FRAMEWORK

1.1 SUMMARY

The aims of this study are to extend the established high-resolution sequence stratigraphic framework of the Madison Formation of Wyoming and southern central Montana (Sonnenfeld, 1996a, 1996b; Elrick, 1990; Elrick and Read, 1991) to the correlative and genetically-related Mississippian carbonate ramp, ramp margin, and basin strata of the central Montana trough and Antler foreland basin in order to examine and discriminate the controls on depositional processes and the resulting stratigraphic architecture through space and time in tectonically-active settings. Herein is an outcrop-based, high-resolution sequence stratigraphic study of two ramp-to-basin transects, one in central Montana and the other in southwestern Montana and east-central Idaho, in order to examine these deposits across two coeval margins with differing subsidence, hydrodynamic, and physiographic configurations and histories.

The thesis to be tested is whether independent measurements of system response to global and local forcings will allow disentanglement of primary controls on deposition and allow us to gain understanding of the roles and interplay of these controls, in particular eustasy and tectonics, on the system's architectural development. Conversely, insight into the geodynamic evolution of western North America, glacioeustatic changes, and variations in global climate and oceanographic systems during the greenhouse-to-icehouse transition is sought to be gained.

The focal product of the study is a series of high-resolution sequence stratigraphic cross-sections and time-slices incorporating new outcrop measured sections and measured sections previously collected by members of the Comparative Sedimentology Laboratory (Smith et al., 2000, 2001, 2004) in a series of transects across the Madison ramp system. The results of the study include resolution of sequential foreland basin subsidence, carbonate sediment production and progradation, subsidence and uplift of foreland basin structures along a carbonate shelf edge, diachronous subsidence of discrete depocenters, and eustasy.

1.2 INTRODUCTION

The Mississippian period was one of the most significant times of global change of the Phanerozoic and, perhaps, in Earth history. Two critical global events characterize the Mississippian: the assembly of the Pangean supercontinent (Veevers and Powell, 1987) and the cooling of global climate which was marked by the onset of major Gondwanan glaciation. This period is also characterized by major changes in the earth's biotic system, which may be related to global changes in the carbon cycle. Two of the Phanerozoic's most prominent marine mass extinctions, the Frasnian-Famnenian and Viséan-Namurian (Webster and Groessens, 1990; Ziegler and Lane, 1987), bracket the Lower Mississippian, and at the same time vascular land plants greatly expanded, which significantly altered the global carbon cycle by drawing down atmospheric levels of CO₂ through enhancement of chemical weathering rates and burial of organic carbon (Bernier, 1990).

The transitional nature of this time not only spanned the globe but also regionally impacted the western margin of North America. In the Late Devonian and Early Mississippian, an arc system impinged on the passive margin of western North America and a foreland developed in response to compression and the loading of the Roberts Mountain allochthon onto the continental lithosphere during the Antler orogeny (Roberts et al., 1958). A series of linked basins formed along the western North American margin (Johnson and Pendergast, 1981) in response to subsidence associated with the orogeny and may have acted as storage areas for organic carbon further removing CO₂ from the atmosphere (Saltzman et al., 2000). The records of the global greenhouse to icehouse transition, supercontinent assembly and associated mantle dynamics, and regional reconfiguration from a passive margin to a foreland is archived the carbonate sediments of the Madison Group and equivalents in the northern US Rockies.

Production of carbonate sediments is largely dependent on a number of primary controlling factors including, light (water depth and turbidity), temperature, salinity, and nutrients (Bathurst, 1975; Lees and Buller, 1972; Hallock and Schlager, 1986; Schlager, 1992), which are further forced by secondary processes such as sedimentation rate, climate, water quality and oceanic circulation, tectonic setting, antecedent topography, compaction, and the evolution of carbonate producing organisms. Carbonate sediment

production is dominantly water depth-dependent, and as such, sea-level change is thought to largely control the architecture of carbonate depositional systems primarily through multiscale eustatic sea-level changes and subsidence (e.g., Kendall and Schlager, 1981; Crevello et al., 1989; Loucks and Sarg, 1993). The Lower and middle Mississippian of western North America encompass a time and space where most of the first- and second-order controls on carbonate production are in flux: increasing amplitude of glacioeustatic sea-level change in response to Gondawanian icesheet expansion; variable antecedent topography and subsidence rates and changing patterns in ocean circulation due to the compressional tectonic setting; and cycles of decimation and evolution of carbonate producing organisms in association with the Late Paleozoic mass extinction events. The expansive temporal and secular extent of the Lower to middle Mississippian Madison system provides an opportunity to examine earth history during this period of radical change through the unfiltered lens of a system which is sensitive to and directly impacted by these changes at all relevant scales. The major reorganizations in the primary and secondary controls of carbonate production, transport and storage during the Lower and middle Mississippian allow testing of paradigms of carbonate ramp development during times of large gradients in forcing functions where the system is far from equilibrium; system readjustment to these stresses; and near-equilibrium, steady state processes.

This study addresses three fundamental issues associated with development of the Madison ramp and the evolution of the Antler foreland basin: the deconvolution of relative sea-level controls on carbonate sedimentary architecture development; the tectonic framework for accommodation development in a foreland setting; and the evolution of the foreland basin and geodynamics of the setting. One aspect of this study is the examination of the interplay of eustasy and tectonics at all temporal and spatial scales using high-resolution sequence stratigraphy and attempt to extract the subtle signals that tectonic and eustatic processes contribute to the architecture of the carbonate system. It is particularly critical to resolve the high-resolution architecture of the system which lies below seismic resolution to improve predictive models of carbonate facies distributions in active tectonic settings. Second, foreland basin geometry is a function of the thrust load which is emplaced, the rheological properties of the lithosphere upon which the load was emplaced, and the loading of the basin by sedimentary infill. By examining the

changing distribution of accommodation space through time as indicated by changes in the distributions and thicknesses of carbonate lithofacies, lithospheric response to loading can be calculated. This analysis is used to constrain the timing, location, and magnitude of thrust load emplacement as revealed in carbonate facies patterns. Lastly, carbonate ramps in foreland settings are predicted to be both spatially and temporally restricted and are generally considered as relatively minor constituents of foreland depositional settings; however, the Madison ramp apparently contradicts these model predictions, as it was both a spatially expansive ($>> 100,000 \text{ km}^2$) and long-lived system ($\sim 15 \text{ Ma}$) and contributed up to 1500 m of carbonate sediment to the foreland basin fill. The third aspect of this project is addressing the disparity between the modeled and the observed carbonate responses to foreland basin subsidence by quantitatively assessing the mechanisms of differential subsidence across the region and examining the genetic implications for carbonate ramp development.

1.3 WHY STUDY THE MADISON?

The Madison Group and lateral equivalents is ideal for this study for the following reasons:

1. The Madison is a large epicontinental ramp, which is well-exposed regionally in relatively autochthonous outcroppings from its furthest up-dip extent to the laterally equivalent basin over an area of $\sim 300,000 \text{ km}^2$ (Maughan, 1983). This makes the Madison an ideal setting for studying the evolution of a low-angle ramp setting at all spatially- and temporally-significant scales.
2. A large volume of work on the high-resolution sequence stratigraphy and diagenesis of the Madison Formation in Wyoming (Westphal et al., 1999, 2004; Smith et al., 2000, 2001, 2004; Sonnenfeld, 1996a, 1996b; Elrick, 1990; Elrick and Read, 1991) will enable us to examine the ramp at a comprehensive, large scale and allow us to build on the regional stratigraphic and diagenetic framework already in place for updip areas.
3. The Madison provides an archive which is sensitive to changing climate, biogeochemistry, and tectonics during a period of major global and regional climatic transition and tectonic reorganization. By examining the arrangement, evolution and distribution of architectural elements, we can look at the local and regional controls on deposition incrementally as the systems steps through time.

4. The Madison system is bounded by two distinct orthogonal margins with differing subsidence, antecedent topography, and hydrodynamic conditions and histories. Here, these paradigmatic controls on carbonate deposition can be tested and their roles assessed. Additionally, this configuration provides a ready test bed for comparative study between the margins as well as the fill of the adjoining foreland basin and aulacogen.

1.4 DISCUSSION

1.4.1 Deconvolution of Relative Sea-Level Controls on Architecture Development

Changes in the architecture of marine strata are directly related to the change in available space for deposition, or accommodation space. Accommodation space is a function of several variables, namely, eustatic sea level and relative tectonic motion (i.e., subsidence or uplift). Unfortunately, as these variables normally act in concert, that poses an inherent problem in assessing the relative contribution of each. It has generally been shown that well-developed regional unconformities and the supergroup- to group-scale architecture of the strata they bound are related to tectonic processes (Sloss, 1963; Quinlan and Beaumont, 1984; Tankard, 1986). These tectonically-driven unconformities typically bound the continental-scale first-order megasequences of Sloss (1963) as well as regional second-order supersequences (Quinlan and Beaumont, 1984), and tectonic processes control these long-term accommodation development trends. At shorter temporal scales (third- to fifth-order) in carbonate systems, however, eustatic sea-level change apparently is the dominant process controlling accommodation development, even in tectonically active basins (Vail et al., 1977; Giles and Dickinson, 1995; Giles, 1996; Giles et al., 1999).

An example of this phenomenon comes from the Late Devonian of Utah and Nevada. Giles and others (1999) demonstrate that in the Late Devonian, forced regressive shoreface sandstones were repeatedly deposited in downslope positions in response to third-order eustatic sea-level change; however, the forced regressive deposits stack in an overall retrogradational pattern, which is inconsistent with the Devonian coastal onlap curve, which shows eustatic sea level fall at this time. They conclude tectonic subsidence drives long-term accommodation development at the scale of the third-order composite sequence (and larger scale), while eustasy modulates accommodation at third-order and shorter time scales. Preliminary work of this study has shown regional correlation of

third-order sequences across the study area, implying eustatic control on third-order packaging in the Madison.

1.4.2 Tectonic Framework for Accommodation Development in a Foreland Setting

Foreland basins provide a unique setting for the study of the interaction of tectonics and eustasy in accommodation development. Foreland basin development is a direct function of flexure of the lithosphere by topographic loads, both the tectonically-emplaced thrust load and the sedimentary load, and subsurface loads due to subduction-related processes. Basin subsidence and geometry is controlled by the density and geometry of the thrust load, rheology of the lithosphere upon which the load is emplaced, the volume and density of the sedimentary infill, and the amount of erosion across the system that functions to redistribute loads system-wide. These processes generally result in the geologically instantaneous development of an asymmetric basin which is deepest adjacent to the emplaced load (foredeep; e.g., Decelles and Giles, 1996) and gradually shallows away from it. The distal margin of the basin forms as the plate elastically flexes in a regional isostatic response that supports the load. In many foreland basin settings, where the elastic thickness of the lithosphere is low (i.e., the plate is weak; Figure 1.1), uplift will occur on the distal margin and accommodation will decrease. This zone of uplift is known as the forebulge (Jacobi, 1981). Cratonward of the forebulge is the backbulge basin (Turcotte and Schubert, 1982) which generally forms an intrashelf basin of long wavelength and low amplitude and experiences orders of magnitude lower rates of subsidence than the foredeep. The net result is that as thrusting occurs a regionally coherent antiphase accommodation pattern develops across the foreland basin: the foredeep and backbulge basin experience net accommodation increase while accommodation decreases across the forebulge.

Stacking pattern analysis of foreland basin strata provides a method for observation and determination of antiphase accommodation relationships. Stacking pattern analysis relates vertical changes in cycle thickness and the proportions of facies which make up the cycle to changes in accommodation space. Results of this analysis highlight spatial variability in accommodation patterns and reveal the nature of the lithospheric response to loading. Additionally, as the thrust load migrates across the foredeep, tectonic inversion occurs as the forebulge is downwarped and the former

backbulge is uplifted. These inversion relationships are observable through time by examining vertical and lateral variations in water depth sensitive facies and spatial stratal thickness patterns. This analysis acts to constrain the geodynamics of the system specifically the timing and location of emplacement of thrust loads and physical properties of the load.

1.4.3 Foreland Basin and Geodynamic Evolution

The geometry of carbonate systems in foreland basin settings is directly linked to the flexural profile of the distal foreland setting (Dorobek, 1995). The gradual slope of the distal foreland provides the ideal setting for homoclinal ramp development nearly to the exclusion of other carbonate depositional geometries (Dorobek, 1995). During phases of tectonic quiescence, carbonate ramps are modeled as aggrading to slightly prograding and partly filling the foreland basin. This is due to sedimentation rate equaling or exceeding relative sea level rise, and as a result the system is able to keep up with or outpace subsidence. The critical subsidence rate beyond which the carbonate system cannot keep up has been modeled as approximately 1 m/ky (Dorobek, 1995). This rate puts a finite limit on the lateral extent of ramps in foreland settings, and typically predicts ramp widths of between 5 km to 40 km depending on lithospheric strength, weaker for the former and stronger for the latter (Figure 1.2). Additionally this critical subsidence rate places a temporal constraint on the expression of the carbonate ramp. As the thrust load migrates cratonward, subsidence rates increase across the basin and the 1 m/ky threshold value propagates landward across the distal foreland. The result is that carbonate ramps are predicted to backstep, or move landward, through time in direct response to load migration.

Observations of the Madison ramp appear to be in conflict with the general model of carbonate ramps in foreland basins as described above. Dorobek and others (1991) and Dorobek (1995) proposed a geodynamic model for the evolution of the northern U.S. Rockies from Late Devonian to Early Pennsylvanian time. Their model was based on regional isopach data, detailed measured sections, and one-dimensional Airy isostatic modeling of selected outcrop localities. Subsidence analyses indicated that there was contemporaneous episodic subsidence which affected an area extending 800 km from the foredeep to the epicratonic platform (Dorobek, 1995), and isopach maps revealed a series

of paleotectonic elements across this region. The paleotectonic elements typically had wavelengths of 50-200 km and amplitudes of 50-350 m, were often oriented at high angles to the thrust load, and were spatially coincident over the 50-60 million year evolution of this stratigraphic sequence. Although the paleotectonic elements were spatially coherent over the period of loading and deposition, these regions commonly experienced tectonic inversions, with depocenters becoming paleohighs and vice versa through time (Dorobek, 1995). Palestructures were observed to geographically coincide with preexisting structural trends related to Proterozoic extension and were interpreted to have been reactivated during Antler convergence (Dorobek, 1995). Dorobek and others (1991) concluded that complex patterns of differential subsidence across the region could not be easily reconciled with a simple flexural model of vertical loading of elastic plates. Instead, they stated that differential subsidence could be explained by some combination of four possible mechanisms: flexure of mechanically independent, fault-bounded blocks by subregional loads; reactivation of Proterozoic structure by transmission of compressive in-plane stress; waxing and waning of compressive in-plane stress due to episodic convergence along the Antler orogenic belt; and sublithospheric processes occurring beneath the Antler foreland plate (Figure 1.3).

This study quantitatively assesses the possible mechanisms for differential subsidence observed regionally across the Madison ramp and adjacent foredeep (cf., Dorobek et al., 1991; Dorobek, 1995) and examines the genetic implications for carbonate ramp development in a complex foreland setting. In particular, this study parameterizes and constrains the various previously published conceptual models of Antler foreland evolution (e.g., Dorobek et al., 1991; Dorobek, 1995) and tests other models which attempt to explain complex spatial subsidence patterns in foreland settings either through flexural processes (e.g., Quinlan and Beaumont, 1984; Tankard, 1986) or brittle, fault-related processes (e.g., Bradley and Kidd, 1991; Waschbusch and Royden, 1992). This study also attempts to reconcile the foreland basin evolution archived in the stratigraphic record with published tectonic studies (Roberts et al., 1958; Smith and Ketner, 1968; Johnson and Pendergast, 1981; Speed and Sleep, 1982; Murphy et al., 1984; Trexler and Cashman, 1991) on the emplacement and evolution of the thrust load of the Roberts Mountain allochthon.

1.5 PREVIOUS WORK

1.5.1 Geologic Setting

The Lower to middle Mississippian (Kinderhookian-Meramecian) Madison Group and equivalents, here forward referred to as the Madison system or simply the Madison, developed on a westward-thickening pericratonic ramp, which was approximately 1600 km long and 400 km wide and extended from the Canadian Arctic to New Mexico (Maughan, 1983; Figure 1.4). The Madison ramp was located approximately 0°-10° north of the paleoequator (McKerrow and Scotese, 1990) where it was bordered to the east by the Transcontinental Arch, the west by the Antler foreland basin, and the north by the central Montana trough, an aulacogen/continental re-entrant system, and the intracratonic Williston Basin (Figure 1.4). Water depths were generally shallow over the ramp, while deeper marine conditions existed in the Antler foredeep, central Montana trough, and Williston Basin (Reid and Dorobek, 1993). Two cross-sections were constructed in this study: both are anchored to a trunk trending perpendicularly and extending from northwest of the Transcontinental Arch in Wyoming to just north of the Wyoming-Montana interstate border; from there the cross-sections branch with one segment continuing north into the central Montana trough and the other snapping off normal to the paleobathymetric gradient of the Antler foreland basin to the southwest (Figure 1.5). The Madison system was studied in a series of widely spaced (30 – 100 km apart), well preserved outcroppings, which were uplifted and exposed during the Jurassic-Cretaceous Sevier and Cretaceous-Eocene Laramide orogenies.

1.5.1.1 Litho- and Biostratigraphy

Extensive research on the lithostratigraphy and biostratigraphy of the Madison system has been completed over the last 60 years beginning with the work of Andrichuk (1955a, 1955b, 1958). Regional correlation was primarily based on biostratigraphic information which has been detailed by the work of numerous geologists and paleontologists of the US Geological Survey (Dutro and Sando, 1963a, 1963b; Mamet and Skipp, 1970, 1971; Sandberg, 1967; Sando, 1960a, 1960b, 1972; Sando et al., 1959, 1969, 1975). Sando (1976) summarized the evolution of the Mississippian system of the northern US Rocky Mountains region by compiling and integrating these data sets. Three cycles are described Sando for deposition in this region: Cycle I comprises deposition of

the Madison Group from Kinderhookian-Meramecian time during an initial phase of transgression; Cycle II is marked by karsting and erosion across much of Montana and Wyoming, extending from early Meramecian-Chesterian time; Cycle III is marked by renewed transgression beginning in the middle Meramecian but not reaching parts of the area until Pennsylvanian time.

The Madison Group and stratigraphic equivalents disconformably overlies the Upper Devonian Jefferson Formation in Montana and Idaho, while the Madison Formation of Wyoming lies on an angular unconformity, where the underlying formations get progressively older to the southeast with sub-Madison rocks ranging from Devonian-Cambrian in age (Sandberg and Klapper, 1967; Figure 1.6). The Madison system is dominantly composed of limestone across the study area, but considerable amounts of dolomite are also present, especially in updip locations in Wyoming, and argillaceous material is common in downdip locations in the lower part of the stratigraphic section (Kinderhookian Paine Limestone of Montana; Kinderhookian-lower Meramecian McGowan Creek, Milligen, and Middle Canyon Formations of Idaho; Sandberg, 1976; Figure 1.7). Additionally, two regionally extensive collapse breccias of Osagean age have been correlated with thick (up to 30 m) undissolved evaporite deposits in the subsurface of the Williston Basin (Middleton, 1961; Roberts, 1966; Figure 1.8). In middle Mississippian time (middle Meramecian), sea level fell across the region (Figure 1.9). This event led to downstepping of the carbonate system into the Antler foreland basin and contemporaneous karsting across the former ramp-top in Wyoming and Montana (Sando, 1988). The downstepped ramp (Scott Peak Formation) subsequently prograded across the Antler foreland basin in Idaho and filled the basin during the remaining Meramecian (Rose, 1976; Figure 1.9). In the Late Mississippian (Chesterian), the region was again flooded and deposition of mixed clastics and carbonates of the Amsden Formation, Big Snowy Group, and South Creek and Surrect Canyon Formations occurred across the study area (Figure 1.5).

1.5.1.2 Sequence Stratigraphy

Significant amounts of work have been done on the high-resolution sequence stratigraphy of the Madison Formation at the regional (Elrick, 1990; Elrick and Read, 1991; Sonnenfeld, 1996a, 1996b; Smith et al., 2000, 2001, 2004) and reservoir scales

(Crockett, 1994; Moore, 2001; Westphal et al., 1999, 2004). This study uses the sequence stratigraphic framework of Sonnenfeld (1996a, 1996b) and extends it into the central Montana trough and Antler foreland basin.

Sonnenfeld (1996a, 1996b) asserts that the Madison Formation is comprised of six sequences of third-order duration. The sequences are defined on the basis of unconformities which can be resolved either through evidence of exposure or through changes in accommodation space trends from decreasing to increasing accommodation. The third-order sequences are composed of subordinate sequences of fourth-order duration, which in turn are composed of high-frequency cycles, which make up the fundamental building block of the sequence/cycle hierarchy. Sequences of all durations are composed of transgressive and highstand systems tracts, which are divided by a maximum flooding surface or zone.

The six third-order sequences of the Madison are stacked into two composite sequences (Mitchum and Van Wagoner, 1991; Sonnenfeld, 1996a, 1996b) of approximately third-order duration. These composite sequences further stack into an overall second-order supersequence, which is bound by regionally extensive unconformities (Rose, 1976; Sando, 1988).

1.5.1.3 Regional Tectonics and Geodynamics

During the Upper Devonian to Lower Mississippian, the western margin of North America was transformed from a passive margin, which had persisted since the Late Proterozoic, to a compressional foreland. At this time the poorly understood Antler orogeny occurred along a 2300 km stretch of western North America extending from southern California to British Columbia (Burchfiel and Davis, 1981; Gehrels and Smith, 1987; Miller et al., 1992). Many authors have discussed the plate tectonic setting the Late Devonian-Early Mississippian margin (Burchfiel and Davis, 1972, 1975; Silberling, 1973; Dickinson, 1977; Speed 1977; Nilsen and Stewart, 1980; Miller et al., 1984; Burchfiel and Royden, 1991; Figure 1.11) and, although there is much disagreement, the general consensus is that the Antler orogeny represents a collision of an arc with North America and the subsequent emplacement of the Roberts Mountain allochthon via thrust loading. Loading of the allochthon onto the North American margin produced a flexural downwarp of the continental lithosphere, forming the Antler foreland basin (Speed and

Sleep, 1982; Johnson and Pendergast, 1981). This basin was subsequently filled with several kilometers of clastic sediments derived from the orogenic belt in the adjacent foredeep (Speed and Sleep, 1982) as well as hundreds to thousands of meters of carbonates in distal settings along the craton margin (Rose, 1976; Figure 1.12). Deposition of the Madison system occurred along the craton margin in this distal foreland setting of the Antler orogenic belt (Reid and Dorobek, 1993).

The Antler foreland basin of Utah and Nevada has many of the classic characteristics of peripheral foreland basin settings (Dickinson, 1974; Decelles and Giles, 1996; Figure 1.13) including a well-developed, flexurally-controlled, cross-sectional profile complete with a foredeep adjacent to the emplaced load (i.e., the Roberts Mountain allochthon); a forebulge in flexural response to the loading; a backbulge basin on the continental side of the forebulge; and a shoaling, downwarped pericratonic hinge zone (Speed and Sleep, 1982; Giles and Dickinson, 1995; Giles, 1996; Giles et al., 1999). In contrast, the Montana margins of the Madison system seem not to display this flexurally-dominated profile.

The southwestern Montana margin, which faces the Antler foredeep, is relatively high relief, is complicated by a series of re-entrants, and does not display any flexural characteristics (Peterson, 1985; Figure 1.14). Dorobek and others (1991) suggested that underlying Proterozoic rift-related faulting may contribute to this atypical foreland basin configuration, and suggest that strain may have been accommodated flexurally by mechanically independent, fault-bounded segments in response to subregional vertical loading (Figure 1.15). The central Montana trough, which borders the Madison ramp to the north, is an aulacogen which was variably active during the Paleozoic and is likely controlled in basement-rooted faults (Peterson, 1985; Dorobek et al., 1991; Figure 1.16). The response of the central Montana trough to Antler-related loading is problematic as the aulacogen is oriented nearly perpendicular to the direction of compression. Rather, subsidence in the central Montana trough may be in response to in-plane stress associated with the inferred arc-continent collision (Dorobek et al., 1991). Additionally, based on one-dimensional subsidence analysis of several measured sections in Montana and Idaho, Dorobek and others (1991) concluded that the vast majority of accommodation space

created by tectonic subsidence occurred during the early Kinderhookian, pre-Madison deposition, and only insignificant subsidence occurred during Madison deposition.

This project began as an outgrowth of a Comparative Sedimentology Laboratory study (Smith et al., 2000, 2001, 2004) examining the regional distribution of reservoir quality dolomite of the Madison Formation within a high-resolution sequence stratigraphic framework. Smith and coworkers looked at a series of outcrops and cores along a dip-oriented transect extending from Hartville Canyon in southeastern Wyoming to Benbow Mine in the Beartooth Mountains of southern central Montana. The intent of the current project is to continue the transect of Smith and coworkers and extend it out across two independent ramp margins and into the adjacent basinal settings of the Madison system (Figure 1.17). The thesis to be tested is whether independent measurements of system response to global and local forcings will allow disentanglement of primary controls on deposition and allow us to gain understanding of the roles and interplay of these controls (e.g., eustasy and tectonics) on the system's architectural development. Conversely, insight into the processes themselves (e.g., the geodynamic evolution of western North America, glacioeustatic changes, and variations in global climate and oceanographic systems during the greenhouse-to-icehouse transition) may also be gained.

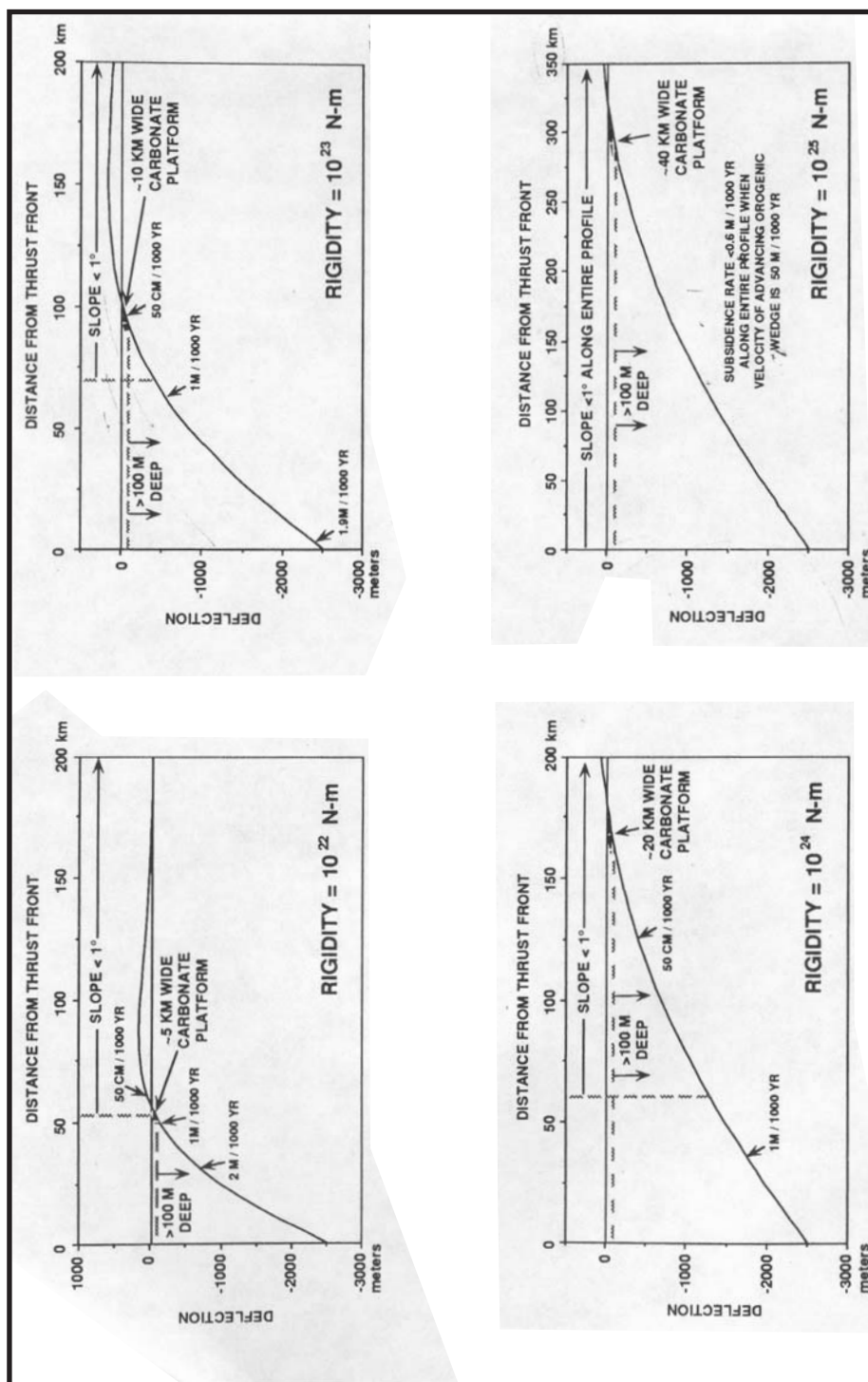


Figure 1.1: Initial flexural profiles of foreland showing when water-filled, the optimum position for carbonate ramp development. All models assume a 5 km thick orogenic wedge and vary the flexural rigidity of the lithosphere upon which the wedge was emplaced. Carbonate ramp width is controlled by the strength of the plate, with stronger plates capable of supporting wider ramps. This is a function of subsidence, which is lower across a strong plate than a weak plate. From Dorobek (1995).

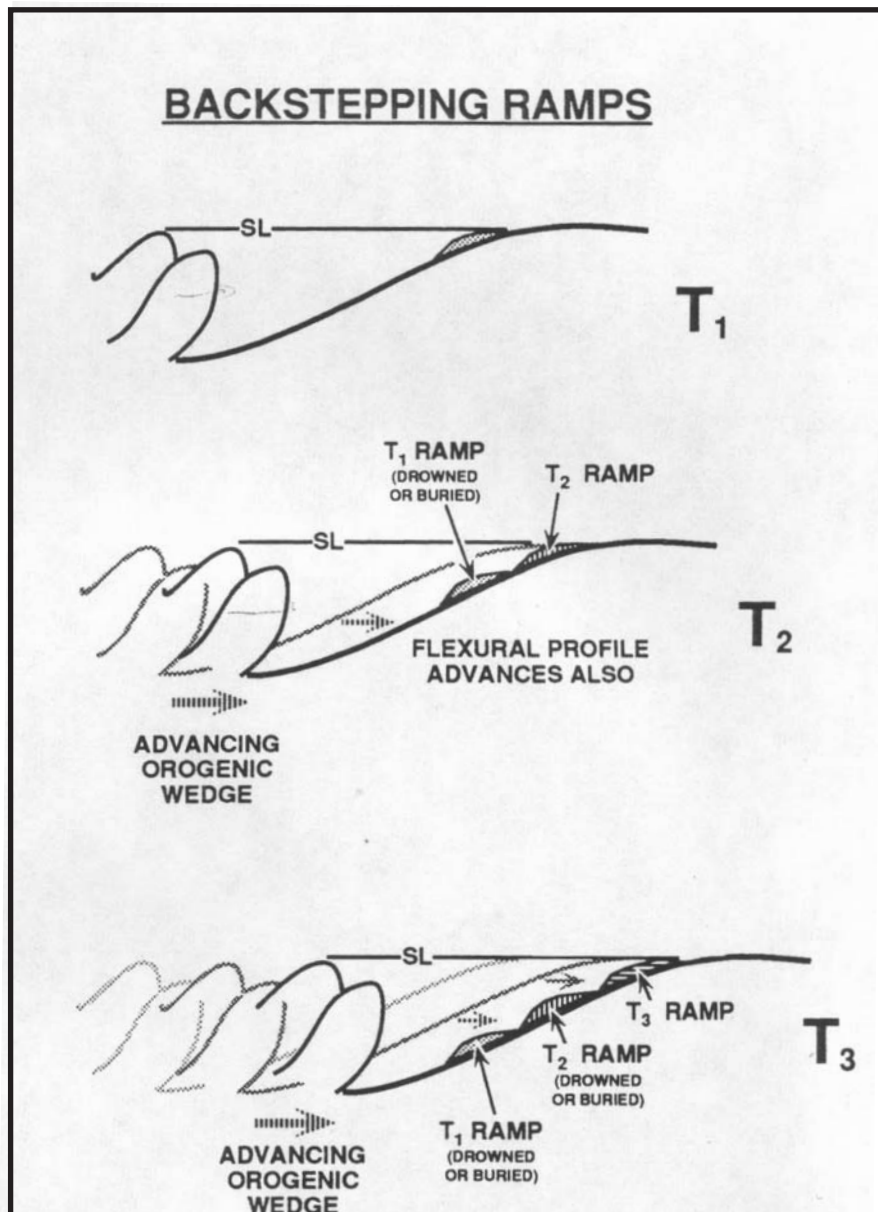


Figure 1.2: Conceptual models of foreland basin carbonate ramps during active convergence. As the load emplaced on the craton migrates forward, so does the flexural profile generated by the load. Carbonate ramps which develop on the distal side of the foreland respond to increasing subsidence by backstepping or drowning. From Dorobek (1995).

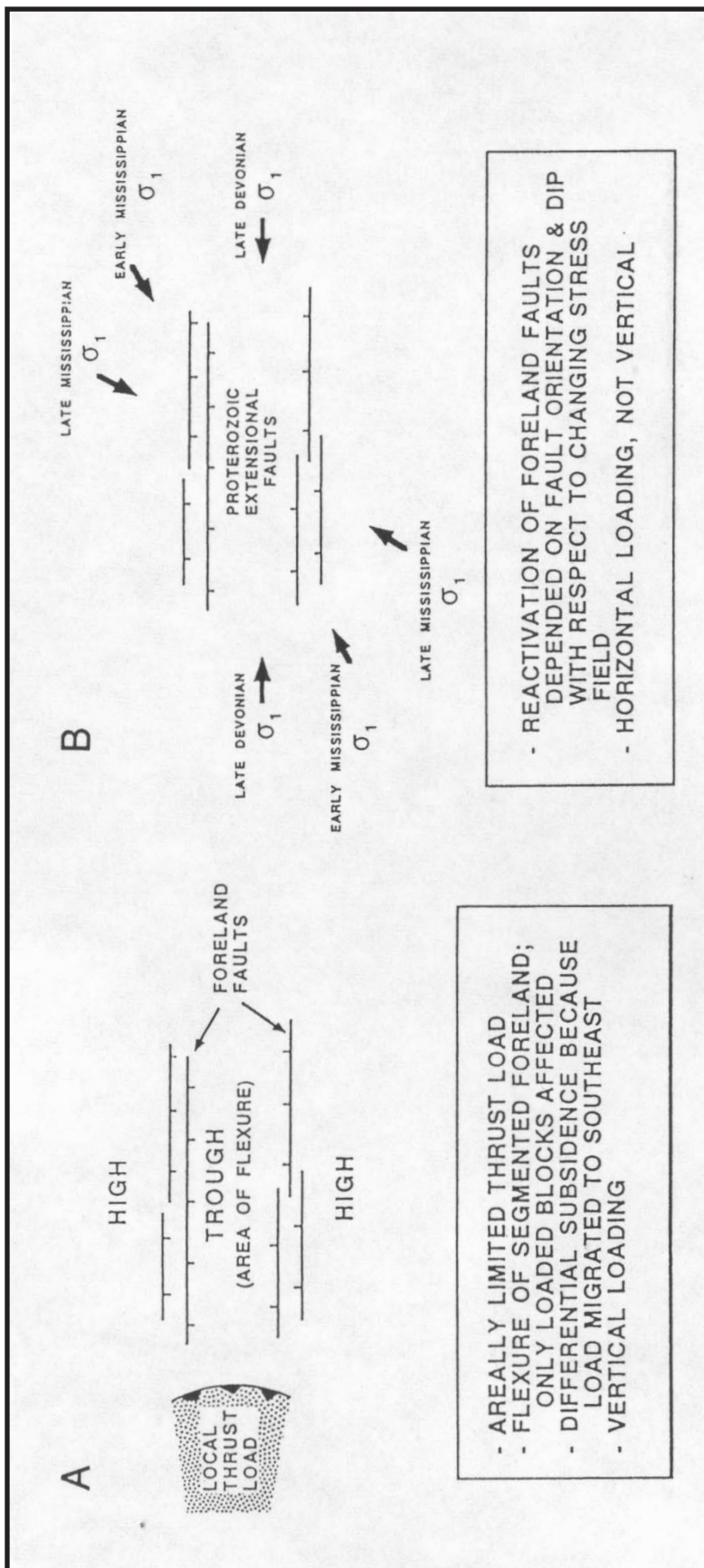


Figure 1.3: Generalized conceptual models invoked to explain differential subsidence observed across the Antler foreland basin of Idaho and Montana. A) Differential subsidence due to subregional vertical loading, which may have been due to emplacement of local thrust loads onto mechanically independent blocks of broken foreland lithosphere. B) Differential subsidence as a result of regional horizontal stress, where in-plane stress due to convergence may have activated movement along old Proterozoic faults. From Dorobek and coworkers (1991).

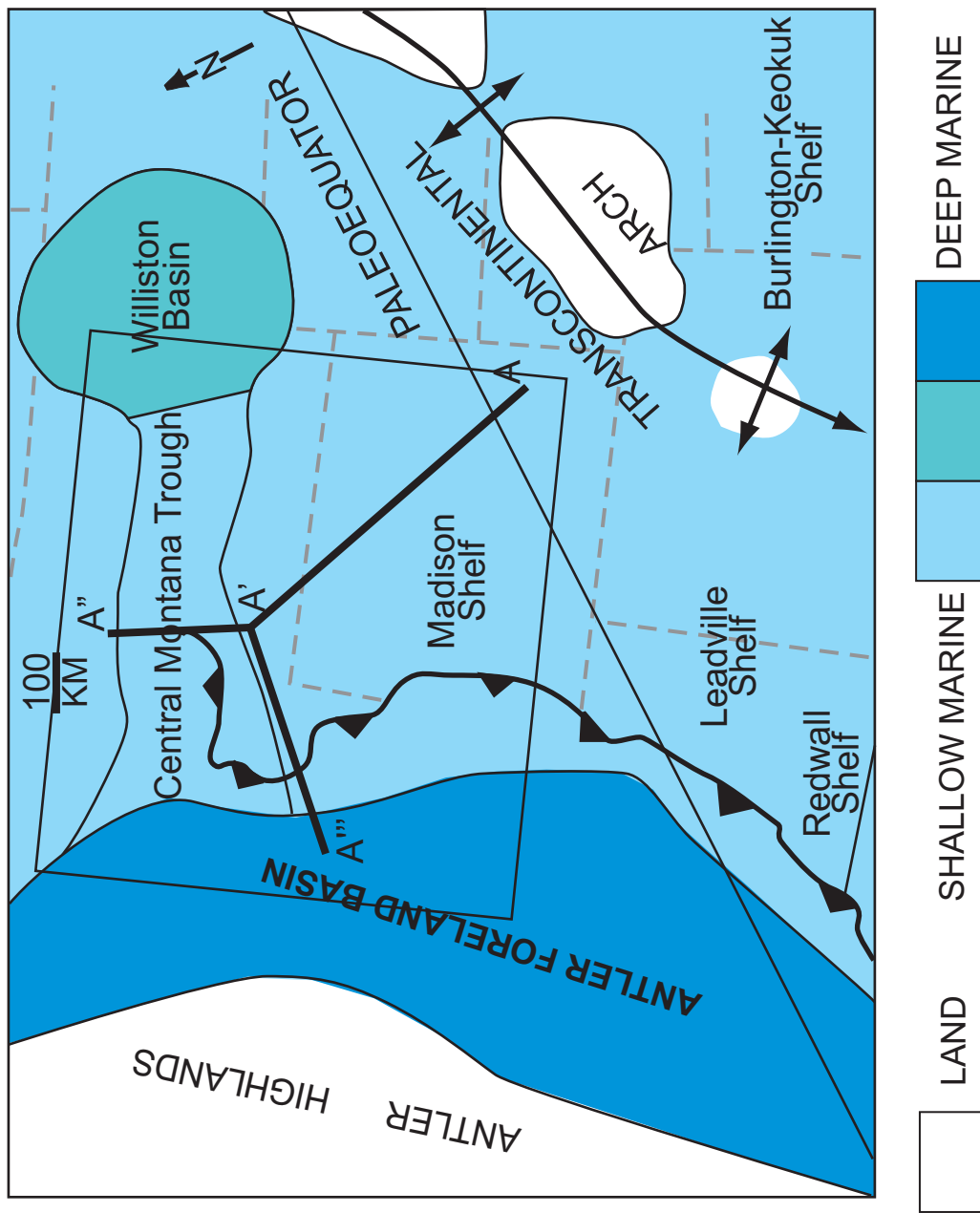


Figure 1.4: Paleogeographic map of the western United States during the Early Mississippian (from Gutschick and Sandberg, 1983). Contours are the interpreted water depths during sequence IV of the Madison of Gutschick and Sandberg. A-A', A'-A'', and A'-A''' in the boxed area denote the cross-section locations of this study.

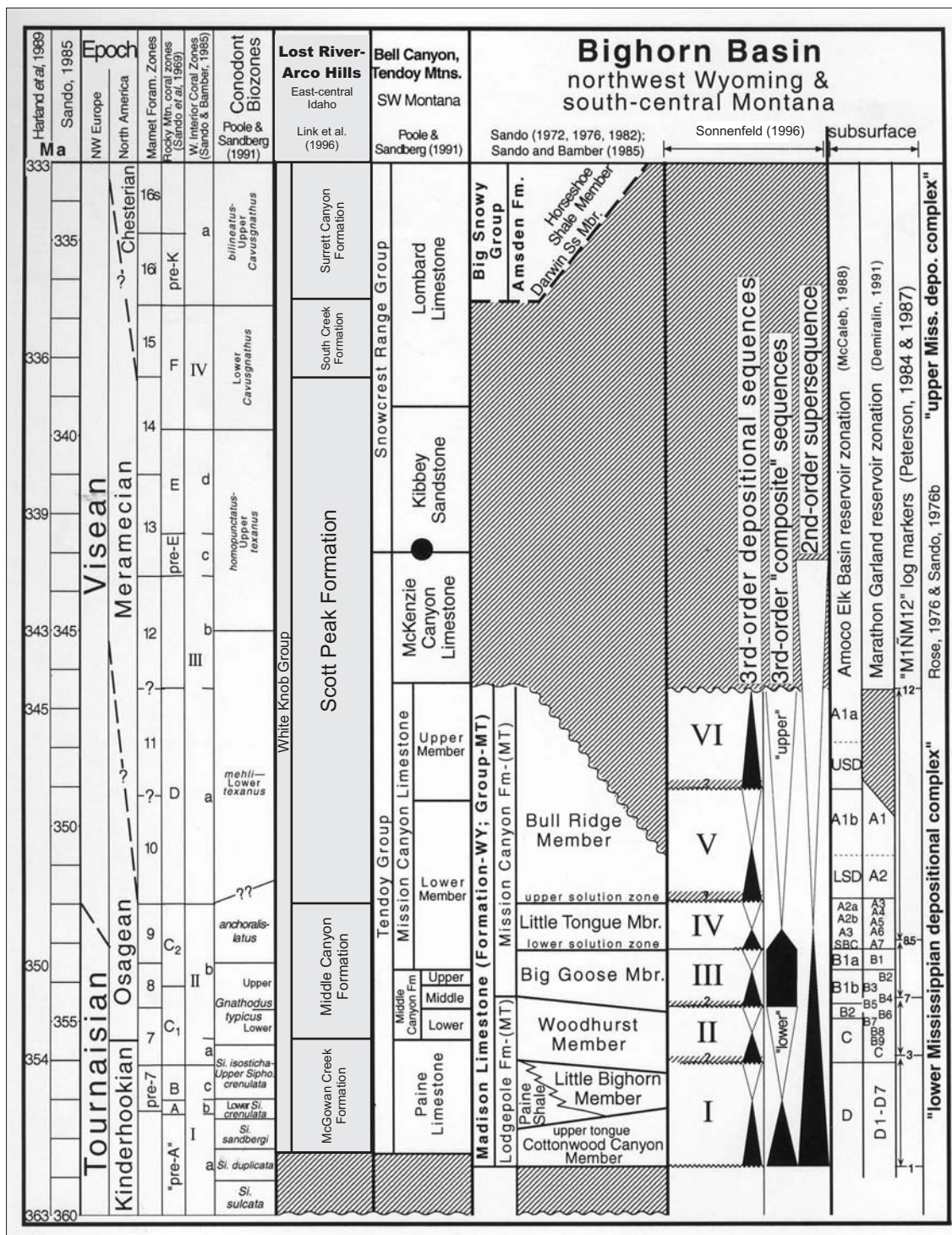


Figure 1.5: Chronostratigraphic chart illustrating the time relationships between the Madison Formation, Group, and its lateral equivalents. Triangles represent changes in accommodationspace, with black triangles showingincreased accommodation and white triangles decreased. Areas of diagonal pattern are hiatuses. Modified from Sonnenfeld (1996b).

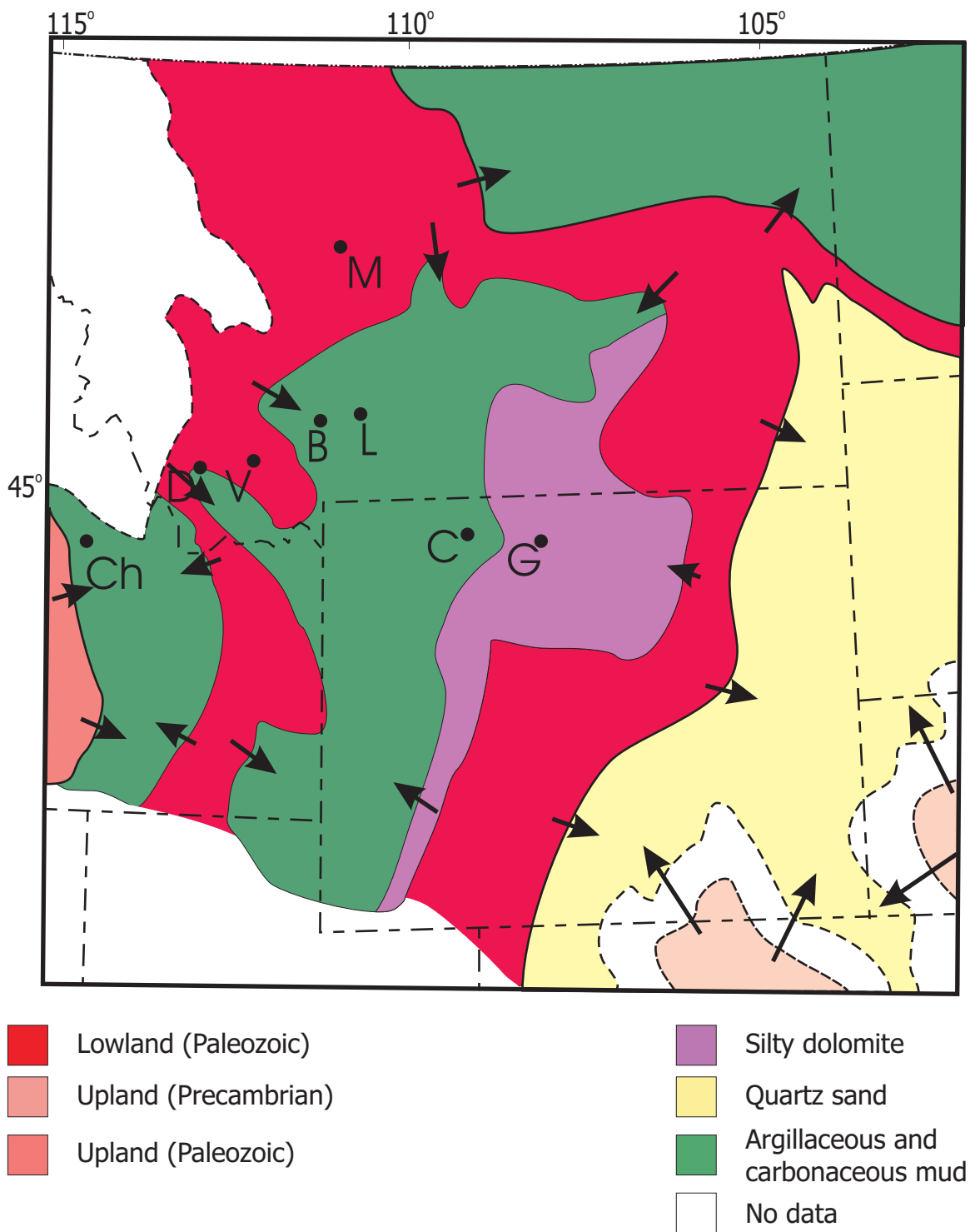


Figure 1.6: Summary facies map of pre-Madison depositional conditions in the northern US Rocky Mountains. This shows the early Kinderhookian landscape pre-inundation by the basal Mississippian transgression. The map represents conditions during Cycle I, Phase I of Sando (1976) which corresponds to composite biozone pre-7, A. Locations: C = Cody, WY; G = Greybull, WY; B = Bozeman, MT; D = Dillon, MT; L = Livingston, MT; M = Monarch, MT; V = Virginia City, MT; Ch = Challis, ID. Modified from Sando (1976).

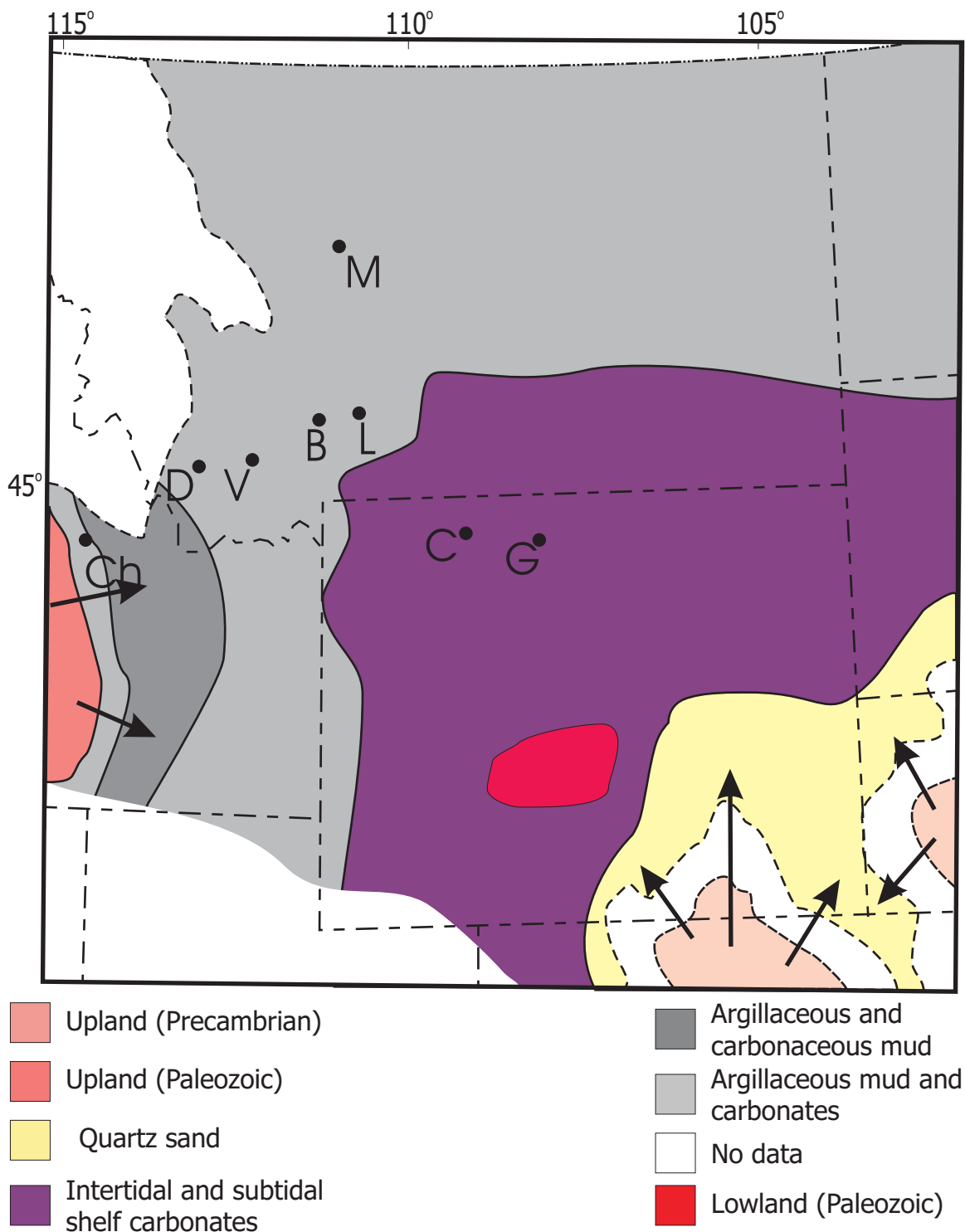


Figure 1.7: Summary facies map of early Madison depositional conditions in the northern US Rocky Mountains. This shows the latest Kinderhookian depositional conditions after full inundation by the Cyle I transgression has occurred and shows broad distribution of argillaceous facies across Montana and Idaho. The map represents conditions during Cycle I, Phase III of Sando (1976) which corresponds to composite biozone pre-7, B. See Figure 1.6 for locations. Modified from Sando (1976).

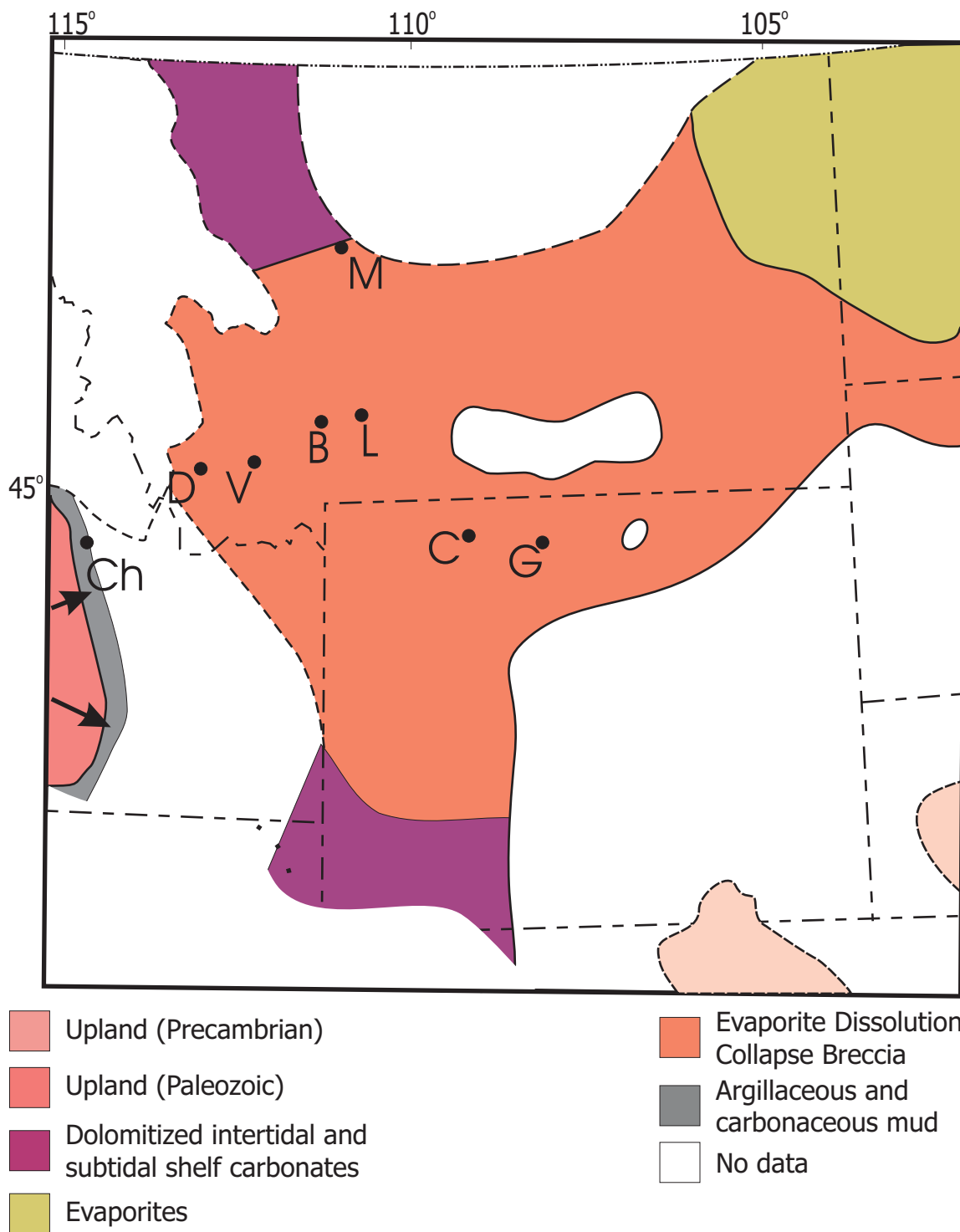


Figure 1.8: Summary facies map of late Madison depositional conditions in the northern US Rocky Mountains. This shows the early Meramecian distribution of facies and the broad distribution of evaporite and related evaporite dissolution collapse breccias across Montana and Wyoming. The map represents conditions during Cycle I, Phase VII of Sando (1976) which corresponds to composite biozone 10, D. See Figure 1.6 for locations. Modified from Sando (1976).

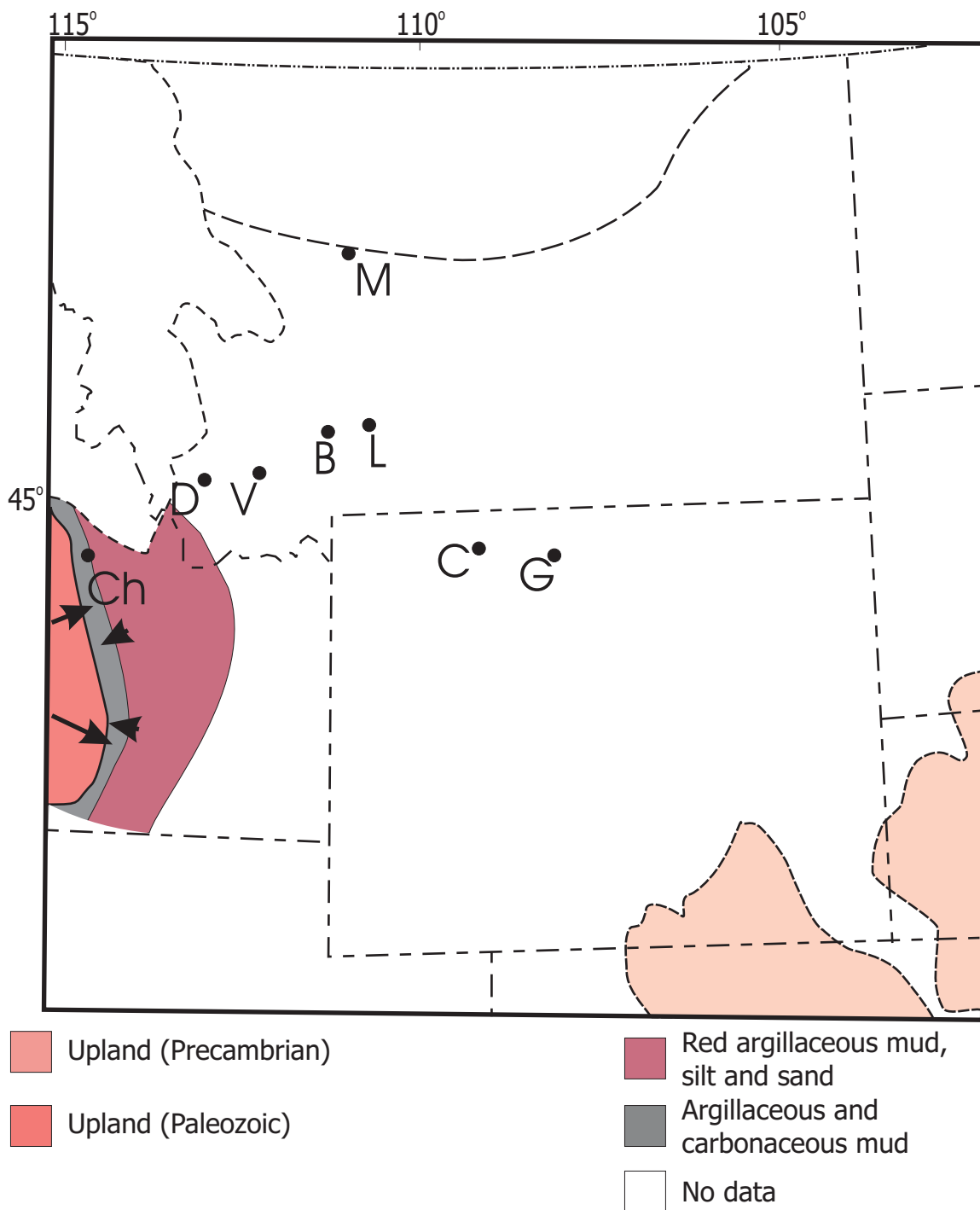


Figure 1.9: Summary facies map of post-Madison depositional conditions in the northern US Rocky Mountains. This shows the limited latest early Meramecian distribution of facies and the development of a karst plain across Montana and Wyoming. The map represents conditions during Cycle II which corresponds to composite biozone 12. See Figure 1.6 for locations. Modified from Sando (1976).

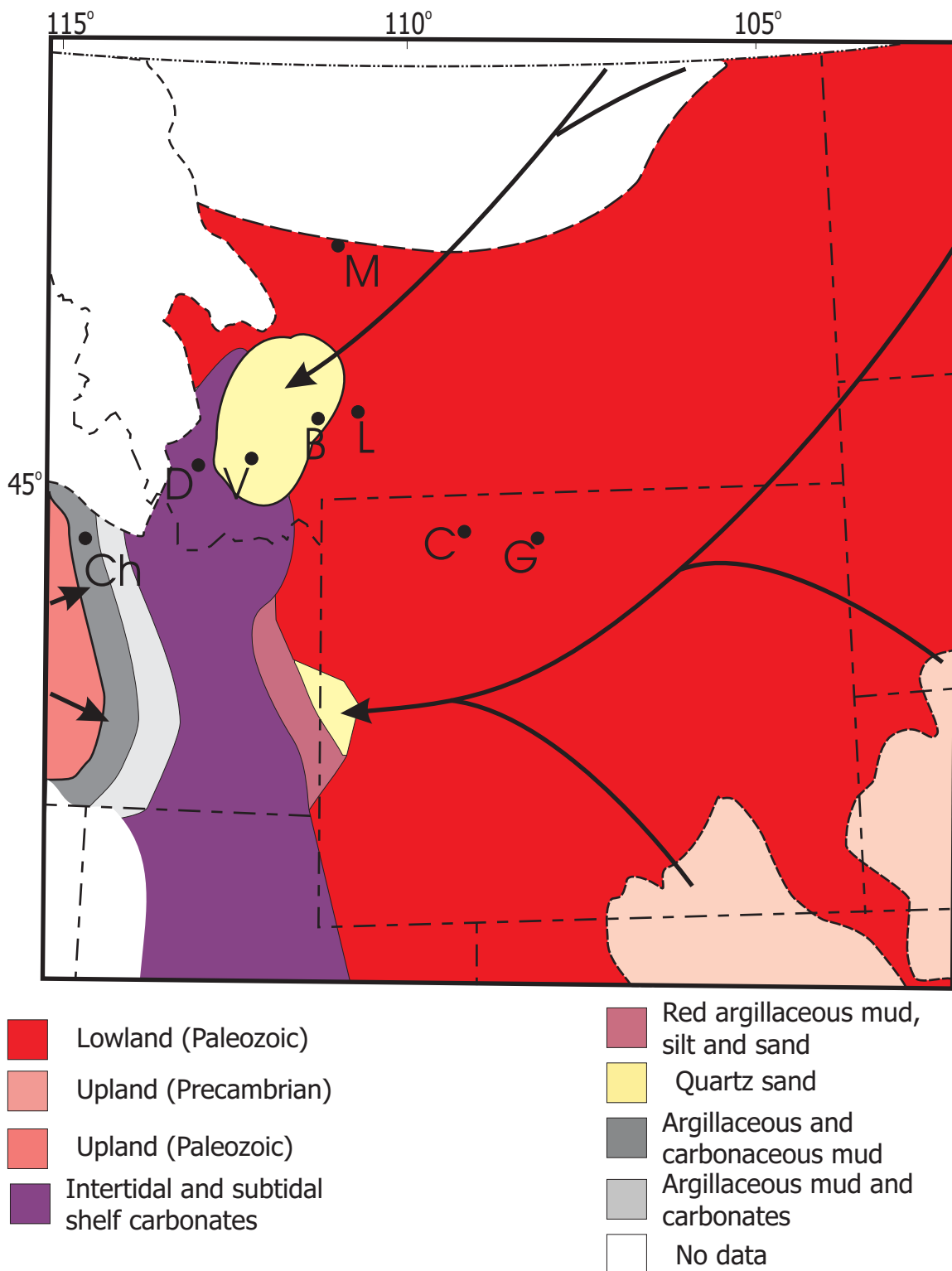


Figure 1.10: Summary facies map of post-Madison and Scott Peak depositional conditions in the northern US Rocky Mountains. This shows the latest Meramecian distribution of facies and the re-inundation of the karst plain across Montana and Wyoming. The map represents conditions during Cycle III, Phase II which corresponds to composite biozone 15, F. See Figure 1.6 for locations. Modified from Sando (1976).

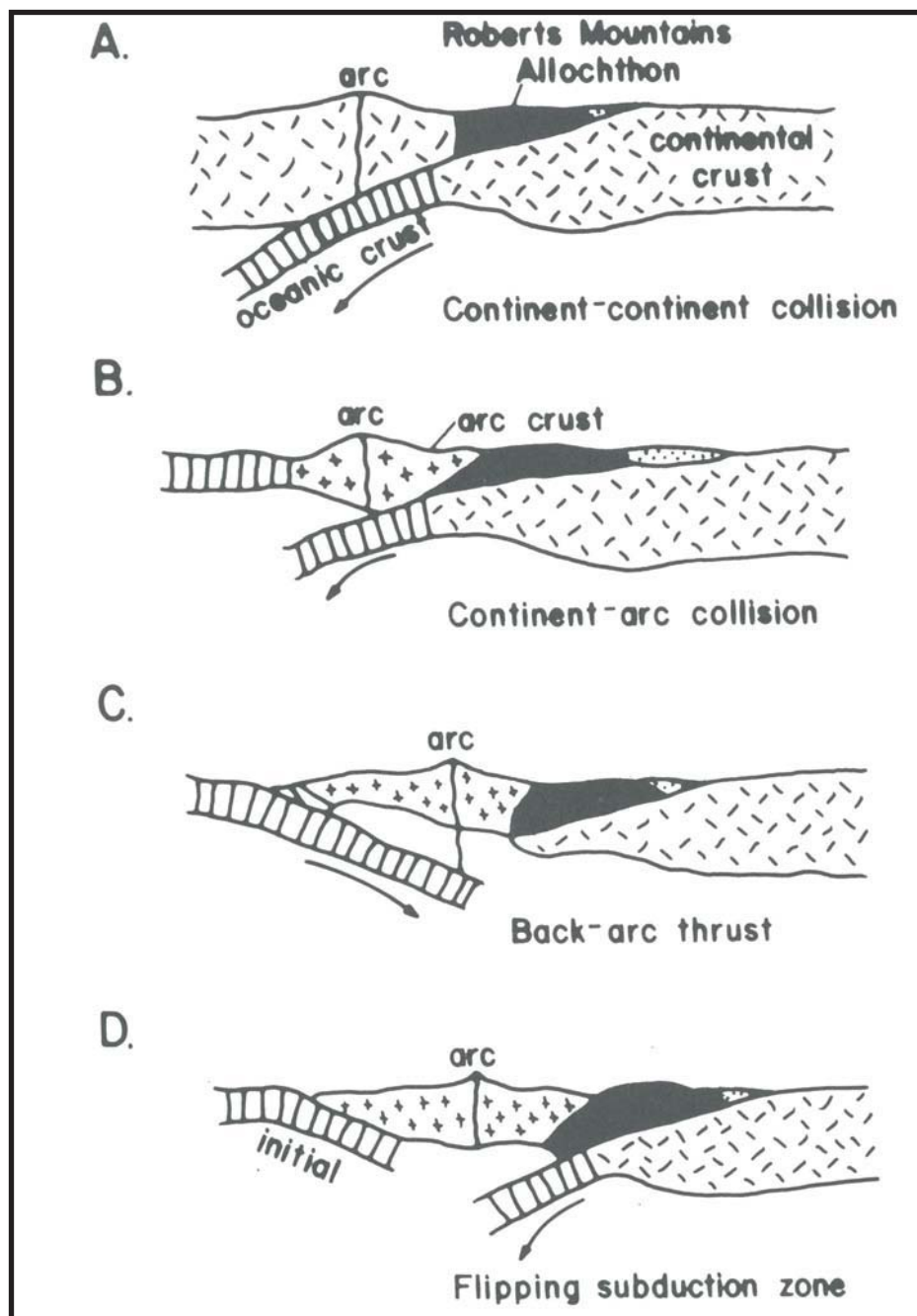


Figure 1.11: Summary of conceptual models of the Antler orogeny showing various configurations of the collision of North America with an arc system in cross-section (west is on the left). A) The continent-continent collision model with a west-dipping subduction zone. B) Continent-island arc collision again in a west-facing subduction setting. C) Back-arc thrust emplacement model for the Roberts Mountain allochthon. This model shows eastward subduction of the oceanic plate. D) A conceptual model showing flipping of the subduction zone and obduction of the Roberts Mountain allochthon on to North America.

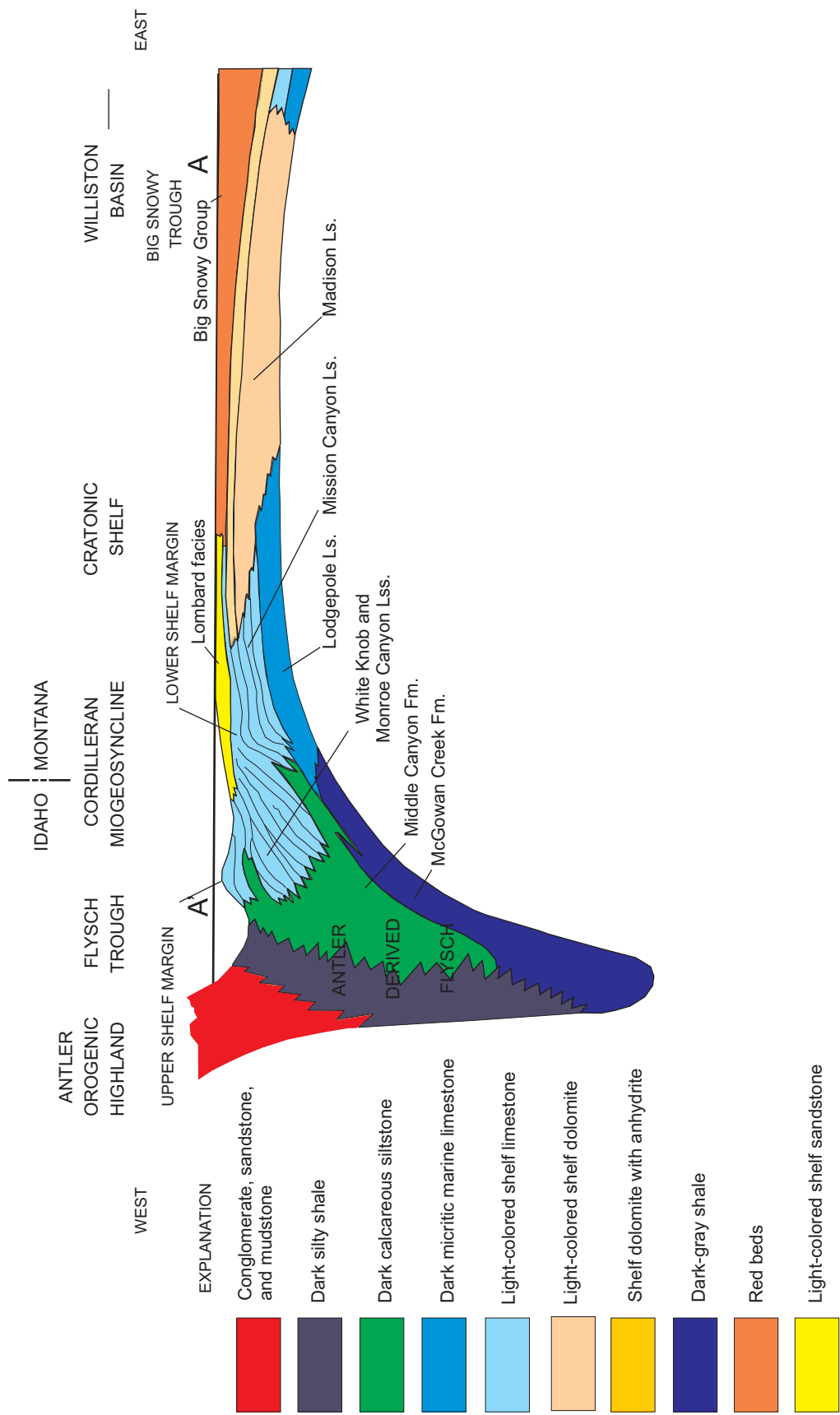


Figure 1.12: Formation-scale cross-section (top) across the Antler foreland basin displaying the geometry of the prograding Mississippian Madison carbonate ramp (modified from Rose, 1977).

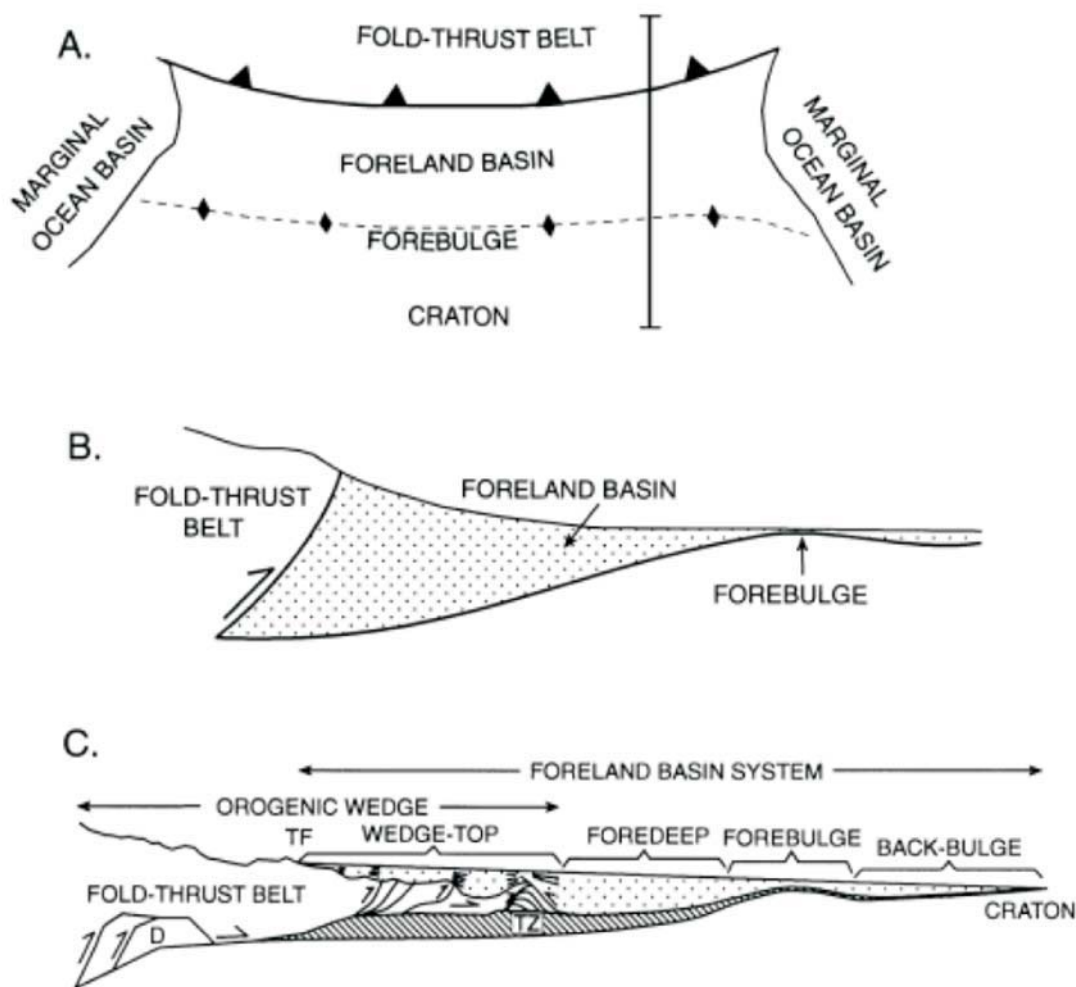


Figure 1.13: A) Plan view of “typical” foreland basin bordered by marginal marine basins. Line indicates location of cross-sections. Although this cartoon is largely schematic, the scale is on the order of 10^2 - 10^3 km. B) Schematic cross-section which is generally accepted for foreland basins, although it is grossly oversimplified. Approximately 10 times vertical exaggeration. C) Revised cross-section of foreland basin system depicting the wedge-top, foredeep, forebulge, back-bulge, and cratonic hinterland depositional settings. From Decelles and Giles (1996)

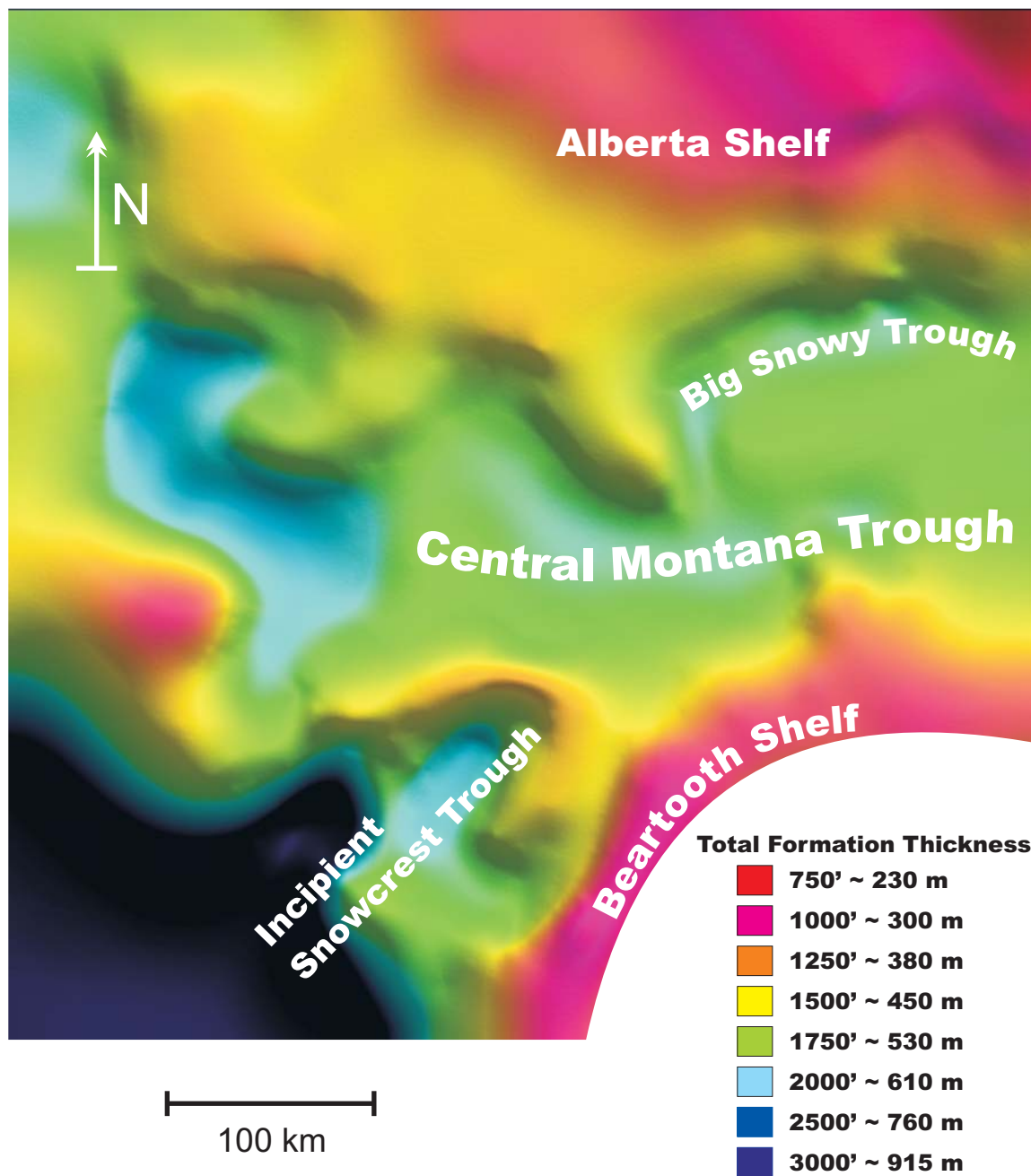


Figure 1.14: Thickness and paleotectonic elements of the Lower and middle Mississippian Madison Group in western Montana (modified from Peterson, 1985)

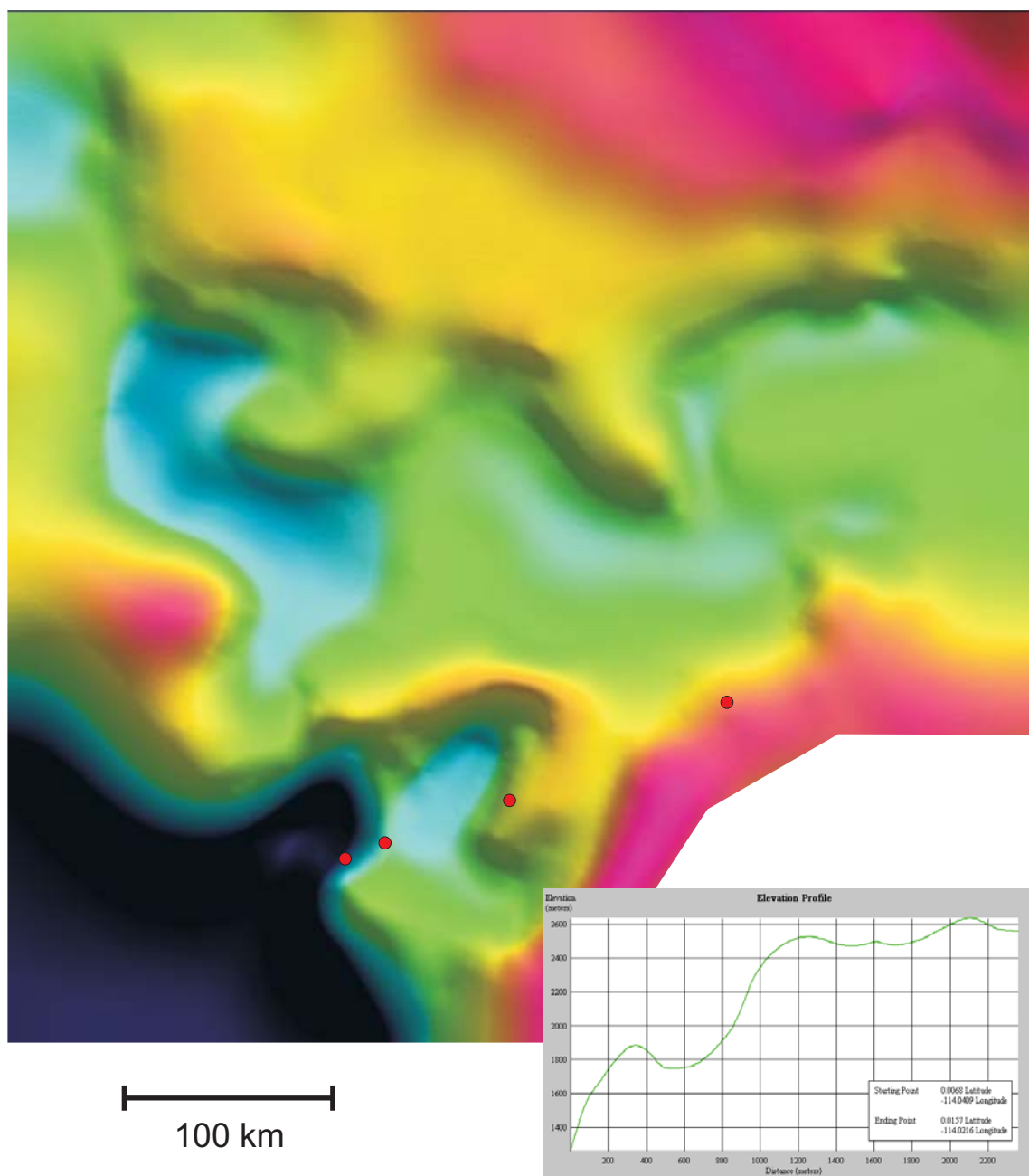


Figure 1.15: Surfaced isopach map showing, reproduced from Figure 1.14 with overlain outcrop section locations (red dots). The profile in the lower right indicates the variation in thickness (+y to the bottom) of Madison-equivalent strata through the transect A'-A'' from Figure 1.4. Significant variability in thickness especially to the southwest is indicative of differential subsidence across the study area towards the Antler foredeep basin. Non-uniform increases in thickness to the southwest may indicate that small-scale faults acted to segment the area and modify the expected accommodation space for sediment accumulation there.

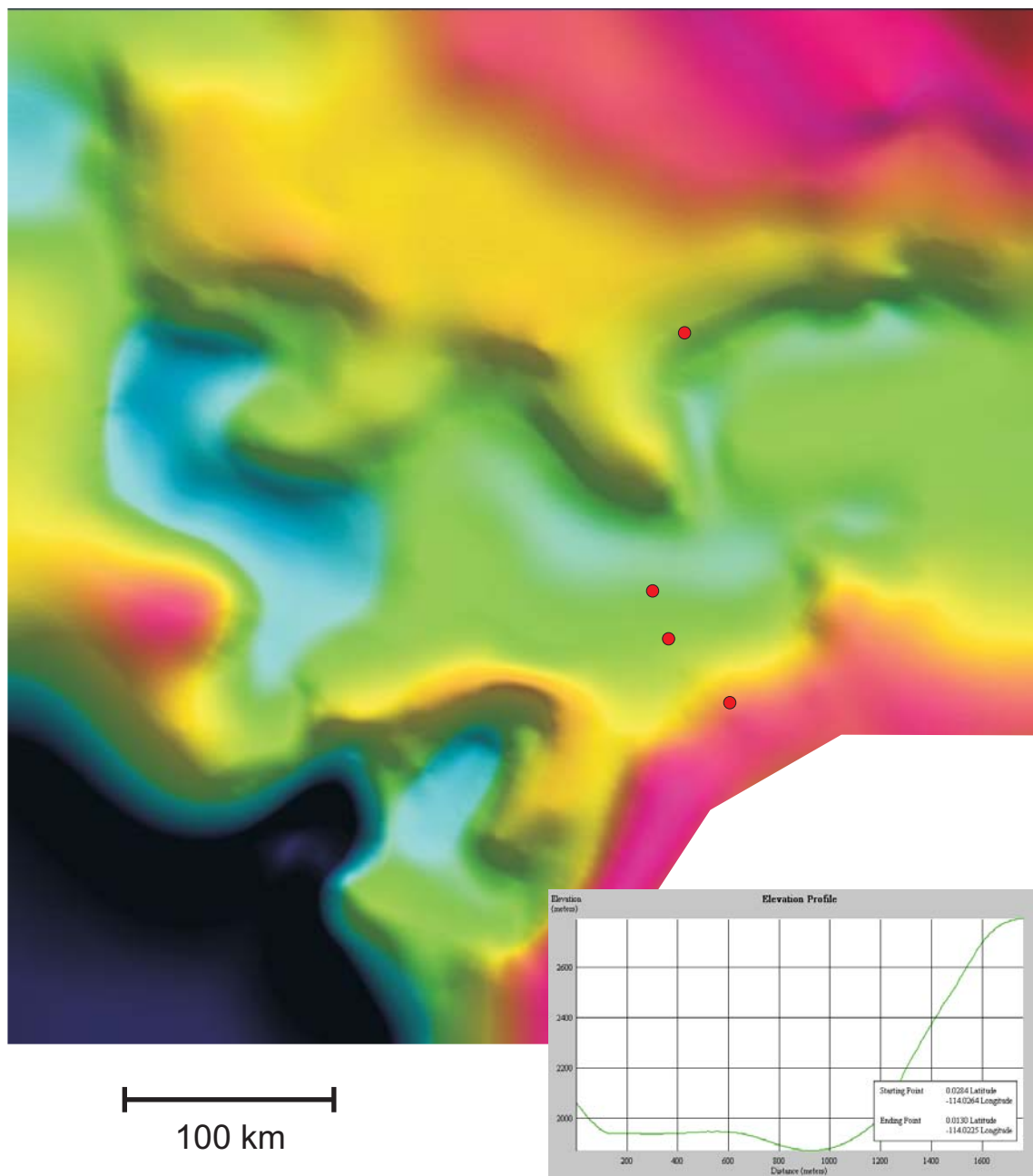


Figure 1.16: Surfaced isopach map showing, reproduced from Figure 1.14 with overlain outcrop section locations (red dots). The profile in the lower right indicates the variation in thickness (+y to the bottom) of Madison-equivalent strata through the transect A'-A'' from Figure 1.4. Significant increases in thickness are observed from south to north in this profile. This profile indicates that the central Montana trough was a slightly asymmetric depocenter during Madison time with the thickest accumulations in the southern part of the cross-section.

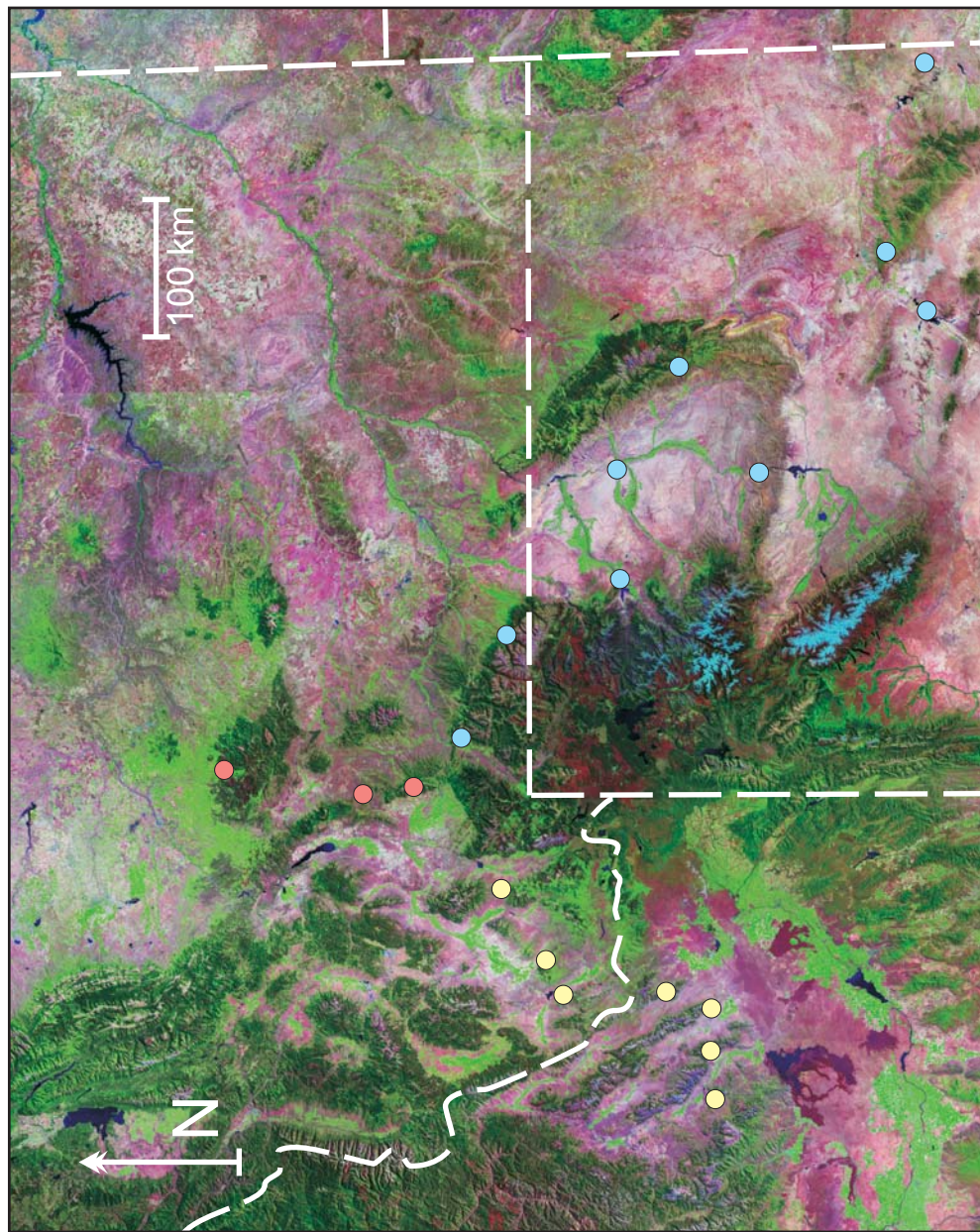


Figure 1.17: Location map showing the locations of outcrop measured sections and sampling localities. Light blue dots indicate sections used in the main trunk (A-A' in Figure 1.4) of the down-dip cross-sections. The red dots are sections which are used in the central Montana trough cross-section (A'-A'' in Figure 1.4), while the yellow dots are those sections which make up the Antler foreland basin cross-sectional profile (A'-A''' in Figure 1.4) North is toward the top of the map.

CHAPTER 2. FACIES DESCRIPTION AND DEPOSITIONAL ENVIRONMENTS

2.1 OVERVIEW

Facies of the Lower and Middle Mississippian carbonate strata of the Madison Group and equivalents can be divided into four major depositional groups based on their position on the depositional profile (Burchette and Wright, 1992). They are the basin, outer ramp, mid-ramp, and inner ramp (Figure 2.1). Each major subdivision represents a specific depth-energy zone along a graded homoclinal ramp profile corresponding to the dominant hydrodynamically-controlled base level position. The interfaces between depozones are lines of average energy below and above which the dominant depositional processes recorded in the strata change in an observationally demonstrable way.

Storm deposition is inferred to have controlled much of the facies partitioning along the ramp profile. The average positions along the profile where fairweather and storm wave bases impinged upon the substrate play a critical role in subdividing the ramp into discriminable facies belts. Based on the inferred position of these horizons, as based on repeatable, objective analysis of strata in outcrop (Aigner, 1984), the ramp profile can be portioned into the area below storm wave base, one between storm and fairweather wave base and a third above fairweather wave base. Based on these hydrodynamic parameters coupled with the resultant graded ramp profile, depozones can be defined along the profile length: the basin depozone is defined as the area at the toe-of-slope and basinward, and lying below the storm wave base and the pycnocline in times where the water mass is stratified; above the toe-of-slope but below storm wave base is the outer ramp; the mid-ramp is confined to the area on the profile between storm and fairweather wave base; and the inner ramp is the broad energy belt from the strandline out to fairweather wave base. Each of these facies belts can range from a few to hundreds of kilometers in width, and not all facies described in this chapter coexist in time. The presence or absence of a particular facies is highly dependent on a range of controls from ramp morphology and sea level state to climate and water mass stratification.

2.2 METHODS

Facies were described based on outcrop observation of lithology, bed thickness, and sedimentary structures. Additionally calibration of outcrop facies was performed by

the examination of approximately 350 thin sections, where allochemical composition and microfabrics were examined. Classification of depositional textures follows that of Dunham (1962) and the subsequent modification of Embry and Klovan (1971).

2.3 BASIN DEPOZONE

The basin depozone is defined here as stretching from the lower slope near the pycnocline, when present and identifiable, to the toe-of-slope and basinward and is composed of four facies characterized by two end members resulting from distinct sets of sedimentary processes. The dominant depositional style of the first end member from suspension and rarely punctuated by distalmost turbidity flows, which were likely induced by catastrophic storms or tsunamis. The facies characteristic with these processes are the cherty peloid/skeletal calcisiltite, the bedded chert facies, and argillite/shale facies. The other end member has features consistent with mass wasting and accumulation at or near the toe-of-slope or incipient mass wasting compatible with lower slope failure. The polymict breccia is the dominant facies along with distal turbidites, which characterize this end member. In addition, the suspension-dominated facies commonly are heavily deformed by syndepositional incipient failure features like contorted bedding, water-escape structures, soft-sediment faulting, and s- and z-folding.

These facies are broadly distributed across Montana and Idaho during deposition of the Paine Member of the Lodgepole Limestone (Figure 2.2). They are considerably more areally restricted during the remaining deposition of the Madison system. In the central Montana trough intrashelf basin, these facies are common throughout the Kinderhookian (Lodgepole Limestone), but absent during the Osagean and Meramecian. In the Antler foreland setting of southwest Montana and east-central Idaho, however, these facies are commonly found during the Kinderhookian and Osagean and during the Meramecian in the proximal foreland of central Idaho.

2.3.1 Cherty Peloid/Skeletal Calcisiltite Facies

This facies is a major component of the Middle Canyon Formation (Osagean-Meramecian) found at locations Bell-McKenzie Canyon, Copper Mountain, East Canyon, and Antelope Creek. It consists of dark gray to black limestone with dark brown to black chert and is thinly bedded to very thinly bedded (*sensu* Ingram, 1954). Beds typically

alternate on an approximately 1-10 cm scale between irregular, commonly nodular limestone layers and beds or bedding-parallel nodules of chert. The limestone typically has a wackestone to packstone texture with allochemical composition of micropeloids and microskeletal fragments (Figure 2.3A). The overall allochem size fraction is calcisilt in size (1-61 μm) with rare larger skeletal fragments composed of crinoid columnals, brachiopods, rugose corals, and bryozoans (up to 2.5 mm). Occasional to rare massive, medium bedded, coarse crinoidal packstone-grainstone interbeds occur interspersed within generally monotonous successions of this facies. Primary sedimentary structures are generally absent within beds and beds are typically homogenous in texture although rare to common bedding-parallel laminations do occur. Soft-sediment deformation is common especially tight s- and z-folds with amplitudes of up to 2 m and contorted bedding present. The chert is dominantly composed of sponge spicules which are matted and display a felted texture.

The cherty peloid/skeletal calcisiltite facies is interpreted to be deposited below storm wave base within an intermittently stratified water mass. This interpretation is based on the presence of a low diversity fauna dominated by sponge spicules (Wilson, 1975). Alternating periods of homogenous and laminated bedding suggest varying presence or absence of infaunal burrowers corresponding with changes in the water mass from aerobic to dysaerobic conditions. Calcisilt beds are interpreted as derived from the carbonate production area up-dip. The fine size of grains suggests long transport distances for these materials probably delivered as distal fine-grained turbidites. Rare coarse grained crinoid beds likely represent sediment gravity flows and turbidites which were generated during extreme energy events on the more proximal parts of the ramp.

2.3.2 Bedded Chert Facies

This facies, like the above one, is restricted to southwestern Montana and east-central Idaho during the Osagean and Meramecian. It is dominated by thin to very thin beds of spiculitic chert with few to rare limestone stringers or interbeds (Figure 2.3B). The bedded chert facies is generally black or brown in color and occurs in uniform, continuous beds. Large (> 2 mm), well preserved silicified crinoid columnals, up to 2.5 mm, are rare to common, sometimes floating within the bedded chert. The chert commonly contains parallel or wavy laminations, but bedding is commonly contorted and

sometimes disrupted by soft-sediment deformation. Limestone stringers are typically composed of graded, fine- to medium-sized crinoid debris, 0.15-1.33 mm wide, with rare silicified brachiopods. Medium to thick massive beds of coarse crinoid debris, up to 5mm in diameter, occur rarely.

The bedded chert facies is interpreted to have been deposited below storm wave base in a largely dysaerobic setting. The predominance of sponge spicules, lack of a diverse macrofaunal community, and lack of burrowing suggest poorly oxygenated waters in this setting (Wilson, 1975). Background sedimentation appears to have been dominated by deposition of sponge spicules. The occasional graded limestone stringers are indicative of turbidity flows periodically punctuating deposition. Massive structureless crinoidal grainstone beds were likely formed by periodic sediment gravity flows, either grain flows or turbidites. Soft-sediment deformation within the chert suggests that these beds were deposited along the slope perhaps near the toe-of-slope.

2.3.3 Argillite/Shale Facies

This facies occurs predominantly during the Paine Shale member of the Lodgepole Limestone in intrashelf central Montana trough at locations Sacagawea Peak and Monarch (Elrick, 1990), in southwest Montana at Baldy Mountain, Ashbough Canyon, and Bell-McKenzie Canyons, and also in east-central Idaho from the Kinderhookian through the Osagean (McGowan Creek and Middle Canyon Formations; Sandberg, 1975). The argillite/shale facies is typically has a calcareous component as well and has a color ranging from medium gray to tan gray to black (Figure 2.3C). This facies is typically poorly exposed. Where exposed, the facies is commonly fissile with very low skeletal content. The skeletal content consists mainly of whole, small, thin-shelled brachiopods, up to 500 μm wide, with occasional phosphatized grains like ramose and fenestrate bryozoans, shark teeth, and fish scales. Glauconite and pyrite are common authigenic minerals occurring within the argillite/shale facies. Rare microskeletal (33-100 μm) wackestones and packstones with thin to medium bedding are typically the only beds resistant enough to weather out of the hillsides.

This facies is interpreted as deposited on the lower slope and basin floor. The rare occurrence of macrofossils implies this facies was deposited far from the area of carbonate sediment production perhaps in a dysphotic or aphotic setting (Read, 1985).

Further, the lack of burrowing is suggestive of dysoxic conditions here. The sometimes competent limestone bed is likely due to distal turbidity flows reaching the basin floor or surrounding slope apron. Authigenic mineral production implies very slow sedimentation rates and pyrite deposition furthers the argument of dysoxia in this environment.

2.3.4 Polymict Breccia Facies

The polymict breccia facies is known only from a single locality, the Bell-McKenzie Canyon section. It is a breccia where the matrix is typically yellow gray to medium gray and clasts medium to dark gray and brown gray (Figure 2.3D). It occurs in discrete units from 1-52 m thick, which have finite lateral extent creating overall lens shaped bodies. These lenses can be traced out along the outcrop and extend at least 500 m laterally where it grades into fine-grained peloidal/skeletal calcisilt fine-grained turbidites which are commonly contorted. There is no evidence of channelization of the breccias into the underlying strata. Clasts are typically 50 cm in width although larger clasts are up to 5 m in length and are typically subangular to subrounded and have moderate to low sphericity. The clasts are mostly composed of peloid/skeletal calcisiltite with subordinate amounts of lime mudstone and crinoidal packstone to grainstone. The breccia itself is matrix supported with the matrix dominantly composed of lime mud with subordinate microskeletal and micropeloidal components.

These breccias are interpreted as resedimented slope carbonates which formed during debris flow processes. The disorganized, mud-supported texture of these breccias and generally small clast size suggests a relatively low-energy event with short transport distance over a low-angle slope. These breccias likely accumulated at or near the base-of-slope (Burchette and Wright, 1992), and their overall rare occurrence and limited spatial distribution suggest that this was not a major slope process and likely recorded only rare events of slope failure.

2.4 OUTER RAMP DEPOZONE

The outer ramp depozone is defined as the area from storm wave base to the pycnocline, where this location is identifiable. Deposition in this area is typified by infrequent storm reworking and is subsequently dominated by suspension deposits and frequent resedimentation of up-dip derived materials and infrequent traction and local

reworking occurring during large storm events. The dominant facies of this zone are very finely to finely interbedded couplets of alternating limestone and argillite. Here the limestone and argillite couplets alternately represent deposition under storm conditions and non-storm influenced events, respectively. This facies is broadly distributed across Montana during the Paine and Woodhurst Members of the Lodgepole Limestone and interfingers basinward with the cherty thinly bedded limestones of the basin depozone and strongly storm-influenced deposits of the mid-ramp in the landward direction.

2.4.1 Limestone/Argillite Couplets Facies

This facies is broadly distributed across Montana during the deposition of the Kinderhookian Lodgepole Limestone. It consists of medium gray limestone beds interbedded at a fine scale with yellow to orange weathering argillite beds, which contain up to 60% siliciclastic silt (Elrick, 1990). The limestone is typically variable in texture from lime mudstone to crinoidal wackestone to peloidal packstone to grainstone and rare very thin brachiopod packstones-grainstones. Limestone beds are generally thin to very thin with rare medium bedding and are sometimes graded or have thin graded laminae (Figure 2.4). Wave ripples and other traction features are rare to absent. The dominant allochems of the limestone couplet are disarticulated pelmatozoans, brachiopods, rugose corals and bryozoans (0.17 – 1 mm in width) which commonly are concentrated along scours at the base of the beds. Bioturbation of the limestone couplets is highly variable with laminae either nearly pristinely preserved or completely obliterated with common *Zoophycos* trace fossils. In contrast, preservation of whole delicate fossils commonly in life position occurs in the argillaceous portion. *In situ* rugose and syringoporid-type corals, fenestrate and ramose bryozoans, as well as articulated crinoid columnals are common within the argillaceous matrix material.

The bimodal nature of this facies and component lithotypes suggests a strong external driver to deposition. Scouring and graded laminations and bedding of the limestone couplets are interpreted as turbidity flows representative of distal storm deposits but below storm wave base. These observations are consistent with the general lack of wave ripples and other obvious storm features common in deposition within storm wave base. Additionally, the highly variable nature of bioturbation is suggestive of changes in water conditions from aerobic to dysaerobic through time. The argillite

couplets are interpreted as background sedimentation dominated by settling of material from suspension through the overlying water column, which was likely material derived from the Antler highlands to the west and brought into the area via currents. The high abundance of diverse macrofauna commonly preserved in the argillite couplets suggests good water conditions likely within the deeper photic zone. Relatively high sedimentation rates were likely required for burial and exceptional preservation of these fossils in life position (Elrick, 1990). Argillaceous background sedimentation was commonly interrupted by turbidity pulses of material derived from the major carbonate production areas landward of the outer ramp during periods of storm activity (Aigner, 1985).

2.5 MID-RAMP DEPOZONE

This depozone records a progression upwards in storm energy along the graded ramp profile. Five facies make up the mid-ramp facies association, which lies along the swath of the ramp between storm and fairweather wave base. The hydrodynamic conditions change along the profile of the mid-ramp from unidirectional turbidity flows to oscillatory impingement of wave energy along the sediment-water interface to combined flow of both wave energy and downslope directed current flow as energy proceeds up along the bathymetric profile. Aigner (1985) documented this energy-base level progression in the description of storm-proximality cycles, which related the lateral variation of facies to the vertical succession of strata observed in both cores and outcrops of Recent and Ancient storm-dominated successions.

The progression along a storm-dominated tract of a graded homoclinal ramp profile can be subdivided based on the occurrence of graded, that is turbidity-related, beds, hummocky cross-stratified or combined flow strata, and trough cross-stratified resulting from unidirectionally flowing traction currents (Aigner, 1985). An idealized tempestite would have a scoured base overlain by graded beds, which would then be followed by hummocky cross-stratification overlain by wave ripple laminations. This sequence would then be capped by a mud drape. The degree of amalgamation of beds, and hence the presence or absence of the mud cap and its thickness if present, provides additional indication of the degree and frequency of storm reworking of sediments along the storm-graded profile. These facies are commonly distributed across most of Montana

throughout the Woodhurst Member of the Lodgepole Formation as well as the Mission Canyon Formation at Bell-McKenzie Canyon.

2.5.1 Graded Peloidal/Skeletal Packstone-Grainstone Facies

This facies is typically medium to dark gray in color, and fine to medium bedded. The lithology of the facies is dominated by mixed peloidal and skeletal grains with packstone to grainstone texture (Figure 2.5A). This composition can vary from nearly completely peloidal to nearly completely skeletal reflecting changes in source area for the allochems. Bases of these beds are typically scoured and the scour surface is usually overlain by graded coarse to medium skeletal material, up to 3.5 mm wide, or finely graded peloids, 60-140 μm in width, but generally an admixture of the two is dominant. Depending on the degree of amalgamation, the peloidal/skeletal packstone-grainstone is typically overlain by very fine to finely bedded argillaceous material, which is normally moderately to heavily bioturbated and occasionally capped by iron-stained firmgrounds or hardgrounds. In addition to the abundant graded fabrics observed at the bed base, this facies rarely to commonly displays hummocky cross-stratification and parallel and wave ripple laminations. Skeletal material is abundantly composed of crinoid debris as well as debris derived commonly from rugose corals, brachiopods, and bryozoans. Argillaceous rip-up clasts derived from the overlying drapes are locally common as well.

The typical graded texture of this facies owes to deposition by turbidity flows. The scour surfaces associated with the bases of the graded bed also provide evidence of this facies being deposited under turbid flow conditions and accounts for the locally abundant rip-up clasts of associated argillaceous beds. Thinning of the overlying argillaceous drapes and amalgamation of graded beds has been interpreted to indicate shallowing within the middle ramp (Aigner, 1985). Additionally, shallowing within the middle ramp is indicated by the the increased abundance of oscillatory and combined flow sedimentary structures like hummocky cross-bedding and wave ripple lamination (Aigner, 1985). Diverse open marine macrofauna and abundant bioturbation of intervening argillaceous drapes also attest to the deposition of the graded peloidal/skeletal packstone-grainstone facies in normal salinity conditions within the photic zone. However, this facies, when dominated by non-skeletal allochems, is indicative of

transport of allochems from restricted ramp-top areas where open marine fauna are limited or absent.

2.5.2 Oolitic Packstone-Grainstone Facies

This facies is distributed over the same area as the graded peloidal/skeletal packstone-grainstone facies, but its distribution is particularly concentrated within the Woodhurst Member of the Lodgepole Limestone in the central Montana trough intrashelf basin. This facies is dominantly medium bedded with subordinate thin and thick bedding. It is typically composed of ooid, which range from 100-400 μm in size, and micritized grains although admixed skeletal grains are common to abundant (Figure 2.5B). Iron staining of the oolitic grains is common and these beds sometimes weather red but otherwise weather to a light gray to a medium gray color. Skeletal grains are sometimes disarticulated and are composed of pelmatozoan, brachiopod, bryozoan, and rugose coral debris, ranging in size from 100-1000 μm . Sedimentary structures are commonly hummocky cross-bedding and wave ripple and parallel laminations. This facies is usually moderately to well-sorted, so grading is difficult to observe and moderate to intense bioturbation is occasionally observed. Amalgamation of beds is common and tabular cross-beds may be observed in the amalgamated bed sets when bedding is not completely obliterated and massive. Textures are generally packstone to grainstone with few argillaceous drapes or incorporated argillaceous intraclasts.

This facies is interpreted as redeposited rather than resulting from *in situ* ooid shoal deposition based on the presence of hummocky cross-stratification, abundant micritization of grains, and common red-staining of oolitic cortices indicating long seafloor residence time. Furthermore, the admixture of open marine macrofauna adds evidence for a number of sources of the sand-sized components of this facies, both areas of abiotic, restricted sand production and skeletal open marine settings. Rare argillaceous drapes and intraclasts and common amalgamation suggests that the redeposited ooid packstone-grainstone facies was deposited in the shallow mid-ramp near fairweather wave base (Aigner, 1985).

2.5.3 Skeletal Packstone-Grainstone Facies

The skeletal packstone-grainstone facies is commonly medium to thick bedded and occurs as light to medium gray in color. This facies is commonly graded with

scoured bed base, exhibits hummocky cross-stratification, and has parallel and wave rippled laminae (Figure 2.5C). Like the ooid packstone-grainstone facies, it has rare to common argillaceous drapes and argillaceous intraclasts and is commonly amalgamated. When these beds are amalgamated, trough and planar cross-bedding is common. Allochemically, this facies is composed of pelmatozoan debris with subordinate amounts of disarticulated bryozoans, rugose corals, brachiopods and rare overturned syringoporid-type corals. Peloids and micritized grains are common to abundant. The texture of this facies is typically grainstone and packstone with grain sizes ranging from 80-1000 μm , but skeletal rudstones dominated by crinoid columnals are also common.

Like the ooid packstone-grainstone facies, this facies is interpreted as deposited as a part of the storm-dominated mid-ramp rather than as a part of an *in situ* sand shoal based on the abundant oscillatory and combined flow sedimentary structures present (Aigner, 1985). The heavy micritization commonly observed on the component skeletal grains suggests that these grains spent a significant amount of time on the seafloor before they were incorporated into the tempestite deposit. The small amount of argillaceous material associated with or incorporated into this facies suggests that it was deposited in high-energy conditions near fairweather wave base.

2.5.4 Massive Crinoidal/Skeletal Facies

This facies is typified by accumulations of massive, thick to very thick bedded crinoidal grainstone and commonly rudstones with subordinate packstone textures. These strata usually weather to a medium gray color and sometimes are cliff-forming due to their massive texture. Stringers of chert are commonly the only indicators of bedding within these accumulations. The pelmatozoan grainstones are usually structureless although rare to common planar, trough, and bidirectional cross-bedding do occur (Figure 2.5D). Admixed with the pelmatozoan debris are commonly bryozoans with brachiopods and rugose and large *in situ* syringoporid-type corals rare to locally abundant. Other allochems locally present include coated and micritized grains as well as occasional to rare gastropods. Grain sizes range from fine to very coarse sand (125-1000 μm).

The crinoidal skeletal facies is interpreted to represent a shallow subtidal meadow of crinoids which lived *in situ* upon an autochthonous substrate of crinoid debris. This facies is likely akin to similar skeletal bank deposits observed in the modern of the

Persian Gulf (Purser, 1973), especially the Pearl Barrier Bank region (Purser and Evans, 1973), and Shark Bay (Hagan and Logan, 1974), where sediments of this type accumulate in 5-20 m water depth. The lack of lime mud preserved within this facies suggests that it was either not produced here or was more likely winnowed by wave energy. This facies is interpreted to have accumulated at or just below fairweather wave base in a wave-agitated environment.

2.5.5 Bioturbated Wackestone-Packstone Facies

This facies is nearly ubiquitously deposited during Madison time, but its spatial distribution generally expands from near the Wyoming border in Montana during the Lodgepole Limestone deposition to southwestern and central Montana during Mission Canyon Limestone deposition and east-central Idaho during the deposition of the Scott Peak Formation. It is typically medium bedded but also has thick and very thick bedding. Its color varies widely from medium to dark brown-gray. Bioturbation is generally moderate to intense, commonly giving outcrops of this facies cliff-forming character. The texture is wackestone-packstone with grainstone stringers from 1-15 cm thick and tens to hundred of centimeters long are common and sometimes the only heterogeneity in this normally homogenized unit (Figure 2.5E). Irregular chert beds, nodules and chert stringers also help to indicate bedding in massive beds of this facies. Allochems include open marine macrofossil debris, like pelmatozoans, brachiopods, rugose corals, and rarely gastropods and benthic foraminifera, as well as occasional to common ooids, peloids and pellets. Macrofaunal elements are generally disarticulated and add to the usually poorly sorted texture of the near-shoal facies. Grain sizes reflect the poorly sorted nature of this facies with very fine to very coarse sand grain sizes (67 μm – 1.7 mm).

The intense bioturbation of this facies makes precise identification of its depositional environment difficult. The best indicators of its precise position along the ramp profile are commonly allochemical composition and contextual evidence from underlying and overlying strata. The thoroughly-churned, bioturbated character of this facies does, however, speak to the fact that conditions were good below the sediment-water interface for extensive burrowing by infaunal biota. This facies is likely not restricted solely to one position along the ramp, but likely was distributed commonly in a number of different settings as is supported by its broad distribution in space and time

through the Madison system. Abundant and occasionally coarse skeletal material within this facies suggests that it was deposited in quiet subtidal environments within close proximity to skeletal shoals in these cases. Additionally, stringers of skeletal grainstone which are still preserved as coherent units likely were brought into this depositional environment during storm events. The bioturbated wackestone-packstone facies typified by high abundance of oolitic and peloidal allochems likely accumulated in protected environments in relative proximity to the localities of production of these grain types. In this case it is probable that these near-shoal facies were actually deposited in subtidal setting landward of ooid shoals where ooid sands were actively being produced. This facies is then interpreted to have been deposited in energy-restricted subtidal settings within proximity to sand-sized material, where sand-sized material could be introduced during high-energy events.

2.6 INNER RAMP DEPOZONE

The inner ramp depozone lies along the tract from fairweather wave base landward to the strandline. The associated facies of this depozone are subject to a great spectrum of depositional energies and processes, from wave- and tide-dominated barrier bars and shoals to low-energy proximal lagoonal deposits, and highly variable extrinsic environmental factors like water quality, ranging from open marine to stenohaline conditions. The width of this facies belt is highly variable during deposition of the Madison system. It ranges from very narrow shoreline-attached skeletal and coated grain sand systems to broad mud-rich lagoonal settings which span hundreds of kilometers bounded seaward by detached barrier bar systems. Expansion and contraction of barrier-controlled inner ramp depositional systems is a common theme of the Madison Group and equivalents. Changing shallow-water facies arrangements and introduction and exclusion of facies types are indicative of an ever reorganizing depositional system with variable geometries due to changing long-term accommodation conditions across the shelf. Accordingly, the facies described within this section commonly, if not usually, are not all laterally coexisting at the same moment in time. For instance, the lack of an effective barrier system precludes the development of extensive back-barrier and

lagoonal facies, and humid and arid tidal flat deposits would not be expected to occur in close spatial proximity at the same time.

Within the overall inner ramp depozone, three facies associations can be subdivided: the shoalwater/barrier, lagoonal, and peritidal associations. These facies belts are subdivided based on energy and base level states and water conditions, dominated by salinity state. The shoalwater/barrier facies association is composed of two facies which exhibit both wave- and tide-dominated sedimentary structures. They are the ooid grainstone shoal facies and skeletal grainstone shoal facies. In comparison, the lagoonal facies association is composed of three facies which show decreasing wave energy in a distal (seaward) to proximal (landward) lateral arrangement. In this depozone, textures grade laterally from the peloidal grainstone facies to the bioturbated peloidal wackestone-packstone facies to the low-energy pellet/restricted fauna wackestone to mudstone facies. The peritidal facies association is composed of facies associated with the most proximal areas of carbonate sediment production and storage, specifically in the intertidal to supratidal zones. Five facies make up the peritidal facies association and they are the pisoid packstone to grainstone facies, the algal laminite facies, the mudclast conglomerate facies, the evaporite solution collapse facies and the marginal marine shale/siltstone facies.

2.6.1 Shoalwater/Barrier Facies Association

This association is composed of two facies which are broadly distributed across the Madison shelf in space and time. These facies have grain-supported textures. The facies either occur in association with shoreline-detached sand systems or shoreline-detached barrier bar and shoal systems. The presence or absence of a barrier system and the effectiveness of the barrier system play a critical role in the presence or absence and spatial distribution of all other inner ramp facies.

2.6.1.1 Cross-Bedded Ooid Packstone-Grainstone Facies

The cross-bedded ooid packstone-grainstone facies is typically composed of ooid to ooid-skeletal grainstones. The facies weathers white in outcrop and because of common very thick bedding this facies commonly forms prominent cliffs in outcrop. Occasionally bedding also is medium to thick. Planar and trough cross-beds are common and bidirectional cross-bedding is rare to occasional (Figure 2.6A). Allochems are

dominated either by ooids, ooids and peloids, or either of these admixed with skeletal grains. Skeletal grains are mostly abraded pelmatozoan debris, commonly with subordinate amounts of bryozoans, brachiopods, rugose corals and rare syringoporid-type corals which are typically preserved in growth position. Ooids have a radial microfabric and range from superficially coated peloids <100 μm in diameter to coarse sands up to 1 mm across. In the central Montana intrashelf basin, oolitic intraclast which are platy to rounded and up to 10 cm in diameter are common. These intraclasts are composed of ooids, peloids, and composite grains.

Based on the abundant cross-bedding, this facies is interpreted as being deposited in shallow subtidal to intertidal conditions. The dominance of ooids and abiotic grains suggests that elevated salinity conditions, as normal marine fauna were excluded from the deposit. In the cases where skeletal allochems were incorporated, the abraded nature of the grains suggests that these grains had a long residence time on the seafloor. Commonly pelmatozoan grains act as the nuclei of the ooids, and it follows that an intimate link between the sand belts must exist.

2.6.1.2 Cross-Bedded Skeletal Packstone-Grainstone Facies

The cross-bedded skeletal packstone-grainstone facies occurs across the entire Madison shelf; however extensive deposits are accumulated at the Bell-McKenzie Canyon section where skeletal grainstone is the dominant facies type during deposition of the Mission Canyon Limestone. Like the ooid grainstone shoal facies, planar and trough cross-bedding are abundant within this facies with subordinate amounts of bidirectional cross-bedding (Figure 2.6B). This facies is commonly thick bedded but very thick bedding and subordinate amounts of medium bedding also occur. The facies is medium gray in color and dominated by pelmatozoan debris and textures range from rare packstones to occasional rudstones. Grain sizes typically range from medium to very coarse sands (125-1000 μm wide) with some rudstone textures (> 2 mm width). Other subordinate allochems are bryozoans, brachiopods and rugose corals. Syringoporid-type corals also occur *in situ* but with rare frequency. Peloids and ooids are rare to occasional in occurrence.

This facies is interpreted, like the cross-bedded ooid facies, to have been deposited in shallow subtidal to intertidal conditions. Common tidal sedimentary

structures like trough, planar, and herringbone cross-stratification show that this facies underwent continual reworking by tidal currents. The dominance of open marine faunal allochems is strong evidence that this facies was deposited in open marine conditions. The fresh appearance of skeletal grains is indicative of deposition at or near the site of skeletal sediment production. Tidal currents removed any lime mud which may have been produced in the carbonate factory here.

2.6.2 Lagoonal Facies Association

The lagoonal facies association is comprised of three facies which illustrate waning energy conditions along the lateral profile from shoal to lagoon. These facies compose a typical transect across the lagoon from the distal back barrier bar setting to the supratidal depozone. The broad deposition of these facies across Montana during the Mission Canyon Formation attests to the development of extensive effective barrier bar and shoal systems during deposition at this time. Attenuation of circulation over a broad shallow area also likely attributed to the wide distribution of lagoonal facies across the Madison shelf. Less extensive lagoonal deposits were common during the deposition of the Upper Cyclic Member of the Scott Peak Formation in east-central Idaho.

2.6.2.1 Peloidal/Micropeloidal Wackestone-Grainstone Facies

The peloidal/micropeloidal wackestone-grainstone facies is broadly distributed and occurs throughout Mission Canyon Formation deposition across most of Montana and is common during the Lower and Upper Cyclic Members of the Scott Peak Formation in Idaho. It is composed of dark brown to gray to light tan limestone and subordinate amounts of dolomite. This facies is typically moderately to intensely burrowed. Rare flaser bedding is preserved within this facies. The texture is generally grainstone with subordinate amounts of packstone present. As a result it is commonly massive in outcrop and occasionally forms cliff of several meters in height. Bedding is typically of medium thickness with common thick to very thick beds. Stringers to nodules of chert typically aligned with bedding commonly form the only clear indication of bedding. This facies is similar to other near-shoal facies although the allochemical composition of the peloidal grainstone facies is typically dominated by abiotic grains,

especially peloids and micritized and unmicritized ooids as well as rare calcispheres and ostracods, with rare to occasional open marine skeletal grains or stringers of open marine skeletal grains (Figure 2.7A). Skeletal allochems range from abraded pelmatozoans, brachiopods, and bryozoans to benthic foraminifera, gastropods, and ostracods. Peloids range in size from 100-400 μm in width while skeletal grains tend to be very fine to fine sand size and micropeloids range from 35-70 μm . This facies has an overall homogenized appearance due to intense burrowing.

The peloidal/micropeloidal wackestone-grainstone facies is interpreted to have been deposited in a shallow subtidal environment within lower energy conditions. Wave energy was high enough to winnow most lime mud produced and initially deposited in this area, indicating close proximity to the barrier system. Rare preservation of flaser bedding indicates periodic tidal energy within this environment. Additionally, periodic high energy conditions are indicated by the introduction of open marine fauna into this environment. Conditions below the sediment-water interface were apparently conducive to heavy burrowing by infauna (Tedesco and Wanless, 1995). Differentiation of this facies from the near-shoal facies is based on contextual evidence from the subjacent and superjacent beds. The peloid grainstone facies is typically underlain by the bioturbated peloidal wackestone-packstone facies and overlain by ooid grainstone shoal facies. This is differentiated from the near-shoal facies which is deposited in close association with open marine faunal-dominated facies such as the massive crinoidal/skeletal facies. Similar facies associations have been observed in the Persian Gulf, where hypersaline lagoons behind the Great Pearl Bank barrier are rich in pelleted sands and poorly fossiliferous (Purser and Evans, 1973).

2.6.2.2 Bioturbated Peloidal Wackestone-Packstone Facies

The bioturbated peloidal wackestone-packstone facies is typically yellow gray to buff in color and usually medium to thick bedded with occasional very thick beds. It is commonly structureless due to moderate to intense bioturbation. Like the peloid grainstone facies, nodular chert is typically the major indicator of bedding in this facies. Rare wave ripples and parallel laminations are generally the only sedimentary structures preserved within this environment. Peloids, ostracods, microskeletal fragments, and calcispheres are the dominant allochems in this facies (Figure 2.7B). Grain sizes are

similar to those of the peloidal/micropeloidal wackestone-grainstone facies, but the size range is typically skewed towards the smaller size fractions. Peloids range from 50-120 μm , while ostracods range from 150-500 μm , and rarely other skeletal debris can reach widths exceeding 2 mm.

This environment is interpreted as lying laterally between the peloidal grainstone facies and pellet/restricted fauna facies. This facies lateral succession of facies has been interpreted by Sonnenfeld (1996a) as an indication of increasingly attenuated circulation and increasing restriction landward. The facies likely represent pellets which are increasingly uncemented in the landward direction. Attenuated circulation results in decreased cortical and intergranular cements and as a result the pellets lose their integrity and are squashed into a wackestone texture as decreasing amounts of structurally-sound peloids are being formed or moved into this depositional environment. Low diversity, thin-shelled fauna indicate restricted conditions of deposition. Allochems were likely transported in during storm events and the rare wave ripple and parallel laminae preserve evidence of high energy conditions interacting with the bottom here. This facies is interpreted to have been deposited in a restricted subtidal lagoonal setting. This setting is analogous to the pelleted lagoonal deposits observed in the modern Persian Gulf (Purser and Evans, 1973).

2.6.2.3 Pellet/Restricted Fauna Mudstone-Wackestone Facies

This facies is light gray to buff in color. Although typically calcitic across Montana, this facies is the most commonly dolomitized facies in the region. This broad facies belt extends spatially across Montana during deposition of the Mission Canyon Formation and east-central Idaho during the time of Scott Peak Formation deposition. This facies is structureless except for rare graded laminae and wave ripples (Figure 2.7C). It is generally thin bedded and occasionally medium bedded. Bioturbation is low to occasionally moderate. The texture is dominantly mudstone with occasional wackestone beds. Allochems are dominated by euryhaline fauna especially ostracods, which are usually 150-500 μm across. Other typical allochems are calcispheres and peloids as well as microskeletal debris, all of which tend to range in size from 50-150 μm . Chert nodules are rare to occasional and appear to form after evaporite nodules.

This facies is interpreted to have been deposited in shallow environments within the most proximal portion of the lagoon adjacent to the peritidal environments. Lime mud is interpreted to have been both locally produced and deposited through suspension after being brought up into the water column during periodic storm events. Associated allochems were introduced to the restricted inner lagoon during this time and were deposited by traction currents which were preserved in the rare wave ripple and parallel laminae. Replacement of interpreted evaporite nodules by chert suggests that deposition occurred in this area under highly restricted condition with generally poor circulation and possibly hypersaline conditions.

2.6.3 Peritidal Facies Association

As suggested by this facies association's name, facies of this group refer to deposition "around the tides." The peritidal facies association is interpreted to represent the suite of depositional environments which existed between the restricted inner lagoon and the uppermost supratidal environments. These depositional environments encompass the wide range of environmental and energy regimes that are associated with strandline deposition. The peritidal deposits herein described are predominantly those of the low-energy tidal zones and the associated supratidal mud flat environment.

2.6.3.1 Pisoid Packstone-Grainstone Facies

This facies is commonly deposited within the central Montana intrashelf basin during the Mission Canyon Formation and is common during deposition of the McKenzie Canyon Formation at the Bell-McKenzie Canyon outcrop location in southwest Montana. The pisoid packstone to grainstone facies is typically light to medium gray in color and is usually thin to medium bedded. The texture is dominantly grainstone with subordinate packstone. Allochemically, this facies is composed of abundant pisoids with abundant micritized and coated grains and lesser amounts of calcispheres. In particular, ostracods and gastropods are almost exclusive. Fenestrae are common throughout this facies. It is occasionally cross-bedded (Figure 2.8A)

The pisoid packstone to grainstone facies is interpreted as deposited in intertidal to very shallow subtidal environments. Grainstone textures suggest that this facies was at least partially wave agitated. This likely winnowed away any mud which may have been deposited. The fauna present is typical of that of other restricted settings in the inner

lagoon. This restricted fauna further promotes the idea that this facies was deposited in an overall restricted energy setting in potentially a highly saline to hypersaline water mass. This facies has been interpreted in the subsurface of the central Montana trough and Williston Basin as forming island complexes (Petty, 1996), and it is possible that similar island deposits may be reflected in the outcrop examples described here.

2.6.3.2 Algal Laminite Facies

The algal laminite facies has a broad distribution similar to that of the lagoonal facies associations. It is widely distributed across Montana during the deposition of the Mission Canyon; however, its distribution in east-central Idaho during the Scott Peak Formation is much less common and rather infrequent. The fabric of this facies is dominated by crinkly to irregular laminations at the mm-scale which are typically undulatory (Figure 2.8B). This facies is devoid of burrowing and skeletal debris. It is typically medium gray in color and is at least partially dolomitized. Rare domal stromatolites are associated with this facies which have amplitudes of 1-5 cm and wavelengths of usually 10 cm. Rare fenestrae are also associated with this facies.

The algal laminite facies is interpreted to have been deposited in the supratidal to upper intertidal environments. It is interpreted to have formed by trapping and binding of sediments by algae (Hardie and Ginsburg, 1977). The barren nature of the algal laminite facies suggests highly evaporitic conditions which prevented burrowers from mechanically destroying the laminations. The rare domal stromatolites may indicate deposition controlled by similar processes but occurring in a shallow subtidal rather than supratidal setting.

2.6.3.3 Mudclast Conglomerate Facies

This facies is typically tan to medium gray in color and is usually thinly bedded. It is commonly dolomitized, especially the mud matrix which surround the mudclasts (Figure 2.8C). The matrix may also be composed of peloids. Mudclasts and mudchips range in size from 2-7 cm in length and 1-2 cm in height and are typically elongate. The mudclast conglomerate facies occasionally shows lamination but clasts are commonly unoriented.

The mudclast conglomerate facies is interpreted to result from periodic storm energy impinging upon the supratidal mudflat and ripping up desiccated muds deposited

here. The mudclasts are then redeposited over the same supratidal area and mud infill between the clasts results from settling of mud from suspension.

2.6.3.4 Red Shale/Siltstone Facies

This facies is dominated by siliciclastic silt and clay and is typically red in color. It is nearly always very thinly bedded with occasional thin beds and extremely rare medium beds. The only carbonate typically present is microcrystalline dolomite about 20 μm across. It is commonly friable and always barren of fossils. It is interpreted to have been deposited during periods of extended subaerial exposure. Clastic sediments were likely derived from eolian transport onto the exposed former tidal flats.

2.6.4 Evaporite Solution Collapse Breccia Facies

These breccias are distinguished from other breccias by their high lateral continuity, flat strataform bases and irregular tops, and by the associated strata within which they are bedded (Figure 2.9). These breccias are typically 15-100 cm thick and contain clasts of other peritidal facies. The matrix is nearly always dolomitized and clasts are commonly dolomitized. The clasts are typically angular and range in size from 1-2 cm to 15-30 cm. The breccia fabric is generally clast supported with a chaotic arrangement of the clasts.

This breccia is interpreted to have formed when bedded evaporites deposited on the supratidal mudflat were dissolved out and the overlying strata collapsed into the void. It is also possible that the evaporites were deposited during times of initial sea level rise and subaqueous deposition of evaporites occurred in shallow hypersaline waters. This process is inferred to have driven the accumulation of thick evaporite sequences deposited in the subsurface in time-equivalent strata of the central Montana trough and Williston Basin (Roberts, 1967). Broad sheet-like regionally-correlative breccia deposits up to 20 m in thickness which have been deposited across Wyoming and additionally exposed in the outcrops of the central Montana trough are interpreted to have resulted from dissolution of these thick accumulations of subaqueously-deposited evaporites.

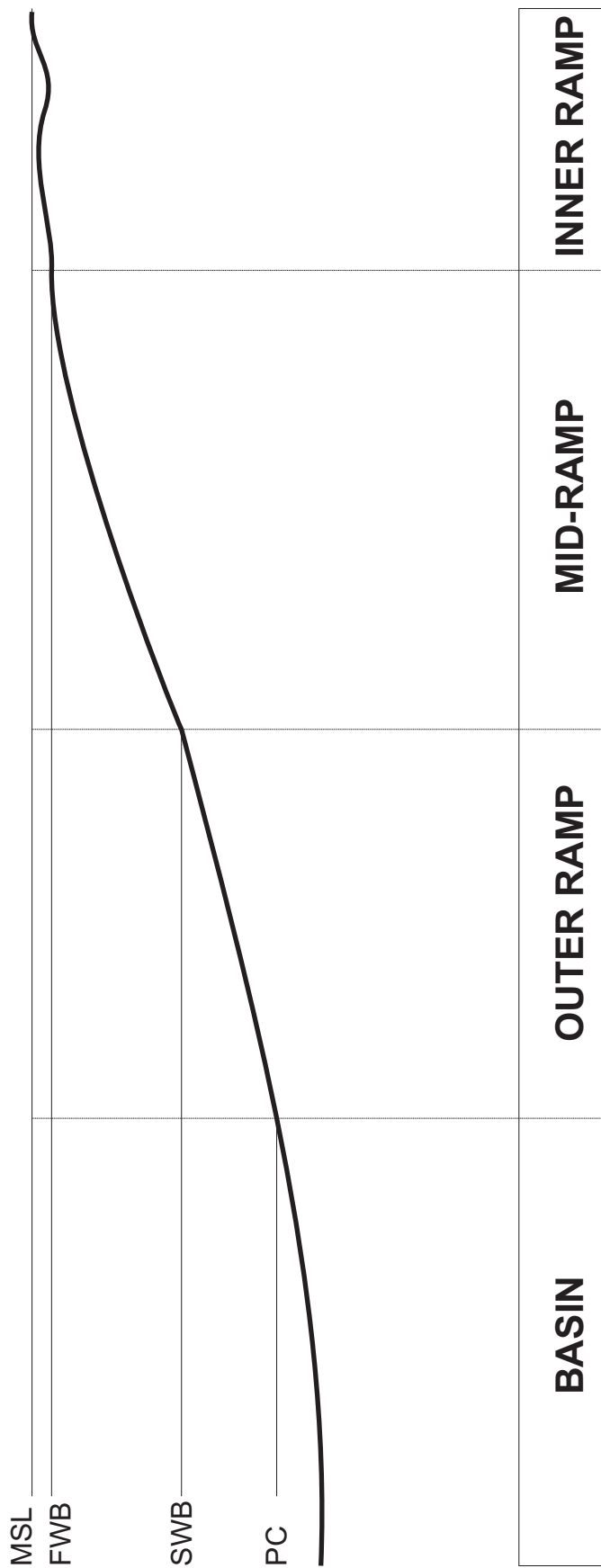


Figure 2.1: Homoclinal ramp profile illustrating the subdivision of depocenters across the ramp. The basin depozone makes up the area at or near the toe-of-slope and below the pycnocline (PC), when expressed. Only the highest energy events impinge upon the bottom in this depozone. The outer ramp depozone lies between the pycnocline and storm wave base (SWB). Deposition here is only rarely affected by reworking by storm events. The mid-ramp depozone makes up the area between storm and fairweather wave bases (FWB) and is an area of frequent reworking by storm events. The area between fairweather wave base and mean sea level (MSL) is the inner ramp depozone. This area can be further subdivided into a shoal/barrier zone which is the area of highest energy on the ramp, two subtidal zones, one seaward and one landward of the shoal/barrier zone, and a peritidal zone at or near the shoreline.

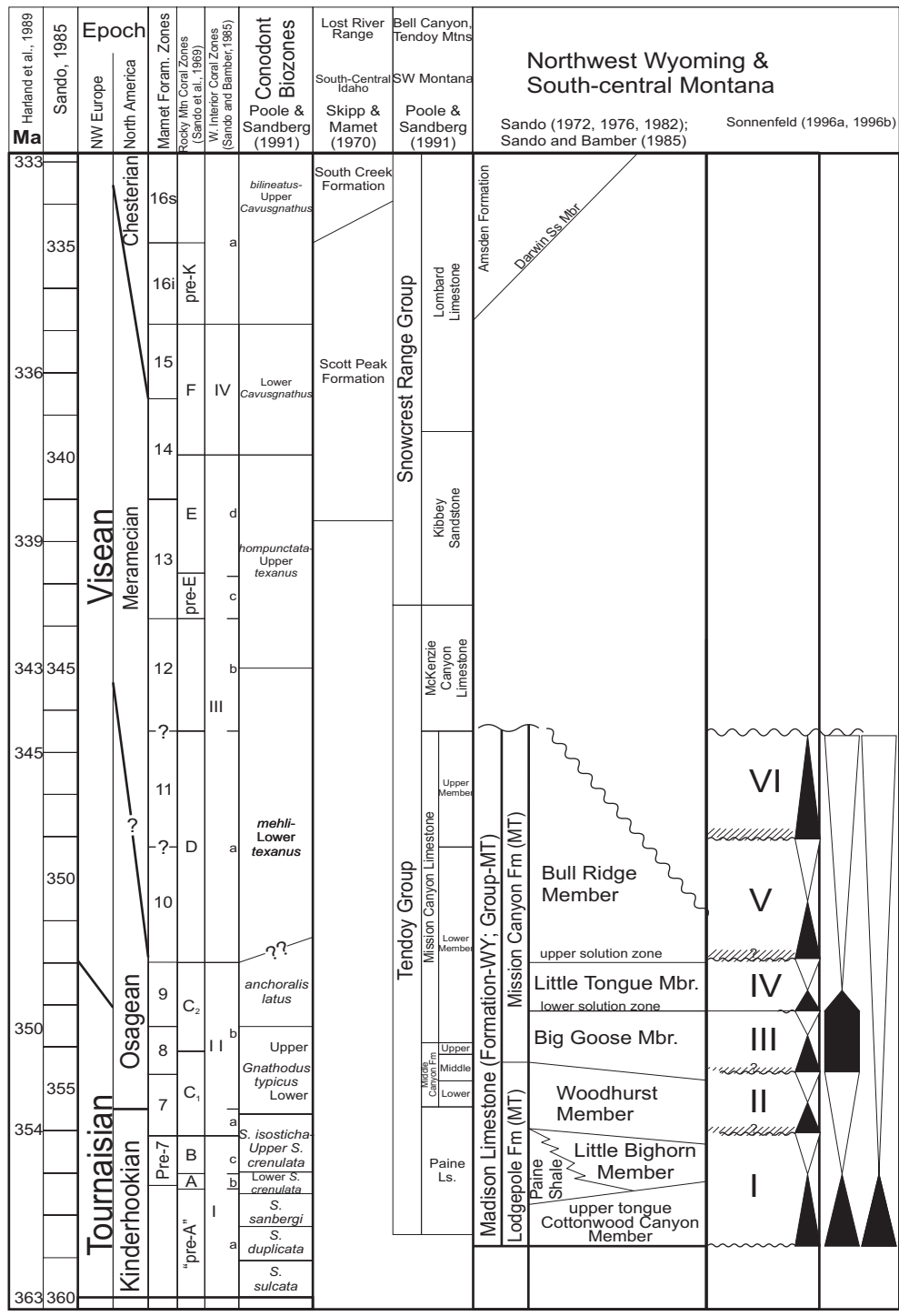
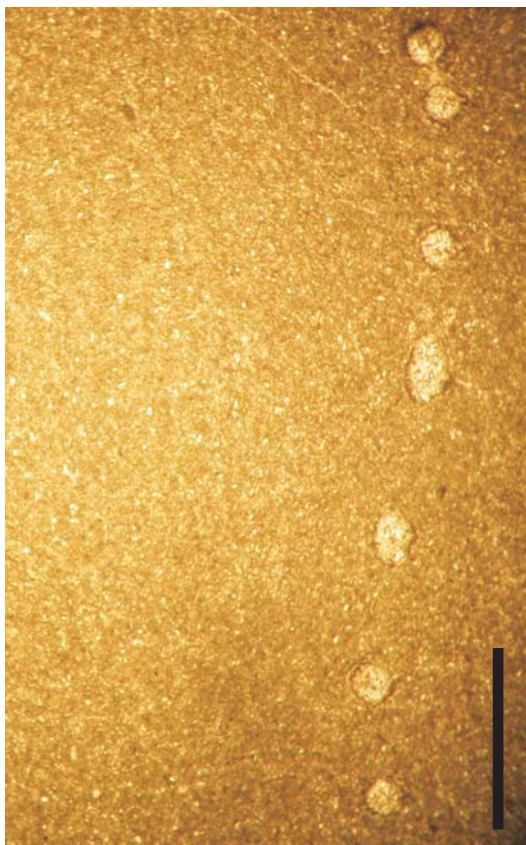
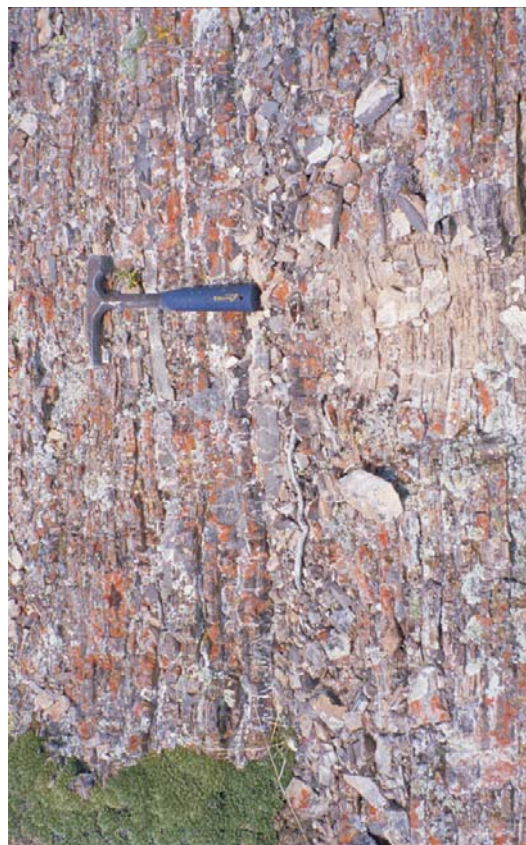


Figure 2.2: Chronostratigraphic chart summarizing the regional relationships of lithostratigraphic units in southern and southwestern Montana (Sando, 1972,1976, 1982; Sando and Bamber, 1985; Poole and Sandberg, 1991) and east-central Idaho (Skipp and Mamet, 1970) to established biostratigraphy (Poole and Sandberg, 1991; Sando and Bamber, 1985; Sando et al., 1969) and sequence stratigraphy (Sonnenfeld, 1996a,b).

Figure 2.3: Summary graphic of the facies of the basin depozone. A) Photomicrograph of the cherty peloid/skeletal calcisiltite facies of the basin depozone. The calcisilt contains both peloidal material, seen here as the darker micritic components and microskeletal components, the transparent very fine grains. The larger sparry grains near the bottom of the photomicrograph are a cross-section through a fenestrate bryozoan. Bryozoans are commonly the only macrofaunal elements that occur within this facies. Scale bar is 1 mm long. From Middle Canyon Formation at Bell-McKenzie Canyon section. B) Bedded chert facies of the basin depozone. Thin to very thin beds of dark gray to tan brown chert, which pinch and swell laterally. This facies is dominantly composed of sponge spicules with minor amounts of crinoidal and other macrofaunal debris. The light to medium gray interbedded material is typically peloidal/skeletal calcisiltite. Rare crinoidal grainstone beds punctuate sedimentation in this facies. Hammer is ~30 cm long. From Middle Canyon Formation at the Bell-McKenzie Canyon section. C) Argillite/shale facies of the basin depozone. This tan gray to buff colored unit is dominantly composed of siliciclastic silt and clay with admixed lime mud. It is typically finely laminated, as seen here, or fissile. Dewatering of the sediment is well preserved here in the convoluted and contorted bedding seen at the center of the photo. Below this dewatered zone, the strata are moderately bioturbated, although some fine lamination is preserved. Coin is ~2.5 cm across. From Lodgepole Limestone at the Ashbough Canyon section. D) Polymict breccia facies of the basin facies association. The clasts in the photo range from <5 cm to ~1 m in width. Clasts here are light tan to tan gray to dark gray and are most commonly composed of peloidal/skeletal calcisiltite with occasional wackestones with crinoidal and microskeletal debris. In this photo clasts are angular and the breccia is clast supported. The matrix here is composed predominantly of lime mud. Hammer is ~30 cm in length and lies parallel to bedding in the section but perpendicular to the bedding of this coherent block within the breccia. From Lodgepole Limestone at the Bell-McKenzie Canyon section.



A



B



C



D



Figure 2.4: Limestone/argillite couplets facies of the outer ramp facies association. The light gray, finely bedded strata are the limestone couplets, while the argillite couplets are the tan to tan gray very thinly bedded units. The limestone couplets here are texturally wackestone to packstone. Nodular bedding is common especially in the lower part of the photo. Thin lenticular bedded limestone is more common near the top, where beds laterally swell and pinch out against one another. The very top part of the photo shows limestone beds which are partly amalgamated. Hammer is ~30 cm long. From Lodgepole Formation at the Ashbough Canyon section.

Figure 2.5: Summary graphic of the facies of the mid-ramp depozone. A) Graded peloidal/skeletal grainstone facies of the mid-ramp facies association. Coarse tan gray skeletal debris scours underlying buff-colored mudstone at the base of the coin. The bed grades up into fine peloidal packstone with fine laminae. At the top wave ripples and hummocky cross-stratification of laminae of skeletal/peloidal grainstone are interleaved with laminae of mudstone. The mudstone deposited from suspension at the top of the photo is structureless and has a shattered appearance. At the bottom of the photo, red stained firmgrounds and hardgrounds illustrate periods of slow or non-deposition within the suspension-dominated mudstones. Coin is ~2.5 cm across. From Lodgepole Limestone at Livingston section. B) Ooid packstone to grainstone of the mid-ramp facies association. Solution seams subdivide partly amalgamated redeposited oolite beds, one at the base of the coin and one just above the top of the coin. The lower two oolitic units have packstone textures while the top unit grades from grainstone at its base with some scour evident to packstone at the top of the photo. Minor amounts of skeletal material have been incorporated into these beds including brachiopod fragments. Coin is ~3 cm wide. From Lodgepole Formation at the Monarch section. C) Skeletal packstone to grainstone facies of the mid-ramp facies association. Light to medium gray is fine skeletal grainstone and buff is dolomitic mudstone. Coarse skeletal lag scours into the underlying mudstone. This is overlain by hummocky cross-stratified finer skeletal grainstone. The upper part of this amalgamated grainstone shows ripple lamination deposited under oscillatory flow conditions. The skeletal grainstone unit is capped by buff-colored suspension deposited mudstone. Coin is ~3 cm across. From Lodgepole Limestone at Livingston section. D) Massive crinoidal/skeletal facies of the mid-ramp depozone. Moderately well sorted crinoidal grainstone with minor admixed rugose coral, brachiopod, and bryozoan debris. A crinoidal packstone texture is more evident near the bottom of the photo. Coin is ~3 cm wide. From Mission Canyon Formation at the Bell-McKenzie Canyon section. E) Bioturbated wackestone-packstone facies of the mid-ramp facies association. Buff wackestone to packstone with stringers and small nodules of chert. Moderately bioturbated with faint laminations still present. Skeletal grains can be observed in both the chert and limestone, including whole crinoid columnals and articulated crinoid columnals. Due to the bioturbation, the precise depositional environment of this facies is not clear; however, laminations attest to deposition by traction currents. Large and whole fossils suggest deposition proximal to a skeletal bank or shoal. Coin is ~3 cm across. From Lodgepole Limestone at Livingston section.



A



B



C



D

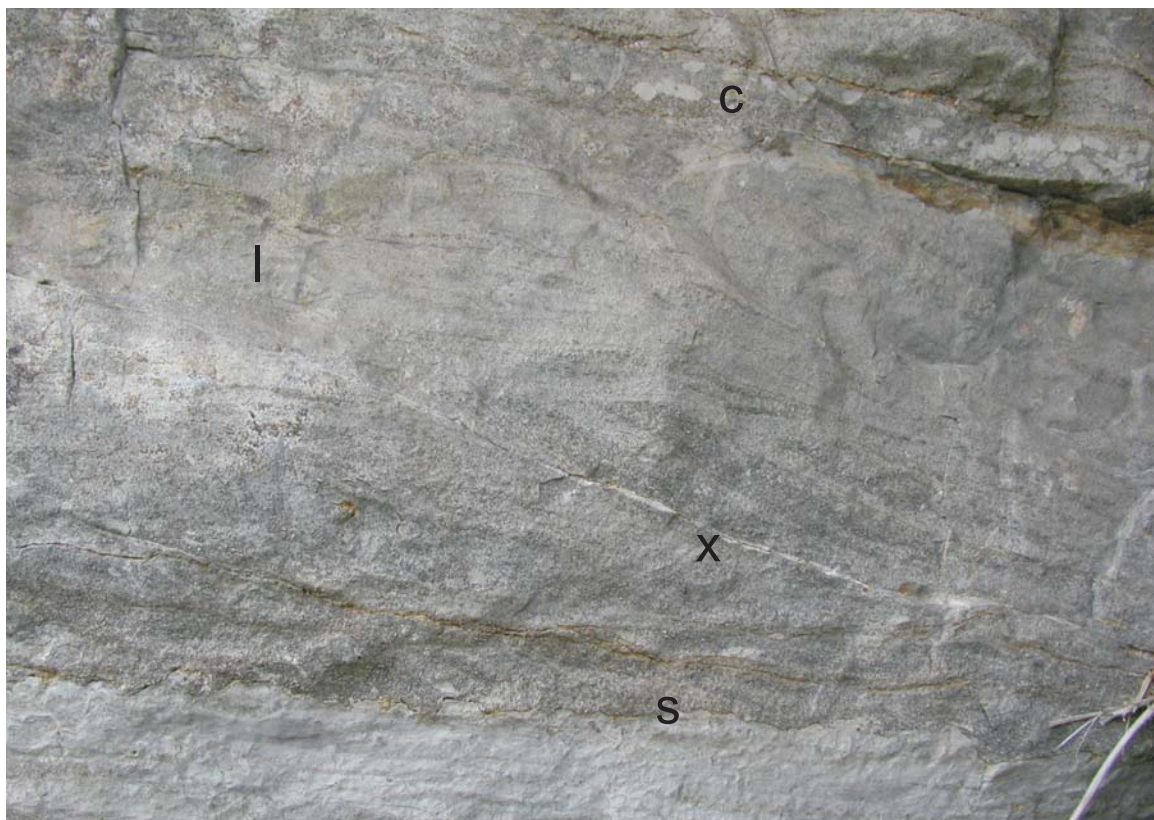


E

Figure 2.6: Summary graphic of the facies of the shoalwater/barrier facies association of the inner ramp depozone. A) Cross-bedded ooid grainstone facies of the inner ramp depozone and shoalwater/barrier facies association. This example shows a mixed ooid and skeletal grainstone shoal with tabular to trough cross-bedding and birectional cross-bedding 2/3 of the way up the photo. The skeletal grainstone laminae, the tan gray textured laminae, clearly define the bedding in the otherwise massive medium gray oolitic laminae. Packstone textures are evident near the bottom of the photo. This grainstone body is interpreted as being deposited in tide-influenced conditions. Coin is ~ 3 cm across. From Mission Canyon Formation at the 16 Mile Creek section. B) Cross-bedded skeletal grainstone facies with trough cross-bedded skeletal grainstone (x) in the middle of the photo are composed of crinoidal, brachiopod, rugose, coral and bryozoan debris. Planar to trough cross-beds are apparent within the facies, and scour of the underlying bioturbated wackestone is clear at the base (s). The skeletal grainstone shoal is overlain by plane laminated peloidal packstone which grades upward in to peloidal wackestone (l). At the very top of the photo, scour by the successive unit has scoured into the wackestone incorporating clasts (c) of the underlying facies into the base of the shoal bed. Cross-bed sets are ~20 cm high. From Mission Canyon Formation at 16 Mile Creek section.

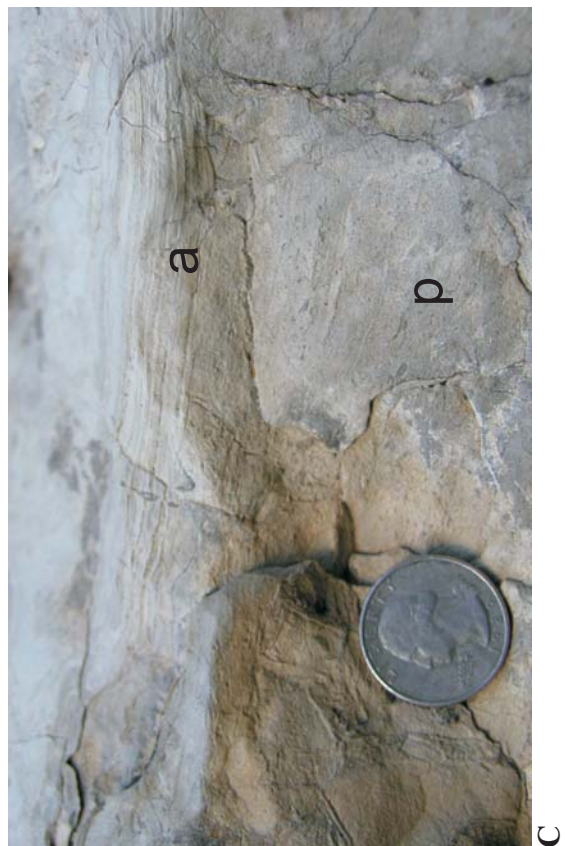
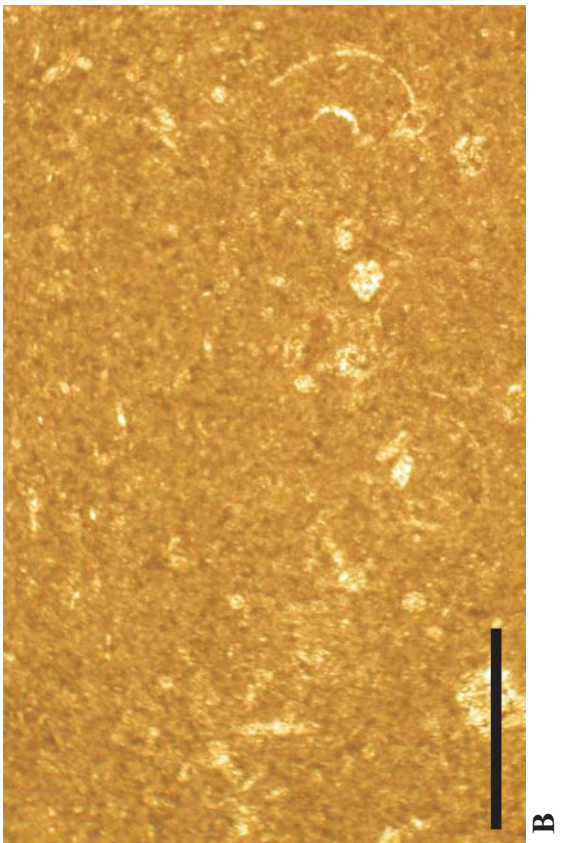
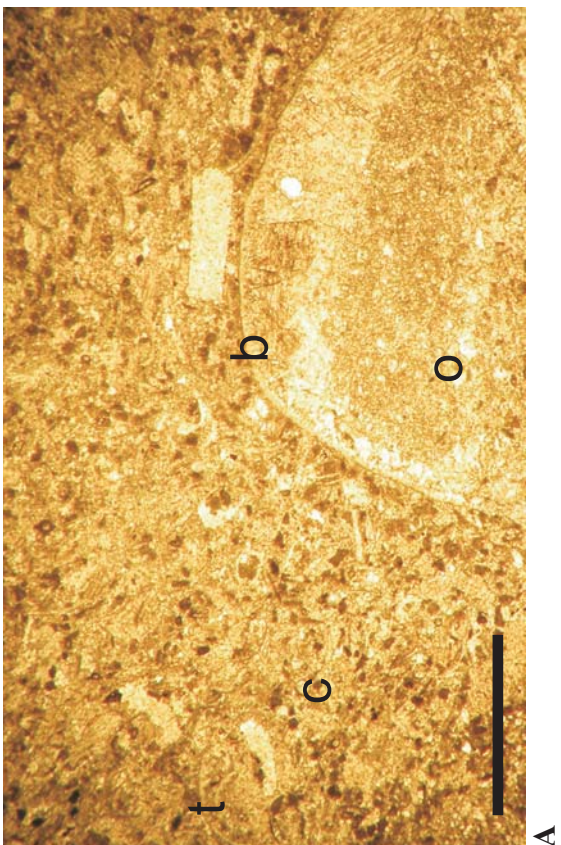


A



B

Figure 2.7: Summary graphic of the facies of the lagoonal facies association of the inner ramp depozone. A) Peloidal grainstone facies of the inner ramp depozone and lagoonal facies association. This photomicrograph shows a bimodal distribution of peloids, both larger dark micritic peloids, and fine, sparry peloids which make up the bulk of the sediment in this same. Allochems indicative of both open marine and restricted conditions are abundant, from thick shelled open marine brachiopods (b) and echinoid spines (e) to thin shelled brachiopods (t) and ostracods (o) and calcispheres (c) indicative of restriction. Open marine fauna were likely washed into a generally more restricted energy and circulation setting during a high-energy event such as a storm. Scale bar is ~1 cm wide. From Mission Canyon Formation at 16 Mile Creek section. B) Bioturbated peloidal wackestone-packstone facies of the inner ramp depozone and lagoonal facies association. Fine micritic peloids which may in fact be pelletal in origin, are the dominant grain in this photomicrograph. Admixed with the pellets are a thin shelled fauna dominated by ostracod debris. This facies is interpreted to have been deposited in a lagoon with restriction. Scale bar is ~1 cm wide. From Mission Canyon Formation at 16 Mile Creek section. C) Pellet/restricted mudstone to wackestone facies shows well preserved parallel laminae (p), where the laminae are defined by skeletal fragments. The lower part of the photo shows the commonly fractured appearance of this mud-dominated facies. At the top of the photo crinkly, very fine laminations of the algal laminitic facies (a) can be seen capping the pellet/restricted mudstone to wackestone facies. This indicates deposition of the pellet mudstone to wackestone facies in very shallow subtidal conditions with low energy and elevated salinity which prevented infaunal burrowing. Coin is ~3 cm across. From Mission Canyon Formation at the 16 Mile Creek section



B

A

C

Figure 2.8: Summary graphic of the facies of the peritidal facies association of the inner ramp depozone. A) Pisoid packstone to grainstone facies of the inner ramp depozone and peritidal facies association. This photo shows a poorly sorted pisoid packstone with tabular cross-bedding. A wide range of pisoid sizes are observed within the overall fining upward trend in the lower and middle part of the photo. In this case, these grains are highly micritized, giving them a very dark gray color which contrast with the medium to dark gray matrix limestone. Although cross-bedded pisoid packstones are uncommon, it does support the idea that occasionally pisoids may have been stacked in high-energy shoals which aggraded to sea level and may have formed island complexes in the central Montana trough. Coin is ~ 2.5 cm across. From Mission Canyon Formation at the 16 Mile Creek section. B) Algal laminite facies composed of very finely laminated dolomitic mudstone. This facies is interpreted to have been deposited on the supratidal mud flat where occasionally washed in mud was trapped and bound by algae living there. Pencil tip is ~ 3 cm long. From Mission Canyon Formation at the Baldy Mountain section. C) Mudclast conglomerate facies of the inner ramp depozone and peritidal facies association. This photo illustrates a typical peritidal succession of the Mission Canyon Formation. At the bottom of the photo, pustular algal mats (p) are seen. These mats are then ripped up when storm energy impinged on the tidal flat, and clasts of the algal mat (c) can be observed in the overlying strata. Laminated packstones (l) with stringers of skeletal grainstone and mudclasts can be seen in the middle of the photo. The top of the photo is dominated by a mudclast conglomerate where light gray, elongate, rounded muclasts have been deposited in a darker micritic matrix. This unit is then capped by bioturbated lagoonal wackestones with pellets and restricted fauna. Pencil is ~ 15 cm long. From Mission Canyon Formation at the 16 Mile Creek section.



B



A



c



Figure 2.9: Evaporite solution collapse facies of the inner ramp depozone and peritidal facies association. Approximately 2 m of breccia overlies a strataform base of thinly to very thinly bedded peritidal facies. The clasts within the breccia are angular and average about 20 cm but range from <5 cm to 100 cm or more. The clast composition is dominated by peritidal and shallow subtidal facies of lagoonal affinity. The matrix in this case is largely dolomitized. This breccia resulted from dissolution of original bedded evaporites and collapse of the overlying carbonate clasts into the void space. In this case, stacked supratidal evaporites have been leached and associated peritidal facies have collapsed into the space created by their absence. Jacob staff at right of photo is ~ 1.6 m long. From Mission Canyon Formation at the Monarch section

CHAPTER 3. SEQUENCE STRATIGRAPHY AND FACIES ORGANIZATION

3.1 OVERVIEW

Genetic units are the building blocks of a stratigraphic succession. They are defined as the smallest scale of organization of beds or bedsets which form in response to changes in the ratio of accommodation space to sediment supply. The base level changes result from changes in hydrodynamic energy either due to increase or decrease of relative sea level or absolute energy changes in the water column due to process changes such as changes in storm frequency or barrier efficiency. As depositional facies (Figure 3.1, 3.2) are high fidelity recorders of changes in bathymetry and system energy, the record preserved reflects the concomitant changes in environmental conditions. A genetic unit, or cycle, is the smallest sedimentary packet which records one transit of accommodation space from minimum to maximum and back to minimum as observed at a single location. The record of the accommodation space, or room for sediment accumulation, is a critical factor in understanding the distribution of facies and evolution of facies distributions in time. Additionally, at the genetic unit scale, vertical facies associations are most likely to reflect coeval lateral facies associations and provide the best information on lateral facies distributions. That is, Walther's law is more likely applicable at the cycle scale rather than at the sequence scale, where dislocation of facies belts is likely and non-Waltherian facies successions are expected.

Two hemicycles define a couplet which composes the genetic unit. During the period where the change in sedimentation rate is lower than the increase in accommodation space, the transgressive hemicycle is deposited. This subunit is composed of a facies assemblage showing overall increasing bathymetry and accompanying changes in hydrodynamic energy. The regressive hemicycle is that hemicycle which records the period when sediment supply exceeds the rate of accommodation space creation. The symmetry, that is the relative proportion of facies preserved within the transgressive versus regressive hemicycle, of the cycle contains important information on the overall accommodation setting of the depositional system. Because paradigmatically carbonate cycles have been considered to be coarsening upward, many workers have used purely asymmetric cycles to describe successions of facies. In this context, the surface coinciding with minimum accommodation in the cycle

also coincides with the surface of maximum accommodation. Although purely asymmetric cycles are observed within the Madison Group, they are the exception rather than the rule. Additionally purely asymmetric cycles are an end-member case along with purely symmetric cycles, which illustrate instantaneous accommodation development for the former and balance between accommodation and sedimentation for the latter. The continuous variation between end-members, cycle thickness changes, and the relative proportion of facies within genetic units provides information on the changes in accommodation through time.

Genetic units may form as a result of autogenic or allogenic forcing functions. That is cycles may form in response to changes in accommodation space which result from local changes in sediment rate, such as full aggradation of sediments to base level, or from global effects like eustatic sea level rise. Genetic units contain no unique information which record the cause of their creation and only relate information of their local setting; however, when long-term patterns of stacked genetic units are observed, the overall trends within cycle thickness and facies proportions within the cycles yield information on secular variation on accommodation (Sonnenfeld, 1996a, 1996b). The temporally-significant accommodation trends relate to other accommodation cycles observed elsewhere on the ramp. Symmetric yet static, or stationary, variation in environmental conditions which yields a succession of cycles that vary little in thickness and facies content are indicative of aggradation of the area over that series of cycles. Progradation or backstepping occurs when symmetric or asymmetric but non-stationary variation in environmental conditions yields a succession of cycles that vary with discrete changes in cycle thicknesses and component facies. The amount of facies offset between genetic units may indicate the degree of forcing and proximity to a sequence boundary.

Sequence stratigraphy is concerned with the hierarchical arrangement of the genetic units into nested orders of accommodation development. Within this arrangement higher order cycles and sequences are embedded within lower order sequences. Here, genetic units form the stratigraphic monad, and lower order sequences are composed of these cycles. These sequences then nest to form the next lower order sequence. A sequence has been defined as a relatively conformable succession of genetically related strata bounded by unconformities or correlative conformities (Vail et al., 1977).

Sequences can then be subdivided into systems tracts which are genetically related intervals of strata which formed during specific increments of a relative sea level cycle.

Systems tracts can further be defined by their types of bounding surfaces, their geometry, and position within a sequence. The basal most systems tract is the shelf margin or ramp margin wedge. It overlies the sequence bounding unconformity or its relative conformity depending on the amount of relative sea level fall. Cycles which make up the ramp margin wedge typically stack in a aggradational to slightly progradational pattern, as they onlap the sequence boundary in a landward direction (Elrick, 1990). The ramp margin wedge is bound on its upper surface by the transgressive surface. The transgressive systems tract, or TST, is marked by retrogradational deposition of cycles and backstepping of the locus of carbonate sediment production. The TST overlies the ramp margin wedge in a downslope position and strata downlap onto the ramp margin wedge; however, the TST directly onlaps the sequence boundary landward of the shelf margin in a progressively landward direction. The TST is bound on top by the maximum flooding surface, or MFS. The MFS marks the most landward position of the deepest water facies within a sequence, and also marks the transition from backstepping of cycles to progradational and/or aggradational stacking. The uppermost systems tract within a sequence is the highstand systems tract or HST. The HST is marked by downlapping of cycles onto the MFS in a seaward direction and progradationally and aggradationally stacked cycles. The HST is capped by the sequence boundary, which marks the time of negative accommodation space across the system.

3.2 GENETIC UNITS

3.2.1 Slope-to-Basin Cycles

Slope-to-basin cycles in the Mississippian Madison Group are composed of poorly cyclic to symmetric cycles of 1-10 m thickness, which are dominated by fine-grained carbonates and associated argillaceous beds (Figure 3.3). These cycles typically begin with bioturbated calcisiltites at the base, which increasingly become laminated and show increased abundance intercalated argillaceous beds progressing upward through the cycle. The maximum deepening within the cycle is placed at the position of greatest abundance of non-carbonate sediments, either argillite and shale or bedded chert. Above this position, the succession typically is made up of first laminated calcisiltites and is

often capped by bioturbated calcisiltite. Rare pelmatozoan-dominated grainstone beds interrupting the overall symmetry of the cycle are indicative of rare turbidity and/or grain flow deposits with enough mass and energy to reach this distal setting.

The cycles are representative of deposition below storm wave base and perhaps below the pycnocline or oxygen-minimum zone. The high abundance of argillaceous material suggests overall slow carbonate sedimentation rates, likely with punctuated introduction of fine carbonate sediment into the slope and basinal environments during storm events (Reid, 1991). Redeposition of carbonates onto the slope and into the basin most likely occurred as a function of storm frequency and the proximity of the area of storm reworking to these sediment storage areas (Elrick, 1990). Based on these ideas, it can be inferred that cyclicity within basinal and slope sediments reflects the retreat and approach of storm wave base during a sea level transit cycle. Changes in bioturbation likely reflect changes in the level of bottom water oxygenation.

3.2.2 Outer Ramp Cycles

Outer ramp cycles are typically composed of slightly asymmetric cycles of 1-10 m in thickness. These cycles are often difficult to recognize because the facies making up the cycles are typically insensitive to bathymetric changes on the scale characteristic of the 10-40 m amplitude sea-level changes driving cyclicity at this temporal scale (Elrick, 1990). Outer ramp cycles are predominantly composed of the limestone/argillite couplet facies (Figure 3.4). Cycles can be distinguished within bedsets of the limestone/argillite couplets based on changing proportions of grain-rich material incorporated to the limestone couplet as well as the proportion of argillite that makes up the couplet (Elrick, 1990). That is, grain-rich limestone is expected nearer the top of the cycle, while thicker argillite intervals are expected near the maximum deepening of the cycle.

Individual couplets within the Lodgepole Formation have been interpreted to represent periodic changes in storm activity from storm-dominant periods to those times where limited or no storm activity occurs (Elrick, 1990). Spectral analysis of the individual couplets revealed a sub-orbital periodicity (0.7-2.9 kyr) within the Lodgepole succession and were attributed to high-frequency variations in paleoclimatic conditions (Elrick, 1990).

Outer ramp cycles, like the slope-to-basin cycles, are attributed to the proximity of the site of sediment storage to the position where storm wave base impinges on the ramp (i.e., the middle ramp to outer ramp transition). Carbonate sediments making up outer ramp cycles are an admixture of locally produced as well as transported materials. Local production is recorded by the preservation of articulated fossils often found in growth position. This further supports the idea that deposition was occurring within a well-oxygenated water column. The graded grain-rich beds near the cycle tops indicate the increasing impact of storms as storm wave base moved down the ramp during relative sea-level fall. Relative sea-level fall likely reflects both the aggradation of the outer ramp into shallower water depths as well as eustatic sea-level fall.

3.2.3 Middle Ramp-to-Foreshoal Cycles

Middle ramp-to-foreshoal cycles are generally 1-10 m thick and are composed of a wide variety of depositional facies. Depositional facies range from limestone/argillite couplets at the lower bathymetric limit to skeletal and peloidal packstones to grainstones to redeposited ooid, skeletal and peloidal packstone to grainstones to crinoid bank facies to near-shoal and shoal facies at the top (Figure 3.5). Sedimentary structures vary from graded bedding near the base indicative of turbidity flow to ripple lamination and hummocky cross-stratification consistent with storm-type traction conditions to parallel laminations and planar, trough, and bi-directional cross-stratification demonstrative of higher energy deposition within fairweather wave base and into the intertidal zone. Cycles of this type have been previously documented within the Lodgepole Limestone in southern and central Montana by Elrick (1990) and in southern Montana by Sonnenfeld (1996a, 1996b).

These cycles are generally symmetrical with cycle tops indicated by the maximum amalgamation of grainstone beds. The maximum deepening within a cycle can occasionally be recognized by firmgrounds or hardgrounds which are typically ripped up and incorporated in the overlying beds. In some cases brachiopod shell lags indicate relative sediment starvation and winnowing at the time of maximum deepening within the cycle.

Cycles of this type were deposited under conditions of direct storm influence. Unlike the outer ramp and slope-to-basin cycles, here storm energy directly impinged

upon the seafloor both in the form of unidirectional and oscillatory flows. Sediments stored on the middle ramp were produced locally or transported only very short distances, which further separates them genetically from basinward deposits. Cyclicity here, although certainly influenced by storm wave base transit during sea level rise and fall, is more likely controlled by aggradation of middle ramp sediments up to base level consistent with a graded clinoform profile.

3.2.4 Restricted Subtidal Cycles

Restricted subtidal cycles range from 1-10 m thick, typically asymmetric, and dominated by facies with relatively low amounts of fossil material and faunal diversity (Figure 3.6). Cycle bases tend to be heavily bioturbated packstones and grainstones with normal marine fauna commonly incorporated within a peloidal and muddy matrix. Ooid also are frequently admixed within this setting further highlighting the proximal position of deposition of this facies with respect to the sand shoal belts. Moving up through the cycle, several compositional and structural changes are commonly observed: the amount of bioturbation and the amount of shoal-derived allochems decrease rapidly. Typically the texture of the rock initially remains packstone to grainstone; however, the composition is dominated by peloids with fauna limited to ostracods and rare thin-shelled brachiopods and gastropods, indicative of restriction. Increased restriction is observed within cycles as the amount of pelleted material decreases and carbonate mud becomes the primary sedimentary constituent, with mudstones capping these cycles.

Unlike the coarsening-upward trend observed within the cycles so far documented, restricted subtidal cycles display increasingly muddy textures from the bottom to the top of the cycle. This pattern is in response to diminished effective wave energy in the back-barrier setting with increased efficiency of the shoal barrier system and attenuation due to expansion of the restricted shelf or lagoon with progradation of the barrier system (Sonnenfeld, 1996a). The effect of decreased hydrodynamic energy on the restricted shelf is manifold and ranges from decreased winnowing of carbonate mud to decreased input of skeletal and coated grain allochems by storm washover to increased salinity due to limited exchange between the shelf and open marine waters seaward. The net effect is to increase the carbonate mud content and decrease the skeletal content both in terms of total volume as well as diversity of fauna. Additionally peloid production and

the presence of other coated grains tend to attenuate in a landward direction as a result of the low energy hydrodynamic regime.

3.2.5 Peritidal Cycles

Peritidal cycles are generally less than 2 m thick and present information on the accommodation development along the shoreline within each cycle. As an extension of this, stacks of peritidal cycles provide a high fidelity record of sea level change and accommodation change often associated with sequence boundaries, with peritidal cycle sets thinning toward sequence boundaries and thickening above (Sonnenfeld, 1996a).

Peritidal cycles (Figure 3.7) may include any or all of the following facies, listed here in a shallowing-upward trend: peloidal grainstone, bioturbated peloidal wackestone-packstone, pellet restricted fauna mudstone-wackestone, pisoid packstone-grainstone, algal laminites, mudclast conglomerates, evaporite solution collapse breccias, and marginal marine shale/siltstone (Sonnenfeld, 1996a). Microkarst is common atop cycle boundaries, reflecting periods of exposure. The overall trend in sedimentary texture is increasing amounts of mud and sedimentary structures tend to be increasingly well preserved with decreasing water depth and increasing restriction. Algal textures, dessication features and appearance of evaporite-related textures, and mudchip conglomerates tend to dominate supratidal deposition on the tidal flat.

In addition to the overall thinning of peritidal cycle sets nearing sequence boundaries, relative facies proportions also provide information on the overall accommodation evolution of the peritidal depositional setting. Typically as the tidal flats step seaward in response to decreasing accommodation, the relative proportion of subtidal facies decrease and a proportionate increase in first intertidal and finally supertidal facies occurs. Increased development of microkarst horizons on cycle tops provides further evidence of overall long-term decreases in accommodation across the shelf.

3.3 SEQUENCE STRATIGRAPHY

The hierarchical arrangement of cycles and sequences within the Madison was first recognized by Sonnenfeld (1996a, 1996b). He observed a five-fold hierarchy with small-scale cycles of 5th-order duration as the basic atomic unit of stratigraphic organization within the succession. The small-scale cycles were embedded within

sequences inferred to be of 4th-order magnitude, which formed the intermediate scale. Typically 5-11 intermediate-scale cycles would in turn stack to form longer term transgressive-regressive cycles of 3rd-order duration. Intermediate-scale cycles could usually be correlated regionally, unlike the 5th-order cycles, but significant amounts of uncertainty with these correlations existed at times during the evolution of the system because cycles of this scale regionally onlap and downlap. Intermediate-scale cycles were often of the same thickness as the 3rd-order sequences, but they could be distinguished based on the amount of facies offset between cycles and the degree of subaerial exposure on the cycle tops (Sonnenfeld, 1996a). Six third-order sequences of 2.2 Myr average duration were regionally identified (Figure 3.8). These sequences provide the best information on accommodation evolution of the system because of their regional lateral extent and because they can be correlated over the area. The third-order sequences were observed to be arranged into two composite sequences also of 3rd-order duration based on their overall stacking geometries, facies motifs, and geomorphic profiles. At the largest temporal scale, Sonnenfeld posited that the entire Madison made up an overall second-order supersequence bounded by interregional unconformities, likely related to far-field tectonic activity in the Antler and Ancestral Rocky Mountain orogenic belts. Beyond simply their enormous lateral extent, the supersequence-bounding unconformities exhibit the greatest amount of erosion and facies belt shifts of any other unconformities, further illustrating their role as master surfaces within the evolution of the system.

The five-fold hierarchy of Sonnenfeld (1996a, 1996b) is adopted here and is the framework for work extending beyond the bounds of the Bighorn basin of Wyoming, where it was developed by Sonnenfeld. This study, however, focuses not only on expanding the framework into time-equivalent successions down-dip from the Madison Limestone of Wyoming (Figure 3.9, 3.10) but also expand the framework temporally and to look at the nature of the downshift of facies belts into the Antler foreland basin during the top-Madison karsting event associated with the Madison supersequence boundary. In this study, an additional 3rd-order sequence beyond the 6 3rd-order sequences identified within the Kinderhookian-Meramecian succession by Sonnenfeld is identified here. This sequence previously was documented in locations in south-central Montana by Elrick (1990) and is here integrated with the regional sequence stratigraphic framework of

Sonnenfeld. Additionally 7 3rd-order sequences of Meramecian-Chesterian age are identified and examined. These sequences are then examined within an expanded spatial and temporal framework in order to understand their evolution within the broader scope of accommodation change at the composite sequence and supersequence scale.

3.3.1 3rd-Order Sequence Evolution and Organization

Fourteen third-order sequences which can be regionally correlated have been identified within this study. Three sequences of third-order duration compose the Lodgepole Formation of Montana, the lowermost formation within the Madison Group. These sequences have been previously documented by Elrick (1990) in the area of southern and central Montana, and are here extended into southwestern Montana. The Mission Canyon Formation is comprised of 4 third-order sequences, as described by Sonnenfeld (1996a, 1996b) in the upper Madison Formation of Wyoming and the Mission Canyon Formation of south-central Montana. These sequences are shown here to be regionally correlative into central and southwest Montana and east-central Idaho. Additionally, seven third-order sequences can be regionally correlated within the McKenzie Canyon, Middle Canyon, and predominantly Scott Peak Formation of southwestern-most Montana and east-central Idaho, making up the lowermost portion of the supersequence overlying the Madison. The Big Snowy Group of central and northwestern Montana and Big Snowy Formation of southwestern Montana and South Creek and Surrect Canyon Formations of east-central Idaho make up the rest of the overlying supersequence (Sando, 1976).

3.3.1.1 Lodgepole Sequence 1

Lodgepole sequence 1 (LP1) overlies a regional angular unconformity which was beveled and karsted as a result of tectonic uplift and exposure (Sonnenfeld, 1996a). The unconformity extends from latest Devonian-earliest Mississippian age in the Antler foreland basin of Idaho, while in updip locations the base LP1 directly overlies progressively older strata of Devonian, Ordovician and Cambrian age (Sando and Sandberg, 1987). Highly variable thicknesses of the overlying basal siliclastics has been interpreted to have resulted from irregular erosion along the unconformity surface and resulting relief (Elrick, 1990). This sequence has been recognized by other workers in

both Montana and Wyoming (depositional sequence 1, Elrick, 1990; sequence I, Sonnenfeld, 1996a, 1996b)

The thickness of this sequence ranges from 0-80 m, with the thickest accumulations within the central Montana trough and in southwestern Montana. The sequence pinches out in a basinward direction either due to non-deposition or later submarine erosion (Huh, 1967). Across the study area, the basal portion of the sequence is equivalent to the Cottonwood Canyon Member of the Lodgepole Limestone. This interval is represented by condensed fine siliciclastic deposition with minor admixed silt-sized dolomite making up the carbonate present in this interval. The upper part of the sequence is represented by the Paine Member of the Lodgepole Limestone across Montana, an argillaceous limestone unit. The sequence is composed of approximately four 4th-order cycles which can be correlated across much of central Montana (Figure 3.11, 3.12), with the lower one and a half cycles defining an overall aggradational to subtly retrogradational interval making up the transgressive systems tract (TST). The upper two and a half cycles make up the highstand systems tract (HST) characterized by overall shallowing of facies and minor progradation (Figure 3.13, 3.14).

3.3.1.1.1 Transgressive Systems Tract

The basal portion of LP1 across the study area is composed of poorly outcropping shale and fine dolomite. This interval is characterized by condensed sedimentation as evidenced by abundant glauconite present within thin carbonate beds. This unit makes up the Cottonwood Canyon Member of the Lodgepole Limestone. At Livingston, in the most proximal position within the study area, mid-ramp cycles of redeposited skeletal packstones and grainstones overlie the basal siliciclastics of the Cottonwood Canyon Member and deepen upward into outer ramp limestone/argillite couplets. Further downdip, in central Montana, middle ramp deposits pass into outer ramp deposits typified by interbedded limestone/argillite couplets, which stack into vaguely shallowing upward intermediate-scale cycles typical 10 m in thickness. Further basinward in southwestern Montana, the outcrop is typically poor with rare outcroppings of shale (Figure 3.15), and the entire sequence thins to approximately 10 m thickness at Bell and McKenzie Canyons before becoming unidentifiable further downdip. Maximum deepening within this succession is difficult to pinpoint. This is due to the relative bathymetric insensitivity of

the outer ramp and basinal facies making up the systems tract. The maximum flooding surface (MFS) at Livingston likely falls within a stack of increasingly argillaceous and upward-fining wackestones and packstones which overlie lenticularly-bedded packstone and grainstone deposits with crinoidal debris. Further downdip, the MFS is placed within the most argillaceous, poorly fossiliferous beds of outer ramp or basinal affinity, likely indicative of a carbonate starved setting due to the large distance from the area of carbonate production and perhaps dysoxic conditions.

3.3.1.1.2 Highstand Systems Tract

The highstand systems tract is represented at location Livingston by shallowing upward outer ramp limestone/argillite couplets which shallow into increasingly skeletal-rich packstones and grainstones of middle ramp affinity. No evidence of exposure atop the mid-ramp deposits, makes distinguishing a precise sequence boundary here equivocal at best in this locality.

In increasingly distal locations in central Montana, limestone/argillite couplets typically are overlain by decreasingly argillaceous and increasingly amalgamated peloidal and skeletal packstones with wavy bedding at location 16 Mile Creek (Figure 3.16). Again, an unequivocal sequence boundary cannot be picked at any of the section locations in these downdip locations because of a lack of definitive exposure; however, the sequence boundary is placed within a middle ramp deposits indicative of decreasing accommodation concomitant with sea-level fall.

In southwestern Montana within the section at Baldy Mountain, the HST can be identified. At Baldy Mountain, however, the highstand deposits are largely covered and interpreted as argillaceous and the sequence boundary is placed just above a single lenticular crinoidal grainstone bed. Limited exposures further downdip lead to the inference that deposits at these locations are carbonate poor and likely highly argillaceous. The sequence boundary is placed within an extensive covered interval withshaly float at location Ashbough Canyon. At the Bell-McKenzie Canyon section location, the sequence boundary location is chosen within poorly exposed calcisilt limestones in an overall argillaceous succession.

3.3.1.2 *Lodgepole Sequence 2*

Lodgepole sequence 2 (LP2) correlates with the lower half of the Woodhurst Member of the Lodgepole Formation across the study area. This sequence was previously documented by Elrick (depositional sequence 2, 1991) and corresponds to the lower portion of Sonnenfeld's (1996a, 1996b) sequence II. LP2 has an age of lowermost Osagean and occurs within Mamet foraminifer biozone 7 with the LP1-LP2 sequence boundary approximately coinciding with the Kinderhookian-Osagean boundary (Sando, 1984). This sequence is 0-115 m in thickness, thinning downdip into Idaho where Osagean strata have yet to be biostratigraphically resolved in many locations (Huh, 1967). LP2 is composed of approximately five 4th-order cycles which are observed to display overall retrogradational followed by progradational stacking in the most proximal parts of the study area (Figure 3.17; Figure 3.19). Distally, however, in the southwestern part of the study area, this pattern becomes less apparent.

3.3.1.2.1 *Lowstand Systems Tract*

Directly overlying the LP1-LP2 sequence boundary at section location Livingston (Figure 3.19), in the most proximal position of the study area, are trough cross-bedded crinoidal grainstones. The cross-bedded crinoidal package overlies partly amalgamated, lenticularly bedded skeletal and crinoidal packstones, which capped a cycle with a base of partly argillaceous, fine bioturbated skeletal and peloidal wackestone and packstone. This crinoidal package has previously been interpreted as a ramp margin wedge by Elrick (1990). The single intermediate-scale cycle is dominated by crinoid bank deposits, which developed during the relative sea-level lowstand coeval with the exposure of much of the ramp updip to the south in Wyoming (Sonnenfeld, 1996a). This crinoid bank was of limited spatial extent, however, as it is not observed at any other location within the study area.

3.3.1.2.2 *Transgressive Systems Tract*

Deposition directly above the LP1-LP2 sequence boundary elsewhere within the study area is markedly more argillaceous and carbonates are dominantly calcisilts consistent with outer ramp to basinal deposition. In the central Montana trough, deposition is dominated by vaguely cyclical stacks of limestone/argillite couplets. In southwestern Montana, the sediments become increasingly argillaceous and outcrop

poorly in many locations (Figure 3.20). The increasing argillaceous content upsection is consistent with the interpretation that little carbonate was produced *in situ* at this locality at this time and very little carbonate could be delivered from the carbonate sediment production locations updip.

The maximum flooding surface for LP2 is difficult to pinpoint across the study area. It is chosen at section Livingston within a series of thickening-upward cycles of limestone/argillite couplets at the top of a covered interval, which poorly outcrops likely due to its high argillaceous content (Figure 3.19). The same criteria were used to place the maximum flooding surface within outer ramp deposits in the central Montana trough and at section Baldy Mountain along the southwest transect. Further downdip in southwestern Montana, the TST of LP2 poorly outcrops and was placed within an extensive covered interval with shaly float at location Ashbough Canyon.

3.3.1.2.3 Highstand Systems Tract

Intermediate-scale cycles at proximal locations are observed within the highstand systems tract of LP2 are observed to be decreasingly argillaceous and display cross-bedding indicative of deposition under traction. At Livingston, the overall amount of argillaceous material decreases upward, while the carbonate beds which are composed of both peloidal and skeletal packstones and grainstones increase in thickness (Figure 3.19) and amalgamate upwards. Additionally beds at the top of the sequence are waved rippled and have flaser bedding indicative of deposition under tidal influence. The sequence is capped by a structureless crinoidal grainstone. Downdip at section Sacagawea Peak, the HST displays decreasing amounts of argillaceous and increasing amounts of oolitic and skeletal beds with swaly cross-bedding.

The observed patterns are indicative of overall shallowing and increased influence of first from storm energy impinging on the sea floor, as evidenced by increased traction features. At the top of the sequence at Livingston, tidal currents become the dominant process as evidenced by well-developed flaser bedding. A similar pattern is observed throughout the central Montana area, where this sequence is capped by regionally extensive decreasingly argillaceous middle ramp deposits made up of oolitic and skeletal packstones and grainstones. In southwestern Montana, overall shallowing is observed however little to no evidence of storm influence can be documented. Rather in these

localities, shallowing is interpreted from overall decreased argillaceous content and increased carbonate deposition. Additionally, increased macrofaunal content suggests that these waters may have been increasingly better ventilated during this time.

Like LP1, the position of the top sequence boundary is equivocal, as no exposure is observed on the tops of any cycles within the study area. The upper sequence boundary of LP2 is chosen across the study area based on the shallowest observed facies deposited before abrupt deepening is observed in association with sea-level rise at the initiation of sequence LP3. In the central Montana trough, the sequence boundary is chosen atop the oolitic and crinoidal grainstone-capped mid-ramp cycle, which is overlain by cross-bedded ooid grainstone shoals. This criterion was previously employed to discriminate the top of depositional sequence 2 by Elrick (1990) in central Montana. In southwestern Montana, the sequence boundary is placed atop the least argillaceous, thickest outer ramp and basinal deposits observed.

3.3.1.3 Lodgepole Sequence 3

Lodgepole Sequence 3 correlates with approximately the upper half of the Woodhurst Member of the Lodgepole Formation and the lowermost part of the Mission Canyon Formation across the study area in Montana. LP3 ranges from 130 m thick in southwestern Montana and thins to zero basinward in east-central Idaho (Huh, 1967). This sequence corresponds to much of Mamet foraminifer zone 7 and is of Osagean age (Sando, 1984). This sequence was previously documented in southern and central Montana by Elrick (depositional sequence 3, 1990) and correlates to the upper portion of Sonnenfeld's sequence II in Wyoming (Sonnenfeld, 1996a, 1996b). Approximately five intermediate-scale cycles make up LP3, which are organized into overall retrogradationally and progradationally stacking patterns (Figures 3.21-25). These patterns can be best observed at location Sacagawea Peak within the central Montana trough.

3.3.1.3.1 Lowstand Systems Tract

In the most updip location within the study area at location Livingston, the lowstand systems tract is composed of one 4th-order cycle of peritidal and intertidal deposits, including pisolitic grainstones and oolitic grainstone shoals. This systems tract, however, is expressed variably across the region. In southwestern Montana at section

Bell-McKenzie Canyon, a 53 m thick polymict conglomerate is observed (Figure 3.26). This package is interpreted as a debris flow which resulted from slope failure, which may have occurred during the maximum sea-level drop which occurred at the LP2-LP3 sequence boundary.

Within the central Montana trough, however, a significantly different pattern of organization is observed near the axis of the trough at location 16 Mile Creek within this systems tract. A ramp margin wedge is observed at this location, which is made up stacked cross-stratified and wave rippled ooid grainstones and is approximate 10 m thick (Figure 3.27). Like the crinoid bank deposited in LP2, these ooid shoals are interpreted to be deposited during the maximum sea-level fall associated with the sequence boundary, in this case the LP2-LP3 boundary. These oolitic shoal deposits are observed to vertically aggrade and make up a significant portion of the lower part of the systems tract here. Directly above these shoal deposits, a tabulate coral-microbial boundstone bioherm is observed at section 16 Mile Creek. This bioherm is interpreted to have formed during rapid sea-level rise and accommodation development during the transgressive systems tract. A similar mound has been documented at location Sacagawea Peak by Elrick (1990).

3.3.1.3.2 Transgressive Systems Tract

In the most updip location within the study area at Livingston, the transgressive systems tract is composed of one and a half 4th-order cycles of bioturbated skeletal and peloidal wackestones-grainstones with minor oolitic packstones-grainstones. Progressively through this systems tract, the bioturbated skeletal and peloidal wackestones-grainstones show decreasing bed thickness and increasing amounts of argillaceous material being incorporated. This pattern is amplified downdip in southwestern Montana. At location Baldy Mountain, outer ramp cycles show decreasing amounts of carbonate and increased amounts of argillaceous material. Within this systems tract, large intervals poorly outcrop which is indicative of basinal deposits stepping back onto the outer ramp along this transect.

The flanks of the central Montana trough show similar patterns to those observed in more proximal locations. Middle ramp deposits show decreasing storm influence, such as decreased abundance of combined oscillatory and traction structures, and backstep

beyond the limits of the study area at locations Sacagawea Peak and Monarch. Outer ramp depositional environments are observed across most of the trough during this interval.

The maximum flooding surface of LP3 is chosen across the study area at the occurrence of the maximum landward position of the deepest water facies. In southwestern Montana, it is chosen atop significant covered intervals which are inferred to contain the most argillaceous material and hence the least carbonate and greatest distance from the carbonate source area updip. Updip at section Livingston, the MFS is chosen atop a middle ramp cycle which shows the most argillaceous material, least amalgamation, and least evidence of storm influence. Further downdip in the central Montana trough, the MFS is chosen among the thinnest bedded carbonates within outer ramp cycle which contain the greatest amount of argillaceous material at locations Sacagawea Peak and Monarch. Near the axis of the trough at location 16 Mile Creek, the MFS is placed near the top of the coral-microbial bioherm which vertically aggraded into the space created during the flooding event and provides a reliable marker of accommodation creation (Figure 3.27).

3.3.1.3.3 Highstand Systems Tract

The highstand systems tract of LP3 is marked by the wide distribution of inner ramp facies belts both toward the Antler foreland basin along the southwestern transect and into the central Montana trough. One and a half intermediate-scale cycles compose this systems tract over the study area. In the most landward position of the study area at location Livingston, both cross-bedded skeletal and oolitic grainstones are observed to near the top of the sequence and overlie laminated and wave-rippled skeletal and peloidal packstones and grainstones (Figure 3.28).

The HST of LP3 in southwestern Montana is characterized by overall deeper water deposition than that observed in the central Montana trough. In this part of the study area, the HST is dominated by increasing storm influence. This observation is most apparent at location Baldy Mountain where outer ramp deposits at the base of the systems tract are overlain by middle ramp deposits with decreasing argillaceous material and increasing amalgamation and evidence of traction deposition. Further downdip, basinal argillaceous and chert-rich calcisiltites are overlain by increasingly carbonate-rich outer

ramp deposits at location Ashbough Canyon, while aggrading basinal deposits mark deposition within this systems tract at location Bell-McKenzie Canyon.

In the central Montana trough and updip at section Livingston, the sequence boundary is placed atop the thinnest bedded amalgamated grainstone shoals within a stack of grainstone shoal cycles. The thinnest bed is interpreted to represent deposition under extremely limited accommodation conditions. In southwestern Montana because a lack of evidence of exposure, similar difficulty in selecting a sequence boundary like that of sequences LP1 and LP2 persist over much of the area. At locations Ashbough Canyon and Baldy Mountain, the sequence boundary is placed at the sharp, erosional contact between outer ramp deposits just below graded, redeposited oolitic and crinoidal grainstones. These beds are interpreted as turbidites which were deposited with the lowstand of the overlying sequence.

3.3.1.4 Mission Canyon Sequence 1

Mission Canyon sequence 1 (MC1) is equivalent to Sonnenfeld's sequence III (Sonnenfeld, 1996a, 1996b) in Wyoming and southern Montana. The base of this sequence lies within approximately 10 m of the lithostratigraphic boundary between the Mission Canyon and Lodgepole Limestones in most localities in Montana with the exception of Bell-McKenzie Canyon. This boundary is within Mamet foraminifer zone 8 (Sando, 1984). The sequence varies in thickness from 202 m in the proximal Antler foreland basin at Bell-McKenzie Canyon to 54 m landward in southwestern Montana at Livingston. The sequence also thins basinward in east-central Idaho and reaches an indeterminate thickness within the axis of the foreland basin.

Unlike the Lodgepole Limestone Sequences, this sequence marks a significant shift in facies types and arrangement of facies belts and has been suggested to represent a change in depositional morphology from a ramp to a shelf system (Sonnenfeld, 1996a, 1996b). Within this sequence a shift occurs from a dominantly storm-graded profile to one dominated by shallow water, often restricted deposition (Sonnenfeld, 1996a, 1996b).

Approximately five 4th-order cycles make up this sequence. Unlike the earlier Lodgepole sequences, where shallowing-upward cycles dominated the depositional cycle, within this sequence fining- and muddying-upward cycles are common. These cycles are typical of restricted lagoonal-type settings where as accommodation over the system

decreases, energy cannot be effectively propagated over the system. As a result, carbonate mud increasingly is deposited within the system (Figure 3.29).

3.3.1.4.1 Lowstand Systems Tract

The LP3-MC1 sequence boundary marks a dramatic seaward shift in facies belts due to relative sea-level fall. The sharp erosive contact which marks this boundary at sections as far seaward as Ashbough Canyon in southwestern Montana and into the axis of the central Montana trough delineates this major fall in accommodation. Atop the boundary, oolitic and crinoidal grainstones were deposited (Figure 3.30). These grainstones overlie dominantly bioturbated, argillaceous skeletal and peloidal packstones of sequence LP3.

As sea level progressively dropped, the carbonate factory stepped out into the previously distal localities and established shallow water sediment factories in these areas as sea level initially rose within the MC1 sequence. At this time broad tracts of the middle and outer ramp became centers of primarily oolitic sand generation. During the initial rise, ooid shoals developed as far seaward as section Baldy Mountain and rapidly backstepped to section Livingston within a single intermediate-scale cycle, approximately 110 km, onlapping the LP3-MC1 sequence boundary (Figure 3.31, 3.32).

In the central Montana trough, the LST follows a generally similar evolution to that of the southwestern margin. Dominantly oolitic sands were redeposited within the trough and focused particularly at the axis of the trough at section 16 Mile Creek. Similarly to southwestern Montana, the shallow water carbonate sand factories downshifted, in this case into the trough itself, where they were established themselves for much of the sequence.

3.3.1.4.2 Transgressive Systems Tract

During the transgressive system tract of sequence MC1, the grainstone belts continued to shift landward. This is marked by the landward shift of crinoidal banks in southwestern Montana to a position lying somewhere between sections Baldy Mountain and Livingston. Further basinward, at section Bell-McKenzie Canyon outer ramp and basinal facies interfingers as the outer ramp deposits backstep and are overlain by cherty basinal facies.

In central Montana the TST of MC1 is similarly marked to that in southwestern Montana. On the margins of the trough, deposition of more restricted facies occurred at this time. In these locations deposition was dominated by peloidal packstones and grainstones locally produced in a distal lagoonal setting as well as bioturbated skeletal packstones. As the central Montana trough continued to flood and fill, circulation attenuated across the area. A regional subaqueous evaporite was deposited during this time as exchange between open marine waters further to the west and waters within the trough became limited (Sonnenfeld, 1996a, 1996b). This event is preserved by an evaporite dissolution collapse breccia which can be traced at sections within the trough and as far away as Wyoming (Figure 3.33; Roberts, 1967; Sonnenfeld, 1996a, 1996b).

The maximum flooding surface within this sequence is highly variable in character. At the most basinward locality in southwestern Montana, the MFS is placed within a poorly exposed interval dominated by bedded chert and argillaceous material. This interval is vaguely cyclical and the MFS is chosen atop the thickest covered interval within the bedded chert cycles. Further updip in southwestern Montana, the MFS is chosen atop a cycle dominated by crinoidal grainstone deposition. This horizon marks the maximum landward extent of the shoalwater barrier complex within this sequence. In the central Montana trough, the MFS is chosen atop the evaporite solution collapse breccia. This horizon is chosen for two reasons. First, the evaporites which originally accumulated have been interpreted to have been deposited during sea level rise because rising sea level provides the water volume necessary to accumulate thick, laterally extensive deposits of evaporites (Sonnenfeld, 1996a, 1996b). Secondly, because the facies incorporated within this breccia are of normal marine affinity and it is reasonable to assume that normal marine conditions resumed after deposition of the breccia as relative sea-level continued to rise.

3.3.1.4.3 Highstand Systems Tract

The highstand systems tract of Mission Canyon sequence 1 is composed of cross-bedded peloidal packstones and grainstones with minor fine skeletal debris admixed over most of the study area (Figure 3.32). The exception to this is in southwesternmost Montana at location Bell-McKenzie Canyon where deposition of crinoidal grainstone shoals are inferred to have dominated deposition and in the axis of the central Montana

trough at location 16 Mile Creek where oolitic grainstones make up much of early highstand deposition. In southwestern Montana, the distribution of skeletal and oolitic grainstone shoals extended from landward locations in the early HST to positions along the margin of the Antler foreland basin near the top of the sequence.

The sequence boundary is chosen in the lagoonal portion of the system at the thinnest occurrence of the peloidal wackestones and packstones within a series of stacked aggrading peloidal wackestone-packstone cycles. In southwesternmost Montana, the sequence boundary is chosen atop a series of cycles of calcisiltite and redeposited skeletal and peloidal packstones-grainstones before an abrupt deepening recognized by renewed deposition of bedded chert.

3.3.1.5 Mission Canyon Sequence 2

Mission Canyon sequence 2 is correlative with the lower middle portion of the Mission Canyon Limestone across the study area. This sequence was previously documented by Sonnenfeld (sequence IV; 1996a, 1996b) in southernmost Montana and this sequence correlates with the Little Tongue Member of the Madison Limestone in Wyoming. The Little Tongue Member has an Osagean age and makes up the lower part of Mamet foraminifer zone 9 (Sando, 1984). MC2 is composed of five intermediate-scale, 4th-order cycles (Figure 3.34-3.36). As previously noted Mission Canyon sequence 2 is marked by an abrupt deepening just above the MC1-MC2 sequence boundary. This is most clearly observed along in the proximal Antler foreland basin in southernmost Montana. Here outer ramp deposits are overlain by basinal facies characterized by bedded chert. Over much of the rest of the study area updip of this locality, significant backstepping of facies belts is observed. Extensive progradation marks much of the upper portion of the sequence especially in downdip localities.

3.3.1.5.1 Transgressive Systems Tract

The transgressive systems tract of Mission Canyon sequence 2 is marked by significant backstepping of facies belts. This is especially noticeable within skeletal grainstone shoals deposited along the margin of the Antler foreland basin in southwestern Montana at location Bell-McKenzie Canyon. Within much of the rest of the study area, much of the detailed stratigraphy of this systems tract is obscured by evaporite solution collapse brecciation (Figure 3.34). This major brecciation interval is regionally

correlative and extends as far as the updip limit of the Madison Limestone in Wyoming (Roberts, 1966; lower solution zone of Sando, 1974; Sonnenfeld, 1996a, 1996b; Smith et al., 2004). This regionally extensive breccia has been previously interpreted as brecciation of overlying strata due dissolution of thick evaporite deposits which accumulated during the relative sea-level rise and the initial flood of the platform during this sequence (Sonnenfeld, 1996a, 1996b; Smith et al., 2004).

In southwestern Montana the TST is characterized by stacked crinoidal grainstone shoals, which aggrade at Ashbough Canyon; however, just updip at section Baldy Mountain, these grainstones overlie a basal cycle of lagoonal peloidal packstones. Further downdip in southwesternmost Montana at section Bell-McKenzie Canyon, outer ramp cycles thin vertically and are progressively interbedded with cherty and argillaceous calcisiltites. The deposition of lower energy facies which accumulated in deeper water depths than the subjacent strata of the HST of sequence MC1 indicates overall backstepping of the carbonate sediment production areas at this time.

Over much of Montana, the transgressive systems tract is almost solely composed of evaporite solution collapse breccia (Figure 3.33). These deposits are laterally continuous over hundreds of kilometers. The crinoidal grainstone shoals observed at Bell-McKenzie and Ashbough Canyons aggraded along the margin of the Antler foreland basin (Figure 3.36). I speculate the shoals acted as an effective barrier to circulation and exchange of waters between the open marine Antler foredeep and the restricted shelf back behind this barrier complex. This aggrading barrier system allowed for accumulation of thick evaporites over a massive area as the shelf system was inundated during relative sea level rise.

Although much of the central Montana trough underwent deposition of extensive evaporites during the deposition of the TST of MC2 as inferred from the widespread dissolution collapse breccia zone, the initial transgression within the axis of the central Montana trough and the northern margin of this feature was recorded by the deposition of thinly bedded lagoonal deposits. In particular cycles with peloidal-micropeloidal bases and tidal flat caps are common in the early TST at locations 16 Mile Creek and Monarch (Figure 3.35). Additionally, localized oolitic grainstone shoals also formed intermittently

in these localities during the early TST. This is then overlain by the regionally extensive solution collapse breccia zone.

Like sequence MC1, the MFS is chosen atop the evaporite solution collapse breccia, these evaporites are again interpreted to be deposited in a subaqueous setting during overall sea-level rise. The MFS is chosen atop the least amalgamated crinoidal grainstone beds within a series of crinoid grainstone cycles along the margin of the Antler foreland basin at locality Ashbough Canyon. Further updip at location Baldy Mountain, the MFS is picked at the last occurrence of the crinoidal grainstone, as it is overlain by peloidal packstones of lagoonal affinity, indicating a position behind the crinoidal barrier system to the southwest.

3.3.1.5.2 Highstand Systems Tract

The highstand systems tract of Mission Canyon Sequence 2 marks the first extensive progradation of the carbonate sediment factory into the Antler foreland basin. In contrast deposition over much of the rest of the Montana study area is marked by deposition of aggradationally stacked lagoonal deposits and thin, laterally discontinuous local shoals. The major exception to this is at the axis of the central Montana trough, where less restricted and more energetic hydrodynamic conditions persisted.

Deposition in southwesternmost Montana was marked by deposition of three and a half intermediate cycles. These cycles represent approximately 150 m of crinoidal grainstone deposition with minor intervening cherty, fine skeletal middle ramp deposits (Figure 3.37). More proximally at Ashbough Canyon, thinner crinoidal grainstone cycles make up the the HST with minor accumulation of oolitic grainstones in the late highstand. Skeletal, oolitic, and peloidal grainstone deposition marks the HST at Baldy Mountain and Livingston. The deposits are observed to increasingly amalgamate near the top of the sequence, and the sequence boundary is placed top of the most amalgamated grainstone packages.

In central Montana, the HST is composed of a highly variable assemblage of facies (Figure 3.35). Cycles at Sacagawea Peak variably include oolitic and peloidal grainstones with some skeletal debris and algal laminites of tidal flat affinity. Further downdip at 16 Mile Creek, the early highstand is made up of oolitic grainstones with lesser amounts of peloidal grainstone and evaporite dissolution collapse breccia

intercalated. In the late highstand, ooids become scarce, while peloids become the dominant allochemical component of the stacked grainstones, which continue to be intercalated with thinning evaporite dissolution collapse breccias. The sequence boundary is placed atop amalgamated peloidal grainstones here.

Along the southwestern margin of the Antler foreland basin, deposition of crinoid grainstones filled much of the accommodation space originally produced during the downwarping of the study area by loading during the Antler orogeny. For the first time the carbonate production zone expanded into this province which to this point had solely been receiving redeposited materials from updip. Expansion of the carbonate factory into this province allowed for the expansion of the carbonate province and set the stage for later infill of the foreland basin by carbonates.

3.3.1.6 Mission Canyon Sequence 3

Mission Canyon Sequence 3 has been previously identified by Sonnenfeld (1996a, 1996b; sequence V) in southern Montana and Wyoming and correlates with the lower part of the Bull Ridge Member of the Mission Canyon Formation. Due to limited accommodation over most of the study area, evaporite solution collapse brecciation within the sequence and post-depositional karsting atop the Madison Group in Montana, this sequence is of limited thickness and of variable outcrop character over much of the study area. However, in southwesternmost Montana and in easternmost Idaho, relatively thick accumulations of crinoidal grainstone typify deposition during this sequence (Figure 3.38). Deposition within this sequence likely occurred within the latest Osagean to earliest Meramecian, probably within Mamet foraminifer zone 10 (Sonnenfeld, 1996a, 1996b). The sequence is composed of approximately three 4th-order cycles, and these cycles display overall aggradation within limited accommodation conditions over most of the study area (Figure 3.39), except in the southwestern part of the study area, where accommodation is virtually unlimited in the proximal Antler foreland basin (Figure 3.40).

3.3.1.6.1 Transgressive Systems Tract

The transgressive systems tract is composed of approximately the lower half of one intermediate-scale cycle. Over most of the study area in Montana, the TST poorly outcrops. Where outcrop is available, the base of the sequence is often made up of laterally discontinuous ooid grainstone shoals and aggrading lagoonal deposits. The TST

in Montana is, however, generally dominated by deposition of evaporite solution collapse breccias. This zone has been termed the “upper solution zone” by Sando (1976). Further downdip, this pattern changes and cycles of crinoidal grainstones and calcisiltites make up the TST.

In southwesternmost Montana at Ashbough Canyon, the early TST is characterized by poorly outcropping bioturbated peloidal and skeletal wackestones to grainstones (Figure 3.38). In the late transgression, the crinoidal grainstones overlie the peloidal and skeletal wackestones at Ashbough Canyon, and fine skeletal wackestones and packstones and calcisiltites make up much of the TST downdip at section location Bell-McKenzie Canyon. Further downdip at location Copper Mountain, middle ramp cycles of calcisiltite and skeletal packstones-grainstones which compose the early TST at this location are overlain by argillaceous calcisiltite outer ramp deposits of the middle transgression and a poorly outcropping interval with argillaceous float in the late transgression.

As in sequences MC1 and MC2, the maximum flooding surface is placed atop the solution collapse breccia interval, at most sections where this facies occurs in central Montana (Figure 3.41). This position is chosen because it likely represents the interval of maximum accommodation creation within the sequence at these localities. In southwestern Montana, the selection of the MFS is more precise. At section location Ashbough Canyon, the MFS chosen atop the thickest crinoidal grainstone shoals which overlie the basal transgressive lagoonal deposits. Here bed thickness is used as a proxy to indicate maximum accommodation space development. Further downdip within the proximal Antler foreland basin at section Bell-McKenzie Canyon, the TST is chosen within the thickest cycle of middle ramp deposits, again employing thickness as a proxy for accommodation space.

3.3.1.6.2 Highstand Systems Tract

The highstand systems tract of MC3 is composed of the upper two and a half intermediate-scale cycles. Over much of Montana, the systems tract is composed of aggrading lagoonal and peritidal cycles with limited lateral correlation at the fifth-order scale (Figure 3.41). Within the axis of the central Montana trough at 16 Mile Creek, ooid grainstone shoals vertically stacked and aggraded at this time and directly overlie the

solution collapse breccias of the TST. At location Sacagawea Peak, peritidal cycles are typically microkarsted, especially in the late HST, indicative of exposure at the top of the cycles.

Stacked grainstone shoals in southwestern Montana make up more than 90% of the HST (~30 m) and exhibit increasing amalgamation throughout the highstand (Figure 3.38). The early and middle highstand at Bell-McKenzie Canyon is made up of stacked and partly amalgamated skeletal and crinoidal grainstones, while the late highstand is made up of bi-directionally cross stratified crinoidal grainstone shoals. Further downdip in east-central Idaho, bioturbated skeletal and peloidal wackestones-packstones make up the HST. These deposits become progressively more cherty and argillaceous in distal positions like East Canyon.

In central Montana, the highstand systems tract varies from nearly purely oolitic deposition at 16 Mile Creek to increasingly algal at Sacagawea Peak. At 16 Mile Creek, stacked ooid grainstone shoals are observed to decrease in thickness throughout the HST, with an increasingly peloidal content in the late highstand. In contrast, thin peloidal and oolitic packstones-grainstones become increasingly thin and compose decreasing amounts of up through the HST at Sacagawea Peak. The peloidal and oolitic facies are in turn replaced by increasing amounts of algal laminites.

In southwestern Montana, crinoidal grainstone shoals aggraded and weakly prograded during the HST of MC3 (Figure 3.38). Approximately one small-scale cycle of calcisiltite and peloidal-micropeloidal wackestone to packstone is observed within the early highstand at location Bell-McKenzie Canyon, indicating the rather narrow width of the grainstone belt during the initiation of the highstand. By the late highstand, the crinoidal grainstone shoal belt underwent some expansion, as recorded by deposition of a broad tract of associated storm-influenced middle ramp deposits, which extended as far downdip as location East Canyon in east-central Idaho.

The sequence boundary of MC3 is chosen across much of Montana atop the thinnest cycle of peritidal character (Figure 3.41). This surface typically has been microkarsted and may show some centimeters of relief along with brecciation. The brecciated surface may represent a regolith horizon where minor soil development occurred during exposure. Further downdip, evidence of subaerial exposure on the

crinoidal grainstone shoals is lacking. Instead the sequence boundary must be chosen based on observed accommodation minima patterns. At location Bell-McKenzie Canyon, the sequence boundary is placed atop the most highly amalgamated crinoidal grainstone unit within a set of upward thinning cycles and increasing tidal influence (Figure 3.38). This surface is interpreted as the minimum accommodation package within the sequence here.

3.3.1.7 Mission Canyon Sequence 4

Mission Canyon sequence 4 corresponds with sequence VI of Sonnenfeld (1996a, 1996b), which was initially described in southern Montana and Wyoming. This sequence is of early Meramecian age and the top of the sequence occurs near the top of Mamet foraminifer zone 11 (Sando, 1984) and correlates with the upper part of the Bull Ridge Member of the Mission Canyon Formation. Because of extremely limited accommodation conditions during the deposition of this sequence over much of Montana and post-depositional erosion across this area, this sequence is significantly thinner than almost all the other sequences so far described. However, on the periphery of the Antler foreland basin, this sequence undergoes an expansion in thickness (Figure 3.42). The sequence doubles in thickness over 32 km due to dramatically increased accommodation space created within the foredeep.

3.3.1.7.1 Transgressive Systems Tract

The transgressive systems tract of Mission Canyon sequence 4 is thin, vertically aggrading lagoonal and peritidal cycles with occasional local development of oolitic grainstone shoals across most of Montana. Local development of evaporite solution collapse breccias is also evident at a few locations such as Ashbough Canyon; however, unlike earlier intervals, these breccias tend to be spatially restricted and are more likely related to local evaporite deposition within a sabkha setting (Sonnenfeld, 1996a, 1996b). Additional brecciation is observed at location Baldy Mountain, however, this is interpreted to be of a karst nature marking the top of Madison deposition and regional karsting.

The transgressive system tract is marked by the deposition of stacked crinoidal, skeletal and peloidal grainstones in southwestern Montana. At location Bell-McKenzie Canyon, the grainstones are trough cross-stratified with minor wave rippling and planar

stratification. Further downdip in Idaho, much of the TST is poorly exposed with minor outcroppings of variably argillaceous skeletal and peloidal packstones and grainstones. In up-dip localities like Baldy Mountain, strata are decreasingly skeletal in nature and have increasingly muddy textures. Here, peloidal wackestones-grainstones with minor skeletal and oolitic packstones-grainstones make up the cycles of the TST.

The TST of central Montana is composed of peloidal wackestones-grainstones with minor oolitic beds especially at Monarch. Deposition is attenuated in the southern part of this transect, while section expansion is observed at Monarch and 16 Mile Creek. Additionally, extensive covered intervals obscure the TST especially at Monarch and notably at 16 Mile Creek as well.

In southwestern Montana the TST of MC4 is characterized by deposition of stacked crinoidal grainstone shoals which aggrade and subtly retrograde during this period (Figure 3.43). The late transgression at location Bell-McKenzie Canyon illustrates this retrogradation as thin cycles of mixed skeletal and peloidal packstone-grainstone deposits interfinger with the crinoidal grainstone shoals in the upper two intermediate scale cycles at this location. Further downdip in east-central Idaho, the TST is poorly exposed and it is inferred that this is due to deposition of highly argillaceous outer ramp to basinal facies at these location during this interval.

The maximum flooding surface of this sequence is poorly characterized across much of Montana. The MFS is chosen based on stacking pattern analysis within the thickest small-scale lagoonal or shoal cycle in these updip localities (Figure 3.43, 3.44). Further downdip in locations where accommodation space is not as limited, the MFS is chosen on marked facies transitions. At location Ashbough Canyon, the MFS is placed atop the last crinoidal grainstone shoal cycle, which is then overlain by restricted lagoonal deposits, indicating a seaward shift of these facies belts above the deepening atop the shoals. Further downdip at location Bell-McKenzie Canyon, the MFS is chosen atop the thickest middle ramp cycle, indicative of the maximum landward extent of this facies belt (Figure 3.43). Within the Antler foreland basin in east-central Idaho, the MFS is picked arbitrarily within or atop a significant covered interval at locations Copper Mountain and East Canyon, which is interpreted to be a highly argillaceous interval likely of basinal affinity.

3.3.1.7.2 Highstand Systems Tract

The highstand systems tract of MC4 is poorly developed and/or preserved over much of the study area in Montana. This is due to both lack of deposition due to increasingly limited accommodation space over this area, but it is also in direct response to the extended erosion during protracted exposure which occurred atop this sequence, the master sequence boundary of the Madison supersequence (Sonnenfeld, 1996a, 1996b).

Deposition of the highstand of sequence MC4 is composed of thin cycles of increasingly algally-laminated strata in central Montana. In localities like Sacagawea Peak, peloidal wackestones-grainstones typify the early HST, but algal laminites of tidal flat affinity dominate the late highstand. The exception to this pattern of increasing algal laminite composition with is time in the HST is at 16 Mile Creek where peloidal and oolitic grainstones predominate.

The HST across much of Montana is composed of very thinly bedded peritidal and lagoonal cycles, which make up approximately one and a half 4th-order cycles (Figure 3.42). These cycles are almost always capped by microkarst horizons, are often red stained, and also typically have some siliciclastic silt associated with them. Within the central Montana trough at section 16 Mile Creek, the HST is capped by relatively thick, laterally discontinuous ooid grainstone shoals which make up several of the high-frequency cycles near the very top of the sequence.

The HST in southwestern Montana is composed of amalgamated, trough cross-bedded skeletal, crinoidal, and peloidal grainstones. This pattern is best expressed at Bell-McKenzie Canyon. Bioturbated peloidal and skeletal wackestones-grainstones are observed in downdip localities like Copper Mountain in east-central Idaho. Updip, peloidal wackestones-grainstones with bioturbation and rare planar laminations are observed especially at location Ashbough Canyon.

In southwestern Montana, the HST of MC4 is composed of one and a half intermediate-scale cycles that stack in a prograding fashion and show increasing tidal influence progressing up through the sequence. Further downdip in east-central Idaho at locations East Canyon and Copper Mountain, the HST is dominated by vertically aggrading mid-ramp cycles with strong evidence of storm influence.

The sequence boundary of MC4 marks the top of Madison Group in Montana and indicates cessation of deposition of carbonates and protracted exposure over much of the study area and as far updip as the Transcontinental arch in southeastern Wyoming. The upper karst surface which marks the unconformity is typically infilled with red sandstones and shales of the Late Mississippian Amsden Formation. Further downdip in southwesternmost Montana and into the Antler foreland basin of Idaho, deposition continued while karsting progressed updip. Here, at location Bell-McKenzie Canyon, the sequence boundary is chosen atop the most amalgamated skeletal grainstone shoal with the most pronounced tidal influence, indicating an accommodation minimum within these aggrading to prograding deposits. At section East Canyon in east-central Idaho, the sequence boundary is placed at the base of a crinoidal bank unit which is interpreted to have developed in a downdip position in response to the dramatic sea-level drop which marked the demise of Madison deposition in most of Montana and Wyoming.

3.3.1.8 Scott Peak Sequence 1

The base of Scott Peak sequence 1 (SP1) occurs near the base of the Scott Peak Formation within the Lower Cyclic Member in east-central Idaho at location Copper Mountain (Huh, 1967) and corresponds to the lower portion of the McKenzie Canyon Formation at location Bell-McKenzie Canyon (Sando et al., 1985) in southwesternmost Montana. This sequence is of Meramecian age in Idaho although detailed biostratigraphic dating to Mamet foraminifer zone level of the measured sections used here has not been completed. In Montana, the strata within this sequence have a middle Meramecian age within Mamet foraminifer zone 12 (Sando et al., 1985). This sequence is composed of approximately four 4th-order intermediate scale cycles which demonstrate overall retrogradational followed by progradational stacking geometries and pinch landward of section location Bell-McKenzie Canyon (Figure 3.46).

3.3.1.8.1 Transgressive Systems Tract

The transgressive systems tract of SP1 has a highly variable character across east-central Idaho and into southwestern Montana. This systems tract is composed of one and a half intermediate scale cycles. At a landward position at section Bell-McKenzie Canyon, the intermediate-scale cycles of transgressive systems tract have no lateral updip equivalent and are interpreted to onlap the top-Madison MC4-SP1 sequence boundary in

an updip direction. Here cycles are initially composed of backstepping crinoidal grainstone shoals at the base, which are overlain by highly aggradational near-shoal, skeletal-peloidal packstones-grainstones during the middle TST (Figure 3.47). Near the top of the TST, the crinoidal shoals are observed at the landward limit of deposition at this time at location Bell-McKenzie Canyon.

Further basinward in the proximal Antler foredeep at section Copper Mountain (Figure 3.48), the character of the systems tract changes from a predominance of crinoidal grainstones to bioturbated, argillaceous skeletal strata. Here stacked crinoidal grainstone shoal cycles are overlain by middle-ramp cycles dominated by bioturbated wackestones and packstones. Further downdip at section East Canyon poorly exposed, partly argillaceous calcisiltite beds with lenticular bedding are overlain by highly argillaceous, aggradational calcisiltites with limited bioturbation and extensive covered intervals. This facies succession is interpreted as the progressive deepening of the facies belts and overall increased accommodation space within the Antler foreland basin during relative sea-level rise.

The maximum flooding surface marking the top of the transgressive systems tract of SP1 shows variable character. In the most landward position at section Bell-McKenzie Canyon, the MFS is chosen atop the last crinoidal grainstone shoals within the sequence. At this time, open marine facies and fauna were broadly distributed across the Antler foreland basin, more so than any other time during the development of the sequence, hence marking the maximum deepening during this stratal interval. Further downdip at location Copper Mountain, the MFS is picked atop a covered interval, which is interpreted to represent the only occurrence of argillaceous, outer ramp facies within sequence SP1 there. These beds lie atop aggradationally stacked cycles of mid-ramp deposits, once again indicating the maximum deepening within the sequence. In the most distal location at section East Canyon, the MFS is chosen above an extended covered interval which contained highly argillaceous material in float. The MFS is placed at the top of this interval which was likely made up of argillaceous outer ramp and perhaps basinal facies which accumulated during the maximum time of accommodation development within the sequence.

3.3.1.8.2 Highstand Systems Tract

The upper approximately two and a half 4th-order intermediate scale cycles make up the highstand systems tract of sequence SP1. Deposition during this interval is marked by spatially-expansive skeletal grainstone deposition from a landward position at location Bell-McKenzie Canyon to as far basinward as location East Canyon, which marks the furthest basinward observation of this sequence in the study. Crinoidal grainstone shoal facies downlap onto the MFS of sequence SP1 in proximal positions and onlap middle ramp deposits of the early highstand in more basinward positions.

The HST in the proximal setting at location Bell-McKenzie Canyon is composed of thin bedded deposits dominated by distal lagoonal peloidal packstones and grainstones and near-shoal deposits with admixed normal marine fauna and peloidal material, which appear to track the progradation of the grainstone shoals basinward (Figure 3.47). Further downdip at locality Copper Mountain, crinoidal grainstone shoals overlie a series of early HST bioturbated peloidal, peloidal/skeletal and skeletal wackestones-packstones (Figure 3.48). These middle ramp cycles in turn overlie a thin covered interval with dominantly argillaceous material in float that was interpreted as a small-scale cycle of outer ramp deposits marking the MFS of SP1. The late highstand at section Copper Mountain is composed of one cycle of near-shoal bioturbated skeletal packstones to grainstone which is capped by a very thin packstone before being overlain by crinoidal grainstones of sequence SP2. These deposits indicate the grainstone belt prograded basinward within the sequence beyond location Copper Mountain. At section, East Canyon this observation is confirmed with the observation of a single crinoidal grainstone shoal cycle marking the late highstand here. At section East Canyon, the HST is poorly exposed; however, where it did outcrop strata were dominated by highly bioturbated middle ramp cycles which overlie the covered interval of the top of the TST in this locality.

The top of sequence SP1 is marked in the most proximal location at section Bell-McKenzie Canyon by very thinly bedded peloidal packstones and grainstones. The sequence boundary is chosen atop the most thinly bedded cycle within a succession of progressively thinning lagoonal cycles at this locality. As mentioned above, the top of the HST, and hence the sequence boundary, within the proximal Antler foredeep at section Copper Mountain is marked by a very thinly bedded near-shoal packstone which is

overlain by crinoidal grainstone cycles which begin to increase in thickness and decrease in amalgamation above the top of the sequence here. Most basinward at section East Canyon, the sequence boundary is placed atop the singular amalgamated crinoid grainstone shoal cycle here, indicating minimum accommodation development at this location within sequence SP1.

3.3.1.9 Scott Peak Sequence 2

Scott Peak sequence 2 is characterized by thinning onto the landward periphery of the Antler foreland basin and expansion basinward. Within this the outer ramp depositional facies belt expands basinward as far as location Upper Pahsimeroi, the first biostratigraphically documented middle Mississippian deposition at this locality (Skipp et al, 1971). The sequence is of Meramecian age within the Lower Cyclic Member of the Scott Peak Formation (Huh, 1967) and deposition within the sequence likely occurred within Mamet foraminifer zone 12 based on correlation of biostratigraphic information from location Bell-McKenzie Canyon. At Bell-McKenzie Canyon, this sequence makes up a part of the McKenzie Canyon Formation. Sequence SP2 is composed of four intermediate-scale cycles (Figure 3.49).

3.3.1.9.1 Transgressive Systems Tract

The transgressive systems tract of sequence SP2 is composed of approximately one and a half 4th-order cycles. The early transgressive systems tract of SP2 is characterized by retrogradation of facies belts. During this interval the crinoidal grainstone belt is observed from a medial position within the Antler foreland basin at location East Canyon to a proximal position where this facies makes up the basal unit at location Bell-McKenzie Canyon. During the middle to late transgression, aggradation of muddier, lower-energy facies is observed in proximal positions while retrogradational stacking patterns are more commonly observed further out within the foredeep (Figure 3.50).

At the landward limit of deposition of sequence SP2 at location Bell-McKenzie Canyon, the initial transgression within the systems tract is composed of a thin stack of crinoidal grainstone shoal cycles (Figure 3.49). These cycles are observed to thicken upward and are interpreted to represent the transgressive portion of the lowermost

intermediate-scale cycle of the sequence. These shoal deposits likely overlapped the SP1-SP2 sequence boundary in a landward direction during the initial flood of SP2.

At section location Copper Mountain, the early transgression is marked by the deposition of crinoidal grainstone shoals which overlie the underlying near-shoal bioturbated skeletal and peloidal deposits which marked the top of sequence SP1 (Figure 3.51). Within the early transgression, the crinoidal grainstone shoal cycles are observed to thicken upward and become less amalgamated. Further basinward at section East Canyon, a similar pattern is observed, but the onset of middle ramp deposition occurs earlier within the TST than at the more proximal Copper Mountain section.

Aggrading to subtly retrograding stacked cycles of lagoonal and near-shoal facies are observed to thicken upward at Bell-McKenzie Canyon in response to overall increases in accommodation space during the sea-level rise of the late transgression. Overall deepening at Copper Mountain during this interval is interpreted by the decreased amalgamation of beds and increased bioturbation. The crinoidal grainstone shoals are observed to aggrade and retreat landward within the late TST and are overlain by middle ramp facies which are increasingly argillaceous, as represented by their decreasing outcrop quality.

The maximum flooding surface is chosen for sequence SP2 at the point of maximum accommodation development based on observable facies distributions. In the proximal locality at section Bell-McKenzie Canyon, the MFS is chosen atop a series of aggrading lagoonal cycles, which show subtle retrogradation. The MFS is picked atop a relatively thick bed of near-shoal facies which contains a relative abundance of normal marine fauna, indicative of well-oxygenated, normal salinity conditions. Further basinward, the MFS is chosen atop the thickest stack of middle ramp facies which are then overlain by crinoidal grainstone shoal facies, indicating maximum deepening at the MFS followed by abrupt shallowing above.

3.3.1.9.2 Highstand Systems Tract

The highstand systems tract is composed approximately of the upper two and a half intermediate-scale cycles. Grainstone belt cycles at the 4th- and 5th-order are observed to strongly shift seaward within this systems tract. Crinoidal and oolitic grainstone belts move seaward from an inferred area near the Montana-Idaho border west

out to and beyond location East Canyon. Additionally, outer ramp facies are observed for the first time within the HST of SP2 at location Upper Pahsimeroi.

At the proximal location of Bell-McKenzie Canyon, the highstand systems tract is composed almost completely of thinly bedded shallow-subtidal, muddy lagoonal beds with limited faunal content and peritidal algal laminite facies making up accommodation limited cycles (Figure 3.49). At location Copper Mountain, the highstand of sequence SP2 is dominated by the deposition of oolitic grainstone shoal cycles (Figure 3.45). This marks the first observed occurrence of oolitic deposition within the Idaho portion of the study area. The oolitic grainstone cycles overlie a few partly amalgamated crinoidal grainstone cycles which mark the early highstand here. The oolitic cycles are observed to thin upward and amalgamate within the highstand of the sequence, indicating decreasing accommodation conditions with time. Further basinward at location East Canyon, the HST is composed of thinning-upward crinoidal and skeletal grainstone shoal cycles which are observed to partly amalgamate near the top of the sequence. In the furthest downdip locality at section Upper Pahsimeroi, stacked argillaceous calcisiltite beds are observed and show decreasing incorporation of argillaceous material in the late highstand.

Cycles in the HST at Bell-McKenzie Canyon stack aggradationally and are observed to thin upward toward the sequence boundary. These shallow subtidal-peritidal cycles are inferred to be seaward stepping beyond the aggradation noted here, but the tidal flats are not observed as far as seaward as location Copper Mountain during this interval. Instead in the central part of the Antler foreland basin, oolitic grainstone shoals observed at Copper Mountain are interpreted to pass laterally downdip into skeletal and crinoidal grainstone shoals at East Canyon.

The sequence boundary is chosen based on observed accommodation minima. Within the shoalwater belt of deposition, the sequence boundary is placed atop the thinnest bedded shoal deposits, be they crinoidal or oolitic. Further basinward the sequence boundary is placed atop the most grain-rich, most poorly argillaceous bed which shows some evidence of traction and storm-influence. In the most landward locality at Bell-McKenzie Canyon, the sequence boundary is placed atop the thinnest

bedded peritidal cycle, here indicative of minimum accommodation on the tidal flat before the subsequent transgression.

3.3.1.10 Scott Peak Sequence 3

Scott Peak Sequence 3 is equivalent to the uppermost McKenzie Canyon Formation and likely the lower part of the Kibbey Sandstone in southwestern Montana. In Idaho, the sequence makes up part of the Middle Massive Member of the Scott Peak Formation at location East Canyon and part of the Lower Cyclic Member further basinward. The age of the sequence is Meramecian and falls within zone 13 of the Mamet foraminifer zone system (Mamet et al., 1971). This sequence is composed of as many as six 4th-order cycles which stack into an overall retrogradational pattern followed by moderate progradation (Figure 3.52). This differs strongly from the previous two sequences which showed much higher progradation/aggradation ratios than this sequence.

3.3.1.10.1 Transgressive Systems Tract

The TST of SP3 at Bell-McKenzie Canyon is composed of peloidal packstones-grainstones overlying a thin basal evaporite dissolution collapse breccia, which pass upward into increasingly skeletal and decreasingly peloidal packstones-grainstones. Downdip the basal TST is made up of aggradationally stacked massive and tabular cross-bedded oolitic grainstones at Copper Mountain. In the late transgression, ooid grainstones become increasingly bioturbated and are intercalated with peloidal wackestones-packstones. In turn, further downdip at East Canyon and Upper Pahsimeroi, skeletal allochems become the dominant component making up limestones here. Additionally, argillaceous material is observed to be incorporated within the TSTs of these sections. In the most distal section at Antelope Creek, the TST poorly outcrops but the available outcrops are typically argillaceous calcisiltite beds with chert.

The aggradational to subtly retrogradational character of the early TST is most clearly expressed in the proximal Antler foreland basin at localities Bell-McKenzie Canyon and East Canyon (Figure 3.52). At these localities, the lowermost intermediate-scale cycle is characterized in the case of Bell-McKenzie Canyon of restricted lagoonal and peritidal cycles which show an ability to keep up with accommodation development in the area (Figure 3.53). This is mirrored at locality Copper Mountain where

aggradationally stacked ooid grainstone shoals exhibit an ability to keep up with sea-level rise during the early transgression (Figure 3.54) Initial deposition of these cycles shows admixture of normal marine skeletal material not seen in the previous sequence and indicative of perhaps conditions better suited to this stenohaline fauna. Above the more skeletal rich cycles of the early TST are highly amalgamated tidally-dominated cycles composed of oolitic shoal deposits, which in turn are overlain by increasingly less amalgamated shoal beds, indicating overall deepening and an inability of the shoals to keep up with continuing sea-level rise.

Continued deepening is observed within a facies transition from oolitic shoals to bioturbated mid-ramp peloid wackestones and packstones at the Copper Mountain locality. Updip at Bell-McKenzie Canyon, this deepening is reflected in the deposition of bioturbated oolitic and skeletal packstones and grainstones, indicating increased transport of these materials into the lagoon, as the sand bar belt backstepped into the late transgression.

Further downdip at locations Upper Pahsimeroi and East Canyon, overall deepening during the transgressive systems tract is also represented by aggradation and subtle backstepping, although in a succession of overall deeper water facies. In these localities aggradation of middle ramp cycles are interrupted by an extended interval of covered section. This covered interval represents the backstepping of the middle ramp depozone to a position likely as far back as location East Canyon within this TST. At the study's most distal locality within the Antler foreland basin, at section Antelope Creek, deposition within the TST is marked by the aggradation of argillaceous carbonate cycles at the very base and is marked largely by an extensive covered interval probably corresponding to argillite or shale deposition.

The maximum flooding surface of SP3 is defined in the distal parts of the study area either at the top of a major covered section at sections East Canyon and Upper Pahsimeroi and within a similar covered interval at Antelope Creek. This interval likely corresponds with a period of deepening, minimization of carbonate production due to restriction of the carbonate production areas to a limited tract along the periphery of the Antler foreland basin and preferential accumulation of argillaceous material within the basin. The top of the argillaceous and peloidal cycles at Copper Mountain marks the MFS

at that locality. The MFS is picked at the top of the McKenzie Canyon Formation at locality Bell-McKenzie Canyon, where the least restricted, most open marine deposition of carbonates is observed.

3.3.1.10.2 Highstand Systems Tract

The highstand systems tract corresponds to the upper one and a half intermediate-scale cycles within the sequence. Seaward stepping of grainstone shoal belts is observed within the systems tract, but unlike other Scott Peak sequences, the amount of aggradation observed within the highstand is significantly greater during this sequence than the previous sequences.

In the proximal foreland, oolitic grainstone shoals mark the early highstand, stepping out in the area of Copper Mountain (Figure 3.54). The oolitic grainstones are observed in proximal localities; however, shoal facies are observed as crinoidal grainstone cycles downdip at locality East Canyon. Here the HST is characterized by intermediate-scale cycles with peloidal calcisilt wackestones-grainstones making up the bases, while the tops are composed of crinoidal grainstones. The intermediate-scale cycles stack with upward increasing crinoidal grainstone proportions indicating the seaward stepping of the crinoidal grainstone belt with decreasing accommodation during this systems tract. At locality Upper Pahsimeroi downdip of East Canyon, argillaceous outer ramp cycles of the early highstand give way to first middle ramp deposits and finally a capping crinoidal grainstone cycle. In the most distal locality at locality Antelope Creek, most of the HST is covered with the exception of the very top of the sequence which is composed of a single cycle of middle ramp bioturbated skeletal wackestones and packstones.

The sequence boundary is placed atop the thinnest cycle of crinoidal grainstone shoals at the overall accommodation minimum as defined by the intermediate-scale vertical accommodation trends at locality East Canyon. Downdip of this the sequence boundary is placed atop the crinoidal grainstone cycle capping the underlying middle ramp cycles and marking the maximum downdip extent of the crinoidal sand shoal belt in the sequence. In the updip position, the sequence boundary is placed within a series of ooid grainstone shoals, where the accommodation trends within the vertical stacking patterns at the 5th-order scale reveal a transition from decreasing to increasing

accommodation. Additionally, the facies proportions within those cycles changed from being dominated by the regressive hemicycle to dominated by facies of the transgressive hemicycle. This change adds further evidence allowing identification of that accommodation minimum marking the sequence boundary, within the stacked ooid packstones and grainstones.

3.3.1.11 Scott Peak Sequence 4

This sequence makes up the middle part of the Middle Massive Member of the Scott Peak Formation at localities Copper Mountain and East Canyon, and the upper part of the Lower Cyclic Member at section Upper Pahsimeroi (Huh, 1967). This sequence is within the upper part of Mamet foraminifer zone 13 and basal zone 14 based on biostratigraphic dating in the region of section Upper Pahsimeroi (Mamet et al., 1971). It also corresponds to some thickness of the Kibbey Sandstone updip in southwestern Montana, although this unit has only been poorly dated (Sando et al., 1985). Scott Peak sequence 4 is comprised of approximately four 4th-order intermediate scale cycles, stacked in an overall transgressive-regressive fashion similar to that observed within sequence SP3. Again within this sequence, extensive and nearly symmetrical backstepping and progradation of particularly the grainstone shoal facies belts is observed over the scale of the transgressive-regressive cycle that makes up sequence SP4 (Figure 3.55).

3.3.1.11.1 Transgressive Systems Tract

The transgressive systems tract is made up of approximately one and a half intermediate-scale cycles, which record the retrogradation of the carbonate sediment factory to the periphery of the foreland basin in easternmost Idaho. Crinoidal grainstone shoals are observed across much of Antler foreland basin during the early transgressive systems tract. The crinoidal grainstone belt is observed landward of location East Canyon during the remaining TST. In the proximal foreland at location Copper Mountain, oolitic grainstone shoal cycles aggrade during the TST of SP4 (Figure 3.56). Additionally, the cycles tend to show increasing amounts of bioturbation and overall muddier, packstone textures, while cycle bases typically are composed of cross-stratified grainstone beds. The grainstone belts downramp from Copper Mountain at location East Canyon are composed of skeletal rather than oolitic allochems, illustrating the continued relative

spatial partitioning of these sand belts, which has been the case for the last two sequences. At location East Canyon and Upper Pahsimeroi aggrading crinoidal grainstone cycles are observed during the TST of SP4; however, the cycles are considerably more amalgamated at East Canyon than at Upper Pahsimeroi, indicating less accommodation development in updip positions than further basinward.

Bioturbated skeletal wackestone and packstone cycles of middle ramp affinity make up the middle and late TST in basinward positions. The overall percentage of middle ramp cycles increases from location East Canyon where only the latest TST is made up of the cycles to location Upper Pahsimeroi where the upper half of the TST is composed of middle ramp cycles to location Antelope Creek where middle ramp cycles mark the initial transgression only. At location Antelope Creek, the middle ramp cycles are overlain by an extensive interval of covered section, likely reflecting deepening into outer ramp conditions and increased argillaceous deposition.

The maximum flooding surface of this sequence is chosen atop the extended covered interval just described at location Antelope Creek, which likely reflects the maximum deepening of the ramp and maximum accumulation of argillaceous material in this locality. At section Upper Pahsimeroi, the MFS is chosen based on similar criterion. Here the MFS is chosen within an argillaceous interval of middle ramp cycles, likely reflecting that the major sources of carbonate sediment have moved updip and away from this locality allowing for accumulation of argillaceous material. Further updip at location East Canyon, the MFS is chosen atop the lone middle ramp cycle occurring within this sequence, again indicating the carbonate sand belts were pushed into a proximal position along the foreland basin margin in eastern Idaho at this time. In the proximal foreland at section Copper Mountain, the MFS is picked atop the last oolitic grainstone observed within this sequence (Figure 3.56). Above and below this grainstone are oolitic beds with muddier textures indicating lower energy conditions consistent with offshoal deposition most likely within the distal lagoon just behind an oolitic barrier bar system downdip. The MFS then is appropriately picked at the last, most landward occurrence of the oolitic barrier bar system within the sequence.

3.3.1.11.2 Highstand Systems Tract

The upper two and a half intermediate-scale 4th-order cycles make up the highstand systems tract of sequence SP4. These cycles are interpreted to step seaward from two-dimensional stacking pattern correlations within the foreland basin, but similar to sequence SP3 considerable aggradation occurs within the sequence as compared to sequences SP1 and SP2.

A single high-frequency cycle marks the last occurrence of oolitic facies at the base of the HST at most proximal location at Copper Mountain. Most of the HST at this locality is composed of very thin, aggrading restricted lagoonal cycles. Within this systems tract, abundant, articulated goniatite and orthocone cephalopods were deposited within this lagoonal setting (Figure 3.56; Figure 3.57). Downdip at East Canyon, thick massive accumulations of crinoidal grainstone of the TST and early highstand are overlain by packstones and grainstones of mixed allochemical composition. Here peloidal, oolitic, and skeletal grainstones of the late highstand are interbedded at the meter scale. Further downdip, skeletal and crinoidal grainstones comprise most of the HST at Upper Pahsimeroi and Antelope Creek.

Deposition of the goniatites and orthocones is indicative of periodic wash-ins of these open marine fauna into a low-energy setting capable of preserving them in nearly pristine condition. This fauna is not known from any other locality, which is likely due to higher-energy conditions over the rest of the basin at this time and a lack of preservation. At locality East Canyon, the HST of sequence SP4 marks the preservation of the most intimate association of the until-now spatially distinct sand belts. The early highstand at locality East Canyon is marked by aggradation of highly amalgamated crinoidal sand shoal cycles which directly overlie and likely downlap onto the MFS here. Deepening within the next 4th-order cycle brought bioturbated peloidal packstones and grainstones of middle ramp affinity atop these crinoidal grainstone shoals. This cycle was then overlain by cycles composed of mixed oolitic and skeletal grainstone shoals, which progressively thinned within the remaining HST. Oolitic shoal beds mark the top and base of this stacked grainstone package with skeletal shoal beds making up the intervening strata.

In the most distal part of the foreland basin at localities Upper Pahsimeroi and Antelope Creek, the HST is dominated by aggradational stacks of typically bioturbated

skeletal wackestone and packstone cycles. This is particularly the case at section Upper Pahsimeroi, where increasing storm-influence and amalgamation is observed in the late highstand. At the very last cycle of the HST at this locality, trough cross-bedded crinoidal grainstone marks progradation of the crinoidal grainstone belt out into the basin here. At section Antelope Creek, much of the HST is covered; however, the limited exposure reveals bioturbated skeletal wackestone and packstone cycles indicative of middle ramp deposition. Also like Upper Pahsimeroi, the late HST at locality Antelope Creek is marked by deposition amalgamating packstones and grainstones and is capped by a trough cross-bedded crinoidal grainstone shoal indicative of progradation of this facies belt far into the foredeep at this time.

The sequence boundary of SP4 is placed atop of the crinoidal grainstone shoal deposits at distal locations within the study area. This horizon marks the shallowest water deposition at these positions capping shoaling upward cycling of the middle ramp into fairweather wave base. In the more proximal location at location East Canyon, the sequence boundary is placed atop the upper oolitic grainstone shoal bed. At this time, this location had shoaled into a tidally-influenced setting and the overall thinning of beds within these uppermost shoal cycles indicates that an accommodation minimum had been reached within this stack of grainstones. In the most proximal location at Copper Mountain, the sequence boundary is placed atop a stack of upward thinning proximal lagoonal mudstone cycles, indicating maximum restriction and minimum accommodation along the landward margins of the Antler foreland at the time.

3.3.1.12 Scott Peak Sequence 5

Deposition of Scott Peak sequence 5 is lithostratigraphically equivalent to upper part of the Middle Massive Member of the Scott Peak at locations Copper Mountain and East Canyon (Huh, 1967). This unit is equivalent to the lower Scott Peak at section location Upper Pahsimeroi (Huh, 1967) and is likely of late Meramecian age within Mamet foraminifer zone 14 based on biostratigraphic dating of measured sections in the Upper Pahsimeroi area by Skipp et al. (1971). These strata are likely correlative with the upper part of the Kibbey Sandstone in southwestern Montana. The sequence is comprised of approximately four 4th-order cycles which display a highly aggradational stacking pattern across the Antler foreland basin (Figure 3.58).

3.3.1.12.1 Transgressive Systems Tract

The lower one and a half intermediate-scale cycles make up the transgressive systems tract of sequence SP5. The early TST is composed of highly aggradational, stacked grainstone cycles over much of the study area. In the middle portion of the study area at East Canyon and Upper Pahsimeroi, amalgamated, massive-tabular cross-bedded crinoidal grainstone cycles characterize the early transgression. Updip at Copper Mountain, peloidal grainstone cycles of a distal lagoonal setting dominate deposition within the early TST. Near the TST, oolitic grainstones and skeletal packstones-grainstones occur. At section locations Upper Pahsimeroi and East Canyon, the TST is dominated by grainstone shoal depositional cycles dominated by crinoidal sands. At both localities, highly amalgamated cycles are the dominant stratigraphic element in the early TST (Figure 3.59). Increasingly, however, peloidal packstone-grainstones make up a larger predominance of the middle and late transgression at East Canyon.

The late TST at Copper Mountain is organized into an aggradational to retrogradational series of small-scale cycles which show interfingering of grainstone shoals and middle ramp facies at a fine scale in the distal parts of the study area. The TST is expressed by upward thickening small-scale cycles dominated by peloidal grainstone which tend to become more muddy and bioturbated during the mid-TST. The late TST is characterized by backstepping of the oolitic grainstone shoal belt to this location.

Aggradation of middle ramp deposits is characteristic of deposition in the distal foreland in throughout the TST. Downdip at Upper Pahsimeroi and East Canyon, both sections are affected by increasing accommodation by observable decreases in amalgamation near the top of the TST; however, maximum accommodation development is marked by the appearance of bioturbated calcisiltite deposits above the crinoidal sand shoals at section Upper Pahsimeroi while this is not the case at East Canyon.

In the most basinward location of Antelope Creek, the TST is composed of three intermediate-scale upward thickening middle ramp cycles which are overlain by a thick interval of covered slope with argillaceous material in float. Similar to other sequences, section Antelope Creek records overall deepening within the TST by increasing amounts of argillaceous material being incorporated with carbonate deposits.

Deepening into the middle ramp depozone, marked by deposition of bioturbated skeletal wackestones-packstones, characterizes the maximum flooding surface at section Upper Pahsimeroi. Although middle ramp deposition does continue at this locality during the highstand, the overall thickness of the mid-ramp cycles just above the crinoidal sand shoal cycles, suggests that this was the period of maximum accommodation within the sequence. Further updip at locality East Canyon, the MFS is chosen atop the last cycle of amalgamated crinoidal grainstone below the first the lagoonal cycles, which mark deposition within a decreased energy regime consistent with backbarrier deposition (Figure 3.59). The MFS atop the thickest oolitic grainstone shoal cycle at location Copper Mountain indicative of the most landward extent of the oolitic barrier system during sequence SP5.

3.3.1.12.2 Highstand Systems Tract

The HST of sequence SP5 is made up of the upper three and a half intermediate-scale cycles of 4th-order duration. Unlike earlier Scott Peak sequences, the highstand systems tract of sequence SP5 is considerably more aggradation, with minor skeletal grainstone shoals within this interval. In landward positions along the periphery of the Antler foreland basin, the HST is dominated by aggrading restricted lagoonal cycles, which are interbedded with crinoidal grainstone shoals at the intermediate-scale cycle level. Further basinward, crinoidal grainstone shoals are observed to interbed with storm-influenced middle ramp deposits, which become increasingly dominant in the most distal positions within the study area.

The proximal Antler foreland basin exhibits increasing restriction with upward progression through the HST of sequence SP5. At location Copper Mountain near the margin of the foredeep, oolitic grainstone shoals make up the early highstand and overlain by peloidal lagoonal facies with increasingly muddy textures. Cycles at this location are marked typically by peloidal packstone bases with wackestone to mudstone tops. These cycles are observed to thin upward within the HST of this sequence. Somewhat more distally at location East Canyon, observed 4th-order cycles exhibit similar trends; however, rather than having oolitic or peloidal grainstone bases, in this locality the cycle bases are typically crinoidal grainstones (Figure 3.59). The cycle caps, similar to location Copper Mountain, are dominated by peloidal packstones and

wackestones indicating increasing restriction within the progression of the HST and overall diminishing accommodation. Near the top of the sequence, the cycles become dominated by restricted lagoonal facies to the exception of grainstones, further illustrating the diminished hydrodynamic energy at this setting with time.

In the downdip positions within the Antler foreland basin at locations East Canyon and Antelope Creek, aggrading middle ramp deposits make up most of the HST within sequence SP5. At location East Canyon, although crinoidal grainstones are present within the early highstand, this facies is observed to be only occasionally interbedded with low-angle cross-bedded skeletal packstones and bioturbated wackestone (Figure 3.59). Within the late TST at East Canyon, the crinoidal grainstone deposits become volumetrically less important and two crinoidal grainstone shoal cycles of 5th-order duration cap the HST at this locality. At locality Antelope Creek, upward thinning mid-ramp cycles make up the HST of SP5.

The sequence boundary is picked within the lagoonal portion of the Antler foreland basin at the accommodation minimum defined within a sequence of upward thinning restricted cycles. At location Copper Mountain this is picked at the top of a thin peloidal wackestone bed, below a series of increasingly thick lagoonal cycles. Based on the same criteria, a thin lagoonal wackestone is chosen at location East Canyon as the sequence boundary. At location East Canyon the sequence boundary is chosen atop the thinnest skeletal shoal which lies atop of a sequence of increasingly amalgamated skeletal packstones (Figure 3.59). At location Antelope Creek, the sequence boundary is arbitrarily placed at the base of an extensive covered interval, which likely represents argillaceous depositional conditions within the TST of sequence SP6.

3.3.1.13 Scott Peak Sequence 6

Scott Peak sequence 6 is equivalent to much of the Upper Cyclic Member of the Scott Peak formation at locations Copper Mountain and East Canyon and to a portion of the upper Scott Peak formation at location Upper Pahsimeroi. Based on biostratigraphic information from the Doublespring Pass area near locality Upper Pahsimeroi, SP6 is of late Meramecian-early Chesterian age, probably within Mamet foraminifer zones 14 and 15 (Mamet et al., 1971). This sequence probably correlates with the upper Kibbey Sandstone and perhaps part of the Lombard Limestone in southwest Montana. This

sequence is made up of five 4th-order cycles which stack in a retrogradational followed by progradational pattern, interrupting the pattern of aggradation seen within sequence SP5 (Figure 3.60).

3.3.1.13.1 Transgressive Systems Tract

The TST of sequence SP6 is composed of two and a half 4th-order scale cycles which display overall aggradation stacking of dominantly restricted lagoonal cycles with increasing admixture of normal marine skeletal component with increasing time. This pattern is observed over more of the Antler foreland basin than at any other previous time, where the grainstone shoal facies belts made up a much more significant tract than within this time unit.

At locality Copper Mountain, very thin bedded peloidal wackestone and packstone cycles are overlain by thicker cycles with articulated ramose bryozoans being the dominant fauna. At locality East Canyon, cycles are highly cyclical with relatively thick, amalgamated peloidal grainstones making up the cycle bases with these beds become less and less amalgamated and progressively more muddy toward the top of the cycles (Figure 3.61). Towards the top of the TST, cycles incorporate progressively more normal marine skeletal allochems. At locality Upper Pahsimeroi, a basal restricted lagoonal intermediate-scale cycle is overlain by progressively more skeletal, near-shoal cycles which in turn grade into crinoidal grainstone cycles near the end of the transgression. The TST at locality Antelope Creek is covered, but it can be inferred that this interval was likely argillaceous and probably middle ramp in affinity based on the float within the area.

At proximal localities, the overall pattern observed within the TST of SP6 can be summed by increased accommodation reflected in overall thickening of both bedding and the cycles they composed and a change from muddier to grainier texture, where the grains become increasingly skeletal rather than abiotic. Additionally the three most proximal sections exhibit relatively uniform sediment thickness during the TST. This suggests uniform accommodation increase across a seaward-dipping ramp.

The MFS is chosen at all localities based on accommodation patterns observed at both the 4th- and 5th-order cycle scales as well as the occurrence of the most marine beds within the sequence. At locality Upper Pahsimeroi, the MFS is placed within the small-scale cycle of crinoidal grainstone which is overlain by restricted lagoonal cycles. At locations East Canyon and Copper Mountain, the MFS is placed within the thickest cycles of near-shoal affinity containing the greatest abundance of articulated bryozoans, at locality Copper Mountain, and within a crinoidal grainstone unit at locality East Canyon.

3.3.1.13.2 Highstand Systems Tract

The highstand systems tract within sequence SP6 is made up of the upper two and a half intermediate-scale cycles, and although this sequence is highly aggradational in proximal positions, the oolitic grainstone belt is observed in its maximum seaward extent during this systems tract.

Aggradational stacking of restricted fauna, peloidal lagoonal facies dominates the HST over proximal as well as more basinal localities within this sequence. At locality Copper Mountain, well-developed symmetrical lagoonal cycles dominate deposition within this systems tract. Here, peloidal packstones typically make up the base of the intermediate-scale cycles, while covered intervals make up the cycle tops. These covered intervals are likely muddy carbonates deposited within a highly restricted lagoonal setting. Cycles are observed to thin upward at both the small- and intermediate-scale reflecting overall decreasing accommodation within the HST here. Additionally, depositional textures are observed to become more and more muddy within the late highstand.

At location East Canyon, a very similar evolution within the cycles making up the HST is observed. The most significant observed difference between locality East Canyon and locality Copper Mountain is that the early highstand is significantly more oolitic and skeletal rather than peloidal at locality East Canyon rather than that observed at Copper Mountain (Figure 3.61). Additionally, packstone textures are much more common within the late highstand at East Canyon as compared to that observed at Copper Mountain, but like Copper Mountain beds are observed to thin dramatically near the top of the sequence here.

Similar to locality East Canyon, section Upper Pahsimeroi is composed of a basal skeletal packstone which is overlain by restricted lagoonal wackestones. Unlike section East Canyon, intermediate cycles at locality Upper Pahsimeroi are typically relatively skeletal rather than peloidal, with bioturbated skeletal wackestones-grainstones common at cycle bases and muddier intervals at the top of cycles represented by thin covered intervals. Cycles at this locality are observed to thin upwards toward the sequence boundary here as well.

Although much of the early highstand is inferred to be represented by a thick covered interval at location Antelope Creek, the late highstand here marks a noteworthy appearance in facies. A single 4th-order scale cycle composed of oolitic grainstone marks the late highstand at this locality, indicating a downshift of this facies to its most basinward position noted within the study area. This cycle is overlain by a bioturbated skeletal wackestone cycle of near-shoal affinity and is interpreted to have been deposited within a backbarrier position landward of the prograding oolitic shoal belt.

The SP6 sequence is placed at the minimum accommodation position within the aggradationally-stacked lagoonal cycles that cover much of the study area as determined by stacking pattern analysis of cycles of both 4th- and 5th-order. This is represented a stack of thin wackestones capped by a covered interval at locality Copper Mountain, while a cycle of thin peloidal packstones mark the top of the sequence at East Canyon, and the thinnest packstone bed is chosen as the sequence boundary here. Similarly, the covered interval overlying a thin, thinly-bedded cycle of near-shoal wackestones is chosen as the sequence boundary at location Upper Pahsimeroi. The top of the sequence at location Antelope Creek is marked by the top of the near-shoal cycle overlying the oolitic grainstone shoal cycle here.

3.3.1.14 Scott Peak Sequence 7

Scott Peak sequence 7 is of Chesterian age and correlates with the upper part of the Upper Cyclic Member of the Scott Peak Formation at localities East Canyon and Copper Mountain (Huh, 1967). Further downdip at locality Upper Pahsimeroi, this sequence correlates with upper part of the Scott Peak Formation (Huh, 1967), and based on biostratigraphic study in this area, this sequence is likely within Mamet foraminifer zone 16i (Mamet et al., 1971). This sequence is composed of approximately three 4th-

order cycles which display an overall retrogradational-progradational stacking (Figure 3.62).

3.3.1.14.1 Transgressive Systems Tract

The transgressive systems tract of sequence SP7 is composed of one and a half intermediate-scale cycles, which are stacked in a highly-retrogradational pattern. The grainstone shoal facies belts are observed in landward positions within this systems tract after having occurred as far basinward as had been to this point observed within the study area.

At locality Antelope Creek, bioturbated skeletal wackestones and packstones are observed to overlie the basal crinoidal grainstone shoal deposits. These mid-ramp cycles make up the remaining TST of SP7 at this locality. More proximally at location Upper Pahsimeroi, the grainstone shoals are observed to vertically aggraded within the transgressive systems tract of SP7. Within the TST of SP7, interbedded oolitic grainstone shoal beds are observed to over- and underlie skeletal wackestone and packstone beds of near-shoal affinity, and near the end of the TST at locality Upper Pahsimeroi, crinoidal shoal beds which cap the underlying 4th-order cycle are directly overlain by oolitic grainstones which make up the base of the following cycle.

Proximal to locality Upper Pahsimeroi at section East Canyon, aggradationally-stacked crinoidal sand shoals make up the entire TST (Figure 3.63). These crinoidal shoal beds are observed to thin upward reflecting decreased amalgamation with overall increasing accommodation. Most proximally at locality Copper Mountain, the TST is poorly exposed and where it is, the cycle bases are observed to be composed of bioturbated, skeletal wackestones. Cycle tops here are inferred to be represented by muddy carbonates which are poorly resistant to weathering and hence do not crop out.

Crinoidal grainstone shoal facies are observed from locality Antelope Creek to locality East Canyon at the base of this sequence. This grainstone belt is inferred to onlap the SP6-SP7 sequence boundary in a landward direction during the initial rise of sea level during this sequence. Similar to sequence SP4, an intimate spatial relationship is observed between the oolitic and crinoidal grainstone belts at Upper Pahsimeroi, where interfingering of crinoidal and oolitic grainstones is observed at the small-scale cycle level.

At section Copper Mountain, the maximum flooding surface of sequence SP7 is chosen atop a skeletal-rich peloidal grainstone bed overlying a relatively thin covered interval. This is interpreted to represent the most hydrodynamically-energetic interval concomitant with maximum deepening in this restricted lagoonal setting. Further basinward at locality East Canyon, the MFS is picked atop the last crinoidal grainstone bed above which hydrodynamic energy clearly is reduced and deposition of muddier, non-skeletal carbonates dominate. At locality Upper Pahsimeroi, the MFS is picked atop a non-amalgamated bioturbated skeletal wackestone interval interpreted to represent deposition along the mid-ramp. This is the only occurrence of this facies belt at locality Upper Pahsimeroi within this sequence. At the distalmost locality at Antelope Creek, the MFS is placed atop a covered interval likely represent an argillaceous interval of deposition along the middle ramp, likely coinciding with the maximum deepening here during this sequence.

3.3.1.14.2 Highstand Systems Tract

The highstand system tract of Scott Peak sequence 7 is characterized by the deposition of one and a half intermediate-scale cycles which stack in an aggradational pattern. In the proximal Antler foreland in eastern Idaho, aggradationally stacked lagoonal cycles mark deposition of the HST, while basinward, the skeletal grainstone belt is inferred to step basinward at this time.

The HST is poorly exposed at locations Copper Mountain and East Canyon at this time. Early highstand deposits at location Copper Mountain are observed to be bioturbated peloidal wackestones and packstones with some normal marine skeletal components. The majority of the late HST is covered, likely due to the deposition of muddy carbonates which are structurally incompetent. The HST of sequence SP7 at locality East Canyon also poorly outcrops, but where it is exposed a the lower portion of one intermediate-scale cycle is observed to be composed of dominantly bioturbated peloidal wackestones to packstones with variable amounts of admixed normal marine skeletal allochems (Figure 3.63). These beds are of lagoonal affinity and are interbedded with likely more muddy carbonates which like those at locality Copper Mountain do not outcrop well.

The HST at locality Upper Pahsimeroi is dominated by the deposition of crinoidal grainstone shoals interbedded with near-shoal skeletal wackestones and packstones likely of middle ramp affinity. The late highstand here poorly outcrops, but the observed lithologies are dominantly bioturbated skeletal wackestones with increasing peloidal content near the top of the sequence. This unit is interpreted to have been deposited in a backbarrier setting close to the active shoal. Bioturbated ostracod-rich wackestones and mudstones make up the highstand at locality Antelope Creek, likely representing dysoxic depositional conditions within the water column on the middle ramp during this interval.

The sequence boundary of sequence SP7 is represented across the Antler foreland basin by deposition during the most widespread restriction of the water mass observed within the deposition of the Scott Peak Formation. The sequence boundary of SP7 is placed atop inferred muddy carbonates within a covered interval at localities Upper Pahsimeroi, East Canyon and Copper Mountain, while it is placed atop a thick ostracod-rich wackestone at locality Antelope Creek. At this point, very limited circulation is due to maximum aggradation of the basin by carbonate sedimentation, and attenuation of hydrodynamic energy due to expansive areas of shallow water.

3.3.1.15 Post-Scott Peak Deposition

The Scott Peak Formation is overlain by the South Creek Formation, an argillaceous interval which poorly outcrops across east-central Idaho (Huh, 1967; Figure 3.64). The South Creek Formation is of Chesterian age (Huh, 1967) and represents a drowning of the Scott Peak ramp likely during renewed activity within the Antler orogenic belt. Limited carbonate deposition does occur within the lowermost South Creek, and is best observed at location Upper Pahsimeroi. Here, one and a half intermediate cycles make up the final carbonate dominated period of deposition. Skeletal grainstone shoals make up the basal part of the transgression here and are overlain by bioturbated skeletal wackestone cycles with interbedded mudstones with minor restricted fauna. Carbonate deposition here is capped several small scale cycles of skeletal shoals. Drowning then ensues above this shoal horizon. This abrupt event likely represents a pulse of orogenesis which had a two-fold impact on carbonate deposition: abrupt deepening in response to lithospheric flexural subsidence under an increased tectonic load and shedding of fine-grained siliciclastics into the basin reducing the efficiency of

carbonate sediment production. It is interesting to note that carbonate deposition appears to continue for an additional 4th-order cycle at location Upper Pahsimeroi than at all other locations. This may be due to the fact that perhaps Upper Pahsimeroi was the site of flexural upwarp within the basin in response to flexure while all other localities were within either forebulge or backbulge downwarp settings. If this were the case, Upper Pahsimeroi would've experienced less net subsidence than the other localities, and doubly, it likely would've experienced overall higher energy conditions with less fine siliciclastics entrained in the water mass to stifle carbonate production.

3.4 Discussion

3.4.1 Accommodation, Basin Evolution, and Carbonate Sedimentation: A Comparison of the Central Montana Trough and the Proximal Antler Foreland Basin

The long-term accommodation patterns observed within the evolution of the Madison-Scott Peak system is a direct result of the interaction of flexural subsidence generated by loading of the lithosphere of western North America by orogenic loading in the Antler thrust belt (Speed and Sleep, 1982). In contrast, subsidence within the central Montana trough cannot be directly linked to flexure along the western margin of the plate, and subsidence within this province is likely due to in-plane stress generated by the collision between the arc to the west and North America (Dorobek et al., 1991; Figure 1.3B) and resulting fault-controlled subsidence. The consequence of these processes is that measurably different basins, in terms of aspect ratio, absolute width and depth, and subsidence rate, are set up which serve to accumulate carbonate sediments within them.

Distal steepening of the Madison system is observed to occur in several discrete steps, creating several definable structural domains. The first is the Montana depositional province from just south of location Livingston across the study area, the Madison is observed to undergo a significant vertical expansion due to increased differential subsidence between Montana and Wyoming (Peterson, 1985; Figure 3.65). The second structural domain observed in Montana is the central Montana trough, which's southern boundary lies between locations Sacagawea Peak and Livingston (Peterson, 1985), but an additional ~20% expansion of the section is observed within the approximate axis of the trough at location 16 Mile Creek. The other structural domain is that of the Antler foreland basin which's proximal limit lies between locations Ashbough Canyon and Bell-

McKenzie Canyon (Gutschick and Sandberg, 1983). Across this domain boundary, an additional 100% of sediment accumulation occurs within the period of Madison Group deposition. Moreover up to an additional 600 m of carbonates accumulate within the Antler foreland basin during the time the Madison was exposed from the middle Meramecian to early Chesterian.

The Lodgepole Limestone (sequences LP1-LP3), as previously noted, was deposited on an angular unconformity with significant inherited topography. The initial space generated by downwarping of the lithosphere in response to loading is apparent in the embryonic distribution of facies belts across Wyoming and Montana and the set up of ramp-style deposition in Wyoming. In Montana, within the area of interest of this study, estimates of initial bathymetry are difficult to ascertain due to the lack of bathymetric sensitivity of most of the dominantly mixed redeposited carbonates and argillaceous facies. Estimates of initial water depth range based on total thickness of the Lodgepole Limestone range from 150 m at location Livingston to 250 m downdip in central and southwestern Montana to perhaps greater than 500 m in southwesternmost Montana at location Bell-McKenzie Canyon. These estimates do not account for any non-uniform dynamic motion of the lithosphere during the ~4.4 Myr which elapsed during deposition of the Lodgepole, so these estimates represent absolute maxima of initial bathymetry.

Facies types and distributions within sequences LP1-LP3 is generally similar in both the central Montana trough and in southwestern Montana. In both localities deposition is dominated by thick intervals of argillaceous carbonates throughout this time interval, especially in the TSTs of these sequences. Expansive covered intervals in southwestern Montana, especially at Ashbough Canyon and Bell-McKenzie Canyon, during these sequences point to greater fine clastic input and less production and more dilution of the carbonate material in these locations than in the central Montana trough. This suggests that the source of the clastic input was likely more proximal to southwestern Montana and was likely derived from the recent uplift of the Antler highlands to the west.

The sequential fill of the initial bathymetry generated by downwarping of the lithosphere across Wyoming and central Montana has previously been documented by Elrick (1990) as a series of distally-steepened prograding ramps. This is consistent with

observations from this study, which show a progressive expansion of storm-, wave- and tidally-influenced facies belts at both the sequence and composite sequence scales during the deposition of the Lodgepole Limestone. The geometry of the ramps developed both within the central Montana trough and in southwestern Montana reflects the initial and evolving bathymetry unique to each of these settings. As previously discussed, the initial bathymetry of these settings is significantly different, with a larger amount of accommodation space developed in southwestern Montana (Figure 3.66, 3.67); however, the distribution of this space within the cross-section also plays a critical role in the observed sequence thicknesses and geometries in both areas. The cross-section through the central Montana trough, as defined by isopach mapping, is U-shaped with Livingston along the southern margin, Sacagawea Peak and 16 Mile Creek both lying within the trough, and Monarch lying along the northern slope (Figure 3.67). This contrasts with southwestern Montana where the profile is initially flat in the northeast and slopes increasingly rapidly to the southwest (Figure 3.66). The differences in these configurations result in differences, some subtle while others marked, in the accumulation of sediments during sequences LP1-LP3. While argillaceous carbonates are the dominant fill element in both areas during these sequences, the proportion of other facies within the fill suggest that differences in total accommodation space and distribution of accommodation play a strong controlling role (Figure 3.68; Figure 3.69). The role of total accommodation space is evinced by the narrow distribution and limited of shallow water carbonate facies and preponderance of argillaceous carbonates throughout the Lodgepole in southwestern Montana downdip of Livingston. This is contrasted by significant deposits of storm-influenced packstones and grainstones in the central Montana trough beginning in the HST of LP2 and wave- and tidally-influenced deposits across the trough in the highstand of LP3, including thick accumulations of aggrading oolitic grainstones at 16 Mile Creek in sequence LP3. Although both settings are distally steepened, the distribution of accommodation space across each region also factors into the observed facies and sequence patterns. Most notably, within sequence LP3, thick slope breccias accumulated along the southwestern margin at Bell-McKenzie Canyon. Here, relatively steep slopes led to instability, failure, and mass gravity flows.

Similar features are absent from the central Montana trough, likely indicating that slopes never reached significant steepness for mass failure.

By the end of the deposition of the Lodgepole sequences, a significant shift in depositional patterns is observed across the study area and abrupt shifts in facies belts. This deposition is culminated by the seaward displacement of the grainstone shoal belts during the late highstand of sequence LP3 and during lowstand deposition during sequence MC1 (Figure 3.68-3.70). The dislocation of the grainstone shoal belts into downdip locations across central and southwestern Montana at this time is due to relatively high-amplitude sea-level fall and by its regional extent across both margins suggests that it is due to a eustatic sea-level fall. However, stabilization of the shoal belts in a distal position is likely due to other factors. Aggradation of the seafloor by outer and middle ramp cyclic deposition and maintenance of a graded clinoform profile play key roles in the development of a shoreline-detached barrier system in southwestern Montana and basin-centered aggrading oolitic grainstone belt in central Montana.

Sequence MC1 marks the beginning of shallow water carbonate deposition across central Montana and the permanent displacement of deeper water facies from the trough (Figure 3.69). Abiotic carbonates are abundant across most of the central Montana trough at this time, with oolitic packstones-grainstones, peloidal wackestones-grainstones, and muddy carbonates dominant and limited deposition of open marine skeletal material. Importantly, deposition of evaporite solution collapse breccias are first observed within the trough at this time further indicating relatively limited circulation and restriction and the development of a broad shallow shelf. In southwestern Montana, sequence shapes indicate a more aggraded profile from Ashbough Canyon landward (Figure 3.68). Again, abiotic allochems become increasingly common in these positions along the southwestern margin; however, significant amounts of crinoidal grainstones did accumulate as far downdip as Ashbough Canyon. Seaward of this point, the sequence thickens nearly four times and thick cherty skeletal wackestones-grainstones become the dominant architectural elements at Bell-McKenzie Canyon. The predominance of middle and outer ramp facies in downdip locations and the thickness of MC1 at these locations indicate that the ramp had not fully aggraded into the shallow subtidal, reflecting greater differential subsidence since the initiation of the Madison within the proximal foredeep.

In the central Montana trough, sequences MC2-MC4 are characterized by similar partitioning of facies as observed within sequence MC1 (Figure 3.69). During these sequences, oolitic grainstone deposition is most pronounced at the axis of the trough at 16 Mile Creek, where thick accumulations of aggrading grainstone were deposited. This is contrasted with thickening proportions of evaporite solution collapse breccias to the south at Sacagawea Peak and Livingston as well as a mosaic of shallow subtidal to supratidal facies. The greatest proportion of open marine fauna accumulation occurred to the north at Monarch over this interval, suggesting that a better connection to the open ocean may have existed to the north. Significant variability within the central Montana trough is observed during the deposition of these sequences. Most evidently the section at 16 Mile Creek is observed to be persistently thicker than other sections within the trough throughout this period with the exception of Monarch during sequence MC4. This is indicative of enhanced differential subsidence near the center of the trough as compared to the margins throughout this time interval. Additionally the thickness of sequences at Sacagawea Peak shows high variability during sequences MC2-MC4, which likely reflects fault control on local accommodation at this location. Similarly, thickening of sequence MC4 at Monarch appears to presage the development of the Big Snowy Trough, which fully developed as a successor basin to the central Montana trough in the Chesterian (Peterson, 1985; Figure 3.59). Differential subsidence observed across and within the central Montana trough during the Mission Canyon sequences likely reflects motion along faults within this area which responded to variations in in-plane stress due to the collision along the margin to the west which were transmitted hundreds of kilometers to the east (Dorobek et al., 1991).

As deposition of the Mission Canyon sequences MC2-MC4 in central Montana is marked by aggradation, so too is much of the history of the southwestern margin over this time period (Figure 3.69). During deposition of MC2 extensive grainstone shoal belts developed along the margin of the Antler foreland basin. Skeletal grainstone shoals and crinoid banks were the dominant architectural elements from Bell-McKenzie Canyon to Baldy Mountain and made up an extensive carbonate sand barrier belt setting up an expansive low-energy zone landward (Figure 3.68). Aggrading to prograding crinoidal grainstones made up most of the sediments deposited at Ashbough Canyon, and these

grainstones prograded seaward as far as Bell-McKenzie Canyon where thick accumulations of crinoidal packstones-grainstones interbedded with skeletal and peloidal wackestones-grainstones, formed a sedimentary wedge which began filling the still substantial remaining space in the proximal foreland basin. Further updip skeletal and crinoidal grainstones interbedded with lagoonal peloidal packstones-grainstones and oolitic grainstones, indicating spatial partitioning of carbonate sand belts at this time. In sequences MC3-MC4, establishment of the grainstone barrier system at Ashbough Canyon and Bell-McKenzie Canyon further enhanced the deposition of skeletal-poor, peloidal sediments updip at Baldy Mountain and Livingston. From the HST of sequence MC3 and throughout sequence MC4, Bell-McKenzie Canyon fully aggraded into a shallow subtidal to intertidal setting and this area became the central locus of the skeletal barrier system. The establishment of this barrier system not only increased the deposition of abiotic sediments updip, but also decreased circulation to a level where evaporites began to accumulate as recorded by several intervals of evaporite solution collapse brecciation. Additionally, accommodation space became very limited during the deposition of these sequences in proximal areas. This is reflected in an increasingly wedge shaped sequence geometry observed especially in sequence MC4 and extensive karsting at the top of the Mission Canyon at Baldy Mountain.

3.4.2 System Requirements for Progradation of Carbonate Sand Belts into the Antler Foreland Basin

By the culmination of deposition of the Madison Group in Montana, the shallow water carbonate factory had extended as far downdip as Bell-McKenzie Canyon; however, concomitant deposition in the Antler foreland basin of east-central Idaho had yet to occur (Figure 3.68). Limited carbonate sediment accumulation had occurred as far downdip as East Canyon, but this sedimentation was limited to cherty calcisiltites, much of which was likely derived from sources to the east. In situ carbonate production was extremely limited and a starved basin existed in the Antler foreland basin. Thick covered intervals of tens to hundreds of meters overlying the subjacent Devonian strata in east-central Idaho suggest that fine siliciclastics of the McGowan Creek and Middle Canyon Formations likely made up most of the fill from Kinderhookian-Osagean time. Approximately 500 m of carbonate-poor sediments accumulated in the proximal foredeep

at Copper Mountain, and not until the HST of sequence MC4 did significant *in situ* carbonate sediment production initiate here. The aggradation of fine siliciclastic material derived from the Antler highlands to the west created a template for accumulation of shallow water carbonates in the Antler foreland basin.

During sequence SP1, *in situ* carbonate production began in full in the proximal Antler foreland basin at Copper Mountain. During the HST of this sequence crinoidal banks had established themselves downdip at this position and were interbedded with fine skeletal debris and calcisiltites (Figure 3.68). This systems tract overlies more argillaceous carbonates of the TST. Further downdip at East Canyon, this sequence is dominantly covered with sparse outcrops of argillaceous packstones-grainstones primarily of consisting of bioturbated calcisilts and fine skeletal debris; however, the sequence is capped by crinoidal grainstone indicative of progradation of this facies belt into the central part of the foreland basin. Deposition of middle and outer ramp carbonates in downdip positions is juxtaposed with shallow subtidal to intertidal deposition along the margin of the basin at Bell-McKenzie Canyon. Here shallow water crinoidal and skeletal packstones-grainstones are interbedded with increasingly peloidal grainstones, indicative of a downshifting of the shoal belts to a position just seaward of Bell-McKenzie Canyon by the top of the sequence. This downdip shift in the locus of carbonate sand production is increasingly apparent in sequence SP2. Although the sequence is poorly exposed at Copper Mountain, extensive shallow subtidal to intertidal deposition of skeletal and crinoidal grainstone shoals are observed at East Canyon throughout this sequence. An overall westward tapering wedge of sediment was deposited during this sequence with thick deposits of decreasingly skeletal, increasingly peloidal packstones and grainstones proximally at Bell-McKenzie Canyon and thin argillaceous carbonates distally at Upper Pahsimeroi and Antelope Creek. The sand shoal system developed in the central part of basin appears to be only moderately effective in terms of attenuating circulation of the waters of the proximal foreland, allowing for normal marine fauna to continue to proliferate there.

Rapid downshift of carbonate sand belts and infilling of the distal parts of foreland basin mark the deposition of sequences SP3 and SP4. During these sequences thick packages of oolitic grainstone aggraded and filled the proximal foreland at Copper

Mountain while further downdip at East Canyon and later Upper Pahsimeroi crinoidal and skeletal grainstones acted to infill the foreland basin here (Figure 3.68). Ooids remained partitioned within the proximal foreland basin at Copper Mountain and the ooid shoal belt never prograded as far as East Canyon during this sequence. In sequence SP3, sediments are observed to form a westward-thickening wedge out to the center of the foreland basin at East Canyon and the taper towards the distal periphery at Antelope Creek. From East Canyon landward, shallow water carbonates are able to aggrade at rates greater than or equal to subsidence within the foreland basin at this time, but in downdip localities, limited *in situ* carbonate production and perhaps higher rates of differential subsidence preclude full aggradation of the ramp at this time. This situation, however, was not the case during sequence SP4. During this sequence, crinoidal and oolitic sandbelts prograded downdip and, in the case of the crinoidal grainstone shoals, expanded as far downdip as Antelope Creek by the end of this sequence. During SP4 a westward-thickening wedge of carbonates was deposited from the updip limit at Bell-McKenzie Canyon to Upper Pahsimeroi before tapering westward. Although this sequence is dominantly covered at Antelope Creek, the observed outcrops showed decreasing argillaceous content and increasing skeletal debris, indicative of a productive carbonate factory in this location at this time. In proximal locations basal grainstones are overlain by shallow subtidal skeletal and peloidal packstones to grainstones which are capped by low-energy intertidal to supratidal deposits, indicating decreasing accommodation in the proximal foreland.

The final stage of carbonate fill of the Meramecian Antler foreland basin is marked by the deposition of sequences SP5-SP7. This interval is marked by high rates of aggradation within the foreland basin from Antelope Creek to Copper Mountain (Figure 3.68). This interval marks the highest proportion of accumulation of abiotic sediments within the foreland basin and the interval with the most uniform sequence thickness across the basin. Additionally carbonate sediment production terminates at Bell-McKenzie Canyon at the end of sequence SP5 marking the cessation of the longest continuous carbonate production of any location within the study area. Sequence SP5 forms an eastward-thickening wedge between Antelope Creek and Copper Mountain, indicating increased differential subsidence in the proximal part of the foreland basin.











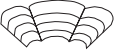

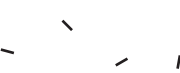

Basal crinoidal grainstones are overlain by peloidal and skeletal wackestones-grainstones at East Canyon, while this sequence is characteristically skeletal downdip at Upper Pahsimeroi and Antelope Creek and peloidal updip at Copper Mountain and Bell-McKenzie Canyon. Numerous thin skeletal and oolitic grainstones are interbedded with peloidal wackestones and packstones at Copper Mountain signaling that bathymetrically-similar facies often substituted locally forming a facies mosaic at this time.

A similar evolution is observed during sequence SP6 across the Antler foreland basin. The sequence is observed to be fairly uniform in thickness across the basin with minor thinning noted at Upper Pahsimeroi. During this sequence the sedimentary fill of the basin is observed to become increasing peloidal and increasingly muddy, especially at East Canyon and Copper Mountain producing an aggrading fill. At Upper Pahsimeroi increased amounts of abiotic sediments are also observed, and open marine fauna is often substituted with lower-energy, euryhaline fauna indicating periodic restriction of the water mass.

Deposition of sequence SP7 is marked by an overall decrease in peloidal sediments and carbonate mud and an increase in skeletal material across the Antler foreland basin. The sequence shape is generally uniform across the foreland basin although some variability in sequence thickening is observed especially at Upper Pahsimeroi (Figure 3.68). The increased amount of stenohaline fauna indicates freshening of the basin presaging the increased subsidence leading to the drowning of the carbonate system at the end of Scott Peak time. The limited carbonate sedimentation above sequence SP7 is composed of thin skeletal and oolitic grainstone shoals which are widespread across the basin. These shoals are overlain directly by shales of the overlying South Creek formation, indicating abrupt drowning and burial of the carbonate system by siliciclastic sediments produced during rejuvenation of tectonism in the Antler highlands to the west.

LEGEND

Allochem symbols

	: Pelmatozoans		: Gastropods
	: Peloids		: Ostracods
	: Ooids		: Foraminifera
	: Rugose corals		: Micritized ooids
	: Bryozoans		: Pisoid/oncoid
	: Tabulate corals		: Intraclast
	: Fine-microskeletal debris	G	: Goniatite and orthocone cephalopods
	: Brachiopods		

Sedimentary structure symbols

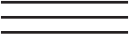

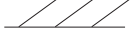










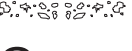
	: Parallel laminations		: Swaly/hummocky bedding
	: Tabular cross-stratification		: Ripple laminations
	: Trough cross-stratification		: Bidirectional cross-stratification
R	: Iron staining		: Sand waves
	: Chert nodules		: Bioturbation
	: Lenticular bedding		: Flaser bedding
Z	: Z-folding	X	: Microkarst
	: Algal laminations	C	: Caliche
	: Fenestrae		: Brecciation
		S	: S-folding

Figure 3.1: Legend for allochem symbols and limestone/dolostone used in logs of the following sedimentary sections.

LEGEND

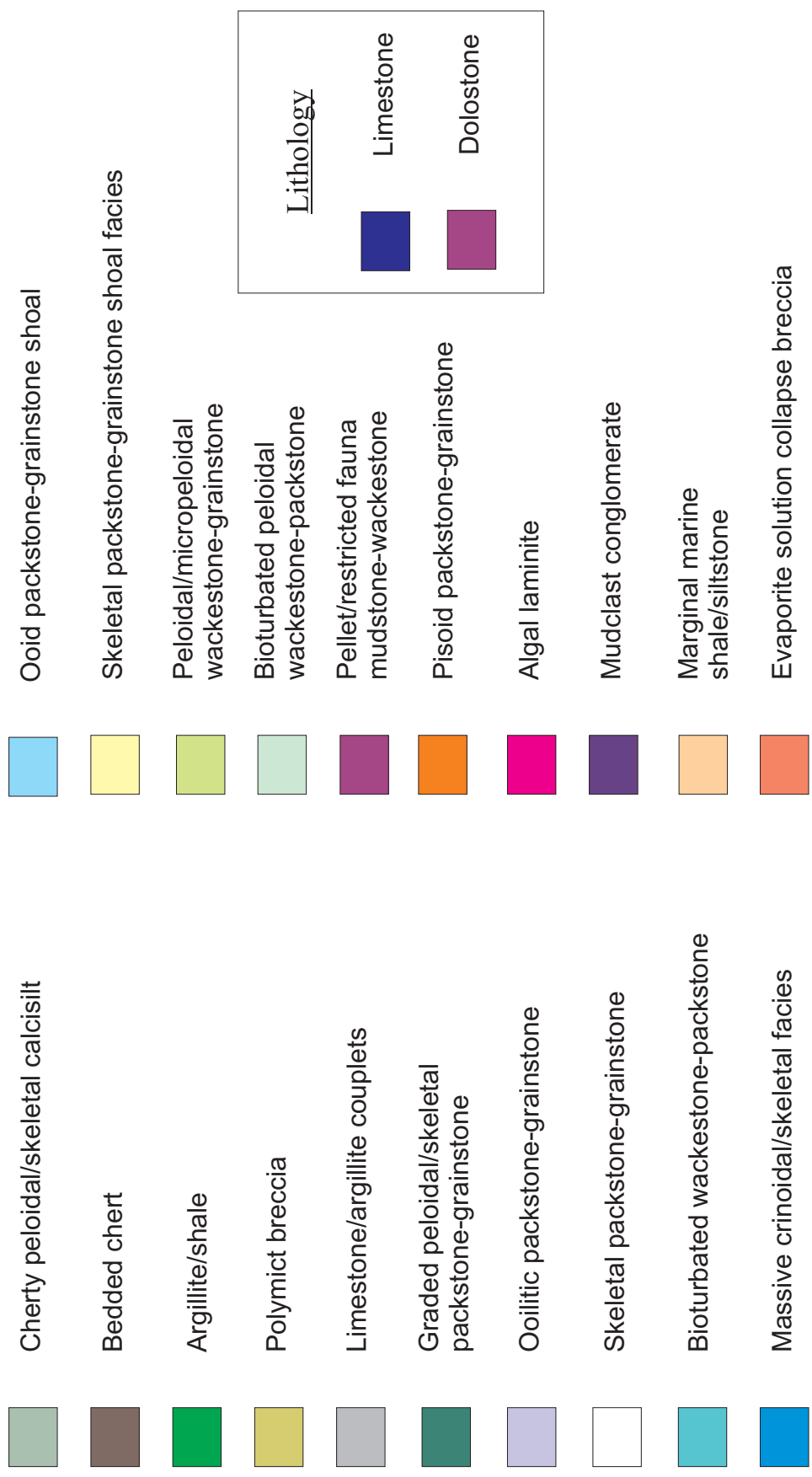


Figure 3.2: Legend for lithologies used in logs of the following sedimentary sections.

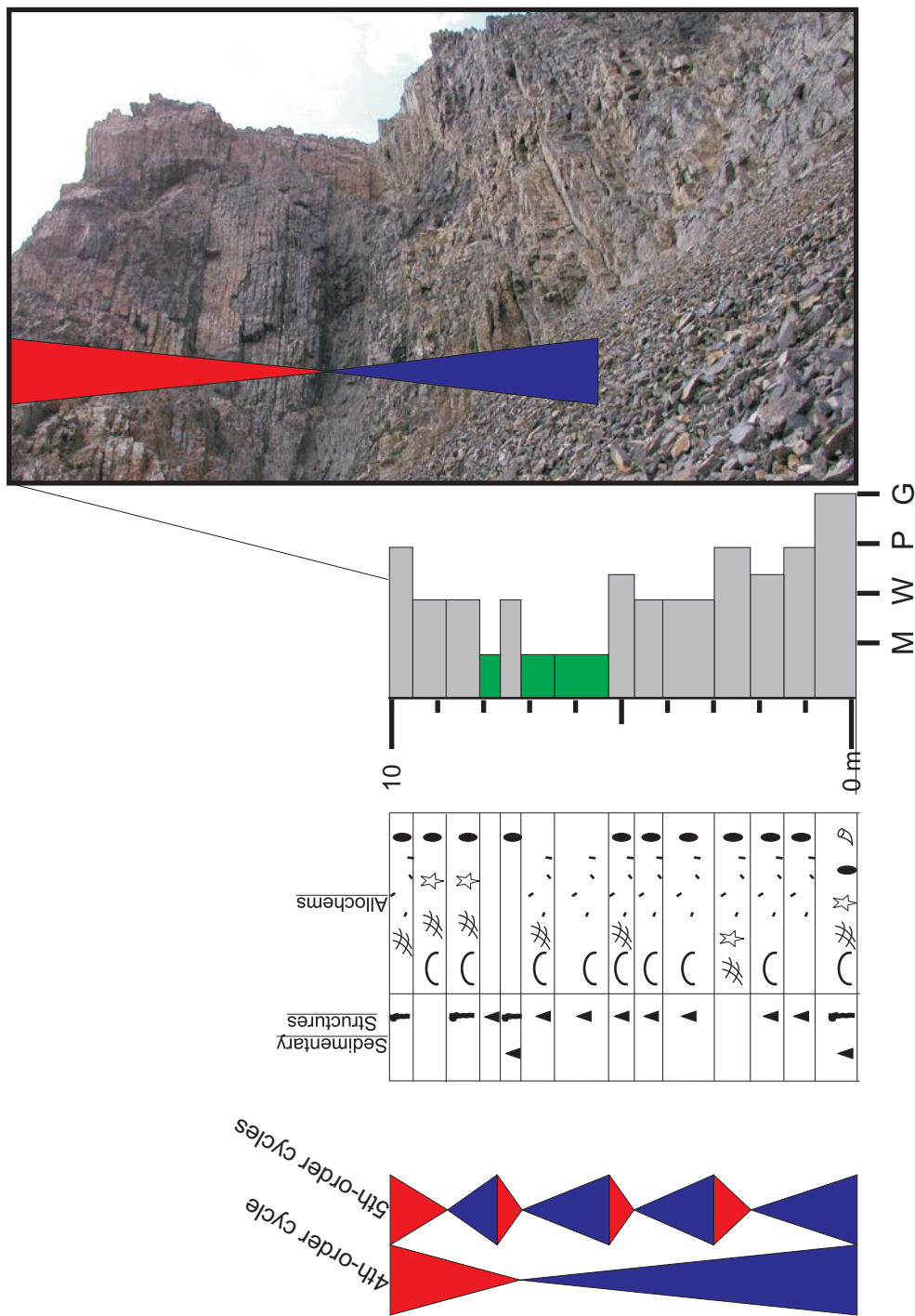


Figure 3.3: Intermediate 4th-order and small-scale 5th-order cycles of basinal affinity. Cherty peloid/skeletal calcisiltite facies are interbedded with the argillite/shale facies, visible within the recessed interval of the outcrop photograph. Here four 5th-order cycles stack to form the single 4th-order intermediate scale cycle visible in the outcrop photograph on the right. Refer to Figure 3.1-3.2 for symbol definitions.

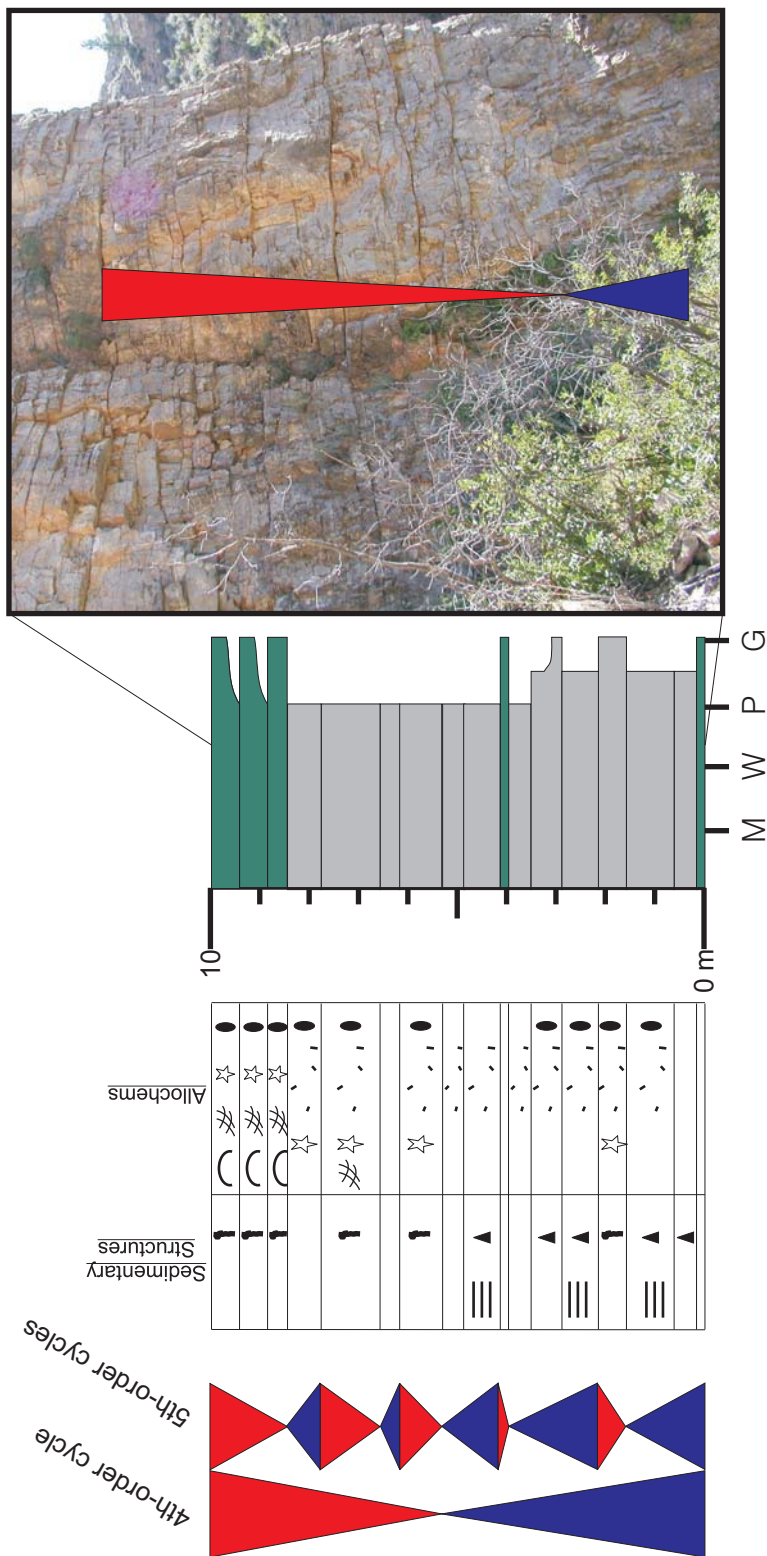


Figure 3.4: Outer ramp cycles at the 4th-order and genetic unit scales. In the outcrop photo, limestone/argillite couplets stack to form meter-scale 5th-order cycles which amalgamate upward. The top of the intermediate-scale cycle here is capped by partly amalgamated redeposited skeletal packstone-grainstones, which coarsen upwards here. Refer to Figure 3.1-3.2 for symbol definitions.

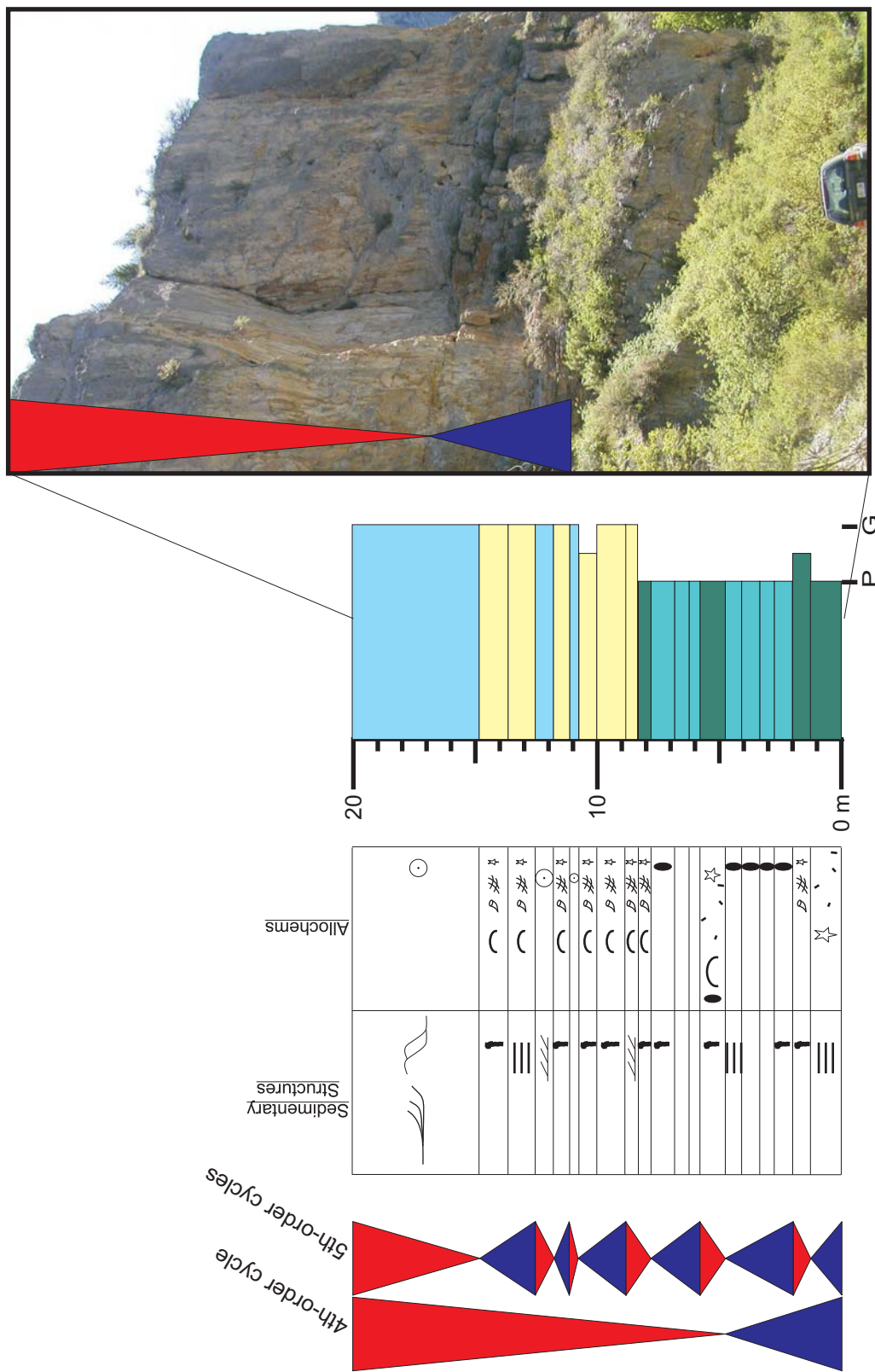


Figure 3.5 An intermediate-scale 4th-order cycle which is composed of middle ramp small-scale cycles at the top and is capped by skeletal and oolitic grainstone shoals at the top. In this example, the both middle ramp and the overlying inner ramp shoal complex cycles are apparent. Refer to Figure 3.1-3.2 for symbol definitions.

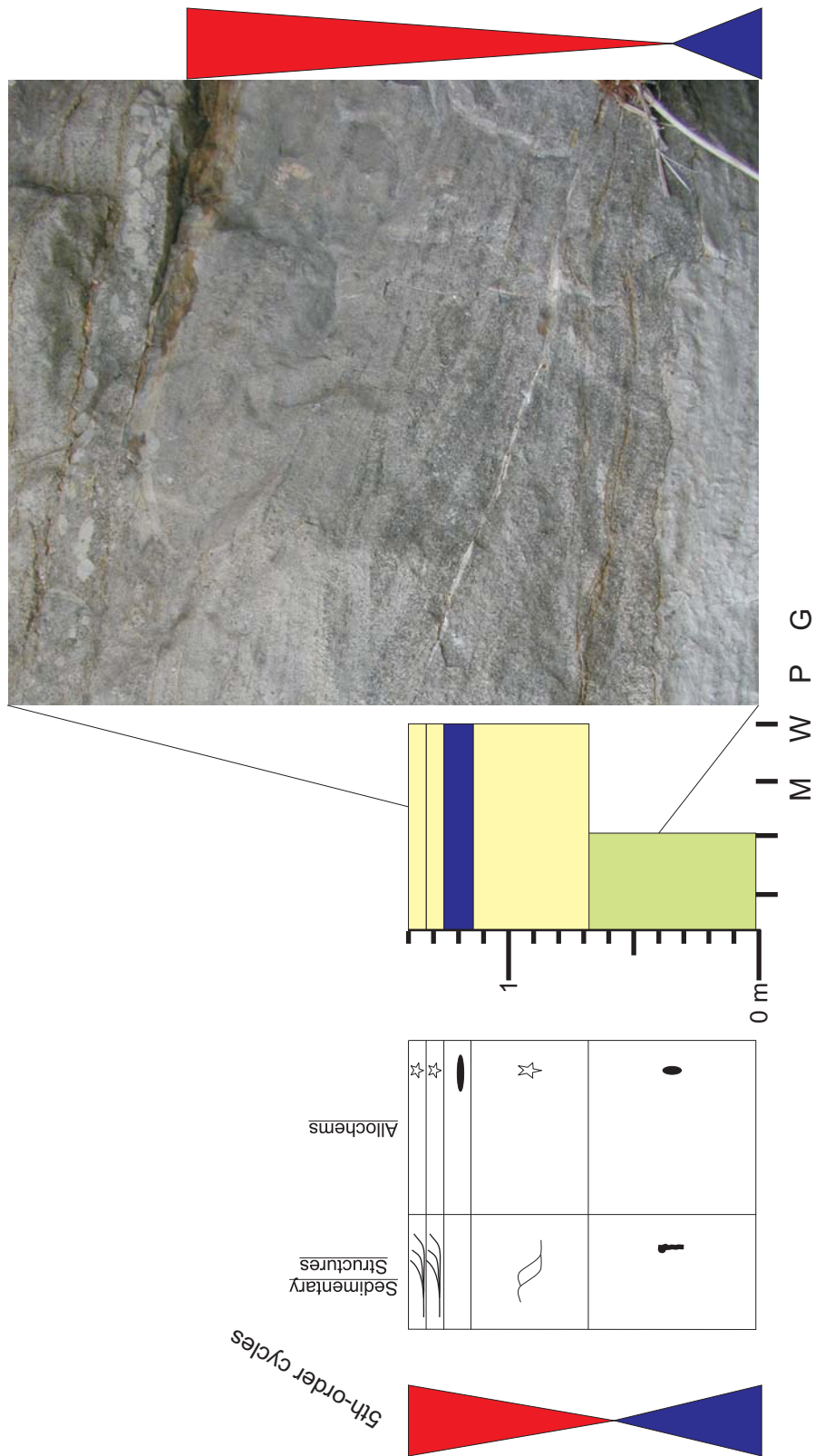


Figure 3.6: The upper part of an intermediate-scale intertidal-subtidal cycle is shown in the outcrop photograph on the right. In the middle is the facies and cycle description for the photograph on the right. Here, bioturbated peloidal wackestones are overlain by tidally-influenced crinoidal grainstones in the lower part of the photo making up the basal small-scale cycle as depicted in the interpretation panel. Bioturbated peloidal wacke-packstones being ripped up and incorporated at the base of the overlying grainstone shoal.

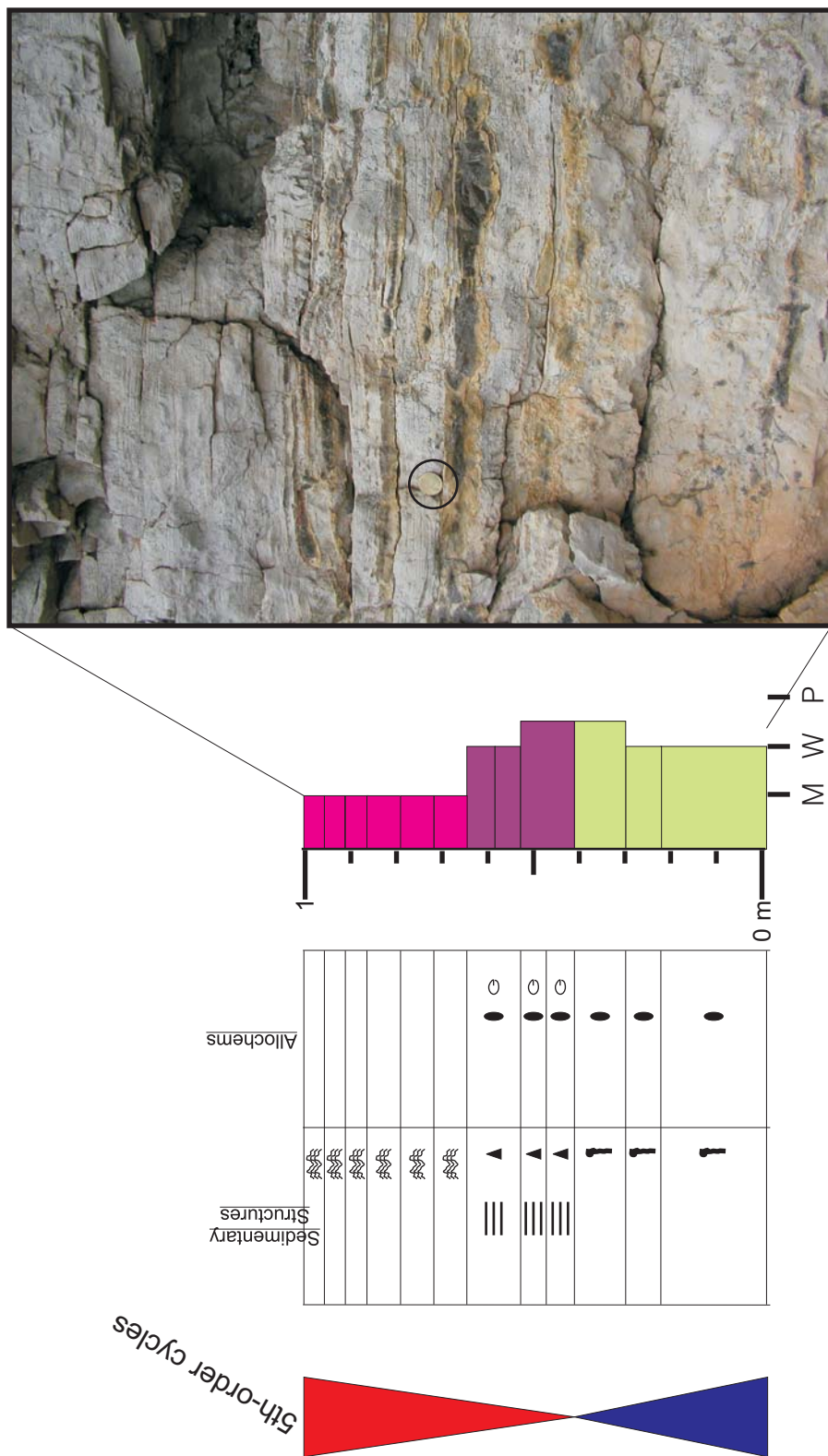


Figure 3.7: The base of the small-scale 5th order shallow subtidal-intertidal cycle is composed of peloidal-micropeloidal wackestone-packstone, which has been heavily bioturbated. These beds are overlain by cherty, parallel laminated, ostracod-bearing micropeloidal wackestone-packstones, which thin upward. The cycle is capped by crinkly-laminated algal laminitic beds. Section Sacagawea Peak. Coin (circled) is approximately 2.5 cm across.

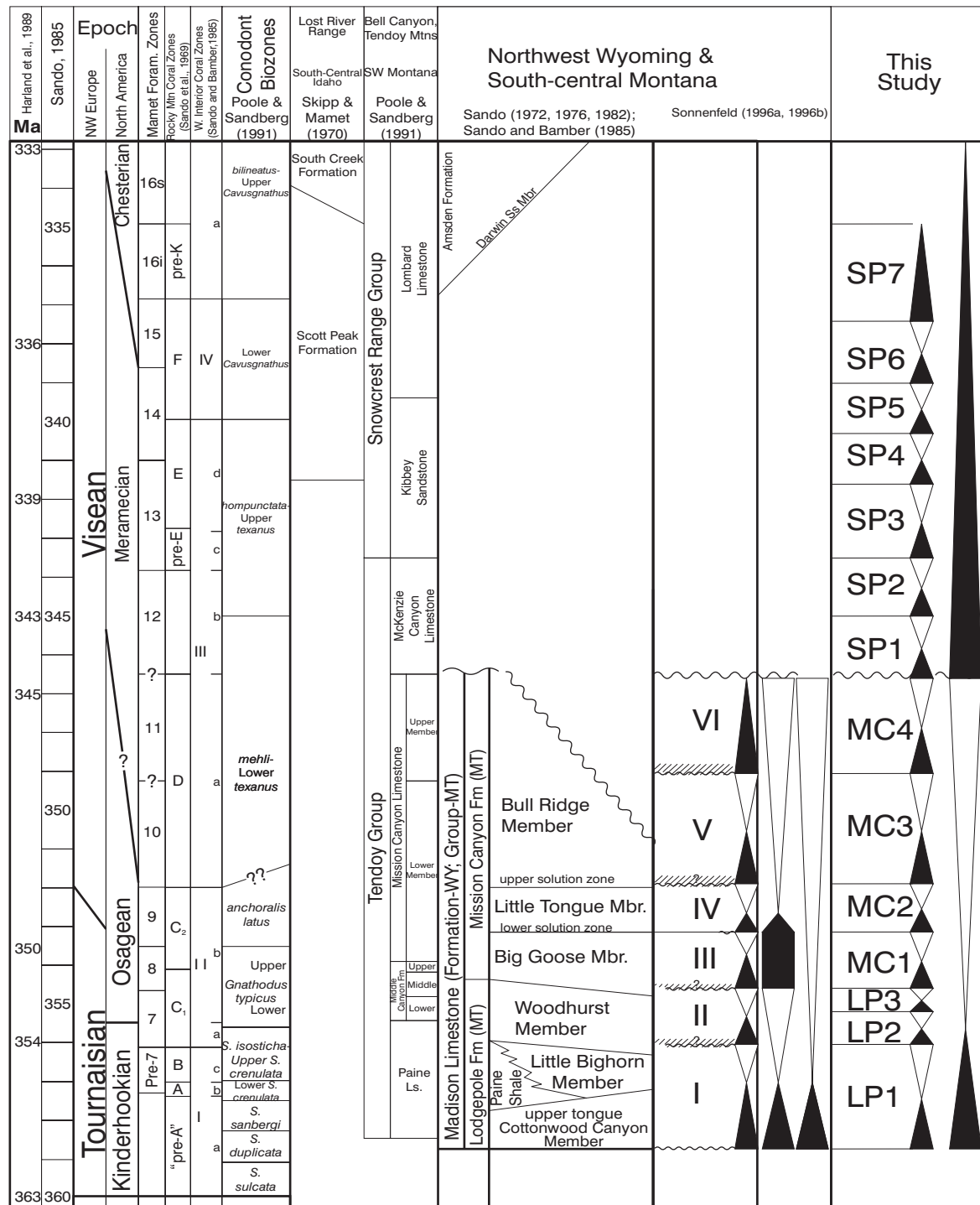


Figure 3.8: Chronostratigraphic chart summarizing the regional relationships of lithostratigraphic units in southern and southwestern Montana (Sando, 1972, 1976, 1982; Sando and Bamber, 1985; Poole and Sandberg, 1991) and east-central Idaho (Skipp and Mamet, 1970) to established biostratigraphy (Poole and Sandberg, 1991; Sando and Bamber, 1985; Sando et al., 1969) and sequence stratigraphy (Sonnenfeld, 1996a,b).

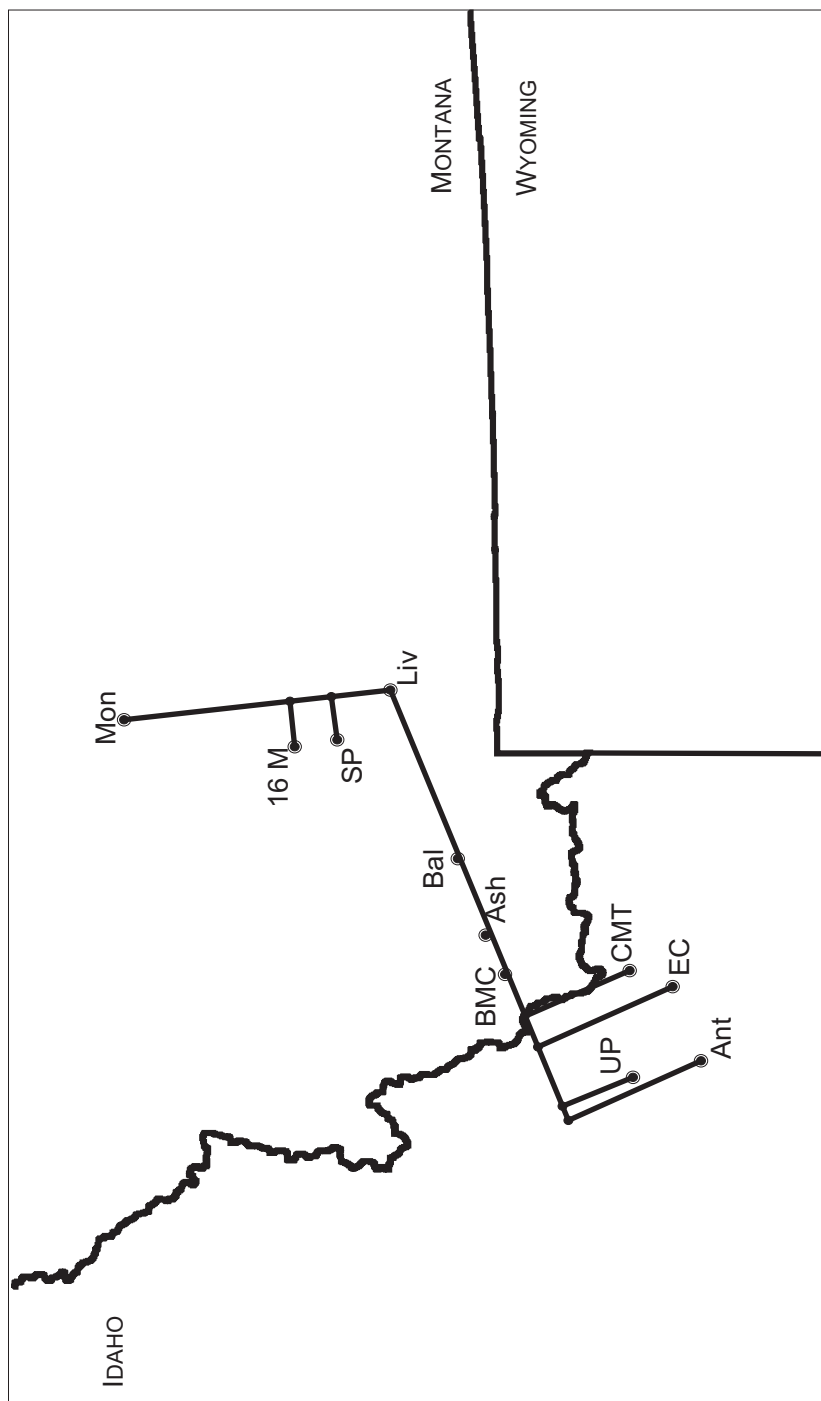


Figure 3.9: Study location map indicating the locations of outcrop measured sections in southwest and central Montana and east-central Idaho as well as the two regional cross-sections. Section localities in Montana are treated as autochthonous and projected directly onto the cross-sections while those in Idaho are allochthonous and must be palinspastically restored (not shown). Abbreviations for sections localities are as follows: 16 M = 16 Mile Creek; Ant = Antelope Creek; Ash = Ashbough Canyon; Bal = Baldy Mt; BMC = Bell and McKenzie Canyons; CMT = Copper Mt; EC = East Canyon; Liv = Livingston; Mon = Monarch; SP = Sacagawea Peak; and UP = Upper Pahsimeroi.

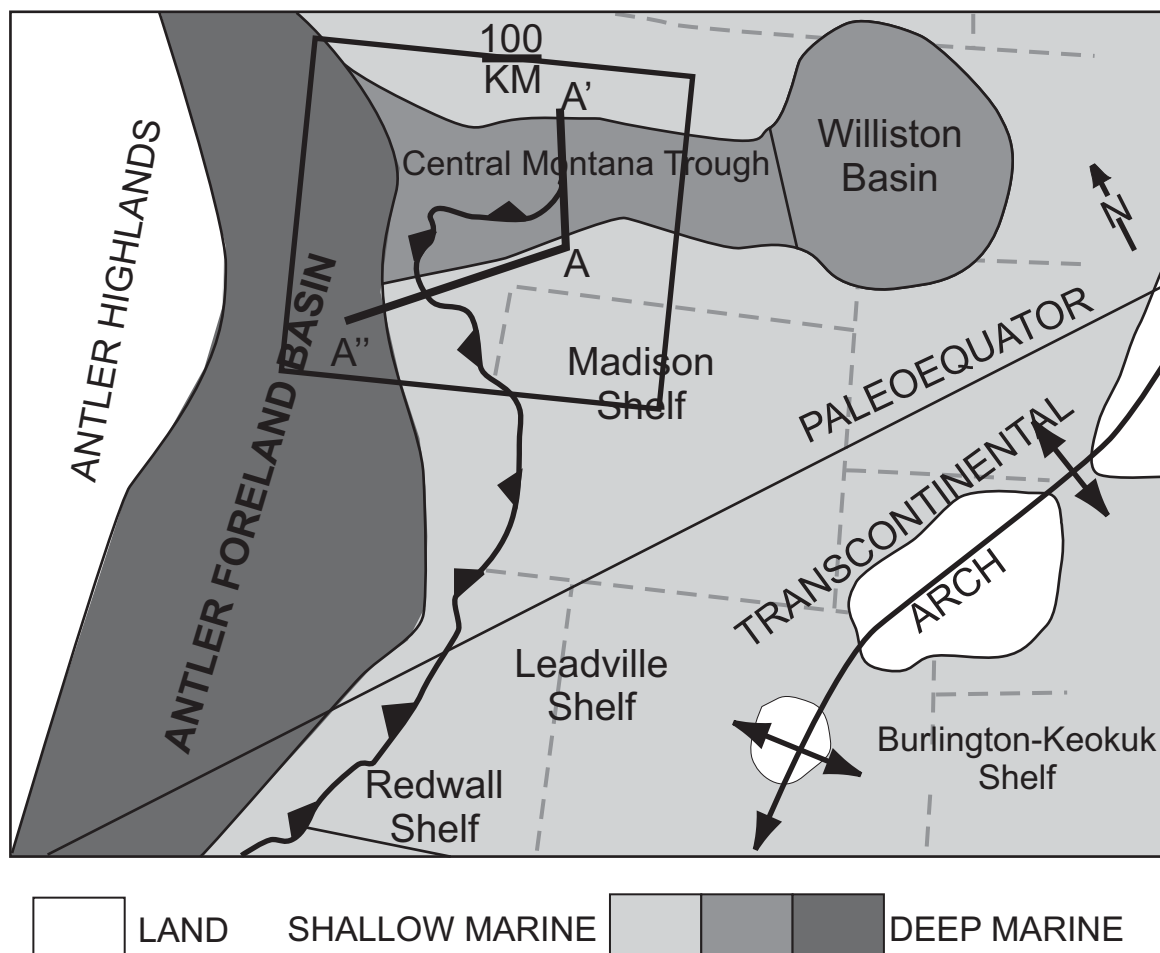


Figure 3.10: Paleogeographic map of the western United States during the Early Mississippian (from Gutschick and Sandberg, 1983) showing the approximate locations of the cross-sections constructed within this study. Contours are the interpreted water depths during sequence IV of the Madison of Sonnenfeld (1996a, b). A-A' and A'-A'' in the boxed area denote the cross-section locations of this study. Cross-section A-A' denotes the transect across the central Montana trough while cross-section A-A'' strikes downdip into the Antler foreland basin.

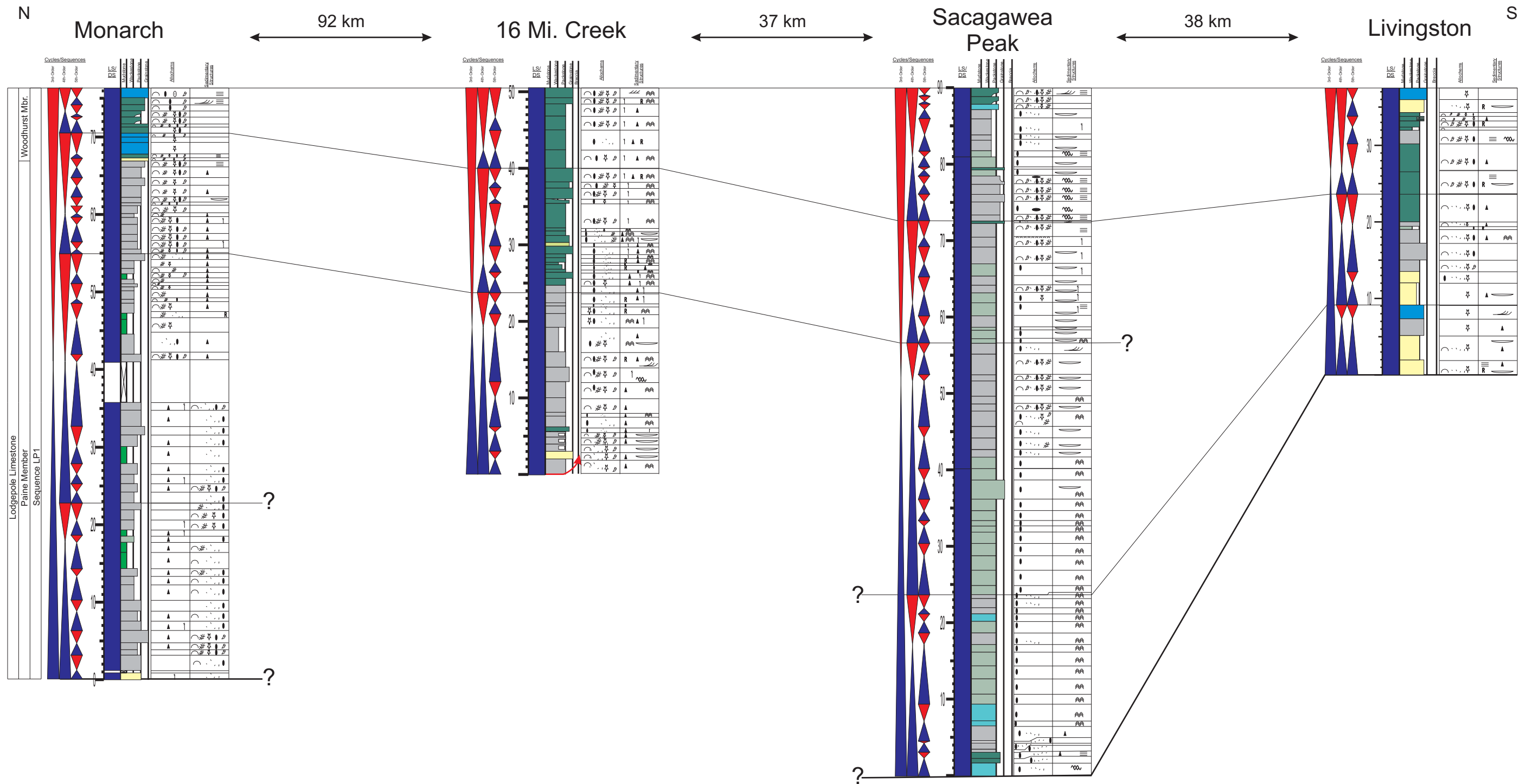


Figure 3.11: Correlation of 3rd- and 4th-order cycles and sequences within sequence LP1 across the central Montana trough. The sequence is observed to thicken to the north into the central Montana trough. 4th-order cycles can generally be correlated across this study area except in the 16 Mile Creek locality which is missing much of the lower part of the sequence due to truncation by faulting. Additionally a single 4th-order cycle is omitted from the most landward section at Livingston. Heavy lines mark 3rd-order sequence boundaries, while the thin lines mark 4th-order cycle boundaries. See Figures 3.1-3.2 for symbol and color keys.

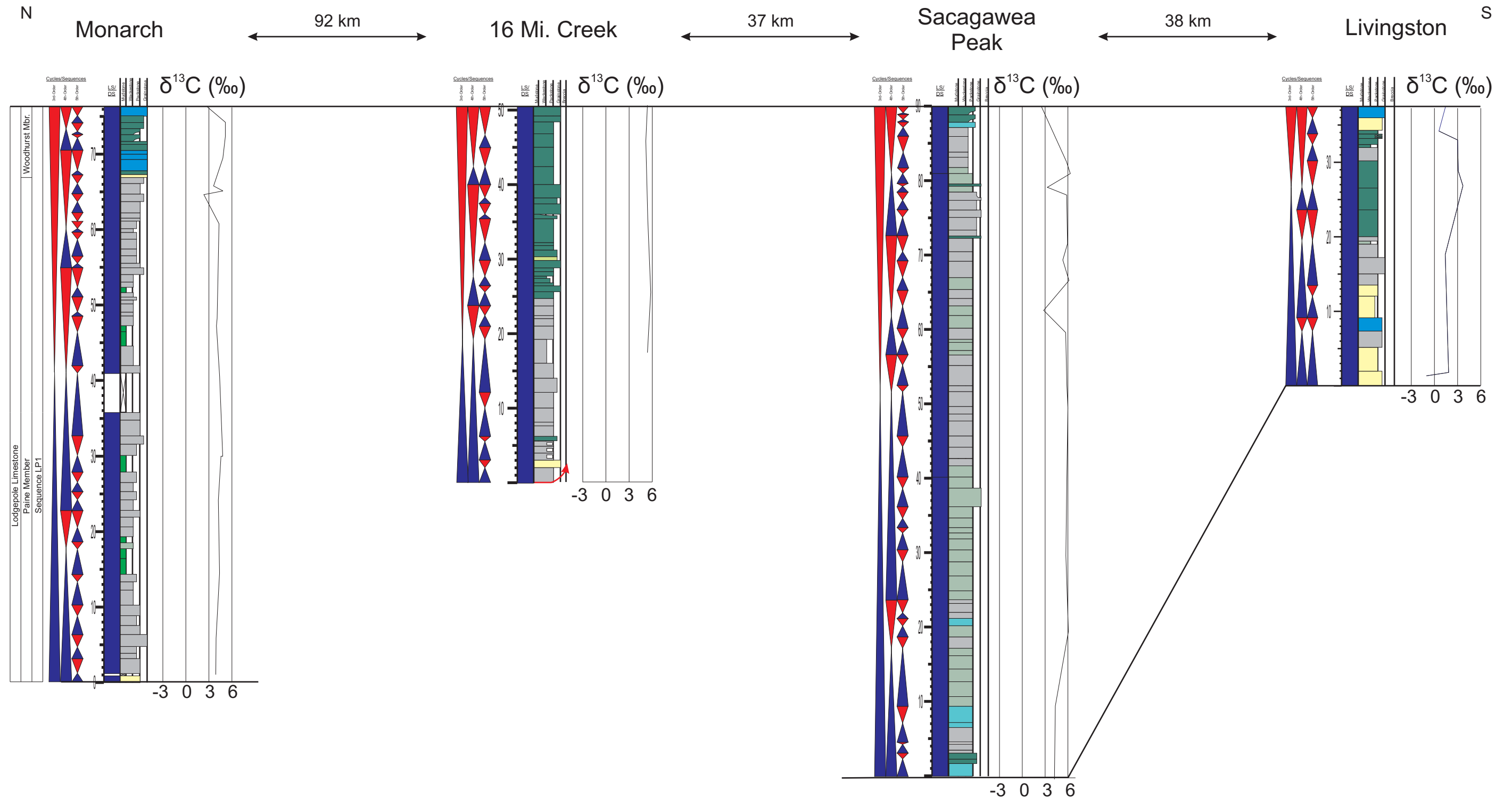


Figure 3.12: Correlation of sequence LP1 across the central Montana trough and associated carbon-13 values measured from the sections. The carbon isotopes are observed to increase from minimum values at the base of the sequence to maximum values near the MFS before returning to a minimum at the top of the sequence. Fault truncation of the lower most part of sequence LP1 at the 16 Mile Creek locality is apparent in the carbon isotope record, which begins near the maximum values for this section. Heavy lines mark 3rd-order sequence boundaries. See Figures 3.1-3.2 for symbol and color keys.

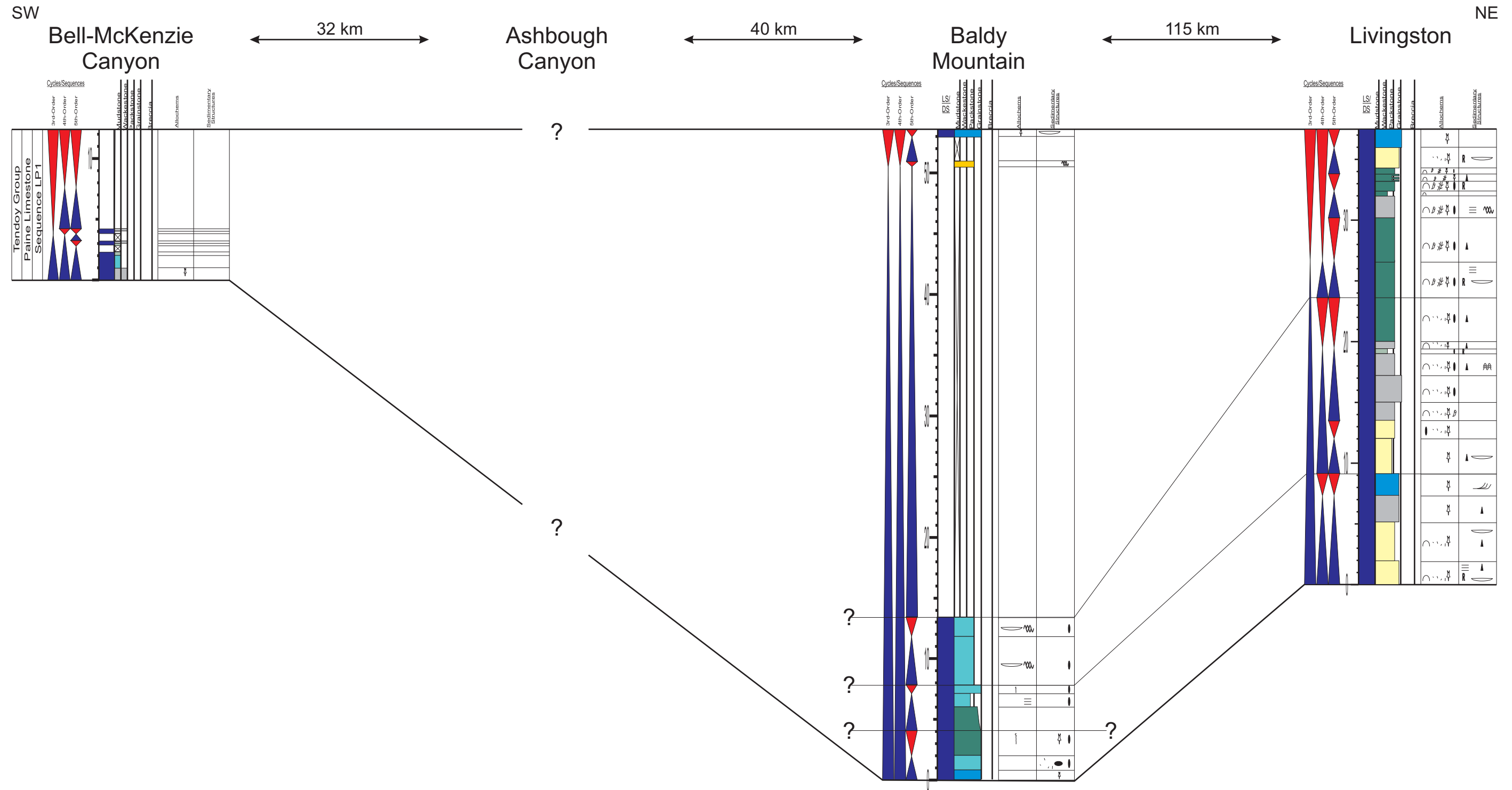


Figure 3.13: Correlation of 3rd- and 4th-order cycles and sequences within sequence LP1 across the southwest Montana. This sequence is observed to wedge basinward. 4th-order cycles are correlated between Baldy Mountain and Livingston; however, an expansive covered interval at the base of the section at Ashbough Canyon prevents further correlation downdip into the Antler foreland basin. Heavy lines mark 3rd-order sequence boundaries, while the thin lines mark 4th-order cycle boundaries. See Figures 3.1-3.2 for symbol and color keys.

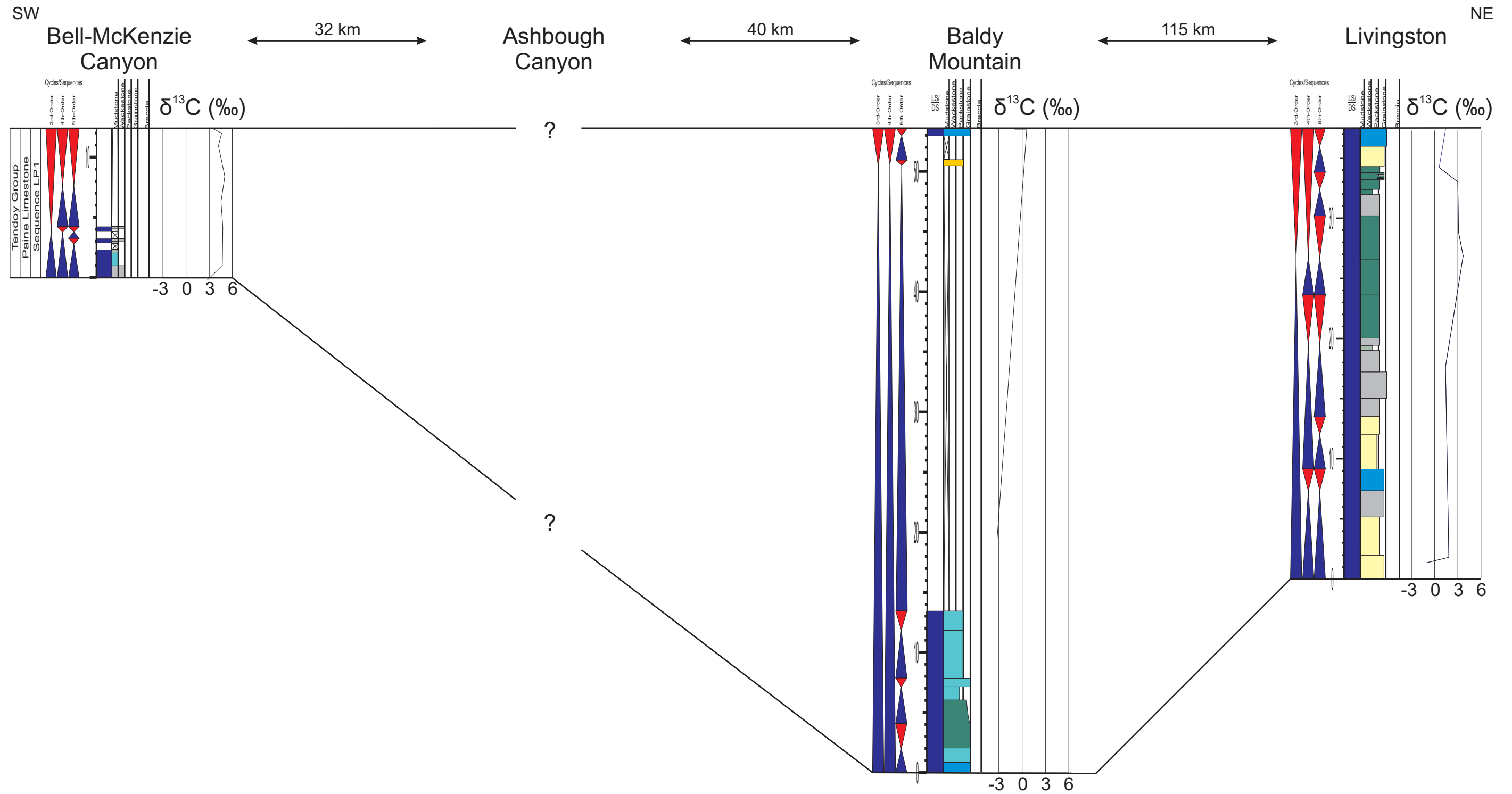


Figure 3.14: Correlation of sequence LP1 across southwest Montana showing carbon-13 isotope variation within the sequence. Carbon isotopes are observed to rise nearly 3 per mille from a minimum at the base of the sequence before falling to a minimum at the top of the sequence. Heavy lines mark 3rd-order sequence boundaries. See Figures 3.1-3.2 for symbol and color keys.

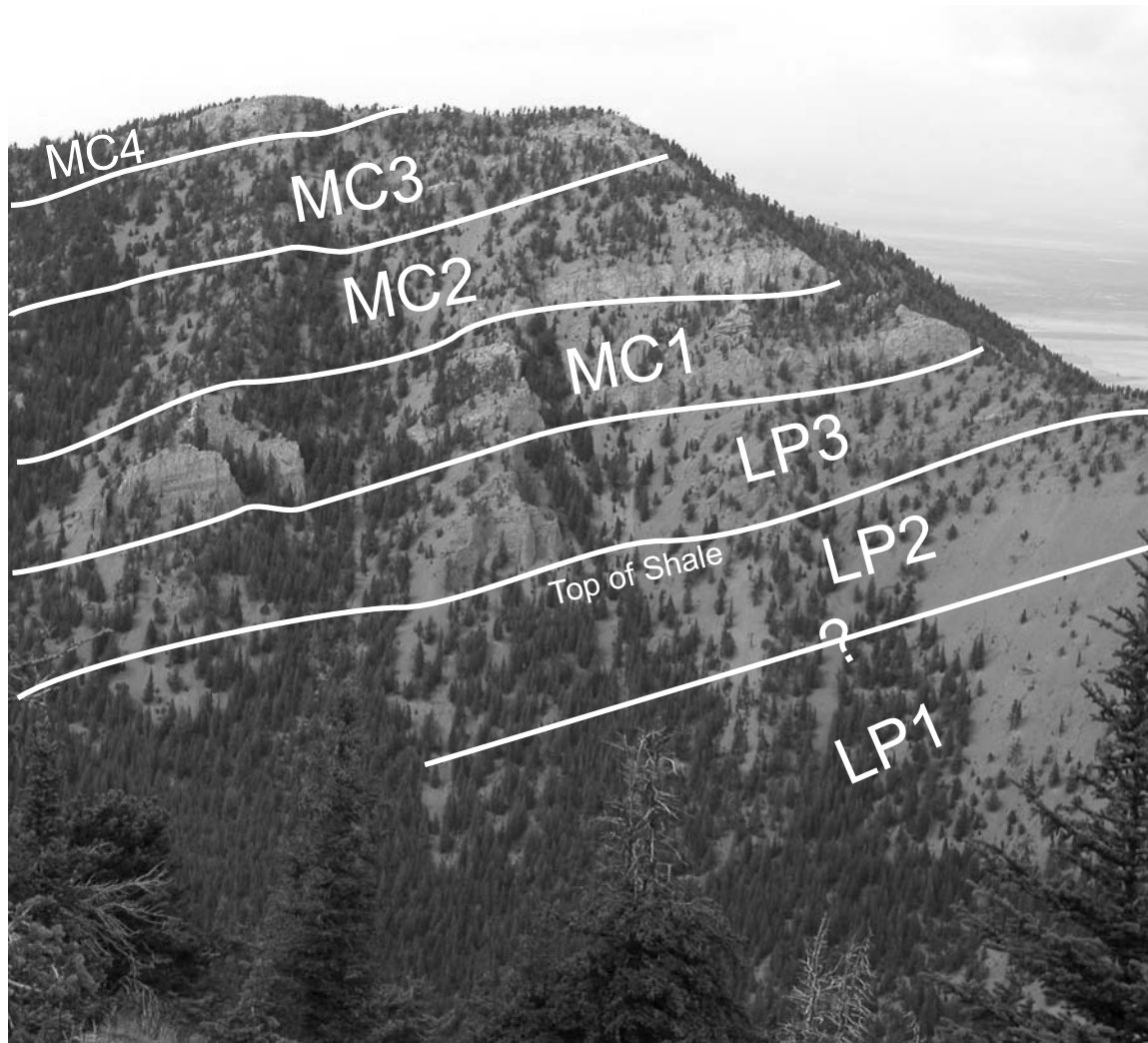


Figure 3.15: Outcrop photograph from Ashbough Canyon showing the Madison Group in this locality. Here approximately 40% of the Lower Mississippian section is a covered slope composed of shale with minor amounts of carbonate deposited during sequence LP1. The blue line marks the top of the shale and base of the HST of sequence LP2. This is in contrast to updip localities where only a few meters of the TST of LP1 are composed of shale. Field of view is approximate 500 m vertically.

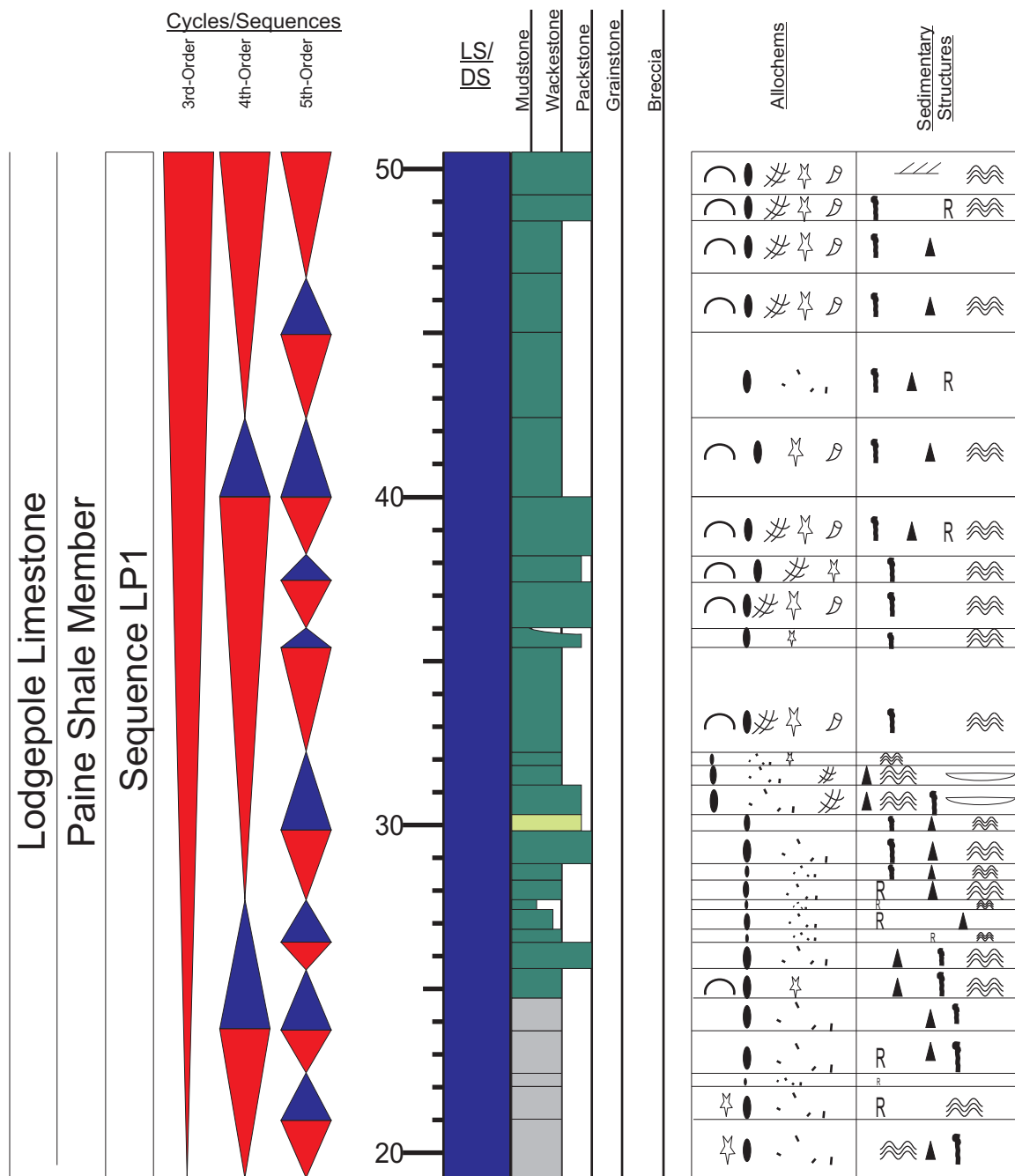


Figure 3.16: The graphic sedimentary log of the highstand systems tract of sequence LP1 from section location 16 Mile Creek within the central Montana trough. This section exhibits an overall pattern of decreasing argillaceous material, increasing skeletal material, and increasing grain size toward the top of the sequence. Additionally, this section exhibits a pattern of increasing amalgamation in the late highstand. Refer to Figures 3.1-3.2 for symbol definitions.

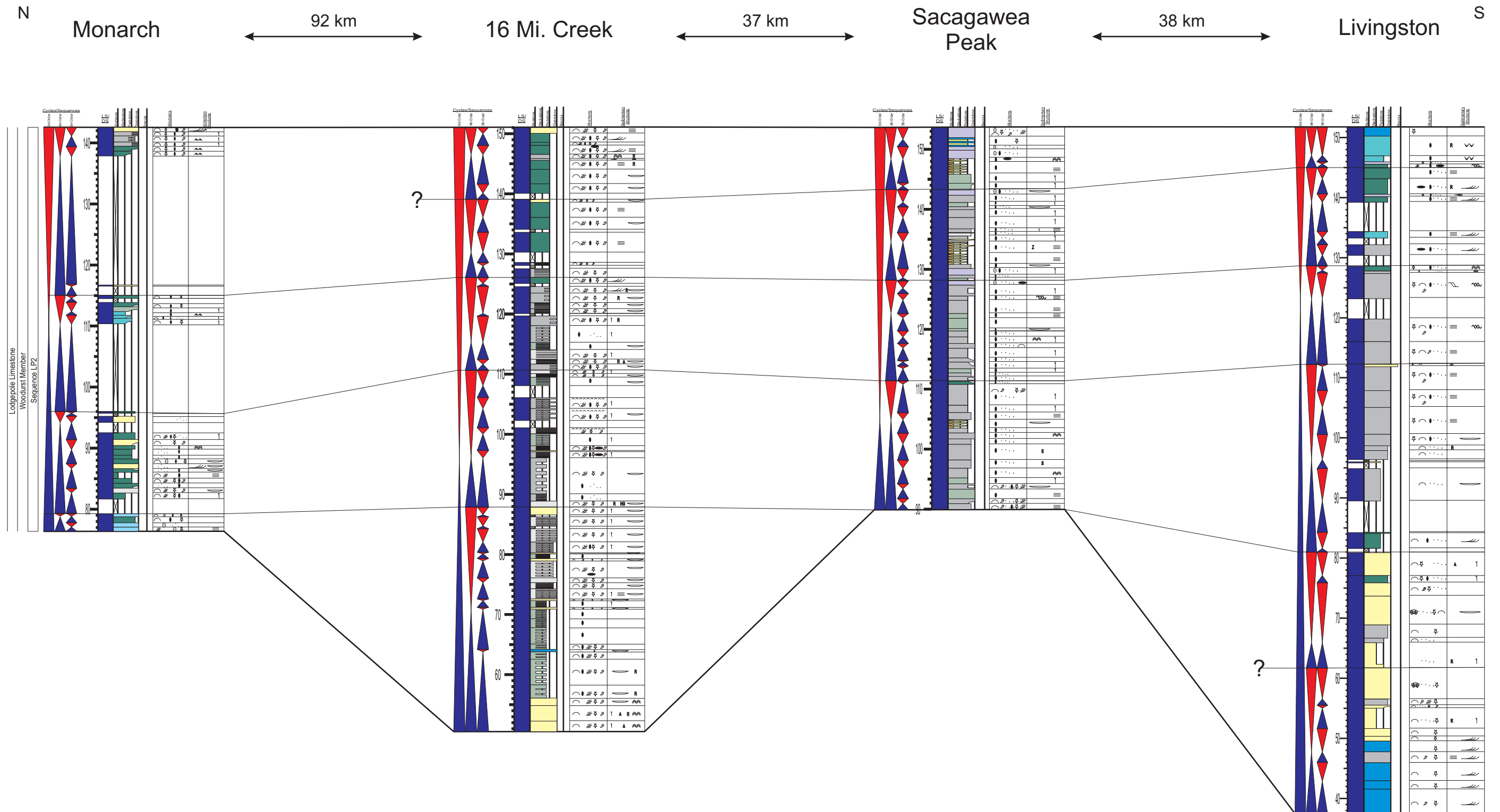


Figure 3.17: Correlation of 3rd- and 4th-order cycles and sequences within sequence LP2 across the central Montana trough. 4th-order cycles can generally be correlated across this study area with the exception of location Monarch where extensive covered intervals exist. Additionally a single basal 4th-order cycle is omitted from the section Sacagawea Peak. Heavy lines mark 3rd-order sequence boundaries, while the thin lines mark 4th-order cycle boundaries. See Figures 3.1-3.2 for symbol and color keys.

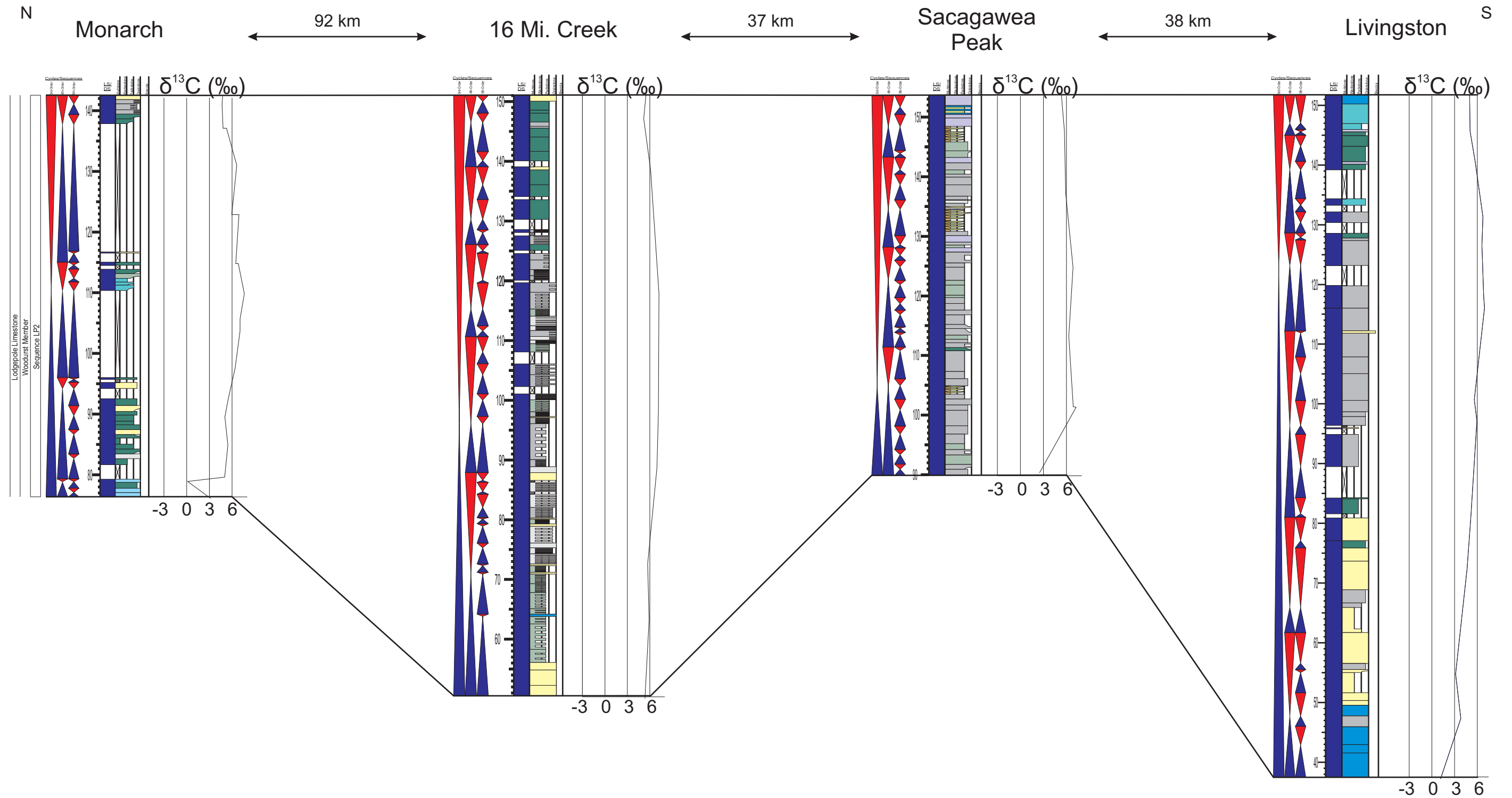


Figure 3.18: Correlation of sequence LP2 across the central Montana trough and associated carbon-13 isotopes values. Carbon isotope values are observed to trend from low values near the base of the sequence to maximum values, up to and exceeding +7‰ in some localities, near the MFS before falling to minimum values at or near the 3rd-order sequence boundary. Heavy lines mark 3rd-order sequence boundaries. See Figures 3.1-3.2 for symbol and color keys.

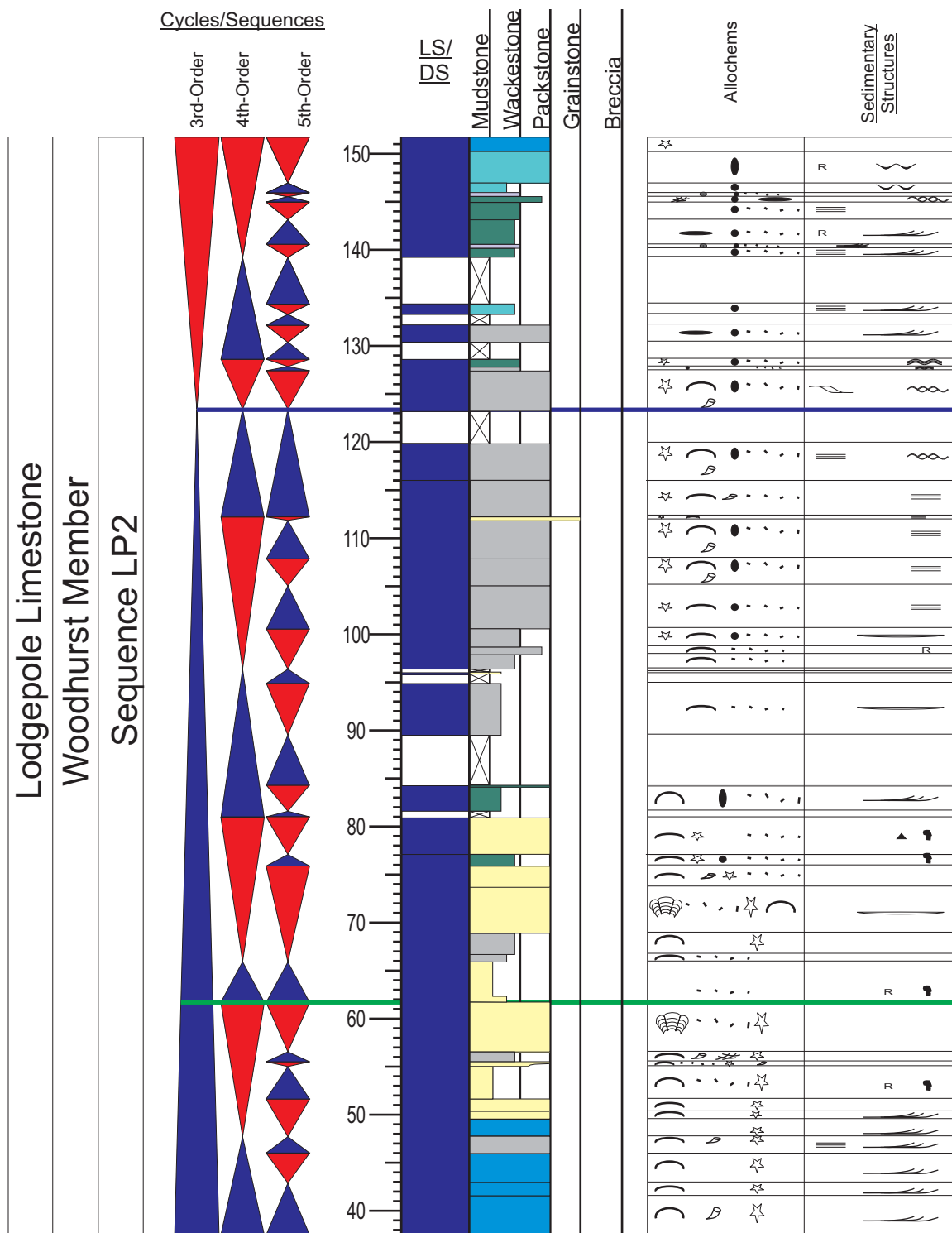


Figure 3.19: The graphic sedimentary log of the sequence LP2 from section location Livingston. This sequence is composed of a lowstand systems tract composed of a single fourth-order cycle, which is overlain by increasingly argillaceous wackestones-grainstones of the TST. The highstand is comprised of one and a half fourth-order cycles which show decreasing argillaceous composition and increasing evidence of traction deposition. Green line is the transgressive surface and the blue line is the maximum flooding surface. Refer to Figures 3.12-14 for symbol definitions.

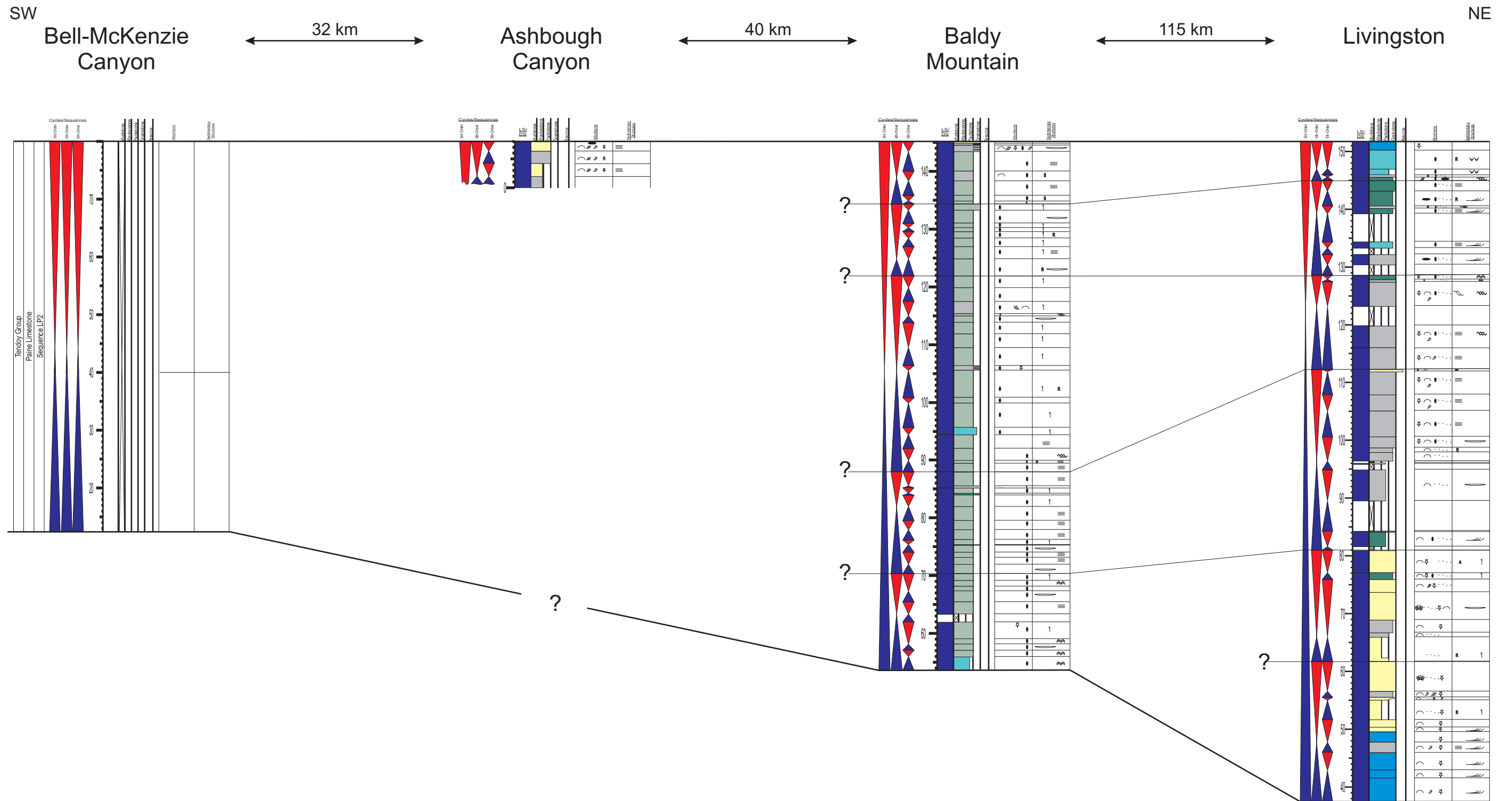


Figure 3.20: Correlation of 3rd- and 4th-order cycles and sequences within sequence LP2 across the southwest Montana. Most 4th-order cycles can be correlated from Livingston to Baldy Mountain; however, a single 4th-order cycle at the base of Livingston cannot unequivocally be correlated. Similar to sequence LP1, 4th-order cycles cannot be correlated further downdip because of a lack of exposure at Ashbough Canyon. Heavy lines mark 3rd-order sequence boundaries, while the thin lines mark 4th-order cycle boundaries. See Figures 3.1-3.2 for symbol and color keys.

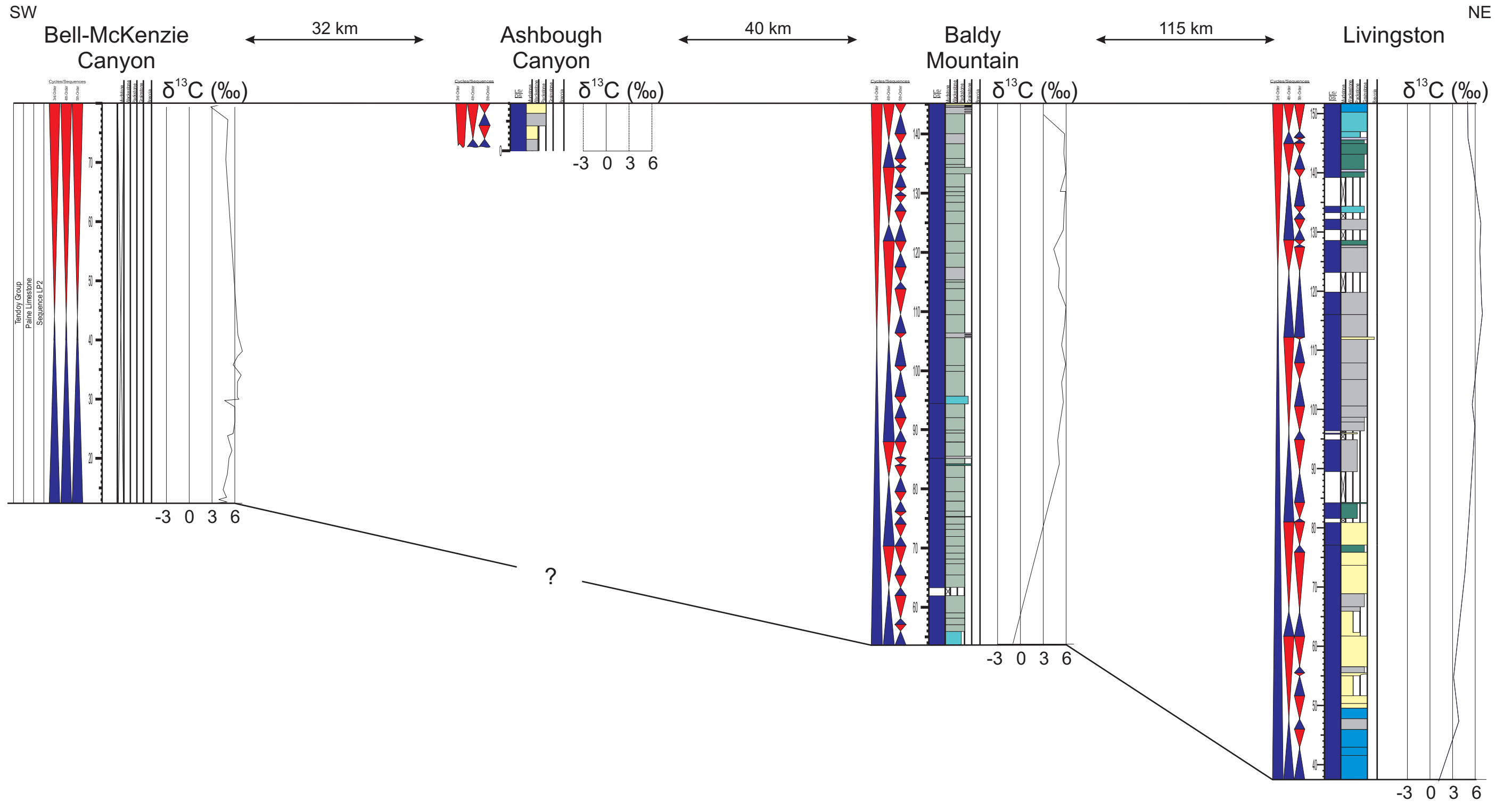


Figure 3.21: Correlation of sequence LP2 across the southwest Montana with accompanying carbon-13 isotope curves for each measured section. Similar to sequence LP1 in southwest Montana and sequences LP1 and LP2 in central Montana, isotope values are observed increased from minima at the basal sequence boundary to maxima near the MFS and return to minimum values at the top of the sequence. Heavy lines mark 3rd-order sequence boundaries. See Figures 3.1-3.2 for symbol and color keys.

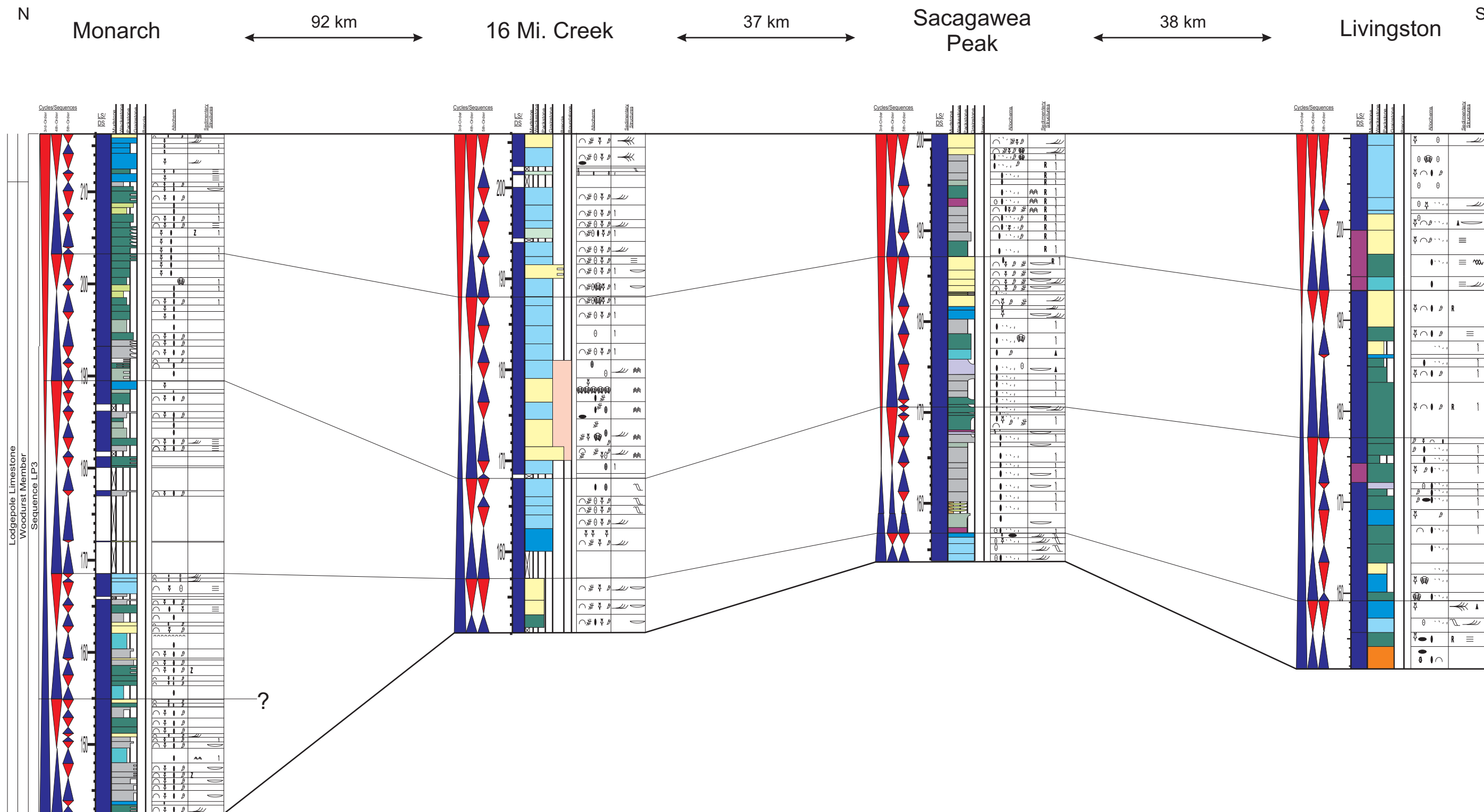


Figure 3.22: Correlation of 3rd- and 4th-order cycles and sequences within sequence LP3 across the central Montana trough. 4th-order cycles can generally be correlated across this study area with the exception of location Monarch which displays an additional 4th-order depositional cycle near the base of the sequence. Heavy lines mark 3rd-order sequence boundaries, while the thin lines mark 4th-order cycle boundaries. See Figures 3.1-3.2 for symbol and color keys.

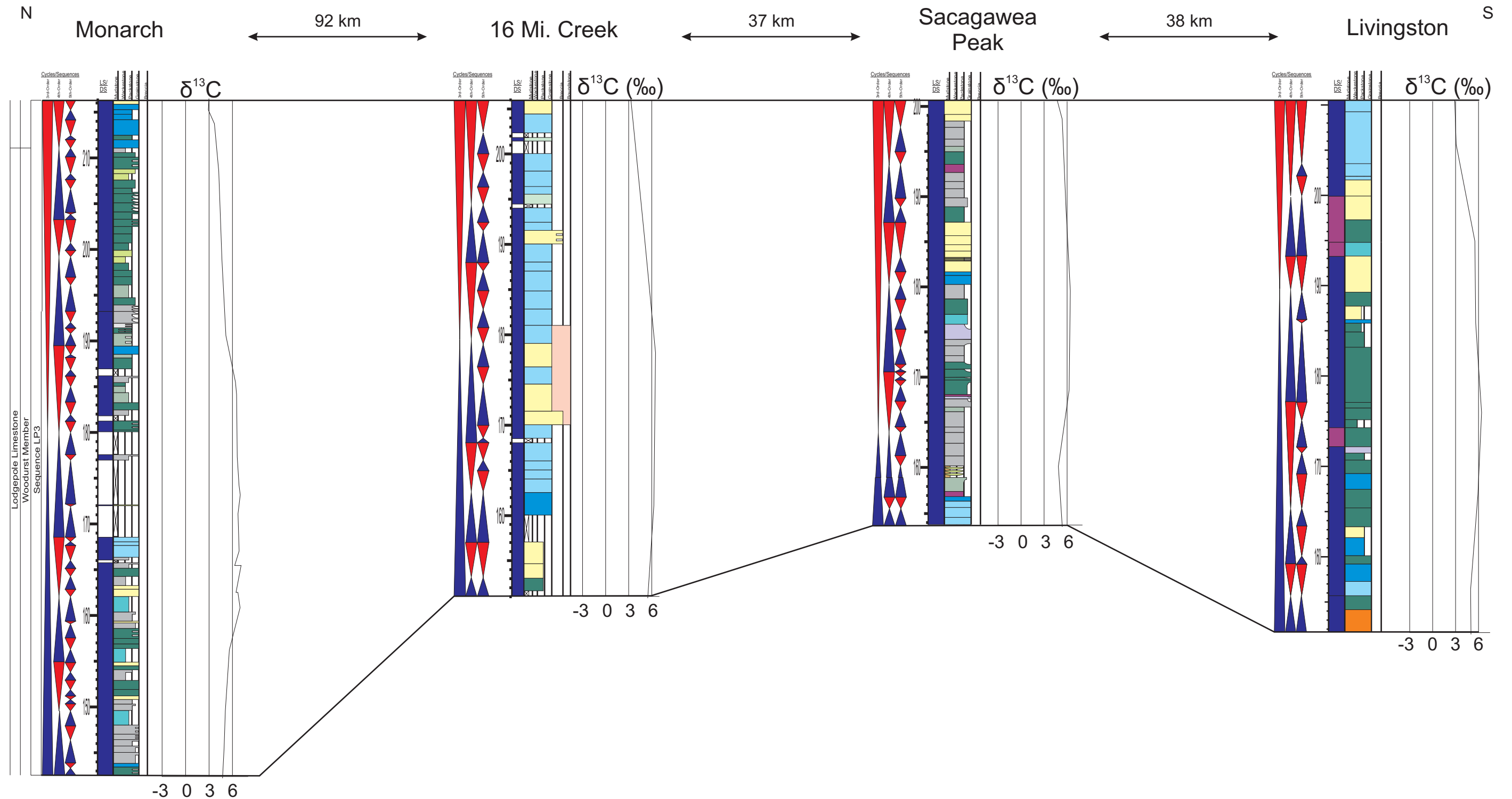


Figure 3.23: Correlation of sequence LP3 across the central Montana trough shown here with accompanying carbon-13 isotope values from the associated outcrop localities. Like other Lodgepole sequences, a trend is observed where C-isotope values rise from minima at the base of the sequence to maxima at or near the MFS of the sequence before falling to minima again at the top of the sequence. In these localities, minima are typically near 3‰ while maxima generally exceed 6‰. Heavy lines mark 3rd-order sequence boundaries. See Figures 3.1-3.2 for symbol and color keys.

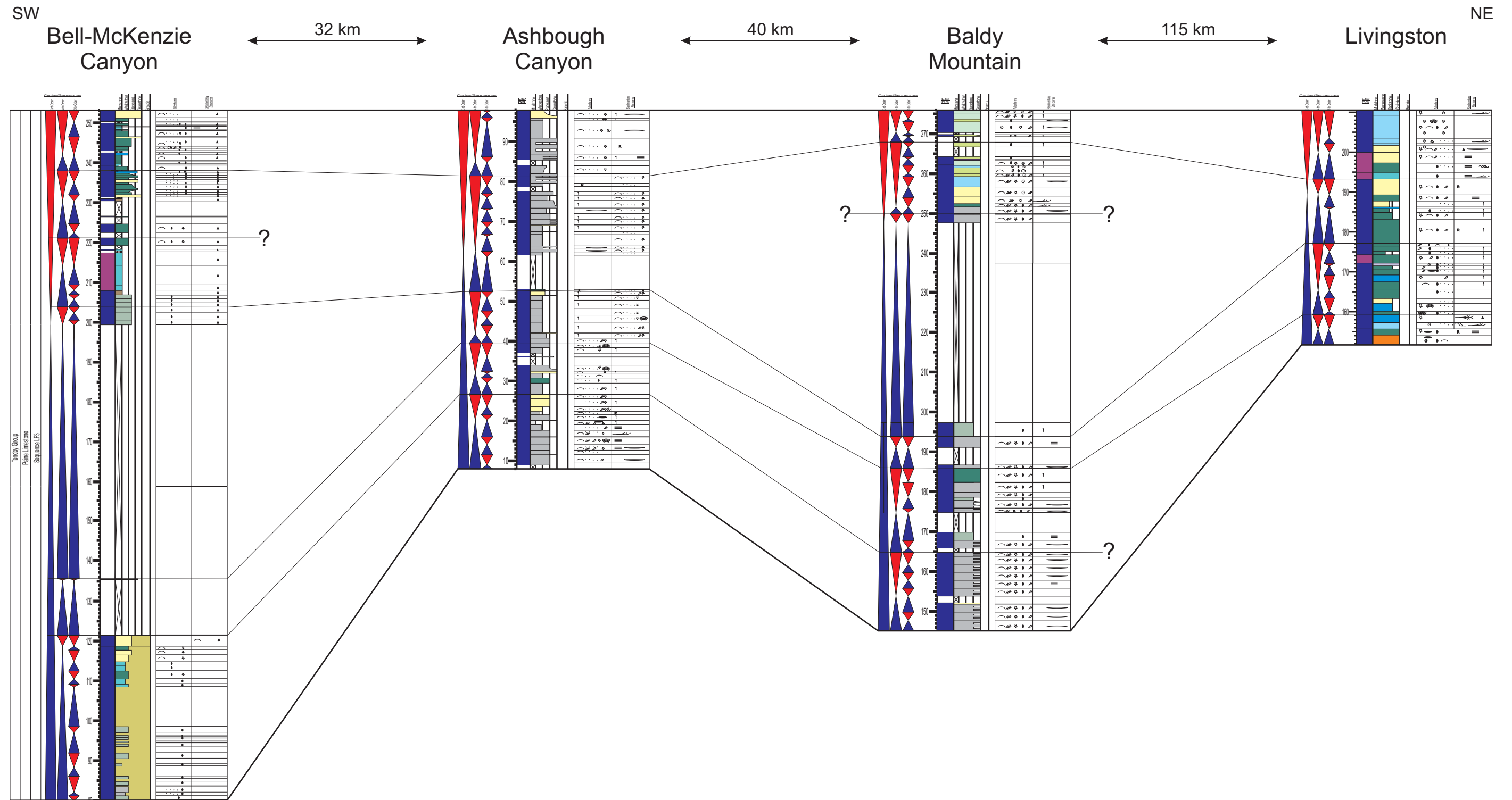


Figure 3.24: Correlation of 3rd- and 4th-order cycles and sequences within sequence LP3 across the southwest Montana. 4th-order cycles are correlated across this study area except in the intervals near the maximum flooding surface, where extensive covered intervals make correlation difficult. Additionally two 4th-order cycles are omitted from the most landward section at Livingston. Heavy lines mark 3rd-order sequence boundaries, while the thin lines mark 4th-order cycle boundaries. See Figures 3.1-3.2 for symbol and color keys.

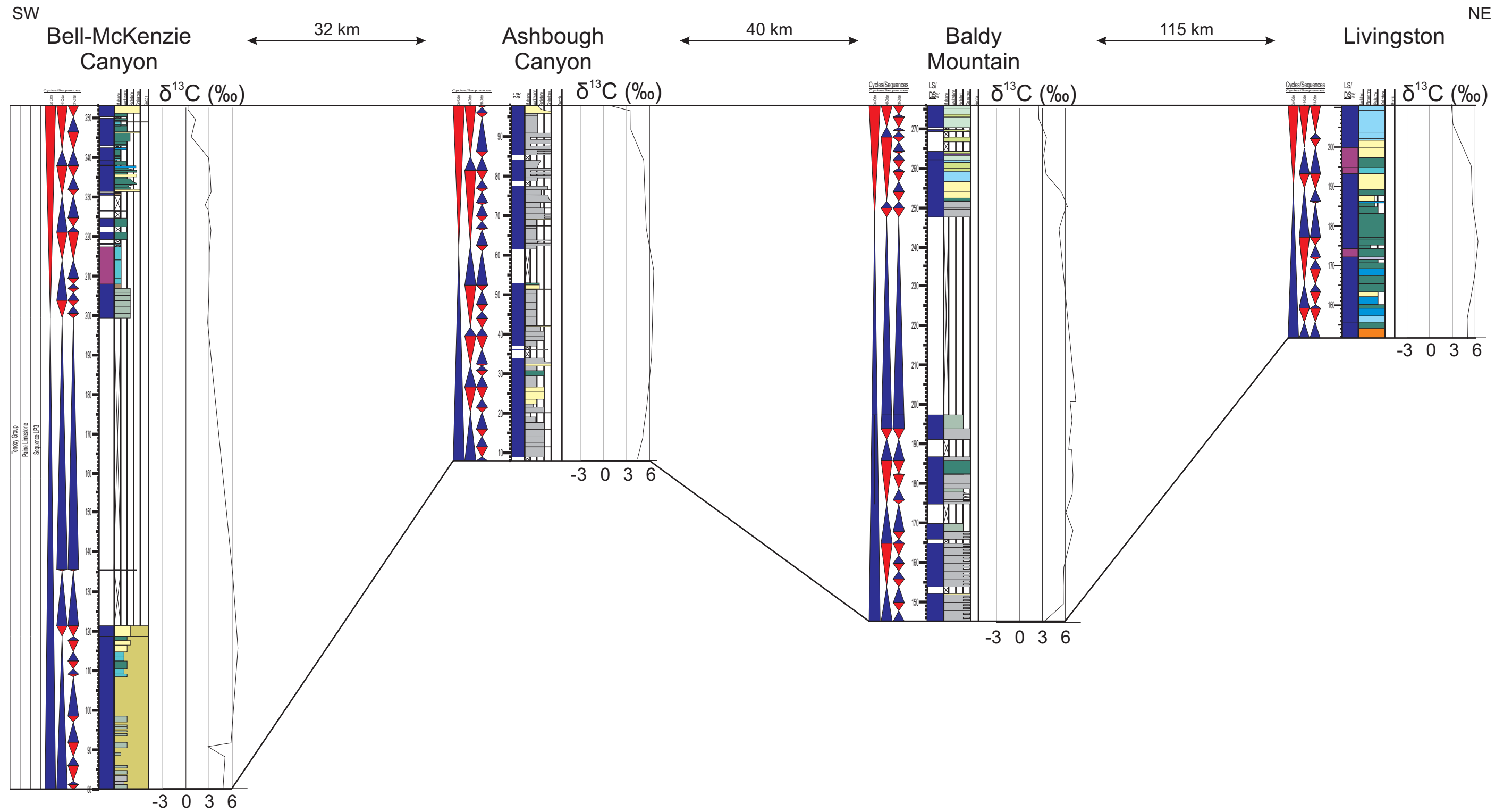


Figure 3.25: Correlation of sequence LP3 across the southwest Montana with associated carbon-13 isotope values. Carbon isotope values are observed to trend from minima of approximately +3‰ near the bas of the sequence, rising to maxima of ~+6‰ near the MFS of the sequence, before falling to $\leq +3\%$. Heavy lines mark 3rd-order sequence boundaries. See Figures 3.1-3.2 for symbol and color keys.

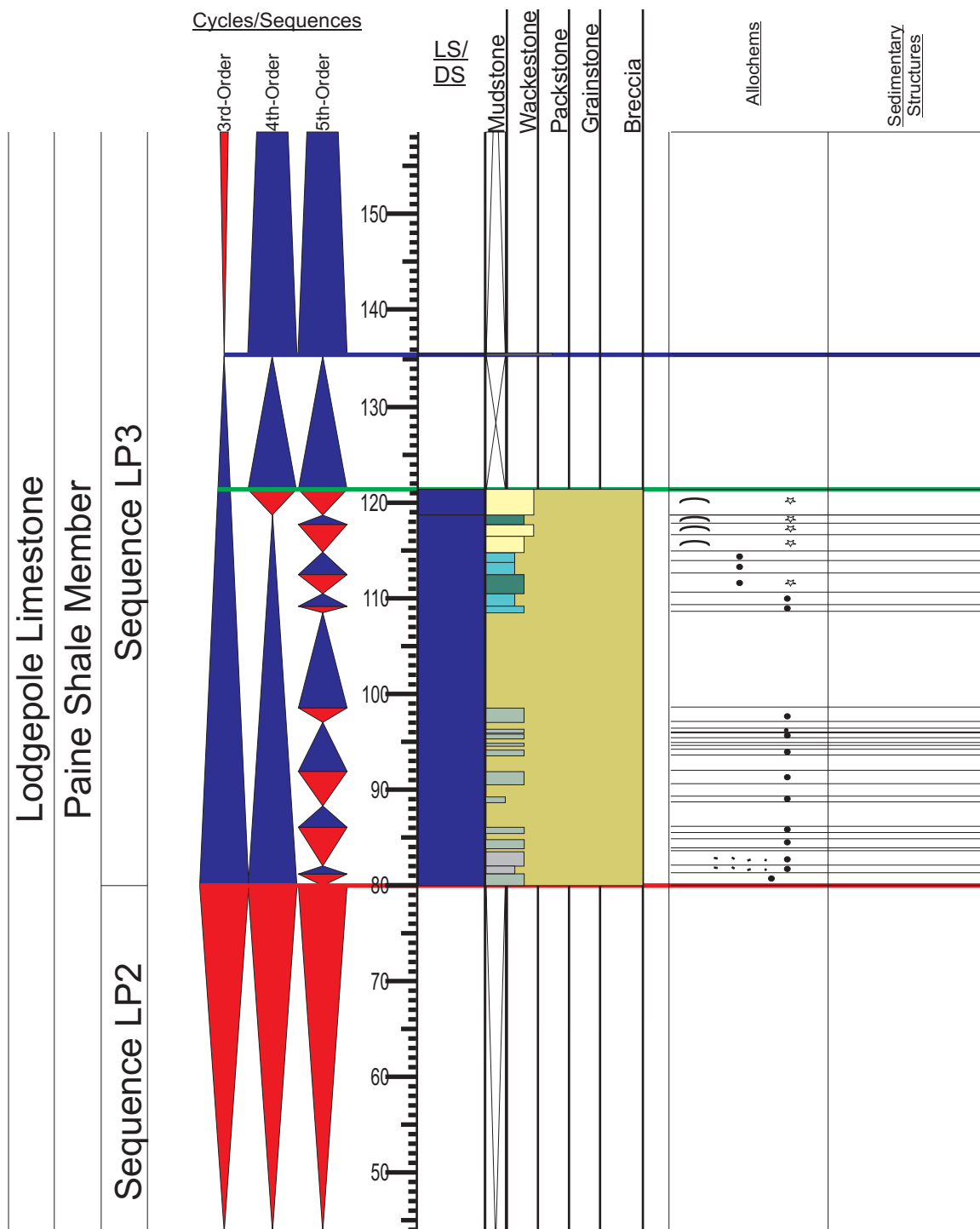


Figure 3.26: The graphic sedimentary log of the sequences LP2 and LP3 from section location Bell-Mckenzie Canyons. Sequence LP3 is composed of a lowstand systems tract made up of a single fourth-order cycle composed of a 53 m-thick accumulation of polymict conglomerate and laterally equivalent in situ calcisilt deposits (both shown). Green line is the transgressive surface, the blue line is the maximum flooding surface, and the red line is the sequence boundary. Refer to Figures 3.12-14 for symbol definitions.

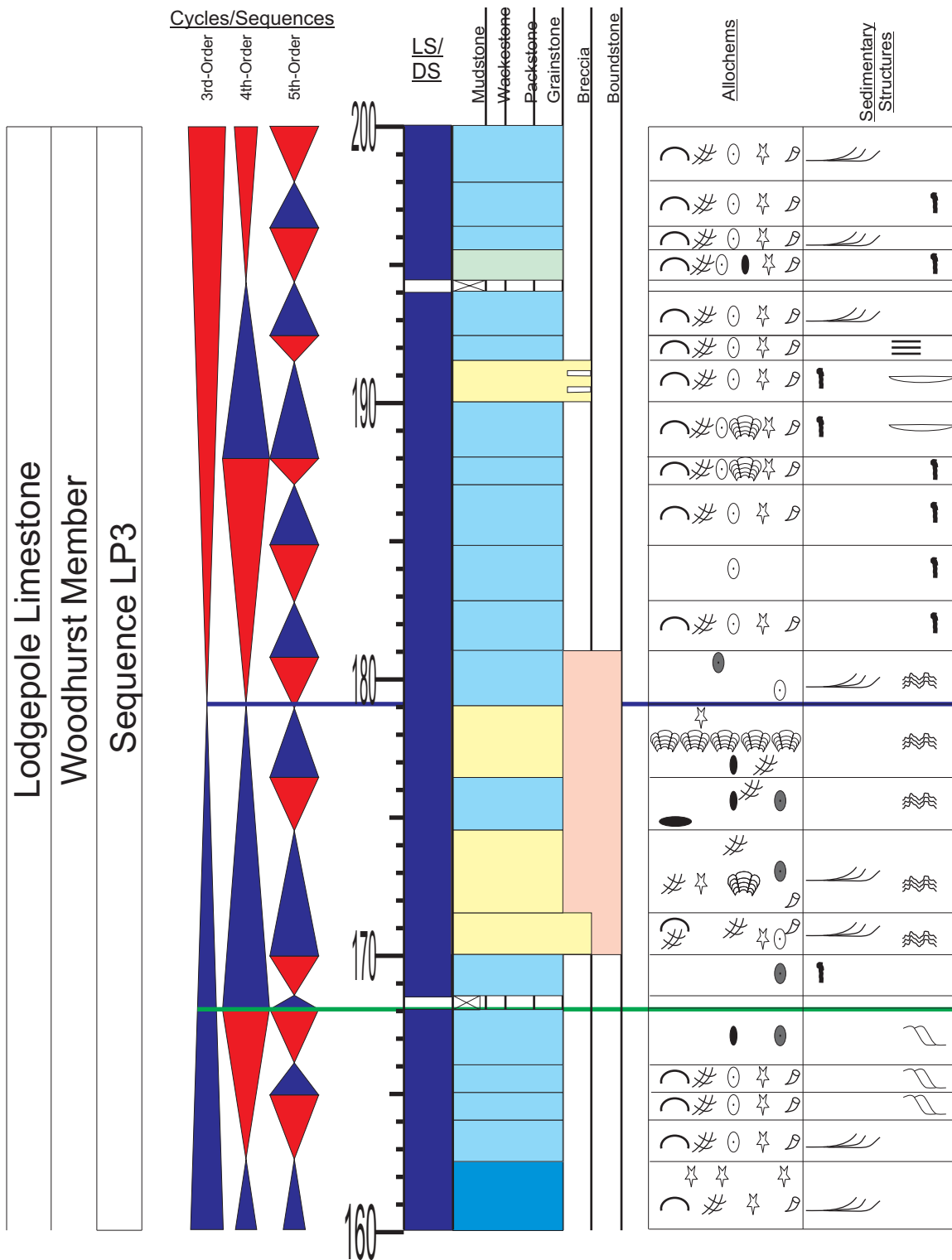


Figure 3.27: The graphic sedimentary log of the sequence LP3 from section location 16 Mile Creek. Sequence LP3 is made up of a lowstand systems tract composed of a single fourth-order cycle composed of trough cross-bedded crinoidal grainstones and oolitic sandwaves. These deposits are overlain by microbial/tabulate coral boundstone (pink). Green line is the transgressive surface, and the blue line is the maximum flooding surface. Refer to Figures 3.12-14 for symbol definitions.

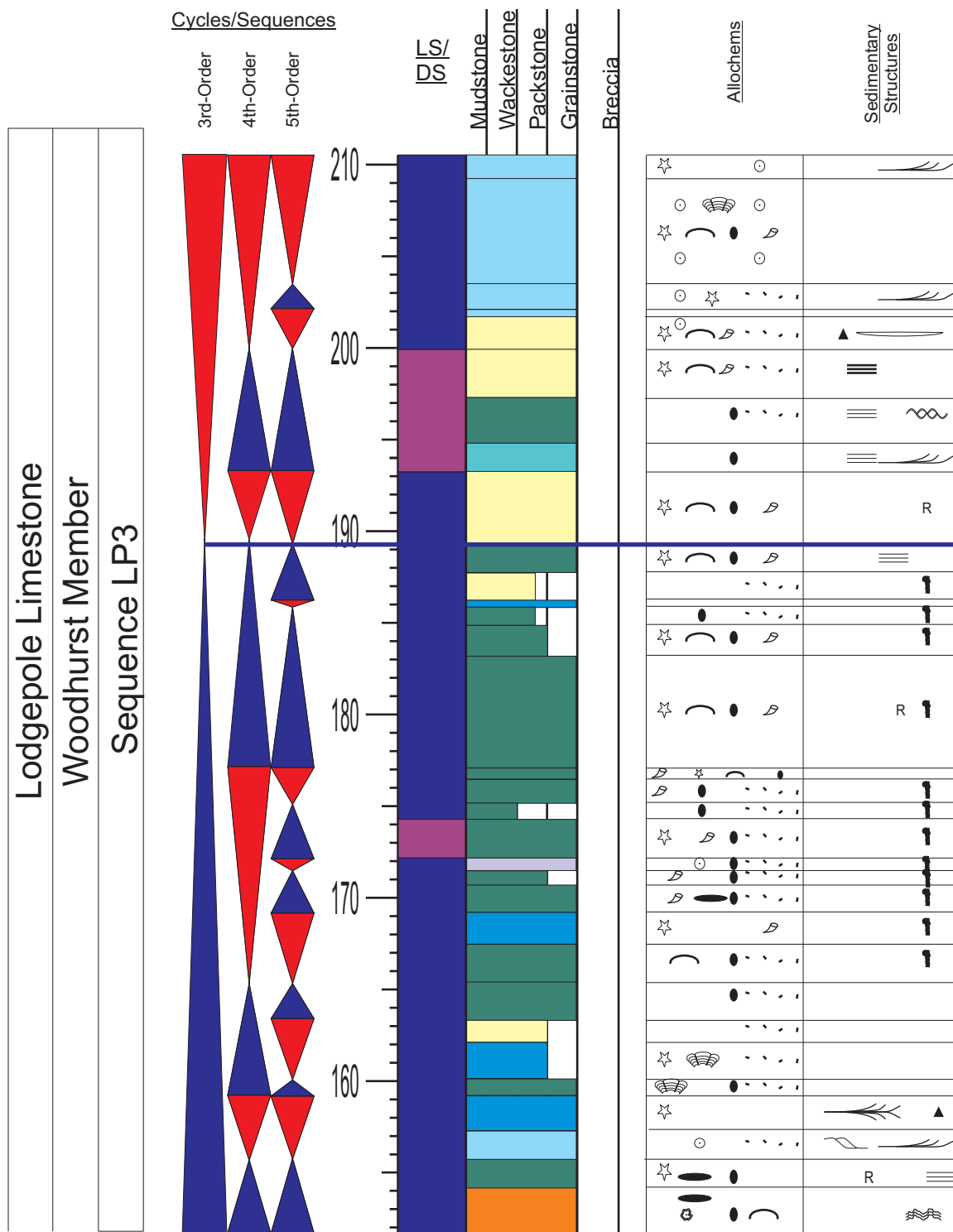


Figure 3.28: The graphic sedimentary log of the sequence LP3 from section location Livingston. The highstand systems tract of Sequence LP3 is composed predominantly by trough cross-bedded oolitic grainstones and increasingly dolomitized skeletal grainstones. The blue line is the maximum flooding surface. Refer to Figures 3.12-14 for symbol definitions.

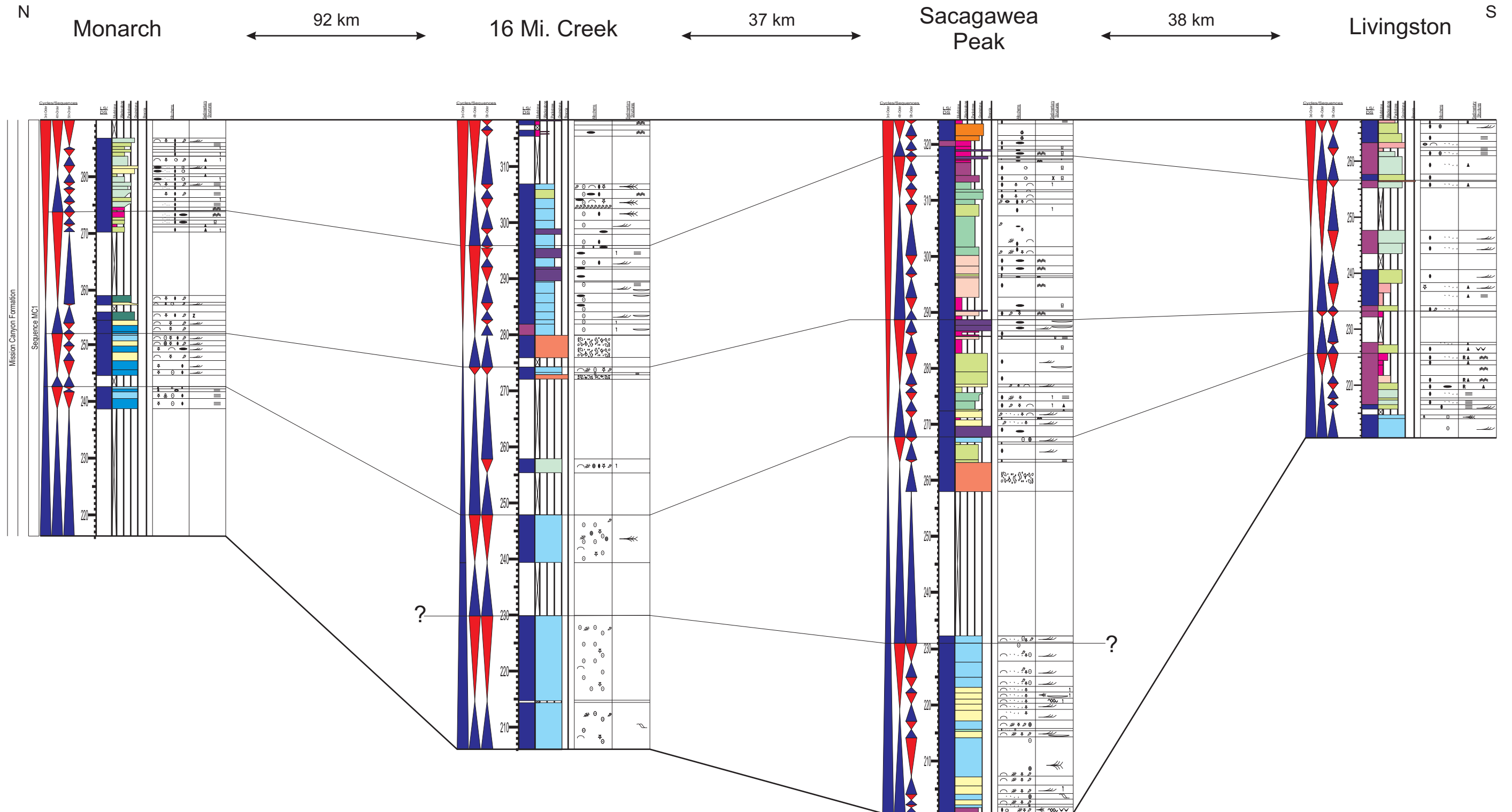


Figure 3.29: Correlation of 3rd- and 4th-order cycles and sequences within sequence MC1 across the central Montana trough. 4th-order cycles can generally be correlated across this study area. Additionally a single 4th-order cycle is omitted from the most landward section at Livingston and at location Monarch along the northern margin of the central Montana trough. Heavy lines mark 3rd-order sequence boundaries, while the thin lines mark 4th-order cycle boundaries. See Figures 3.1-3.2 for symbol and color keys.

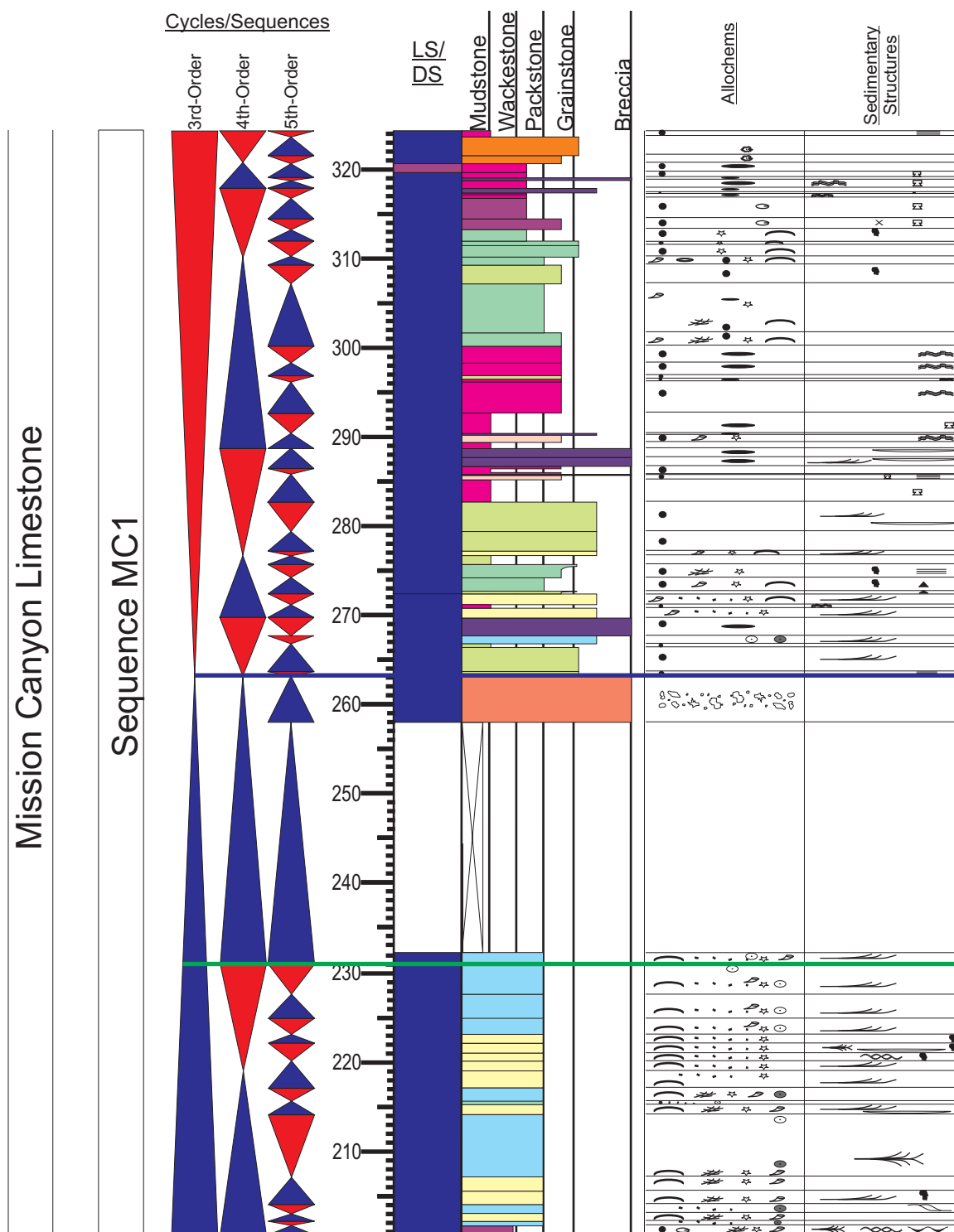


Figure 3.30: The graphic sedimentary log of the sequence MC1 from section location Sacagawea Peak. The lowstand systems tract is composed of stack oolitic and skeletal grainstone shoals. The TST, which overlies these shoals, is predominantly poorly exposed evaporite solution collapse breccia. The highstand systems tract is made up of muddier-textured lagoonal facies and algal laminites. The green line is transgressive surface and the blue line is the maximum flooding surface. Refer to Figures 3.12-14 for symbol definitions.

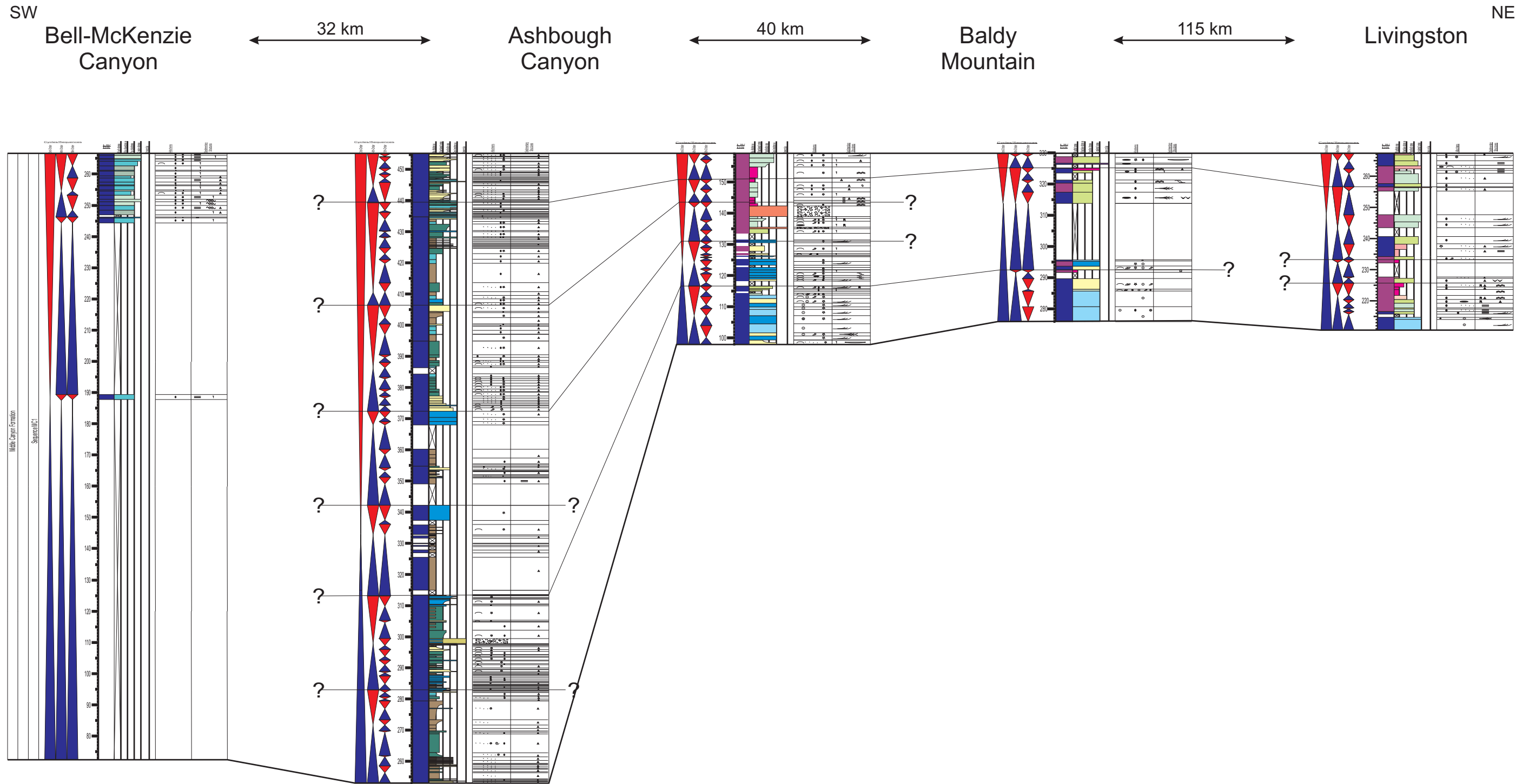


Figure 3.31: Correlation of 3rd- and 4th-order cycles and sequences within sequence MC1 across southwestern Montana and into the Antler foreland basin. The relationship between 4th-order cycles is less clear during this sequence than earlier sequence. The best correlation occurs between Bell-McKenzie and Ashbough Canyons, although significant omissions of sequences does occur at Ashbough Canyon. Additionally, correlation of cycles is inhibited by extensive covered intervals at Baldy Mountain and Copper Mountain. Heavy lines mark 3rd-order sequence boundaries, while the thin lines mark 4th-order cycle boundaries. See Figures 3.1-3.2 for symbol and color keys.

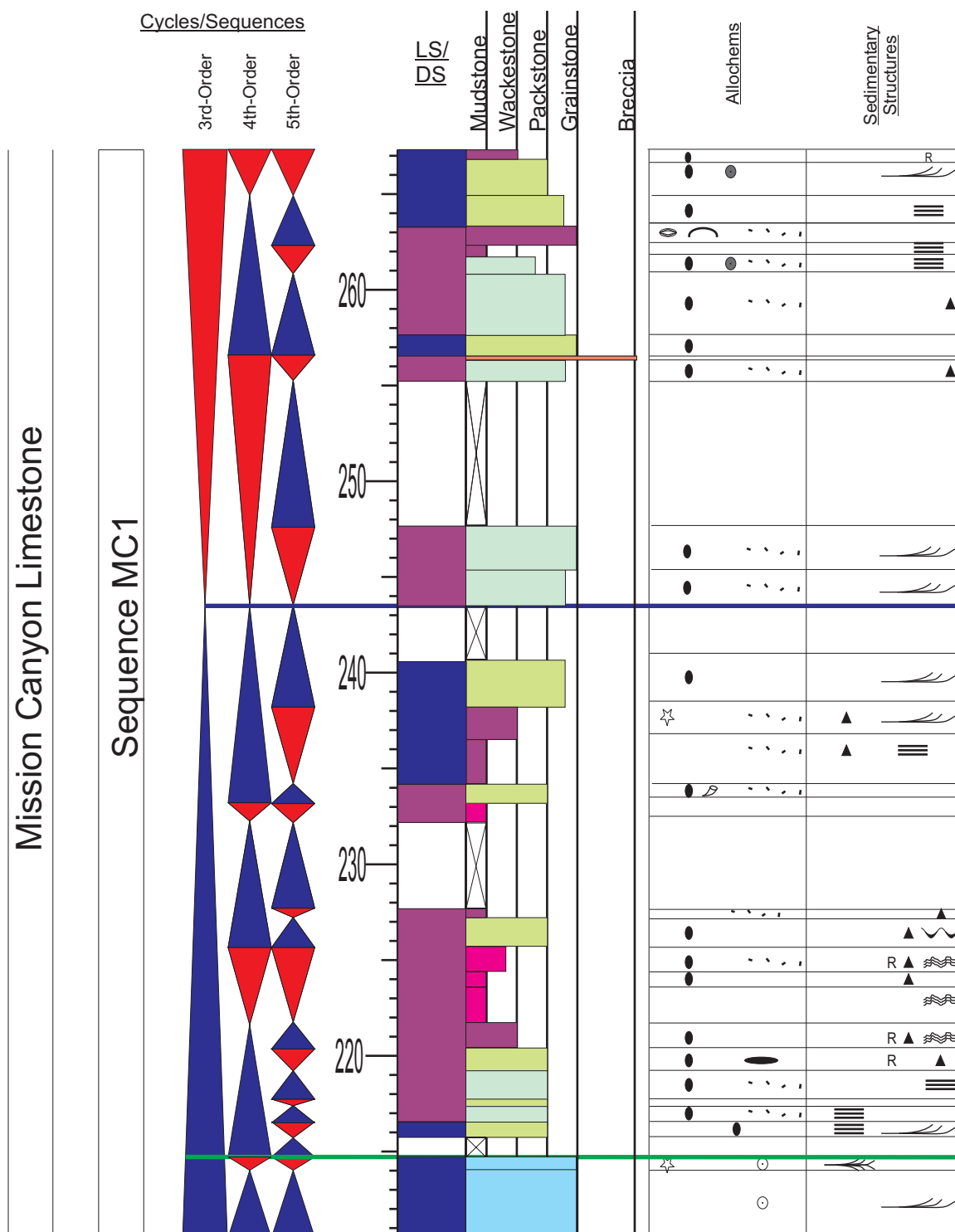


Figure 3.32: The graphic sedimentary log of the sequence MC1 from section location Livingston. The lowstand systems tract of this sequence is made up of oolitic grainstone, while the TST is dominated by muddying-upward cycles of dolomitic lagoonal mudstone-packstones. The highstand systems tract is composed of dolomitized mudstones-grainstone cycles. The green line is the transgressive surface and the blue line is the maximum flooding surface. Refer to Figures 3.12-14 for symbol definitions.



Figure 3.33: Outcrop photograph from section location Monarch sequence MC2, showing an occurrence of evaporite dissolution collapse breccia. Here the breccia sharply overlies carbonates of lagoonal affinity, and the contact between these two units is flat and regular, indicative of the strataform nature of the contact. The staff on the right of the photo (circled) is 1.6 m high.

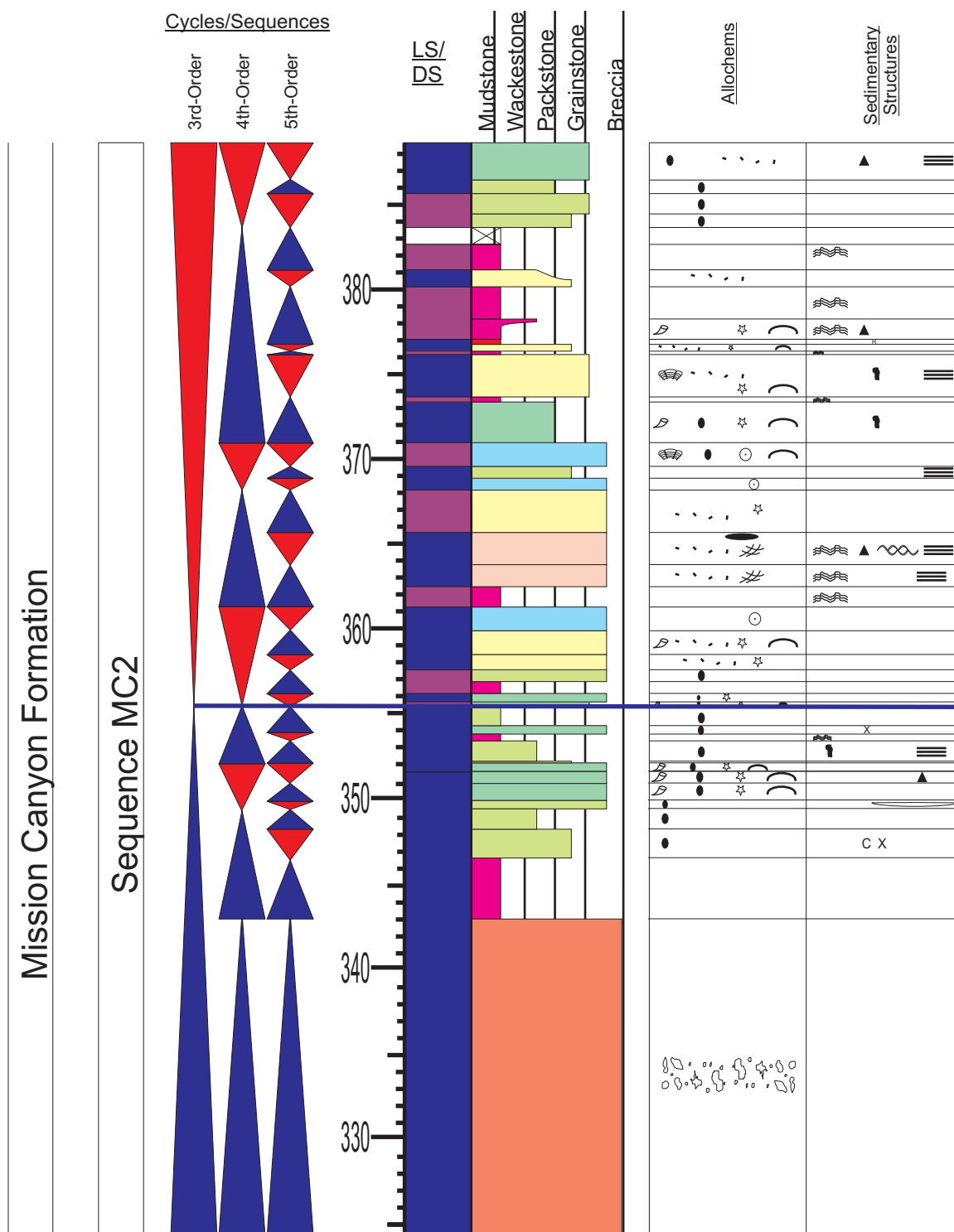


Figure 3.34: The graphic sedimentary log of the sequence MC2 from section location Sacagawea Peak. The TST is dominated by approximately 19 m of evaporite solution collapse breccia, which is overlain algal laminites and peloidal packstones and peloidal and skeletal packstones-grainstones. The highstand systems tract is made up of minor skeletal and oolitic grainstone shoals as well as algal laminites and muddier, partly dolomitized, restricted facies of lagoonal affinity. The blue line is the maximum flooding surface. Refer to Figures 3.12-14 for symbol definitions.

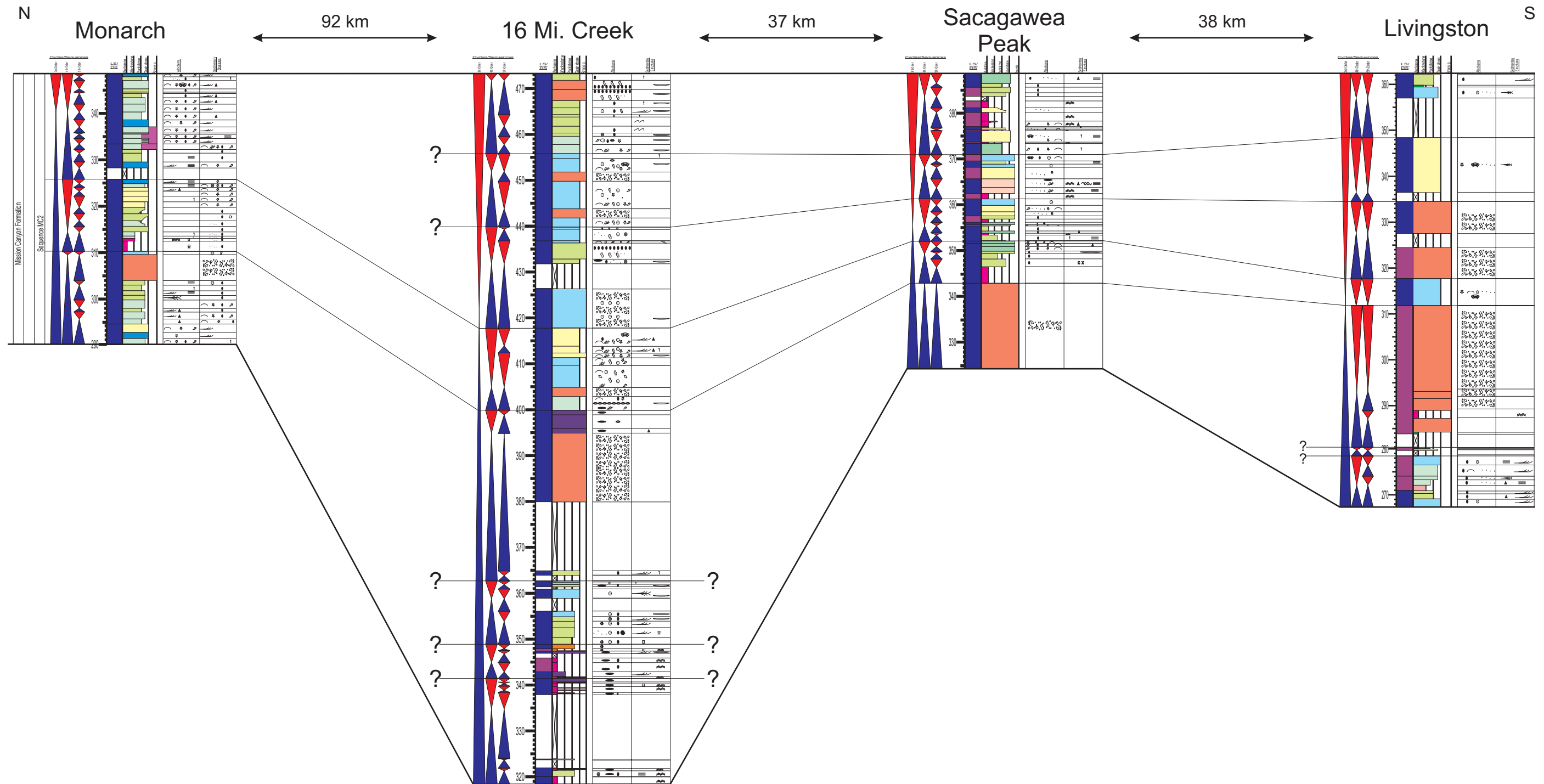


Figure 3.35: Correlation of 3rd- and 4th-order cycles and sequences within sequence MC2 across the central Montana trough. 4th-order cycles can generally be correlated across this study area except between 16 Mile Creek and Monarch, because of expanded section at the 16 Mile Creek locality in the HST. Additionally, cycles at the base of the sequence are only identified locally because of extensive breccia at this time, which obscures the original sequence stratigraphy. Heavy lines mark 3rd-order sequence boundaries, while the thin lines mark 4th-order cycle boundaries. See Figures 3.1-3.2 for symbol and color keys.

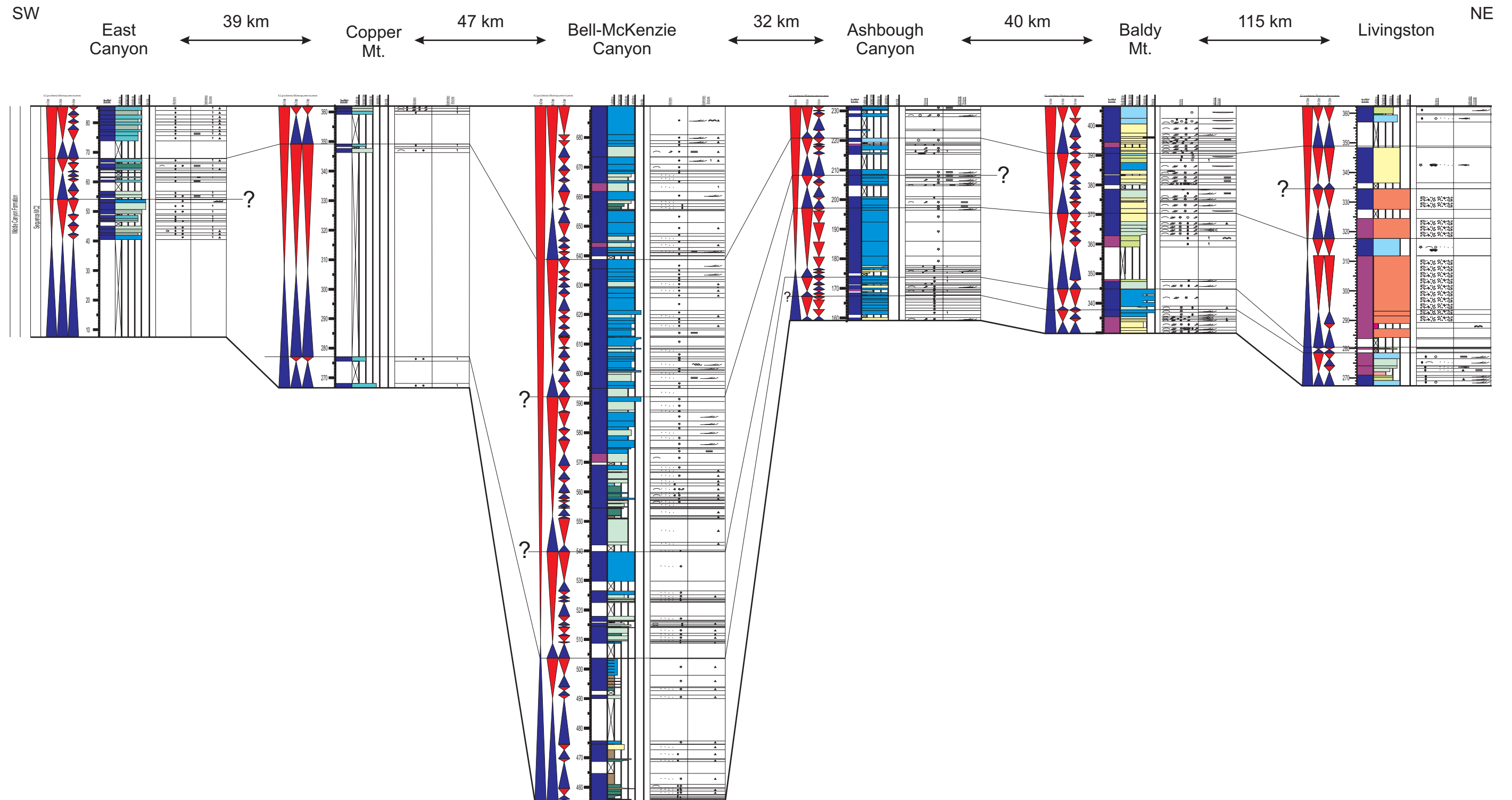


Figure 3.36: Correlation of 3rd- and 4th-order cycles and sequences within sequence MC2 across southwestern Montana and into the Antler foreland basin. 4th-order cycles can generally be correlated across this study area as far downdip as Bell-McKenzie Canyon. At this location, greatly expanded section during this sequence makes correlation of updip and downdip strata tenuous. Heavy lines mark 3rd-order sequence boundaries, while the thin lines mark 4th-order cycle boundaries. See Figures 3.1-3.2 for symbol and color keys.

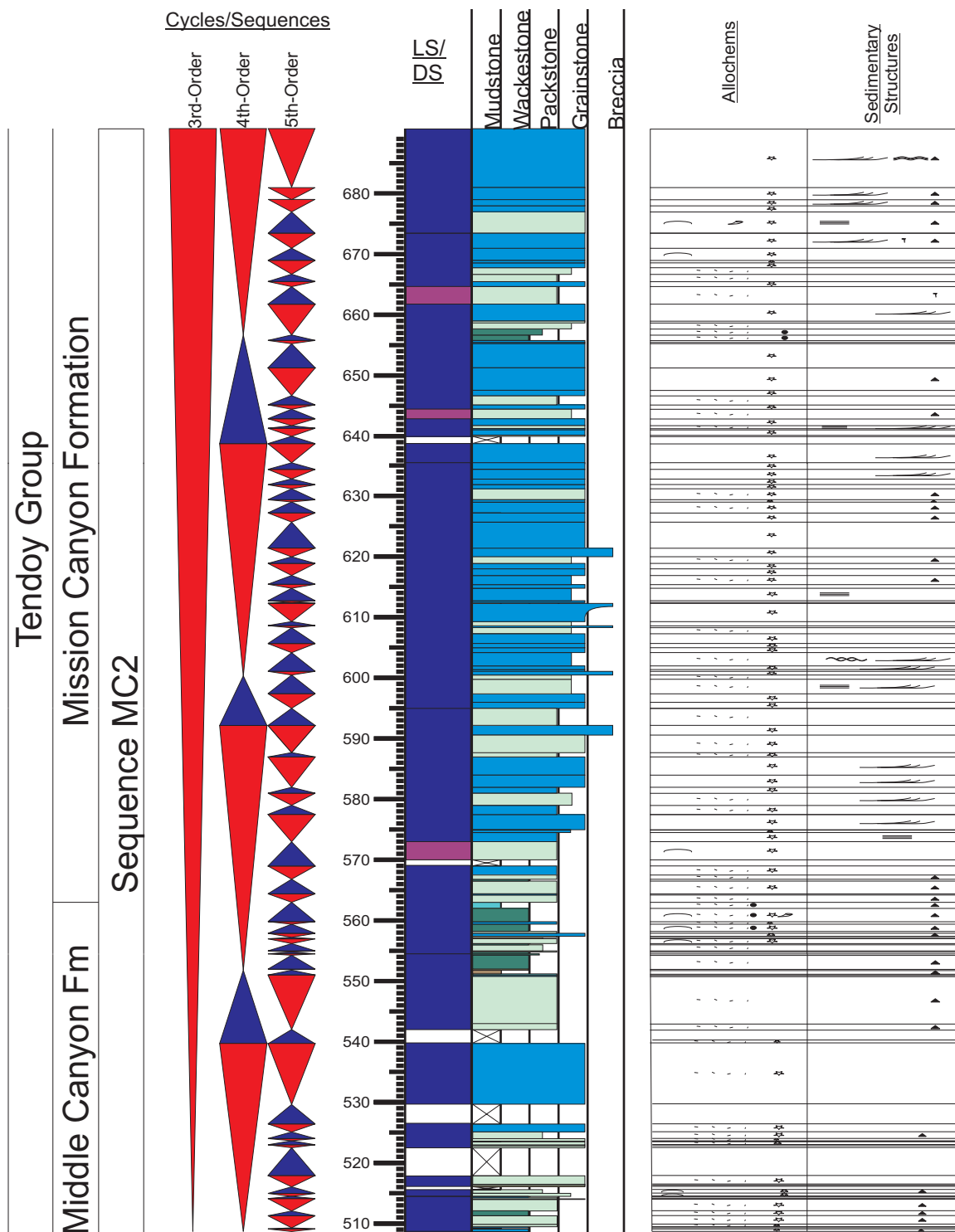


Figure 3.37: The graphic sedimentary log of the highstand systems tract of sequence MC2 from section location Bell-McKenzie Canyons. The HST is dominated by stacked cycles of crinoidal packstones-grainstones and caclisilt wackestones-packstones, with minor bedded chert present. Refer to Figures 3.12-14 for symbol definitions.

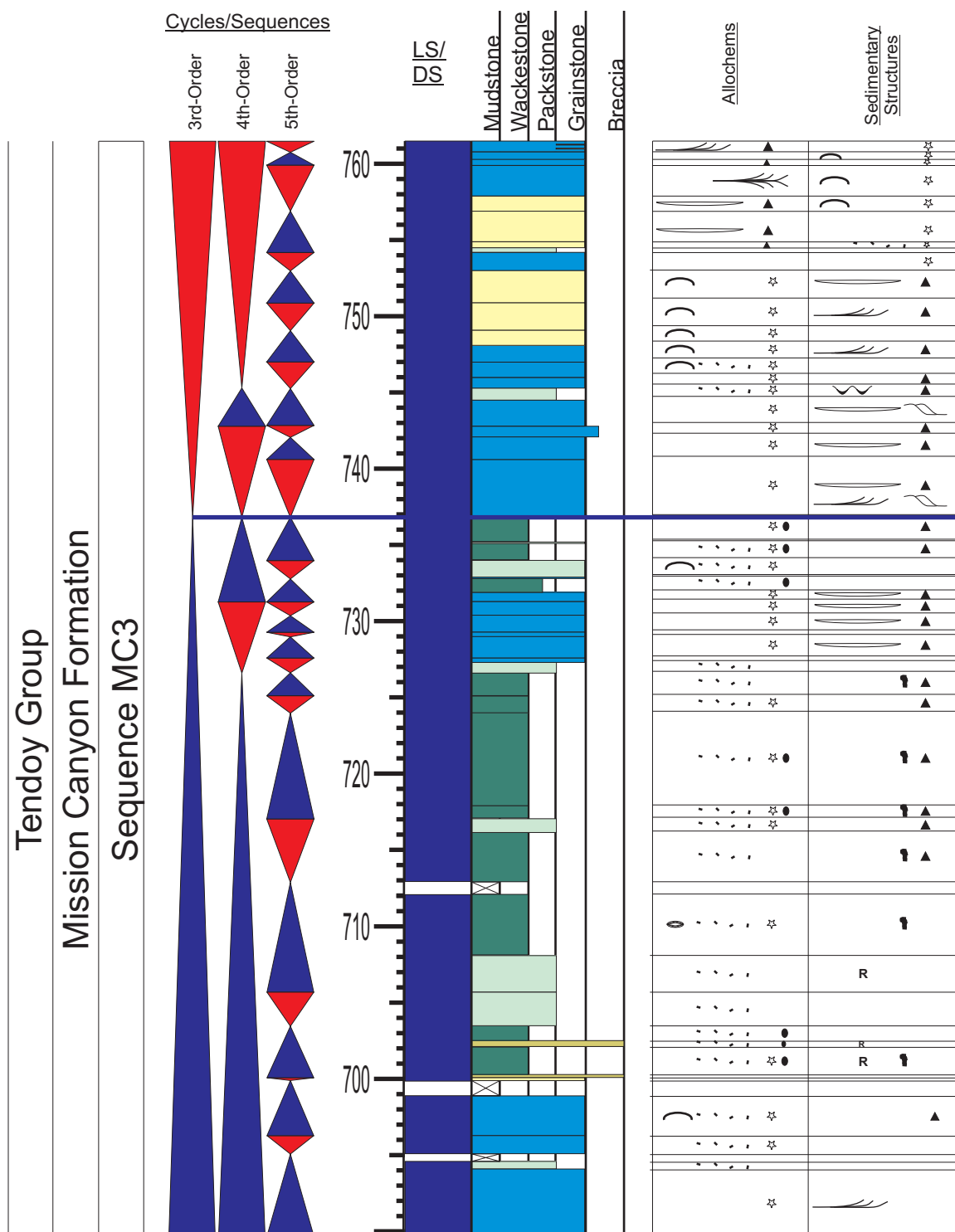


Figure 3.38: The graphic sedimentary log of the sequence MC3 from section location Bell-McKenzie Canyons. The transgressive systems tract is composed primarily of crinoidal grainstone at the base and poorly cyclic calcisiltites in middle and late transgression. The highstand systems tract, in contrast, is made up of stacked crinoidal and skeletal grainstone cycles. The blue line is the maximum flooding surface. Refer to Figures 3.12-14 for symbol definitions.

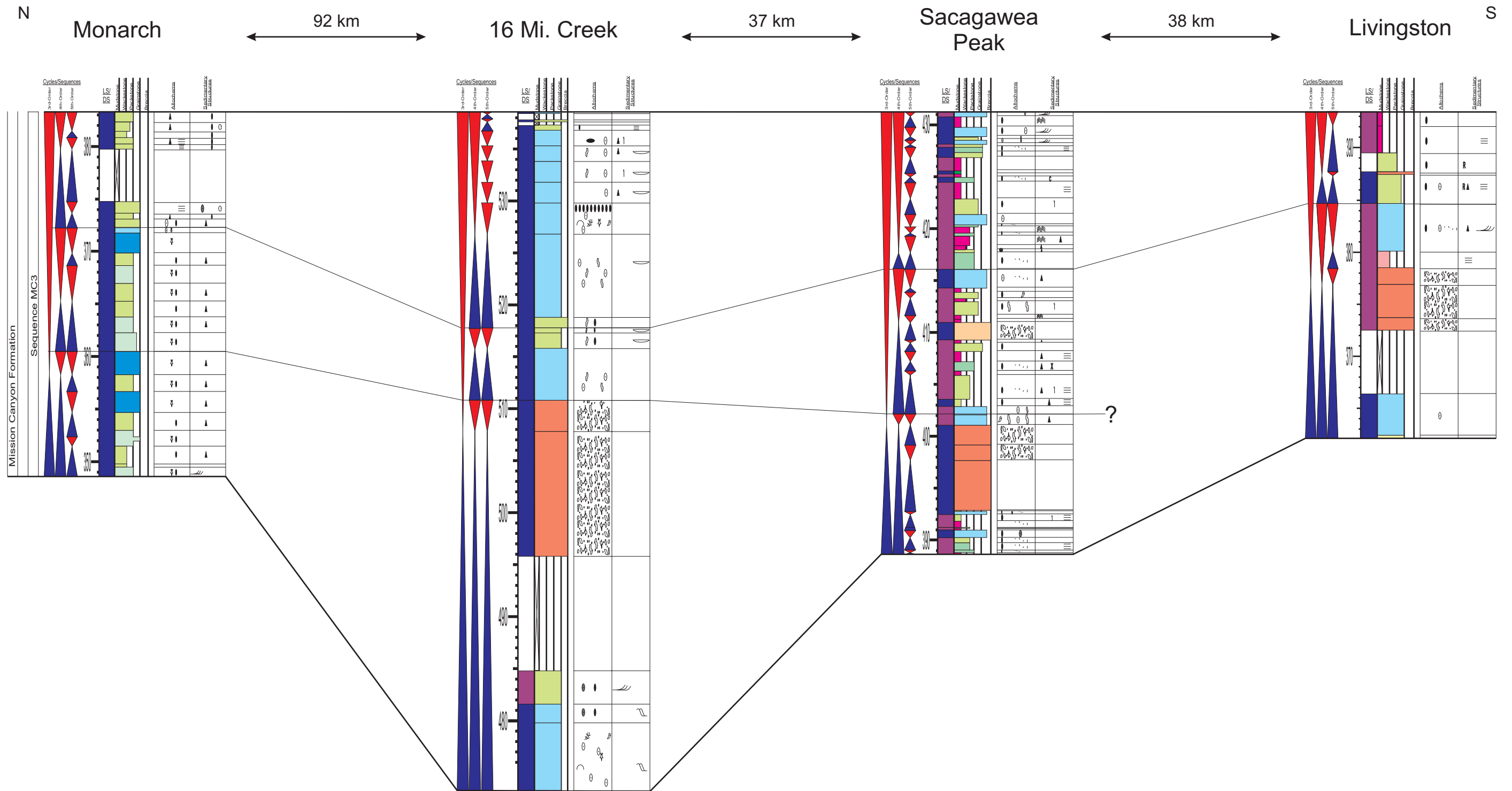


Figure 3.39: Correlation of 3rd- and 4th-order cycles and sequences within sequence MC3 across the central Montana trough. 4th-order cycle correlation is complicated by extensive brecciation near the base of this sequence in the TST. The upper two fourth-order cycles are observed to correlate across the study area. Heavy lines mark 3rd-order sequence boundaries, while the thin lines mark 4th-order cycle boundaries. See Figures 3.1-3.2 for symbol and color keys.

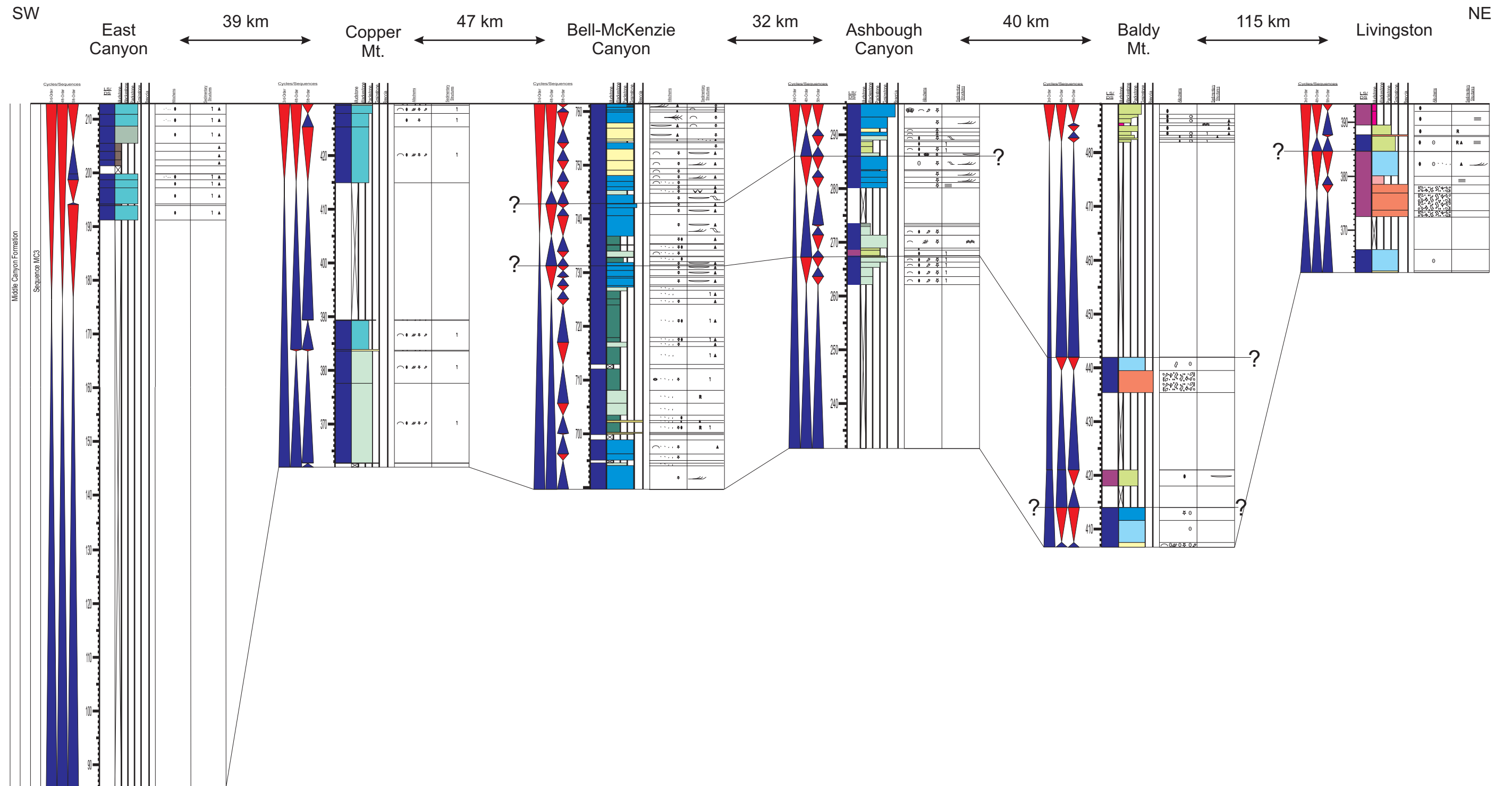


Figure 3.40: Correlation of 3rd- and 4th-order cycles and sequences within sequence MC3 across southwestern Montana and into the Antler foreland basin. Correlation of 4th-order cycles in this sequence across this study area are complicated due to extensive covered intervals in most localities during this time. Heavy lines mark 3rd-order sequence boundaries, while the thin lines mark 4th-order cycle boundaries. See Figures 3.1-3.2 for symbol and color keys.

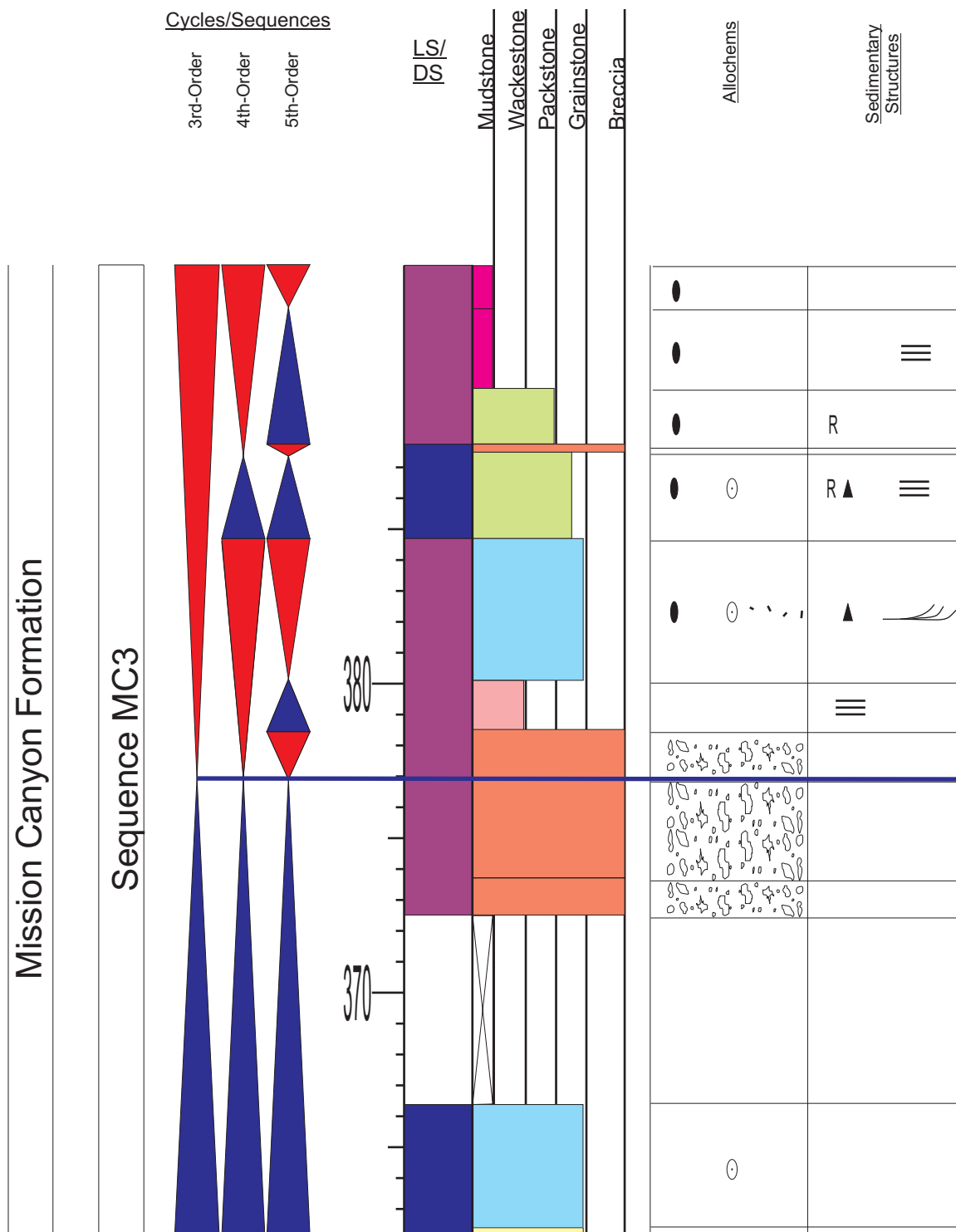


Figure 3.41: The graphic sedimentary log of the sequence MC3 from section location Livingston. The transgressive systems tract in this location is dominated by evaporite solution collapse breccia. The maximum flooding surface of this sequence is placed within the solution collapse breccia zone near its top. Here it is placed at the base of the uppermost discrete breccia package, which is markedly thinner than the lower two, indicative of decreasing accommodation. The blue line is the maximum flooding surface. Refer to Figures 3.12-14 for symbol definitions.

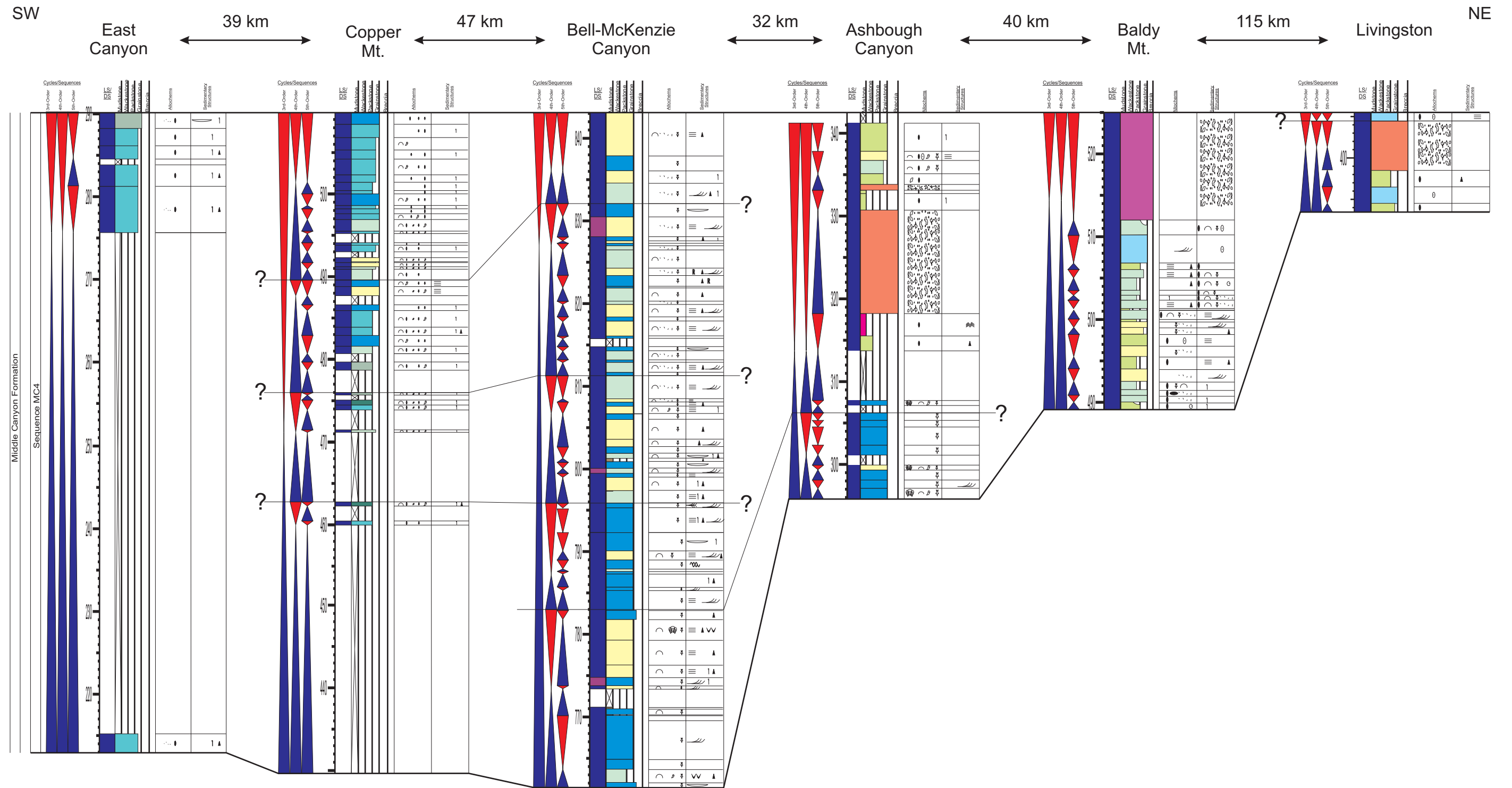


Figure 3.42: Correlation of 3rd- and 4th-order cycles and sequences within sequence MC4 across southwestern Montana and into the Antler foreland basin. Extensive brecciation due to evaporite dissolution and post-Madison karsting make correlations of 4th-order cycles equivocal across the updip sections from Ashbough Canyon to Livingston. Downdip, correlations of cycles is made difficult due to poor exposure in the TSTs of Copper Mountain and East Canyon. Heavy lines mark 3rd-order sequence boundaries, while the thin lines mark 4th-order cycle boundaries. See Figures 3.1-3.2 for symbol and color keys.

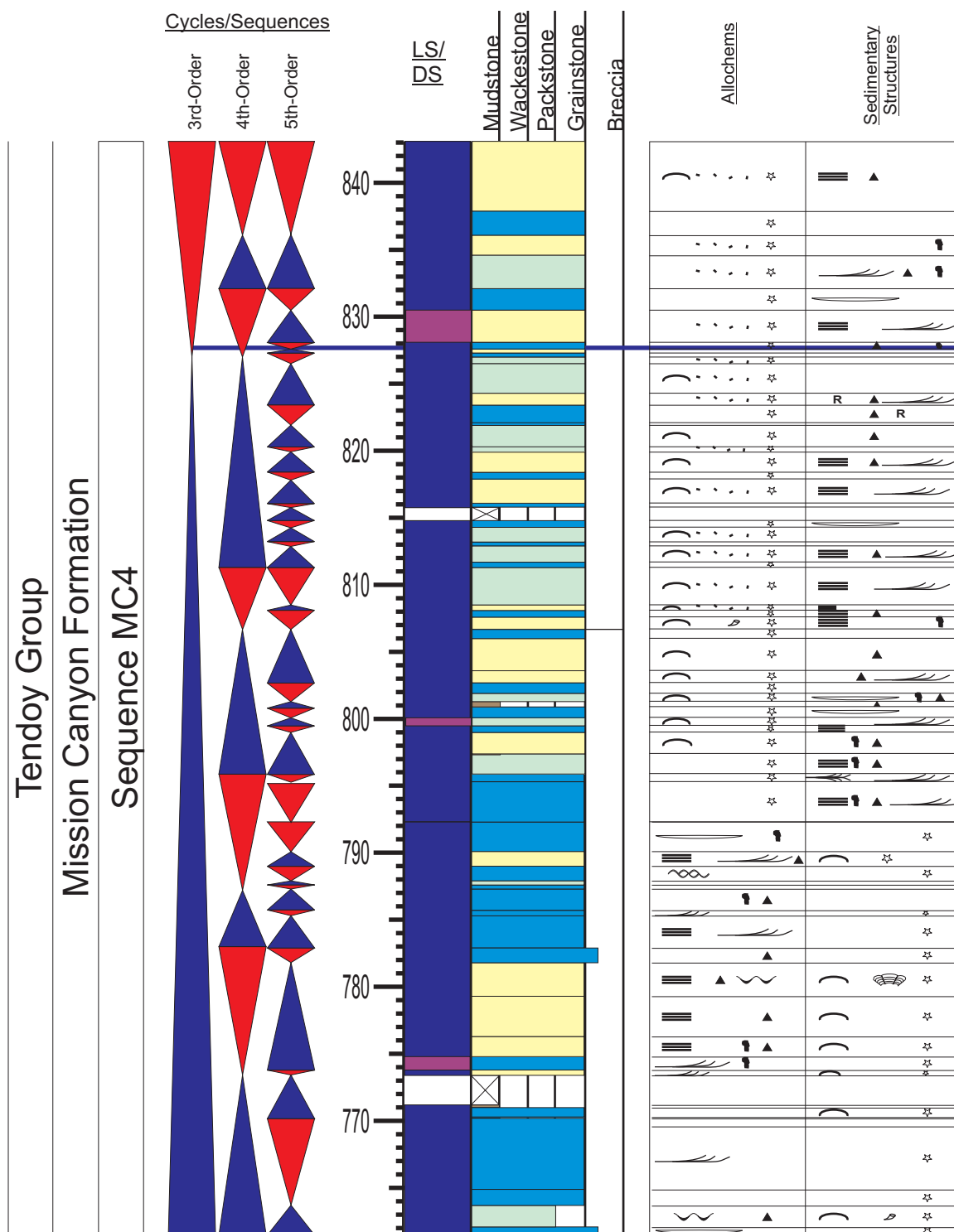


Figure 3.43: The graphic sedimentary log of the sequence MC4 from section location Bell-McKenzie Canyons. The transgressive systems tract is composed primarily of crinoidal grainstone at the base and poorly cyclic skeletal and peloidal packstones-grainstones and calcisiltites in middle and late transgression. The highstand systems tract is made up of partly dolomitized, stacked skeletal grainstone cycles with minor amounts of peloidal sediment. The blue line is the maximum flooding surface. Refer to Figures 3.12-14 for symbol definitions.

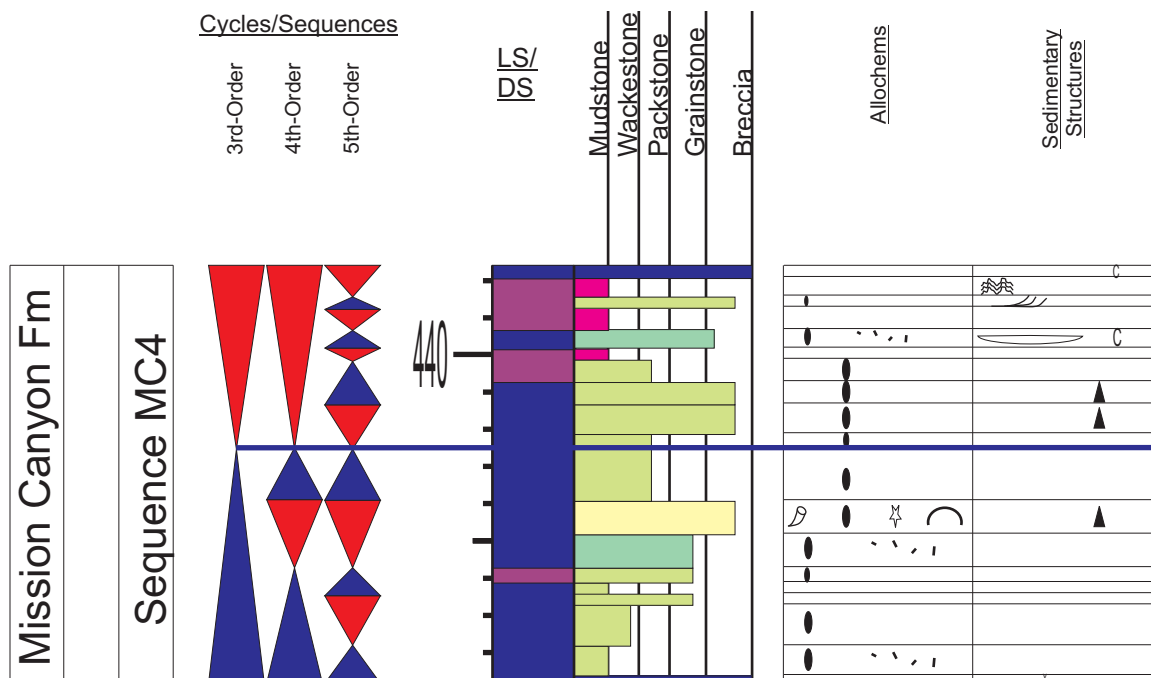


Figure 3.44: The graphic sedimentary log of the sequence MC4 from section location Sacagawea Peak. The transgressive systems tract here is made up of stacks of peloidal mudstone-packstone cycles with minor skeletal grainstones, representing changing energy and circulation within a restricted lagoonal setting. The highstand systems tract is composed of similar facies with increasing contributions from algal laminites in the late highstand. Additionally evidence of exposure is common within the late highstand in the form of minor caliche horizons. The blue line is the maximum flooding surface. Refer to Figures 3.12-14 for symbol definitions.

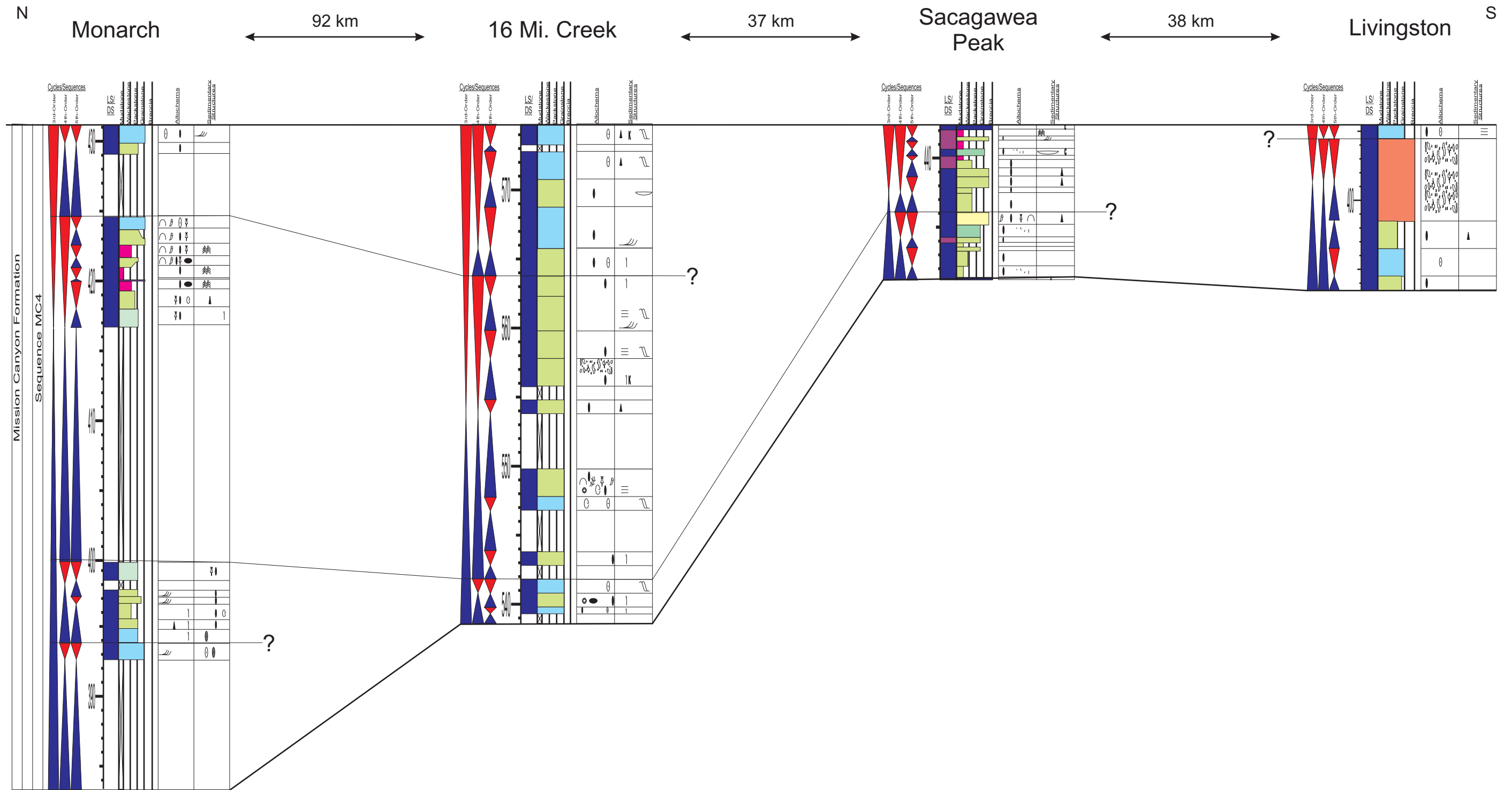


Figure 3.45: Correlation of 3rd- and 4th-order cycles and sequences within sequence MC4 across the central Montana trough. Thin updip sections at Sacagawea Peak and Livingston are observed to correlate poorly with expanded downdip sections at 16 Mile Creek and Monarch. Additionally, this sequence is poorly exposed at Monarch, leading to poor correlation between the downdip localities within this sequence. See Figures 3.1-3.2 for symbol and color keys.

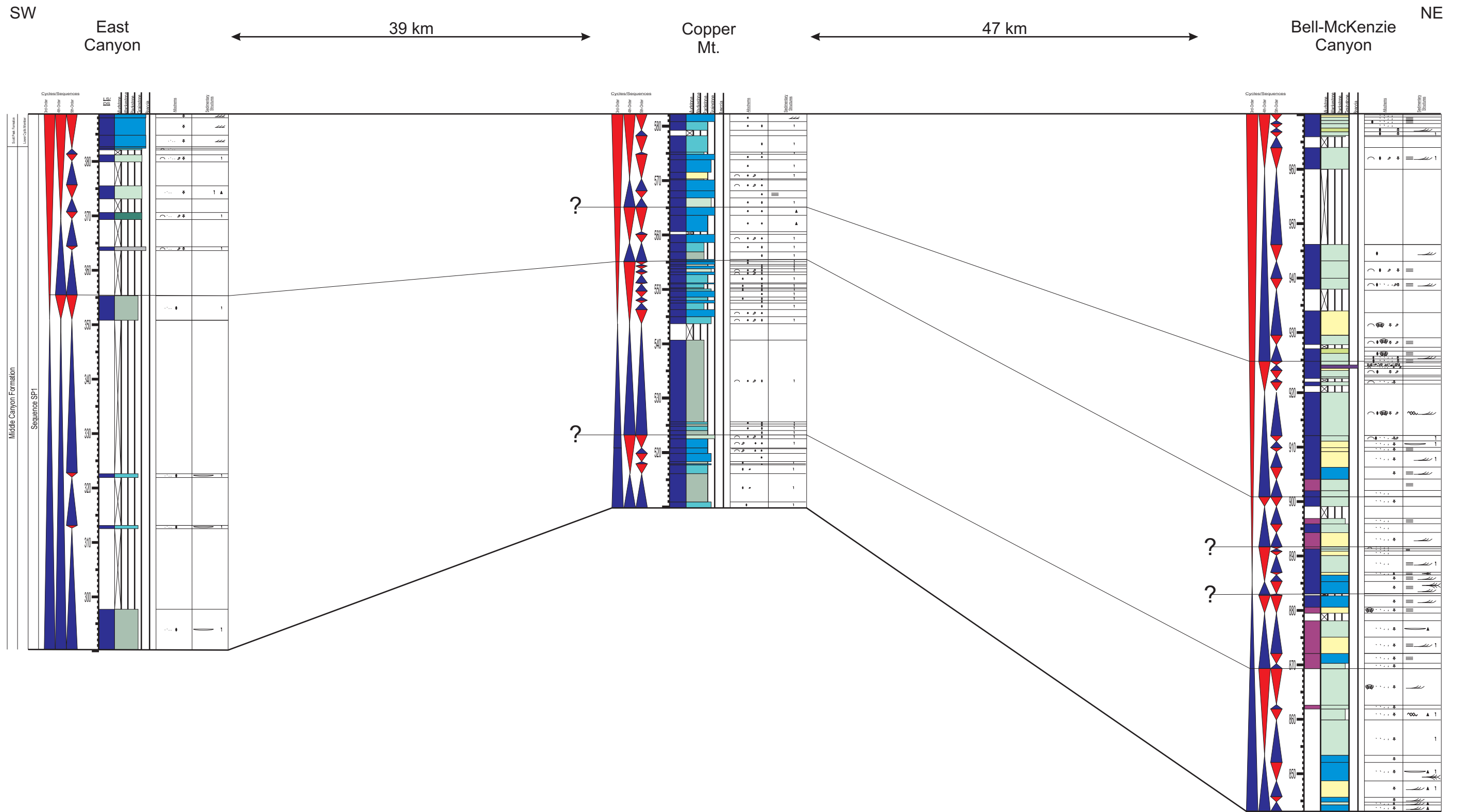


Figure 3.46: Correlation of 3rd- and 4th-order cycles and sequences within sequence SP1 across the Antler foreland basin. 4th-order cycles can generally be correlated across this study area except at location East Canyon, where exposure of this sequence is limited. Additionally, massive, poorly cyclic strata within the TST at Copper Mountain cannot be correlated with identified 4th-order cycles at Bell-McKenzie Canyon. Heavy lines mark 3rd-order sequence boundaries, while the thin lines mark 4th-order cycle boundaries. See Figures 3.1-3.2 for symbol and color keys.

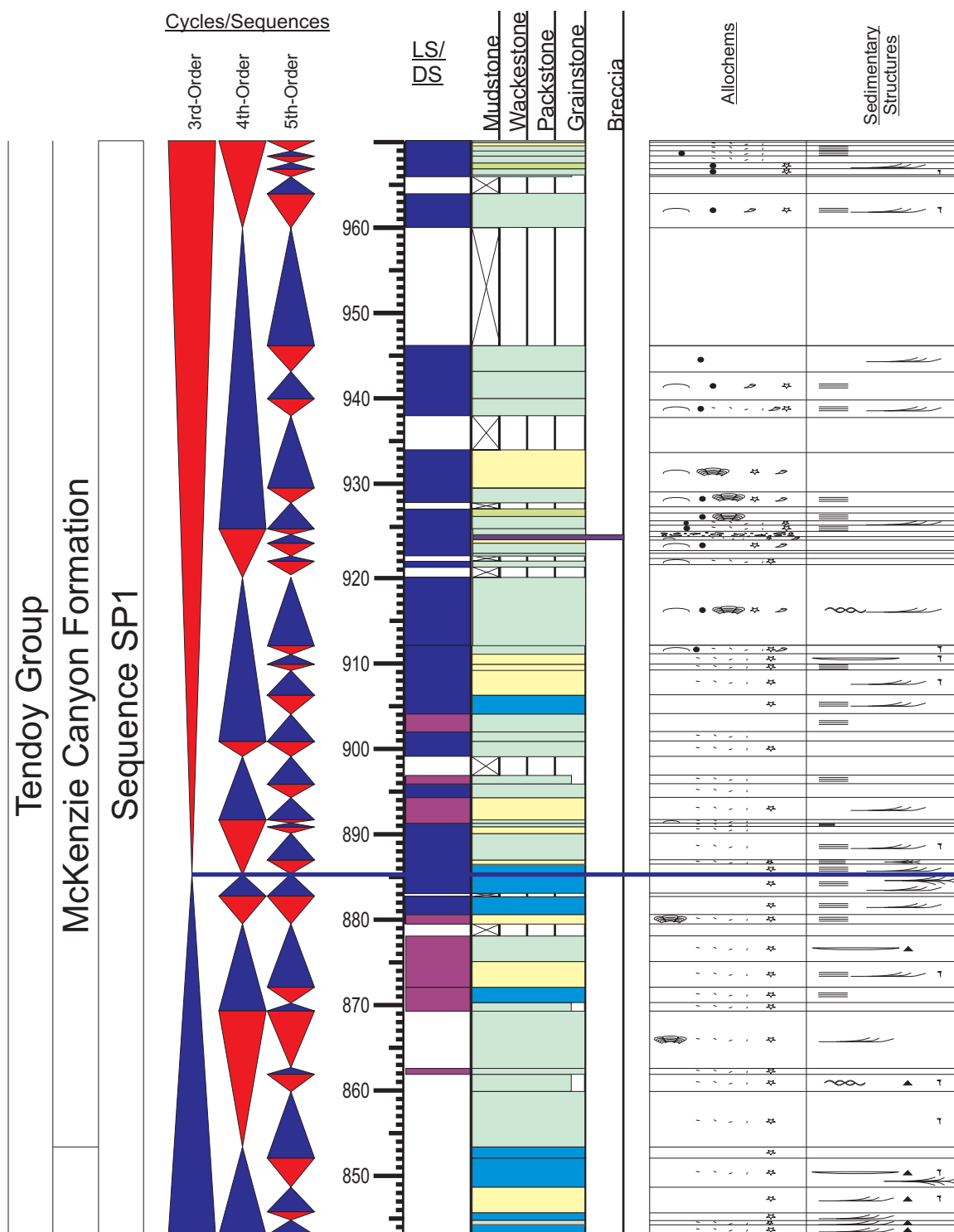


Figure 3.47: The graphic sedimentary log of the sequence SP1 from section location Bell-McKenzie Canyons. The TST is composed primarily of partly dolomitized crinoidal grainstone and skeletal-peloidal packstones-grainstones at the base and predominantly cyclic skeletal and peloidal packstones-grainstones and calcisiltites in middle and late transgression. The HST is made up vaguely cyclical peloidal-skeletal grainstones with numerous intervening covered intervals, which were likely muddier in texture. The blue line is the maximum flooding surface. Refer to Figures 3.12-14 for symbol definitions.

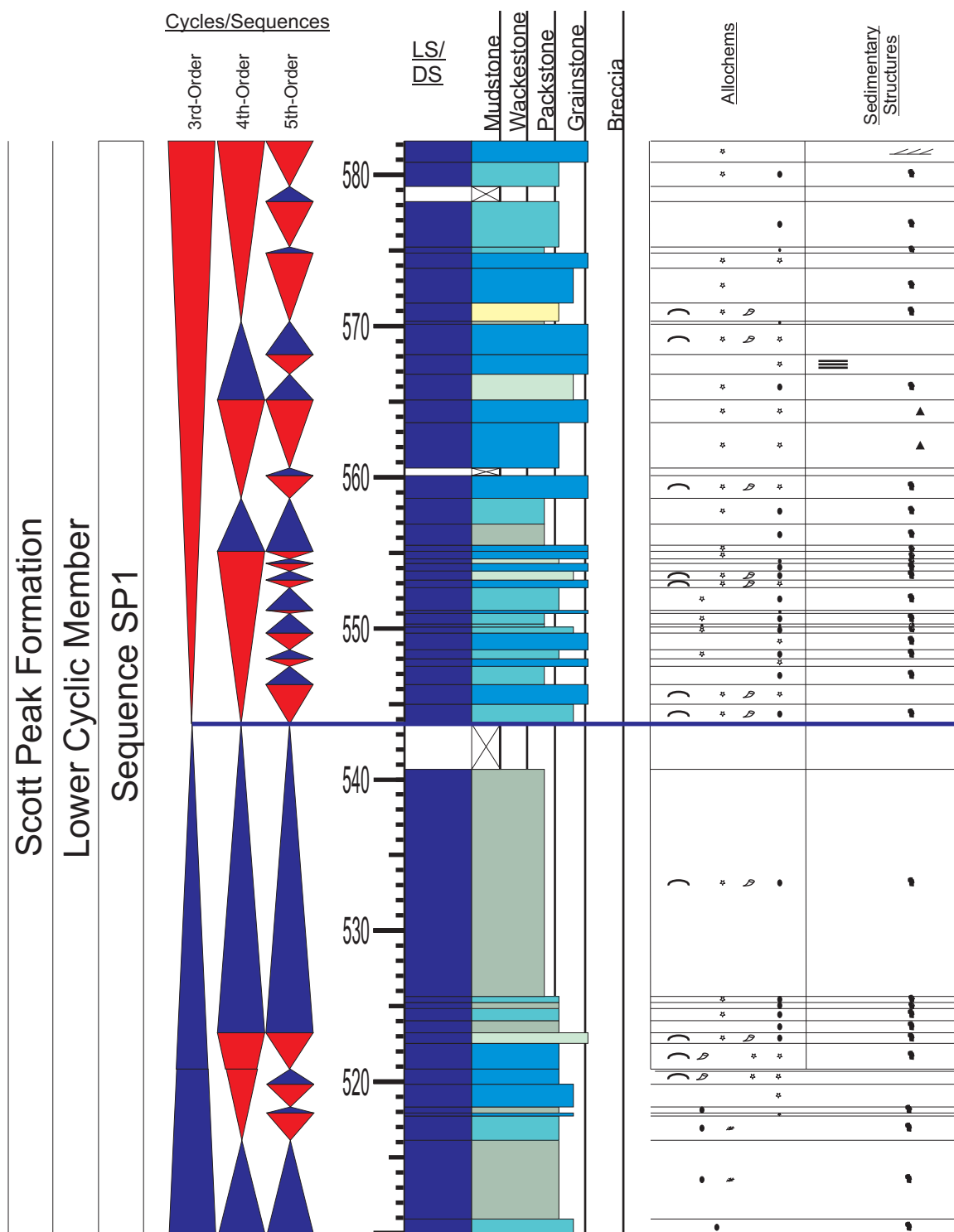


Figure 3.48: The graphic sedimentary log of the sequence SP1 from section location Copper Mountain. The TST is made up of partly argillaceous, bioturbated fine skeletal-peloidal packstones-grainstones with minor crinoidal and peloidal calcisilt packstones-grainstones also present. The HST is composed of crinoidal grainstone interbedded with bioturbated peloidal, peloidal/skeletal and skeletal wackestones-packstones. The blue line is the maximum flooding surface. Refer to Figures 3.12-14 for symbol definitions.

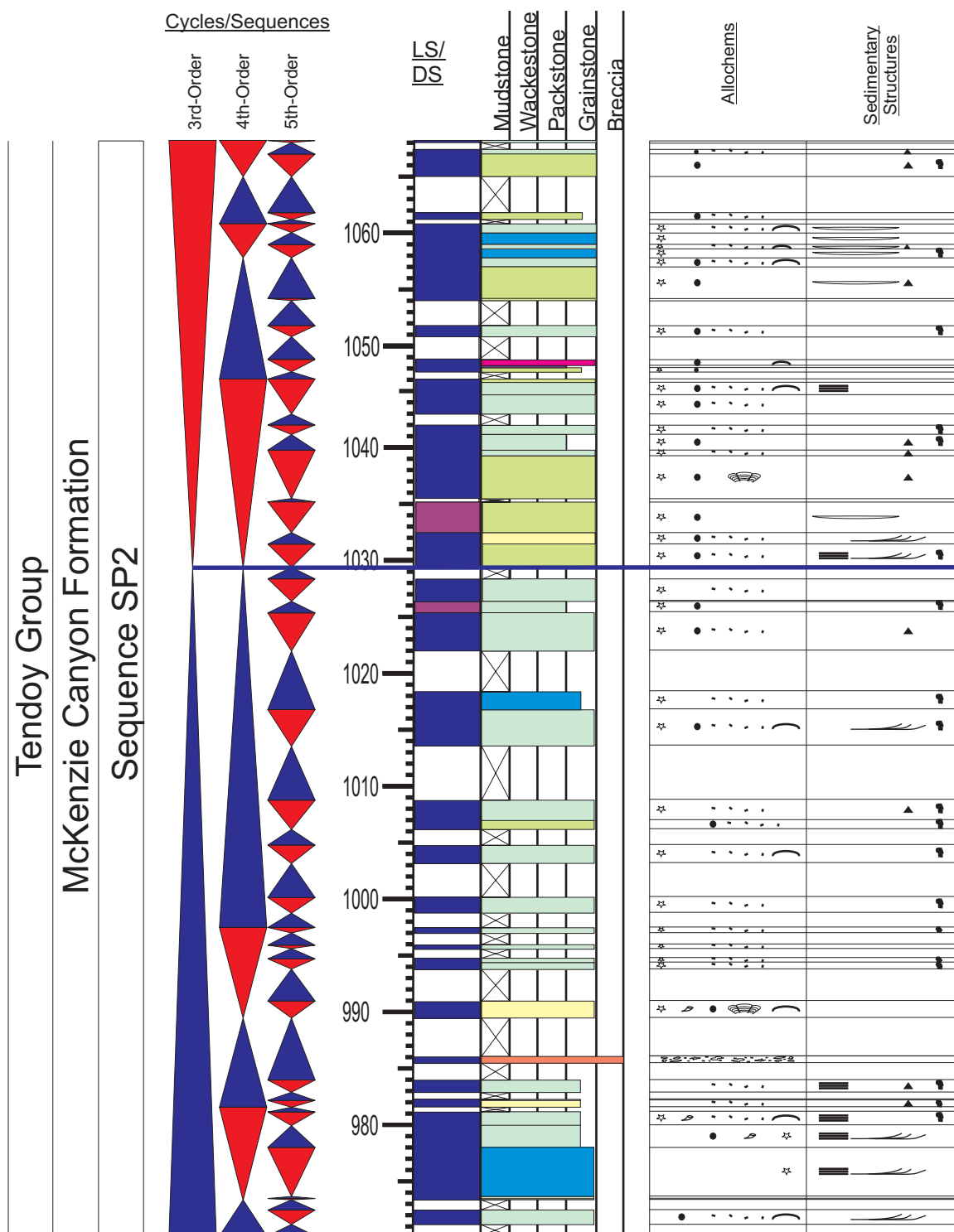


Figure 3.49: The graphic sedimentary log of the sequence SP2 from section location Bell-McKenzie Canyons. The TST is made up of predominantly bioturbated near-shoal facies of skeletal/peloidal packstones-grainstones with significantly covered intervals and minor crinoidal, skeletal, and peloidal packstones-grainstones. The HST is comprised of dominantly peloidal grainstones with minor peloidal/skeletal packstones-grainstones, crinoidal grainstones and algal laminites. The blue line is the maximum flooding surface. Refer to Figures 3.12-14 for symbol definitions.

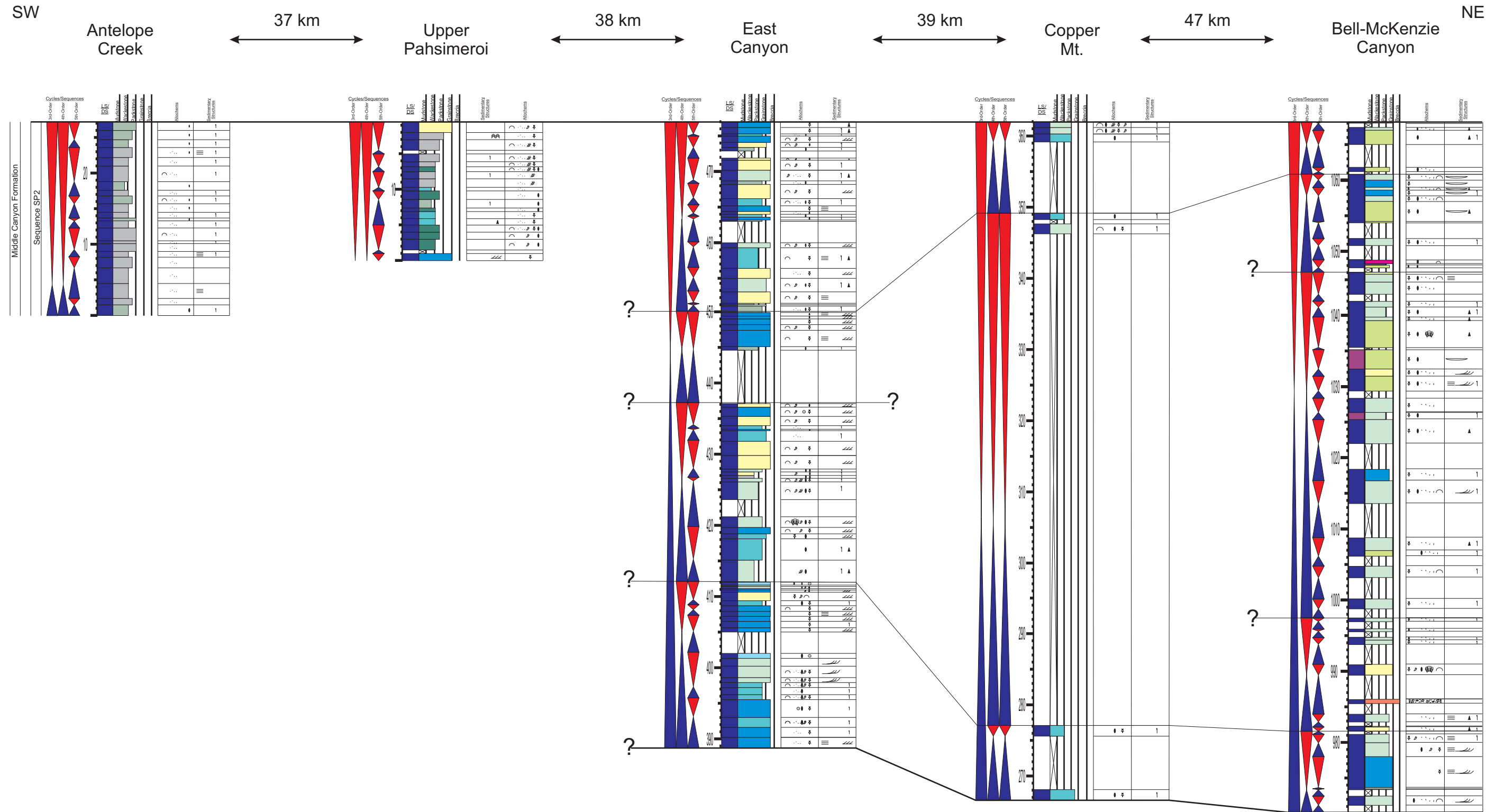


Figure 3.50: Correlation of 3rd- and 4th-order cycles and sequences within sequence SP2 across the Antler foreland basin. Cycles within this sequence are highly local because of poor outcrop quality across the study area at this time. Heavy lines mark 3rd-order sequence boundaries, while the thin lines mark 4th-order cycle boundaries. See Figures 3.1-3.2 for symbol and color keys.

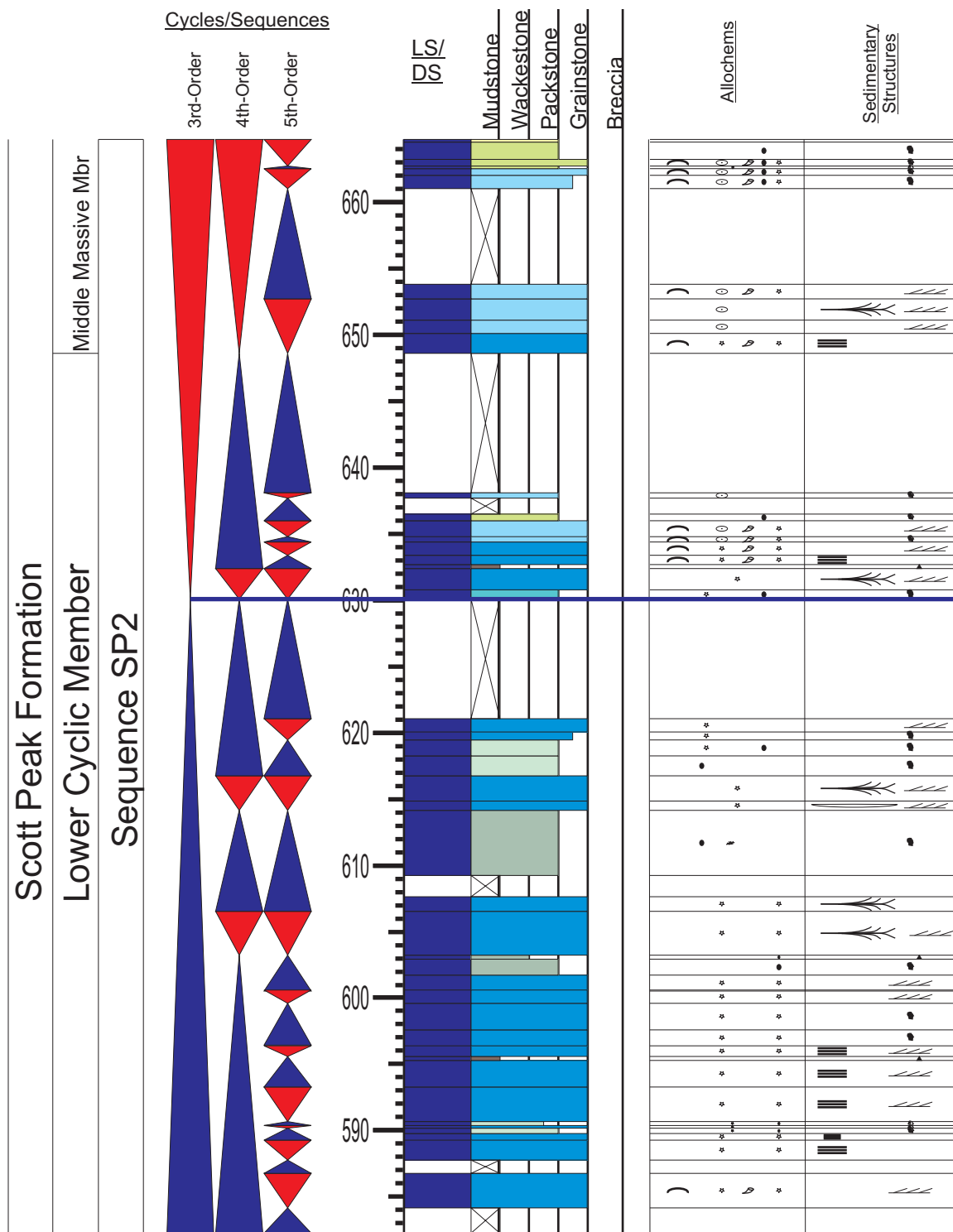


Figure 3.51: The graphic sedimentary log of the sequence SP2 from section location Copper Mountain. The TST is made up of aggradationally stacked subtidal crinoidal grainstone shoals with thin intervening argillaceous peloidal packstones and covered intervals. The HST shows increasing amounts of coated grain grainstones and is capped by muddier backshoal deposits. The blue line is the maximum flooding surface. Refer to Figures 3.12-14 for symbol definitions.

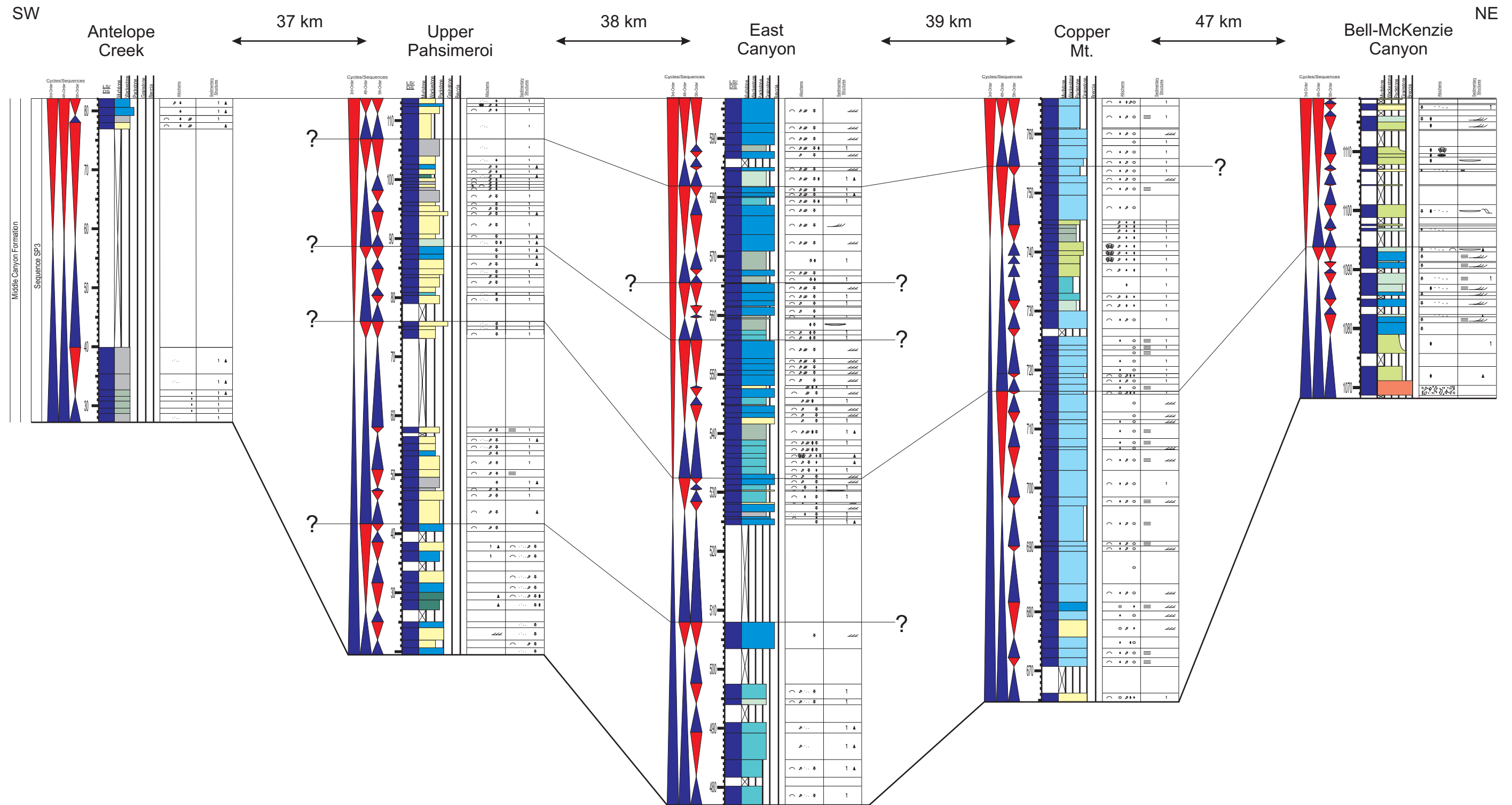


Figure 3.52: Correlation of 3rd- and 4th-order cycles and sequences within sequence SP3 across the Antler foreland basin. 4th-order cycles can generally be correlated across this study area except on the proximal and distal periphery at Bell-McKenzie Canyon and Antelope Creek. At these locations, limited sedimentation occurred in comparison to the central part of the foreland basin, where cycles are more continuous. Heavy lines mark 3rd-order sequence boundaries, while the thin lines mark 4th-order cycle boundaries. See Figures 3.1-3.2 for symbol and color keys.

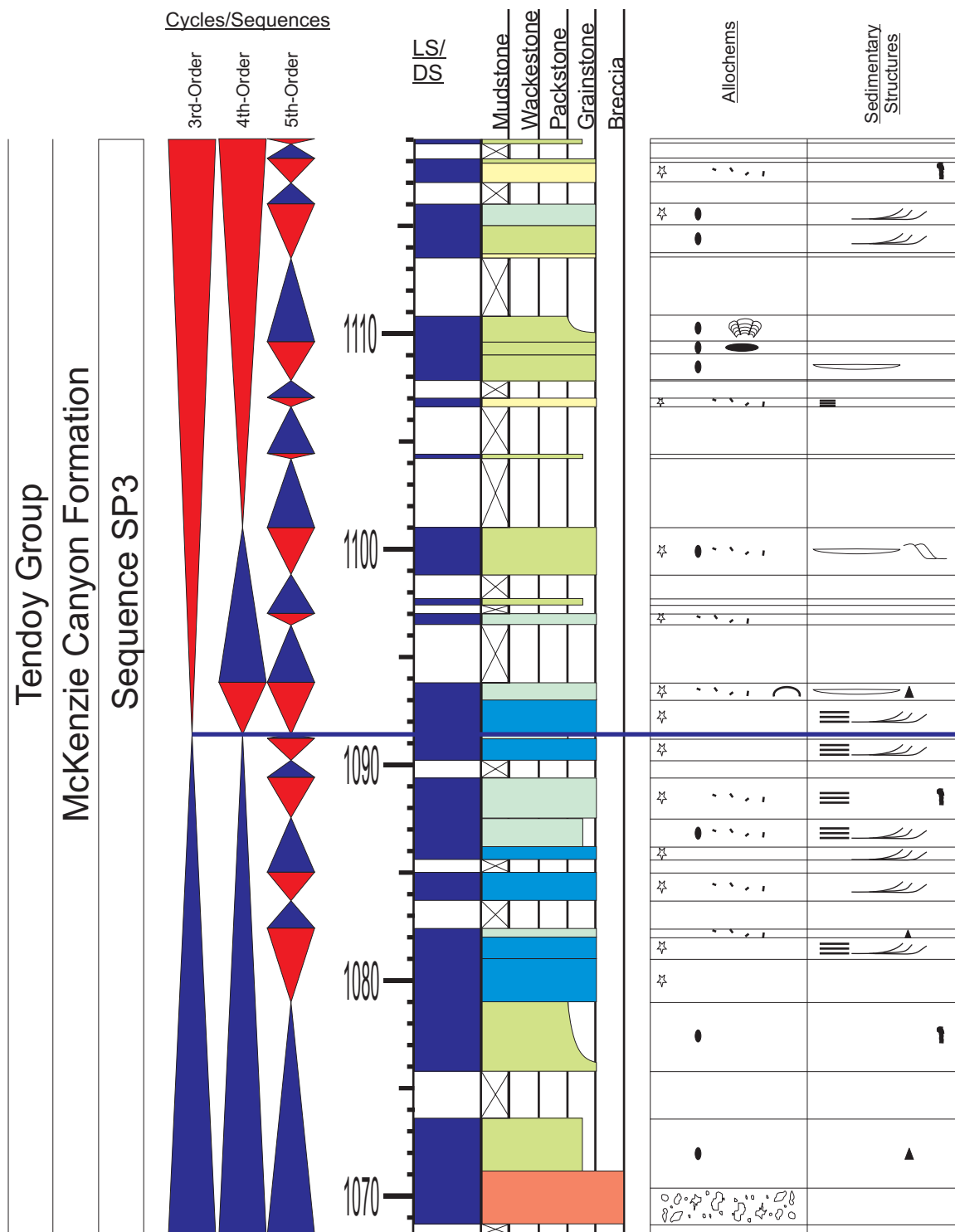


Figure 3.53: The graphic sedimentary log of the sequence SP3 from section location Bell-McKenzie Canyons. The base of the TST is made up of predominantly bioturbated peloidal packstones-grainstones with limited faunal content and lagoonal affinity. This overlain by crinoidal, skeletal, and peloidal packstones-grainstones of subtidal shoal affinity. The HST is comprised of dominantly peloidal grainstones with extensive, likely mud-rich covered intervals, minor peloidal/skeletal packstones-grainstone and, skeletal grainstones. The blue line is the maximum flooding surface. Refer to Figures 3.12-14 for symbol definitions.

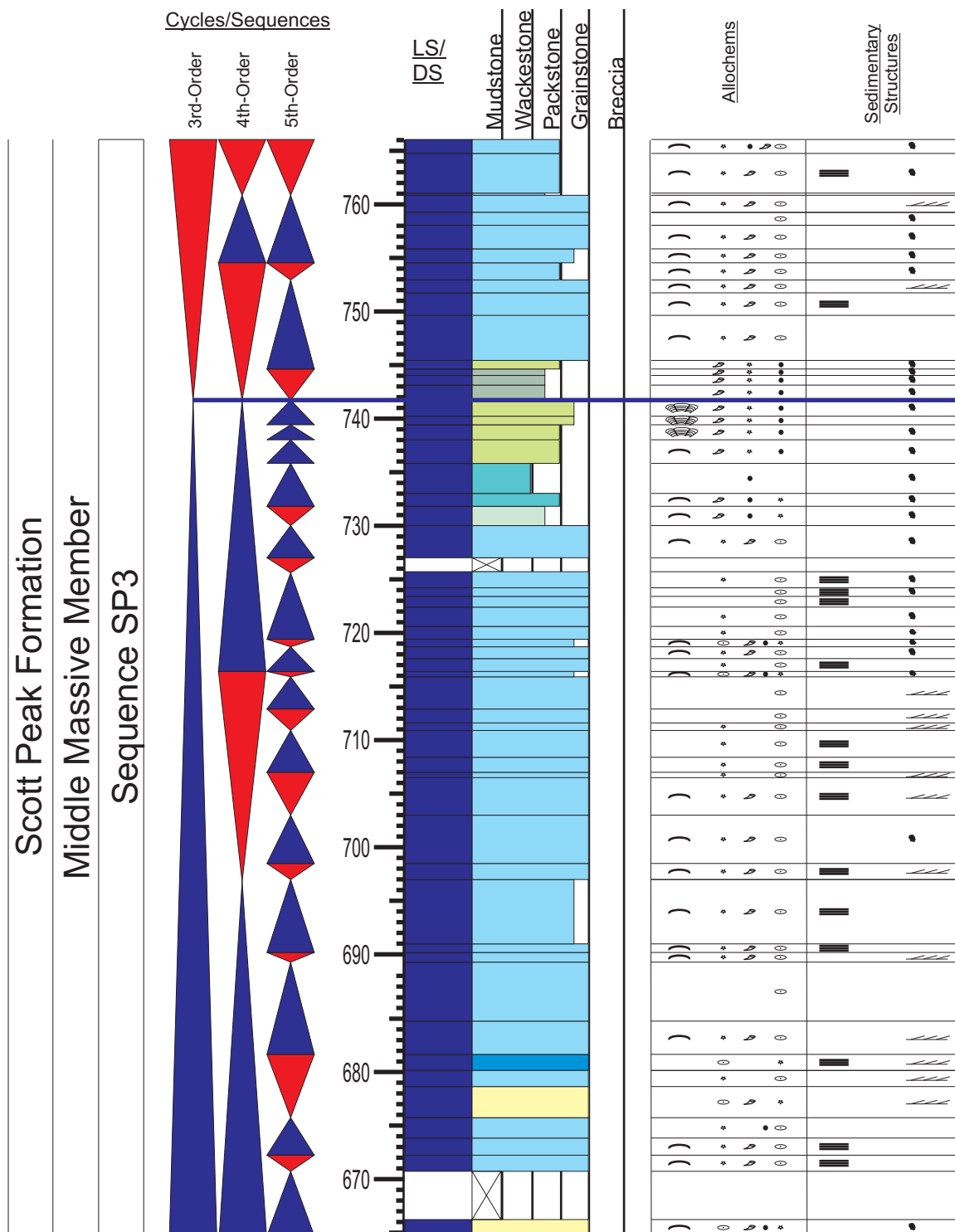


Figure 3.54: The graphic sedimentary log of the sequence SP3 from section location Copper Mountain. The TST is made up of aggradationally stacked subtidal oolitic grainstone shoals with limited skeletal and crinoidal grainstone interbeds and approximately 10 m of peloidal and argillaceous wackestone-packstones in the late TST. The HST is composed of amalgamated, poorly cyclic oolitic packstones-grainstones. The blue line is the maximum flooding surface. Refer to Figures 3.12-14 for symbol definitions.

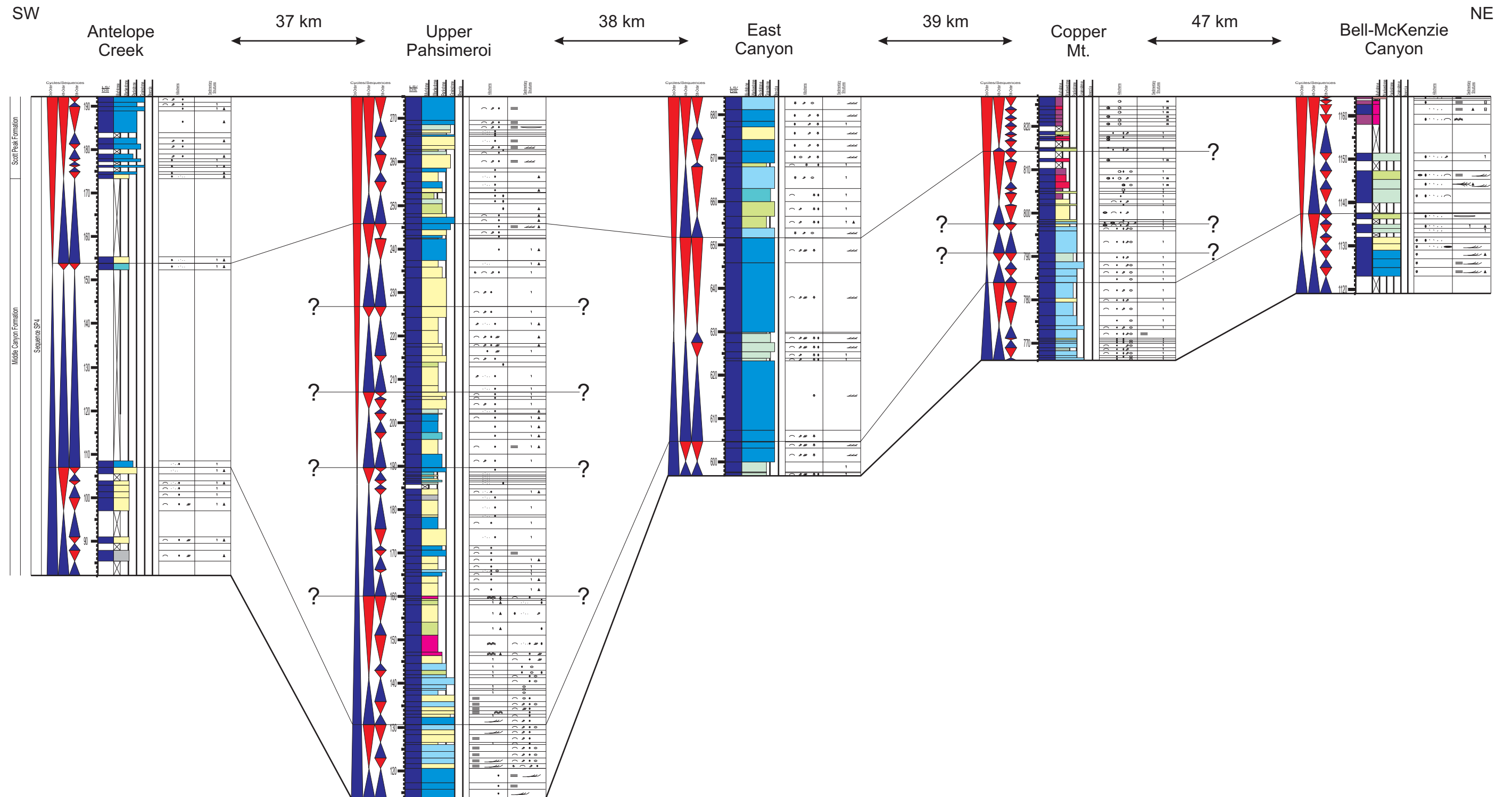


Figure 3.55: Correlation of 3rd- and 4th-order cycles and sequences within sequence SP4 across the Antler foreland basin. Correlation of cycles within this sequence have limited length. This is primarily a function of the deposition of massive crinoidal bank deposits within the central part of the foreland basin at East Canyon. Additionally, limited exposure at the peripheral sections make correlations at this scale difficult. Heavy lines mark 3rd-order sequence boundaries, while the thin lines mark 4th-order cycle boundaries. See Figures 3.1-3.2 for symbol and color keys.

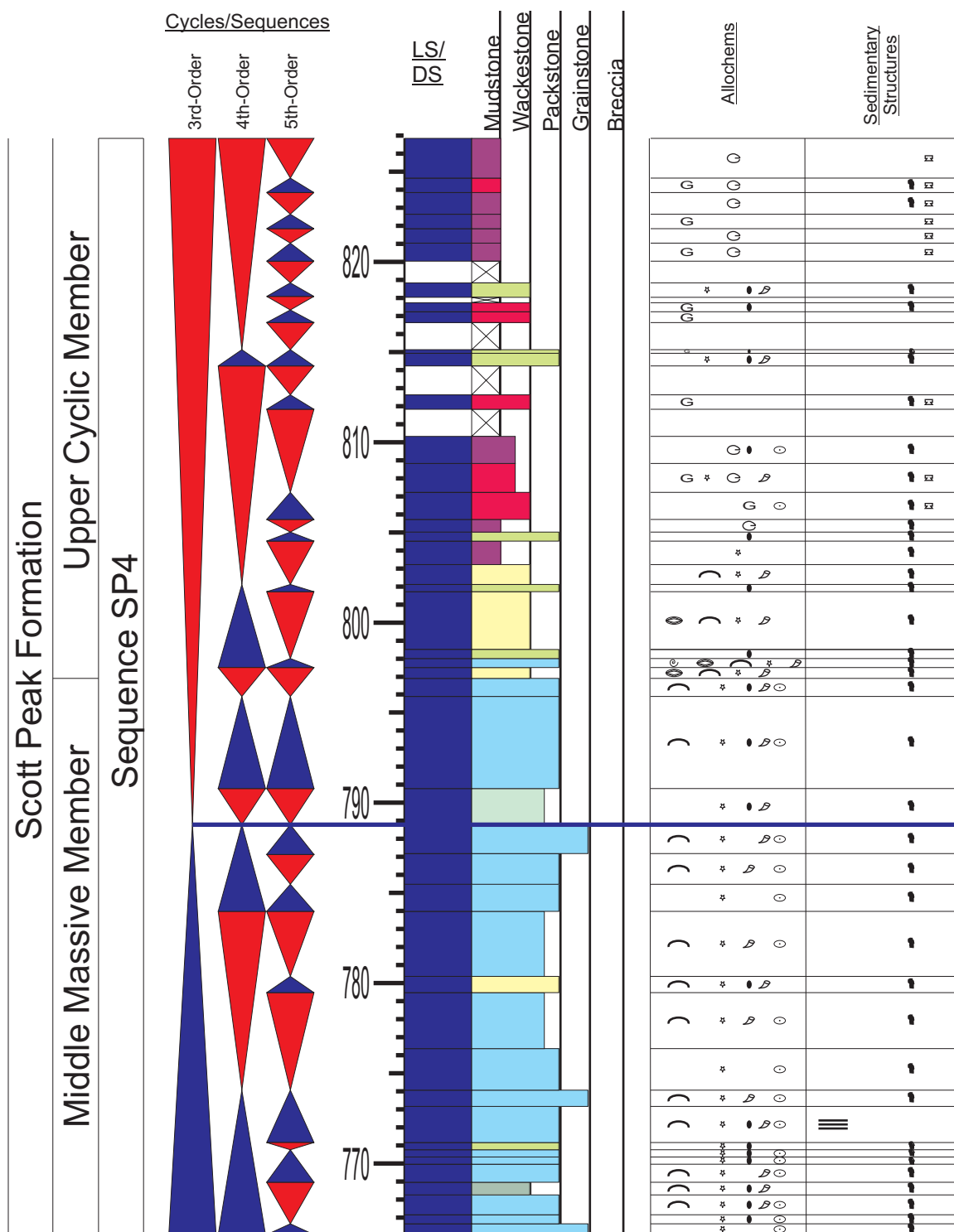


Figure 3.56: The graphic sedimentary log of the sequence SP4 from section location Copper Mountain. The TST is made up of aggradationally stacked subtidal oolitic packstone-grainstone shoals with limited skeletal and peloidal packstone interbeds. The HST is composed of amalgamated, poorly cyclic oolitic packstones-grainstones at the base and becomes progressively muddier, culminating with stacked accumulations of well preserved goniatite cephalopod-bearing mudstone-floatstones. The blue line is the maximum flooding surface. Refer to Figures 3.12-14 for symbol definitions.



Figure 3.57: Well preserved goniatite cephalopods within a cephalopod floatstone bed from the highstand systems tract of sequence Scott Peak 4 at section location Copper Mountain. Accompanying the goniatites are orthocone cephalopods (not shown), bryozoans, ostracods, and calcite cements after fenestrae. Coin is approximately 2.5 cm across. From 806.5 m at section Copper Mountain.

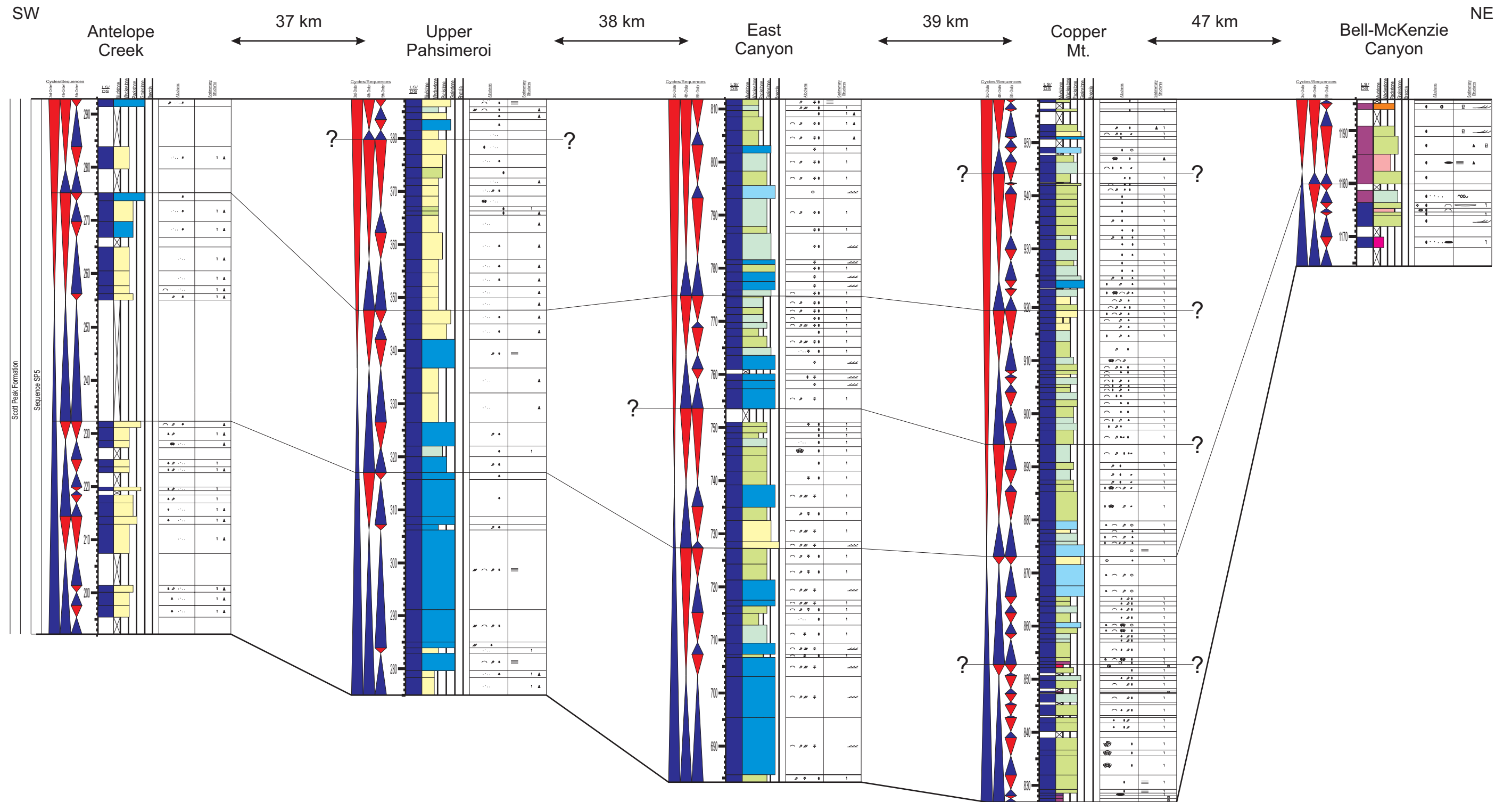


Figure 3.58: Correlation of 3rd- and 4th-order cycles and sequences within sequence SP5 across the Antler foreland basin. 4th-order cycle correlation is observed to have significantly longer length than in previous sequences within the Antler foreland basin. Cycles correlate poorly to Bell-McKenzie Canyon, where deposition is limited as compared to the other sections. Heavy lines mark 3rd-order sequence boundaries, while the thin lines mark 4th-order cycle boundaries. See Figures 3.1-3.2 for symbol and color keys.

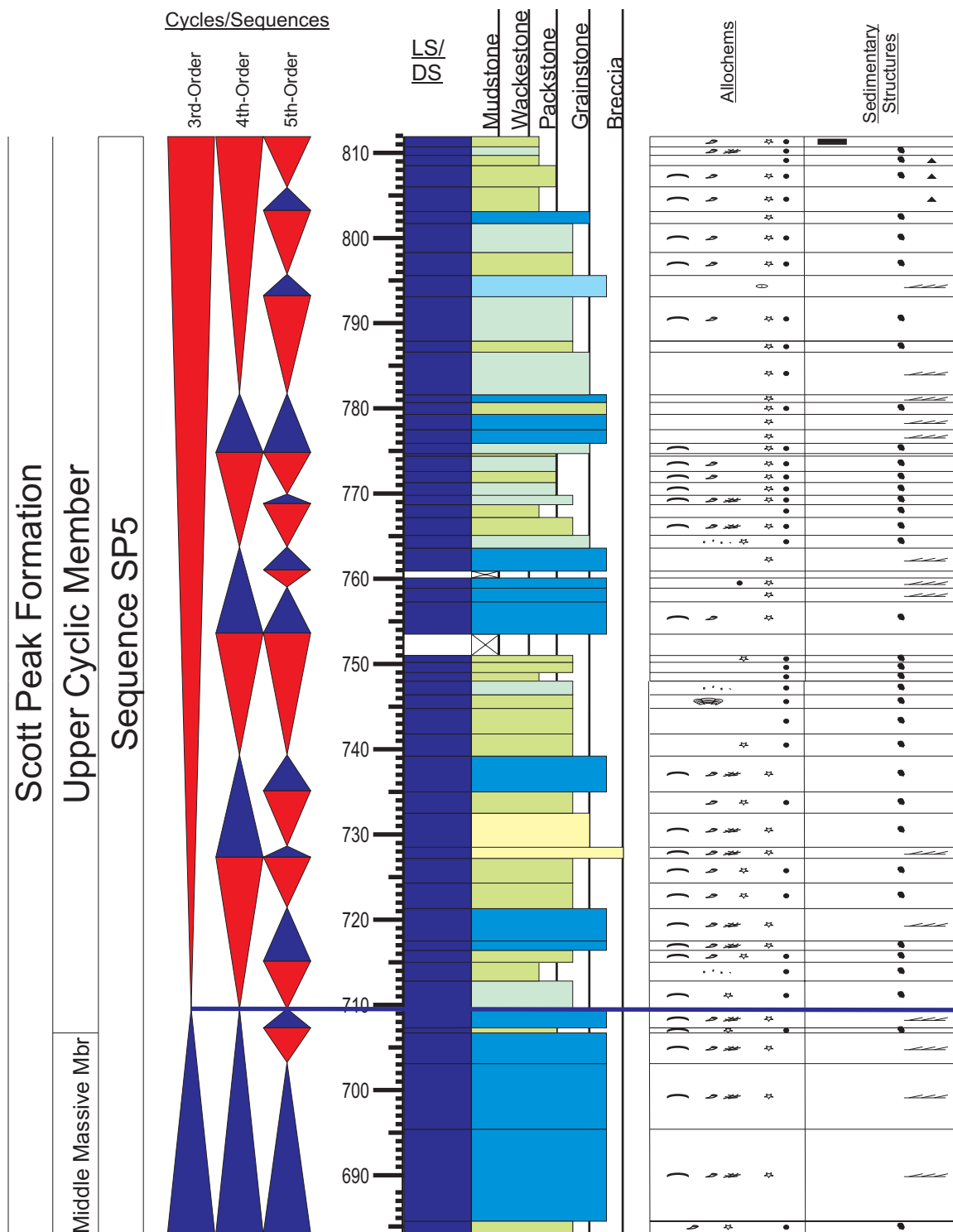


Figure 3.59: The graphic sedimentary log of the sequence SP5 from section location East Canyon. The TST is made up of aggradationally stacked subtidal crinoidal grainstones with limited skeletal and peloidal packstone interbeds. The HST is composed of minor amounts of crinoidal and skeletal packstones-grainstones at the base and becomes progressively more peloidal and muddier, with the top of the sequence marked by the peloidal wackestones with some admixed normal marine fauna. The blue line is the maximum flooding surface. Refer to Figures 3.12-14 for symbol definitions.

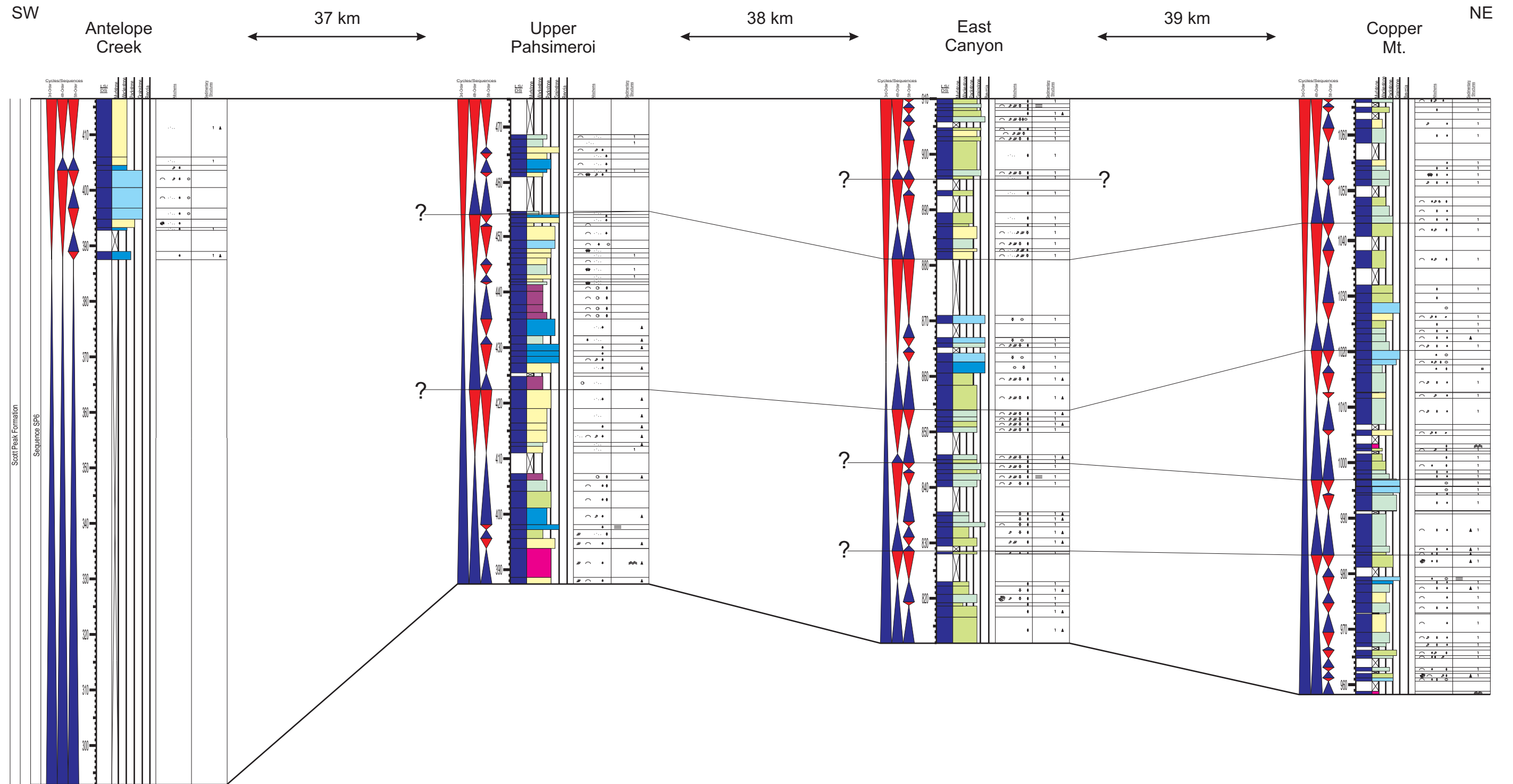


Figure 3.60: Correlation of 3rd- and 4th-order cycles and sequences within sequence SP6 across the Antler foreland basin. Generally uniform depositional thickness is observed across the Antler foreland basin during this sequence. 4th-order cycles are variably correlative across the study area, but correlation with Antelope Creek is tenuous due to a lack of exposed section at this locality. Heavy lines mark 3rd-order sequence boundaries, while the thin lines mark 4th-order cycle boundaries. See Figures 3.1-3.2 for symbol and color keys.

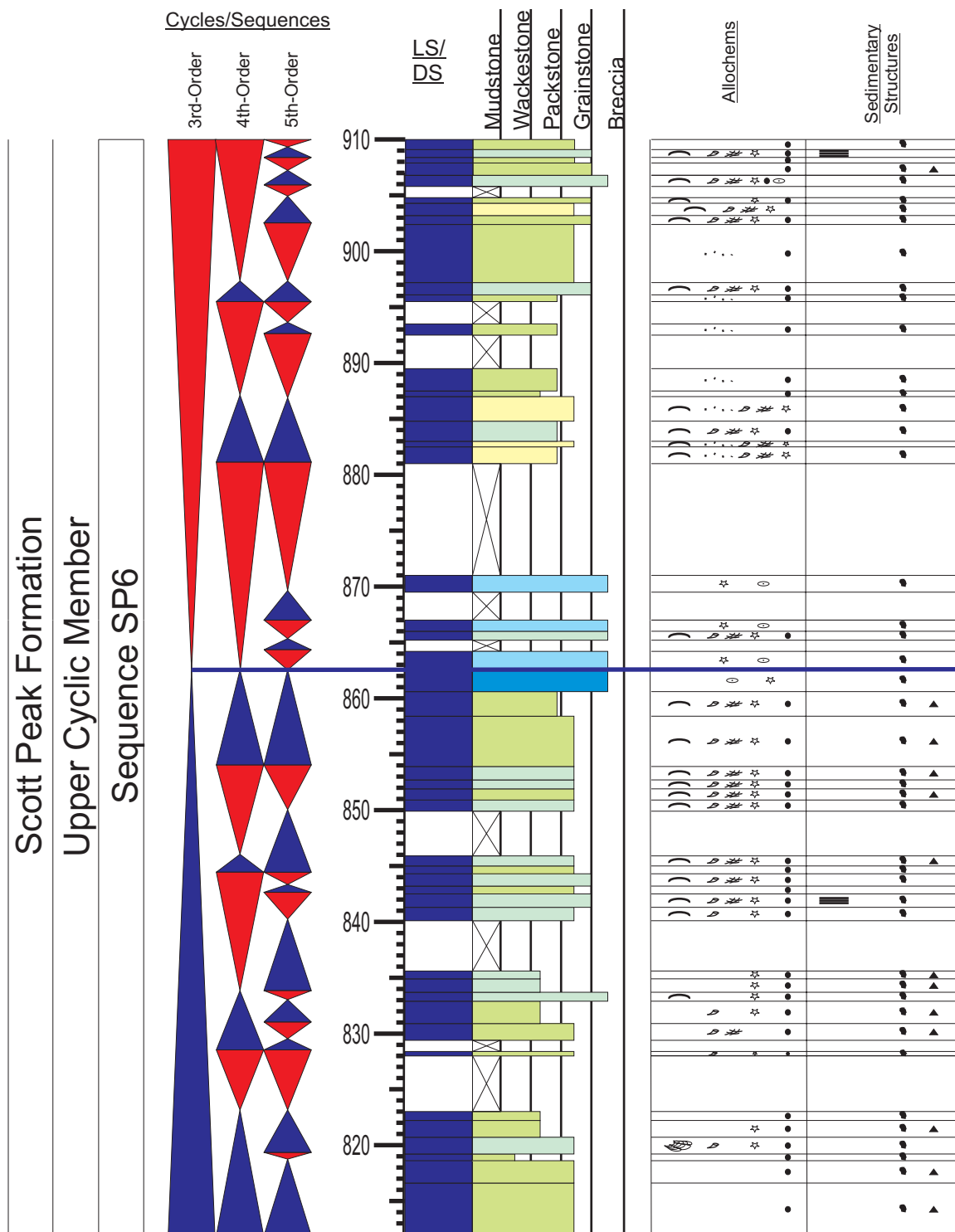


Figure 3.61: The graphic sedimentary log of the sequence SP6 from section location East Canyon. The TST is made up of aggradationally stacked peloidal wackestones-packstones with limited skeletal/peloidal packstone interbeds and common covered intervals. The HST is composed of crinoidal and oolitic packstones-grainstones in the early HST and becomes progressively more peloidal and muddier, with occasional skeletal wackestones-packstone interbedded. The blue line is the maximum flooding surface. Refer to Figures 3.12-14 for symbol definitions.

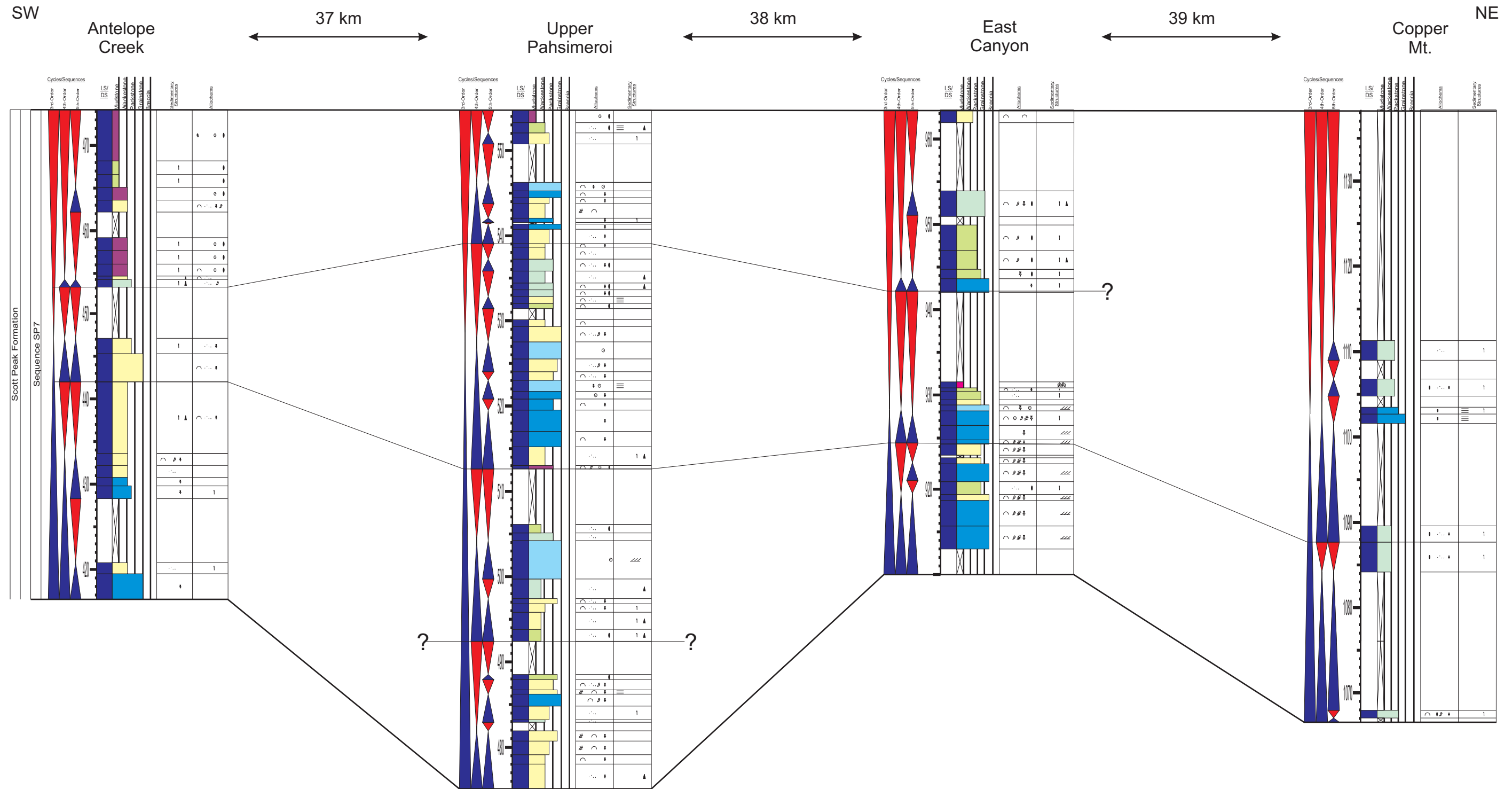


Figure 3.62: Correlation of 3rd- and 4th-order cycles and sequences within sequence SP7 across the Antler foreland basin. The limited quality of exposed section makes correlation of 4th-order cycles within this sequence tenuous, although several cycles do correlate across the basin. Heavy lines mark 3rd-order sequence boundaries, while the thin lines mark 4th-order cycle boundaries. See Figures 3.1-3.2 for symbol and color keys.

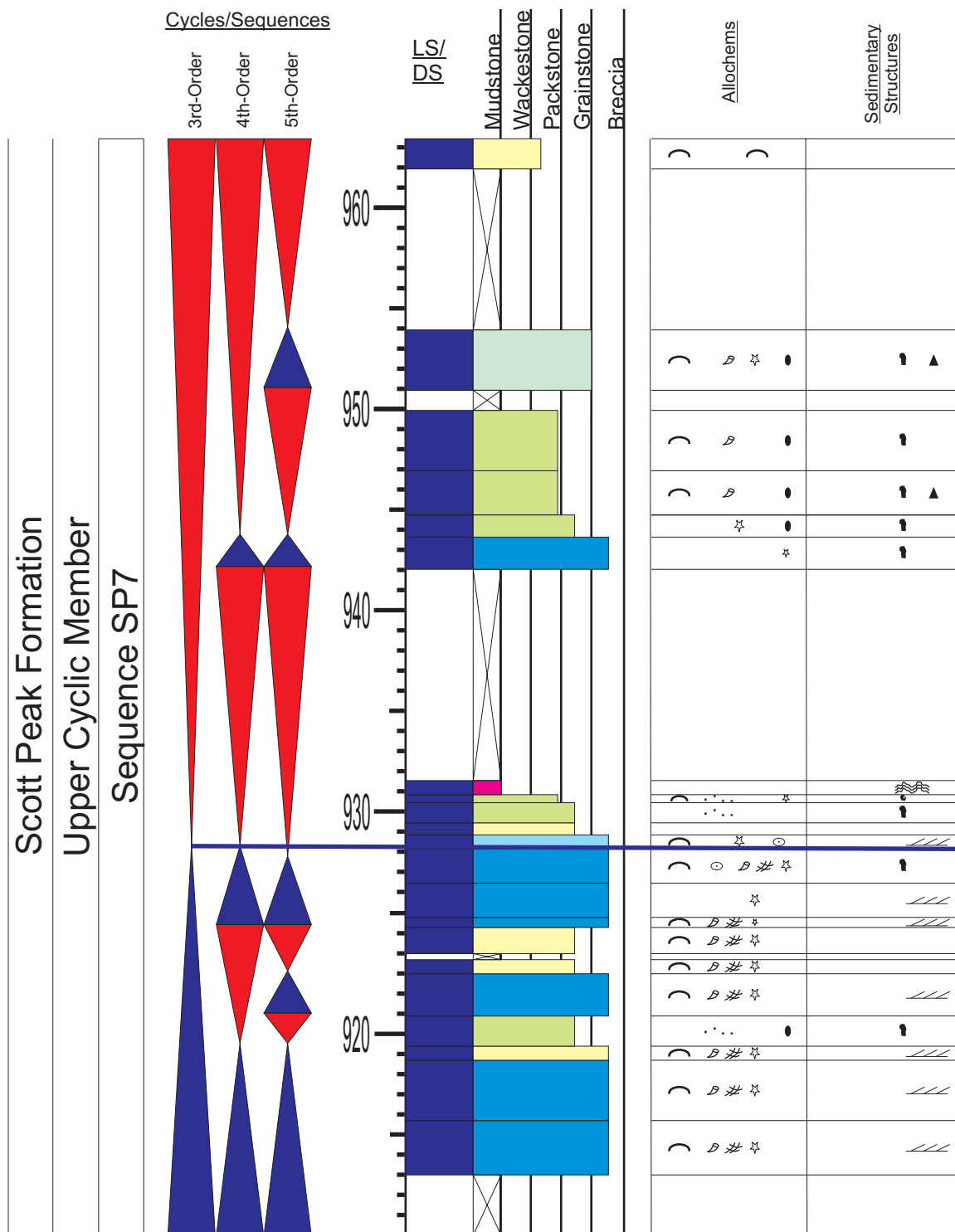


Figure 3.63: The graphic sedimentary log of the sequence SP7 from section location East Canyon. The TST is made up of aggradationally stacked, partly amalgamated crinoidal and skeletal grainstones interbedded with skeletal and peloidal wackestones-packstones. The HST is composed of peloidal wackestones-packstones interbedded with peloidal/skeletal packstone-grainstone and extensive covered intervals which are inferred to be of muddier composition and less competent. The blue line is the maximum flooding surface. Refer to Figures 3.12-14 for symbol definitions.



Figure 3.64: Outcrop photograph of the top of the Meramecian-Chesterian Scott Peak Formation (Msp) and the base of the overlying Chesterian South Creek Formation at section location Upper Pahsimeroi. A sharp contact marks the drowning surface between the shallow water Scott Peak ramp and the deeper water shales of the South Creek Formation. Width of photograph is approximately 1 km.

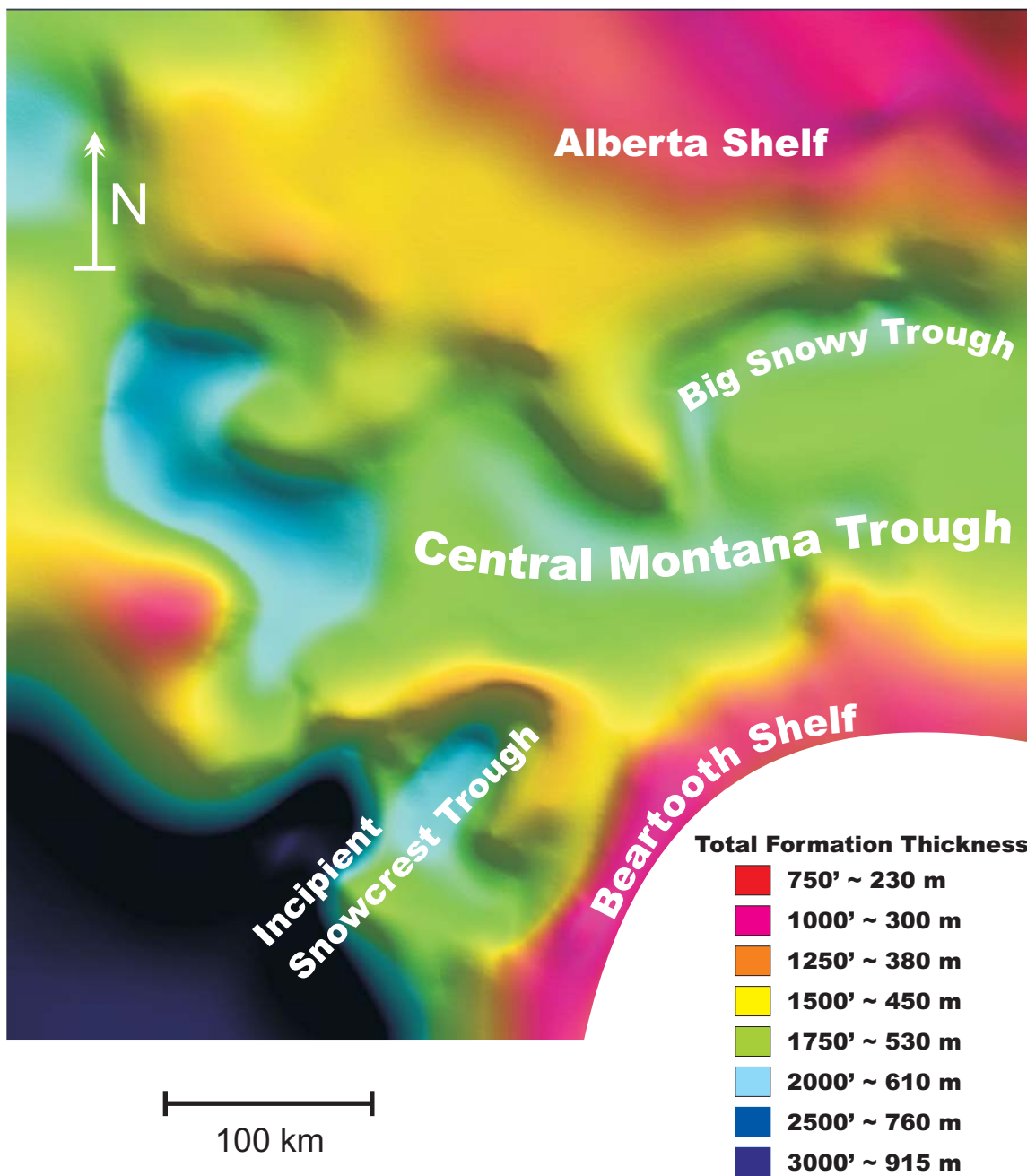


Figure 3.65: Thickness and paleotectonic elements of the Lower and middle Mississippian Madison Group in western Montana (modified from Peterson, 1985)

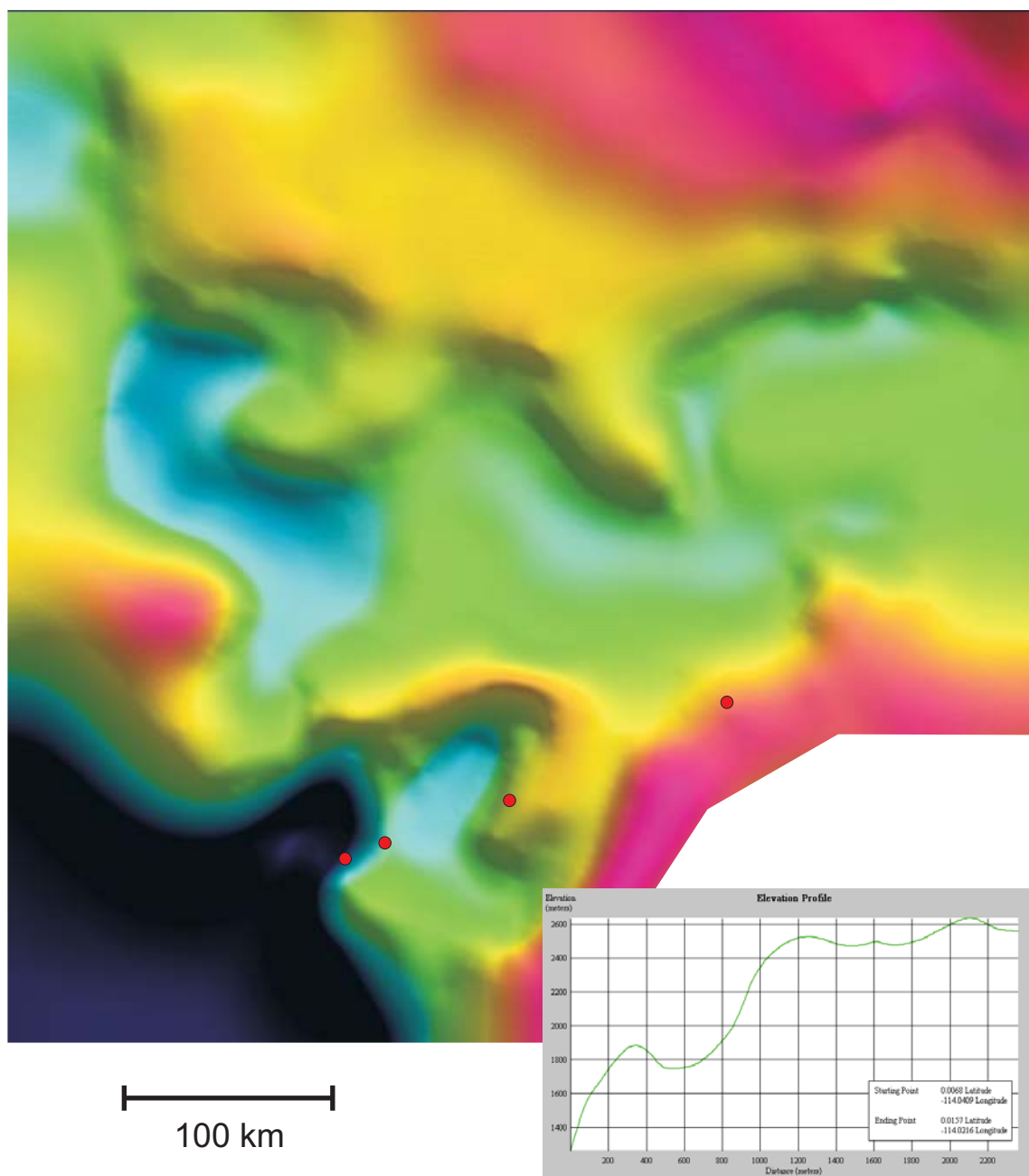


Figure 3.66: Surfaced isopach map showing, reproduced from Figure 3.59 with overlain outcrop section locations (red dots). The profile in the lower right indicates the variation in thickness (+y to the bottom) of Madison-equivalent strata through the transect A'-A'' from Figure 1.4. Significant variability in thickness especially to the southwest is indicative of differential subsidence across the study area towards the Antler foredeep basin. Non-uniform increases in thickness to the southwest may indicate that small-scale faults acted to segment the area and modify the expected accommodation space for sediment accumulation there.

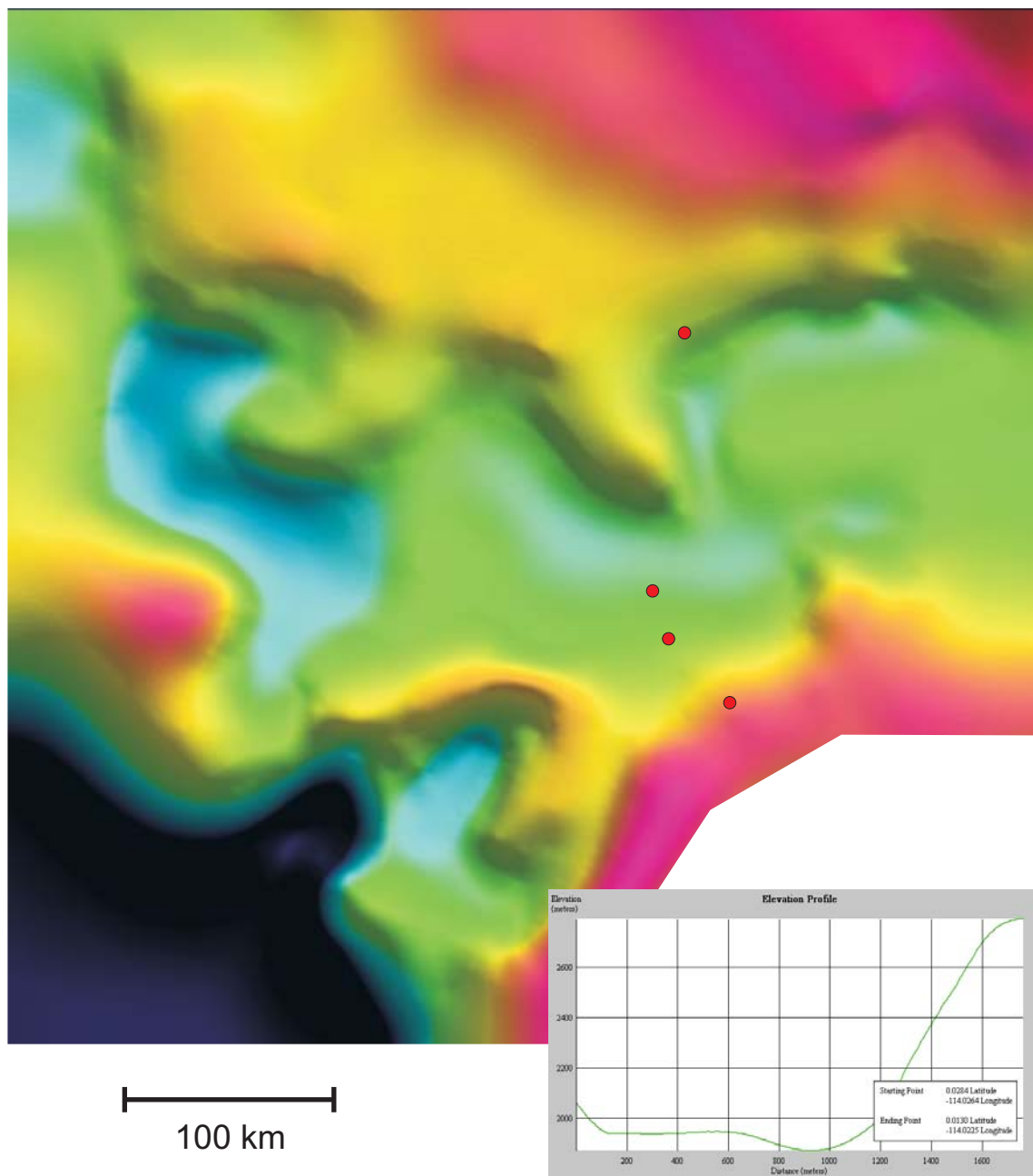


Figure 3.67: Surfaced isopach map showing, reproduced from Figure 3.59 with overlain outcrop section locations (red dots). The profile in the lower right indicates the variation in thickness (+y to the bottom) of Madison-equivalent strata through the transect A'-A'' from Figure 1.4. Significant increases in thickness are observed from south to north in this profile. This profile indicates that the central Montana trough was a slightly asymmetric depocenter during Madison time with the thickest accumulations in the southern part of the cross-section.

SW
A''

NE
A

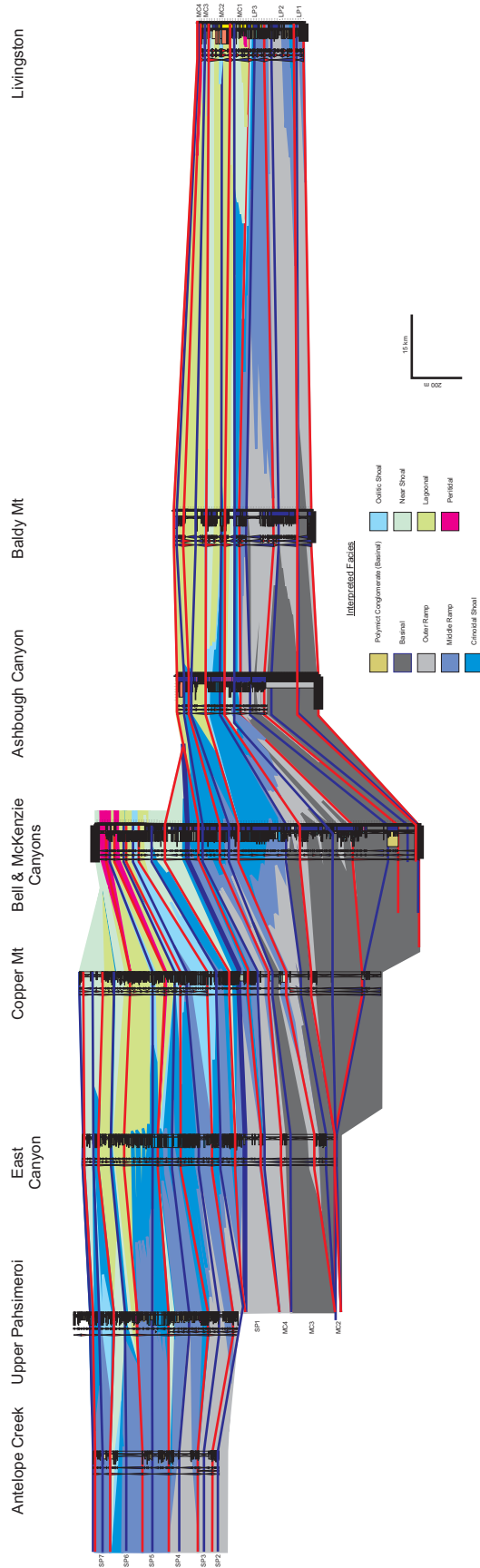


Figure 3.68: Regional sequence stratigraphic cross-section along the transect A-A'' in Figure 3.6 from south-central Montana to the Antler foreland basin. The section is datumed on the top of sequence LP2 for the updip outcrop measured sections (sections Livingston, Baldy Mt., and Ashbough Canyon) and SP7 for the downdip localities to emphasize the overall progradational architecture of the Madison Group and the downstepped nature of the Scott Peak formation.

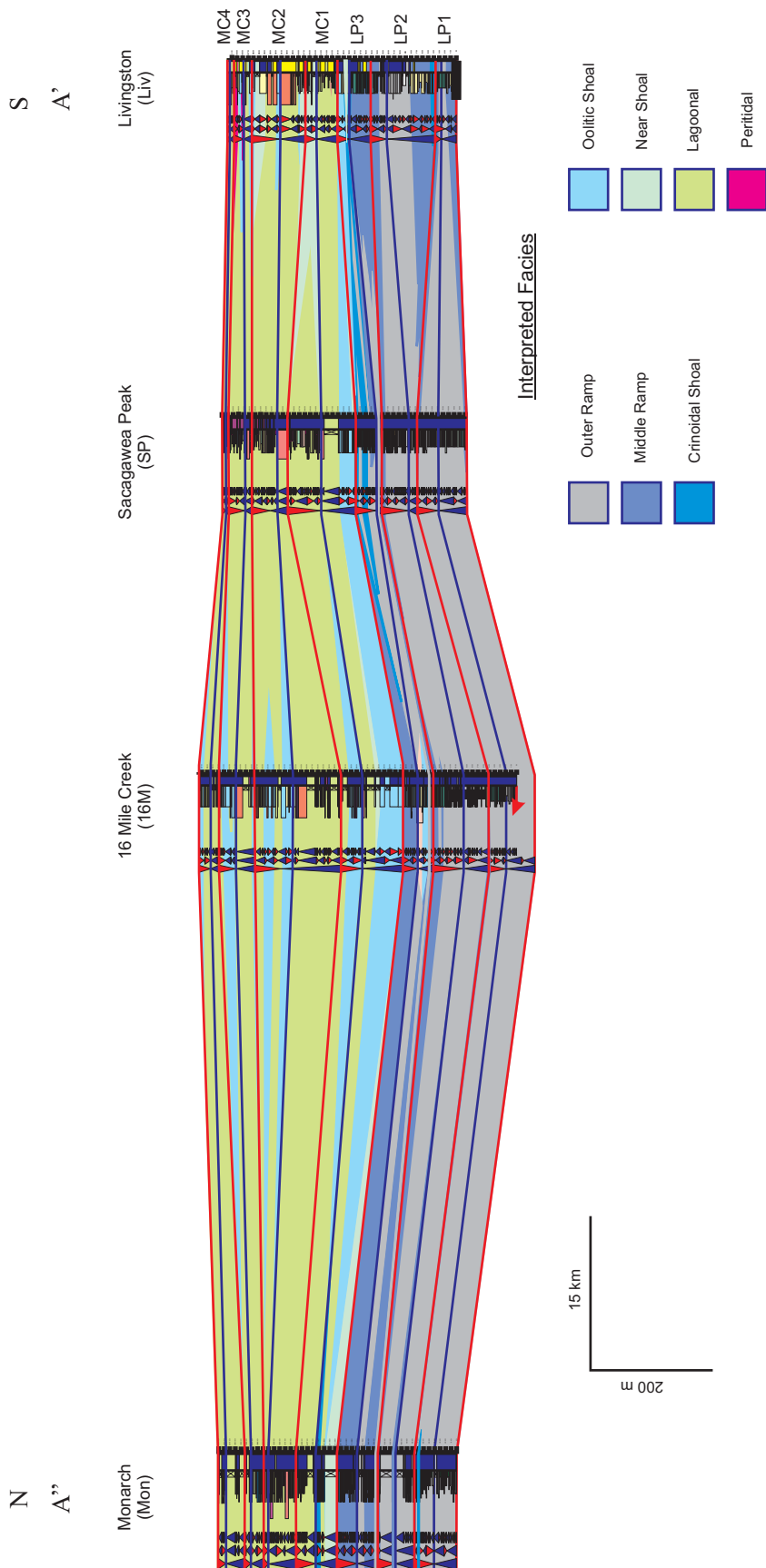


Figure 3.69: Regional sequence stratigraphic cross-section along the transect A-A' in Figure 3.6 from south-central Montana through the central Montana trough. The cross-section is datumed at the MC2 sequence boundary to emphasize the aggradational nature of the fill of the central Montana trough during deposition of the Madison. Marked progradation is notable only during the LP3 highstand.

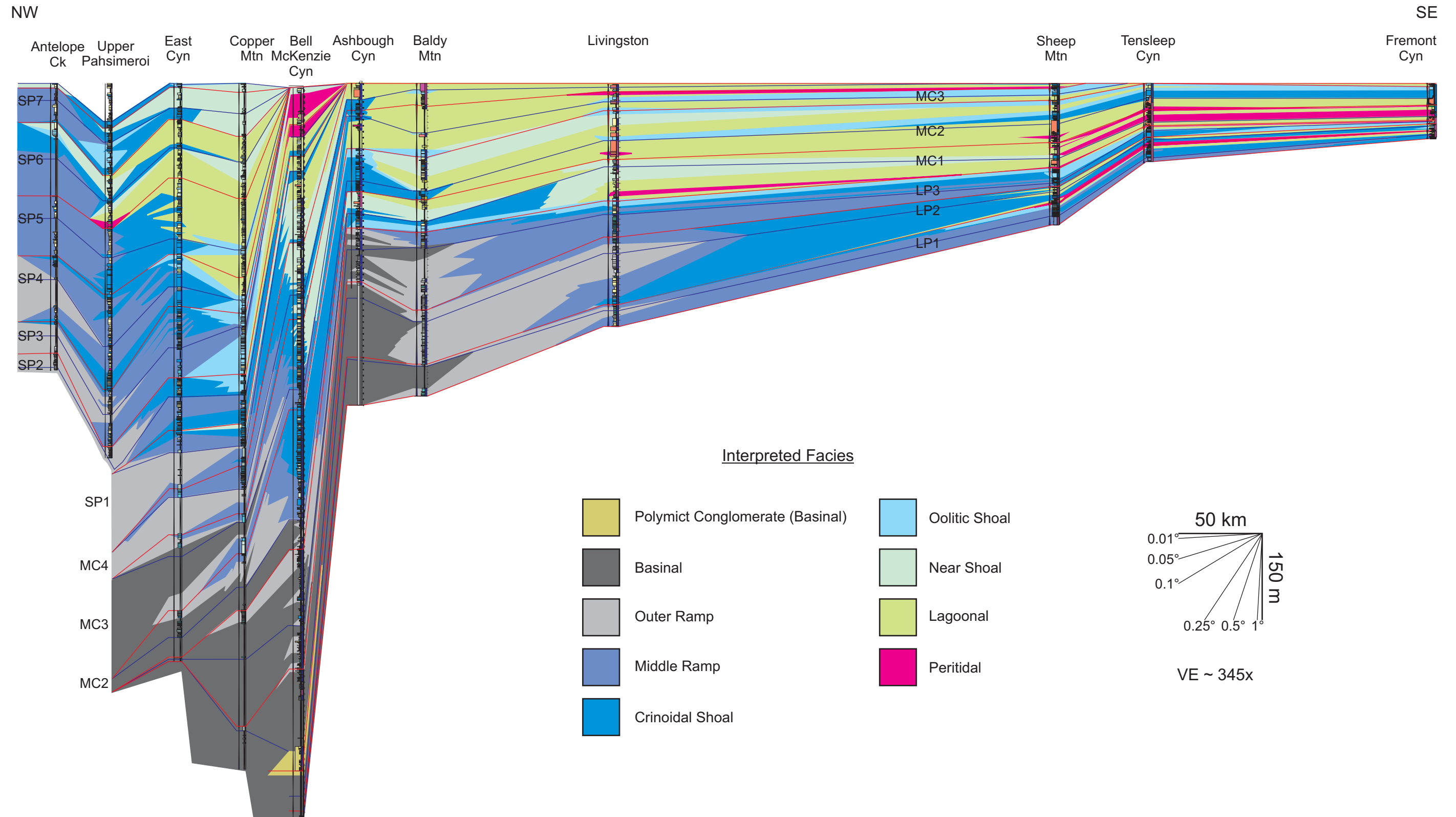


Figure 3.70: Superregional cross-section from extreme updip localities in Wyoming to extreme downdip locations in the Antler foreland basin of Idaho illustrating the overall architecture of the Madison Group and succeeding Scott Peak succession. The section is datumed at top of sequence SP7 in downdip locations and at top Madison supersequence boundary elsewhere. Progradation is characteristic during Lodgepole time (sequence LP1-3) while aggradation dominates Mission Canyon deposition (sequences MC1-4), followed by downstepping and aggradational fill of the Antler foreland during Scott Peak time (sequence SP1-7). Data for sections Sheep Mt., Tensleep Canyon, and Fremont Canyon from Smith et al. (2004).

CHAPTER 4. RECONCILING ANTLER FORELAND BASIN DEVELOPMENT WITH THE MADISON DEPOSITIONAL RECORD: A DYNAMIC FRAMEWORK FOR ACCOMMODATION EVOLUTION

4.1 OVERVIEW

A fundamental problem in regards to carbonate depositional systems and specific to the Madison Group is reconciling the record of extensive carbonate deposits within an environment inhospitable to what is currently understood about the factors which promote their deposition. Foreland basins are a prime example of an environment typically thought to be inhospitable to carbonate deposition (Dorobek, 1995; Chapter 1); however, both in the ancient record and in extant carbonate depositional systems, carbonate sediments are commonly found to be produced and stored in close association with this atypical setting. The Madison Group and genetically related strata of Wyoming, Montana, and Idaho represent a class of spatially large ($\gg 1 \times 10^6 \text{ km}^2$) and temporally long-lived ($\sim 13 \text{ Myr}$; Sando, 1985) carbonate depositional systems with no modern analog. The processes related to the growth, initiation and demise of the Madison Group, however, provide information on how a system of this great scale existed along a collisional margin and coevolved with a developing foreland basin.

In order to address the question of what leads to carbonate sediments contributing a significant proportion of sediments to the overall fill of the basin, controls on carbonate sediment production and storage area need to be constrained. Combinations of tectonic parameters and carbonate sediment production and storage controls that are required can be defined. These controls must act in concert in order to provide conditions suitable to host a large carbonate ramp system in an active flexural setting. The challenge is to develop a self-consistent dynamic tectonostratigraphic framework which is compatible with the physics controlling the geodynamic evolution of the foreland basin and the biologic, physical, and chemical requirements of the vast carbonate depositional system. Carbonate stratigraphy, sedimentary architecture, and facies motifs provide constraints on the distribution of carbonate sediment producing and storage localities and changes in the spatial distributions of these elements through time. By examining these elements, applying the information provided by carbonate sedimentation of the Madison Group and

taking a process-based approach where limits on the geodynamic evolution of the basin are derived from these limits, a self-consistent tectonostratigraphic framework which conforms both with a reasonable lithospheric mechanical model of basin evolution and the geology will result.

The goal of modeling efforts here is to assess whether there is a causal link between orogenesis, load emplacement and long-term lithospheric response to loading and the initiation of carbonate sedimentation, the patterns of carbonate sediment production, dispersal, and storage and changes in these patterns with time, and the ultimate termination of carbonate production. Quantification of temporally-dependent changes in the effective elastic thickness of the lithosphere of western North America when subjected to the load of the Roberts Mountain allochthon for geologically-significant periods of time provides information on the distribution of areas prone to carbonate sediment production and locations for sediment storage and preservation. The general approach adopted here to address this question is to conformably map each third-order stratigraphic sequence identified in outcrop on the modeled deflected lithosphere at appropriate model timesteps. Once a sedimentary package is “deposited”, the modeled lithosphere is then allowed to evolve a timestep and the following sequence can once be deposited on the new topography generated. Each model timestep can then be analyzed to examine the modeled distribution of accommodation space across the system. As the sedimentary record provides information on the water depth at the time of sediment production and deposition, the model is then compared with the observed and a reasonability of fit between the modeled and observed can be obtained, thus “honoring the geology.”

4.2 GEOLOGICAL BACKGROUND

4.2.1 The Antler Orogeny

The Antler foreland basin formed in response to a collision of the former passive margin of western North America with a poorly defined arc system (Nilsen and Stewart, 1980). Recent interpretations suggest that the westward directed subduction of the North American plate beneath the arc began in Middle Devonian time and emplacement of a load upon the North American lithosphere occurred over an 8-10 Myr period from the Late Devonian-Early Mississippian (Dorobek et al., 1991; Johnson and Pendergast, 1981;

Smith and Ketner, 1968, 1977). The load, which is preserved as the Roberts Mountain allochthon in Nevada, has been interpreted as an accretionary prism that was beached on the North American plate margin (Roberts, 1958). Subduction appears to have shut down during the Early Mississippian (middle Kinderhookian) likely in response to buoyant continental crust entering the subduction zone and choking off subduction at this time (Trexler et al., 2004).

The geologic record of the Antler orogeny is poorly preserved, but it was first recognized in central Nevada by Roberts and coworkers (1958). The Antler orogeny was subsequently applied to all Late Devonian-Early Mississippian tectonism along the Arctic and western margins of North America (Johnson and Pendergast, 1981), but the definition of the Antler orogeny was later restricted to events of the time from Idaho to California. The Roberts Mountain thrust fault of central Nevada is the primary structure which preserves a record of the emplacement of allochthonous material onto western North America (Roberts et al., 1958). At least 140 km of throw has been estimated on this fault (Roberts et al., 1958; Stewart and Poole, 1974; Smith and Ketner, 1977). The Roberts Mountain allochthon is composed of a complexly deformed *mélange* of Ordovician-Devonian aged strata of deep water affinity (Kay and Crawford, 1964; Matti and McKee, 1977; Rowell et al., 1979). It has been suggested by Burchfiel and Royden (1991) that this material is a part of a wide accretionary prism which flanked the arc lying to the west. The arc has been interpreted to perhaps lie within the Klamath-Sierran arc of California.

The Antler orogeny has recently been reinterpreted by Trexler and coworkers (2003, 2004). Their work focuses on the reinterpretation of fault contacts and the identification of stratigraphically significant surfaces in northern and central Nevada of Permo-Carboniferous age. In particular, they conclude that a series of angular unconformities were formerly interpreted as thrust faults. Detailed biostratigraphy has shown six unconformities of Carboniferous age and two of Permian age (Figure 4.1). Trexler et al. (2004) have used this new interpretation of these surfaces to define a new chronology of tectonism along the North American margin at this time. They conclude that each unconformity records a pulse of tectonic loading of the margin, which is then followed by a period of tectonic quiescence. The Madison Group and its genetically

related strata of east-central Idaho, herein referred to as the Madison system, are bracketed by two of these surfaces, the Kinderhookian C1 unconformity and the C2 unconformity of Meramecian age. This work suggests that the erosional base and top of the Madison Group and equivalents are likely tectonic in origin and driven by pulsed loading along the western margin of North America.

4.2.2 Elastic Response to Loading

In order to understand the deflection of the lithosphere under the load of the Antler orogeny, an elastic model can be used to understand the shape of the deflection and the geometry of the resulting foreland basin. The lithosphere responds to emplacement of a load not purely by an Airy response but rather by a regional compensation of the load (Vening Meinesz, 1931). That is rather than purely subsiding locally beneath the stress of the emplaced load, the lithosphere flexes. This occurs because the lithosphere has strength and can transmit the stress some distance in order to accommodate the load. The flexure in response to loading is an elastic response and the deflection produced reflects the mechanical properties, initially the elastic properties, of the lithosphere. The deflection under the load produces a characteristic flexure which can be characterized by the flexural parameter, λ , which defines the wavelength and the amplitude of the deflection. The flexural parameter is controlled by the strength of the lithosphere, which in turn can be thought as a measure of the elastic thickness of the lithosphere. The product of this flexure is typically a series of long wavelength, low relief swales and swells.

A retroarc foreland system is defined as the area affected by flexural warping of the lithosphere which lies between the emplaced load and the unaffected cratonic hinterland. The profile produced by the lithosphere in flexure is a predictable damped sinusoidal pattern of lows and highs generally scaled by the flexural wavelength. The product is a series of definable depozones with distinct accommodation patterns, which can be defined between nodal points along the flexural profile and accumulate distinct sedimentary assemblages (Figure 4.2). The largest subsidence produced on the loaded lithosphere lies beneath the mass of the load and extends laterally adjacent to the load. This zone is termed the foredeep (Aubouin, 1965; Decelles and Giles, 1996). The foredeep has a typical width of $\lambda/4$, which is due to the load having finite width and

occupying part of this depozone. Flanking the foredeep on its cratonward side is the forebulge depozone. This depozone rises above the mean elevation of the adjacent craton with an amplitude approximately an order of magnitude less than that of the foredeep. Its characteristic wavelength is $\lambda/2$. The last major depozone cratonward before flexure is attenuated is the backbulge. This zone also has a width of $\lambda/2$, and like the foredeep is characterized by subsidence; however, its amplitude is approximately an order of magnitude less than that of the forebulge.

Typically during an orogeny, the load moves progressively toward the craton. The flexural profile accompanies the movement of the load in a cratonward direction. The implication of the migration of the flexural profile is that tectonic inversion is demanded as migration progresses. As a result areas which were once uplifted upon the forebulge and warped downward into the new foredeep, and backbulge areas are flexed upward atop the forebulge. Additionally the foredeep depozone becomes overridden by the load and potentially incorporated within it. Antiphase accommodation patterns result as a consequence of flexural profile migration as well (Catuneanu et al., 2000). All else being equal, areas within the foredeep and backbulge depozones see increasing accommodation, while accommodation space across the forebulge decreases and could possibly be uplifted to the point where erosion rather than deposition occurs. Patterns of antiphase accommodation space development are diagnostic of flexural partitioning of a foreland basin.

4.2.3 Paleogeography

The Madison system was deposited over a broad area in what is now Wyoming, Montana and Idaho covering an area $\gg 1 \times 10^6 \text{ km}^2$ (Figure 4.3). The system was deposited on a shallow tropical shelf at approximately $0\text{-}10^\circ \text{ N}$, which was positioned along the western margin of North America (Scotese and McKerrow, 1990). The Madison shelf was bordered to the southeast by the Transcontinental arch, which had positive relief at this time, and by a shallow trough, the central Montana trough, and the Williston basin, an intracronic basin, on its north. To the west the shelf was bound by deep water of the Antler foreland basin, which separated the shelf from the Antler highlands further west (Maughan, 1983). The Madison system was deposited over a

period of ~20 Myr in the Lower-Middle Mississippian from Kinderhookian (Tournasian) to Meramecian (Visean) time.

4.2.4 Regional Antler foreland sedimentary architecture

The classic regional cross-sections of the Madison system illustrate the overall geometries and facies relationships across the area of deposition at broad spatial and temporal scales (Rose, 1976; Figure 4.4). Rose's illustrates several key points. First deposition of the subordinate Lodgepole and Mission Canyon Formations of the Madison Group (Madison Limestone of Wyoming) are areally restricted to a broad zone which lay arched between the Williston basin in the east and Antler "flysch trough." These formations are of Kinderhook-Osagean in age and contributed insignificant amounts of carbonate sediment to the foredeep depozone. Rather, the "flysch trough", which lay adjacent to the Antler highlands and occupied the foredeep, received clastic sediments from the uplifted and exposed Antler highlands. Progradation of carbonates into the trough and contribution of significant amounts of carbonate sediments to its fill are limited to Meramecian time.

4.2.5 Madison sequence architecture

The Madison system, as noted above, is bound on its top and base by regionally extensive unconformities which are coincidental with major periods of collision between North America and an arc system to the west. These unconformities mark the base and top of the Madison second order supersequence (Sonnenfeld, 1996a). The Madison Group proper has been documented as being composed of a hierarchy of stratigraphic sequences from second order, 10-100 Myr in length, to fifth order, which are of approximately orbital scale, in duration (Sonnenfeld, 1996a, 1996b; Smith et al., 2004; this volume).

Due to the regional correlation length of sequences of third (1-10 Myr) and lower order, long-term accommodation trends and facies patterns are considered for analysis herein. These packages are considered appropriate because they can be correlated over all significant spatial scales and the quality of the time correlations is greatly aided by chemostratigraphic and biostratigraphic data (Katz et al., in prep; Chapter 3). Additionally, the second-order supersequence boundaries are of apparent tectonic nature as documented by Trexler et al. (2004), while third-order sequence boundaries have been

interpreted as eustatic in nature (Sonnenfeld, 1996a, 1996b; Elrick and Read, 1991; Chapter 3). These observations provide end-members and model constraints for this study and also provide readily testable hypotheses on accommodation development and accommodation controls which can be quantitatively explored here.

At the supersequence scale, the Madison system can be viewed as an overall transgressive-regressive cycle where the Madison shelf is first inundated, then filled by a backstepping carbonate ramp as accommodation space increases and a prograding carbonate platform as the space for sediment accumulation decreases (Sonnenfeld, 1996a, 1996b). The beginning and end of these events are punctuated by collisions along the western North American margin. However, at the third order scale, this general picture is complicated. What comes into focus is rather than a simple relative sea level rise and fall with a tectonic master, the system can be discretized into a stacked series of initially retrograding ramps and then shingled prograding platforms with facies distributions characteristic of eustatic control. When viewed at the intermediate scale, that of the composite third-order sequence scale (approximately formation-scale lithostratigraphically), changes in accommodation and facies motif reveal packaging where the shared forcing functions of tectonic relative sea-level change and eustatic sea-level change become clear.

4.3 METHODOLOGY

4.3.1 Approach

Elastic models of the lithosphere have broadly been applied to examine regional compensation of loads by lithospheric flexure (Vening Meinesz, 1931; Walcott, 1970a, 1972; Speed and Sleep, 1982). In the simplest form, the lithosphere can be modeled as a thin elastic plate overlying an inviscid fluid substrate (Nadai, 1963). Models of this type have been successfully applied to explain the lithospheric response in a variety of settings from seamounts and ocean islands emplaced on oceanic lithosphere (Walcott, 1970b) to orogenic loads, both surface and subsurface, in continental settings (Jordan, 1981). Studies employing elastic models have yielded a number of estimates of the long-term mechanical properties of the lithosphere in many different tectonic settings.

Purely elastic models of the lithosphere, however, have several limitations due to their overly simplistic view of geologically and physically complex materials. Observational evidence shows that elastic models overpredict bending stresses induced by glacial loading and stress drops associated with earthquakes (Watts, 2001). A more critical problem particular to the evolution of foreland basins is that these models are time invariant. This is because elastic deformation is dependent only on the stress of the applied load. Consequently, elastic models fail to account for changes in flexure that result from long-term, static loading. In the case where loads are not static and continue to migrate (i.e., active subduction settings), however, the elastic solution may be appropriate. This is because the load is transient and the underlying lithosphere is never subjected to long-term loading.

In order to examine the secular evolution of lithospheric flexure in response to a static load, a more complex set of material properties for the lithosphere must be employed. The simplest of this class of models is the use of a viscoelastic rather than an elastic rheology. The viscoelastic material response is a combination of a time-invariant elastic component as well as a viscous component, which has strain rate dependence.

Walcott (1970) first applied a viscoelastic plate model to the lithosphere. In this work, viscoelastic response functions for a thin plate overlying an inviscid fluid were derived from the general solution for the elastic plate model of Nadai (1963). Viscoelastic models of lithospheric flexure have been successfully applied to retroarc foreland basin settings. Beaumont (1981) applied a viscoelastic formulation to explain offlapping sediment geometries and erosion patterns in the Alberta foreland basin. Quinlan and Beaumont (1984) later applied a similar model to examine sedimentation patterns, unconformity development, and controls on the development of first-order megasequences of Sloss (1963) in the multistage Appalachian foreland basin.

The modeling approach adopted here is a viscoelastic reformulation of the elastic model of Speed and Sleep (1982). Speed and Sleep (1982) first applied quantitative elastic models of lithospheric flexure to the Antler orogenic system. The elastic modeling of Speed and Sleep (1982) was concerned with active orogenesis in the Antler belt related to load emplacement on the western margin of North America. The modeling effort herein focuses on modeling time-dependent flexure during a period of tectonic

quiescence postdating the original emplacement of the Roberts Mountain allochthon using a forward modeling approach.

The work of Speed and Sleep (1982) provided the initial thin-plate theoretical framework for modeling here. The primary modification of their model was the substitution of an elastic lithospheric rheology with a viscoelastic rheological model. Additionally their published Antler orogeny-specific elastic model experiments provided reasonable estimates of basic model parameters such as load mass and lithospheric elastic thickness and the model results were employed here for initial model validation.

4.3.2 Flexure of an elastic plate

Flexure of the lithosphere can be approximated by the deflection of an elastic beam overlying a weak foundation (Hetenyi, 1979). This idea can be further simplified by considering the foundation as inviscid fluid, which is defined as fluid with zero viscosity. Given this case, Watts (2001) has shown that the deflection of a thin elastic plate under a load can be described by the Fourier transform of the flexure equation

$$D \frac{d^4 y}{dx^4} + (\rho_m - \rho_f) y g = 0 \quad (1)$$

where D is the flexural rigidity, y is the vertical displacement of the deflection, x is the horizontal distance along the beam, ρ_m and ρ_f are the densities of the mantle and fill respectively, and g is the acceleration due to gravity. The flexural rigidity is defined as

$$D = \frac{ET_e^3}{12(1-\nu^2)} \quad (2)$$

where E is the Young's modulus of the plate, T_e is the elastic thickness of the plate, and ν is the Poisson's ratio. Following Watts (2001), an analytic solution for equation (1) can be obtained using the method of quadratics, which yields a solution of the form

$$y = e^{\lambda x} (A_c \cos \lambda x + B_c \sin \lambda x) + e^{-\lambda x} (C_c \cos \lambda x + D_c \sin \lambda x) \quad (3)$$

here A_c , B_c , C_c , and D_c are the constants of integration. λ is the flexural parameter which controls the wavelength and amplitude of the deflection and is defined as

$$\lambda = \left(\frac{(\rho_m - \rho_f)g}{4D} \right)^{1/4} \quad (4)$$

λ defines the characteristic asymmetric shape of the flexural profile of the foreland lithosphere.

In order to obtain a useful solution of the equation (3), several assumptions must be made to solve for the integration constants. The first case involves the assumption that a load, P_b , is applied at some arbitrary point on a beam of infinite length, $x \rightarrow \pm\infty$. The point directly beneath the load is then defined as the origin, (0,0). Applying this boundary condition ensures no deflection occurs at the far edges of the beam, and it is met only in the case where the constants A_c and B_c in equation (3) are zero. Thus,

$$y = e^{-\lambda x} (C_c \cos \lambda x + D_c \sin \lambda x) \quad (5)$$

The second boundary condition requires that the deflection is symmetric about the load. For this to be true, the case where $x = 0$ and $dy/dx = 0$ must be satisfied. Taking the first derivative of equation (5) and solving for $x = 0$ yields

$$dy/dx = C_c(-\lambda) + D_c(\lambda) \quad (6)$$

Equation (6) goes to zero only when C_c and D_c are equal, so equation (5) becomes

$$y = e^{-\lambda x} D_c (\cos \lambda x + \sin \lambda x) \quad (7)$$

D_c can be solved for using a force balance approach, where all downward forces are balanced by upward forces. In this case, buoyant restoring forces of the displaced mantle must balance the load P_b ,

$$P_b = 2(\rho_m - \rho_f)g \int_0^{\infty} y dx \quad (8)$$

and substituting y from equation (7) and integrating gives

$$P_b = \frac{2(\rho_m - \rho_f)g D_c}{\lambda} \quad (9)$$

Substituting D_c from equation (9) back into equation (7)

$$y = \frac{P_b \lambda}{2(\rho_m - \rho_f)g} e^{-\lambda x} (\cos \lambda x - \sin \lambda x) \quad (10)$$

Although the solution given in equation (10) is appropriate for geological applications where a load is emplaced on an unbroken plate, such as an ocean island erupted onto oceanic lithosphere, this consideration is not likely applicable to the case of a foreland basin. In this case where the load is emplaced at or near the edge of the plate, a semi-infinite beam should be considered. The approach to the solution of this problem is

similar to that for an infinite plate. An additional force balance, however, must be considered, that of the bending moments. When these forces are considered, the deflection y of the semi-infinite plate with the load P_b emplaced on its end is

$$y = \frac{2P_b\lambda}{(\rho_m - \rho_f)g} e^{-\lambda x} \cos \lambda x \quad (11)$$

A full treatment of the derivation of this solution is presented by Watts (2001).

Applying equation (11), solutions can be found for the deflection of the lithosphere about a load due to the regional compensation of the load by flexure. Model runs illustrating the variation of the flexural response are performed by varying the load mass and density as well as the flexural rigidity of the plate.

4.3.3 Time-dependent flexure of a viscoelastic plate

Studies of the long-term mechanical properties have shown that the lithosphere, although maintaining most of its strength over geologically-significant time scales, does relax at least part of the stress that was initially applied by loading. Although this process is likely due to a combination of factors, a first approximation can be reached by assuming that part of the lithosphere behaves elastically while the other part behaves viscously. Viscous and elastic materials deform in fundamentally different ways when stressed. An elastic material properties model follows Hooke's law, which relates the stress, σ , to the strain, ε , by Young's modulus, E , while in a viscous model the strain is proportional to the change in deformation. That is in a viscous model, stress is related to the strain rate, $\dot{\varepsilon}$, by the material's viscosity, η . A viscoelastic material model combines both these components. The simplest viscoelastic material model is the Maxwell model. A Maxwell viscoelastic material is commonly depicted by an elastic spring and a viscous dashpot linked in series. Mathematically, this combination is expressed for strain in terms of stress as

$$\varepsilon = \frac{\sigma}{E} + \frac{\sigma t}{\eta} \quad (12)$$

Additionally, after a certain amount of time under stress, the deformation due to elastic and viscous strains become equal in the viscoelastic material. This time is known as the Maxwell relaxation time, τ , and is defined

$$\tau = \frac{\eta}{E} \quad (13)$$

Nadai (1963) solved the general equation for the flexure of a viscoelastic plate overlying an inviscid fluid, which is given by

$$D_0 \frac{\partial^4 y}{\partial x^4} + (\rho_m - \rho_f)g(\tau \dot{y} + y) = 0 \quad (14)$$

where D_0 is the instantaneous flexural rigidity of the plate and \dot{y} is the derivative of y with respect to time. Watts (2001) demonstrated using substitution that flexure of a viscoelastic plate under a periodic load is periodic. Based on this solution, it was shown that a viscoelastic flexural response function could be defined of the form

$$y = \frac{(\rho_f - \rho_m)h \cos(kx)}{(\rho_m - \rho_f)[1 + \frac{D_0 k^4}{(\rho_m - \rho_f)g}]} \left(1 + \frac{D_0 k^4}{(\rho_m - \rho_f)g} [1 - e^{-t/\tau[1 + \frac{D_0 k^4}{(\rho_m - \rho_f)g}]}]\right) \quad (15)$$

where h is the height of the load and k is the wavenumber of the load.

This solution demonstrates the critical behavior of the viscoelastic material property model. The instantaneous response of the viscoelastic plate, that is when $t = 0$, is purely elastic in form, as the no stress has yet to be viscously relaxed. In the infinite limit of time, however, equation (15) approaches an Airy response. This suggests that each viscoelastic flexural profile should have an equivalent purely elastic profile with an equivalent effective elastic thickness. To address this, Watts (2001) compared the viscoelastic and elastic flexural response functions. These functions use a wavenumber parameter in order to relate the Airy response to the flexural response. As a consequence these functions give the flexural response in terms of a unitized load, which allows direct comparison of these model and yields the equivalent flexural rigidity, D_e , for both the purely elastic and viscoelastic profiles (Figure 4.5). D_e is defined as

$$D_e = \frac{(\rho_m - \rho_f)g}{k^4} \left[\frac{1 + \frac{D_0 k^4}{(\rho_m - \rho_f)g}}{1 + \frac{D_0 k^4}{(\rho_m - \rho_f)g} [1 - e^{-t/\tau[1 + \frac{D_0 k^4}{(\rho_m - \rho_f)g}]}]} \right] - 1 \quad (16)$$

Applying equations (15) and (16), results from elastic modeling can be applied to a viscoelastic framework. This allows forward models to be produced which honor the

elastic model parameterizations and constraints first explored by Speed and Sleep (1984) in their dynamic modeling effort of the Antler foreland. Importantly though, the viscoelastic formalization applied here allows for examination of the lithosphere under the load stress when compressional strain rates are approximately zero during intercollisional periods identified by Trexler et al. (2004), and deformation results purely from time evolution of the stress field induced by loading.

4.3.4 Conformable mapping of sequences on modeled flexural profiles

Four outcrop locations in southwest Montana were considered for time-thickness analysis. These outcrops are parautochthonous having been uplifted in Laramide-age, thick-skinned, reverse faults of limited throw (Peterson, 1985) and lying east of the edge of the Jurassic Sevier thrust belt, a highly disturbed, thin-skinned series of nappes (Rodgers et al., 1995). Outcrop localities west of the thrust belt line were not considered for this analysis because they contain no Lower Mississippian carbonate strata and no palinspastic reconstruction of the area is sufficient to resolve their absolute positions on the dip cross-section. An approximate palinspastic restoration where a 30% shortening of the Sevier thrust belt followed by 10% extension due to Cenozoic Basin and Range normal faulting is considered here (Rodgers et al., 1995). This approximation is used to ascertain a restored distance of 358 km from the most basinward outcrop section in southwest Montana to the assumed location of the load in central Idaho.

The third-order stratigraphic sequence scale (~2.2 Myr duration; Sonnenfeld, 1996b) is considered appropriate for analysis of regional accommodation patterns that result from flexural loading of the lithosphere in the Antler foreland basin. This scale is chosen because stratigraphic packages are regionally correlative based on sequence stratigraphic analysis and chemostratigraphic analysis (Chapter 3; Katz et al., in prep), and the duration of each package is of the order of the 1-2 Myr length of the Maxwell relaxation time suggested for the lithosphere (Beaumont, 1978). Thicknesses are linearly interpolated from one outcrop locality to the adjacent localities. For the case of the most basinward section, carbonate sediment thickness is tapered linearly to zero along a line with a slope that ensures that no Lower Mississippian carbonate sedimentation is allowed to occur at the position of the next basinward outcrop section locality. Sediment thickness cratonward of the most updip section is assumed isopachous. The time-thickness plots

that result reveal the overall distribution of accommodation space over the depositional system. This is because the sequence boundaries represent the interval of minimum accommodation space within each mapped interval, thus only minor amounts of unfilled space between the sea surface and water bottom exist.

The initial model surface is assumed to be a seaward-dipping plane with 0.01° dip based on regional isopach maps of Devonian strata of western Montana and eastern Idaho (Peterson, 1985). A load is emplaced on the edge of the semi-infinite beam, with flexural rigidity of $6.48 * 10^{24}$ Nm and Young's modulus of 10^{11} Pa and load parameters of 5 km height, 10 km width, and density of 2800 kg/m^3 (Speed and Sleep, 1982). Carbonate sedimentation is assumed to initiate immediately after load emplacement (i.e., collision rate is zero). Accommodation analysis is performed by first allowing the lithosphere to deflect elastically under the load. The first time-thickness unit (sequence I of Sonnenfeld) is emplaced on this deformed surface with section locations datumed to the modeled flexed lithosphere at the appropriate distance from the load based on the approximate palinspastic reconstruction. The model is then advanced a timestep, which's length is model-run dependent but adheres to chronostratigraphic information. The lithosphere deforms due to viscous relaxation of stress of the load and both the sedimentary package and lithosphere deform in response. This sets up the accommodation conditions for the next sedimentary package, and the process is repeated for subsequent time-thickness packages.

4.4 MODELING RESULTS

4.4.1 Elastic model

The elastic model here applies equation (10) in order to validate the results of Speed and Sleep (1982). Their study produced the original quantitative flexural experiments of deformation of the Antler foreland basin, and the analytic model described therein has been implemented in successive studies of the Antler foreland basin (Wilson et al., 1994) and has been applied more generally to examine sedimentation in foreland settings (Dorobek, 1995). The model here using equation (10), although very similar to the formulation used by Speed and Sleep (1982, Equations 3a, 3b, 4, and 5), employs a significantly different formulation of the flexural rigidity. In their model, Speed and Sleep use a wavenumber, k , which is independent of the flexural rigidity, D .

As a consequence, the model does show variation in the flexural wavelength and the amplitude of the uplift of the forebulge in response to changing load parameters; however, the deflection directly beneath the load is invariant, with respect to variations of load-induced stress. This solution is unreasonable as the maximum stress occurs directly beneath the load, and thus, increased amplitude of the deflection beneath the load with increased load stress is demanded. This behavior is captured within the formulation of the wavenumber, λ , in equation (4), and provides the appropriate solutions to the elastic flexure equations for loads of varying mass.

4.4.2 Viscous stress relaxation

Having solved for the elastic deformation due to emplacement of the load and the flexural regional compensation of the stress induced by the load, the viscous, that is time-dependent behavior, of the plate in flexure can be considered. The simplest treatment of the problem is to employ the time-dependent flexural rigidity, D_e , defined by equation (16) and substitute this expression into the elastic solution for the wavenumber parameter, λ (equation (4)). Using this solution, the relaxation of stresses within the plate by the viscous channel can be viewed in terms of the change in the effective elastic thickness of the lithosphere. D_e , the equivalent flexural rigidity, then expresses the deflection of a viscoelastic plate in terms of an equivalent elastic plate with a lower flexural rigidity than the original plate at time $t = 0$. The time-dependent wavenumber parameter, λ , is then substituted into equation (10). The elastic equation can then be employed using a solution for the wavenumber that is expressed in terms of the effective elastic thickness of the lithosphere and allowing time dependency to be observed within a formerly static formulation. The model is then validated by comparing the solution to the new time-dependent expression at $t = 0$ and the elastic solution, ensuring that the solutions are equivalent under this condition.

The overall effect of viscous stress relaxation can be seen in Figure 4.5. Here, the equivalent flexural rigidity is compared to the initial in terms of t as it relates to the Maxwell relaxation time, τ . Initially, the flexural rigidity is slow to change, but there is a rapid decrease in flexural rigidity as t approaches τ , and when the model reaches $t = \tau$, an approximately 50% decline in flexural rigidity has occurred. This is followed by an asymptotic falloff on long timescales, as the model response approaches that of the Airy

case. As the model progresses from a regionally compensated flexural response of the load to a local response, concomitant changes in the flexural profile occur. Figure 4.5 shows the evolution of the flexural profile as viscous stress relaxation occurs. As the effective elastic thickness of the plate decreases, the flexural wavelength narrows and the amplitude of the deflection increases. The net effect is a migration of the flexural profile back toward the load.

4.4.3 Conformable mapping

Viscoelastic modeling provides a conceptual framework for carbonate deposition in a foreland basin during times between compressional events. An ever narrowing foredeep restricts the areas in the basin where carbonate sediment production is inhibited due to aphotic conditions, a rising forebulge an area prone to high-energy, open marine conditions which are favorable for carbonate sediment production although not storage, and a broad protected backbulge zone would be likely to accumulate carbonate mud and detrital sediments produced on the forebulge and would be prone to restriction and potentially evaporite precipitation. This conceptual framework can be tested quantitatively by conformably mapping sequence thicknesses onto the modeled flexed lithosphere and analyzing the resulting accommodation distribution patterns. In order for a model to be accepted, it must meet the criteria for carbonate sediment production and storage as defined by outcrop analysis over the 200 km long, dip-oriented cross-section (Figure 4.6). All other models are rejected.

Model parameters for the viscoelastic flexure are largely derived from the literature as reasonable values for this tectonic setting. The initial flexural rigidity has been suggested as reasonable for lithosphere of the age of the Wyoming craton. It has also been verified experimentally as the lower limit of solutions for the flexure equation which conform to the constraints from outcrop and satisfy the conditions suitable for carbonate sedimentation over the area of interest (i.e., the thinnest elastic thickness which satisfies the initial model conditions as determined from the stratigraphy).

The remaining parameter to be modeled was the magnitude of the load stress. Using an elastic model, load was varied over 1.3 orders of magnitude across 38 load steps in order to examine the sensitivity of basin geometry to load size and determine the potential range of loads consistent with outcrop data constraints. Load tests revealed that

71% of tested loads produced basins which failed to meet the criterion that the depositional area be below sea level across the entire area of interest. Another 8% were eliminated because they failed to produce a foredeep which could accommodate the amount of clastic sediment that was deposited in the Antler foreland. Of the final 21%, all but four cases were eliminated as unreasonable after one depositional sequence was added and one timestep of basin evolution was invoked. Further addition of stratigraphic time-thicknesses and continued viscous stress relaxation of the modeled lithosphere produced a single model which produced reasonable accommodation patterns over the basin. Results are shown in Figure 4.7.

The initial configuration (Figure 4.8A) shows a downwarped plate under a point load emplaced at 0 km and the basin reaches a maximum depth of 3 km. The foredeep basin extends to 250 km, where it shallows to an initial depth of < 1000 m. The forebulge crest lies at 500 km, and water depths shallow to < 500 m at this locality. A low-amplitude backbulge basin lies between 500 and 750 km and gently shallows away from the load. In Figure 4.8B, sediment thicknesses for sequence I were added atop this initial flexural profile. The result is a basinward-tapering wedge which attains a maximum thickness at the transition between the forebulge and foredeep depozones. Maximum water depths in this area were likely on the order of 100 m, which is consistent with the shale and shaly limestone deposited across the area at this time. Additionally a marked break in slope is observed approximately 350 km from the load, representative of observed abrupt thinning of the sequence at the Montana-Idaho border at this time. In Figure 4.8C, the lithosphere is allowed to relax under the orogenic load at position 0 km for a timestep of 1 Myr. At this model timestep, the sediments of sequence I are observed to deform as the forebulge migrates to a position near 450 km. A distinct backbulge depozone is generated at this time between 350 and 800 km, while abrupt shallowing is observed at 350 km. Additionally, the foredeep is observed to deepen to 3.5 km depth at this time. Figure 4.8D shows the result of the layering of sequence II atop the flexed profile inherited from the model step in Figure 4.8C. Here, sediment thicknesses are observed to reflect the inherited topography from the previous step, with thicker accumulations observed in the backbulge and proximal foredeep areas and thinning overtop of the upwarped sediments of sequence I along the repositioned forebulge. The

carbonate sedimentary wedge is also predicted to extend approximately 100 km further seaward than the underlying sequence I wedge. In Figure 4.8E, the lithosphere is again allowed to relax for a single 1 Myr timestep and deform the overlying sedimentary sequences. A similar pattern to that of Figure 4.8C emerges in this timestep. Again, the forebulge is observed to migrate towards the foredeep, here to a position of approximately 350 km. Again, the backbulge depocenter is observed to increase in amplitude, while the forebulge is uplifted and deforms the overlying packages toward the sea surface. Within the foredeep depozone, the position beneath the model edge at position 0 is observed to exceed 3.5 km in depth, as subsidence is observed to continue in this locality under the relaxing lithosphere.

4.5 DISCUSSION

4.5.1 Introduction to previous modeling

Elastic modeling efforts by Speed and Sleep (1982) of the Antler foreland basin response to emplacement of the Roberts Mountain allochthon demonstrated the importance of consideration of load geometry and margin geometry on Antler foreland basin evolution. Viscoelastic modeling efforts here focus on the problem of flexural evolution of the foreland in response to the already emplaced load and the evolution of the lithosphere in response to the continued presence of the load. The elastic model demonstrates that to the first order, the overall accommodation space available for carbonate sediment production and storage in southwest Montana is compatible with deformation predicted within the constraints of a geologically reasonable elastic parameterization.

The elastic approach, however, is fundamentally flawed. Observations of the behavior of the lithosphere under stress on timescales from days to thousands of years to millions of years to hundreds of millions of years and under various strain rates demonstrate that the lithosphere does not behave in a purely elastic fashion (Walcott, 1970a; Pollitz, 2005; McNutt and Parker, 1978). Rather, a more complex set of material properties must be applied to examine this behavior. By using a simple formulation of a more realistic approximation of lithospheric rheology, namely a Maxwell viscoelastic plate, a reconciliation can be made between a geologically reasonable model of

lithospheric evolution in flexure and the observations of a carbonate depositional system which recorded the high-resolution distribution of space conditions in the far field.

4.5.1.1 Antler foreland basin evolution and accommodation development

Studies of the carbonate strata of the Antler foreland basin in Montana, Wyoming and Idaho have recognized the importance of the influence of tectonics on deposition here. Viscoelastic relaxation has been invoked by Chen and Webster (1994) to explain the overall evolution of the Lower Mississippian Lodgepole Formation of western Wyoming and southeastern Idaho; however, this idea was used as a conceptual framework for their observations and no attempts to place these observations within a quantitative framework was made.

Dorobek et al. (1991) examined regional isopach data and lithofacies patterns, constructed cross-sections and computed subsidence curves for Middle Devonian-Carboniferous carbonates primarily deposited in Montana in an attempt to understand the effects of the onset of collision through postcollision tectonic influence on the stratigraphic systems here. They recognized that although foreland basins are formed in response to loading, most numerical modeling studies of these settings tended to treat the lithosphere as an isotropic medium. They noted that in addition to emplacement of loads, collisions produced high in-plane stresses which could be transmitted hundreds of kilometers inboard of the load. A large number of features existed which could be defined through isopach mapping. These features typically had low amplitudes and short wavelengths and developed at high angles to the collision direction (Figure 4.9), and may reflect underlying heterogeneity within the lithosphere and preexisting weakness. Additionally, these features commonly underwent inversion, that is, areas which were initially low became highs and vice versa over the duration of the time examined.

In the study of Dorobek et al. (1991), differential subsidence induced by loading was considered, however, certain conditions must have been necessary. They suggested that loading may explain subsidence over the region only if the lithosphere was segmented mechanically by previous rifting and the mechanically independent segments were subregionally loaded.

The attempt of work here was not to explain the distribution of all paleotectonic elements, but rather to attempt to explain the general accommodation patterns observed

in an outcrop transect across the distal Antler foreland basin system. Modeling results suggest that first-order accommodation patterns of the distal foreland basin system can be explained within an internally consistent framework of flexure of the lithosphere using geologically reasonable values for lithospheric elastic thickness. Evolution of accommodation space patterns are modeled as a result of the deflection of the lithosphere under the load of the Antler orogenic belt and subsequent relaxation of stress via the viscous channel using a viscoelastic rheology for the lithosphere.

4.5.2 Stratigraphic architecture and facies motifs

Viscoelastic model results, although garnered through an overly simplistic approach, provide an internally consistent view of accommodation development in the distal setting of a foreland basin system. Initially, the load is broadly compensated with a foredeep 250 km in width and 3 km deep directly beneath the load. A broad carbonate ramp is initiated on this surface along the low amplitude forebulge and a broad backbulge setting which extends cratonward beyond the limits of the outcrop data. The lithosphere viscously relaxes stress over a 1 Myr model timestep. At the end of this model timestep, the flexural profile migrates back toward the load, and as a result the maximum deflection of the foredeep increases by several hundred meters and strata deposited on the initial surface are broadly deflected in response, creating the depositional surface for the next sequence. Although some space is filled by the initial package, sufficient space remains for additional sediment accumulation, well within the photic zone (0-100 m water depth). A gentle upwarp (10's of meters) is apparent at the location of the point of maximum uplift along the forebulge, and a gentle trough develops in the backbulge of a similar amplitude. The carbonate sediments, however, act to generally smooth the relief created by the migrating profile. This trend continues throughout the deposition of the sequences until no space remains at the termination of deposition in forebulge and foredeep depozones. The long-term accommodation patterns displayed by the Madison system are compatible with load-induced subsidence followed by migration of the flexural profile due to increasing local compensation of the load. However, this conclusion does not address the role of tectonic subsidence in the evolution of the Madison system at shorter timescales. Sonnenfeld (1996a, 1996b) stressed the importance of recognizing the hierarchical arrangement of cycles and sequences within the Madison

system and recognizing the organization of subordinate sequences into longer-term accommodation packages.

Although this shows that basin geometry is highly sensitive to load stress, even at large distances from the load, it is highly unlikely that the model presented here is the precise solution to the Antler load mass as it emplaced in the Lower Mississippian of central Idaho. Rather, because of the large number of assumptions and simplifications required for this model and uncertainties inherent in the model, it is more reasonable to assume that this solution is nonunique and that a class of solutions exist which satisfy the actual geology and geodynamics of the setting. This results should be used as a guideline for what the potential load mass was within the parameter space defined here.

One of the last hierarchical scales recognized by Sonnenfeld was the third-order composite sequence. The lower composite sequence is composed of sequences I and II of Sonnenfeld, while the upper was made up of the upper four third-order sequences. The composite sequences approximately correspond to the lithostratigraphically defined Lodgepole and Mission Canyon Formations of the Madison Group in Montana. The composite sequence scale is highly relevant to the work presented here as it falls at a timescale which lies between the eustatically-dominated third order sequence scale and the tectonically-dominated second order scale. Additionally this scale was recognized by Sonnenfeld (1996a, 1996b) as marked by a significant change in overall accommodation conditions across the system. The accommodation change forced the reorganization of the depositional system from a high-energy homoclinal ramp to a flat-topped platform dominated by aggradation of mud-dominated carbonates and evaporites.

The question then becomes: is the accommodation change reflected in the change in facies motif and carbonate depositional system architecture at the composite sequence scale causally related to changes in the flexural profile of the lithosphere due to decreased effective elastic thickness? Increased relative amplitude of the forebulge in time would act as an area of high-energy sediment production and encourage vertical stacking of sand bodies in this area. It would also double as a wave break decreasing overall energy input into the backbulge and act as a physical barrier to open marine waters restricting circulation. These factors would promote carbonate mud production and storage in the backbulge, and with enough restriction, the deposition of evaporites, thick packages of

which commonly occur at the base of subordinate third-order sequences in the upper composite sequence (Chapter 3). Additionally, continued tectonic subsidence of the backbulge depozone would promote aggradational stacking in this region as the region would be subject to relative sea-level rise as compared to the rest of the system. The evidence considered supports the interpretation that the change in facies and stratigraphic architecture are consistent with the viscoelastic lithospheric plate model. The available evidence conceptually fits within the quantitative framework developed here.

4.5.3 Regional carbonate stratigraphic architecture and lithospheric strength

Lower and Middle Mississippian carbonate sedimentation is not limited to the Madison shelf of Wyoming, Montana, and Idaho, but rather extends much of the length of the North American margin from California to Canada. However, significant differences in the overall architecture of these systems are apparent from published accounts. Giles (1996) documented the tectonically forced retrogradation of the Lower Mississippian Joana Limestone of the Antler foreland basin in Nevada. The Joana ramp is significantly shorter lived (Kinderhookian only in age) and narrower in width (< 400 km) than the Madison. The work of Giles (1996) shows backstepping of a carbonate ramp system due to migration of the foreland basin in a landward direction due to continued load migration in the Lower Mississippian. Interestingly, the foredeep basin in this part of the system is significantly narrower, extending 270 km from the load edge to the crest of the forebulge. The forebulge is also uplifted and eroded in this locality. Both these factors seem to suggest a marked difference in the lithospheric mechanical properties along strike, here in an area south of the northern Rockies study area.

Regional seismic studies of the western United States seem to present some ideas on the possible causes of this change. Karlstrom et al. (2002; Figure 4.10), as a part of a series of coordinate seismic experiments and geologic studies, showed that the lithosphere of the western US is heterogeneous at the scale of hundreds to several hundred kilometer belts. According to their results, the Madison shelf developed on the Archean Wyoming craton, while the lithosphere of Nevada and Utah is composed of a series of Proterozoic aged slivers. The Joana system was deposited primarily on lithosphere of St. George and Mojave block affinities. It is reasonable then to assume that the heterogeneity observed between the carbonate architectures along strike in the Antler

foreland basin resulted from changes in lithospheric mechanical strength. The Madison system likely developed on lithosphere with a greater elastic thickness than that of the Joana (Figure 4.11), although differences in load size, shape and geometry may have played a role as well. These observations combine to suggest that lithosphere with greater flexural rigidity is necessary in order to host a large, long-live carbonate depositional system in a foreland setting.

4.5.4 Mechanics of decreasing lithospheric effective elastic thicknesses

Modeling efforts of this study have focused on the decrease of the flexural rigidity of a viscoelastic lithosphere, and hence elastic thickness, through time through stress relaxation via the viscous channel. This study does not address the causes of this stress relaxation, however, and due to the limited information and considerable uncertainty of a poorly preserved ancient foreland system, it is not possible to address the question quantitatively. It is, however, important to address the potential mechanics of the behavior of the lithosphere which is preserved in the record of the foreland basin strata.

The lithosphere is fundamentally viscoelastic in nature, meaning that plastic deformation occurs within the lithosphere due to creep especially at high temperatures and low strain rates. This has been shown experimentally through rock mechanics experiments of lithologies of lower crustal and upper mantle affinity (Goetze, 1978; Karato and Wu, 1993). However, this is not necessarily the only mechanism for stress relaxation within the lithosphere, and it should not be construed that the model solutions obtained here reflect this mechanism solely. Rather the model results reflecting decreased flexural rigidity with time should be considered as the sum of a number of processes known to thin the elastic core of the lithosphere. A mechanism critical to this is brittle faulting in the upper crust. Brittle failure of the upper crust primarily through earthquakes is an obvious example of stress relaxation through plastic strain accumulation. The work of Dorobek et al. (1991) clearly demonstrates that movement of faults due to in-plane stress is a significant component of the stress relaxation mechanism of the lithosphere of the Antler foreland system in Montana.

Additionally, recent numerical modeling studies have predicted that under certain circumstances, the lower crust and upper mantle could theoretically decouple, causing a catastrophic decrease in the effective elastic thickness of the lithosphere (Burov and

Diament, 1992). Anomalously low lithospheric elastic thicknesses in modern foreland system have been documented for several orogenic belts including the Andes, Tarim, Kunlun, and Zagros chains (Lavie and Steckler, 1997).

4.6 CONCLUSIONS

This work explores the concepts required to host a large, long-lived carbonate depositional system within a foreland basin setting, and challenges current ideas on the long-term controls on accommodation space development for the Madison carbonate system.

1. Combinations of tectonic parameters and carbonate sediment production and storage controls must act in concert in order to provide conditions suitable to host a large carbonate ramp system in an active flexural setting.
2. Quantification of temporally-dependent changes in the effective elastic thickness of the lithosphere of western North America when subjected to the load of the Roberts Mountain allochthon for geologically-significant periods of time provides information on the distribution of areas prone to carbonate sediment production and locations for sediment storage and preservation.
3. Tectonism along the North American margin in the Lower Mississippian has been demonstrated to be punctuated rather than continuous. That is each regional unconformity observed to bound the Madison supersequence records a pulse of tectonic loading of the margin, which is then followed by a period of tectonic quiescence.
4. The deflection of the lithosphere under the load of the Antler orogeny can be examined by employing an elastic model. This is used to understand the shape of the deflection and the geometry of the resulting foreland basin and show that flexure is consistent with the first-order distribution of accommodation space within the region.
5. In order to examine the secular evolution of lithospheric flexure in response to a static load, a more complex set of material properties for the lithosphere must be employed. A time-dependent viscoelastic rheology is employed to examine the evolution of the lithosphere under a load.

6. The viscoelastic formalization applied here allows for examination of the lithosphere under the load stress when compressional strain rates are approximately zero during intercollisional periods, and deformation of the lithosphere results purely from time evolution of the stress field induced by loading.
7. The overall effect of viscous stress relaxation is decreased flexural rigidity of the plate under maintained loading. As the effective elastic thickness of the viscoelastic plate decreases, the flexural wavelength narrows and the amplitude of the deflection increases. The net effect is a migration of the flexural profile back toward the load.
8. The long-term accommodation patterns displayed by the Madison system are compatible with load-induced subsidence followed by migration of the flexural profile due to increasing local compensation of the load. Although some space is filled by the initial sedimentary package deposited in the modeled scenario, sufficient space remains for additional sediment accumulation, well within the photic zone (0-100 m water depth). A gentle upwarp (10's of meters) is apparent at the location of the point of maximum uplift along the forebulge, and a gentle trough develops in the backbulge of a similar amplitude. The carbonate sediments, however, act to generally smooth the relief created by the migrating profile. This trend continues throughout the deposition of the sequences until no space remains at the termination of deposition in forebulge and foredeep depozones.
9. The distribution of carbonate sedimentary facies tracts also can be predicted from the model results. The increased relative amplitude of the forebulge would act as an area of high-energy sediment production and encourage vertical stacking of sand bodies in this area. Doubly it would act as a wave break decreasing overall energy input into the backbulge and act as a physical barrier to open marine waters restricting circulation. These factors would promote carbonate mud production and storage in the backbulge, and with enough restriction, the deposition of evaporites, thick packages of which commonly occur at the base of subordinate third-order sequences in the upper composite sequence. Additionally,

continued tectonic subsidence of the backbulge depozone would promote aggradational stacking in this region as the region would be subject to relative sea-level rise as compared to the rest of the system.

10. Regional variation of carbonate depositional styles during the Kinderhookian can be attributed to changes in the composition and heterogeneity of the underlying basement terranes upon which these systems developed. The Madison system likely developed on lithosphere with a greater elastic thickness than that of the Joana system of Utah and Nevada (Figure 4.11), although differences in load size, shape and geometry may have played a role as well.

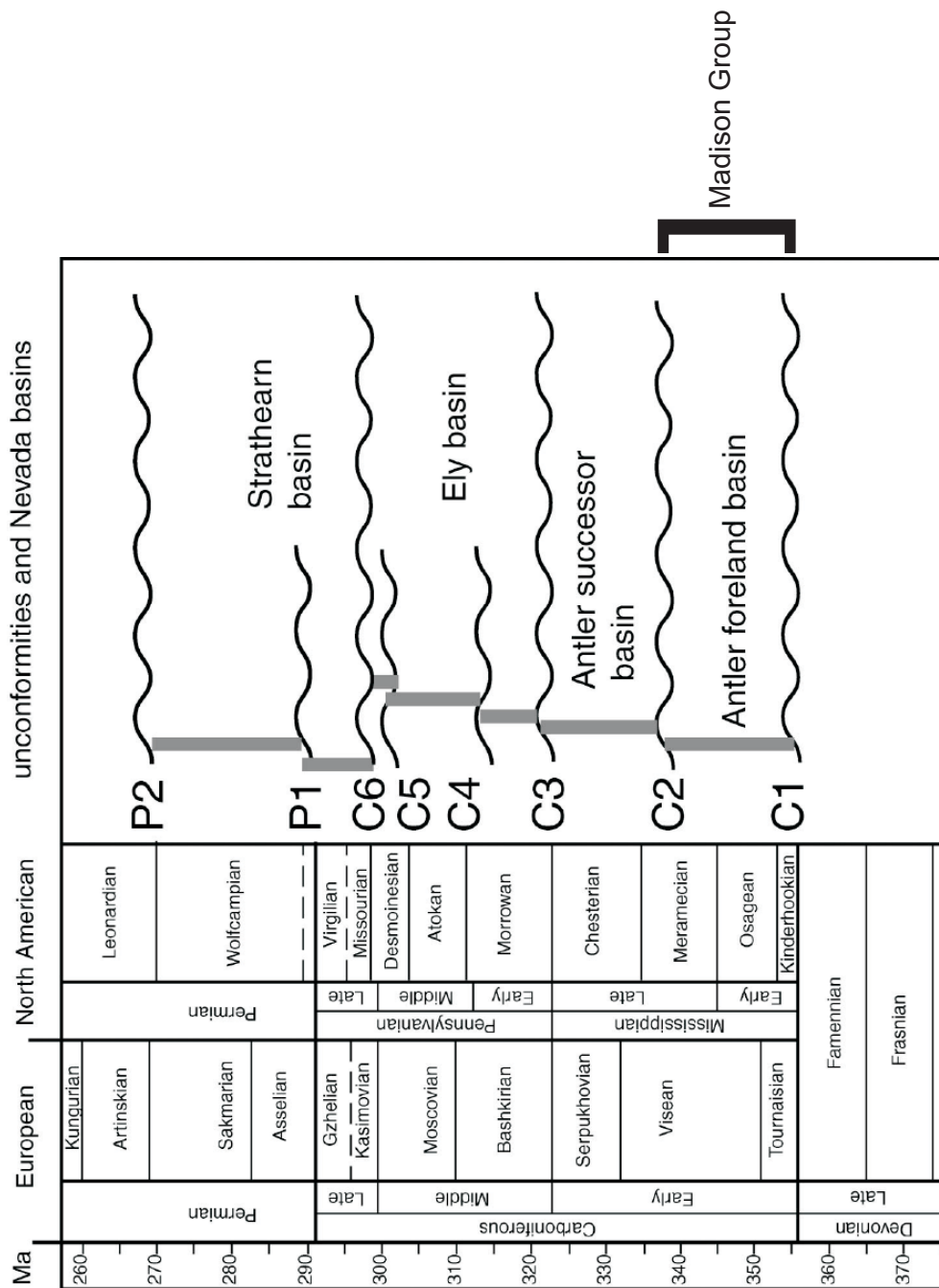


Figure 4.1: Tectonostratigraphic boundaries from the Great Basin, USA, from Carboniferous to Permian time. The boundaries are regional-scale unconformities identified by Snyder and Trexler (2000), Snyder et al. (2000), and Trexler et al. (2004). The Madison Group and equivalent strata of Wyoming, Montana, and Idaho are bounded by the C1 and C2 unconformities, further extending the regional context beyond the borders of the Great Basin. Figure modified from Trexler et al. (2004)

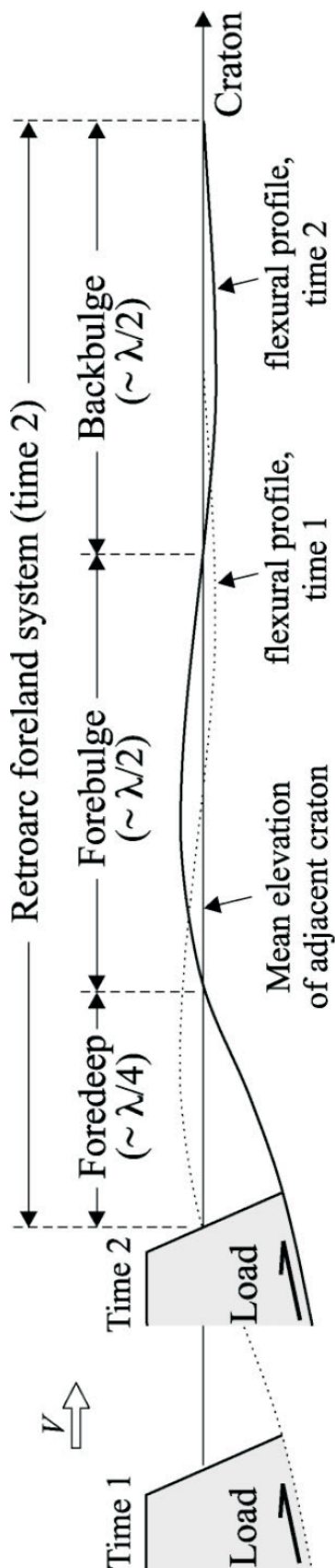


Figure 4.2: Flexural profile of a retroarc foreland basin system. The profile is depicted as migrating cratonward through time as the load migrates from position 1 to position 2 with a velocity, V . The profile is highly vertically exaggerated as the forebulge depozone has an amplitude which is an order of magnitude less than that of the foredeep. Similarly, the backbulge has an order of magnitude less than that of the forebulge. Figure from Catuneanu (2004).

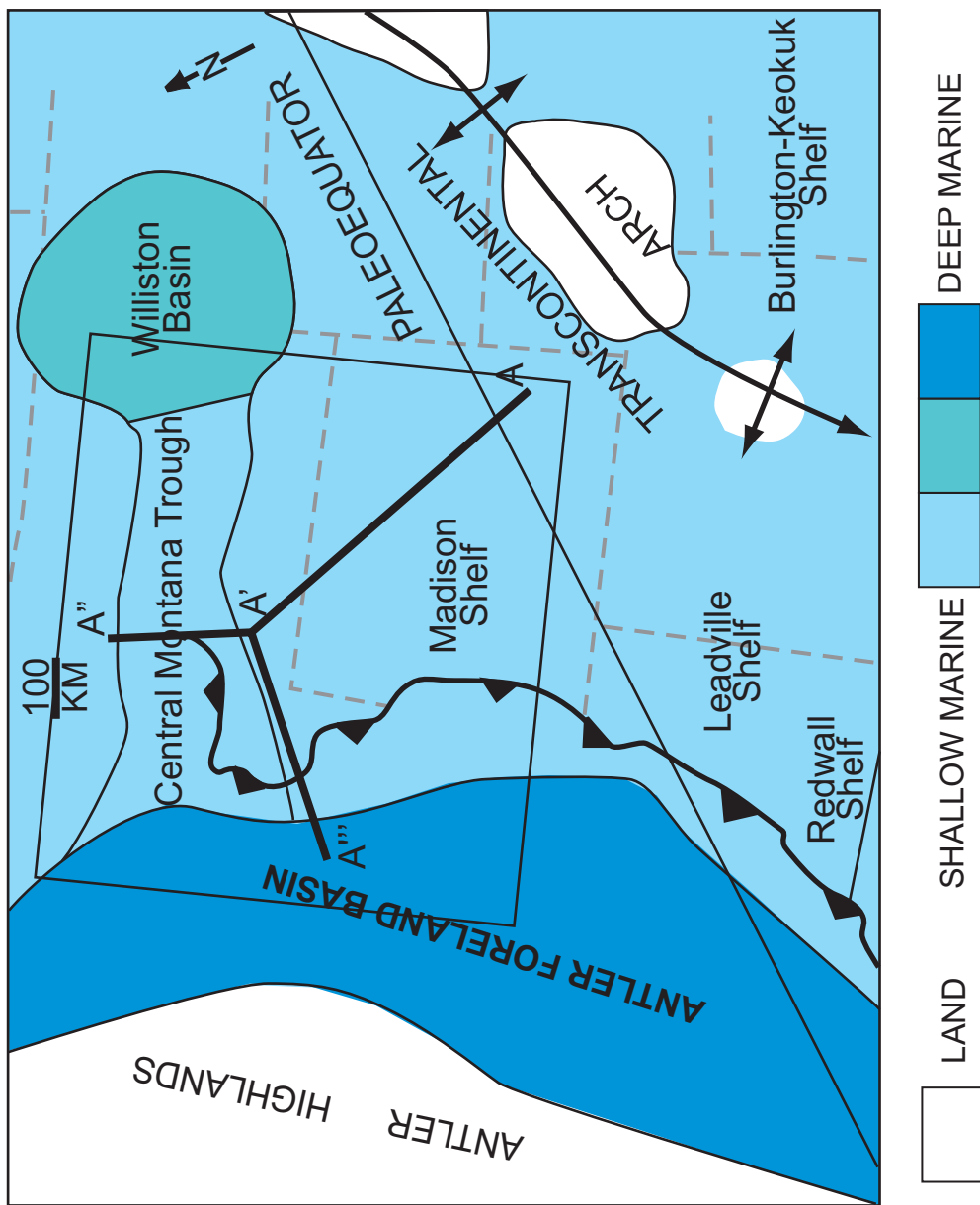


Figure 4.3: Paleogeographic map of the western United States during the Early Mississippian (from Gutschick and Sandberg, 1983). Contours are the interpreted water depths during sequence IV of the Madison of Gutschick and Sandberg. A-A', A'-A'', and A''-A''' in the boxed area denote the cross-section locations of this study.

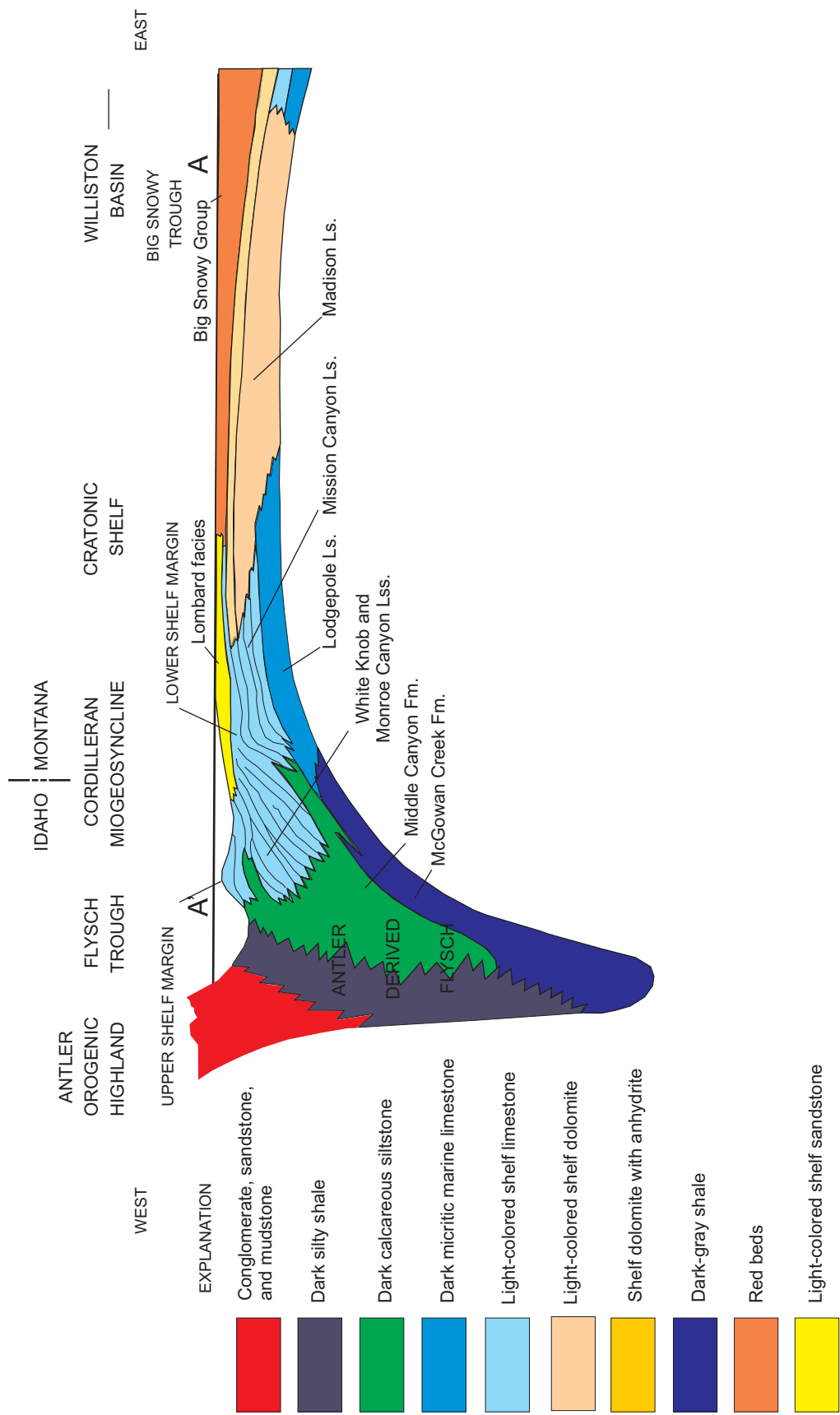


Figure 4.4: Formation-scale cross-section (top) across the Antler foreland basin displaying the geometry of the prograding Mississippian Madison carbonate ramp (modified from Rose, 1977).

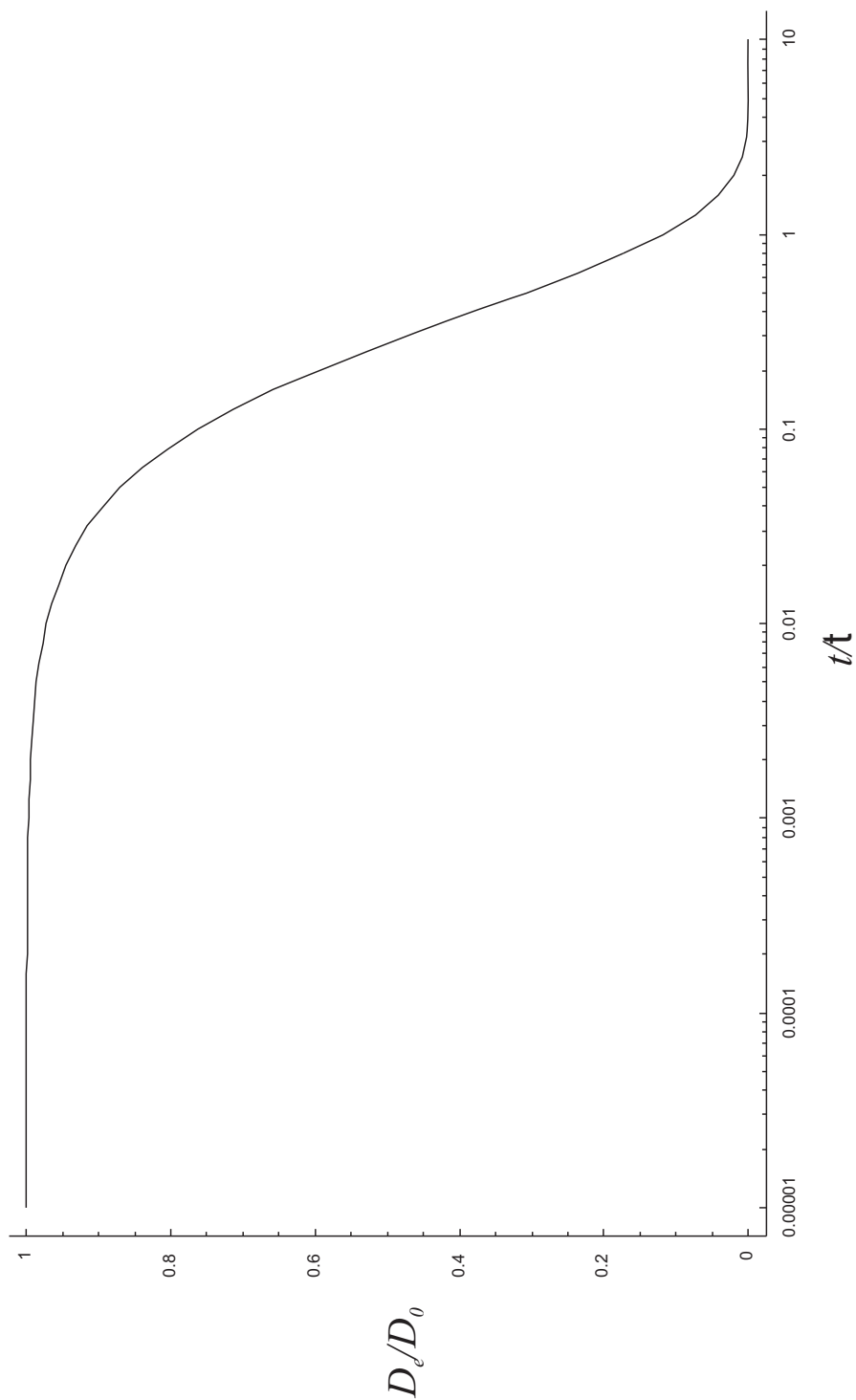


Figure 4.5: A log-linear plot showing the ratio of the equivalent flexural rigidity, D_e , of a viscoelastic material under stress to the initial flexural rigidity, D_0 , of an elastic plate as a function of the ratio of the model time, t , to the Maxwell relaxation time, t . This plot shows that the viscoelastic plate is initially strong and maintains its strength, but as time approaches the Maxwell relaxation time, a dramatic fall-off in strength occurs. At time $t = t$ the flexural rigidity of the plate has decreased by approximately 50%.

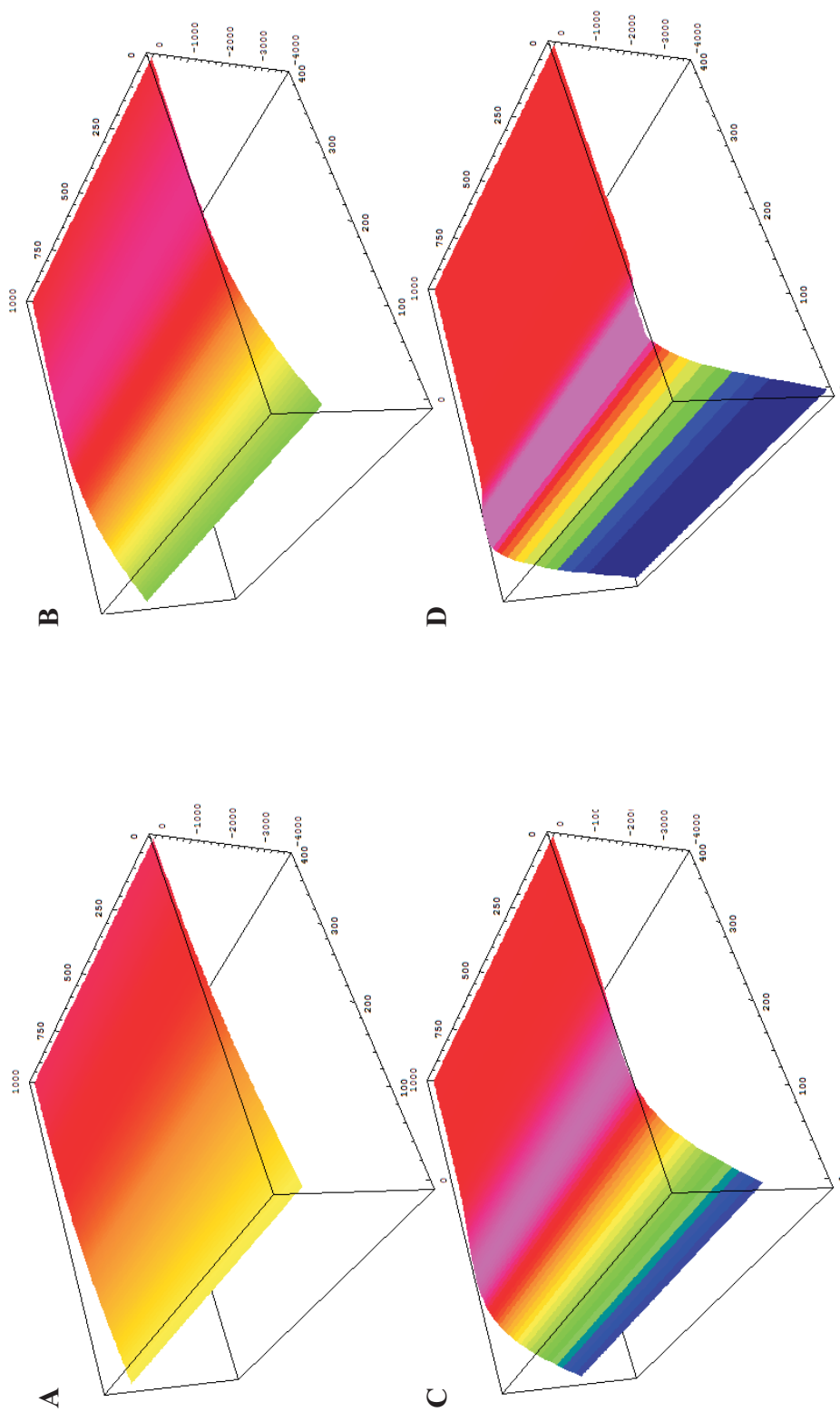


Figure 4.6: A series of plots illustrating viscoelastic relaxation of a semi-infinite broken plate in stress under a line load on its broken edge. (A) shows the initial elastic response of the plate by broad regional compensation of the load. The forebulge crest lies at the edge of the plot 400 km from the load. (B-D) show the progressive migration of the flexural profile back towards the load as stress is relaxed and the load is progressively more locally compensated. As the profile migrates towards the load the wavelength of the flexural profile decreases and the amplitude of the forebulge and foredeep zones increase. Each plot is of the same scale (400 km x 1000 km x 4000 m) and is highly vertically exaggerated to emphasize the rising forebulge (pink) and deepening foredeep (cool colors).

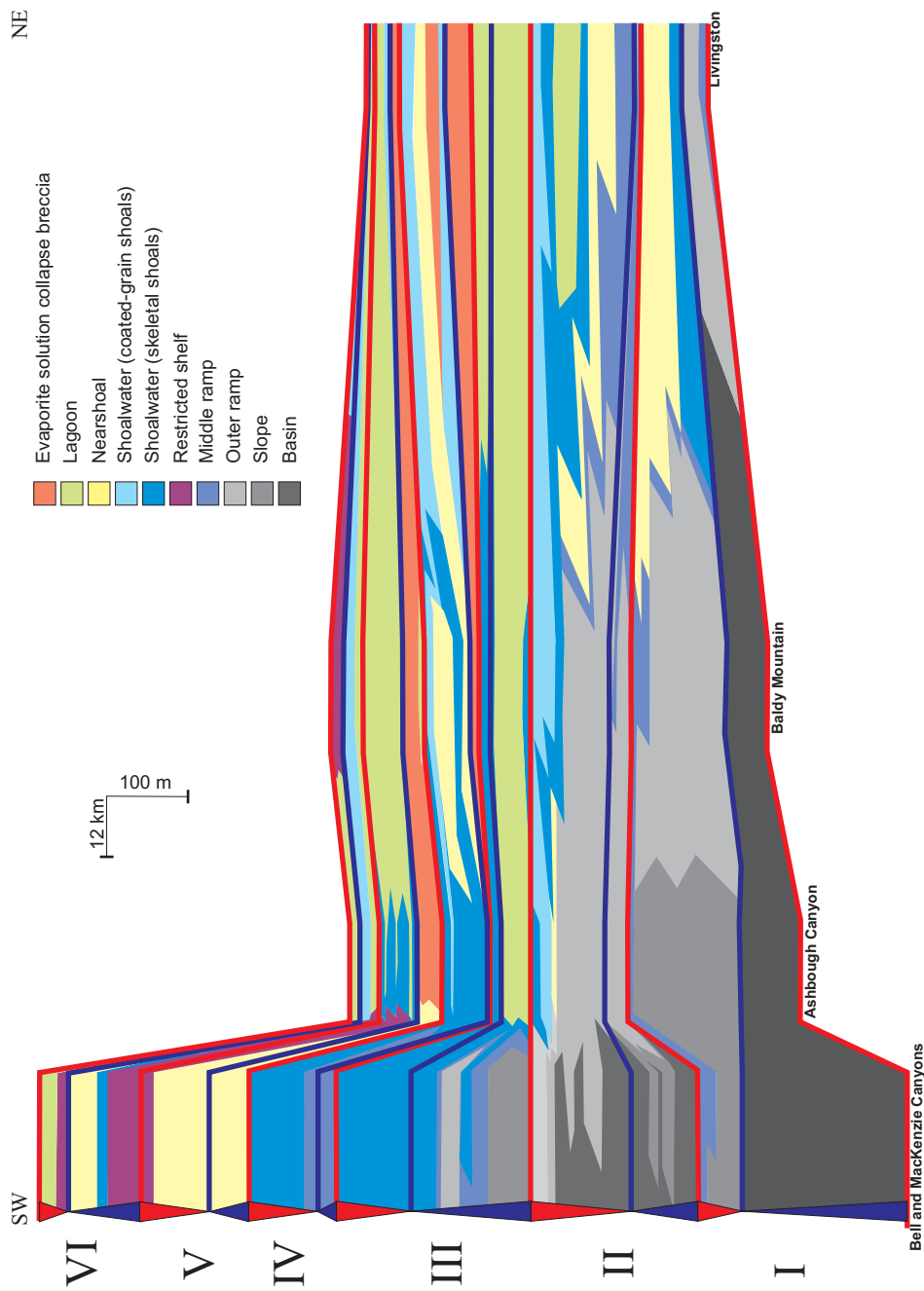


Figure 4.7: Stratigraphic interpretation of the Madison Group through a dip-oriented cross-section from the craton to the northeast to foredeep basin of the Antler foreland in the southwest. The depositional system doubles in thickness for northeast to southwest as it passes into the higher accommodation setting of the foredeep. The six third-order sequences of the Madison Group are shown here. The overall pattern of initial backstepping and aggradation of the carbonate ramp is followed by progradation of shallow water high-energy carbonate sand bodies into the foredeep.

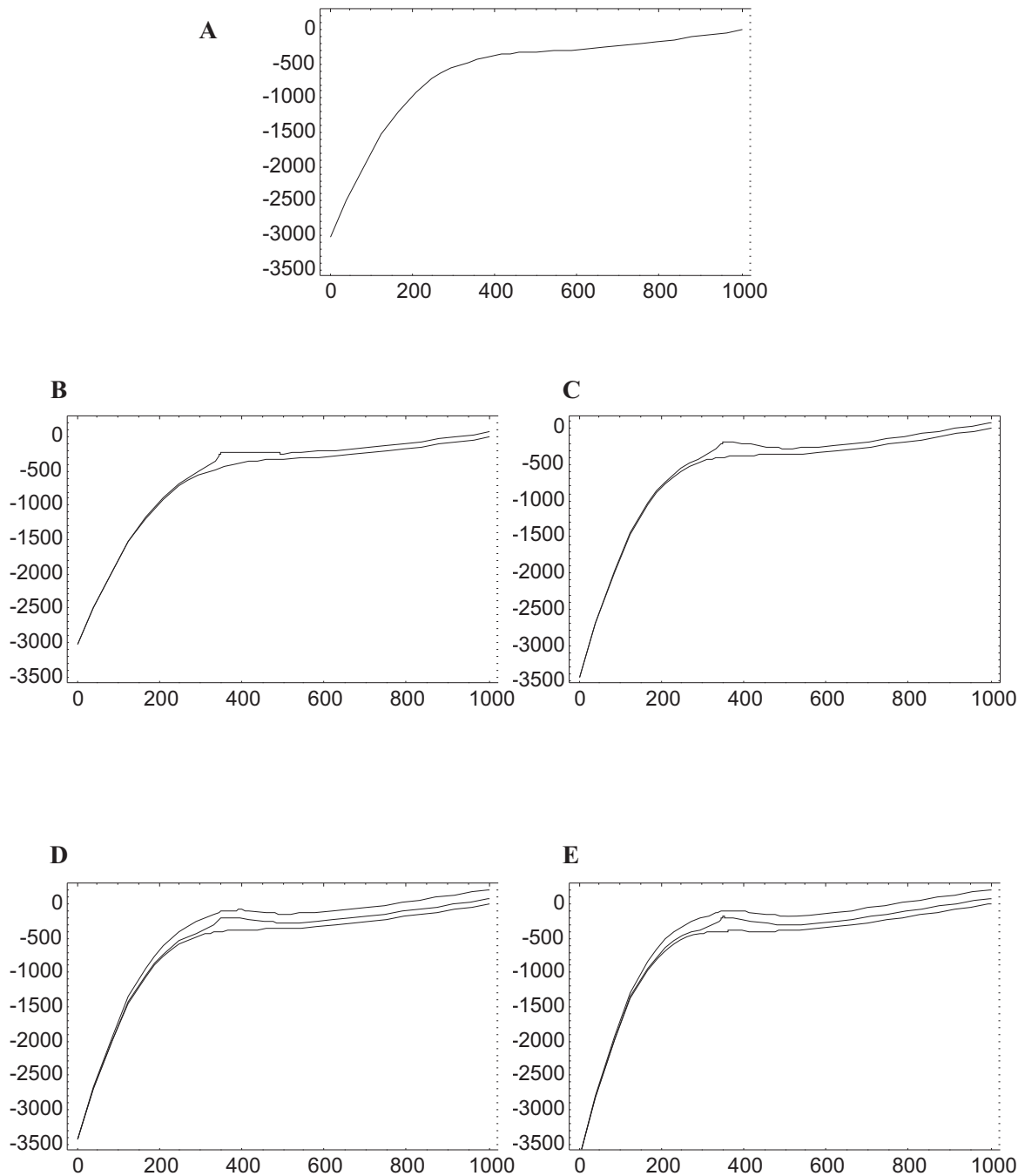


Figure 4.8: Conformable mapping of third-order sequences of the Madison Group onto (A) initially elastically deflected lithosphere. (B) Sequence I “deposited” onto the initial surface of (A). (C) A 1 Myr timestep occurs and the plate viscously relaxes under the stress of the load. The flexural profile migrates back toward the load and uplift and narrowing of the forebulge and deepening of the foredeep adjacent to the load occurs, and the overlying carbonate package is subtly deformed. (D) depicts the layering of the next stratigraphic sequenced, sequence II, onto the newly inherited substrate. (E) depicts the next timestep and the subsequent modification to the lithosphere and overlying carbonate sedimentary packages.

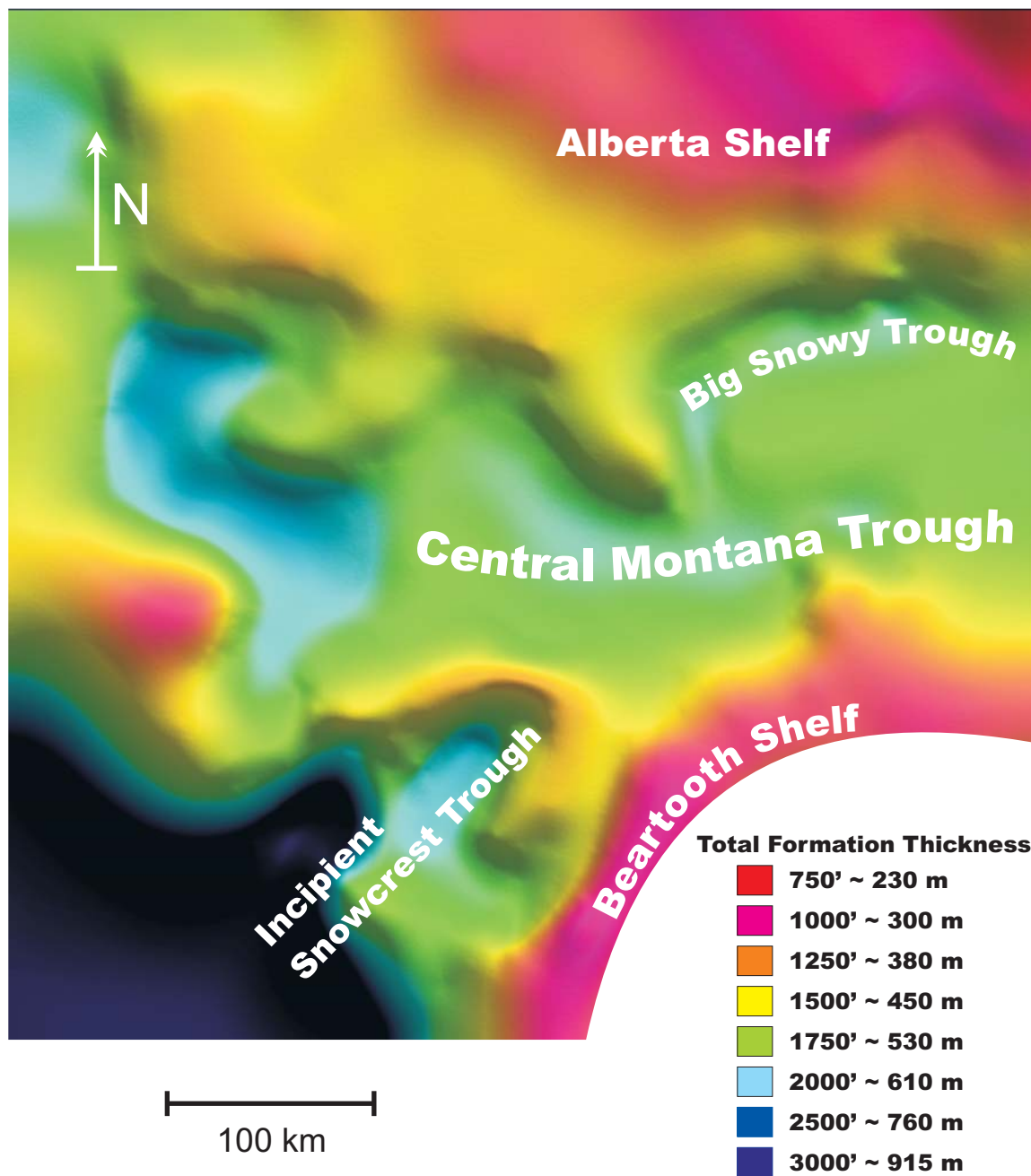


Figure 4.9: Thickness and paleotectonic elements of the Lower and middle Mississippian Madison Group in western Montana (modified from Peterson, 1985)

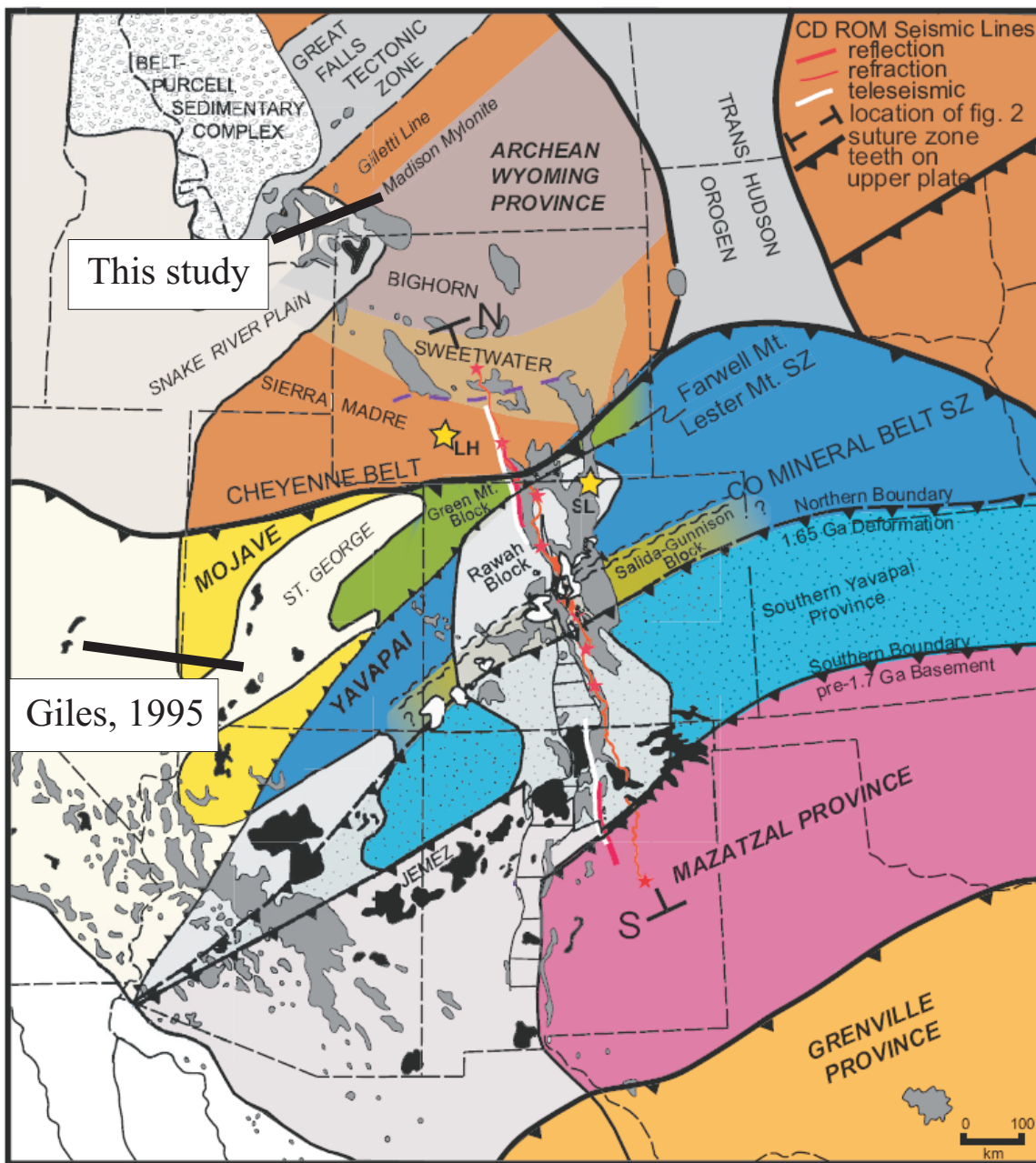
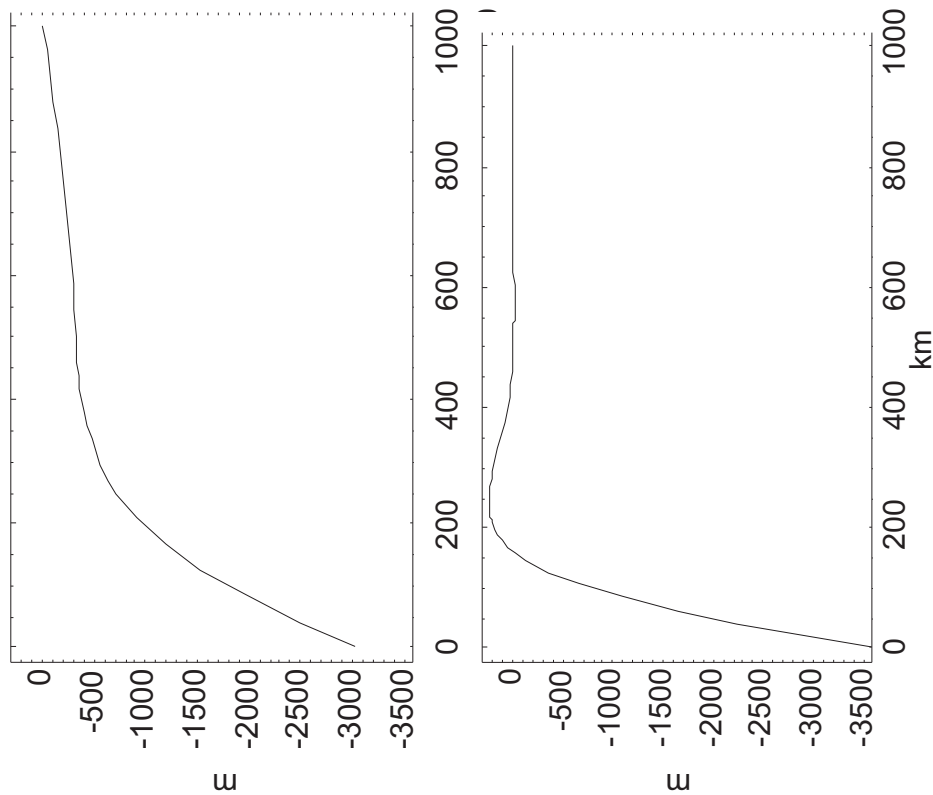


Figure 4.10: Map of tectonic elements of the western US. Locations of this study and the study of Giles (1995) are marked. The Madison shelf developed on the edge of the Archean Wyoming Province while the Joana system developed on slivers of terrains of Proterozoic age. The mechanical differences of these lithospheres of these different blocks likely explain the differences in the stratigraphic development of these contemporaneous carbonate depositional systems

Initial Madison Flexural Profile

-Initial dip = 0.01°

-Elastic thickness = 29.9 km



Initial Joana Flexural Profile

-Initial dip = 0.0°

-Elastic thickness = 13.9 km

Figure 4.11: Two cross-sectional profiles of the initial elastic flexural profiles of in the area of the Madison and Joana carbonate depositional systems. These profiles capture the essential geometries required for deposition of the ensuing carbonates within the forebulge and backbulge areas away from the immediate deflection beneath the load. The Joana profile, which results from no initial dip on the surface and a lower elastic thickness than the modeled Madison profile, has a higher amplitude forebulge and a narrower foredeep than the modeled Madison system. This is consistent with the outcrop observations of Giles (1995).

REFERENCES

- Aigner, T., 1984, Dynamic stratigraphy of epicontinental carbonates, Upper Muschelkalk (M. Triassic), South-German Basin: Neues Jahrbuch fuer Geologie und Palaeontologie. Abhandlungen, v.169, p.127-159.
- Aigner, T., 1985, Storm depositional systems; dynamic stratigraphy in modern and ancient shallow-marine sequences: Berlin, Springer Verlag, 174 p.
- Andrichuk, J.M., 1955a, Carboniferous stratigraphy in mountains of northwestern Montana and southwestern Alberta: Billings Geol. Soc., Guidebook, 6th Ann. Field Conf.
- Andrichuk, J.M., 1955b, Mississippian Madison group stratigraphy and sedimentation in Wyoming and southern Montana: American Association of Petroleum Geologists Bulletin, v. 39, p. 2170-2210.
- Andrichuk, J.M., 1958, Cooking Lake and Duvernay (Late Devonian) sedimentation in Edmonton area of central Alberta, Canada: American Association of Petroleum Geologists Bulletin, v. 42, p. 2189-2222.
- Aubouin, J., 1965, Geosynclines: Amsterdam and New York, Elsevier, 335 p.
- Bathurst, R.G.C., 1975, Carbonate Sediments and Their Diagenesis: Amsterdam, Elsevier, 658 p.
- Beaumont, C., 1978, The evolution of sedimentary basins on a viscoelastic lithosphere: Theory and examples: Geophysical Journal of the Royal Astronomical Society, v. 55, p. 471-4947
- Beaumont, C., 1981, Foreland basins: Geophysical Journal of the Royal Astronomical Society, v. 65, p. 291-329
- Berner, R.A., 1990, Atmospheric carbon dioxide levels over Phanerozoic time: Science, v. 249, p. 1382-1386.
- Bradley, D.C., and Kidd, W.S.F., 1991, Flexural extension of the upper continental crust in Collisional foredeeps: Bulletin of the Geological Society of America, v. 103, p. 1416-1438.
- Burchette, T.P., and Wright, V.P., 1992, Carbonate ramp depositional systems: Sedimentary Geology, v. 79, p. 3-57.
- Burchfiel, B.C., and Davis, G.A., 1972, Structural framework and evolution of the southern part of the Cordilleran orogen, western United States: American Journal of Science, v. 272, p. 97-118.

- Burchfiel, B.C., and Davis, G.A., 1975, Nature and controls of Cordilleran orogenesis, western United States: extensions of an earlier synthesis: *American Journal of Science*, v. 275, p. 363-396.
- Burchfiel, B.C., and Davis, G.A., 1981, Triassic and Jurassic tectonic evolution of the Klamath Mountains-Sierra Nevada geologic terrane, *in*, The geotectonic development of California, v. 1, Englewood Cliffs, NJ, Prentice-Hall.
- Burchfiel, B.C., and Royden, L. H., 1991, Antler orogeny: A Mediterranean-type orogeny: *Geology*, v. 19, p. 66-69.
- Burov, E.B., and Diament, M., 1992, Flexure of the continental lithosphere with multilayered rheology: *Geophysical Journal*, v. 109, p. 449-468.
- Catuneanu, O., Sweet, A.R., and Miall, A.D., 2000, Reciprocal stratigraphy of the Campanian-Paleocene Western Interior of North America: *Sedimentary Geology*, v. 134, p. 235-255.
- Chen, X., and Webster, G.D., 1994, Sedimentology, tectonic control and evolution of a Lower Mississippian carbonate ramp with offshore bank, central Wyoming to eastern Idaho and northeastern Utah, U.S.A: *in* Embry, A.F., Beauchamp, B., and Glass, D.J., eds., *Pangea; Global Environments and Resources*, Memoir - Canadian Society of Petroleum Geologists, v.17, p. 557-587.
- Crevello, P.D., Wilson, J.L., Sarg, J.F., and Read, J.F., eds., 1989, Controls on Carbonate Platform and Basin Development: Tulsa, Society of Economic Paleontologists and Mineralogists, Special Publication No. 44, 405 p.
- Crockett, J.J., 1994, Porosity evolution of the Madison Limestone (Mississippian), Wind River Basin, Wyoming, Unpublished Master's thesis, Louisiana State University, 102 p.
- Decelles, P.G., and Giles, K.A., 1996, Foreland basin systems: *Basin Research*, v. 8, p. 105-123.
- Dickinson, W.R., 1974, Plate tectonics and sedimentation: Society of Economic Paleontologists and Mineralogists, Special Publication 22, Tulsa, p. 1-27.
- Dickinson, W.R., 1977, Paleozoic plate tectonics of the Cordilleran continental margin, *in*, J.H. Stewart, C.H. Stevens, and A.E. Fritsche, eds., *Paleozoic paleogeography of the western United States*, Bakersfield, SEPM Pacific Section.
- Dorobek, S.L., 1995, Synorogenic carbonate platforms and reefs in foreland basins: controls on stratigraphic evolution and platform/reef morphology, *in*, S.L. Dorobek and G.M. Ross, eds., *Stratigraphic evolution of foreland basins*, SEPM Special Publication 52, p. 127-147.

- Dorobek, S.L., Reid, S.K., Elrick, M., Bond, G.C., and Kominz, M.A., 1991, Subsidence across the Antler foreland of Montana and Idaho: Tectonic versus eustatic effects, *in*, E. Franseen and L. Watney, eds., *Sedimentary modeling: Lawrence, Computer simulation and methods for improved parameter definition: Kansas Geological Society Special Volume 233*, p. 231-251.
- Dunham, R.J., 1962, Classification of carbonate rocks according to depositional texture: *in* Ham, W.E., ed., *Classification of Carbonate Rocks: AAPG Memoir 1*, p. 108-121.
- Dutro, J.T., Jr., and Sando, W.J., 1963a, New Mississippian formations and faunal zones in Chesterfield Range, Portneuf Quadrangle, southeast Idaho: *Bulletin of the American Association of Petroleum Geologists*, v. 47, p. 1963-1986.
- Dutro, J.T., Jr., and Sando, W.J., 1963b, Age of certain post-Madison rocks in southwestern Montana and western Wyoming: U. S. Geological Survey Professional Paper, Report: P 0475-B, p.B93-B94.
- Elrick, M., 1990, Development of cyclic ramp-to-basin carbonate deposits, Lower Mississippian, Wyoming and Montana, Unpublished Ph.D. dissertation, Virginia Tech, 170 p.
- Elrick, M., and Read, J.F., 1991, Cyclic ramp-to-basin carbonate deposits, Lower Mississippian, Wyoming and Montana: a combined field and computer modeling study: *Journal of Sedimentary Petrology*, v. 61, p.1194-1224.
- Embry, A.F., and Klovan, J.E., 1971, A Late Devonian reef tract on northeastern Banks Island, NWT: *Bulletin of Canadian Petroleum Geology*, v. 19, p. 730-781.
- Gehrels, G.E., and Smith, M.T., 1987, "Antler" allochthon in the Kootenay Arc?: *Geology*, v. 15, p. 769-770.
- Giles, K.A., 1996, Tectonically forced retrogradation of the Lower Mississippian Joana Limestone, Nevada and Utah, *in*, M.W. Longman and M.D. Sonnenfeld, eds., *Paleozoic Systems of the Rocky Mountain Region, Rocky Mountain Section SEPM*, p. 145-164.
- Giles, K.A., Bocko, M., and Lawton, T.F., 1999, Stacked Late Devonian shorelines and their relation to tectonic subsidence at the Cordilleran Hingeline, western Utah: *Journal of Sedimentary Research*, v. 69, p. 1181-1190.
- Giles, K.A., and Dickinson, W.R., 1995, The interplay of eustasy and lithospheric flexure in forming stratigraphic sequences in foreland settings: an example from the Antler foreland, Nevada and Utah, *in*, S.L. Dorobek and G.M. Ross, eds., *Stratigraphic evolution of foreland basins, SEPM Special Publication 52*, p. 243-281.

- Goetze, G., 1978, The mechanisms of creep in olivine: Philosophical Transactions of the Royal Society of London, Series A: Mathematical and Physical Sciences, v. 288, p. 99-119.
- Gutschick, R.C., and Sandberg, C.A., 1983, Mississippian continental margins of the conterminous United States: *in* D.J. Stanley and G.T. Moore, eds., The Shelfbreak: Critical Interface on Continental Margins, SEPM Special Publication no. 33, p.79-96.
- Hagan, G.M., and Logan, B.W., 1974, Evolution and Diagenesis of Quaternary Carbonate Sequences, Shark Bay, Western Australia: AAPG Memoir 22, 358 p.
- Hardie, L.A., and Ginsburg, R.N., 1977, Layering: the origin and environmental significance of lamination and thin bedding: Johns Hopkins University, Studies in Geology, no. 22, Sedimentation on the modern carbonate tidal flats of Northwest Andros Island, Bahamas, p.50-123.
- Hetenyi, M., 1979, Beams on Elastic Foundations: Ann Arbor, MI, University of Michigan Press, 255 p.
- Huh, O.K., 1967, Mississippian stratigraphy and sedimentology, across the Wasatch line, east-central Idaho and extreme south-western Montana: Unpublished Ph.D. dissertation, Pennsylvania State University, University Park, PA, 230 p.
- Hallock, P., and Schlager, W., 1986, Nutrient excess and the demise of coral reefs and carbonate platforms: *Palaios*, v. 1, 1156-1166.
- Ingram, R.L., 1954, Terminology for the thickness of stratification and parting units I sedimentary rocks: Geological Society of America Bulletin, v. 65, p. 937-938.
- Jacobi, R.D., 1981, Peripheral bulge- a causal mechanism for the Lower Ordovician unconformity along the western margin of the northern Appalachians: *Earth and Planetary Science Letters*, v. 56, p. 245-251.
- Johnson, J.G., and Pendergast, A., 1981, Timing and mode of emplacement of the Roberts Mountain Allochthon, Antler Orogeny: Geological Society of America Bulletin, v. 92, p. 648-658.
- Jordan, T.E., 1981, Thrust loads and foreland basin evolution, Cretaceous, western United States: American Association of Petroleum Geologists Bulletin, v. 65, p. 669-674.
- Karato, S., and Wu, P., 1993, Rheology of the upper mantle: *Science*, v. 260, p. 771-778.

- Karlstrom, K.E., Bowring, S.A., Chamberlain, K.R., Dueker, K.G., Eshete, T., Erslev, E.A., Farmer, G.L., Heizler, M., Humphreys, E.D., Johnson, R.A., Keller, G.R., Kelley, S.A., Levander, A., Magnani, M.B., Matzel, J.P., McCoy, A.M., Miller, K.C., Morozova, E.A., Pazzaglia, F.J., Prodehl, C., Rumpel, H.M., Shaw, C.A., Sheehan, A.F., Shoshitaishvili, E., Smithson, S.B., Snelson, C.M., Stevens, L.M., Tyson, A.R., and Williams, M.L., 2002, Structure and evolution of the lithosphere beneath the Rocky Mountains; initial results from the CD-ROM experiment: *GSA Today*, vol.12, no.3, p.4-10.
- Katz D.A., Buoniconti, M.R., Montanez, I.P., Swart, P.K., Eberli, G.P., and Smith, L.B., Jr., In Press, Timing and Local Perturbations to the Carbon Pool in the Lower Mississippian Madison-Limestone, Montana and Wyoming: *Paleogeography, Paleoclimatology, and Paleoecology*.
- Katz, D.A., Swart, P.K., Eberli, G.P., Buoniconti, M.R., and Smith, L.B., Jr., 2004, Lower Mississippian carbonate geochemistry: Montana and Wyoming, *in*, 2004 University of Miami Comparative Sedimentology Laboratory Research Program Prospectus, Miami, p. 41-42.
- Kay, M., and Crawford, J.P., 1964, Paleozoic facies from the miogeosynclinal to the eugeosynclinal belt in thrust slices, central Nevada: *Geological Society of America Bulletin*, v. 75, p.425-454.
- Kendall, C.G.St., and Schlager, W., 1981, Carbonates and relative changes in sea level: *Marine Geology*, v. 44, p.181-212.
- Lavier, L.L., and Steckler, M.S., 1997, The effect of sedimentary cover on the flexural strength of continental lithosphere: *Nature*, v. 389, p. 476-479.
- Lees, A. and Buller, A.T., 1972, Modern temperate-water and warm-water shelf carbonate sediments contrasted: *Marine Geology*, v. 13, p. 67-73.
- Loucks, R.G. and Sarg, J.F., eds., 1993, *Carbonate Sequence Stratigraphy: Recent Developments and Applications*: Tulsa, American Association of Petroleum Geologists Memoir 57, 545 p.
- Mamet, B.L., and Skipp, B., 1970, Stratigraphic micropaleontology of the type locality of the White Knob Limestone (Mississippian), Custer County, Idaho: U. S. Geological Survey Professional Paper, Report: P 0700-B, p. 118-123.
- Mamet, B.L., Skipp, B., Sando, W.J., and Mapel, W.J., 1971, Biostratigraphy of upper Mississippian and associated Carboniferous rocks in south-central Idaho: *Bulletin of the American Association of Petroleum Geologists*, v. 55, p. 20-33.

- Matti, J.C., and McKee, E.H., 1977, Silurian and Lower Devonian paleogeography of the outer continental shelf of the Cordilleran Miogeocline, central Nevada: *in* J.H. Stewart, C.H. Stevens, and A.E. Fritsche, eds., *Paleozoic paleogeography of the western United States*, Bakersfield, SEPM Pacific Section, p. 181-215.
- Maughan, E.K., 1983, Tectonic setting of the Rocky Mountain region during the Late Paleozoic and Early Mesozoic, *Proceedings of Symposium on the Genesis of Rocky Mountain Ore Deposits: Changes with Time and Tectonics*, Denver, Regional Exploration Geologists Society, p. 39-50.
- McKerrow, W.S. and Scotese, C.R., 1990, Revised world maps and introduction, *in*, W.S. McKerrow and C.R. Scotese, eds., *Paleozoic Paleogeography and Biogeography: Geological Society Memoir 12*, p. 1-12.
- McNutt, M.K., and Parker, R.L., 1978, Isostasy in Australia and the evolution of the compensation mechanism: *Science*, v. 199, p. 773-775.
- Middleton, G.V., 1961, Evaporite solution breccias from the Mississippian of southwest Montana: *Journal of Sedimentary Petrology*, v. 31, p. 189-195.
- Mii, H., Grossman, E.L., and Yancey, T.E., 1999, Carboniferous isotope stratigraphies of North America: Implications for Carboniferous paleoceanography and Mississippian glaciation: *Geological Society of America Bulletin*, v. 111, p. 960-973.
- Miller, E.L., Holdsworth, B.K., Whiteford, W.B., and Rodgers, D., 1984, Stratigraphy and structure of the Schoonover sequence, northeastern Nevada: Implications for Paleozoic Plate Margin Tectonics: *Geological Society of America Bulletin*, v. 95, p. 1063-1076.
- Miller, E.L., Miller, M.M., Wright, J.E., and Madrid, R., 1992, Late Paleozoic paleogeographic and tectonic evolution of the Western U.S. Cordillera, *in*, B.C. Burchfiel, P.W. Lipman, and M.L. Zoback, eds., *The Cordilleran Orogen: conterminous US: Boulder, Colorado*, Geological Society of America, *The Geology of North America*, v. G-3, p. 57-106.
- Mitchum, R.M. and Van Wagoner, J.C., 1991, High-frequency sequences and their stacking patterns: sequence stratigraphic evidence of high-frequency eustatic cycles: *Sedimentary Geology*, v. 70, p. 161-193.
- Moore, C.H., 2001, Carbonate reservoirs: porosity evolution and diagenesis in a sequence stratigraphic framework: Golden, CO, *Developments in Sedimentology* 55, 444 p.
- Murphy, M.A., Power, J.D., and Johnson, J.G., 1984, Evidence for Late Devonian movement within the Roberts Mountains allochthon, Roberts Mountains, Nevada: *Geology*, v. 12, p. 20-23.

- Nadai, A., 1963, Theory of Flow and Fracture of Solids: New York, McGraw-Hill, 705 p.
- Nilsen, T.H. and Stewart, J.H., 1980, The Antler Orogeny, mid-Paleozoic tectonism in western North America: *Geology*, v. 8, p. 298-302.
- Peterson, J.A., 1985, General stratigraphy and regional paleotectonics of the western Montana overthrust belt, *in*, J.A. Peterson, ed., Paleotectonics and sedimentation in the Rocky Mountain region, United States, AAPG Memoir, v. 41, p. 57-86.
- Petty, D.M., 1996, Regional stratigraphic and facies relationships in the Mission Canyon Formation, North Dakota portion of the Williston Basin: *in* M.W. Longman and M.D. Sonnenfeld, eds., Paleozoic Systems of the Rocky Mountain Region, Rocky Mountain Section SEPM, p. 193-211.
- Pollitz, F.F., Submitted, Transient rheology of the upper mantle beneath central Alaska inferred from the crustal velocity field following the 2002 Denali earthquake: *Journal of Geophysical Research*.
- Purser, B.H., 1973, The Persian Gulf: Holocene Carbonate Sedimentation and Diagenesis in a Shallow Epicontinental Sea: New York, Springer-Verlag, 471 p.
- Purser, B.H., and Evans, G., 1973, Regional Sedimentation along the Trucial Coast, SE Persian Gulf: *in* B.H. Purser, ed., The Persian Gulf: New York, Springer-Verlag, p. 211-231.
- Quinlan, G.M. and Beaumont, C., 1984, Appalachian thrusting, lithospheric flexure, and the Paleozoic stratigraphy of the Eastern Interior of North America: *Canadian Journal of the Earth Sciences*, v. 21, p. 973-996.
- Read, J.F., 1985, Carbonate platform facies models: *AAPG Bulletin*, v. 69, p. 1-21.
- Reid, S.K., 1991, Evolution of the Lower Mississippian Mission Canyon platform and Antler foredeep, Montana and Idaho: unpublished, Ph.D. dissertation, Texas A&M University, 105 p.
- Reid, S.K. and Dorobek, S.L., 1993, Sequence stratigraphy and evolution of a progradational, foreland carbonate ramp, Lower Mississippian Mission Canyon Formation, and stratigraphic equivalents, Montana and Idaho, *in*, R.G. Loucks and J.F. Sarg, eds., Carbonate Sequence Stratigraphy, AAPG Memoir 57, p. 327-352.
- Roberts, A.E., 1966, Stratigraphy of Madison Group near Livingston, Montana, and discussion of karst and solution-breccia features: USGS Professional Paper P 0526-B, B1-B23.

- Roberts, R.J., Fegurson, H.G., Gilluly, J., and Hotz, P.E., 1958, Paleozoic rocks of north-central Nevada: Bulletin of the American Association of Petroleum Geologists, v. 42, p. 2813-2857.
- Rodgers D.W., Link, P.K., and Huerta, A.D., 1995, Structural framework of mineral deposits hosted by Paleozoic rocks in the northeastern part of the Hailey 1 degrees X2 degrees Quadrangle, south-central Idaho: U. S. Geological Survey Bulletin, Report: B 2064-A-R, p. B1-B18.
- Rose, P.R., 1976, Mississippian carbonate shelf margins, western United States, *in*, J.G. Hill, ed., Geology of the Cordilleran Hingeline, Denver, Rocky Mountain Association of Geologists, p. 135-151.
- Rowell, A.J., Rees, M.N., and Suczek, C.A., 1979, Margin of the North American continent in Nevada during Late Cambrian time: American Journal of Science, v. 279, p. 1-18.
- Saltzman, M.R., 2002, Carbon and oxygen isotope stratigraphy of the Lower Mississippian (Kinderhookian-lower Osagean), Western United States: implications for seawater chemistry and glaciation: Geological Society of America Bulletin, v. 114, p. 96-108.
- Saltzman, M.R., 2003, Late Paleozoic ice age: ocean gateway or pCO₂?: Geology, v. 31, p. 151-154.
- Saltzman, M.R., Gonzalez, L.A., and Lohmann, K.C., 2000, Earliest Carboniferous cooling step triggered by Antler Orogeny?: Geology, v. 28, p. 347-350.
- Sandberg, C.A., 1975, McGowan Creek Formation, new name for lower Mississippian flysch sequence in East-central Idaho: U. S. Geological Survey Bulletin, Report: B 1405-E, 11 p.
- Sandberg C.A., 1976, Conodont biofacies of late Devonian *Polygnathus styriacus* Zone in western United States: Special Paper - Geological Association of Canada, no.15, Conodont paleoecology, p. 171-186.
- Sandberg, C.A., and Klapper, G., 1967, Stratigraphy, age, and significance of the Cottonwood Canyon Member of the Madison Limestone in Wyoming and Montana: USGS Bulletin 1251-B, 70 p.
- Sando, W.J., 1960a, Distribution of corals in the Madison Group and correlative strata in Montana, western Wyoming, and northeastern Utah: U. S. Geological Survey Professional Paper, Report: P 0400-B, p. B225-B227.
- Sando, W.J., 1960b, Corals from well cores of Madison group, Williston Basin (Montana): U. S. Geological Survey Bulletin, Report: B 1071-F, v. 35, p. 157.

- Sando, W.J., 1972, Madison Group (Mississippian) and Amsden Formation (Mississippian and Pennsylvanian) in the Beartooth Mountains, northern Wyoming and southern Montana: Field Conference - Montana Geological Society, v. 21, p. 57-63.
- Sando, W.J., 1976, Mississippian history of the northern Rocky Mountains region: Journal of Research of the U. S. Geological Survey, v. 4, p. 317-338.
- Sando, W.J., 1984, Syringoporoid corals; guides to the stratigraphy of upper Paleozoic rocks in the Western Interior region: Open-File Report - U. S. Geological Survey, Report: OF 84-0080, 32 p.
- Sando, W.J., 1988, Madison Limestone (Mississippian) paleokarst: a geologic synthesis, *in*, N.P. James and P.W. Choquette, eds., Paleokarst, New York, Springer-Verlag, p. 256-277.
- Sando W.J., Dutro, J.T., Jr., and Gere, W.C., 1959, Brazer dolomite (Mississippian), Randolph Quadrangle, Northeast Utah: Bulletin of the American Association of Petroleum Geologists, v. 43, p. 2741-2769.
- Sando, W.J., Gordon, M., Jr., and Dutro, J.T., Jr., 1975, Stratigraphy and geologic history of the Amsden Formation (Mississippian and Pennsylvanian) of Wyoming: U. S. Geological Survey Professional Paper, Report: P 0848-A, 83 p.
- Sando, W.J., Mamet, B.L., and Dutro, J.T., Jr., 1969, Carboniferous megafaunal and microfaunal zonation in the northern cordillera of the United States: U. S. Geological Survey Professional Paper, Report: P 0613-E, p. E1-E29.
- Sando, W.J., and Sandberg, C.A., 1987, New interpretations of Paleozoic stratigraphy and history in the Northern Laramie Range and vicinity, southeast Wyoming: USGS Professional Paper 1450, 39 p.
- Sando, W.J., Sandberg, C.A., and Perry, W.J., Jr., 1985, Revision of Mississippian stratigraphy, northern Tendoy Mountains, Southwest Montana: U. S. Geological Survey Bulletin, Report: B 1656, p. A1-A10.
- Schlager, W., 1992, Sedimentology and sequence stratigraphy of reefs and carbonate platforms: Tulsa, American Association of Petroleum Geologists, Continuing Education Course Notes Series No. 34, 71 p.
- Scotese, C.R., and McKerrow, W.S., 1990, Revised world maps and introduction: *in* W.S. McKerrow and C.R. Scotese, eds., Palaeozoic Palaeogeography and Biogeography, Memoir - Geological Society of London, v. 12, p. 1-21.

- Silberling, N.J., 1973, Geologic events during the Permian-Triassic time along the Pacific margin of the United States, *in*, The Permian and Triassic systems and their mutual boundary, Calgary, Canadian Society of Petroleum Geologists Memoir 2, p. 345-362.
- Sloss, L.L., 1963, Sequences in the cratonic interior of North America: Geological Society of America Bulletin, vol.74, p. 93-113.
- Smith, J.F., Jr. and Ketner, K.B., 1968, Zone of sedimentary facies change and structural instability in the Carlin-Pine Valley area, Nevada: Geological Society of America Special Paper, p. 335-336.
- Smith, J.F., and Ketner, K.B., 1977, Tectonic events since early Paleozoic in the Carlin-Pinon Range area, Nevada: U. S. Geological Survey Professional Paper, Report: P 0867-C, 18 p.
- Smith, L.B., Jr., Eberli, G.P., and Westphal, H., 2000, Sequence stratigraphic distribution of reservoir-quality dolomite, Madison Formation (Mississippian), Wyoming and Montana: Annual Meeting Expanded Abstracts- American Association of Petroleum Geologists, vol. 2000.
- Smith, L.B., Jr., Eberli, G.P, and Sonnenfeld, M.D., 2001, The sequence stratigraphic and paleogeographic distribution of reservoir-quality dolomite, Madison Formation, Wyoming and Montana: Annual Meeting Expanded Abstracts- American Association of Petroleum Geologists, vol. 2001.
- Smith, L.B., Jr., Eberli, G.P., and Sonnenfeld, M.D., 2004, Sequence stratigraphic and paleogeographic setting of reservoir-quality dolomite, Madison Formation, Wyoming and Montana, , *in*, G.M. Grammer, P.M. Harris, and G.P. Eberli, eds., Integration of Outcrop and Modern Analog in Reservoir Modeling, AAPG Memoir 80, p. 67-92.
- Sonnenfeld, M.D., 1996a, Sequence evolution and hierarchy within the Lower Mississippian Madison Limestone of Wyoming, *in*, M.W. Longman and M.D. Sonnenfeld, eds., Paleozoic Systems of the Rocky Mountain Region, Rocky Mountain Section SEPM, p. 165-192.
- Sonnenfeld, M.D., 1996b, An integrated sequence stratigraphic approach to reservoir characterization of the Lower Mississippian Madison Limestone, emphasizing Elk Basin Field, Bighorn Basin, Wyoming: Unpublished Ph.D. dissertation, Colorado School of Mines, Golden, CO, 437 p.

- Speed, R.C., 1977, Island-arc and other paleogeographic terranes of late Paleozoic age in the western Great Basin, *in*, J.H. Stewart, C.H. Stevens, and A.E. Fritsche, eds., Paleozoic paleogeography of the western United States, Bakersfield, SEPM Pacific Section.
- Speed, R.C. and Sleep, N.H., 1982, Antler Orogeny and foreland basin: a model: Geological Society of America Bulletin, v. 93, p. 815-828.
- Stewart, J.H., and Poole, F.G., 1974, Lower Paleozoic and uppermost Precambrian Cordilleran Miogeocline, Great Basin, western United States: Special Publication - Society of Economic Paleontologists and Mineralogists, v. 22, p. 28-57.
- Tankard, A.J., 1986, Depositional response to foreland deformation in the Carboniferous of Eastern Kentucky: Bulletin of the American Association of Petroleum Geologists, v. 70, p. 853-868.
- Tedesco, L.P., and Wanless, H.R., 1995, Growth and burrow-transformation of carbonate banks; comparison of modern skeletal banks of South Florida and Pennsylvanian phylloid banks of south-eastern Kansas, USA: Special Publication of the International Association of Sedimentologists, v. 23, p. 495-521.
- Trexler, J.H., Jr. and Cashman, P.H., 1991, Mississippian stratigraphy and tectonics of east-central Nevada, *in*, J.D. Cooper and C.H. Stevens, eds., Paleozoic paleogeography of the western United States II, Pacific Section SEPM, v. 67, p. 331-342.
- Trexler, J.H., Jr., Cashman, P.H., Cole, J.C., Snyder, W.S., Tosdal, R.M., and Davydov, V.I., 2003, Widespread effects of Middle Mississippian deformation in the Great Basin of western North America: Geological Society of America Bulletin, v. 115, p. 1278-1288.
- Trexler, J.H., Jr., Cashman, P.H., Snyder, W.S., and Davydov, V.I., 2004, Late Paleozoic tectonism in Nevada; timing, kinematics, and tectonic significance: Geological Society of America Bulletin, v.116, p. 525-538.
- Turcotte, D.L. and Schubert, G., 1982, Geodynamics: Applications of continuum physics to geological problems, John Wiley and Sons, New York, NY.
- Vail, P.R., Mitchum, R.M., Jr., and Thompson, S, III, 1977, Seismic stratigraphy and global changes of sea level: Part 3, Relative sea level from coastal onlap, *in*, C.E. Payton, ed., Seismic stratigraphy: Applications to hydrocarbon exploration, AAPG Memoir 26, p. 63-82.
- Veevers, J.J., and Powell, C.M., 1987, Late Paleozoic glacial episodes in Gondwanaland reflected in transgressive-regressive depositional sequences in Euramerica: Geological Society of America Bulletin, v. 98, p. 475-487.

- Vening Meinesz, F.A., 1931, Une nouvelle methode pour la reduction isostatique regionale de l'intensite de la pesanteur: Bulletin Geodesique, v. 29, p. 33-51.
- Walcott, R.I., 1970a, Flexural rigidity, thickness, and viscosity of the lithosphere: Journal of Geophysical Research, v. 75, p. 3941-3954.
- Walcott, R.I., 1970b, Flexure of the lithosphere at Hawaii: Tectonophysics, v. 9, p. 435-446.
- Walcott, R.I., 1972, Gravity, Flexure, and the Growth of Sedimentary basins at a Continental Edge: Geological Society of America Bulletin, v. 83, p.1845-1848.
- Waschbusch, P.J. and Royden, L.H., 1992, Spatial and temporal evolution of foredeep basins: lateral strength variations and inelastic yielding in continental lithosphere: Basin Research, v. 4, p. 179-196.
- Watts, A.B., 1988, Gravity anomalies, crustal structure, and flexure of the lithosphere at the Baltimore Canyon Trough: Earth and Planetary Science Letters, v. 89, p. 133-144.
- Watts, A.B., 2001, Isostasy and Flexure of the Lithosphere: Cambridge, UK, Cambridge University Press, 458 p.
- Webster, G.D., and Groessens, E., 1990, Conodont subdivision of the Lower Carboniferous, *in*, P.L. Brenkle and W.L. Manger, eds., Intercontinental correlation and division of the Carboniferous System; contributions from the Carboniferous Subcommittee meeting, p. 31-40.
- Westphal, H., Eberli, G.P., Grammer, G.M., and Moore, C.H., 1999, Mississippian Madison Formation – Reservoir evaluation through outcrop to subsurface correlation, Unpublished report, 76 p.
- Westphal, H., Eberli G.P., Smith L.B., Jr., and Grammer, G.M., 2004, Reservoir characterization in the Mississippian Madison Formation, Wind River Basin, Wyoming- AAPG Bulletin
- Wilson, J.L., 1975, Carbonate Facies in Geologic History: Springer-Verlag, New York, 471 p.
- Wilson, E., Preacher, J.M., and Link, P.K., 1994, New constraints on the nature of the Early Mississippian Antler sedimentary basin in Idaho: *in* A.F. Embry, B. Beauchamp, and D.J. Glass, eds., Pangea: Global Environments and Resources: Memoir - Canadian Society of Petroleum Geologists, v. 17, p. 155-174.

Ziegler, W. and Lane, H.R., 1987, Cycles in conodont evolution from Devonian to Mid-Carboniferous, *in*, R.J. Aldridge, ed., Paleobiology of conodonts, Fourth European conodont symposium, Nottingham, UK.

APPENDICES

APPENDIX 1.1

LEGEND













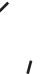
	Peloidal/skeletal calcisilt wackestone-grainstone		Skeletal packstone-grainstone
	Peloidal calcisilt wackestone-grainstone		Intraclast wackestone-conglomerate
	Argillaceous fine peloidal-micropeloidal wackestone-grainstone		Peloidal/skeletal packstone-grainstone
	Argillaceous fine-very fine peloidal/skeletal wackestone-grainstone		Algal laminites
	Micritized-iron stained coated grain-skeletal wackestone-grainstone		Pisolitic floatstone-rudstone
	Oolitic packstone-grainstone		Peloidal-micropeloidal wackestone-grainstone
	Pelmatzoan packstone-grainstone		Siliciclastic sandstone-siltstone
	Peloidal-micropeloidal and ostracod wackestone-packstone		Siliciclastic mudstone/shale
	Polymict breccia		Evaporite dissolution collapse breccia
	Bedded chert		

Appendix 1.1: Legend for lithologies used in logs of sedimentary sections

APPENDIX 1.2

LEGEND

Allochem symbols

	: Pelmatozoans		: Gastropods
	: Peloids		: Ostracods
	: Ooids		: Foraminifera
	: Rugose corals		: Micritized ooids
	: Bryozoans		: Pisoid/oncoid
	: Tabulate corals		: Intraclast
	: Fine-microskeletal debris	G	: Goniatite and orthocone cephalopods

Lithology




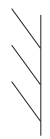










	Limestone
	Dolostone

Appendix 1.2: Legend for allochem symbols and limestone/dolostone used in logs of sedimentary sections

APPENDIX 1.3

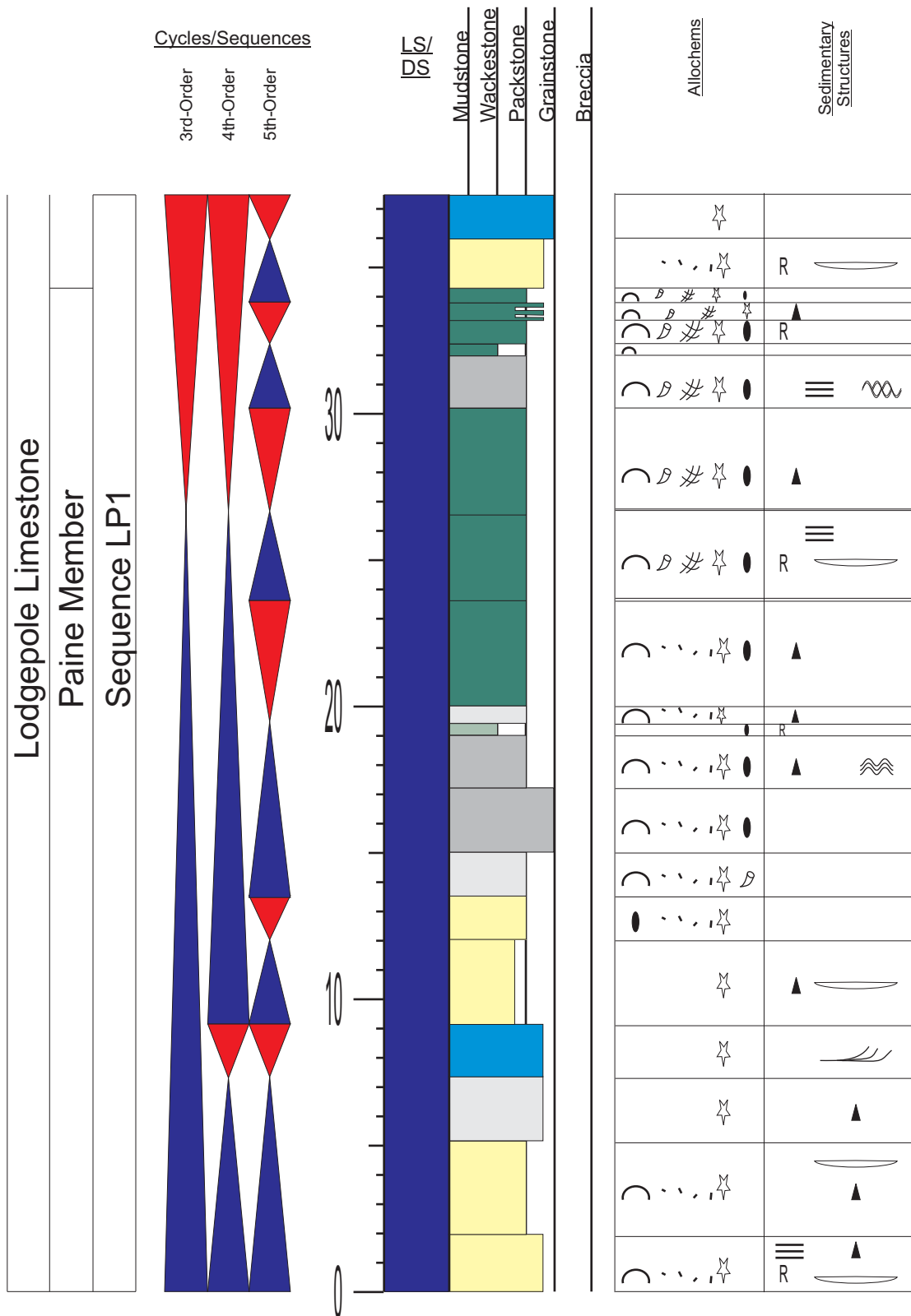
LEGEND

Sedimentary structure symbols

	: Parallel laminations		: Swaly/hummocky bedding		: Algal laminations
	: Tabular cross-stratification		: Ripple laminations		: Fenestrae
	: Trough cross-stratification		: Bidirectional cross-stratification	X	: Microkarst
R	: Iron staining		: Sand waves	C	: Caliche
	: Chert nodules		: Bioturbation		: Brecciation
	: Lenticular bedding		: Flaser bedding	S	: S-folding
Z	: Z-folding				

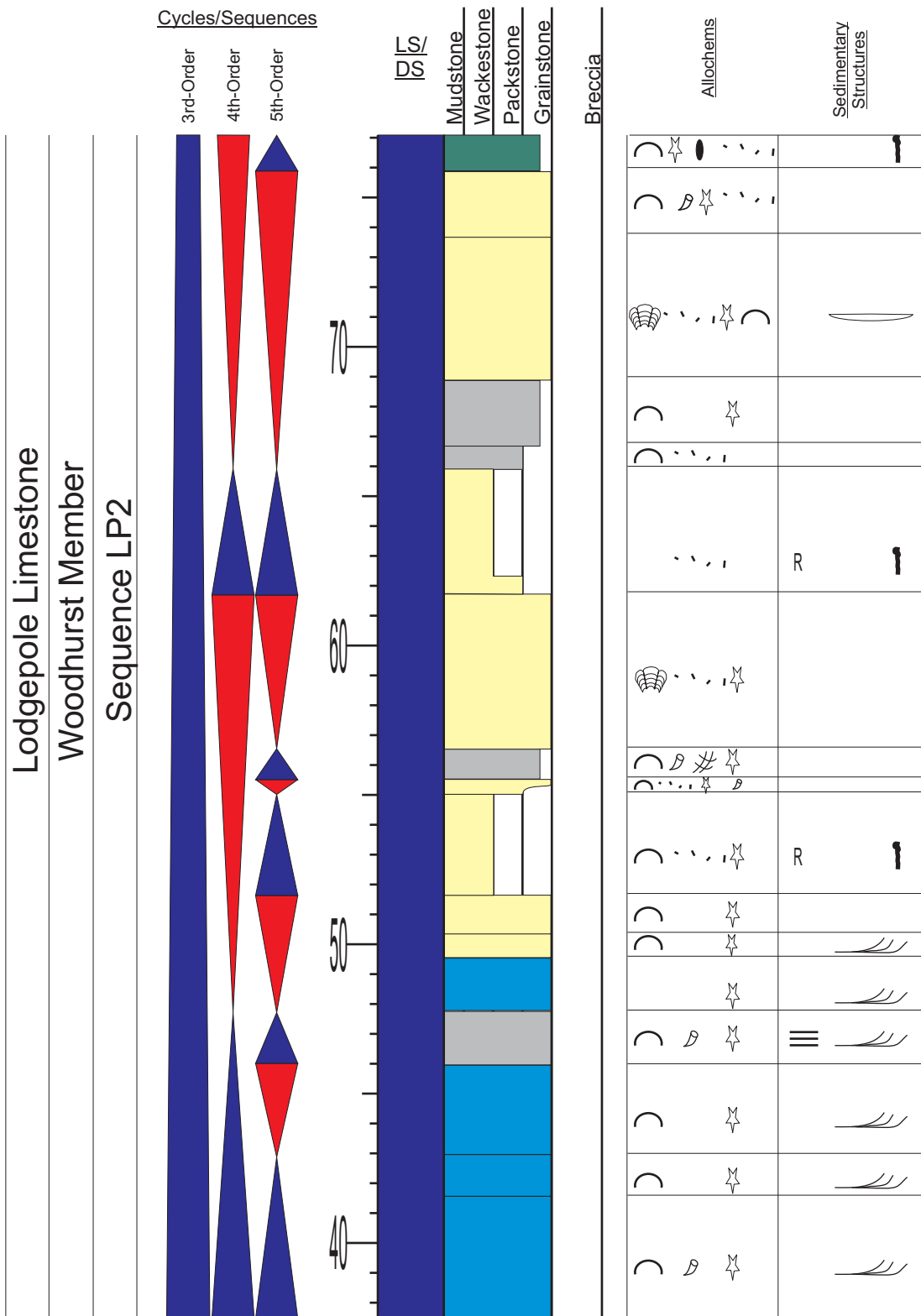
Appendix 1.3: Legend for sedimentary structure symbols used in logs of sedimentary sections

APPENDIX 2.1



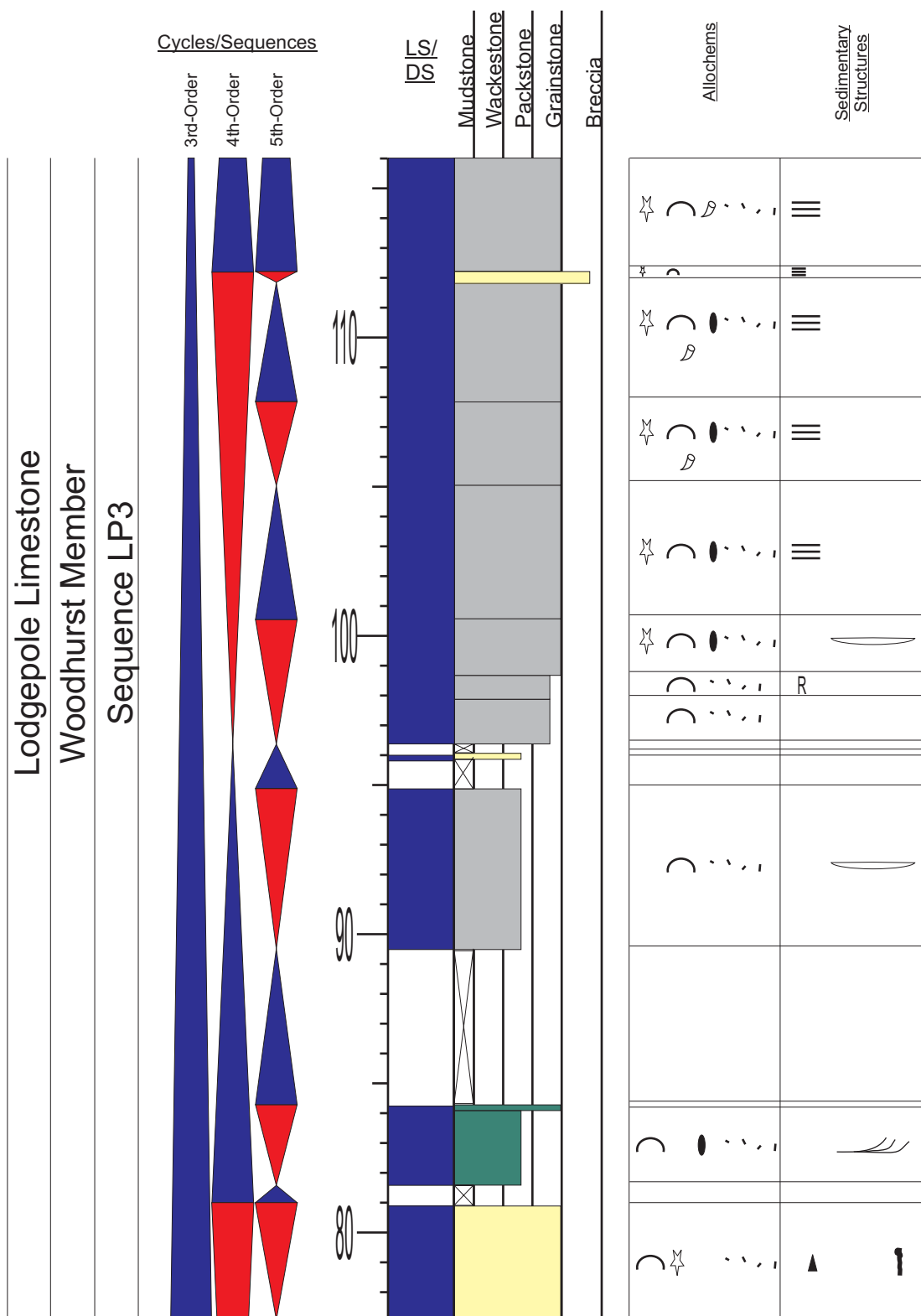
Appendix 2.1: Sedimentary section log for section Livingston. Refer to Appendix 1 for symbols and Figure 3.6 for location.

APPENDIX 2.2



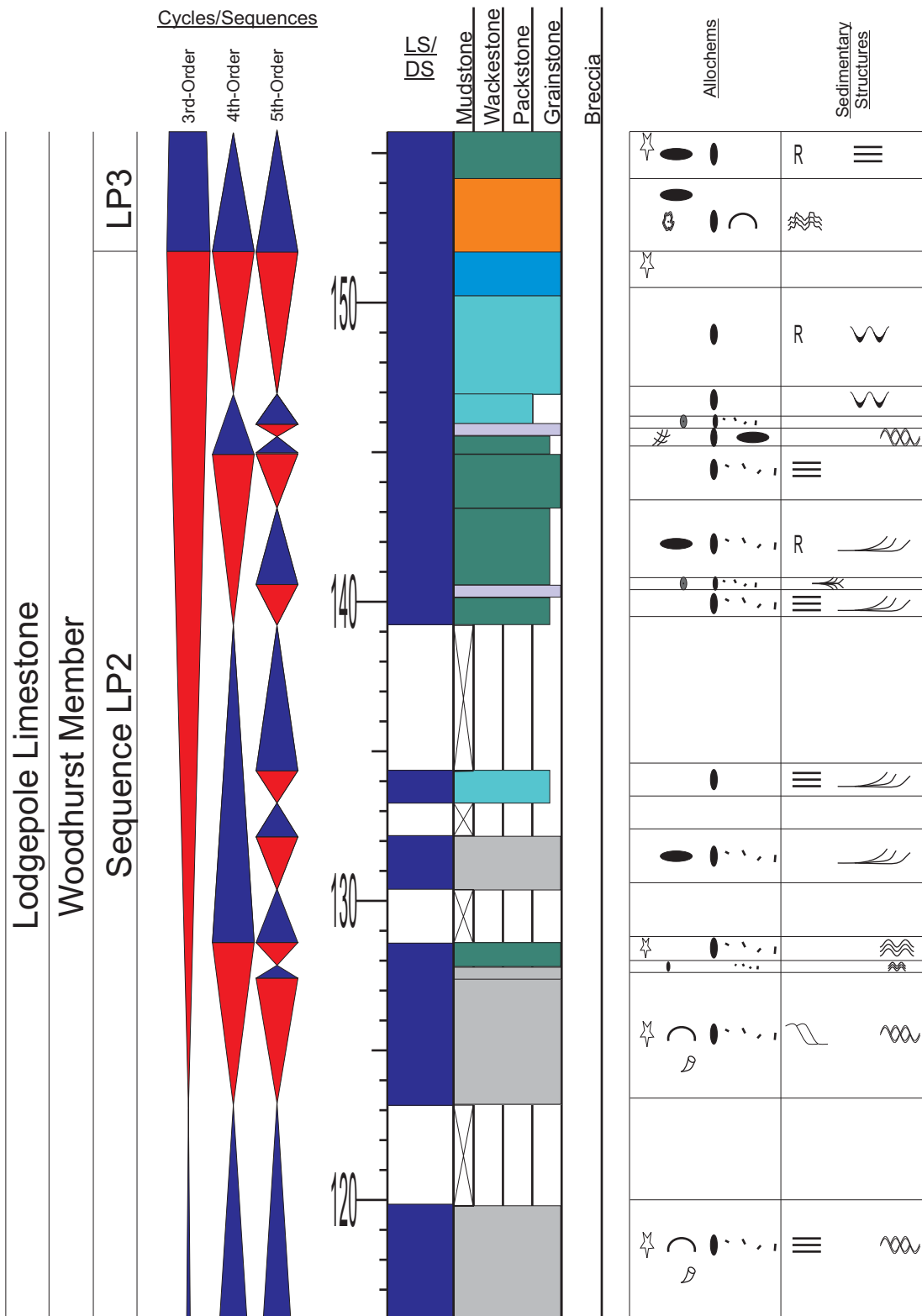
Appendix 2.2: Sedimentary section log for section Livingston (continued). Refer to Appendix 1 for symbols and Figure 3.6 for location.

APPENDIX 2.3



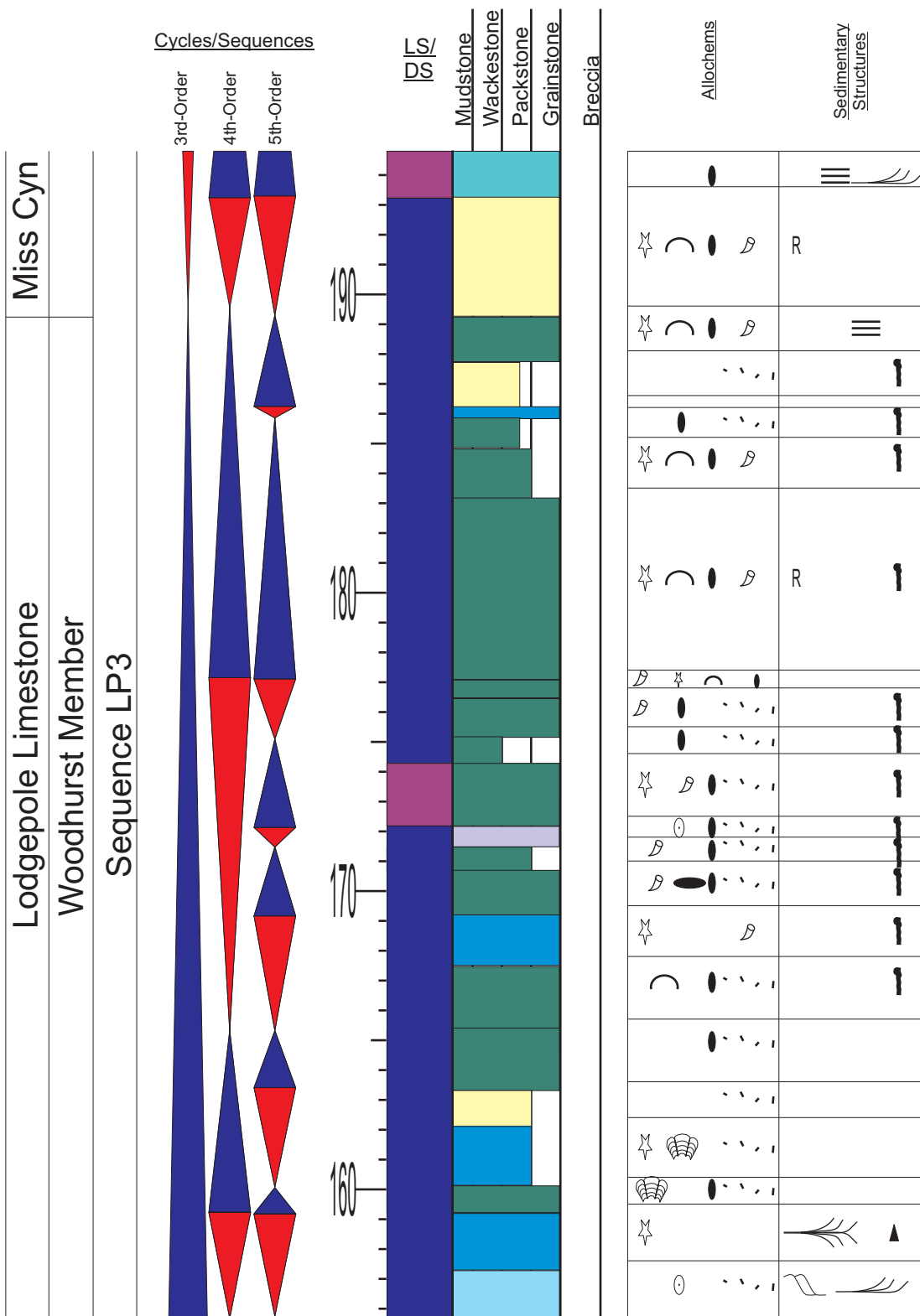
Appendix 2.3: Sedimentary section log for section Livingston (continued). Refer to Appendix 1 for symbols and Figure 3.6 for location.

APPENDIX 2.4



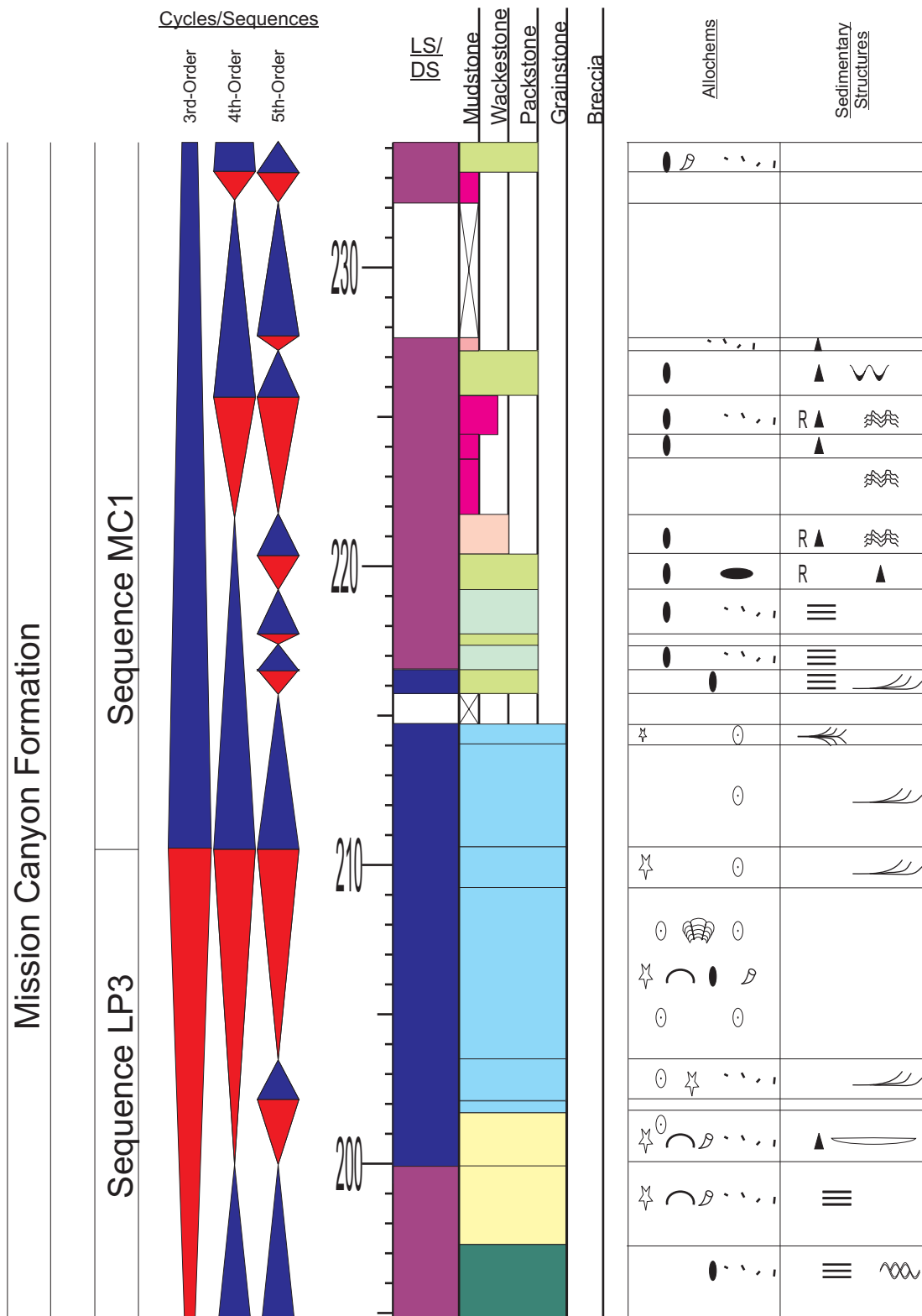
Appendix 2.4: Sedimentary section log for section Livingston (continued). Refer to Appendix 1 for symbols and Figure 3.6 for location.

APPENDIX 2.5



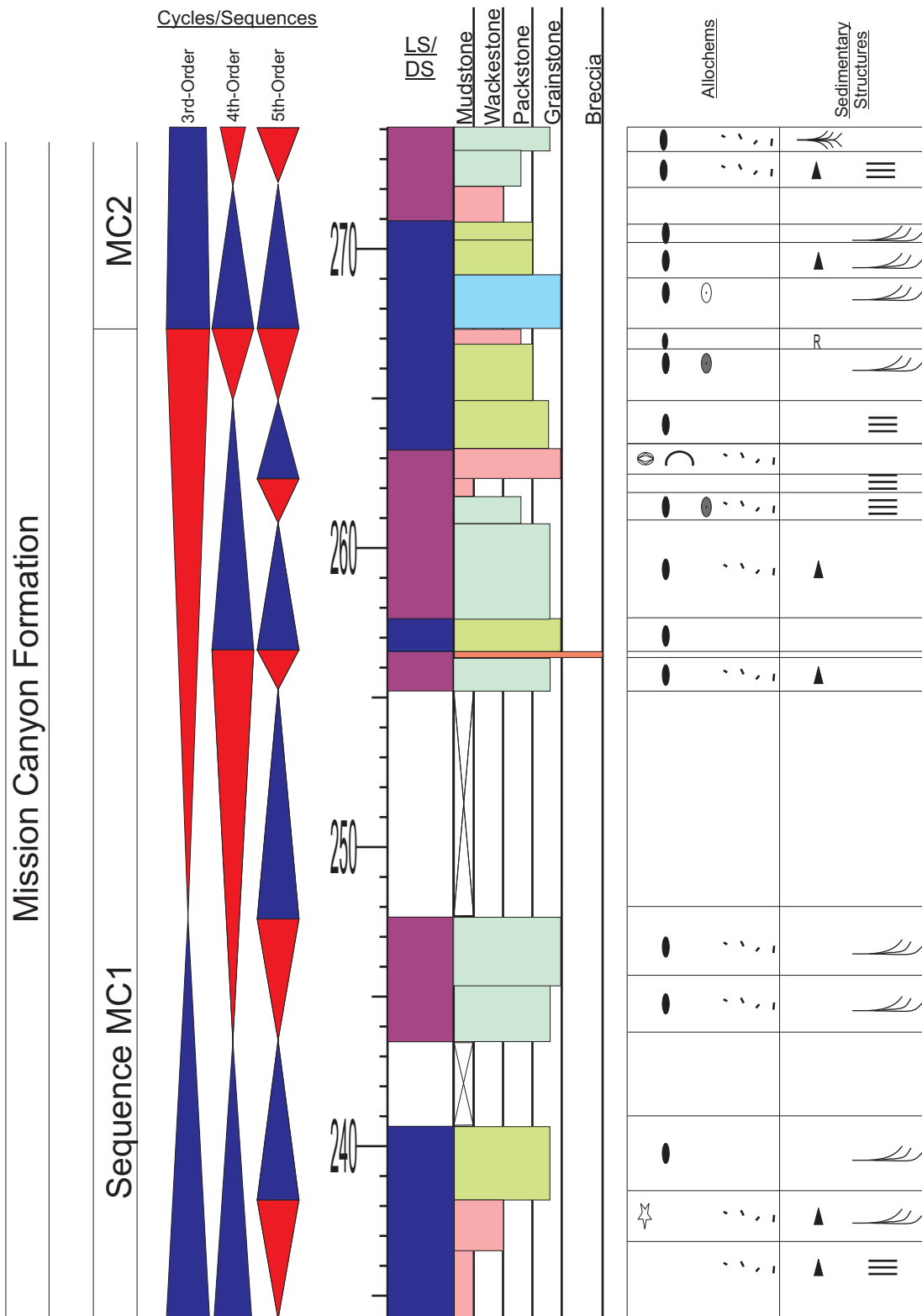
Appendix 2.5: Sedimentary section log for section Livingston (continued). Refer to Appendix 1 for symbols and Figure 3.6 for location.

APPENDIX 2.6



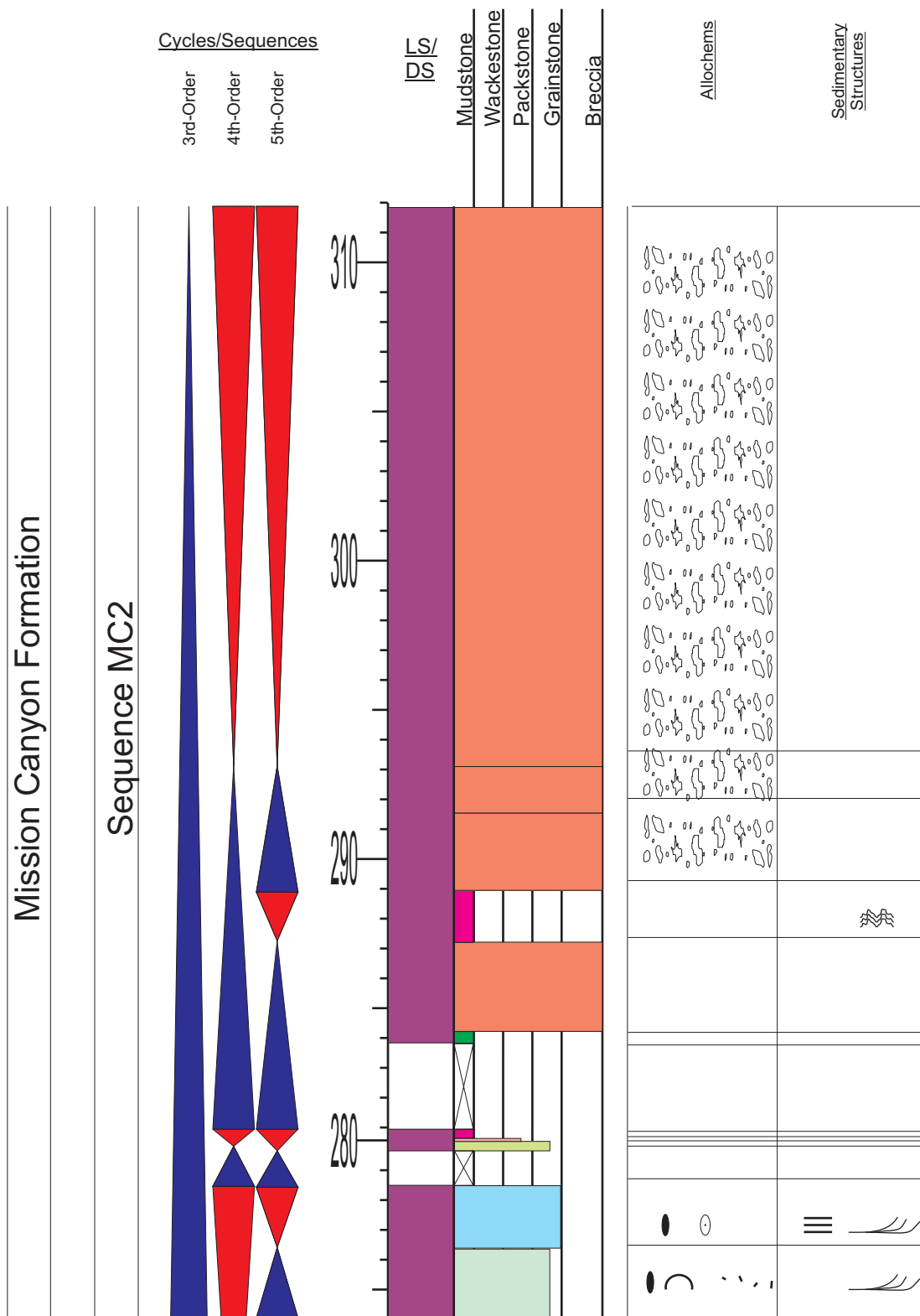
Appendix 2.6: Sedimentary section log for section Livingston (continued). Refer to Appendix 1 for symbols and Figure 3.6 for location.

APPENDIX 2.7



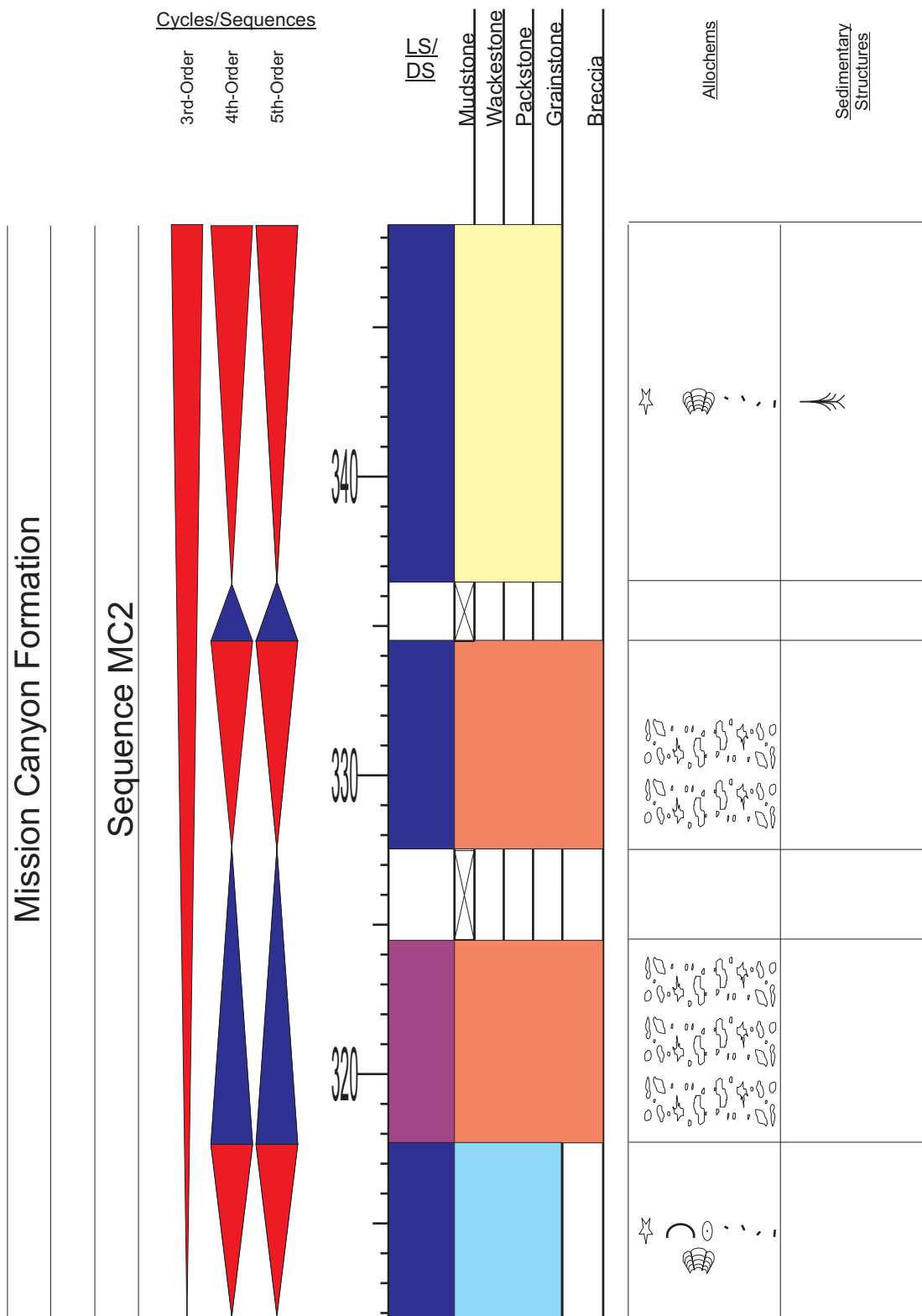
Appendix 2.7: Sedimentary section log for section Livingston (continued). Refer to Appendix 1 for symbols and Figure 3.6 for location.

APPENDIX 2.8



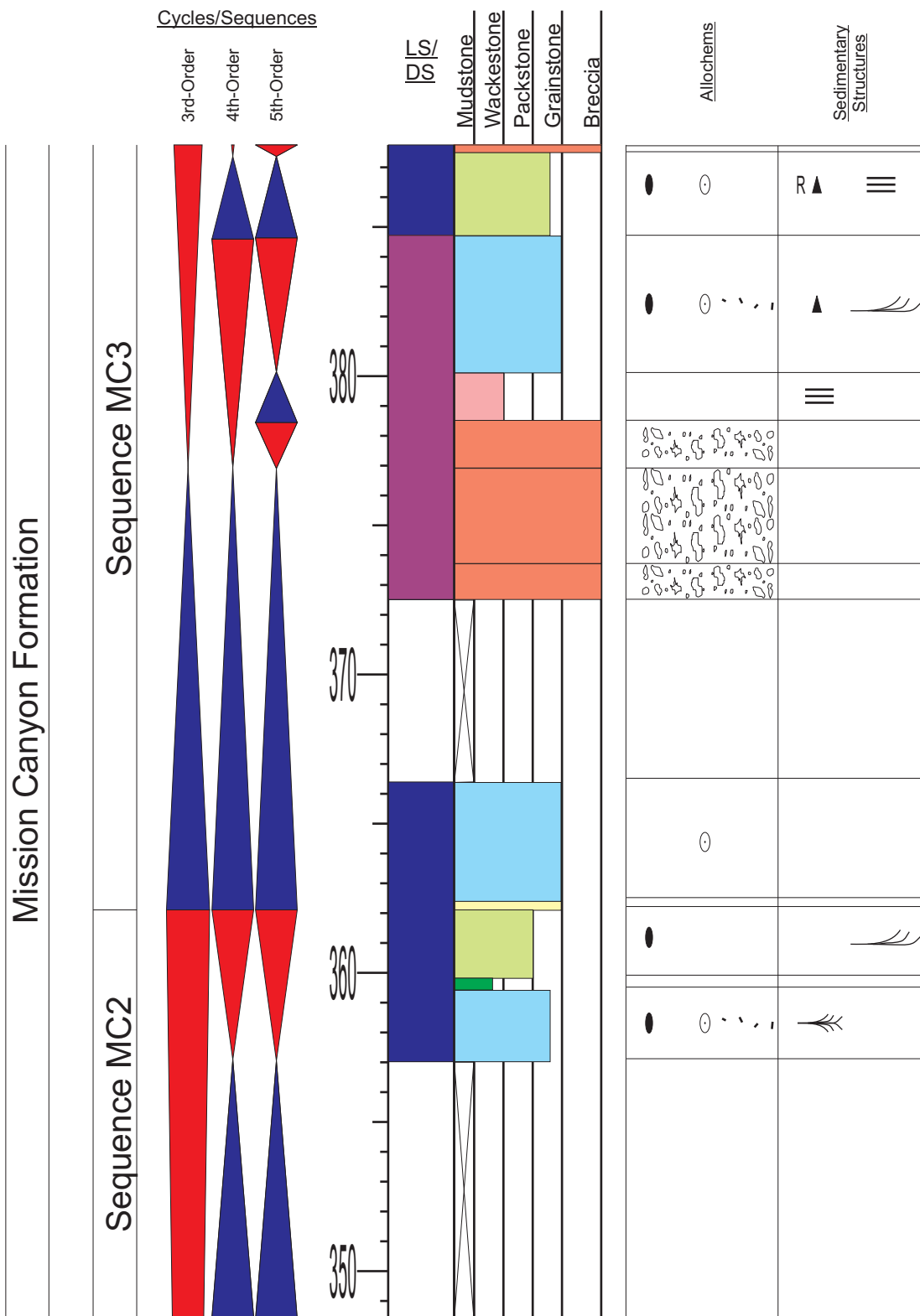
Appendix 2.8: Sedimentary section log for section Livingston (continued). Refer to Appendix 1 for symbols and Figure 3.6 for location.

APPENDIX 2.9



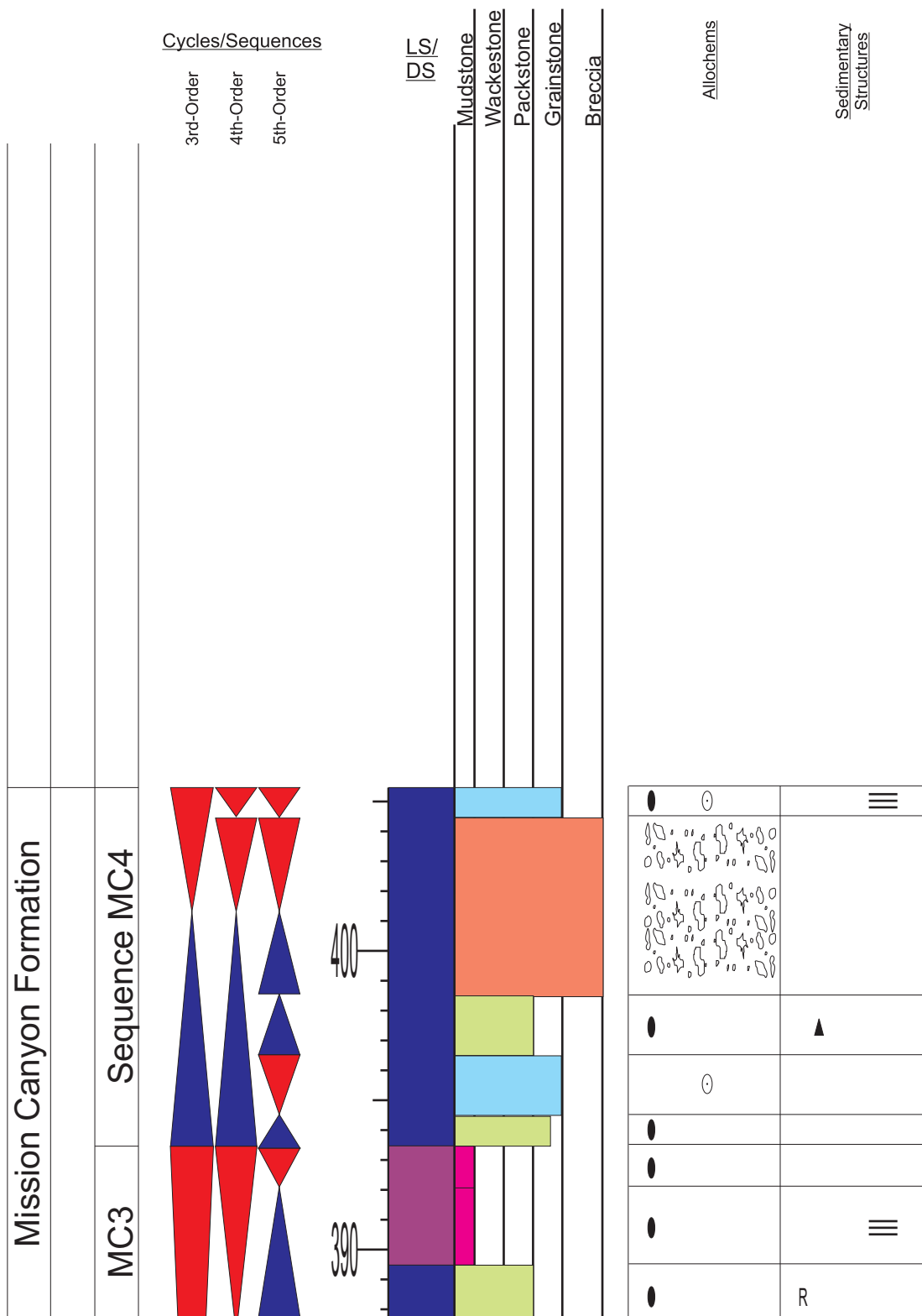
Appendix 2.9: Sedimentary section log for section Livingston (continued). Refer to Appendix 1 for symbols and Figure 3.6 for location.

APPENDIX 2.10



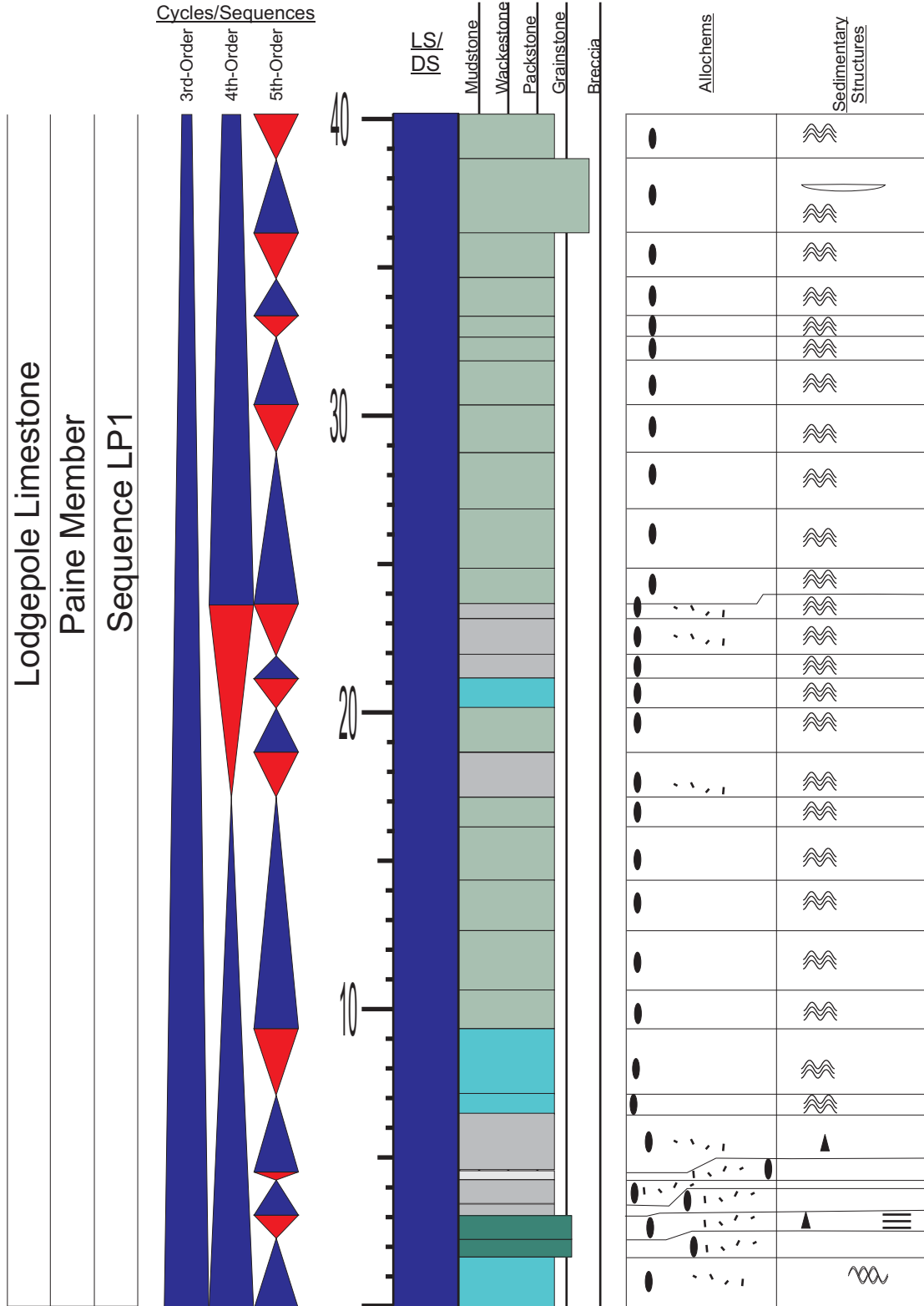
Appendix 2.10: Sedimentary section log for section Livingston (continued). Refer to Appendix 1 for symbols and Figure 3.6 for location.

APPENDIX 2.11



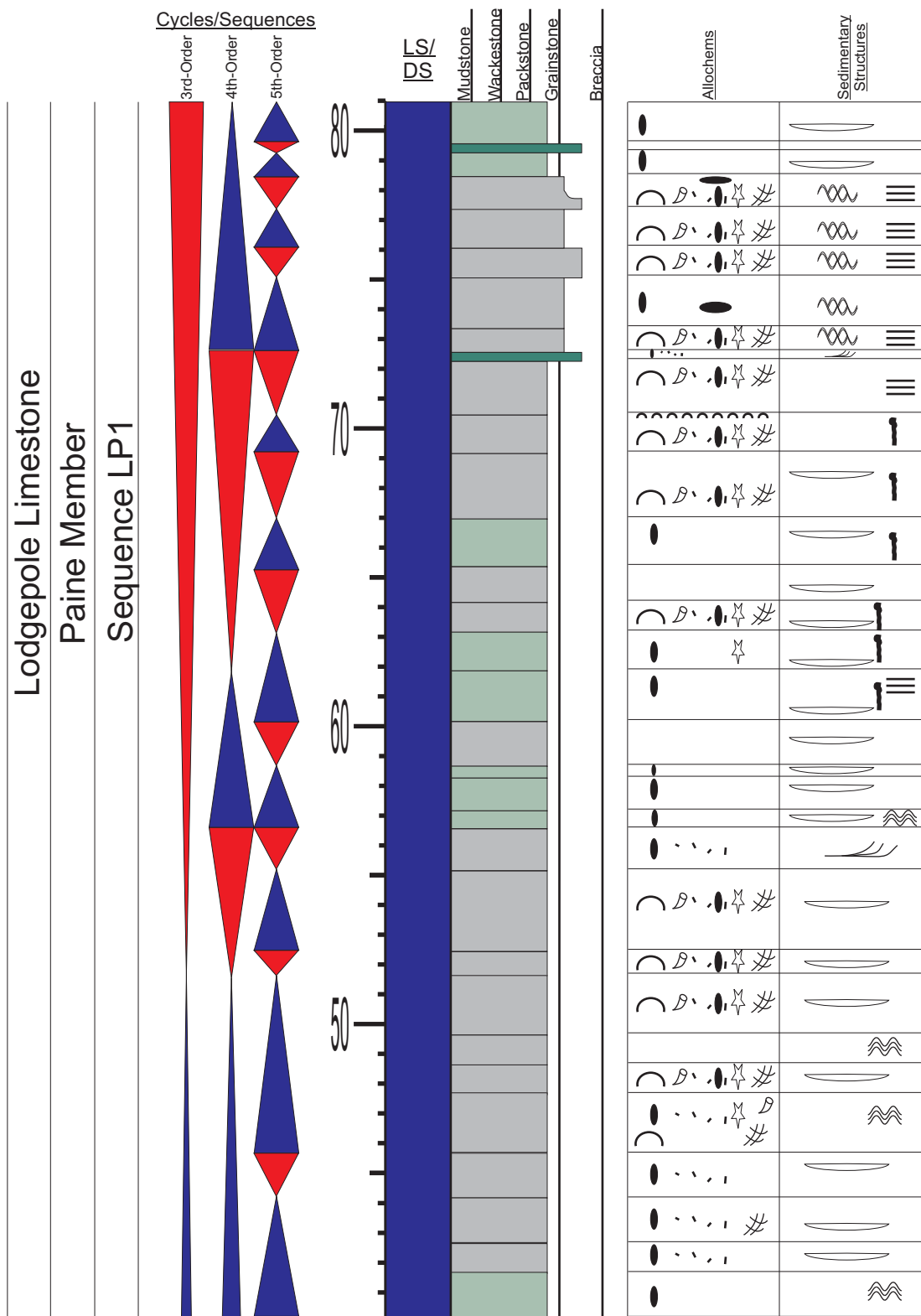
Appendix 2.11: Sedimentary section log for section Livingston (continued). Refer to Appendix 1 for symbols and Figure 3.6 for location.

APPENDIX 3.1



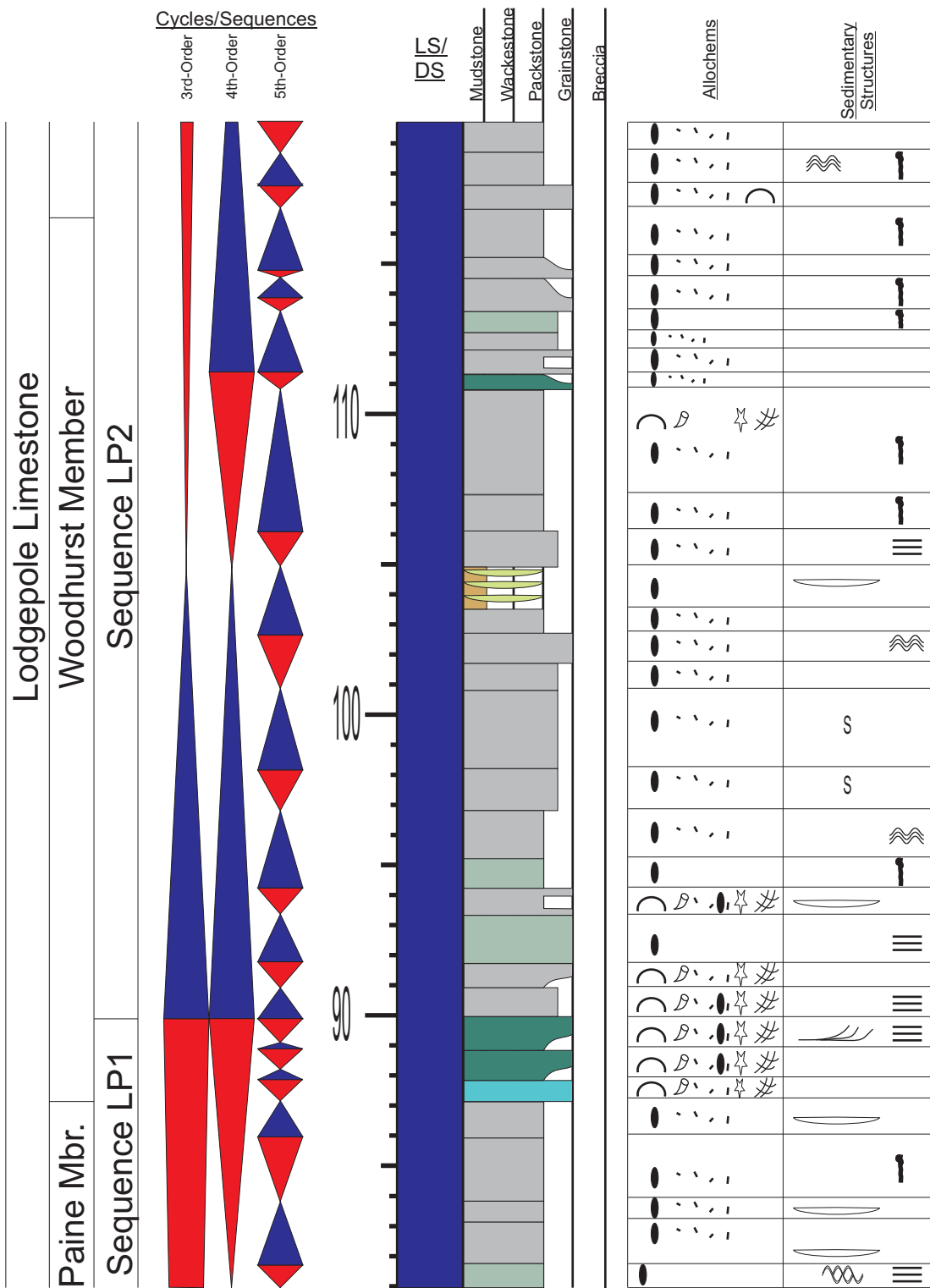
Appendix 3.1: Sedimentary section log for section Sacagawea Peak. Refer to Appendix 1 for symbols and Figure 3.6 for location.

APPENDIX 3.2



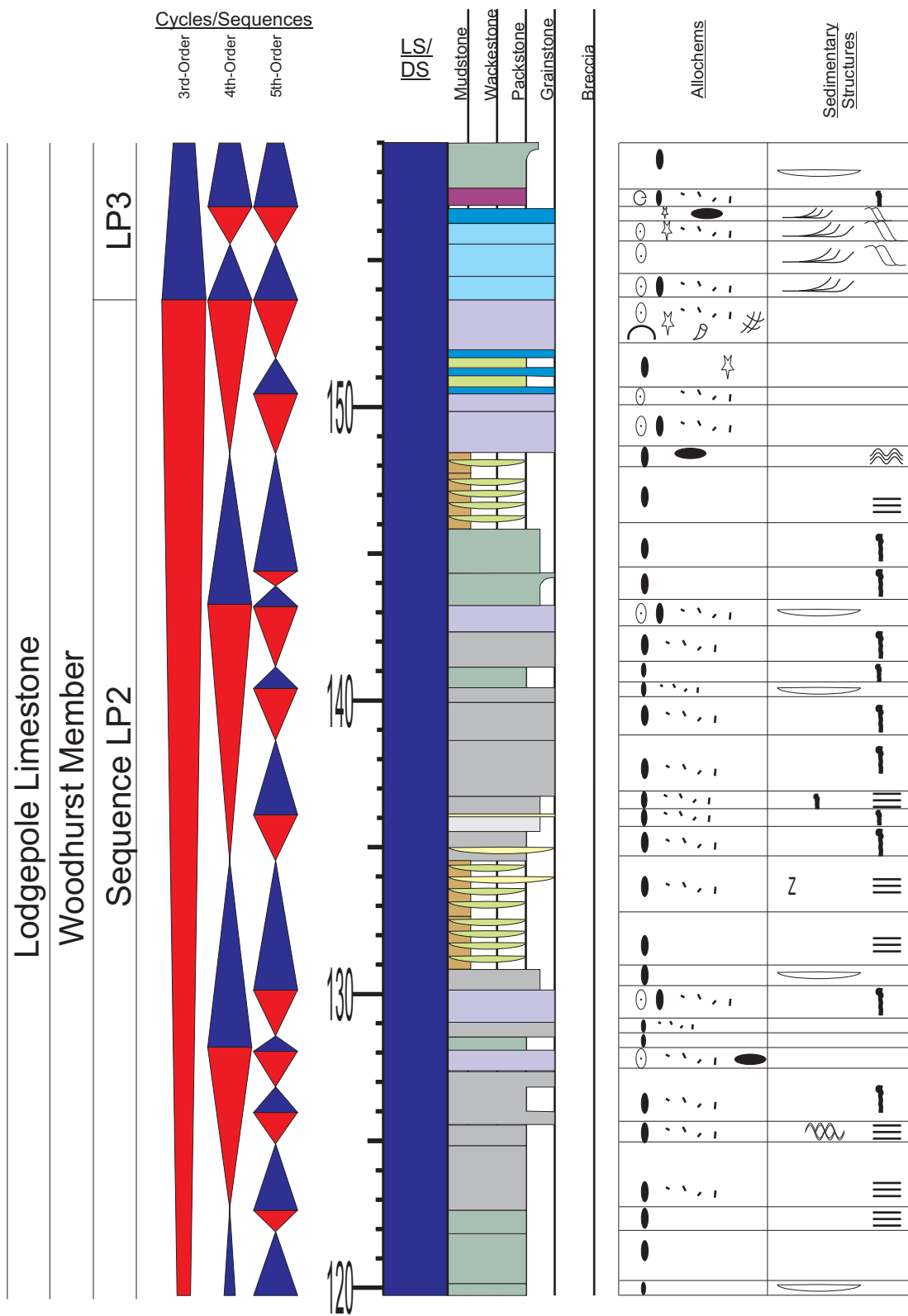
Appendix 3.2: Sedimentary section log for section Sacagawea Peak (Continued). Refer to Appendix 1 for symbols and Figure 3.6 for location.

APPENDIX 3.3



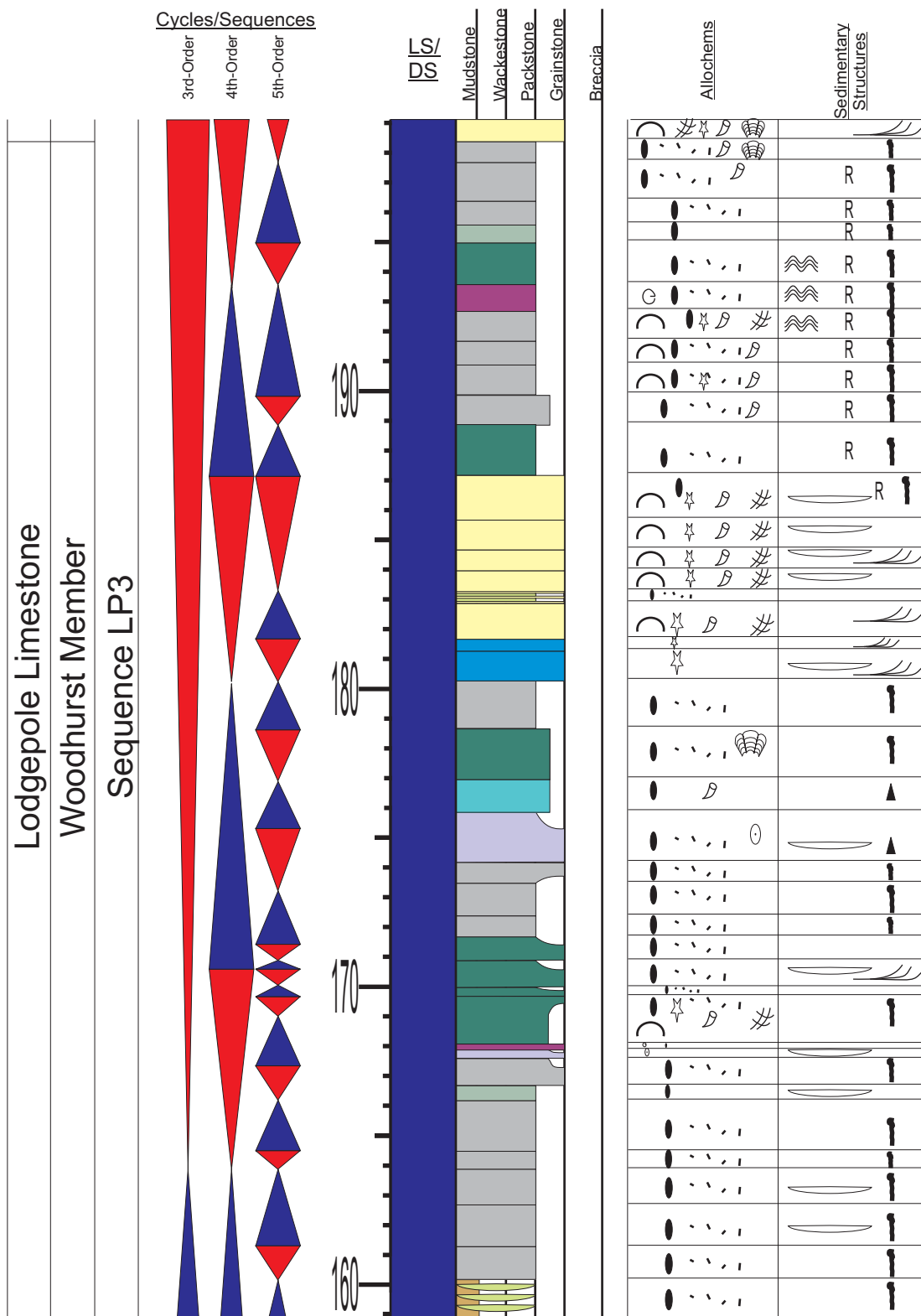
Appendix 3.3: Sedimentary section log for section Sacagawea Peak (Continued). Refer to Appendix 1 for symbols and Figure 3.6 for location.

APPENDIX 3.4



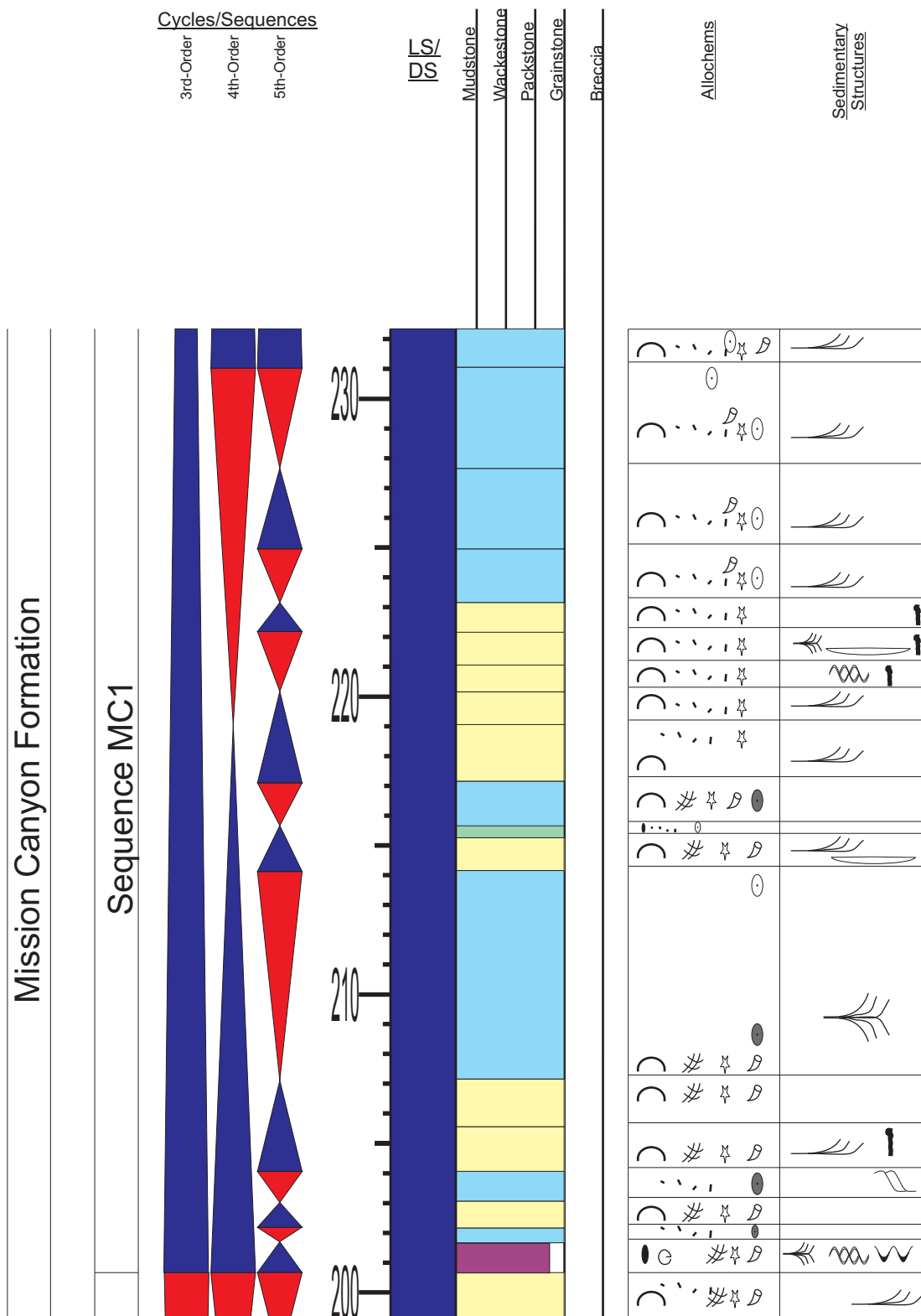
Appendix 3.4: Sedimentary section log for section Sacagawea Peak (Continued). Refer to Appendix 1 for symbols and Figure 3.6 for location.

APPENDIX 3.5



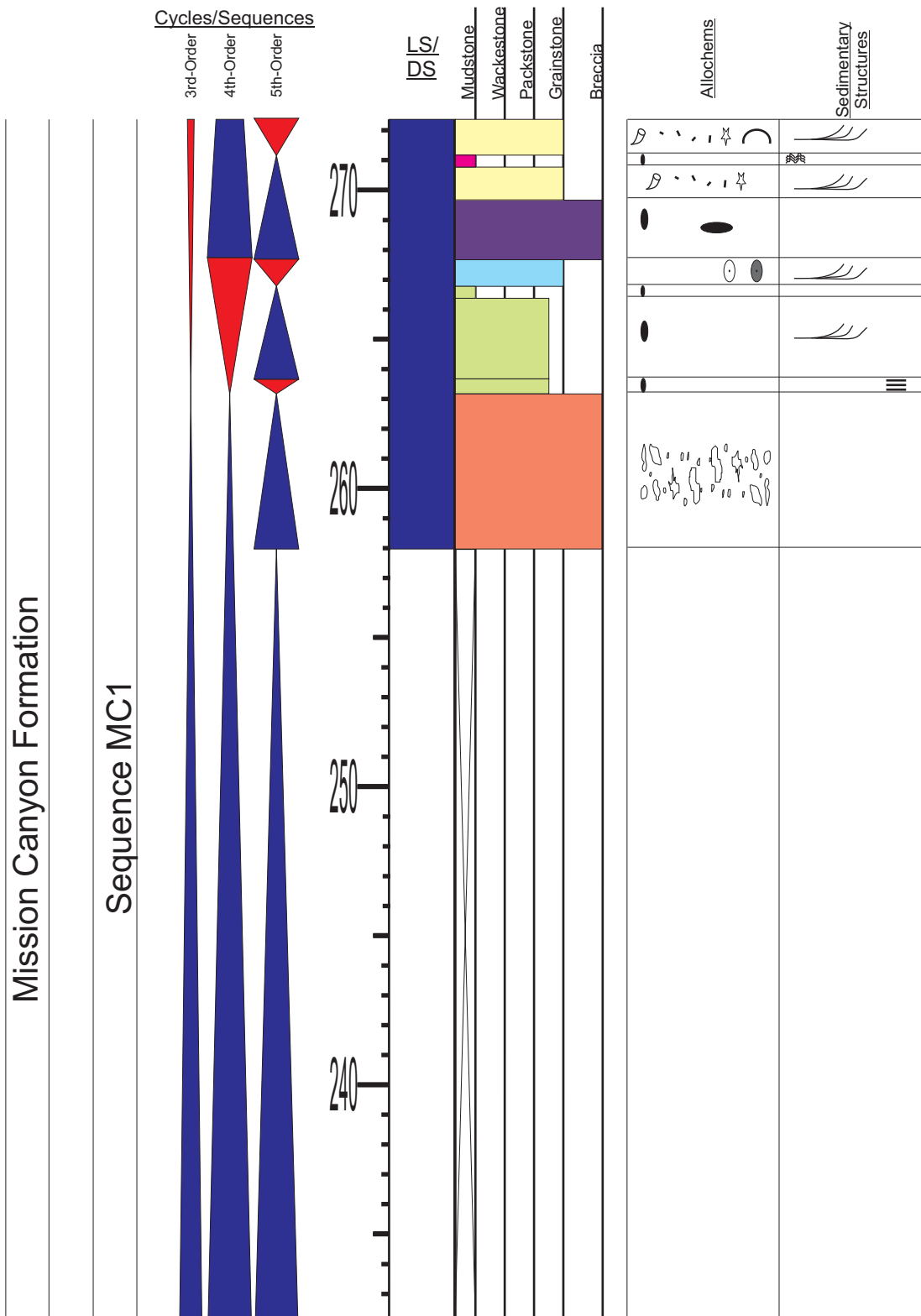
Appendix 3.5: Sedimentary section log for section Sacagawea Peak (Continued). Refer to Appendix 1 for symbols and Figure 3.6 for location.

APPENDIX 3.6



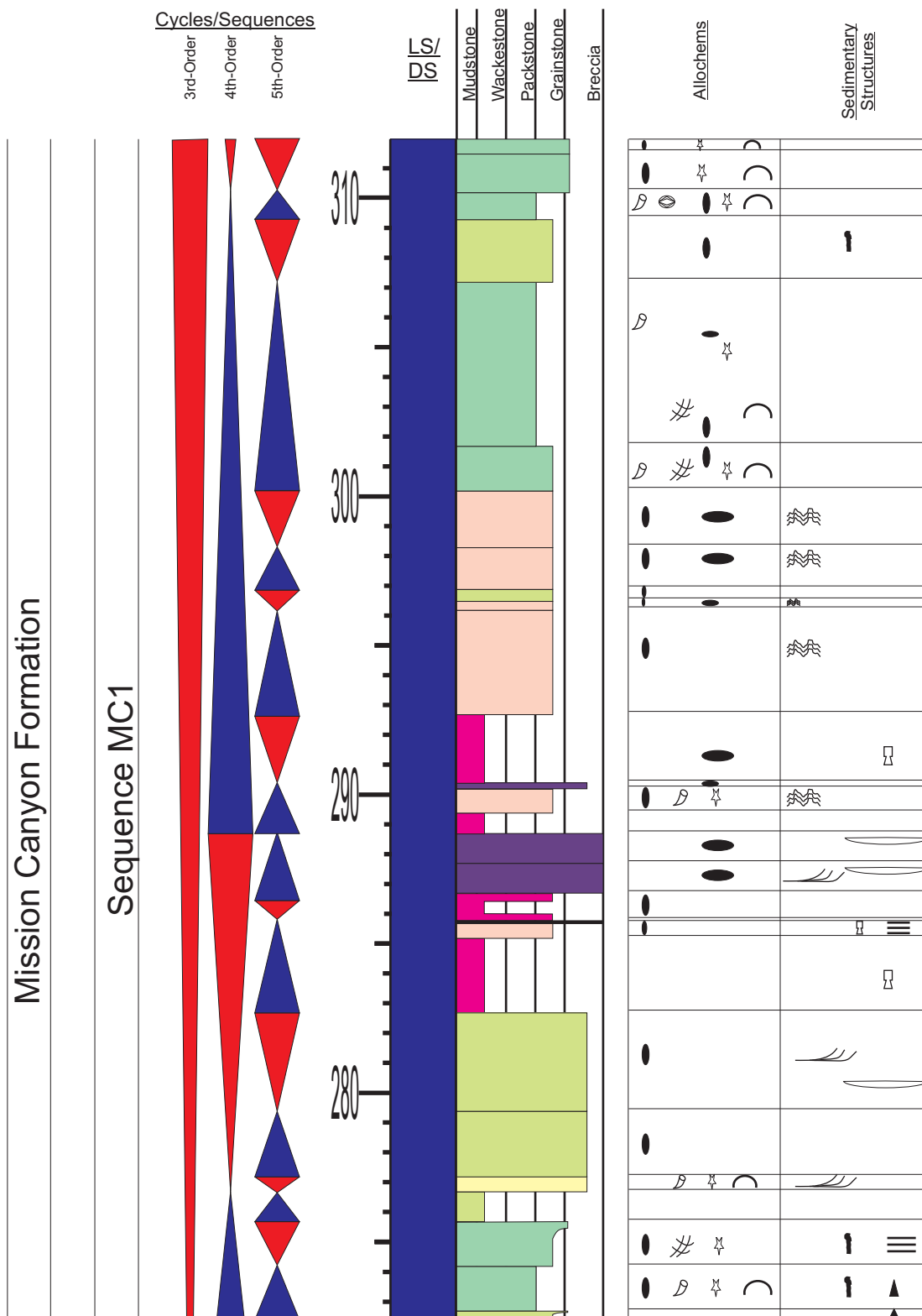
Appendix 3.6: Sedimentary section log for section Sacagawea Peak (Continued). Refer to Appendix 1 for symbols and Figure 3.6 for location.

APPENDIX 3.7



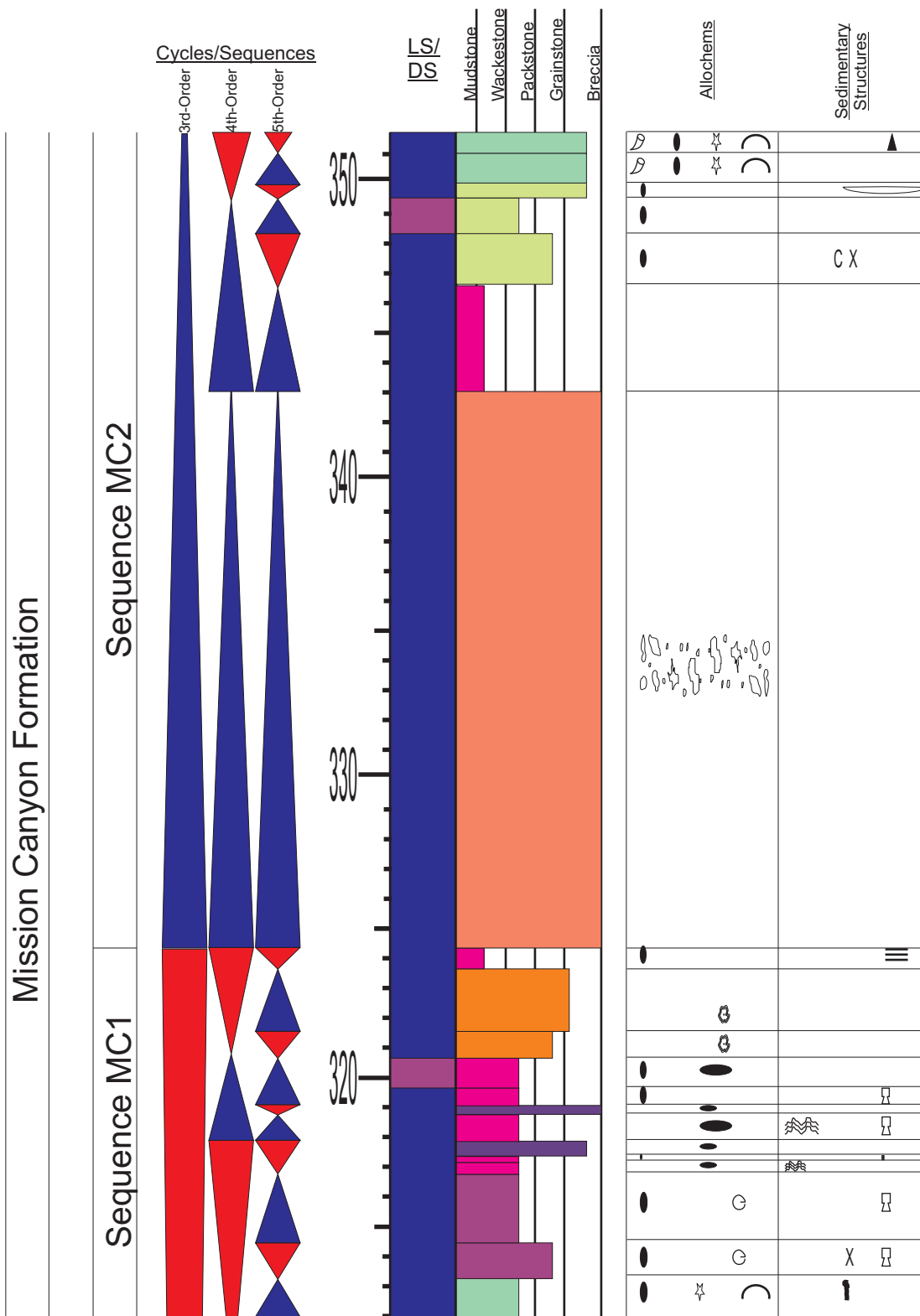
Appendix 3.7: Sedimentary section log for section Sacagawea Peak (Continued). Refer to Appendix 1 for symbols and Figure 3.6 for location.

APPENDIX 3.8



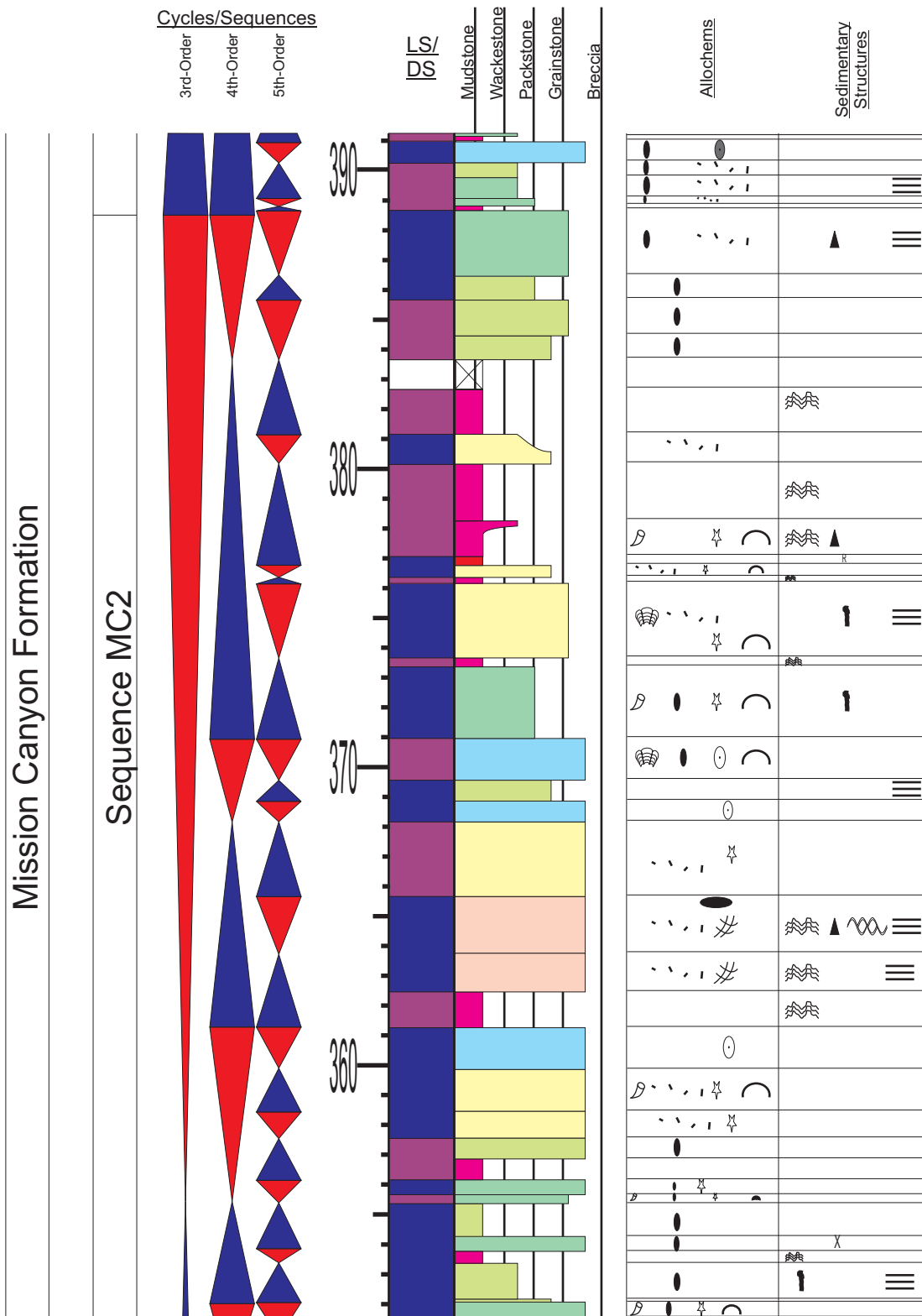
Appendix 3.8: Sedimentary section log for section Sacagawea Peak (Continued). Refer to Appendix 1 for symbols and Figure 3.6 for location.

APPENDIX 3.9



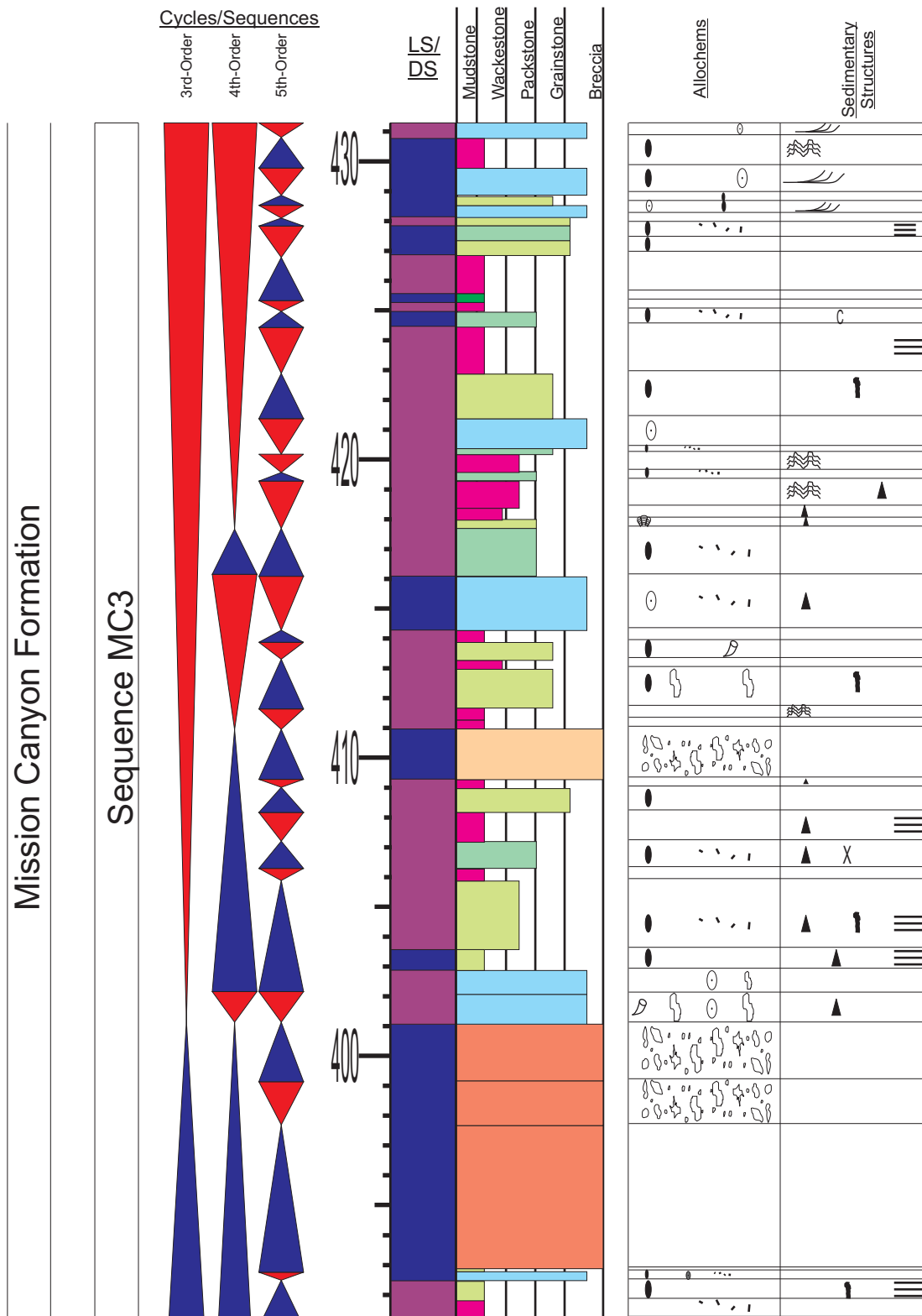
Appendix 3.9: Sedimentary section log for section Sacagawea Peak (Continued). Refer to Appendix 1 for symbols and Figure 3.6 for location.

APPENDIX 3.10



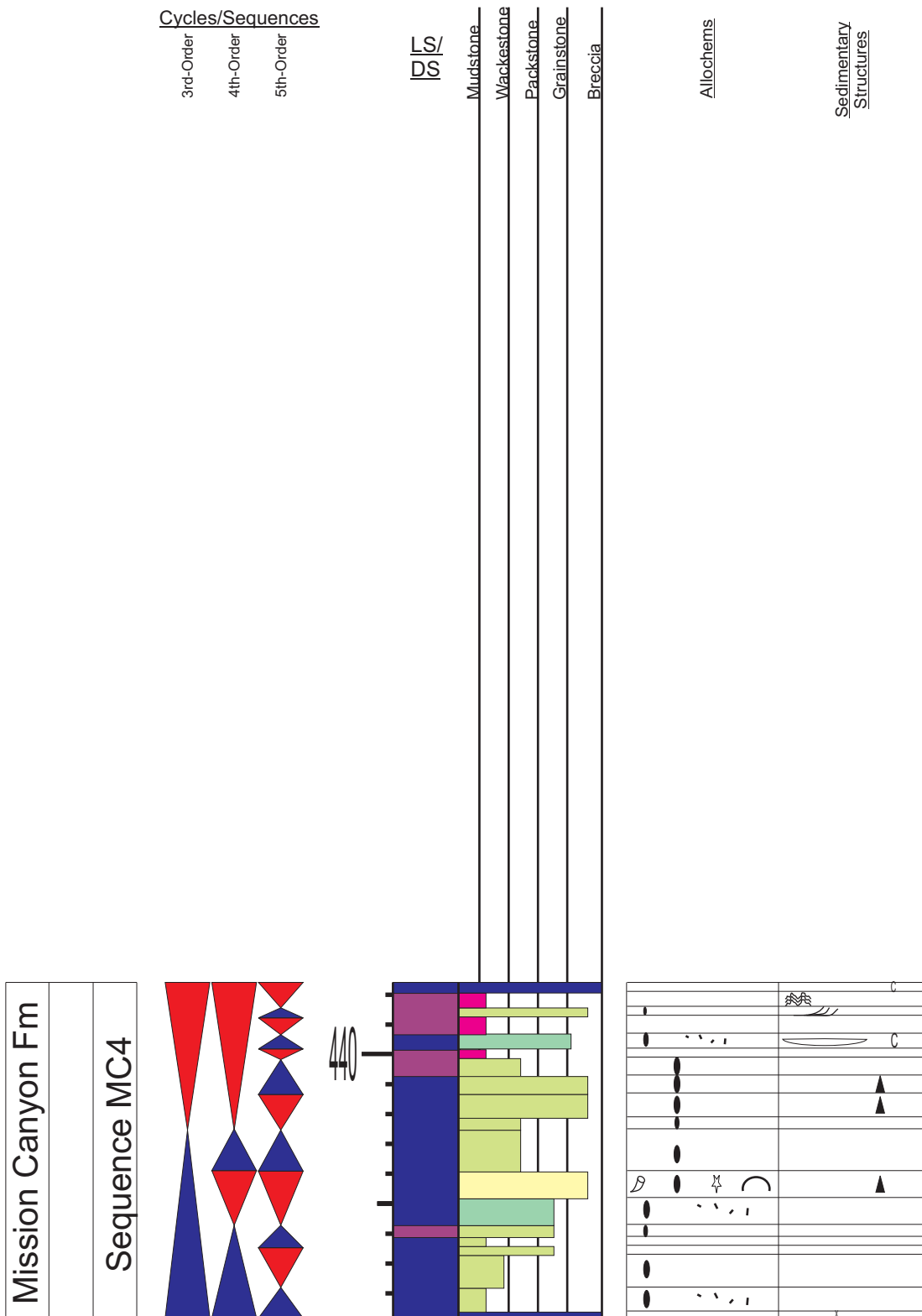
Appendix 3.10: Sedimentary section log for section Sacagawea Peak (Continued). Refer to Appendix 1 for symbols and Figure 3.6 for location.

APPENDIX 3.11



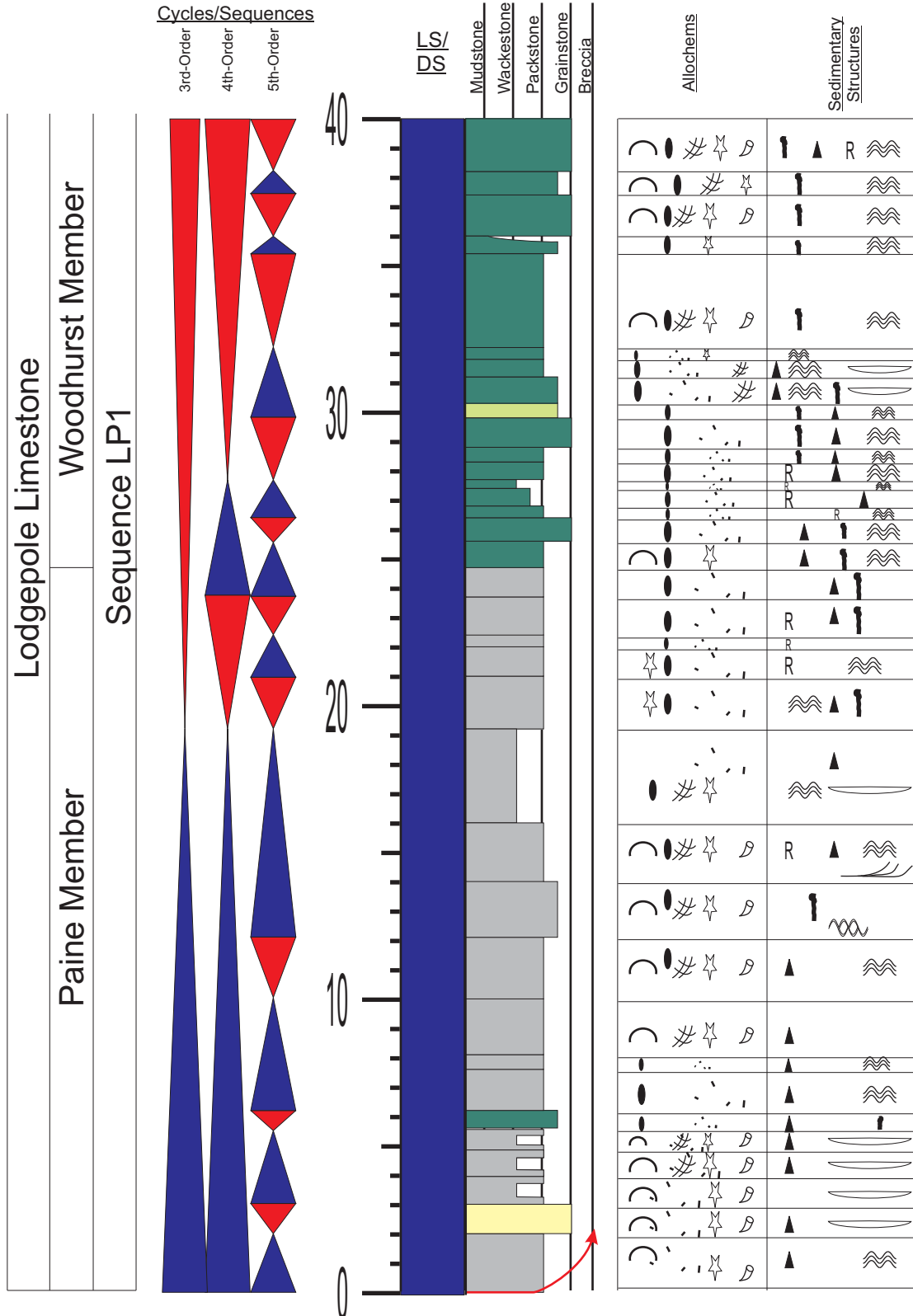
Appendix 3.11: Sedimentary section log for section Sacagawea Peak (Continued). Refer to Appendix 1 for symbols and Figure 3.6 for location.

APPENDIX 3.12



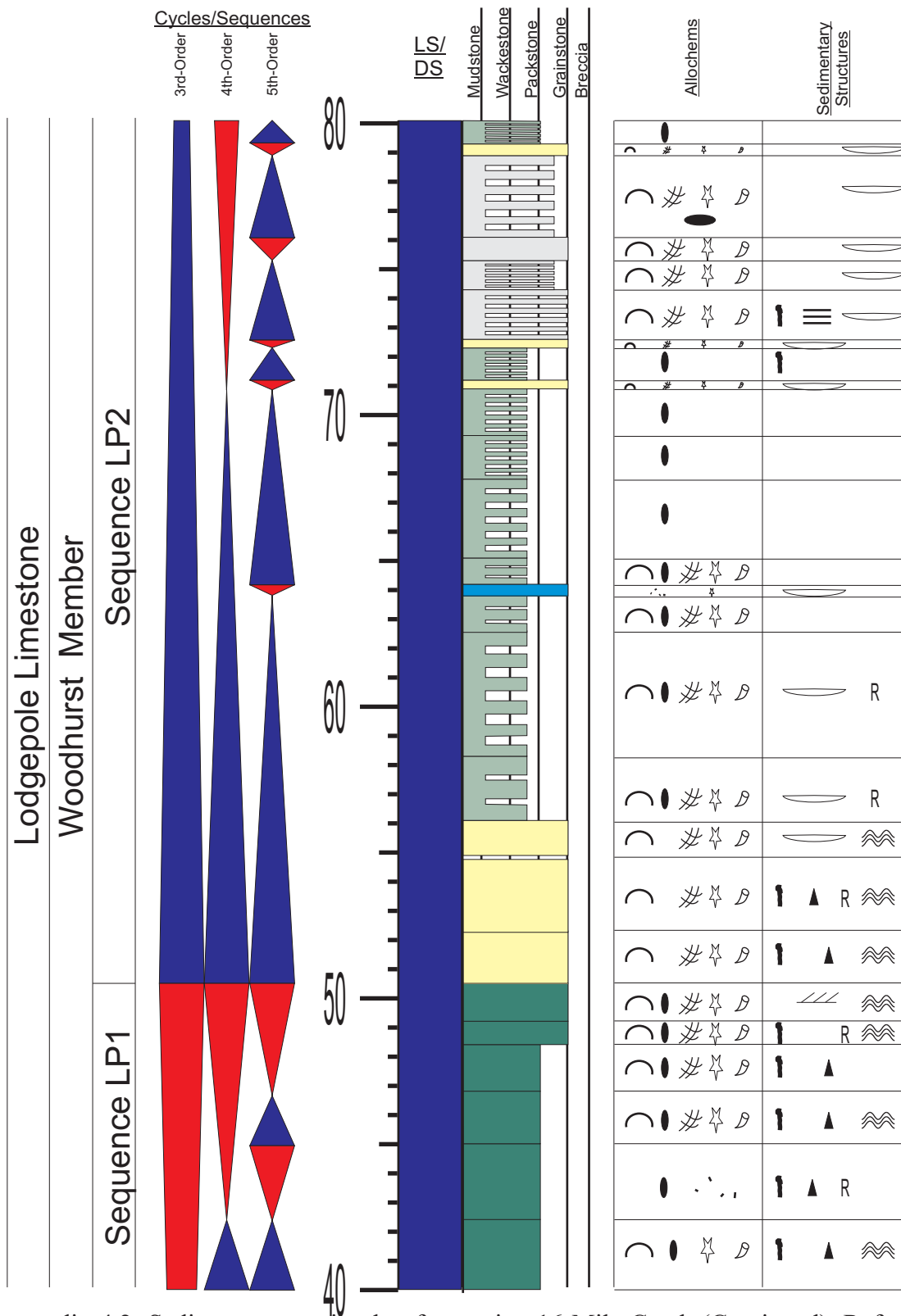
Appendix 3.12: Sedimentary section log for section Sacagawea Peak (Continued). Refer to Appendix 1 for symbols and Figure 3.6 for location.

APPENDIX 4.1



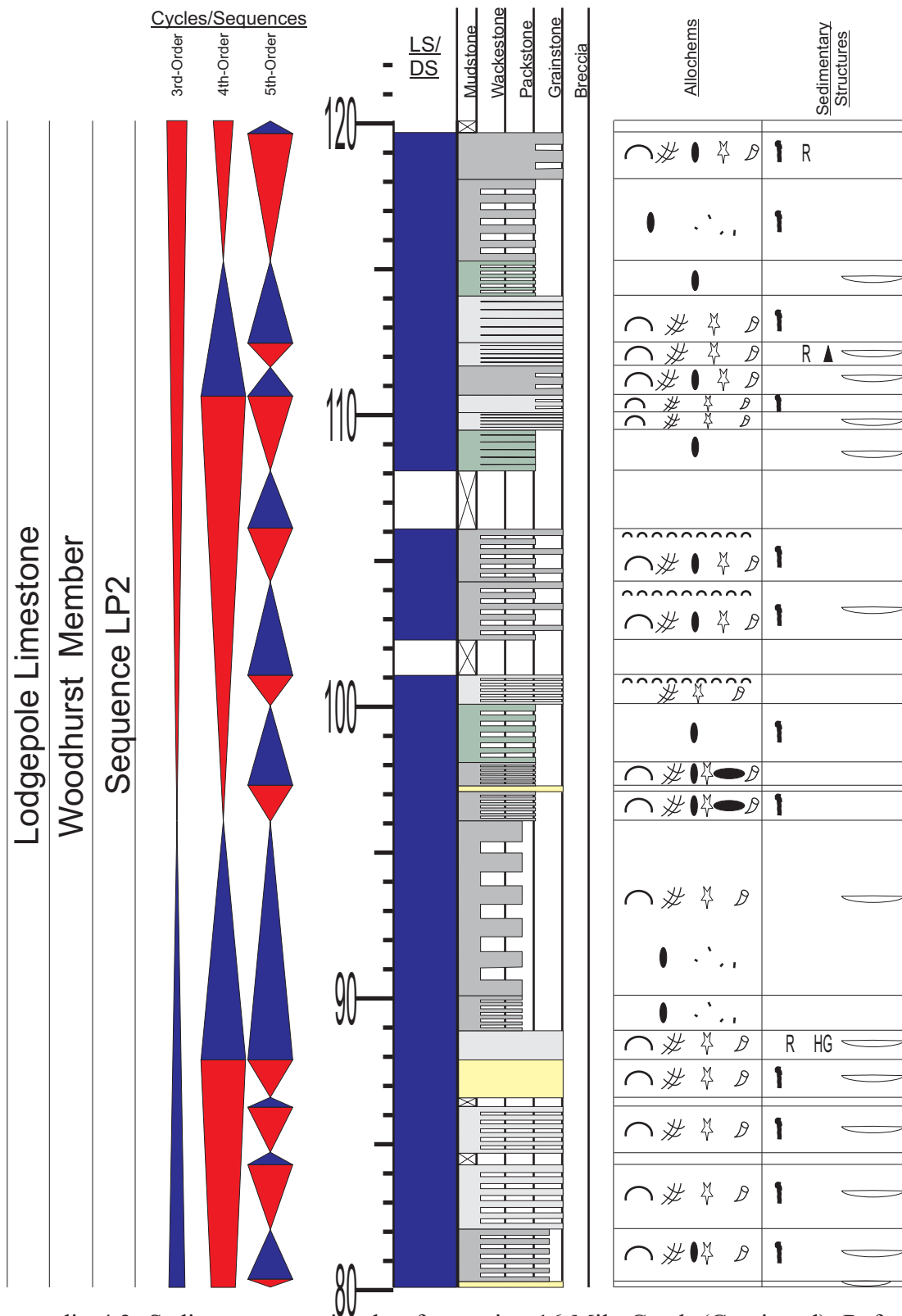
Appendix 4.1: Sedimentary section log for section 16 Mile Creek. Refer to Appendix 1 for symbols and Figure 3.6 for location.

APPENDIX 4.2



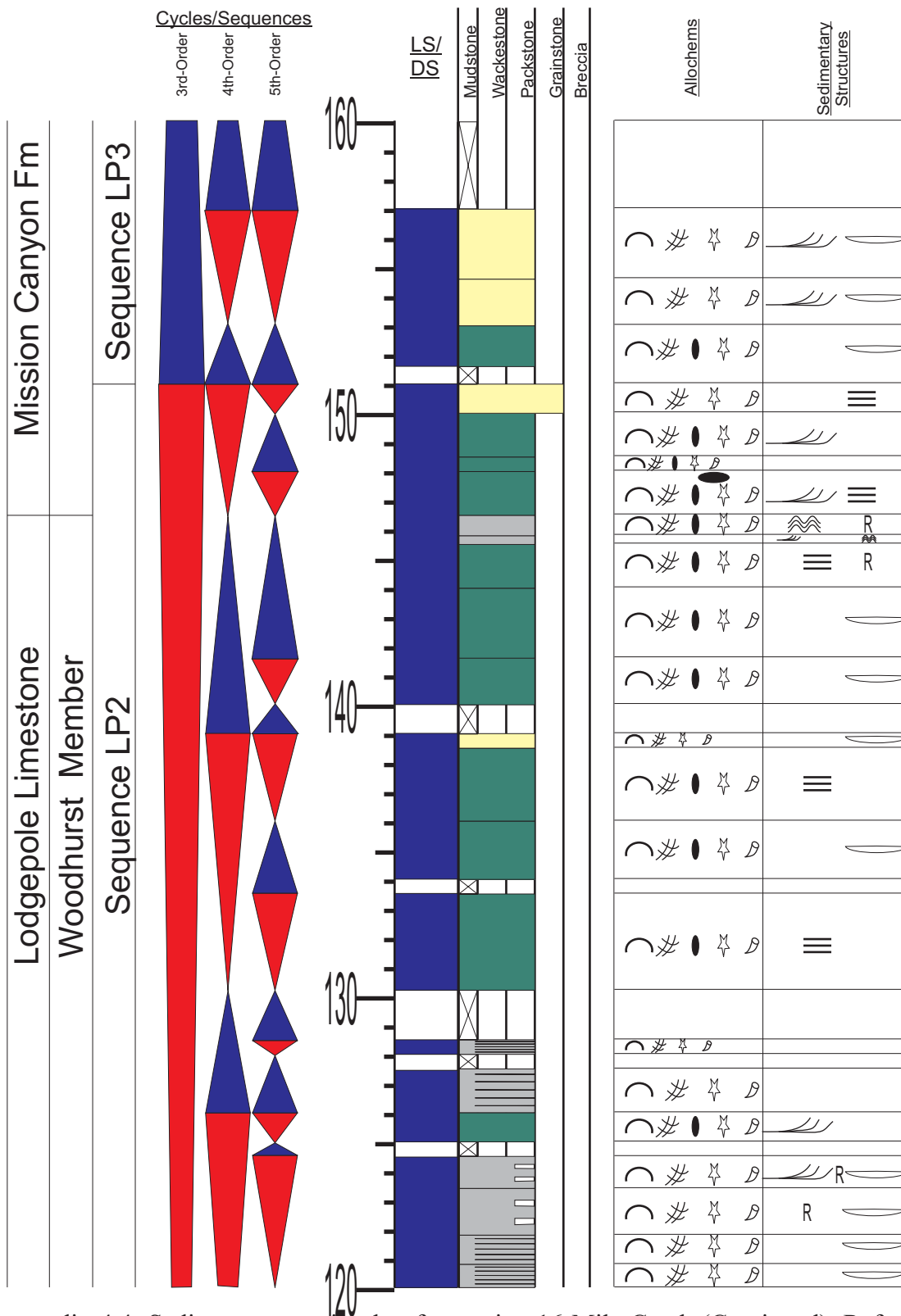
Appendix 4.2: Sedimentary section log for section 16 Mile Creek (Continued). Refer to Appendix 1 for symbols and Figure 3.6 for location.

APPENDIX 4.3



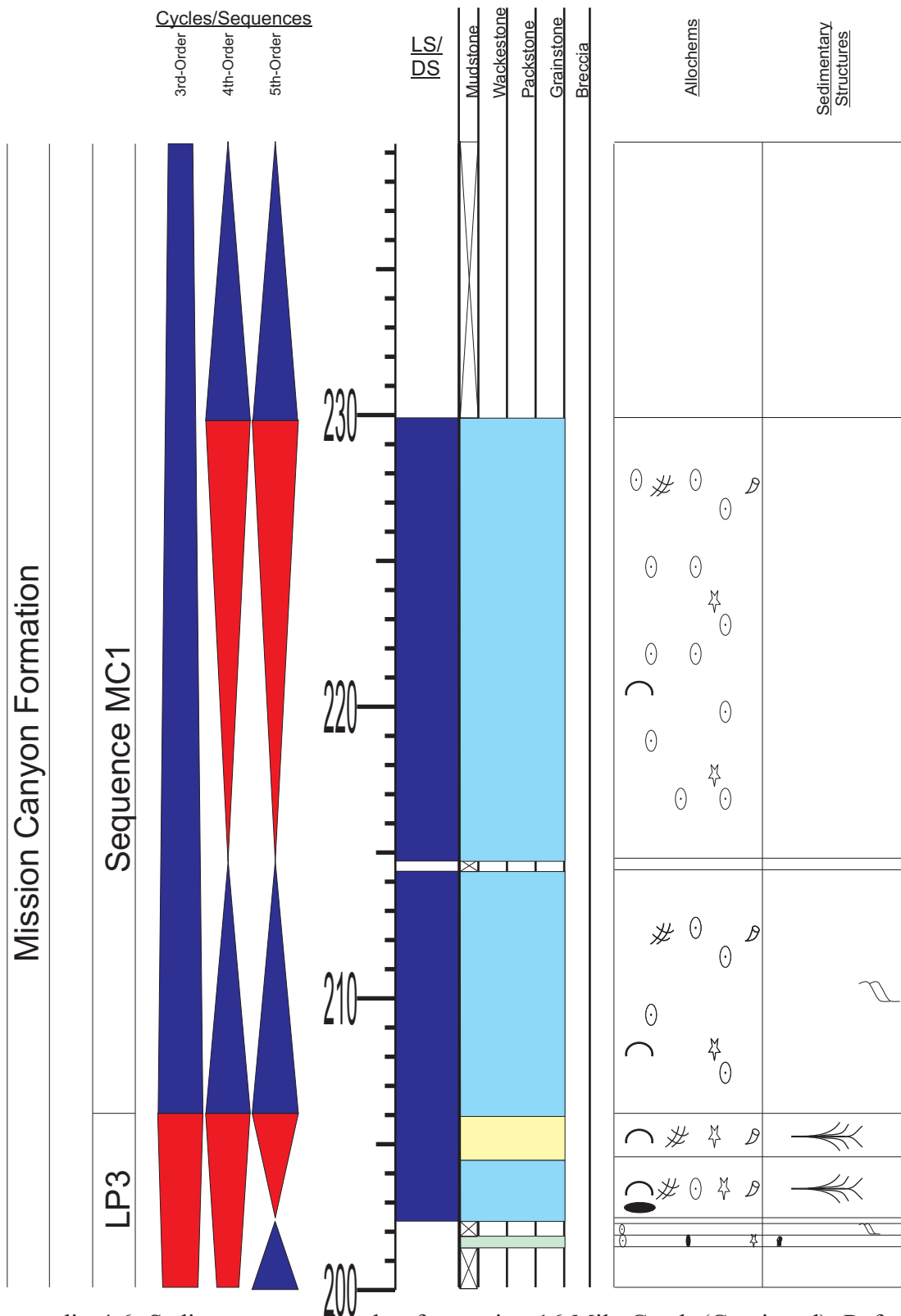
Appendix 4.3: Sedimentary section log for section 16 Mile Creek (Continued). Refer to Appendix 1 for symbols and Figure 3.6 for location.

APPENDIX 4.4



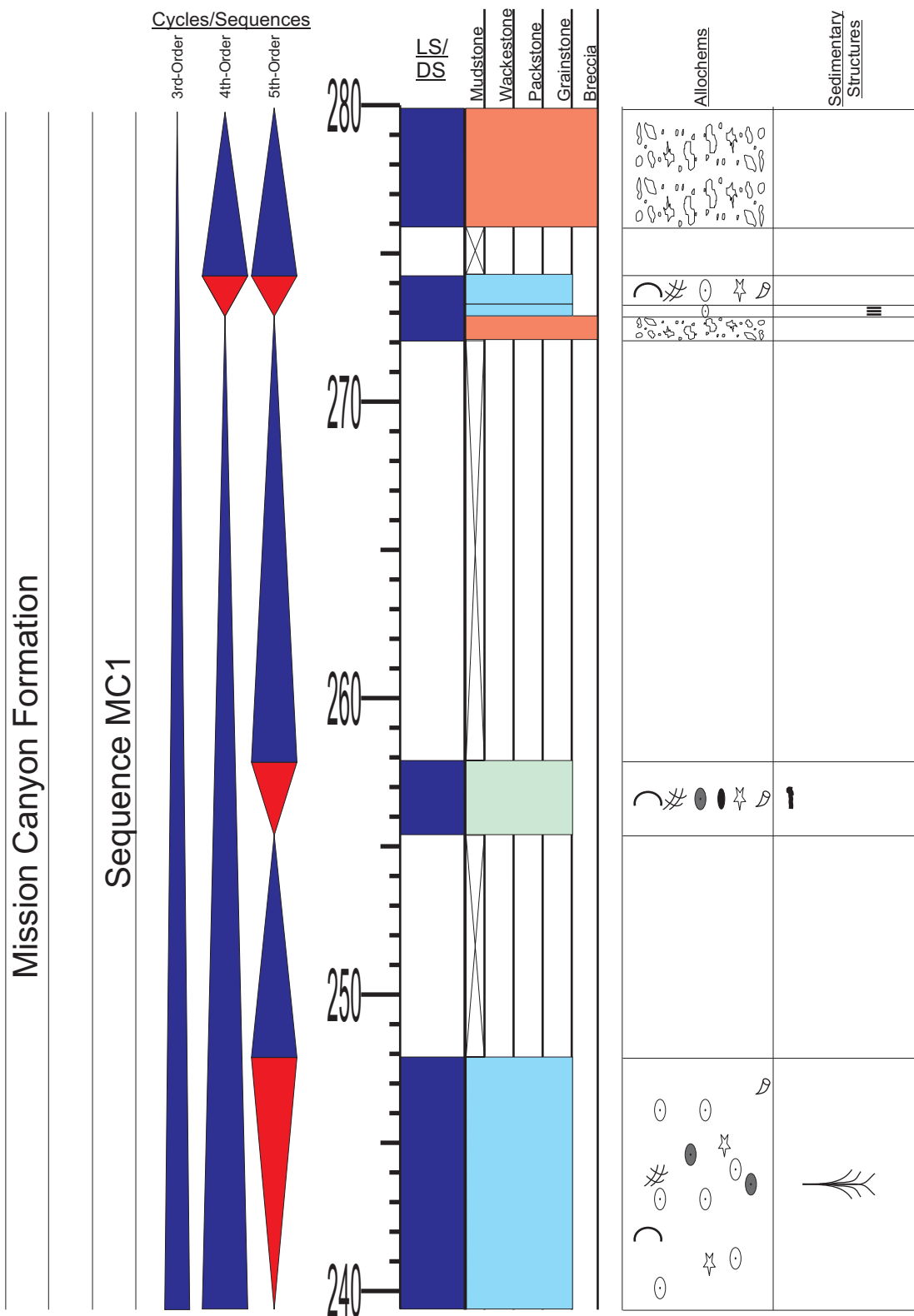
Appendix 4.4: Sedimentary section log for section 16 Mile Creek (Continued). Refer to Appendix 1 for symbols and Figure 3.6 for location.

APPENDIX 4.6



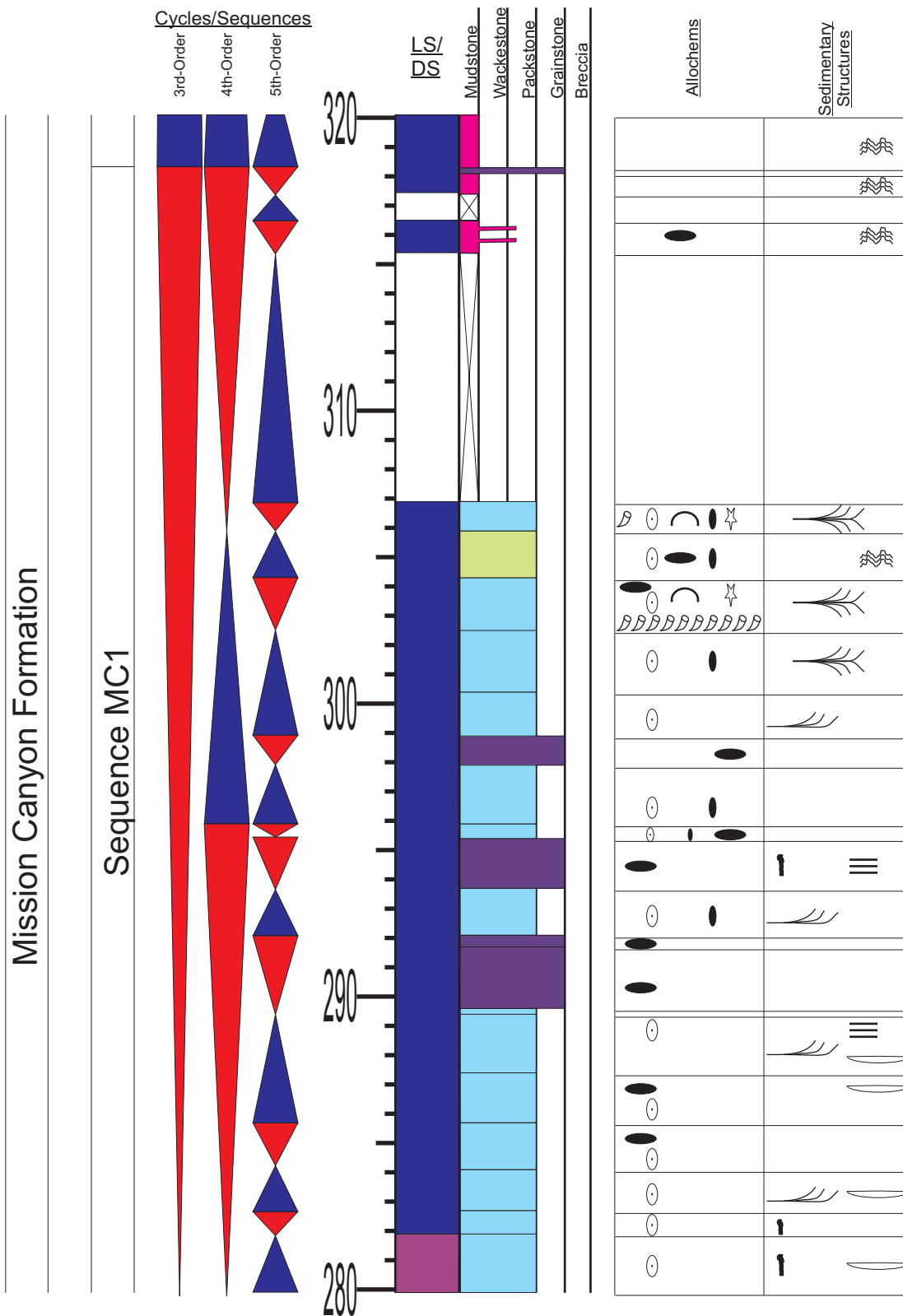
Appendix 4.6: Sedimentary section log for section 16 Mile Creek (Continued). Refer to Appendix 1 for symbols and Figure 3.6 for location.

APPENDIX 4.7



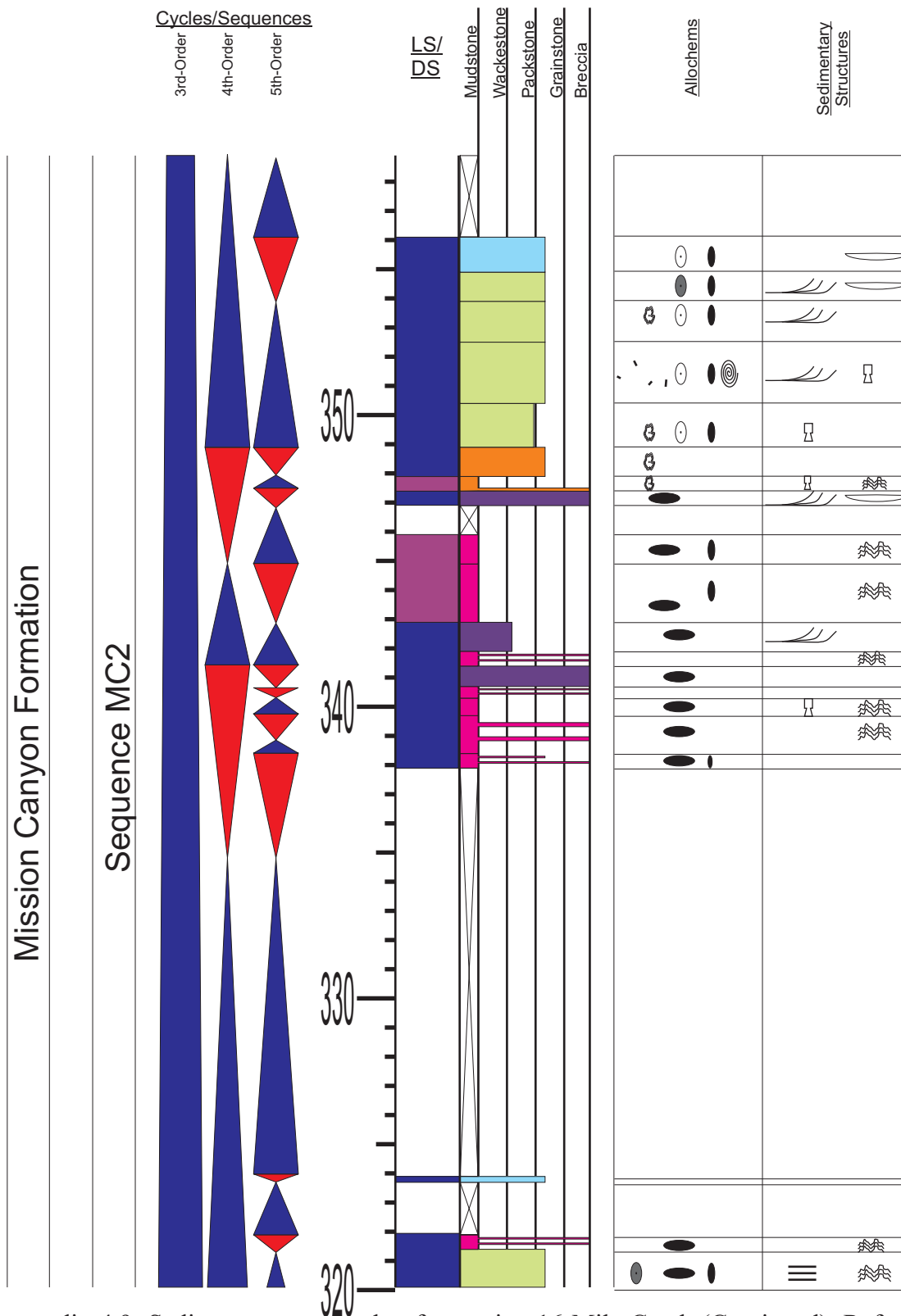
Appendix 4.7: Sedimentary section log for section 16 Mile Creek (Continued). Refer to Appendix 1 for symbols and Figure 3.6 for location.

APPENDIX 4.8



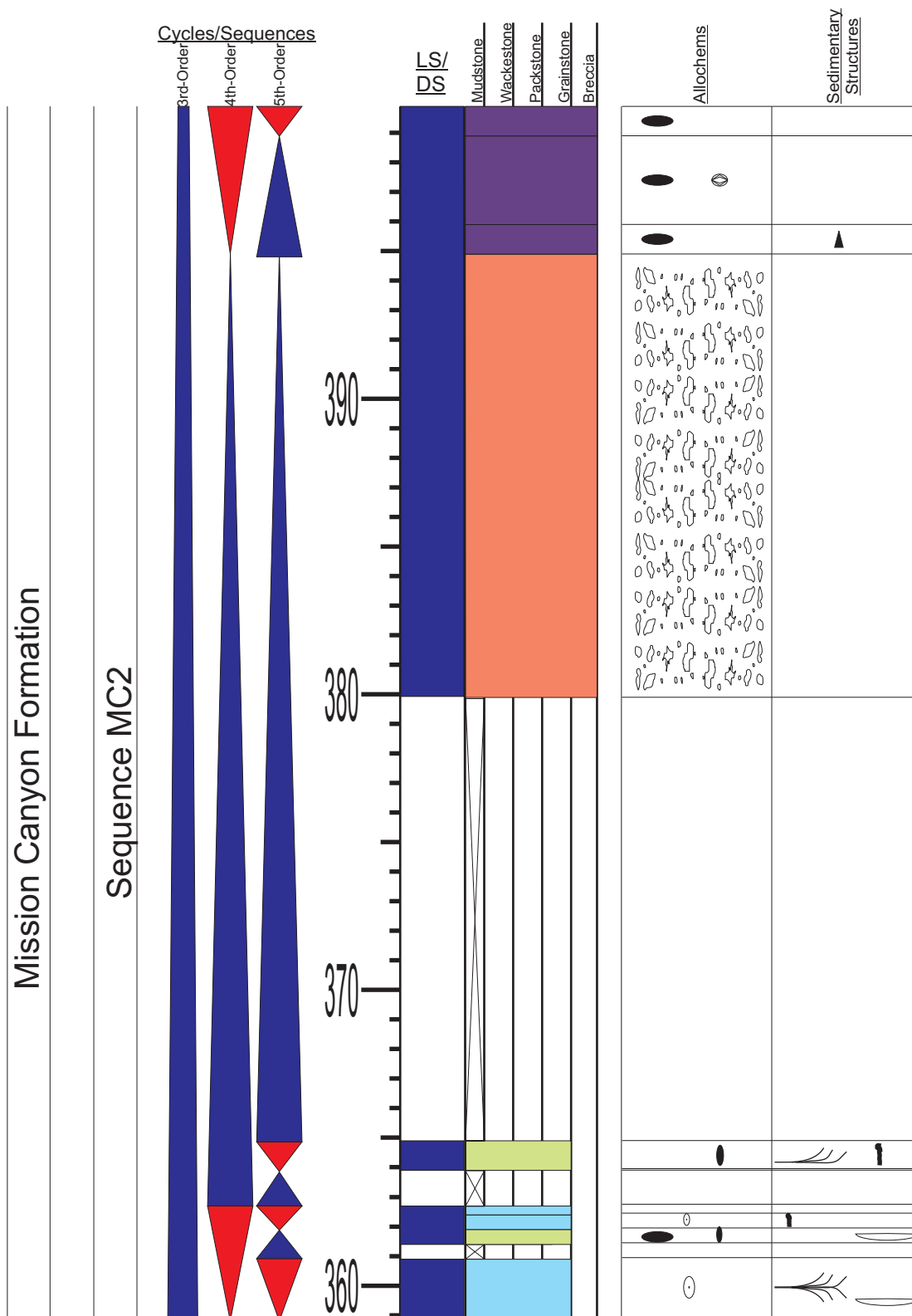
Appendix 4.8: Sedimentary section log for section 16 Mile Creek (Continued). Refer to Appendix 1 for symbols and Figure 3.6 for location.

APPENDIX 4.9



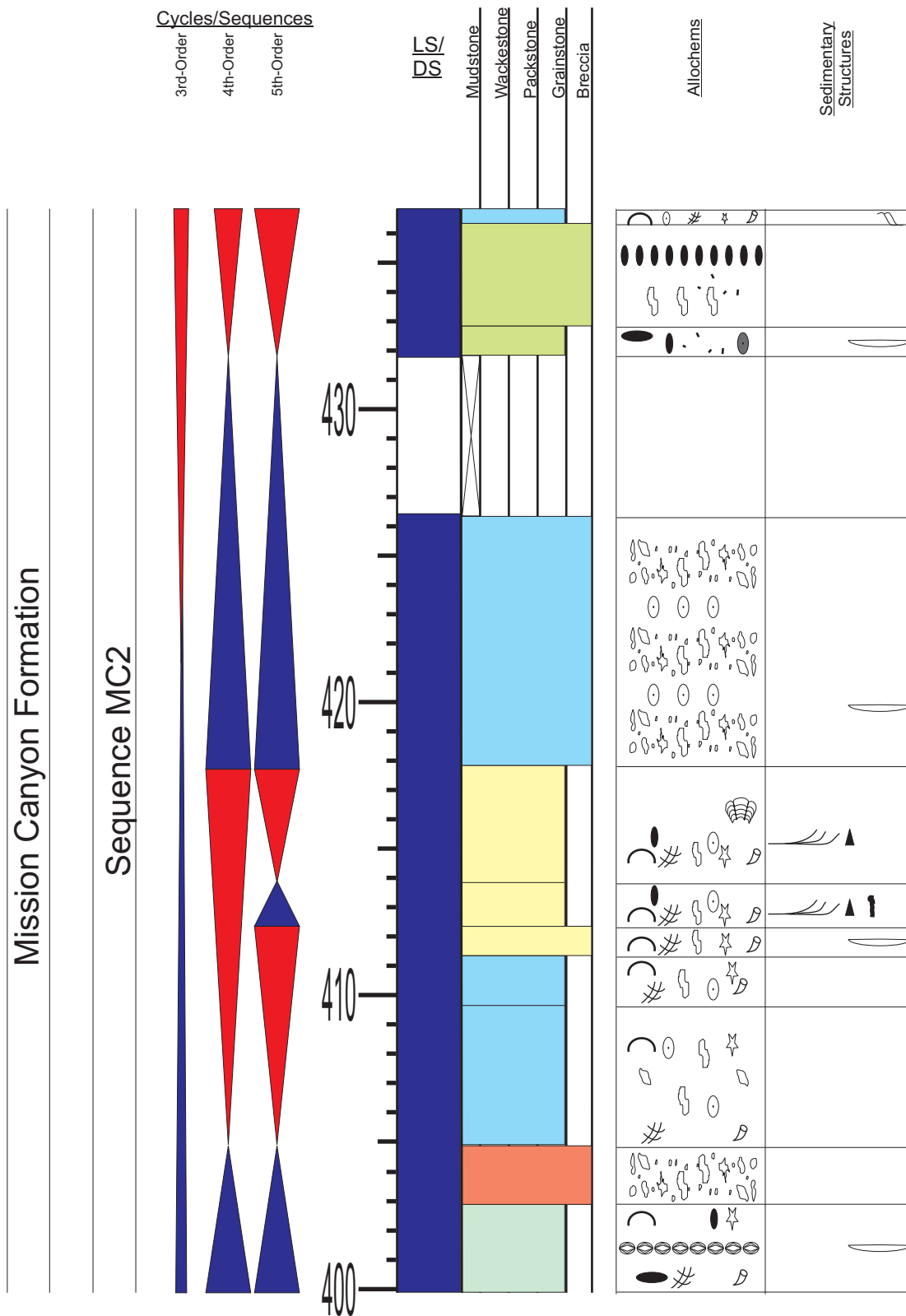
Appendix 4.9: Sedimentary section log for section 16 Mile Creek (Continued). Refer to Appendix 1 for symbols and Figure 3.6 for location.

APPENDIX 4.10



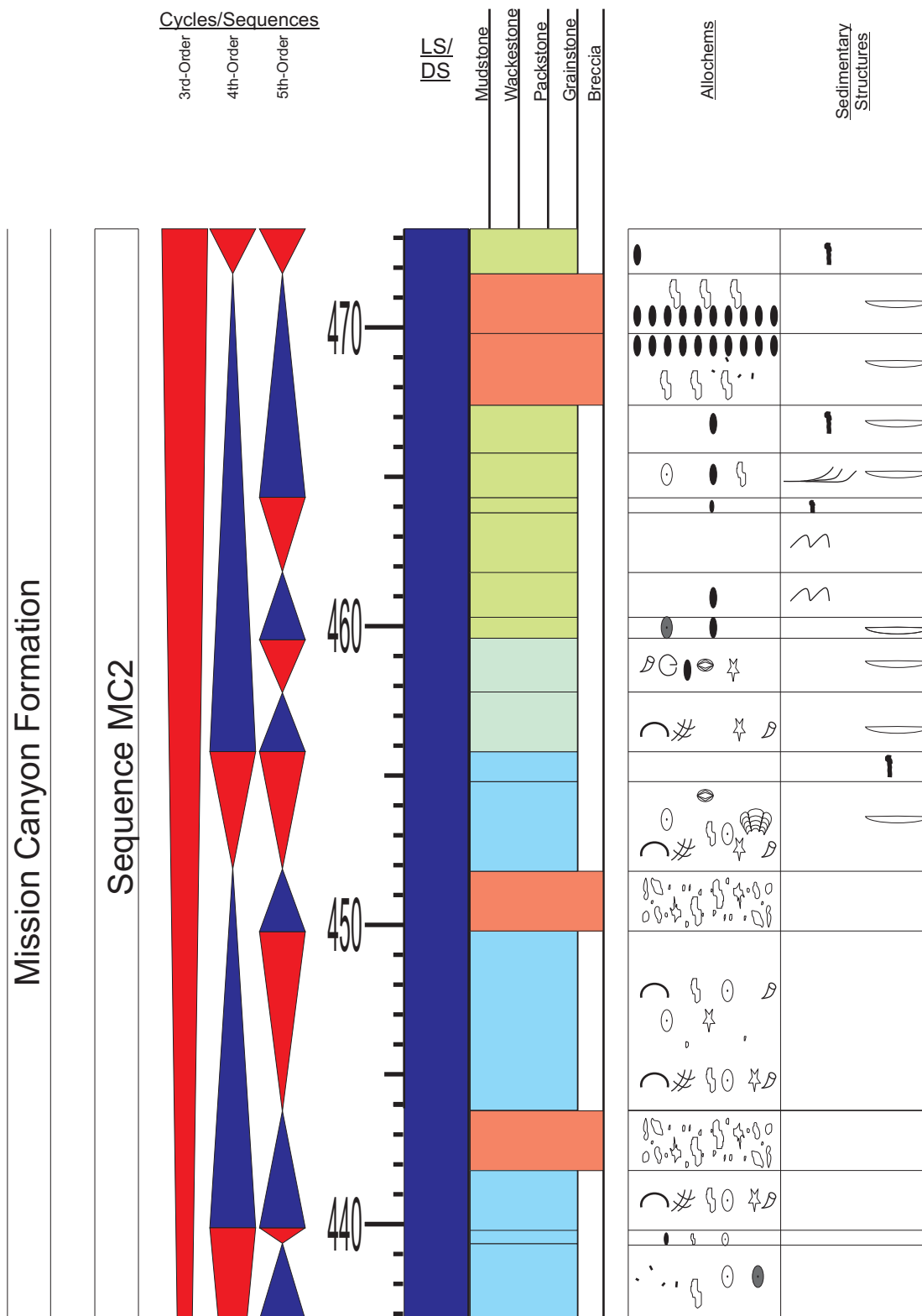
Appendix 4.10: Sedimentary section log for section 16 Mile Creek (Continued). Refer to Appendix 1 for symbols and Figure 3.6 for location.

APPENDIX 4.11



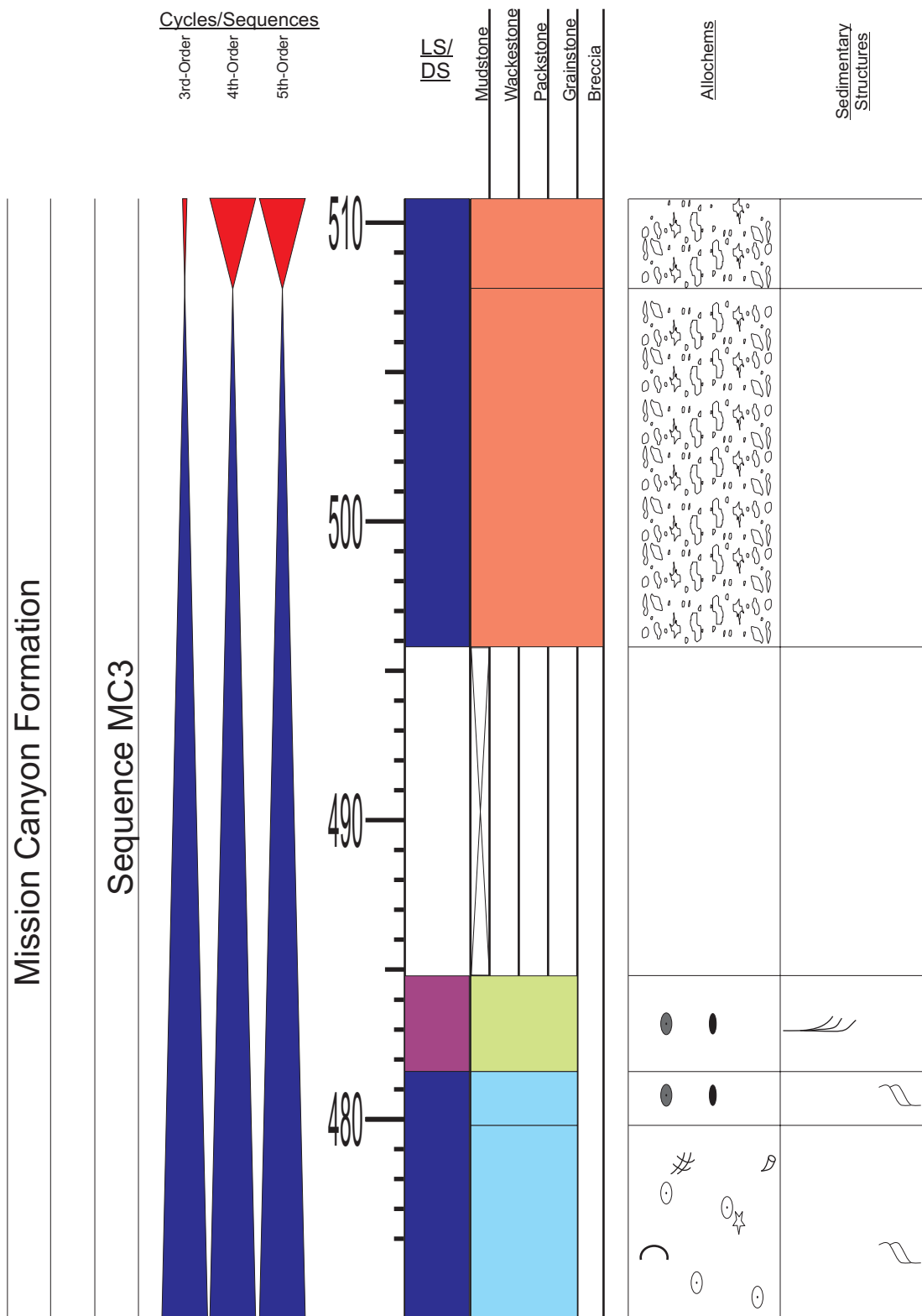
Appendix 4.11: Sedimentary section log for section 16 Mile Creek (Continued). Refer to Appendix 1 for symbols and Figure 3.6 for location.

APPENDIX 4.12



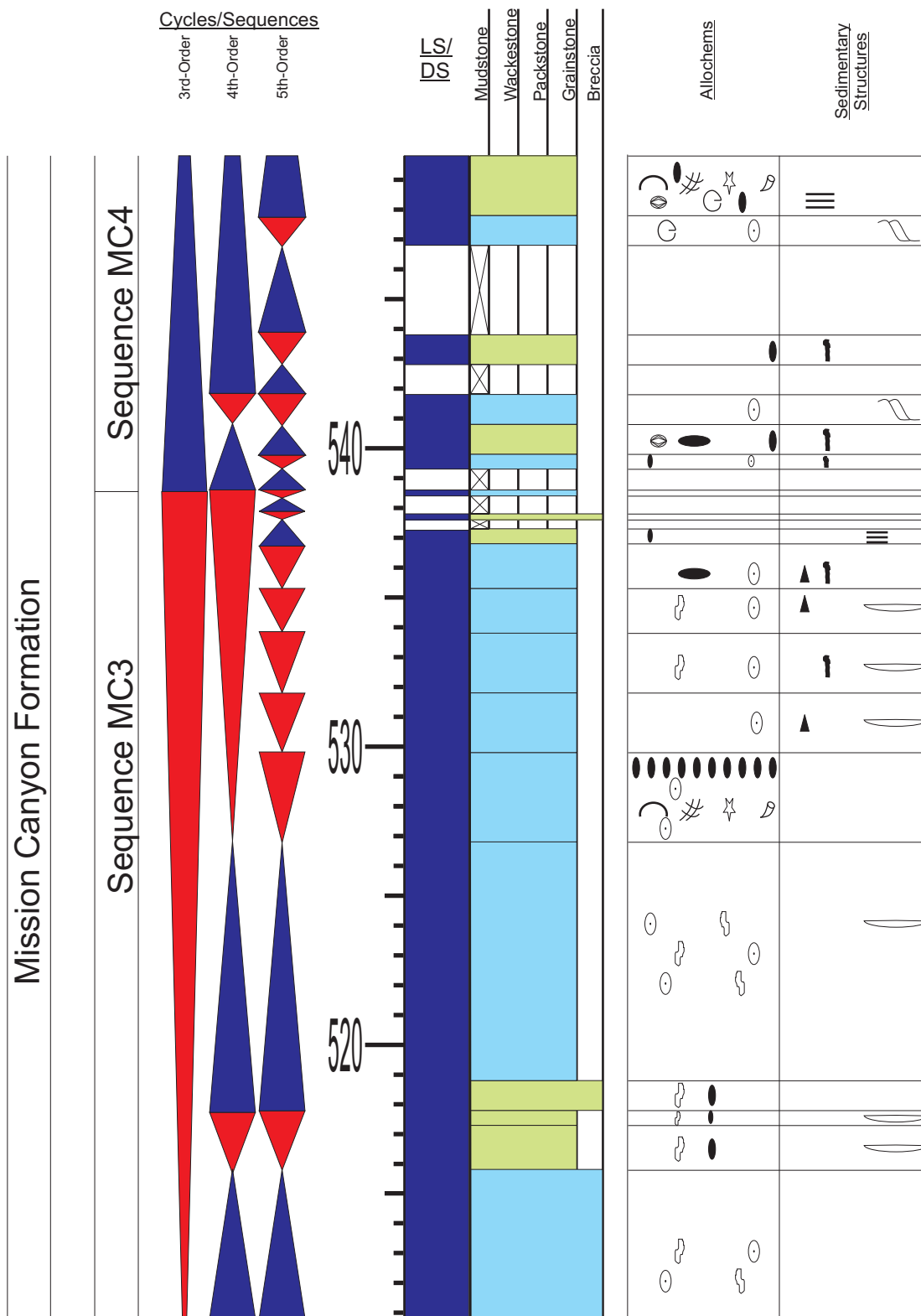
Appendix 4.12: Sedimentary section log for section 16 Mile Creek (Continued). Refer to Appendix 1 for symbols and Figure 3.6 for location.

APPENDIX 4.13



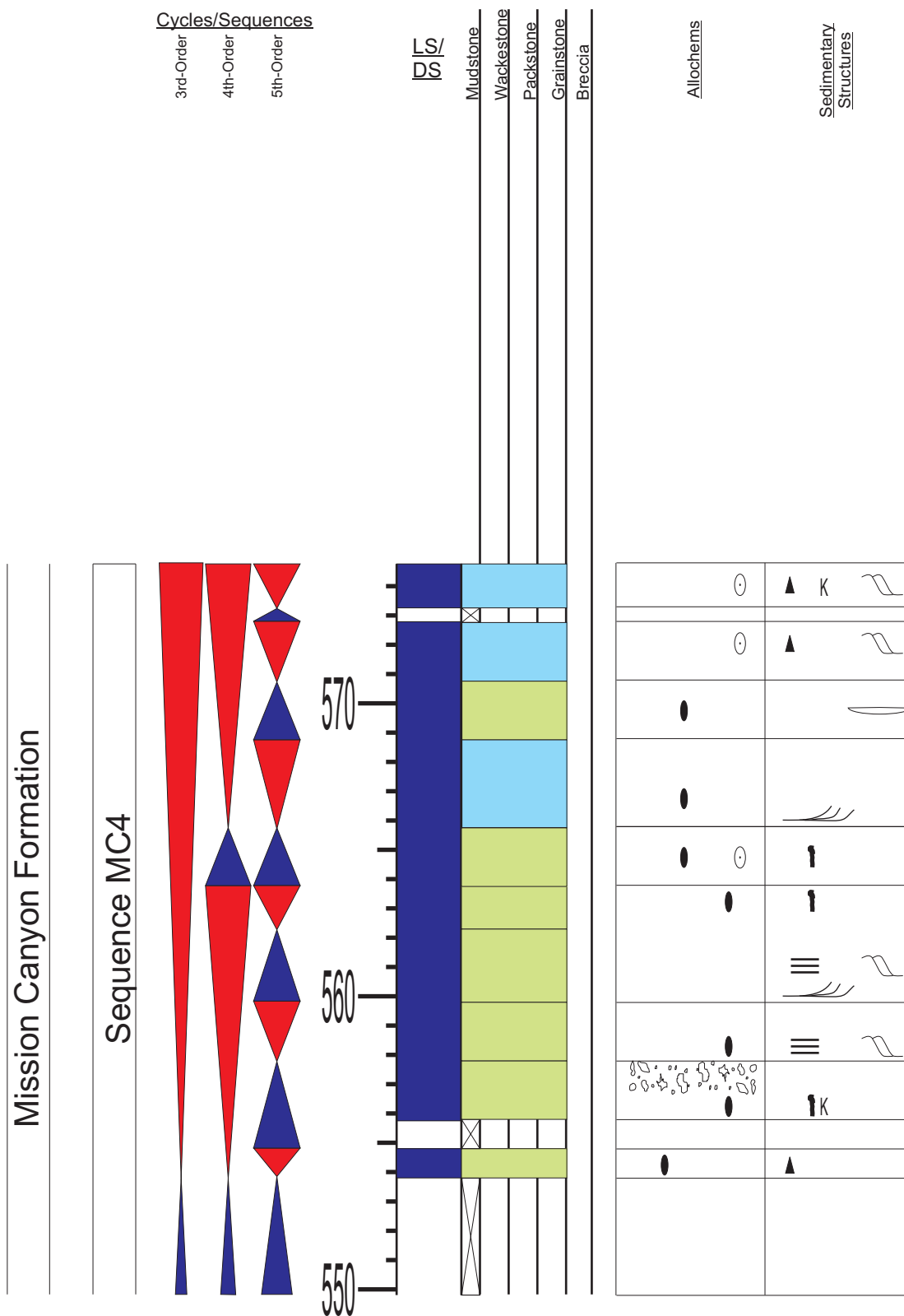
Appendix 4.13: Sedimentary section log for section 16 Mile Creek (Continued). Refer to Appendix 1 for symbols and Figure 3.6 for location.

APPENDIX 4.14



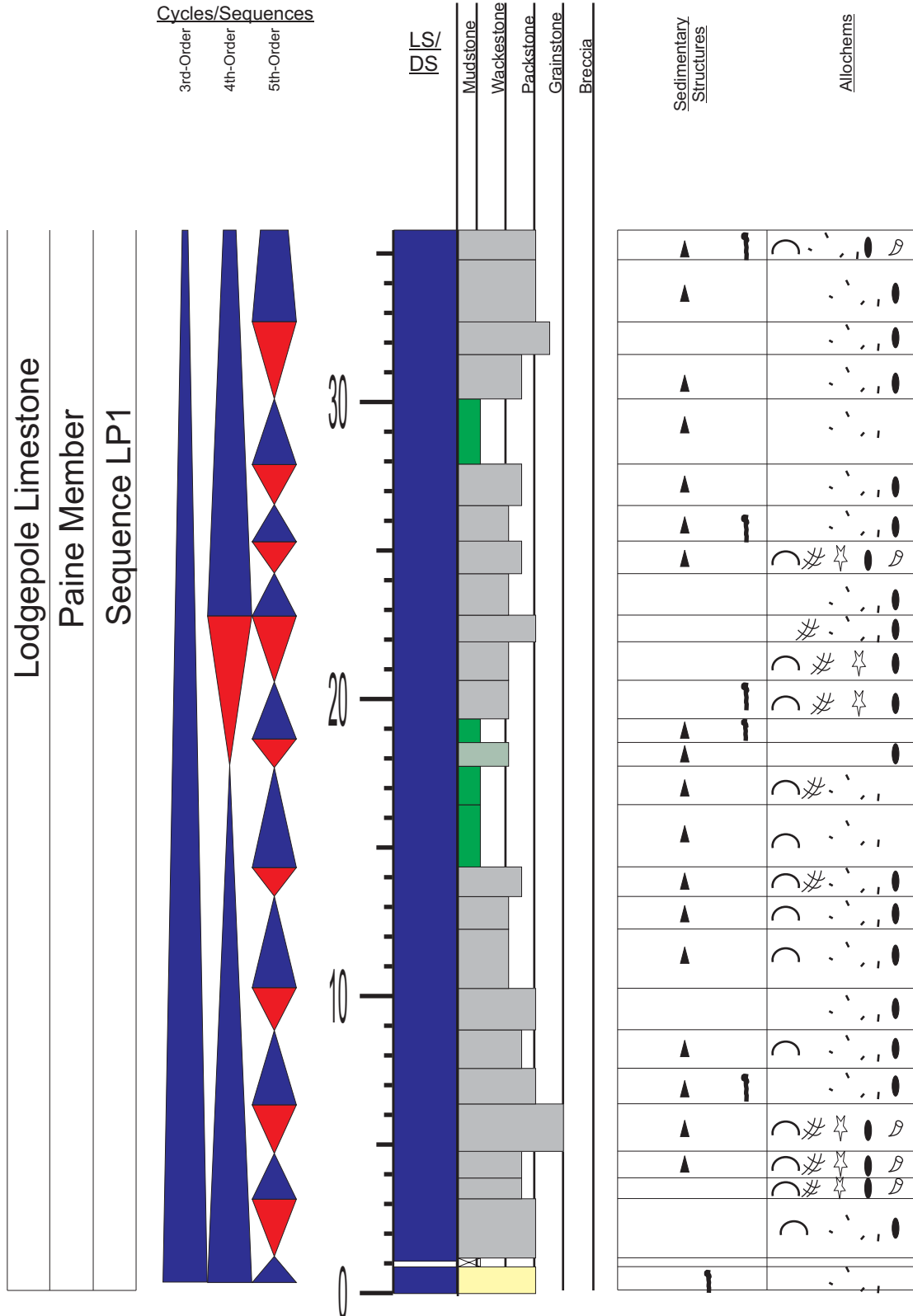
Appendix 4.14: Sedimentary section log for section 16 Mile Creek (Continued). Refer to Appendix 1 for symbols and Figure 3.6 for location.

APPENDIX 4.15



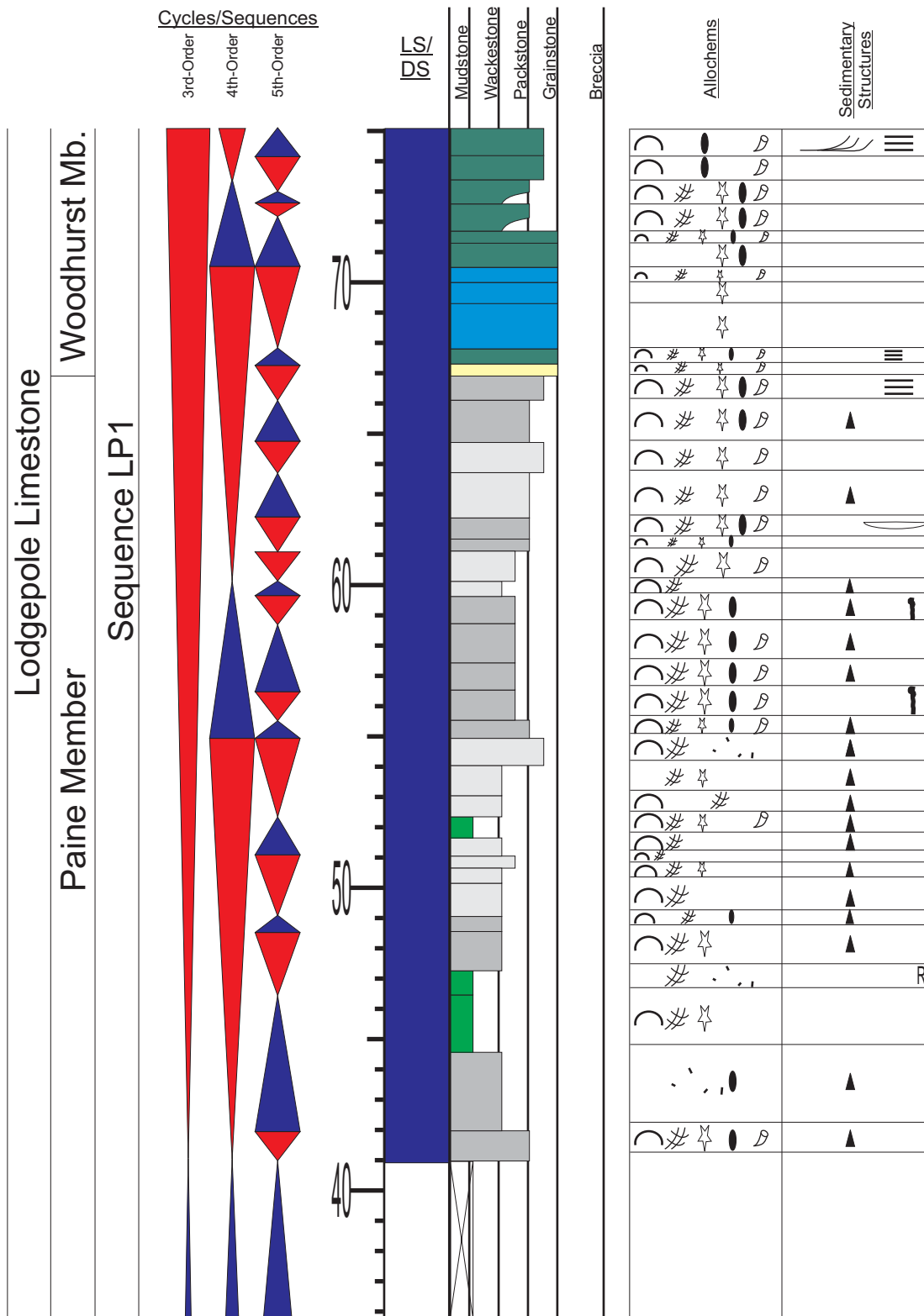
Appendix 4.15: Sedimentary section log for section 16 Mile Creek (Continued). Refer to Appendix 1 for symbols and Figure 3.6 for location.

APPENDIX 5.1



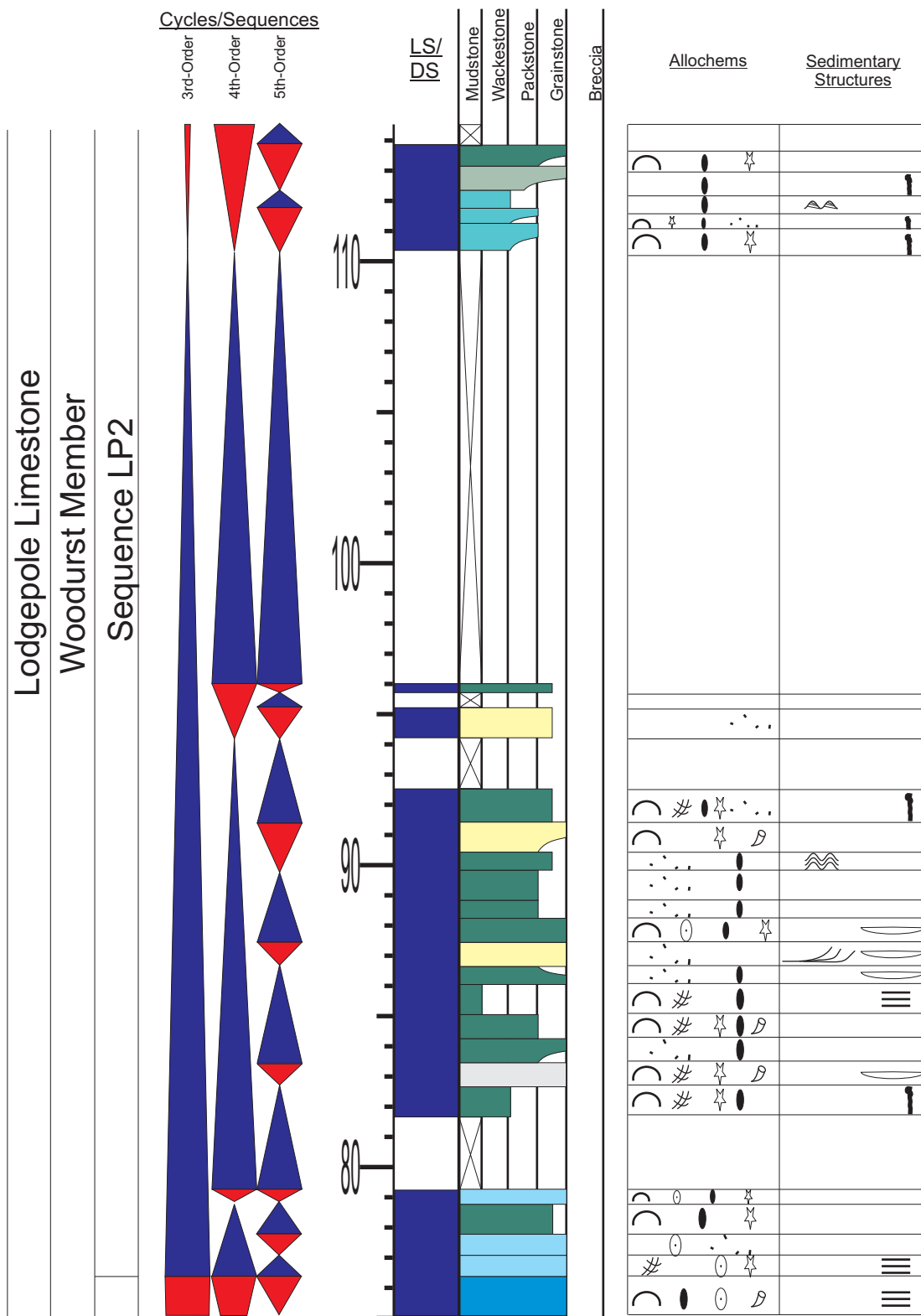
Appendix 5.1: Sedimentary section log for section Monarch. Refer to Appendix 1 for symbols and Figure 3.6 for location.

APPENDIX 5.2



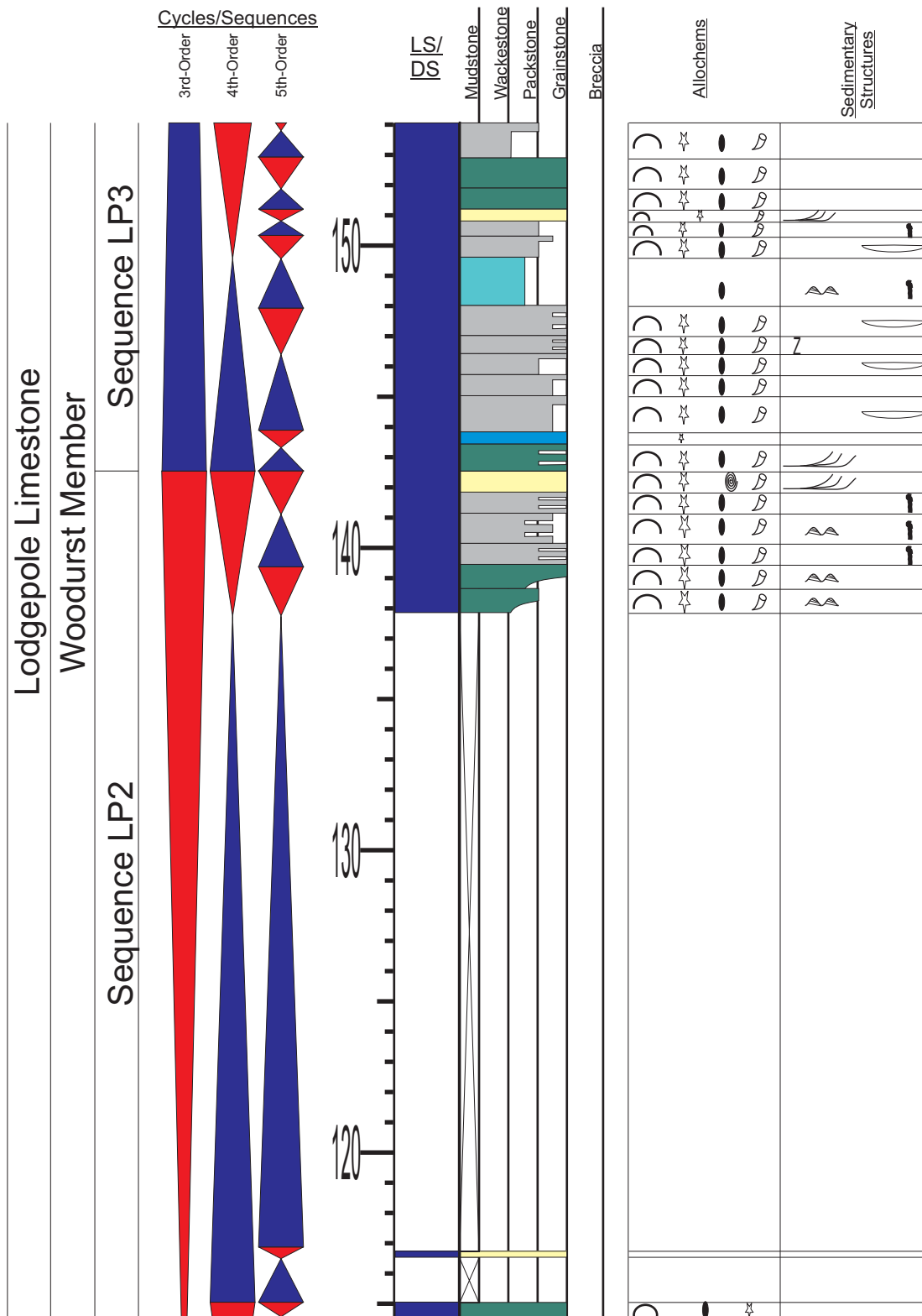
Appendix 5.2: Sedimentary section log for section Monarch (Continued). Refer to Appendix 1 for symbols and Figure 3.6 for location.

APPENDIX 5.3



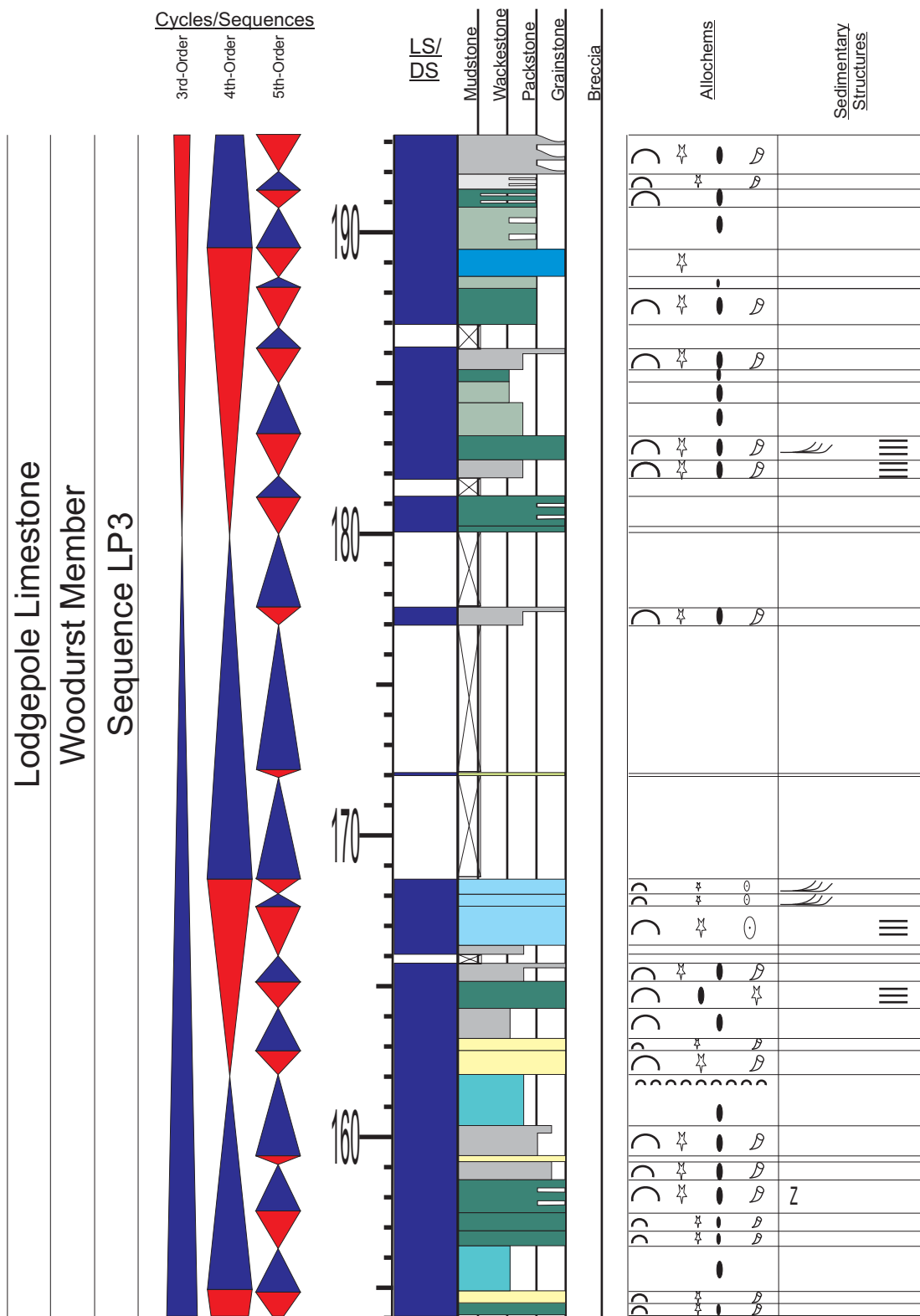
Appendix 5.3: Sedimentary section log for section Monarch (Continued). Refer to Appendix 1 for symbols and Figure 3.6 for location.

APPENDIX 5.4



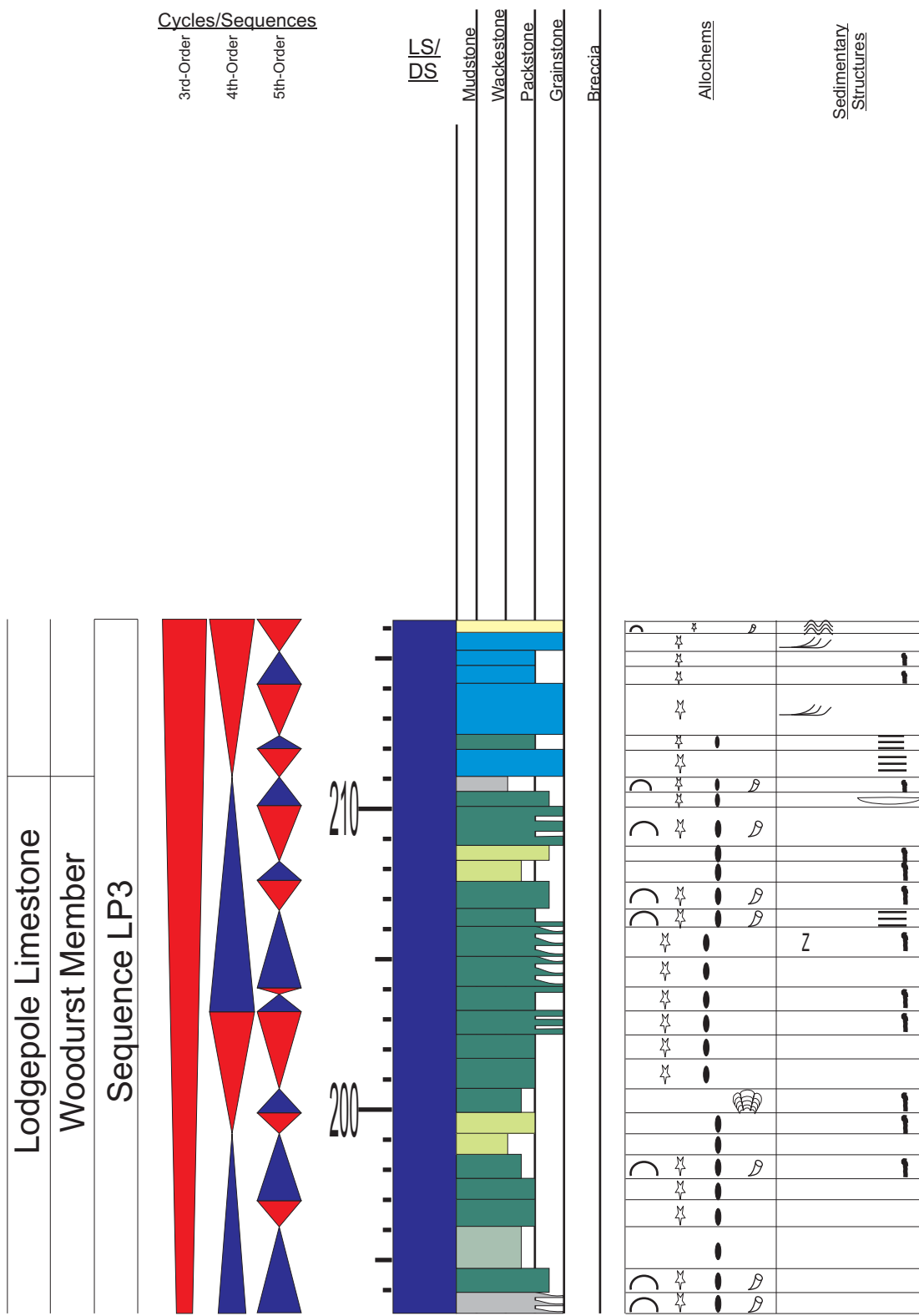
Appendix 5.4: Sedimentary section log for section Monarch (Continued). Refer to Appendix 1 for symbols and Figure 3.6 for location.

APPENDIX 5.5



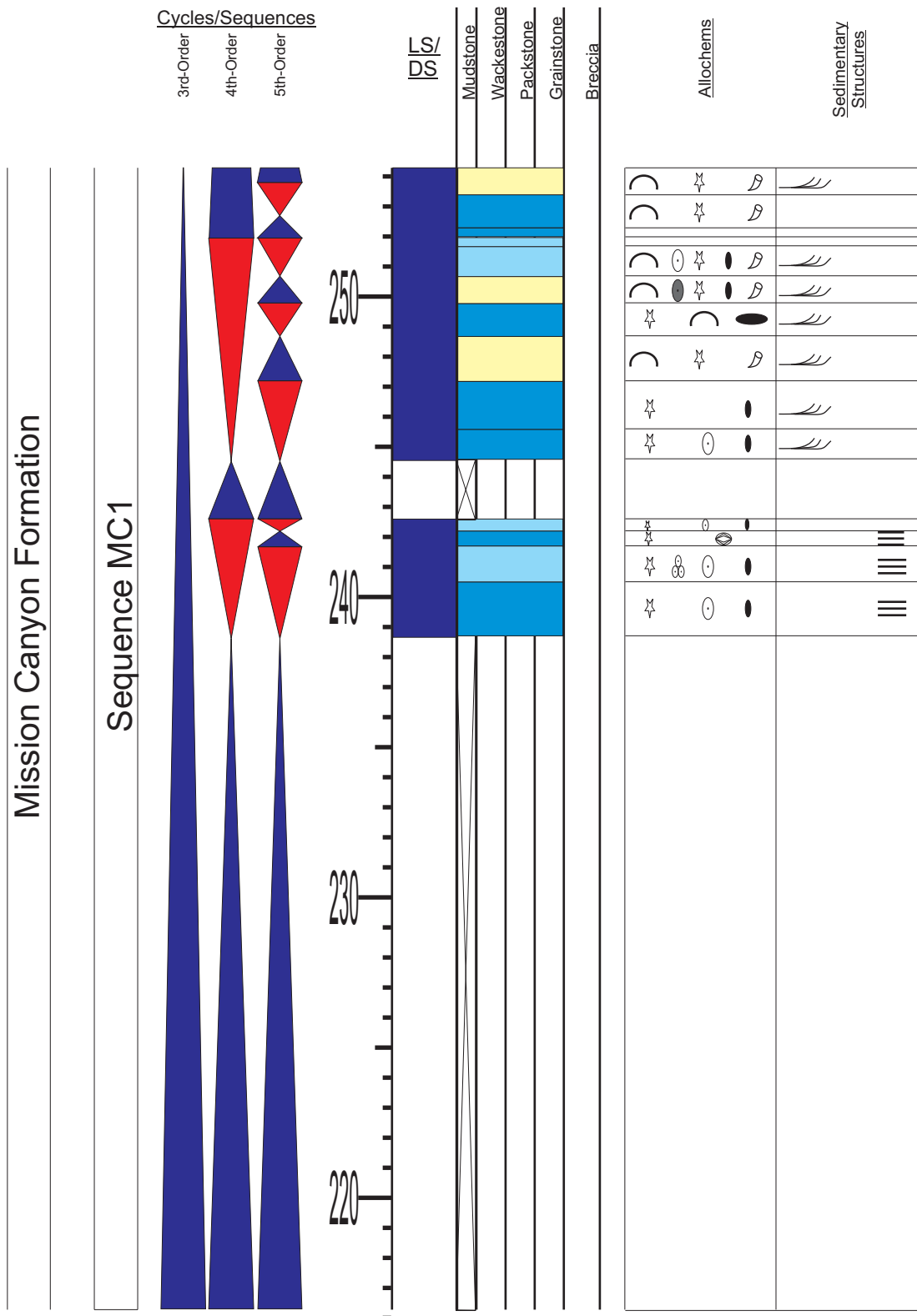
Appendix 5.5: Sedimentary section log for section Monarch (Continued). Refer to Appendix 1 for symbols and Figure 3.6 for location.

APPENDIX 5.6



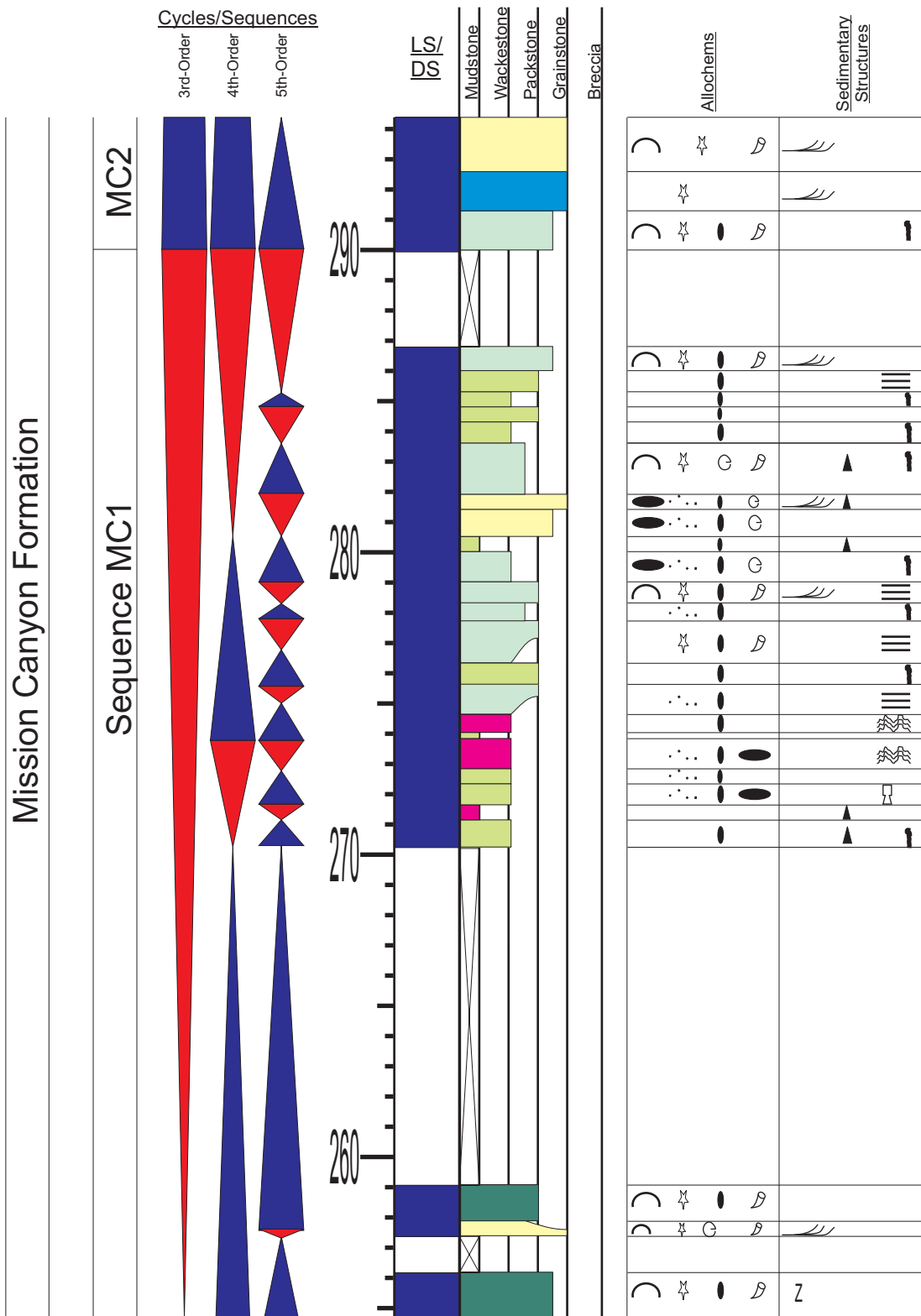
Appendix 5.6: Sedimentary section log for section Monarch (Continued). Refer to Appendix 1 for symbols and Figure 3.6 for location.

APPENDIX 5.7



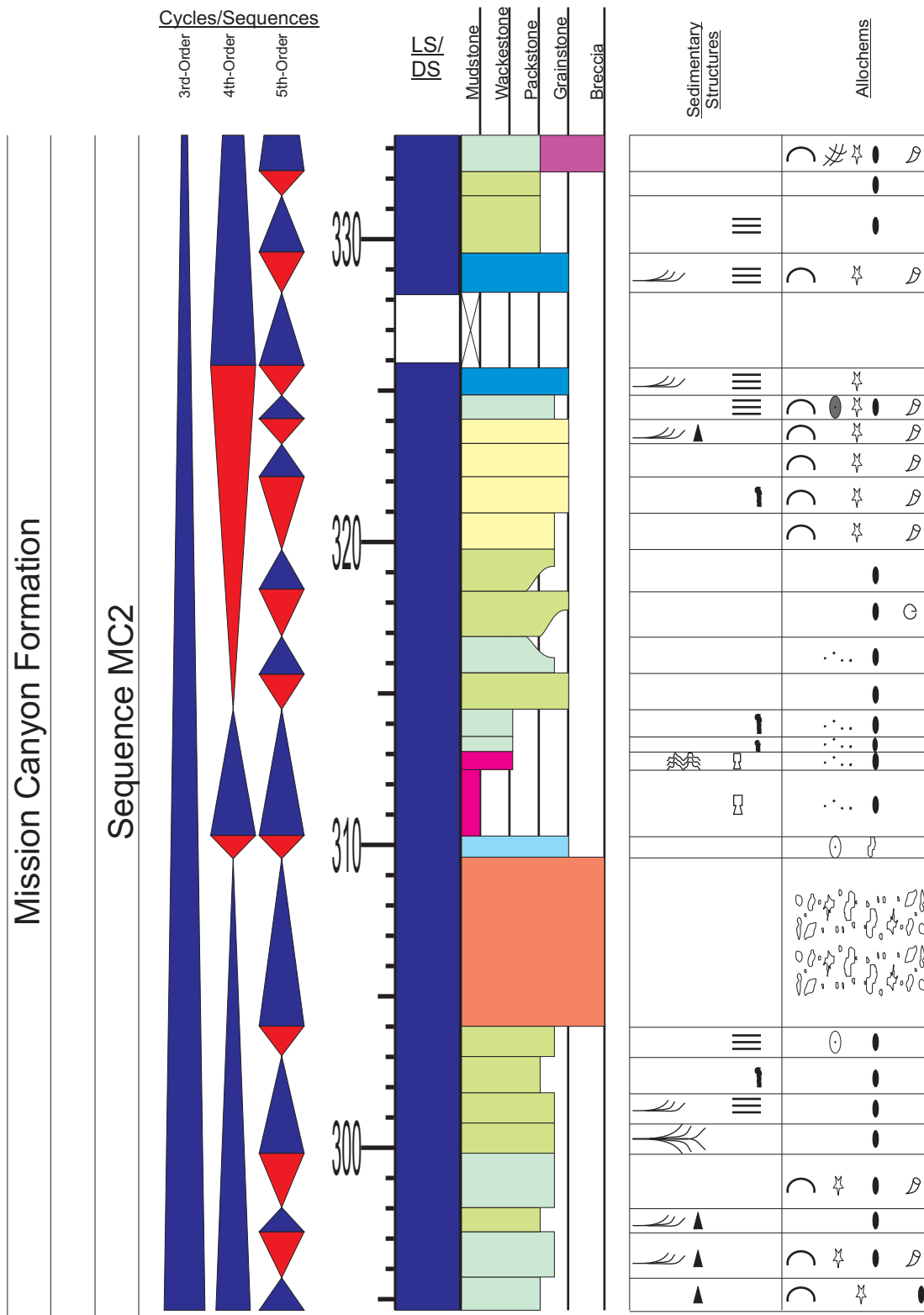
Appendix 5.7: Sedimentary section log for section Monarch (Continued). Refer to Appendix 1 for symbols and Figure 3.6 for location.

APPENDIX 5.8



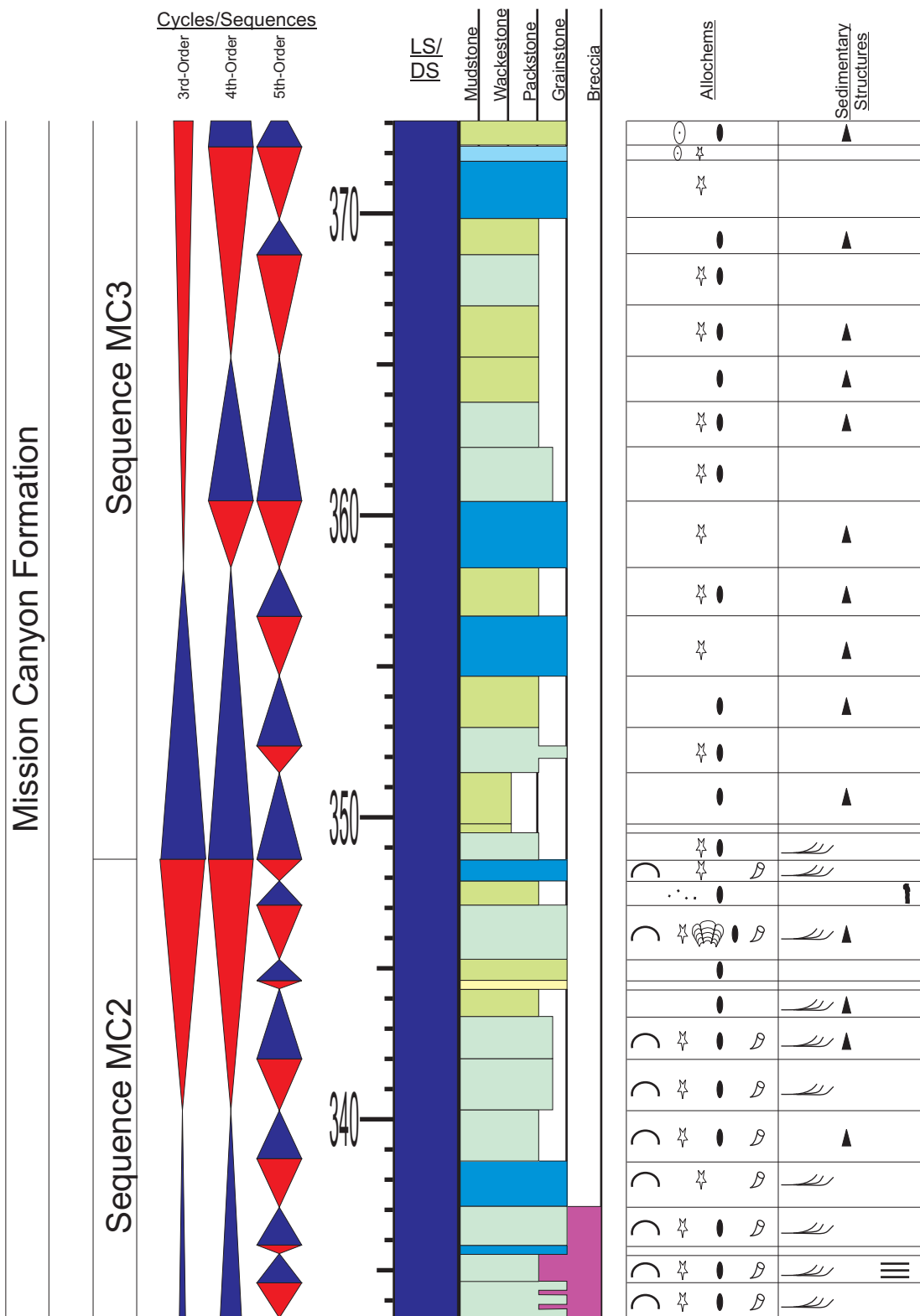
Appendix 5.8: Sedimentary section log for section Monarch (Continued). Refer to Appendix 1 for symbols and Figure 3.6 for location.

APPENDIX 5.9



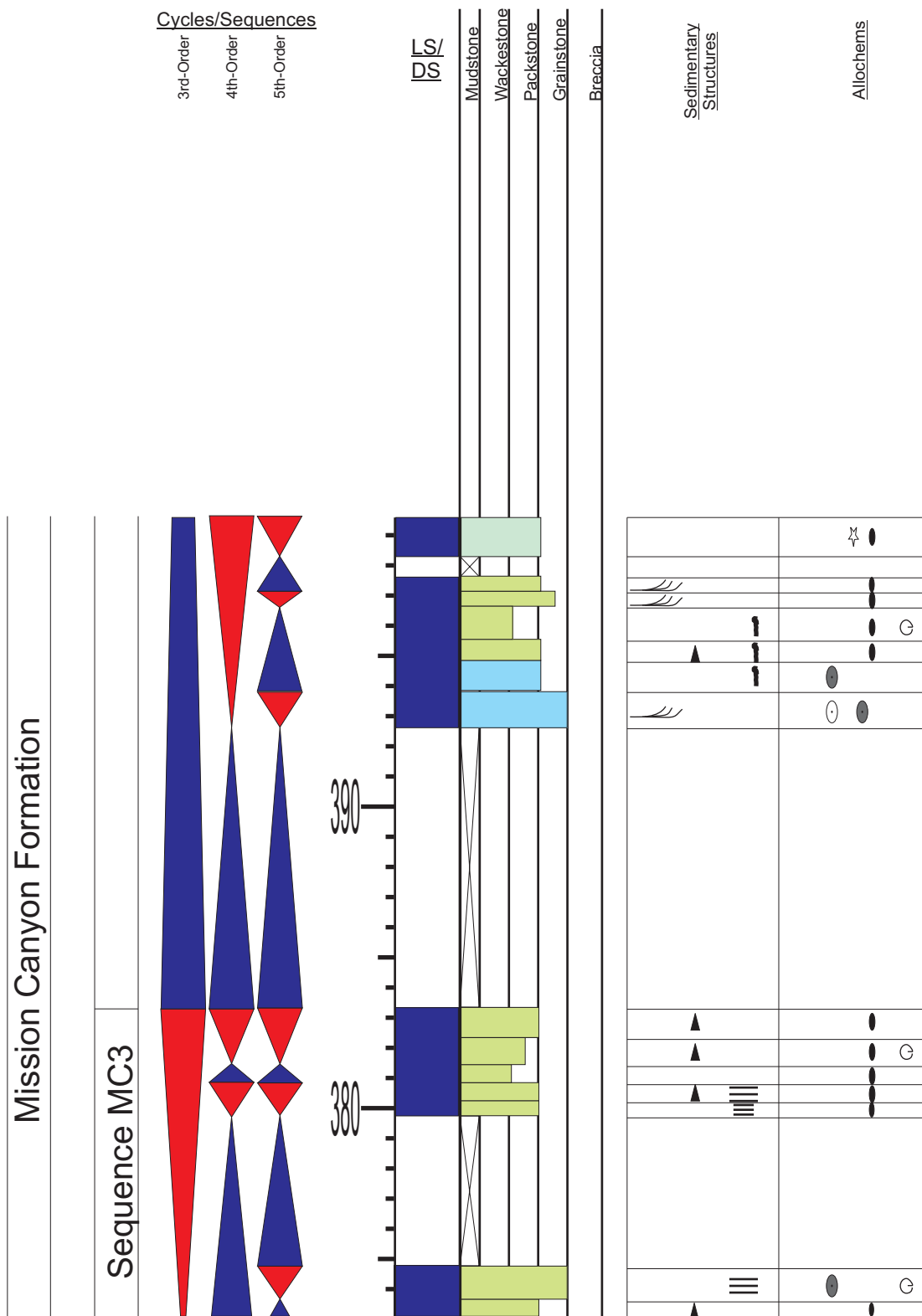
Appendix 5.9: Sedimentary section log for section Monarch (Continued). Refer to Appendix 1 for symbols and Figure 3.6 for location.

APPENDIX 5.10



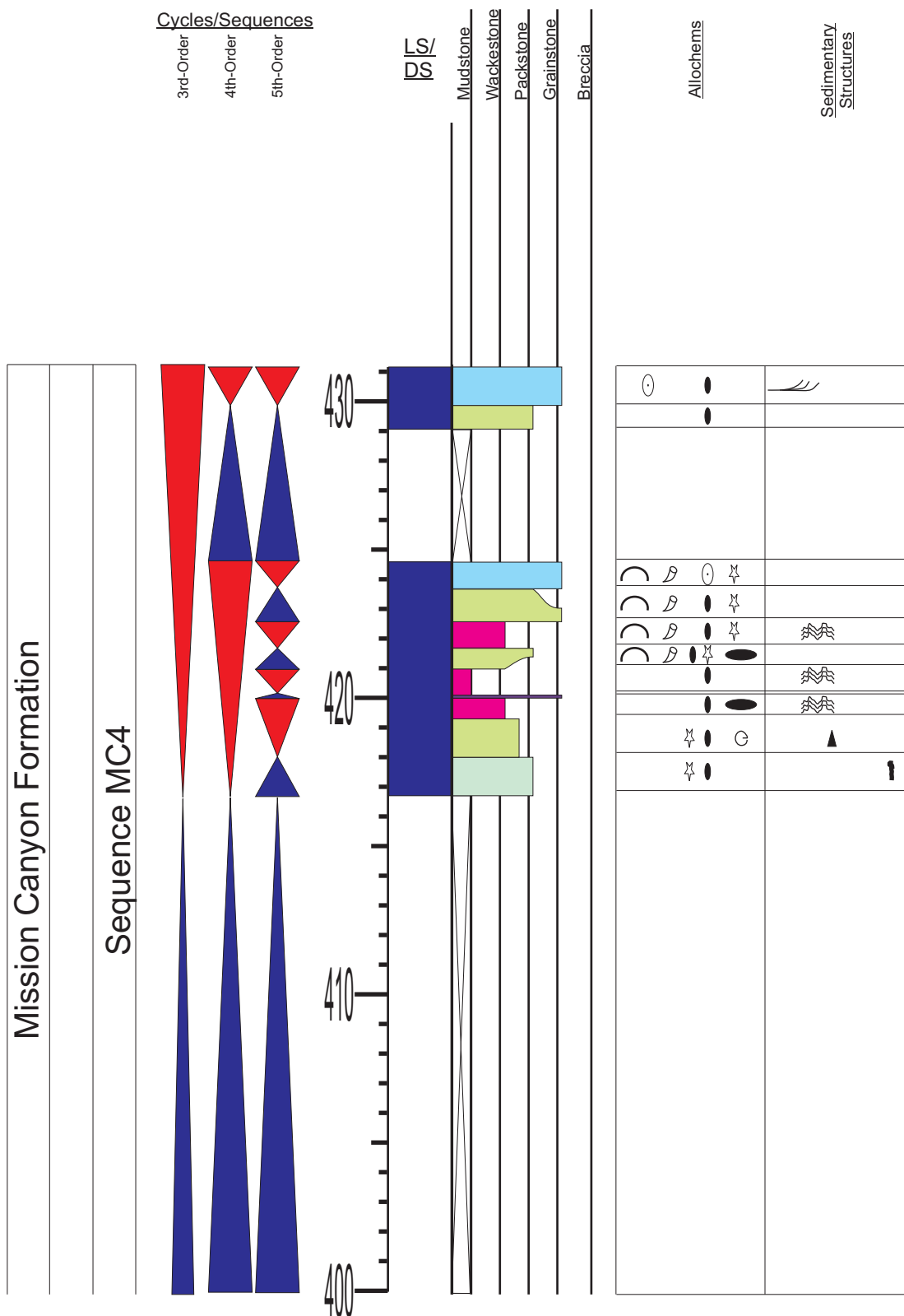
Appendix 5.10: Sedimentary section log for section Monarch (Continued). Refer to Appendix 1 for symbols and Figure 3.6 for location.

APPENDIX 5.11



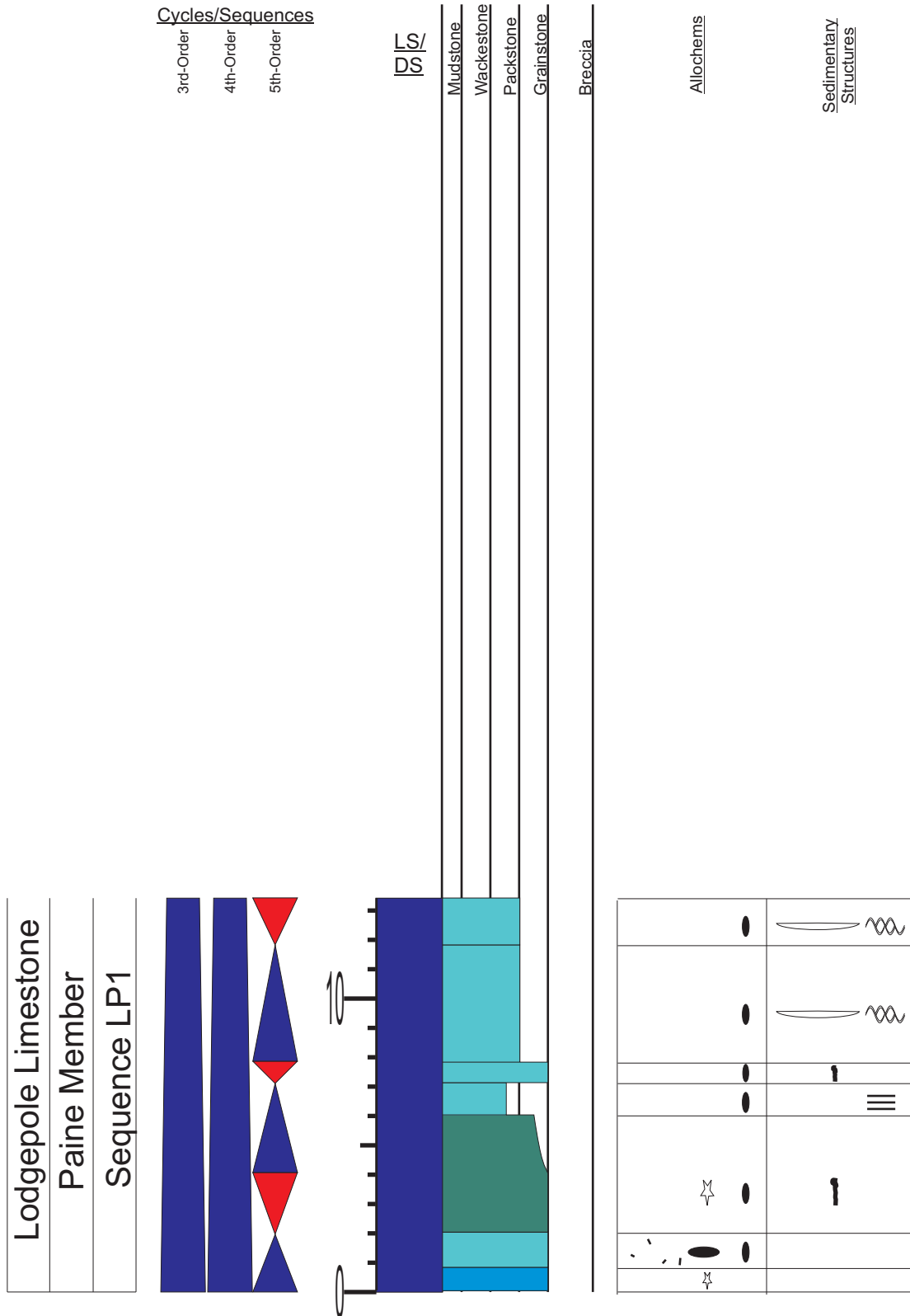
Appendix 5.11: Sedimentary section log for section Monarch (Continued). Refer to Appendix 1 for symbols and Figure 3.6 for location.

APPENDIX 5.12



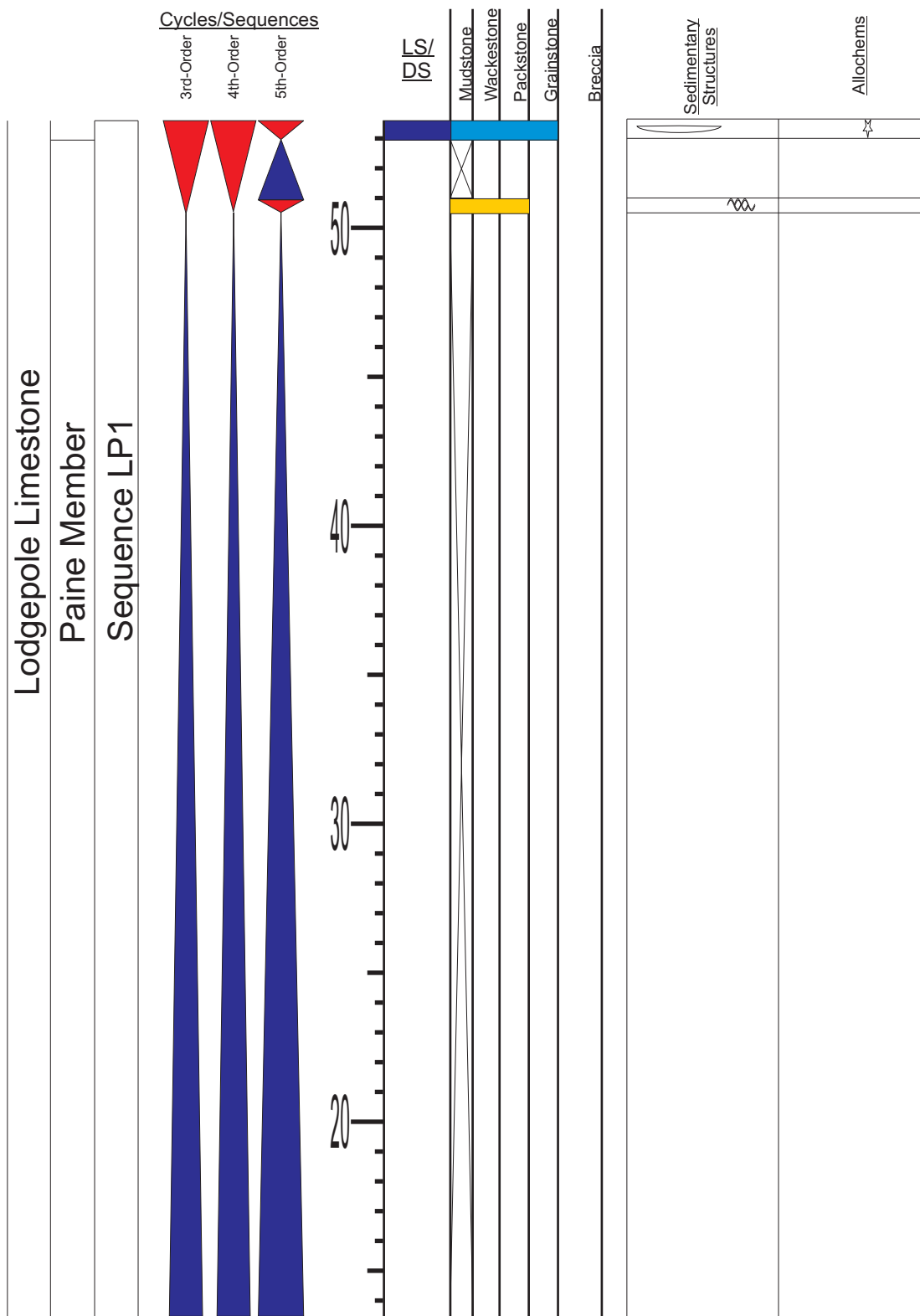
Appendix 5.12: Sedimentary section log for section Monarch (Continued). Refer to Appendix 1 for symbols and Figure 3.6 for location.

APPENDIX 6.1



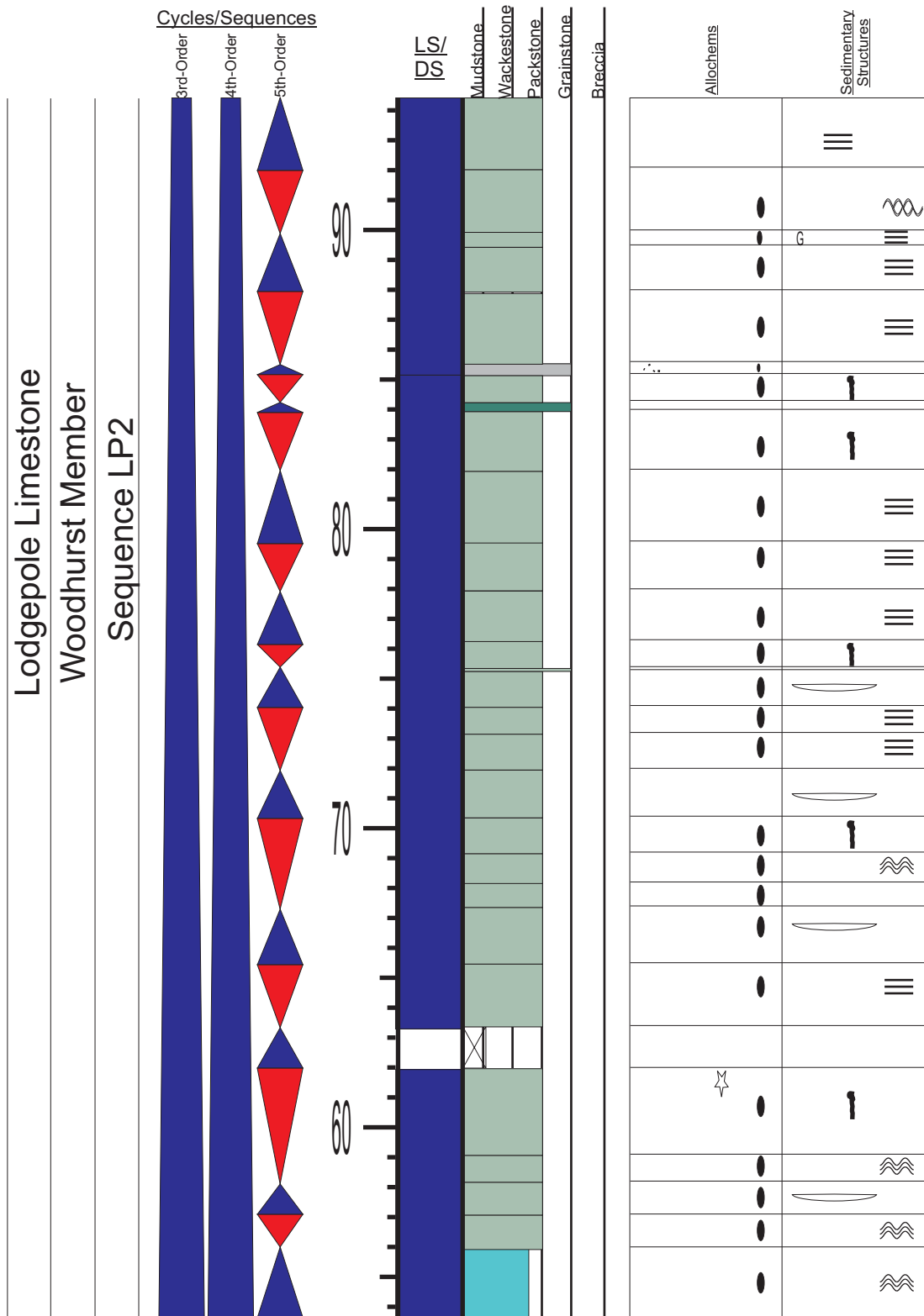
Appendix 6.1: Sedimentary section log for section Baldy Mountain. Refer to Appendix 1 for symbols and Figure 3.6 for location.

APPENDIX 6.2



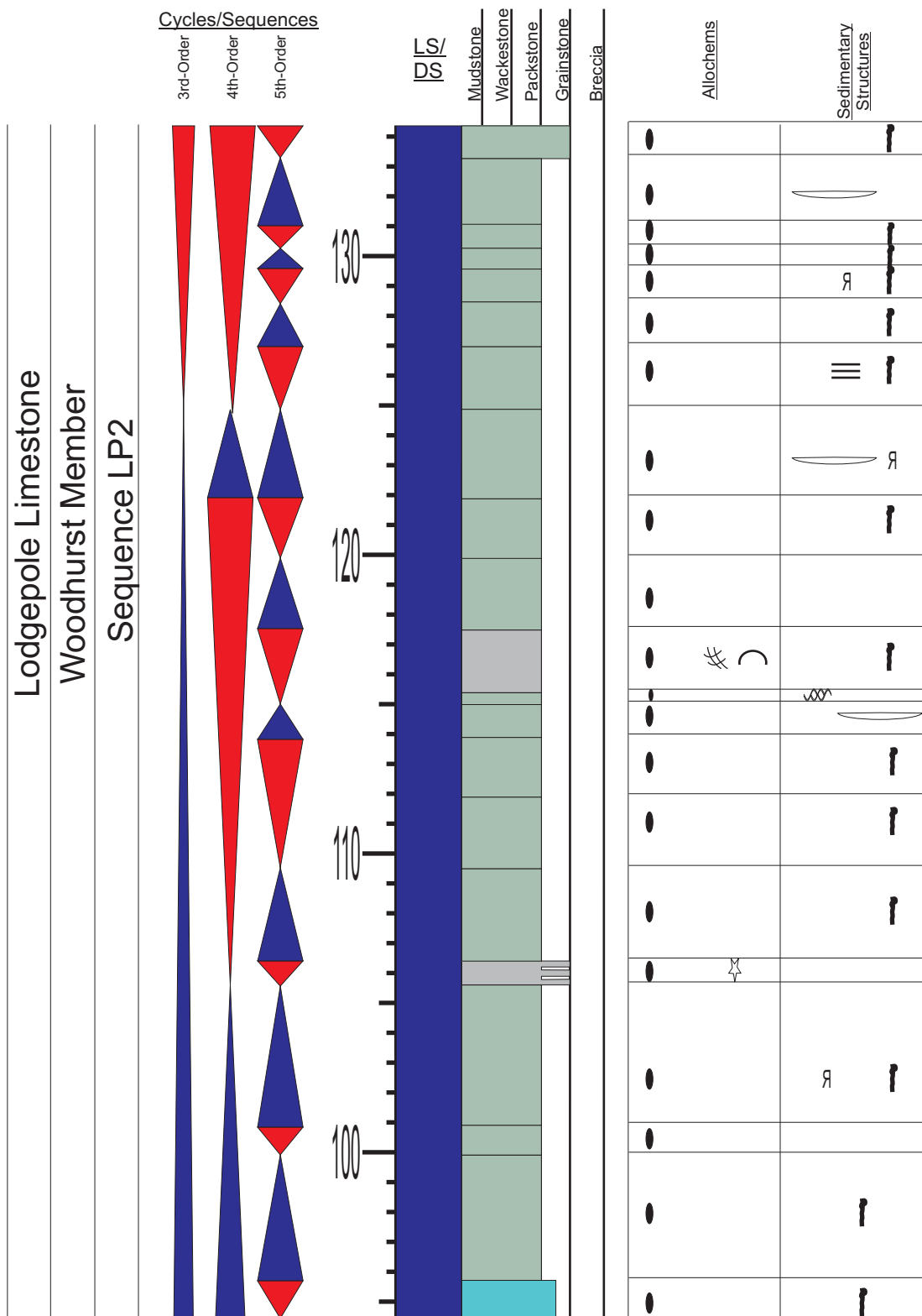
Appendix 6.2: Sedimentary section log for section Baldy Mountain (Continued). Refer to Appendix 1 for symbols and Figure 3.6 for location.

APPENDIX 6.3



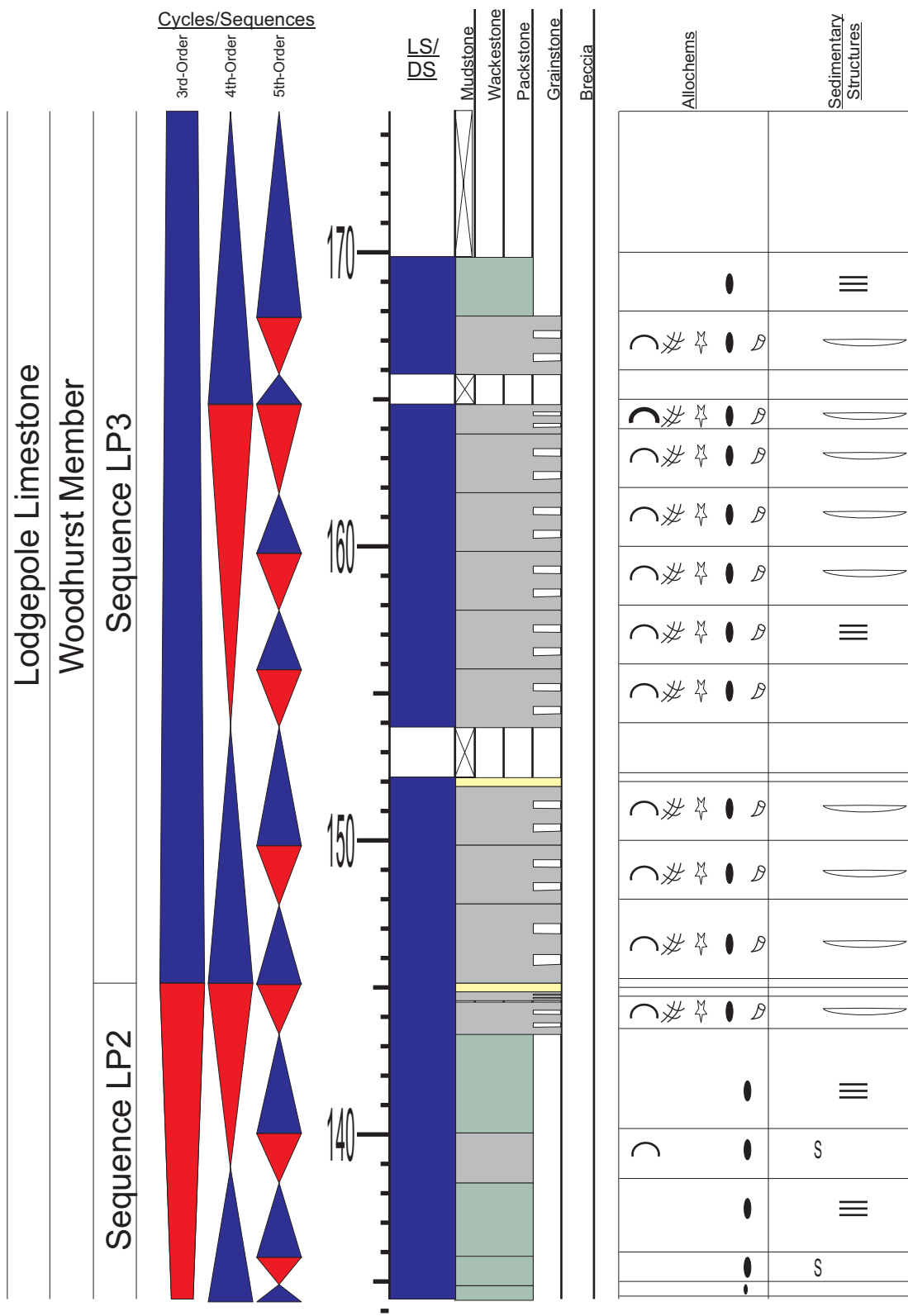
Appendix 6.3: Sedimentary section log for section Baldy Mountain (Continued). Refer to Appendix 1 for symbols and Figure 3.6 for location.

APPENDIX 6.4



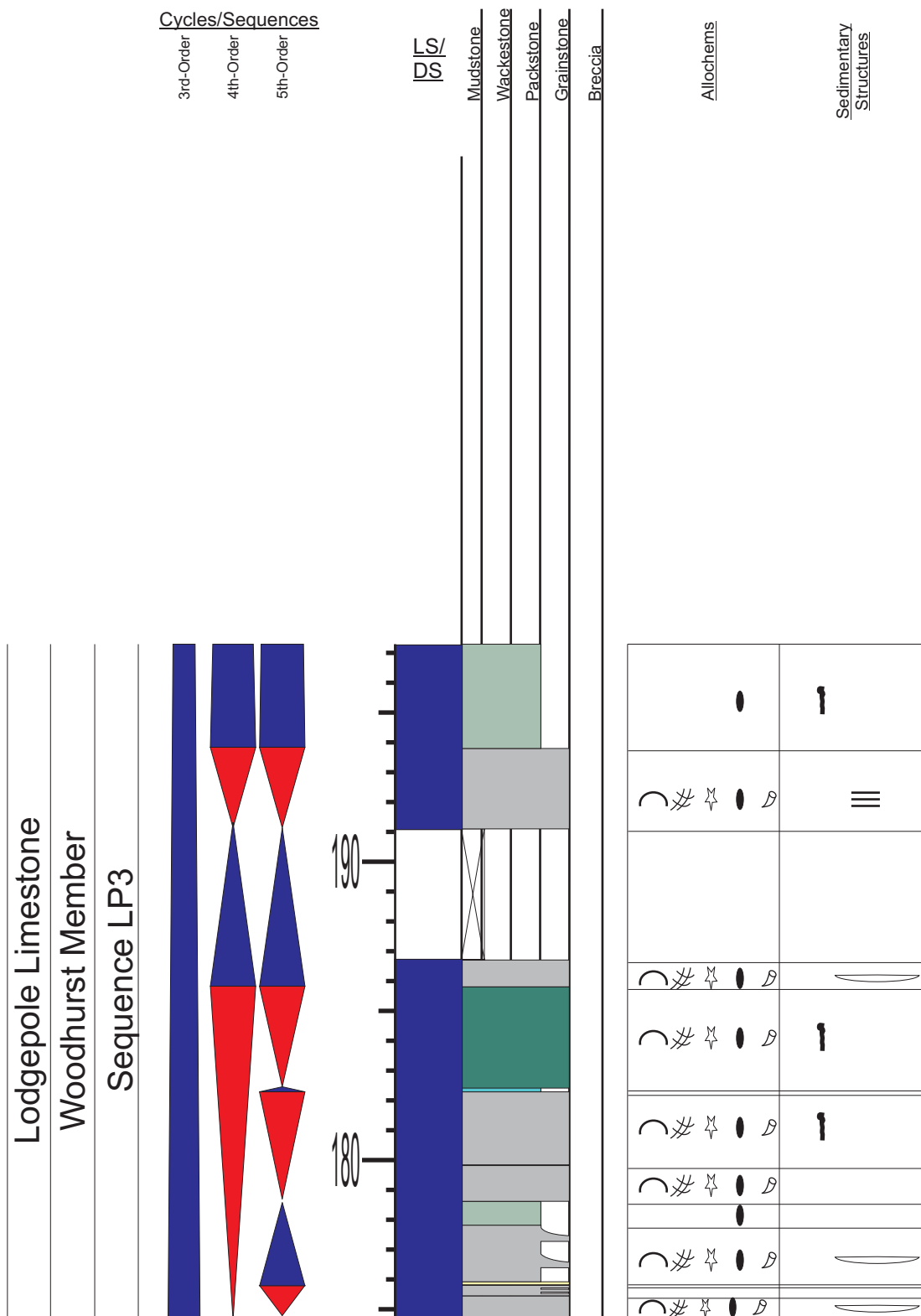
Appendix 6.4: Sedimentary section log for section Baldy Mountain (Continued). Refer to Appendix 1 for symbols and Figure 3.6 for location.

APPENDIX 6.5



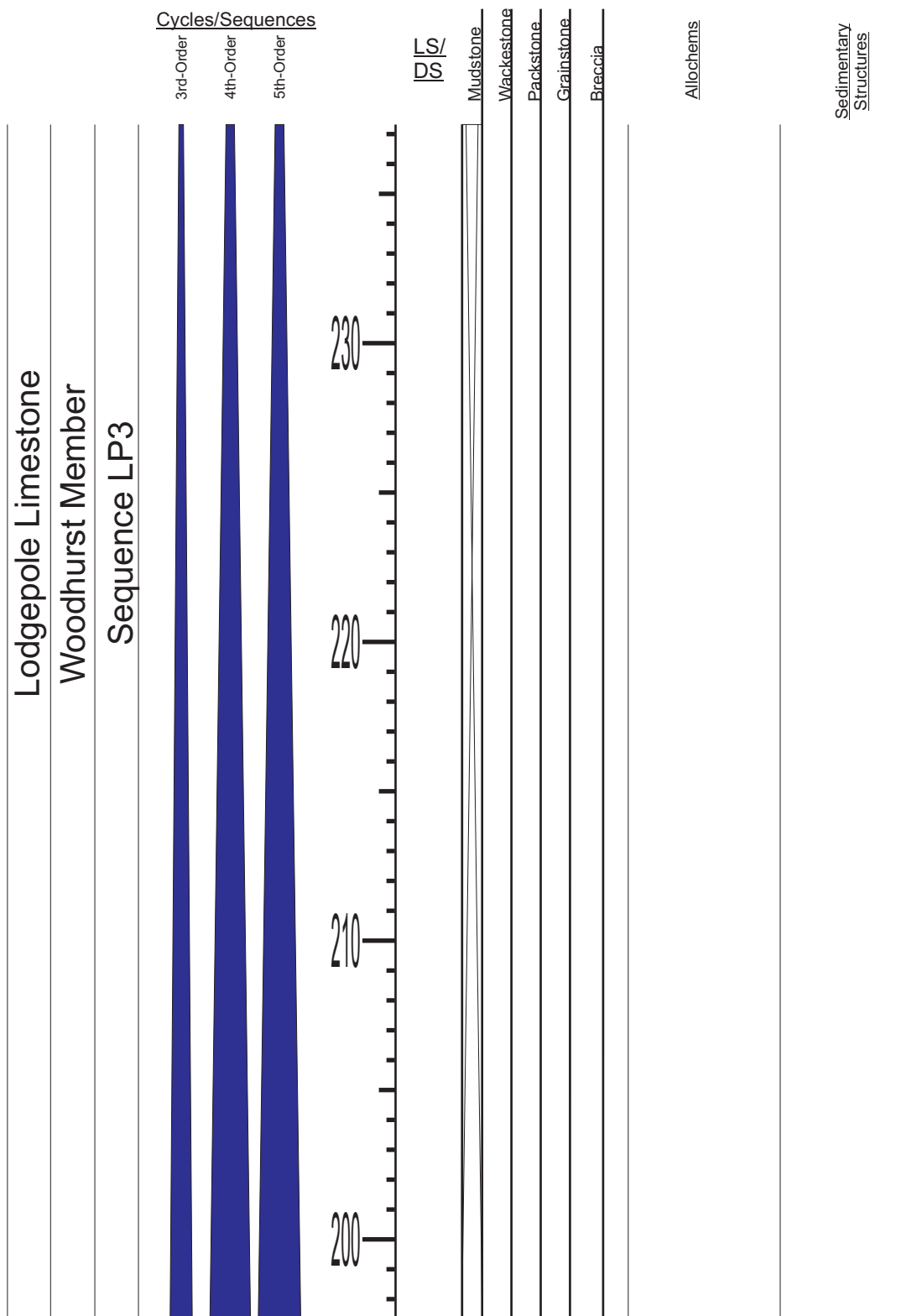
Appendix 6.5: Sedimentary section log for section Baldy Mountain (Continued). Refer to Appendix 1 for symbols and Figure 3.6 for location.

APPENDIX 6.6



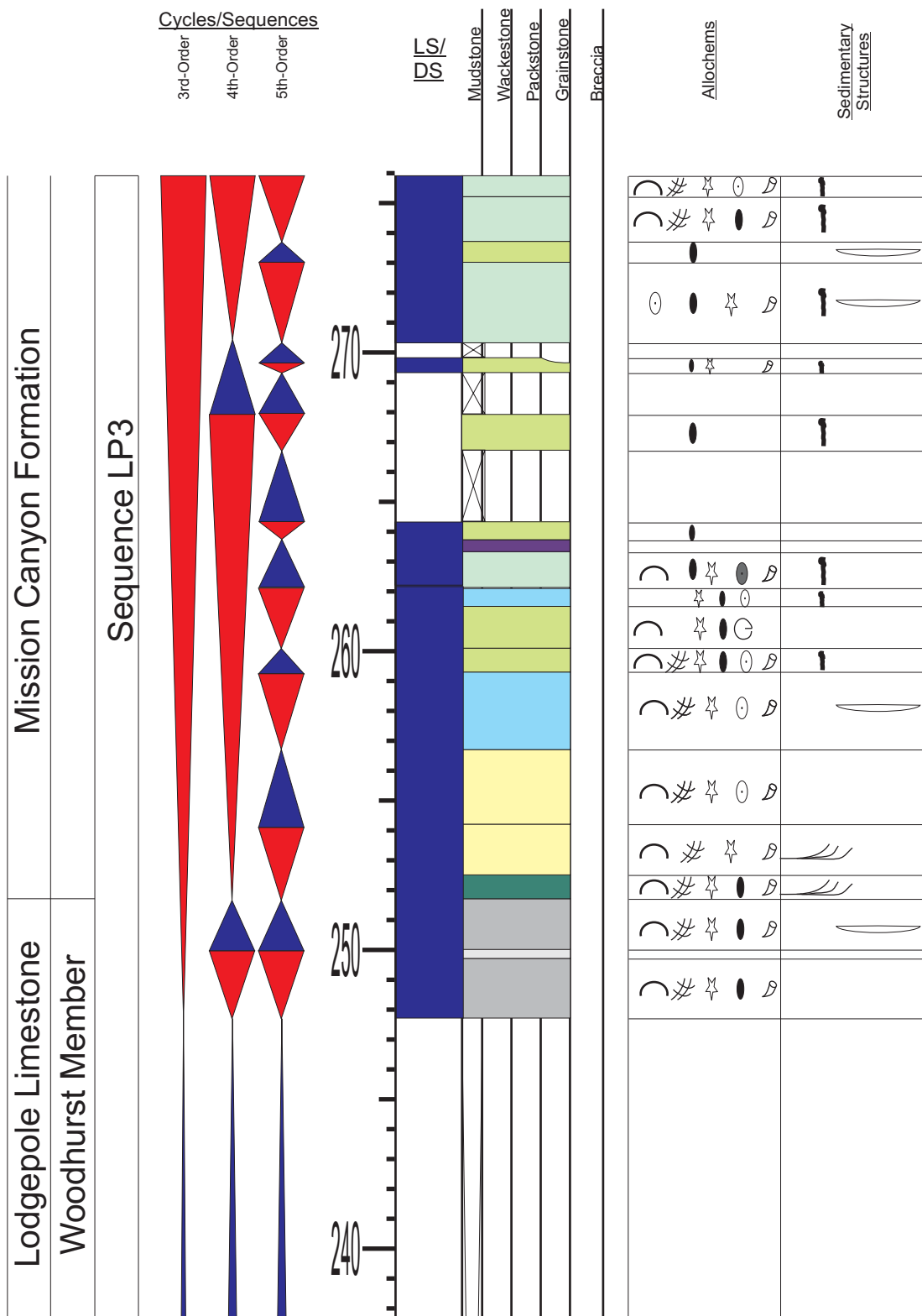
Appendix 6.6: Sedimentary section log for section Baldy Mountain (Continued). Refer to Appendix 1 for symbols and Figure 3.6 for location.

APPENDIX 6.7



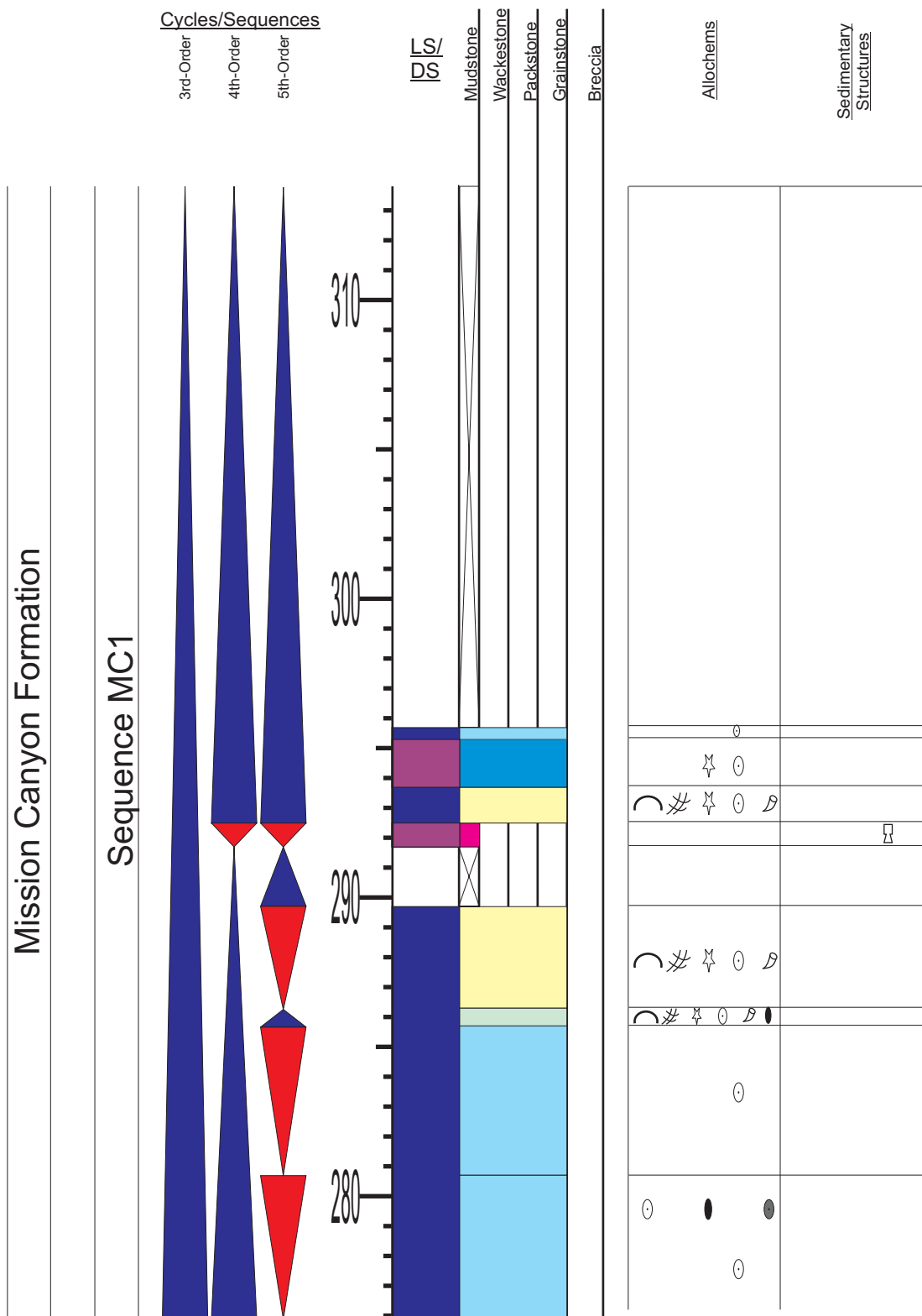
Appendix 6.7: Sedimentary section log for section Baldy Mountain (Continued). Refer to Appendix 1 for symbols and Figure 3.6 for location.

APPENDIX 6.8



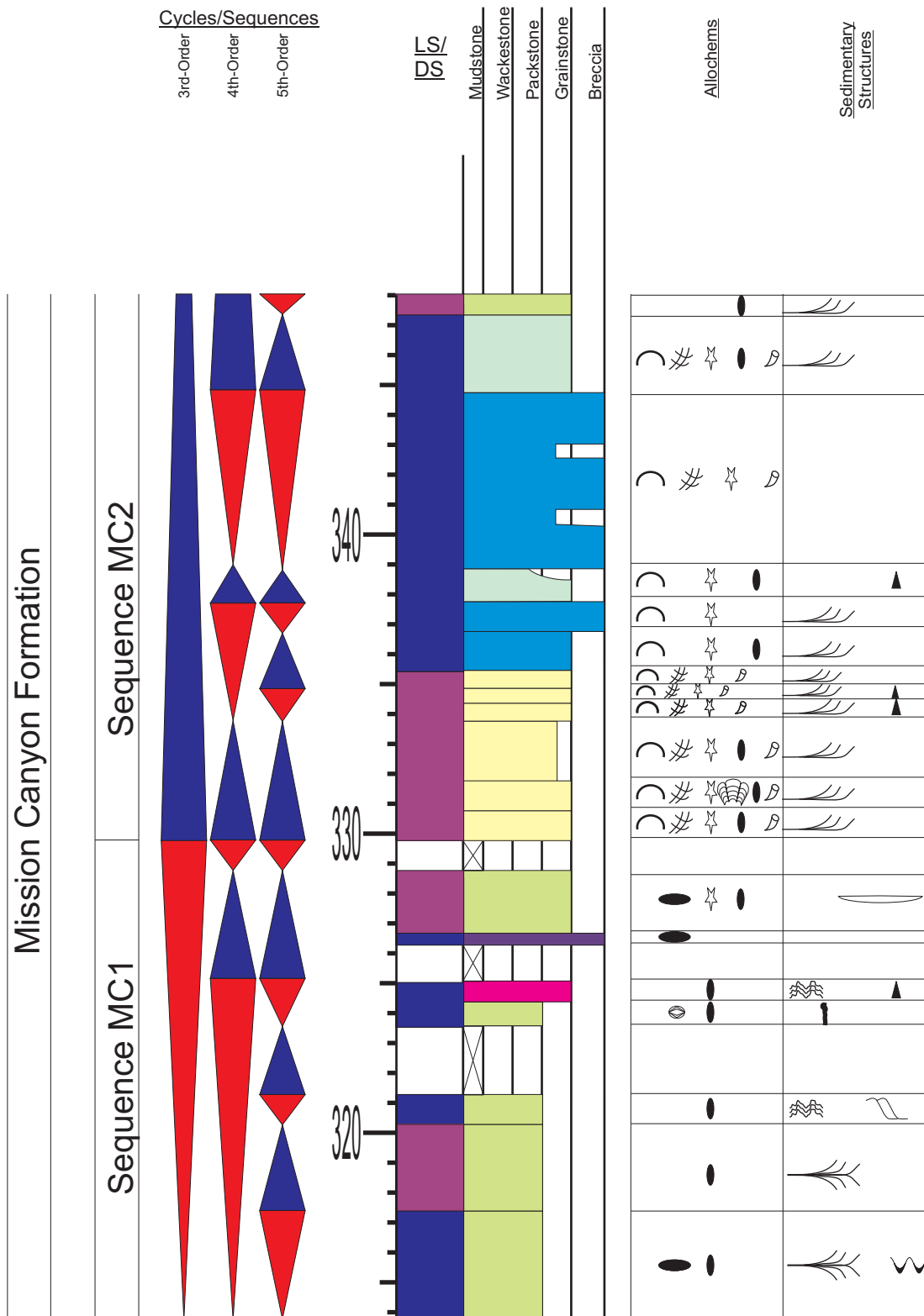
Appendix 6.8: Sedimentary section log for section Baldy Mountain (Continued). Refer to Appendix 1 for symbols and Figure 3.6 for location.

APPENDIX 6.9



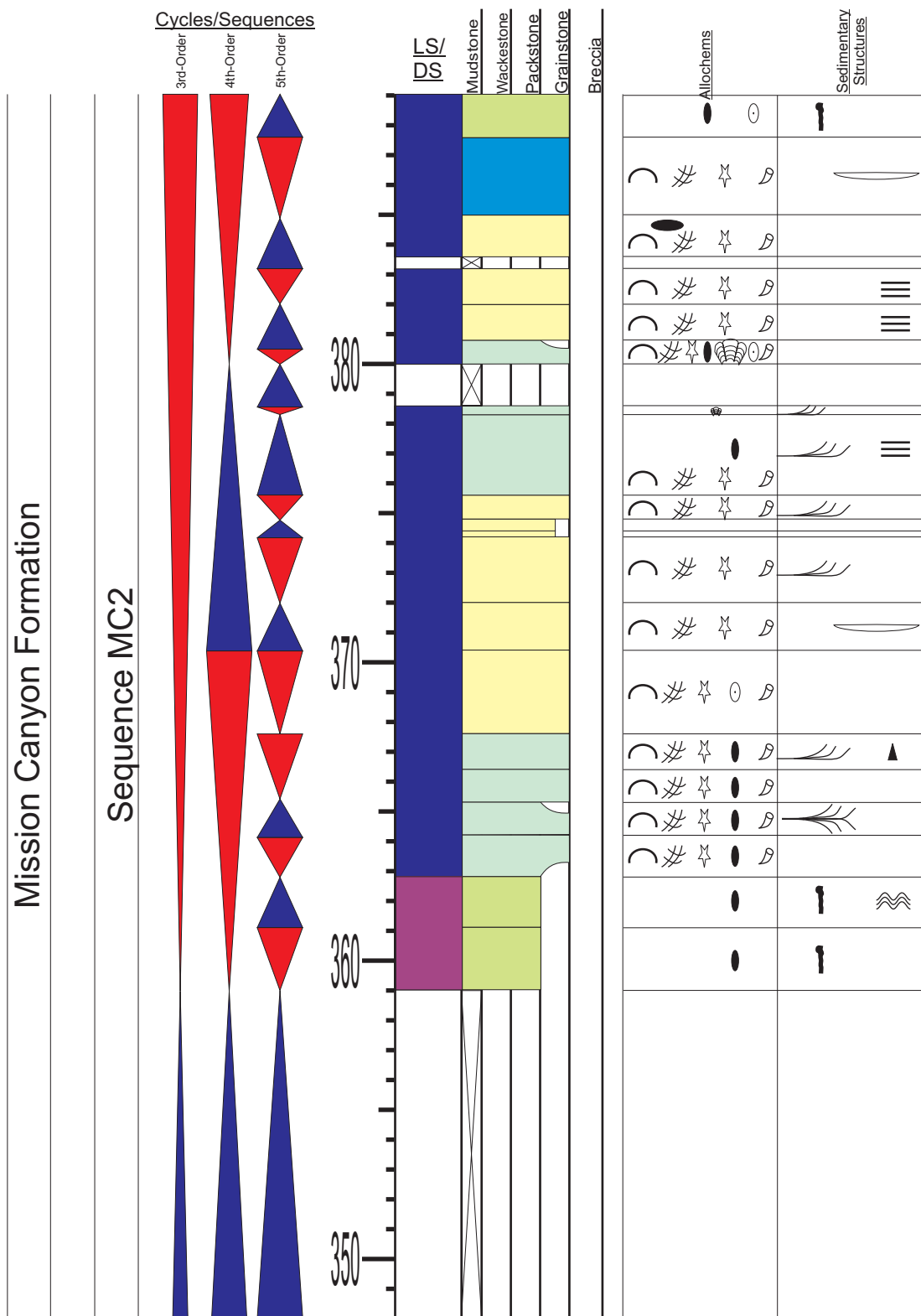
Appendix 6.9: Sedimentary section log for section Baldy Mountain (Continued). Refer to Appendix 1 for symbols and Figure 3.6 for location.

APPENDIX 6.10



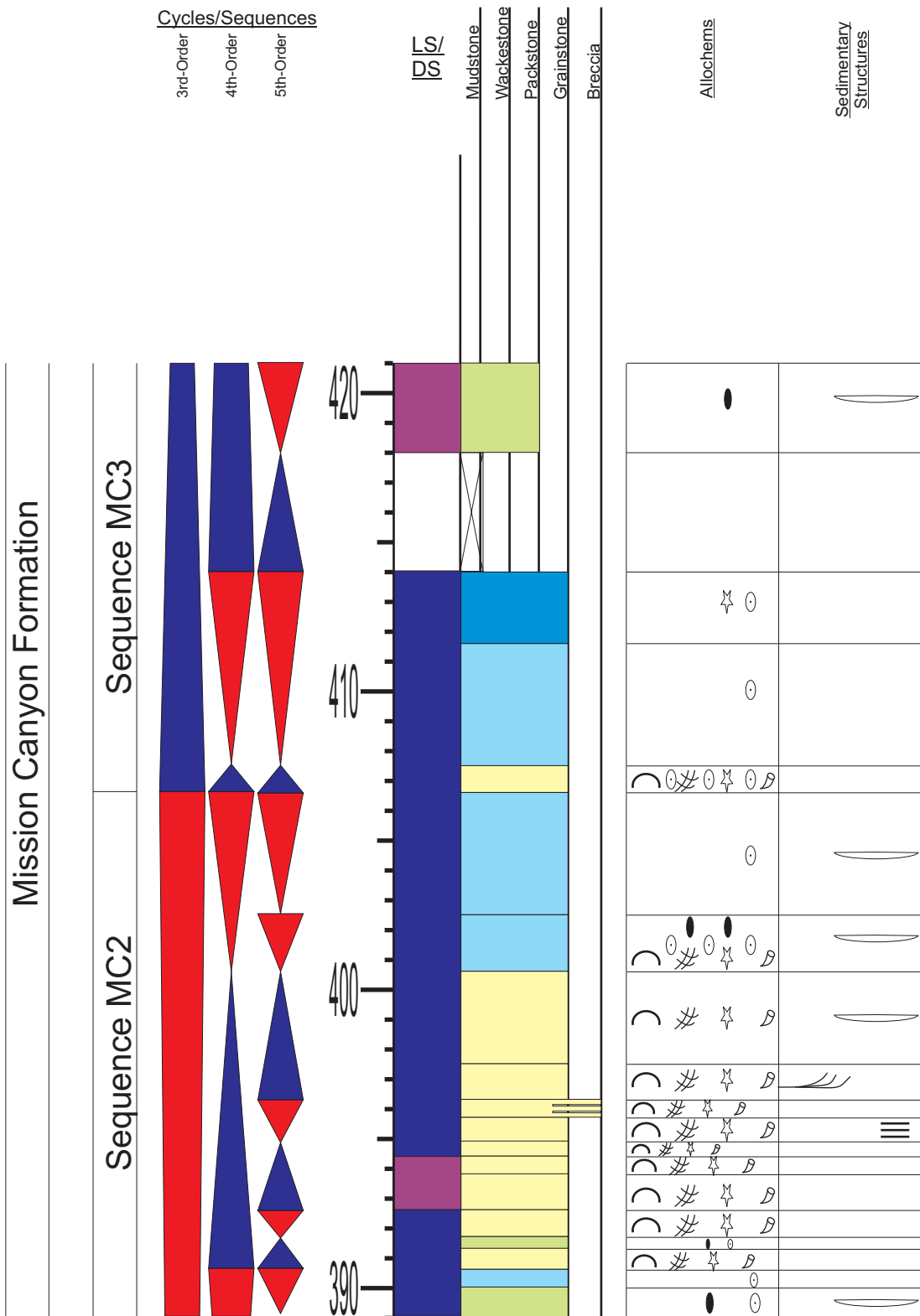
Appendix 6.10: Sedimentary section log for section Baldy Mountain (Continued). Refer to Appendix 1 for symbols and Figure 3.6 for location.

APPENDIX 6.11



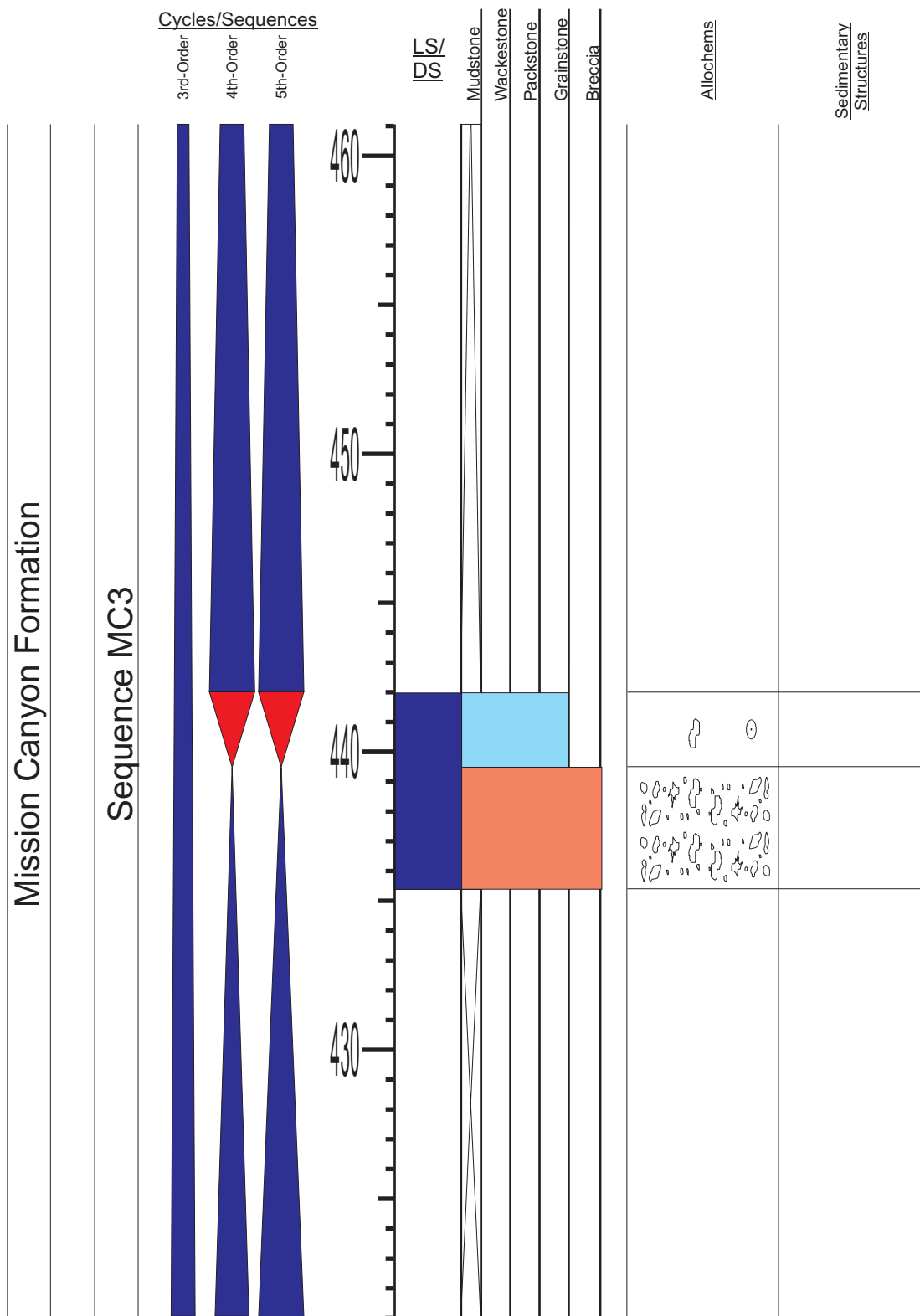
Appendix 6.11: Sedimentary section log for section Baldy Mountain (Continued). Refer to Appendix 1 for symbols and Figure 3.6 for location.

APPENDIX 6.12



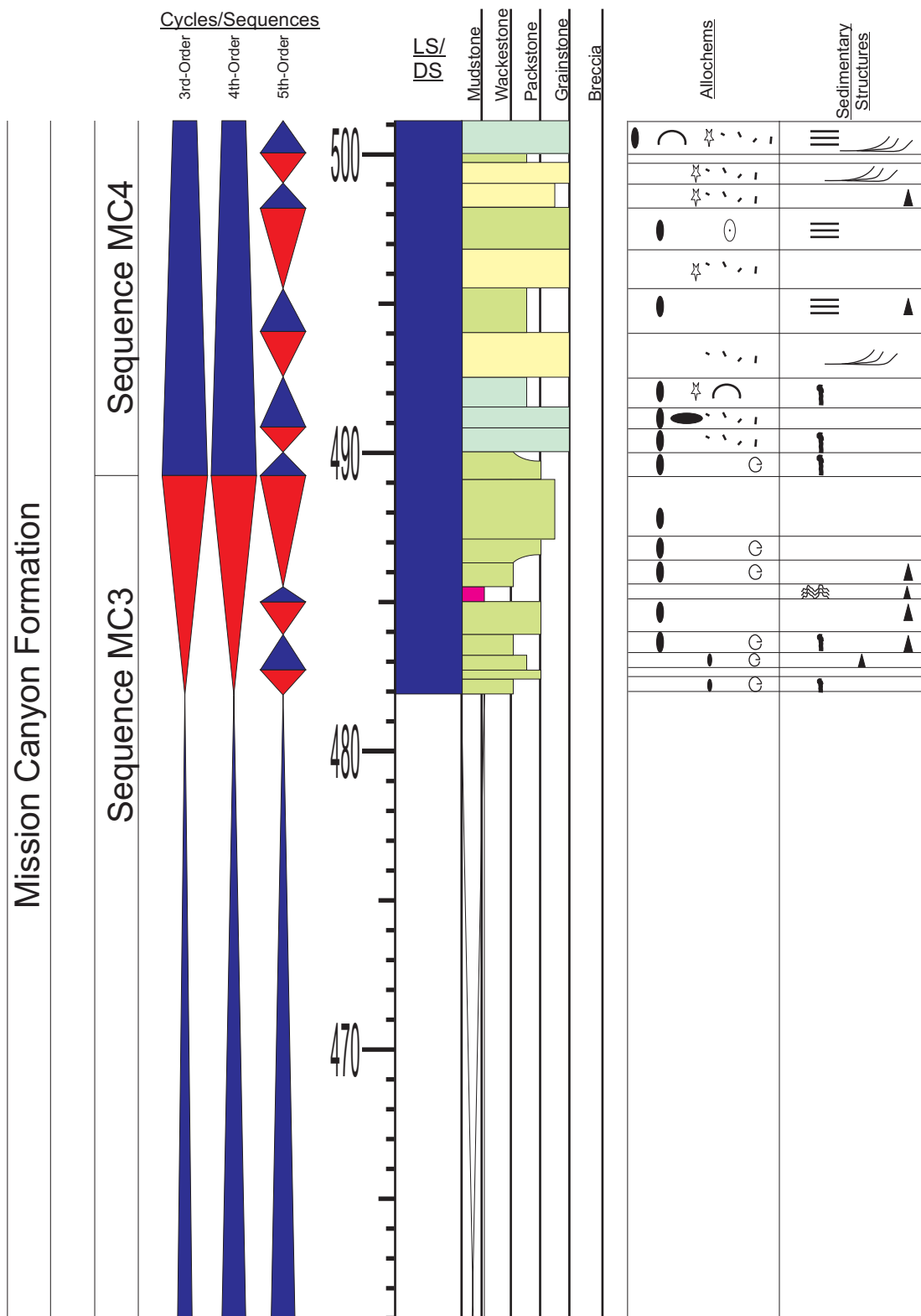
Appendix 6.12: Sedimentary section log for section Baldy Mountain (Continued). Refer to Appendix 1 for symbols and Figure 3.6 for location.

APPENDIX 6.13



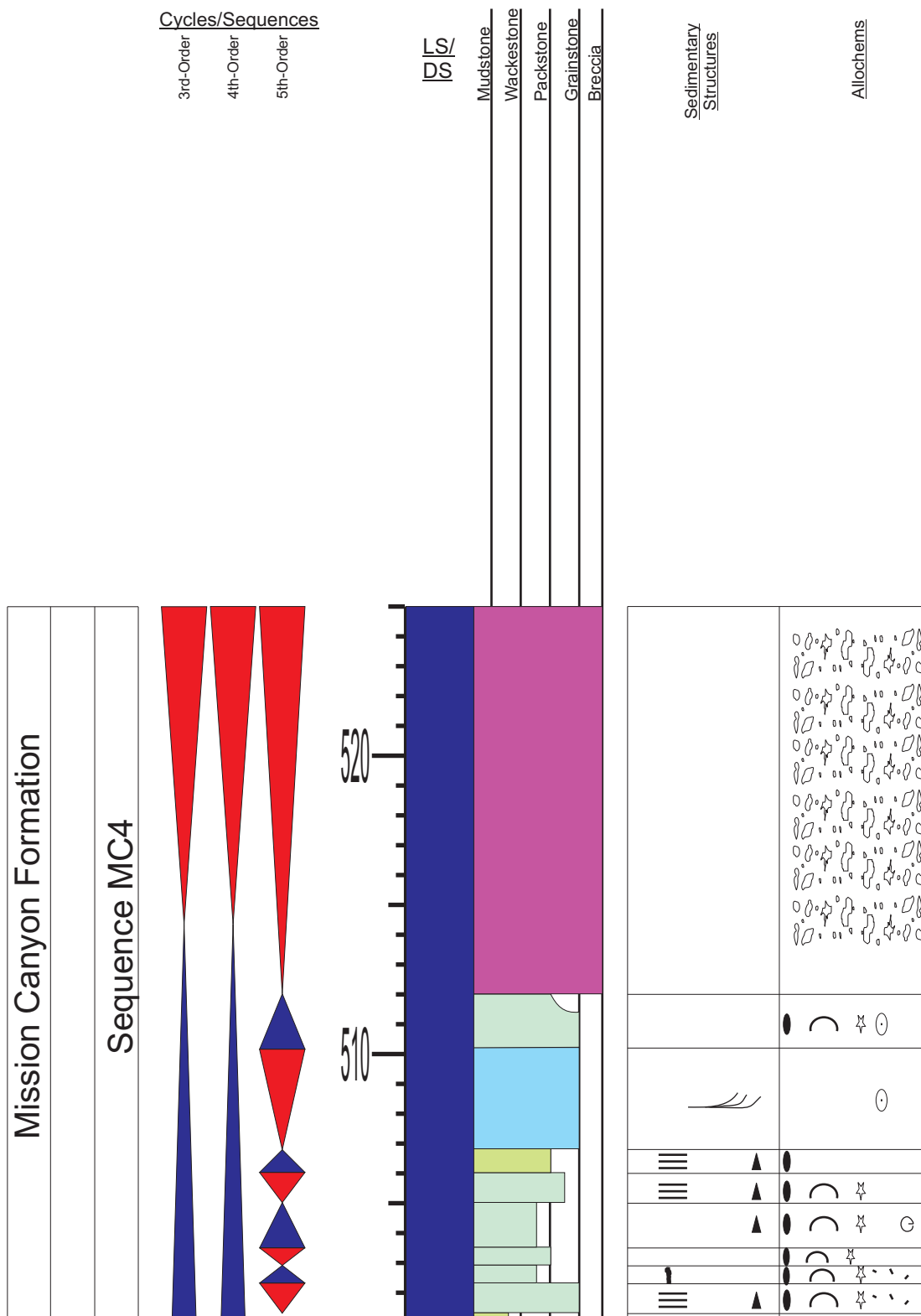
Appendix 6.13: Sedimentary section log for section Baldy Mountain (Continued). Refer to Appendix 1 for symbols and Figure 3.6 for location.

APPENDIX 6.14



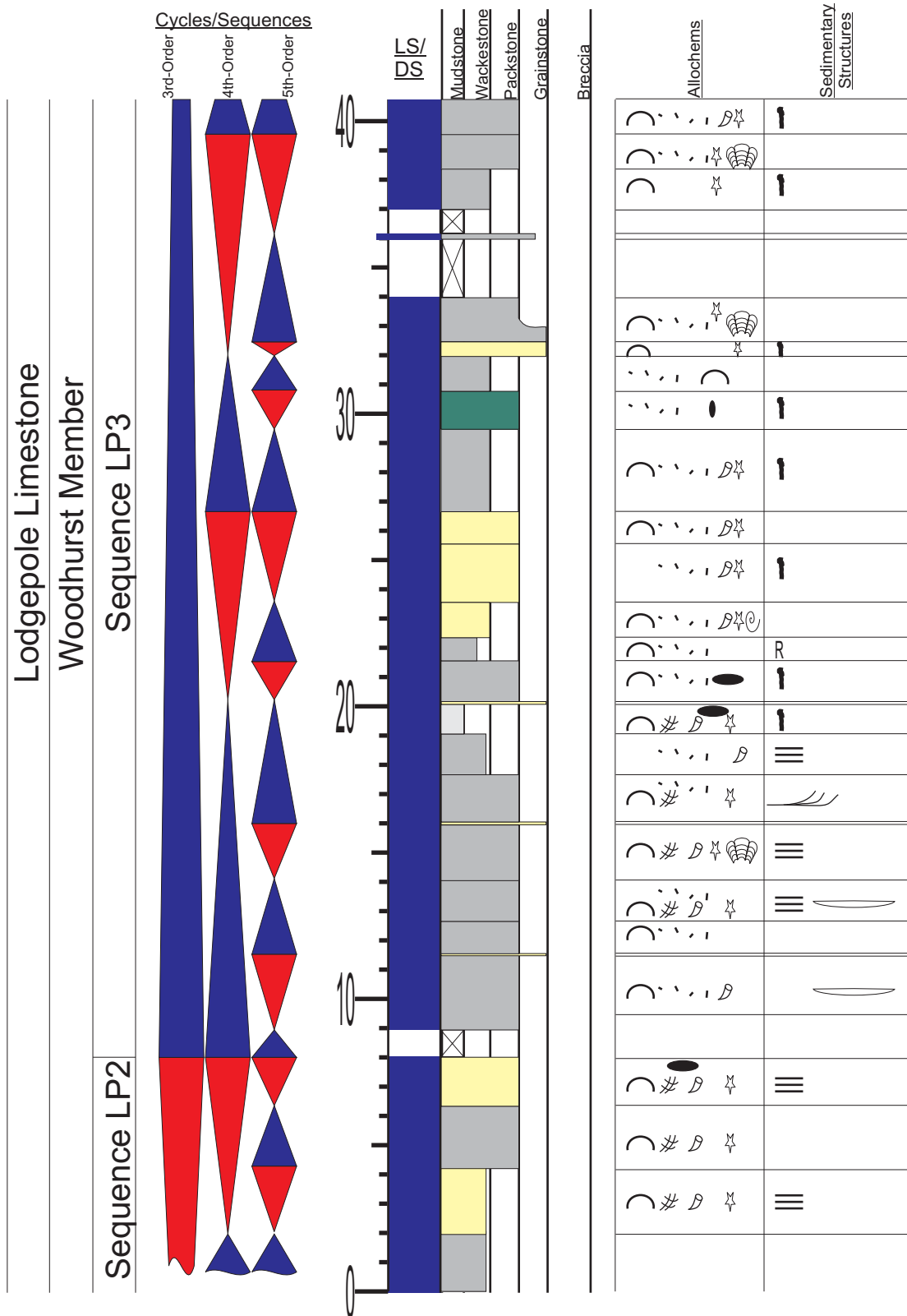
Appendix 6.14: Sedimentary section log for section Baldy Mountain (Continued). Refer to Appendix 1 for symbols and Figure 3.6 for location.

APPENDIX 6.15



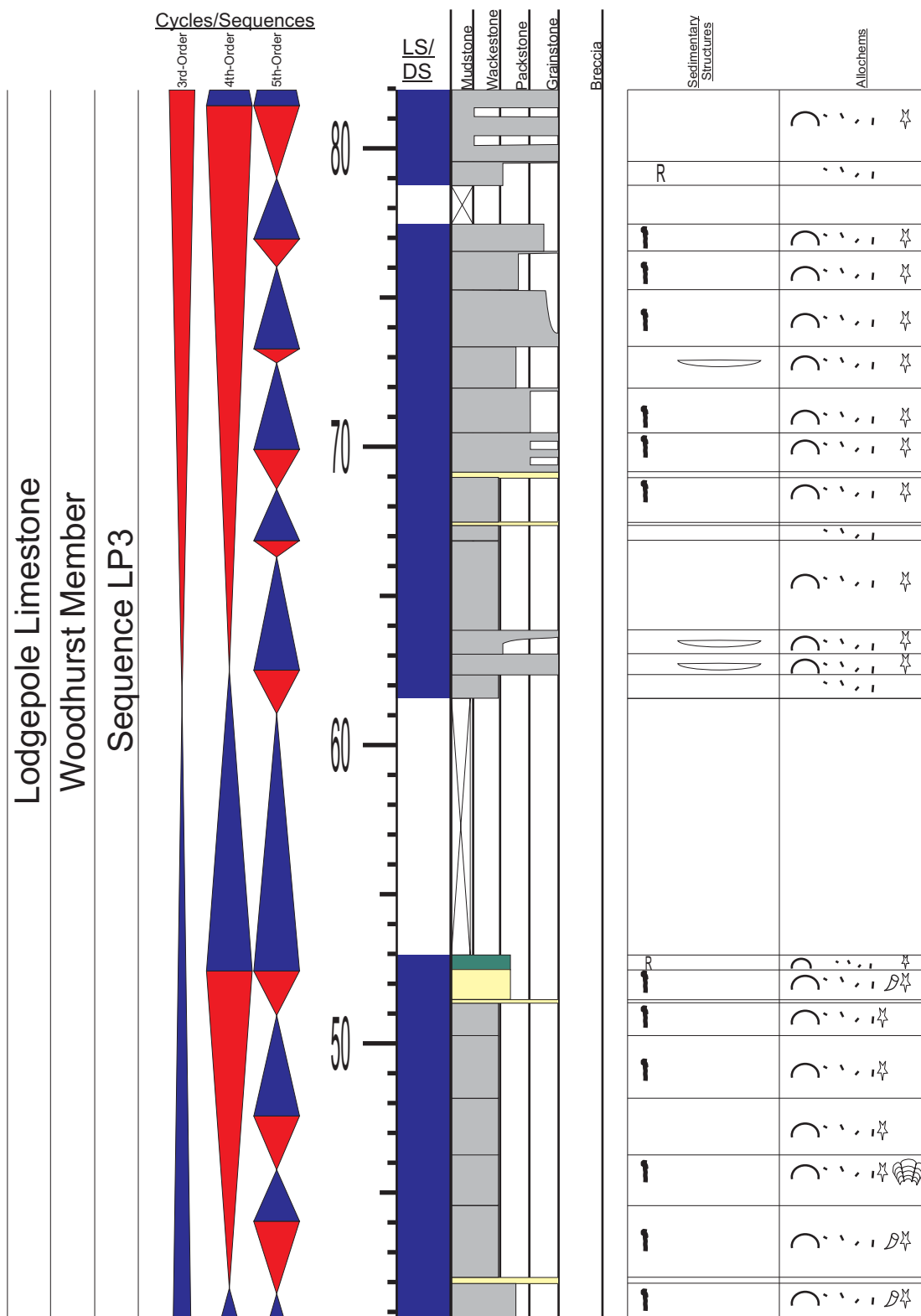
Appendix 6.15: Sedimentary section log for section Baldy Mountain (Continued). Refer to Appendix 1 for symbols and Figure 3.6 for location.

APPENDIX 7.1



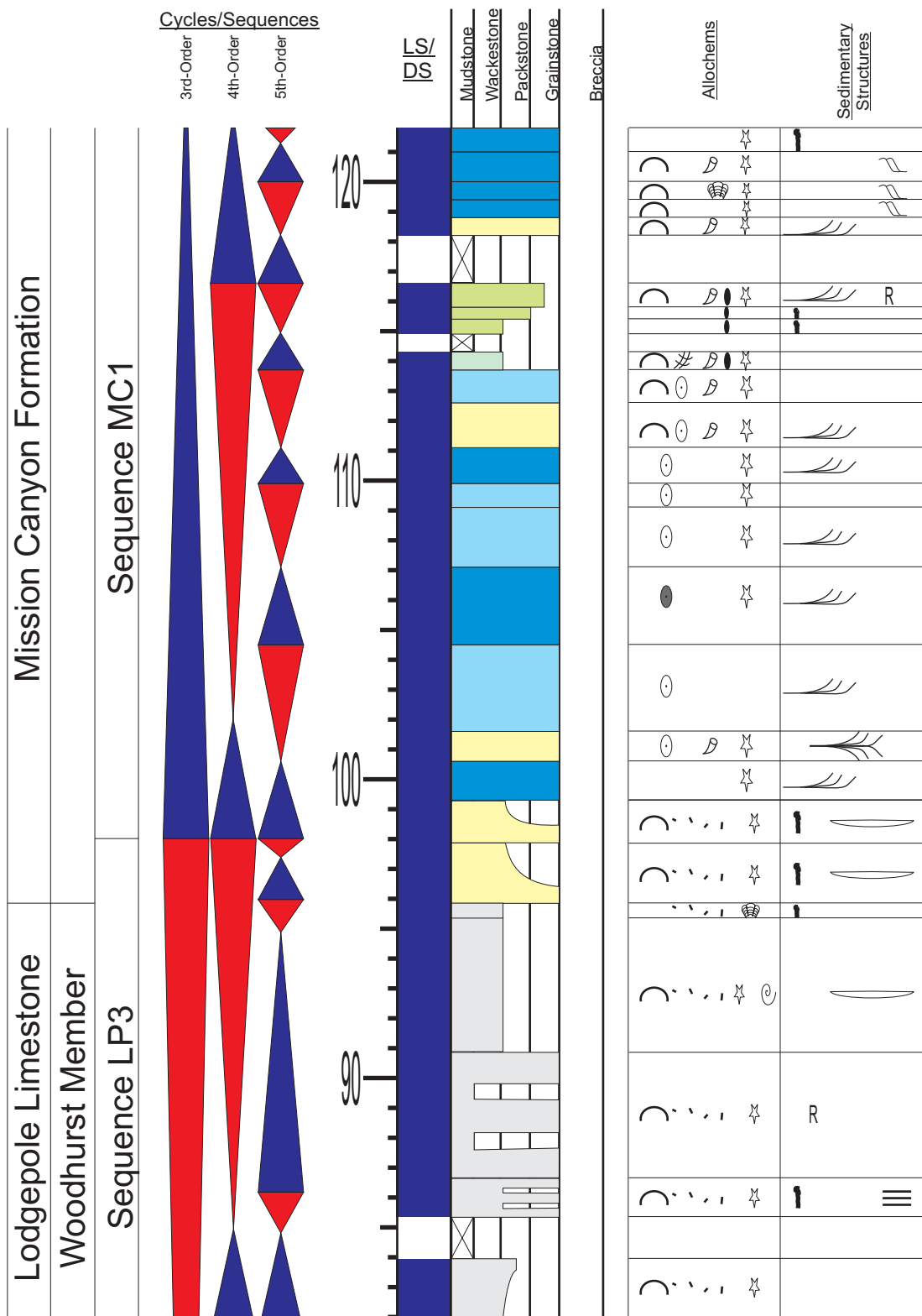
Appendix 7.1: Sedimentary section log for section Ashbough Canyon. Refer to Appendix 1 for symbols and Figure 3.6 for location.

APPENDIX 7.2



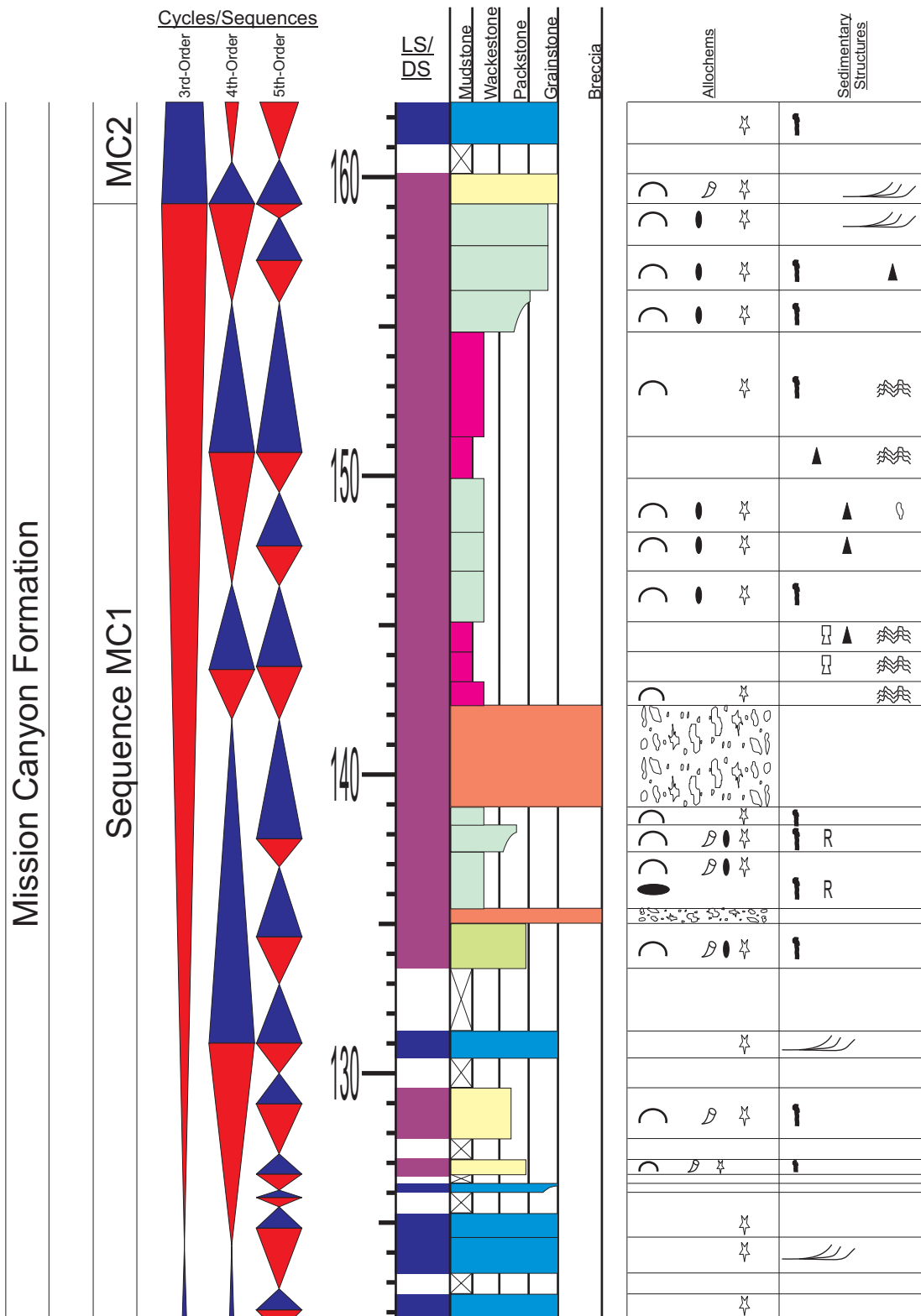
Appendix 7.2: Sedimentary section log for section Ashbough Canyon (Continued). Refer to Appendix 1 for symbols and Figure 3.6 for location.

APPENDIX 7.3



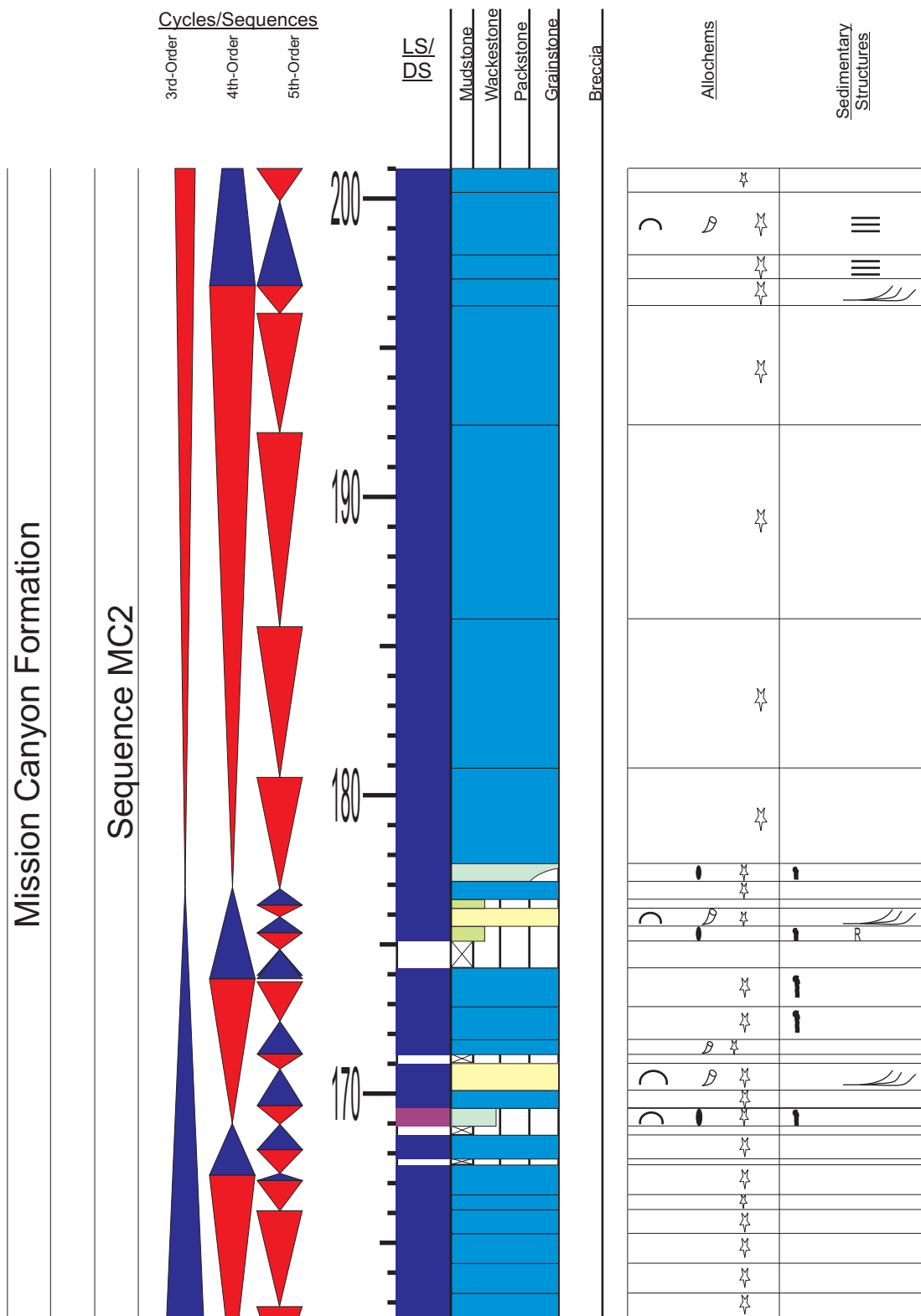
Appendix 7.3: Sedimentary section log for section Ashbough Canyon (Continued). Refer to Appendix 1 for symbols and Figure 3.6 for location.

APPENDIX 7.4



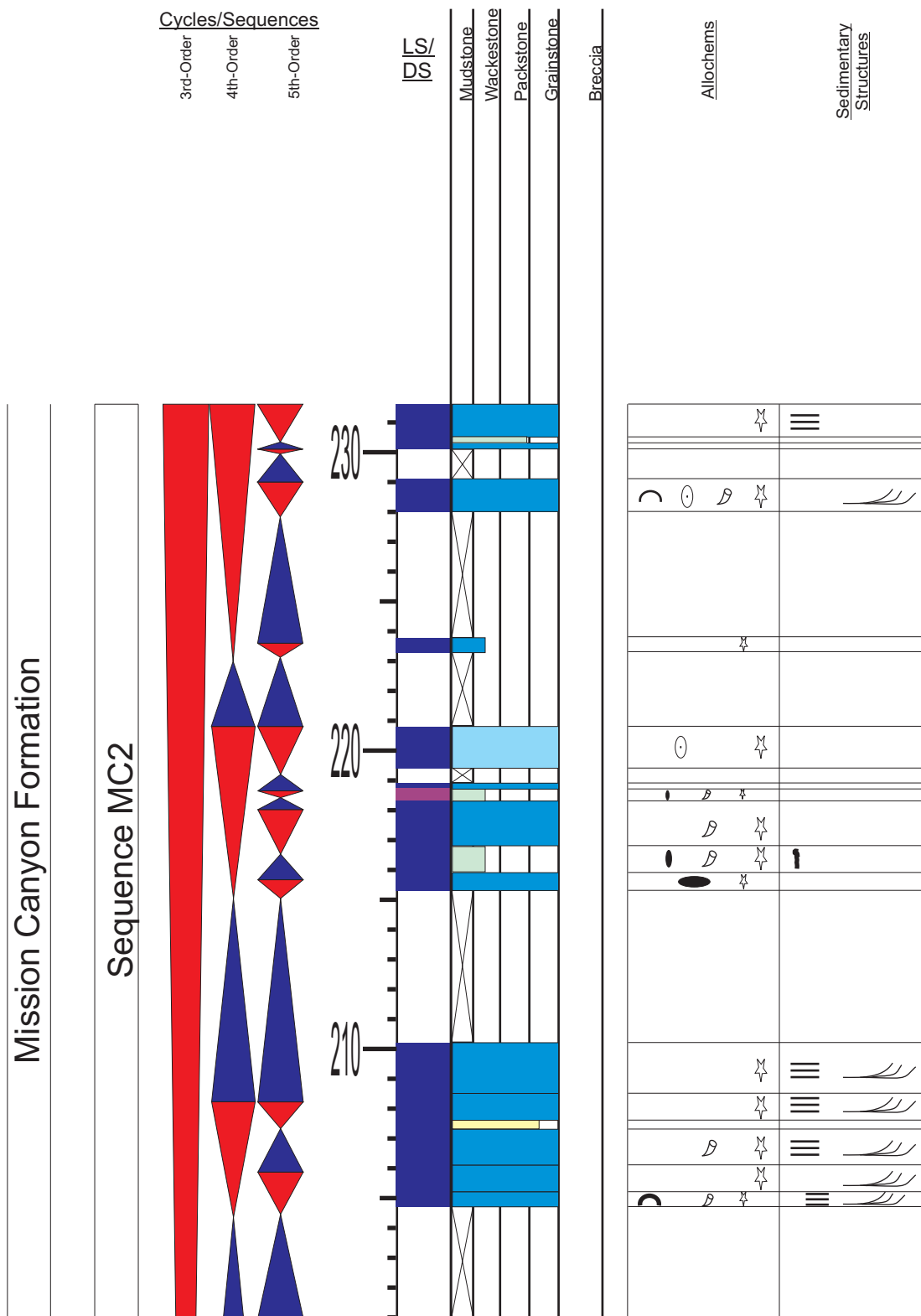
Appendix 7.4: Sedimentary section log for section Ashbough Canyon (Continued). Refer to Appendix 1 for symbols and Figure 3.6 for location.

APPENDIX 7.5



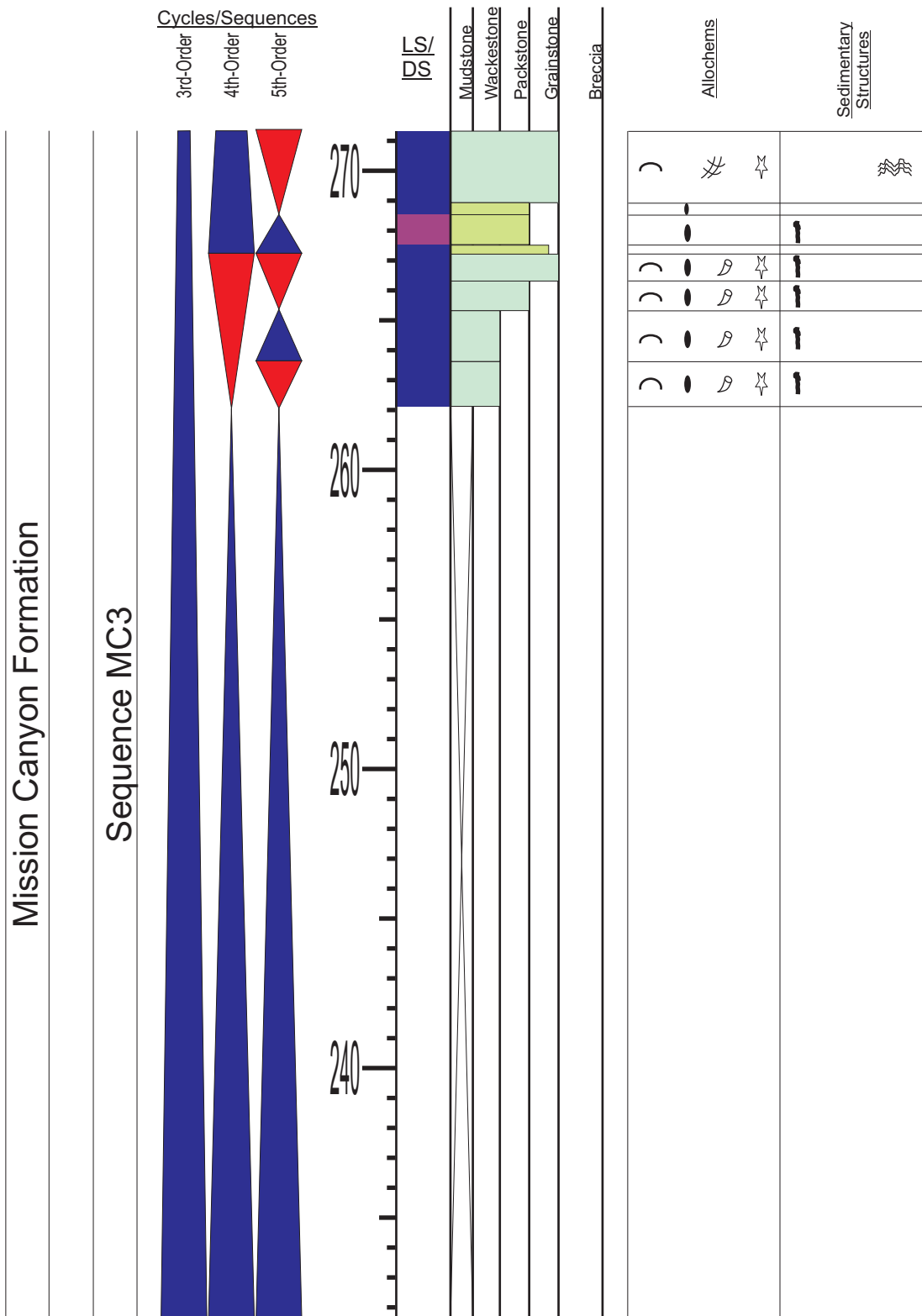
Appendix 7.5: Sedimentary section log for section Ashbough Canyon (Continued). Refer to Appendix 1 for symbols and Figure 3.6 for location.

APPENDIX 7.6



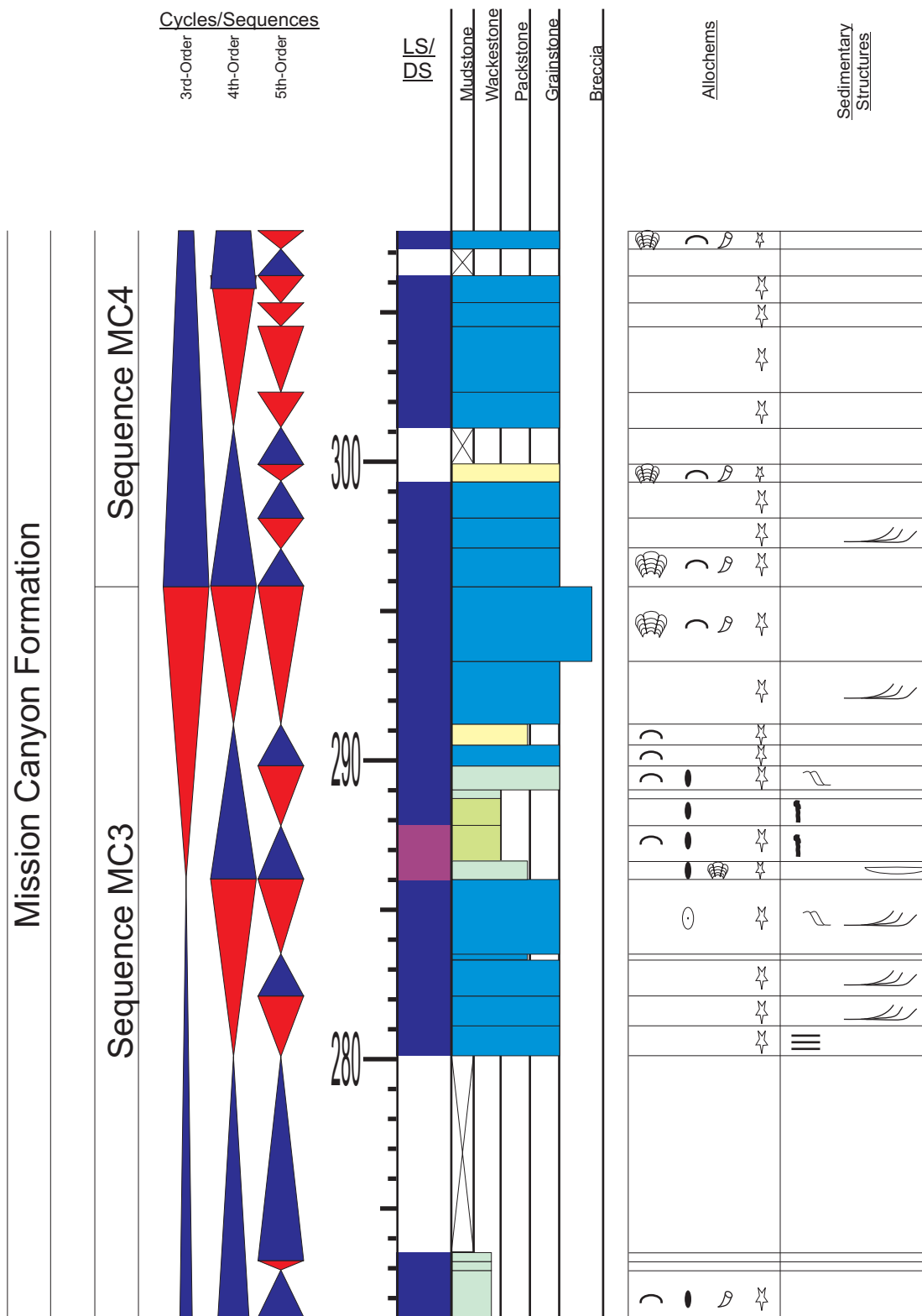
Appendix 7.6: Sedimentary section log for section Ashbough Canyon (Continued). Refer to Appendix 1 for symbols and Figure 3.6 for location.

APPENDIX 7.7



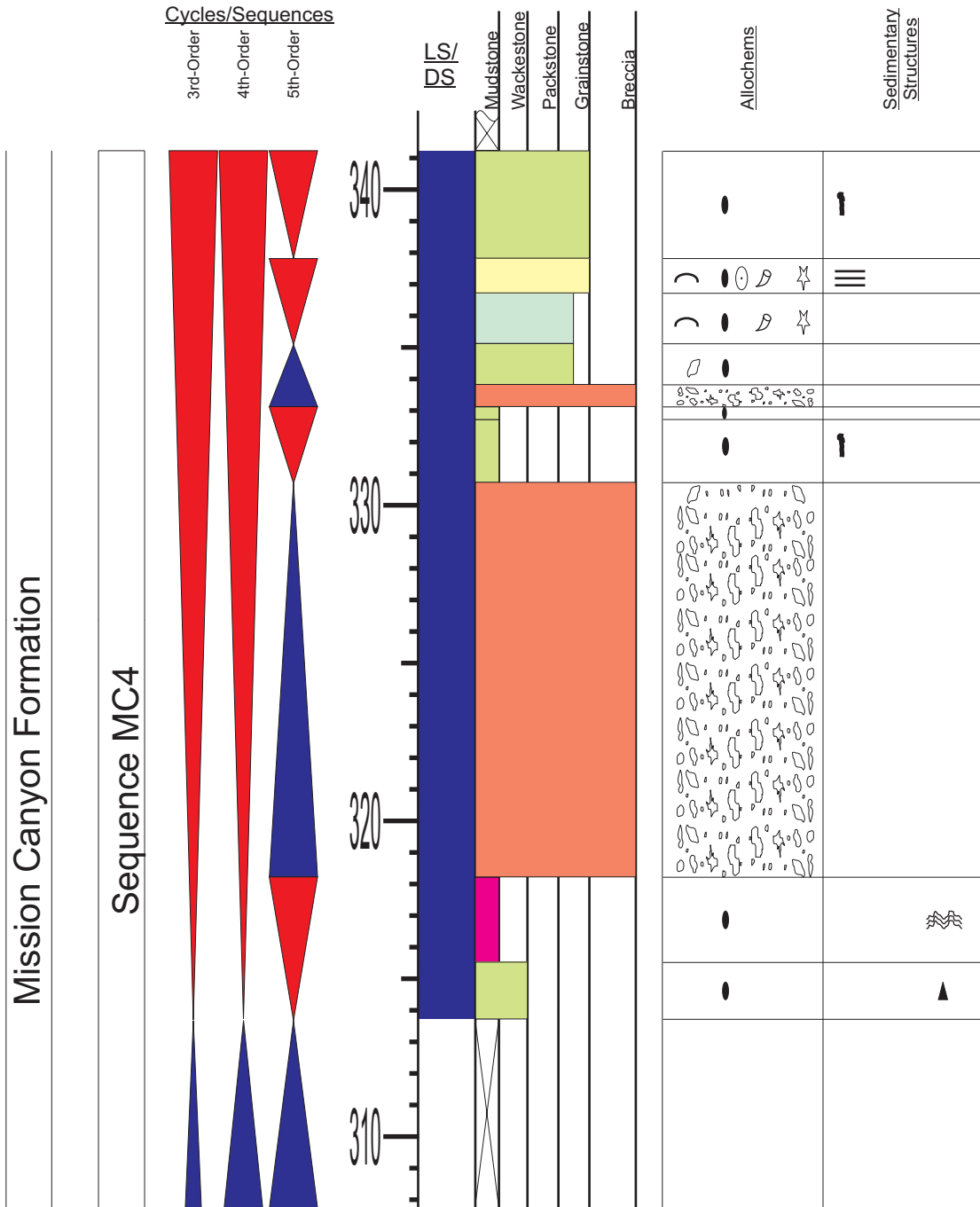
Appendix 7.7: Sedimentary section log for section Ashbough Canyon (Continued). Refer to Appendix 1 for symbols and Figure 3.6 for location.

APPENDIX 7.8



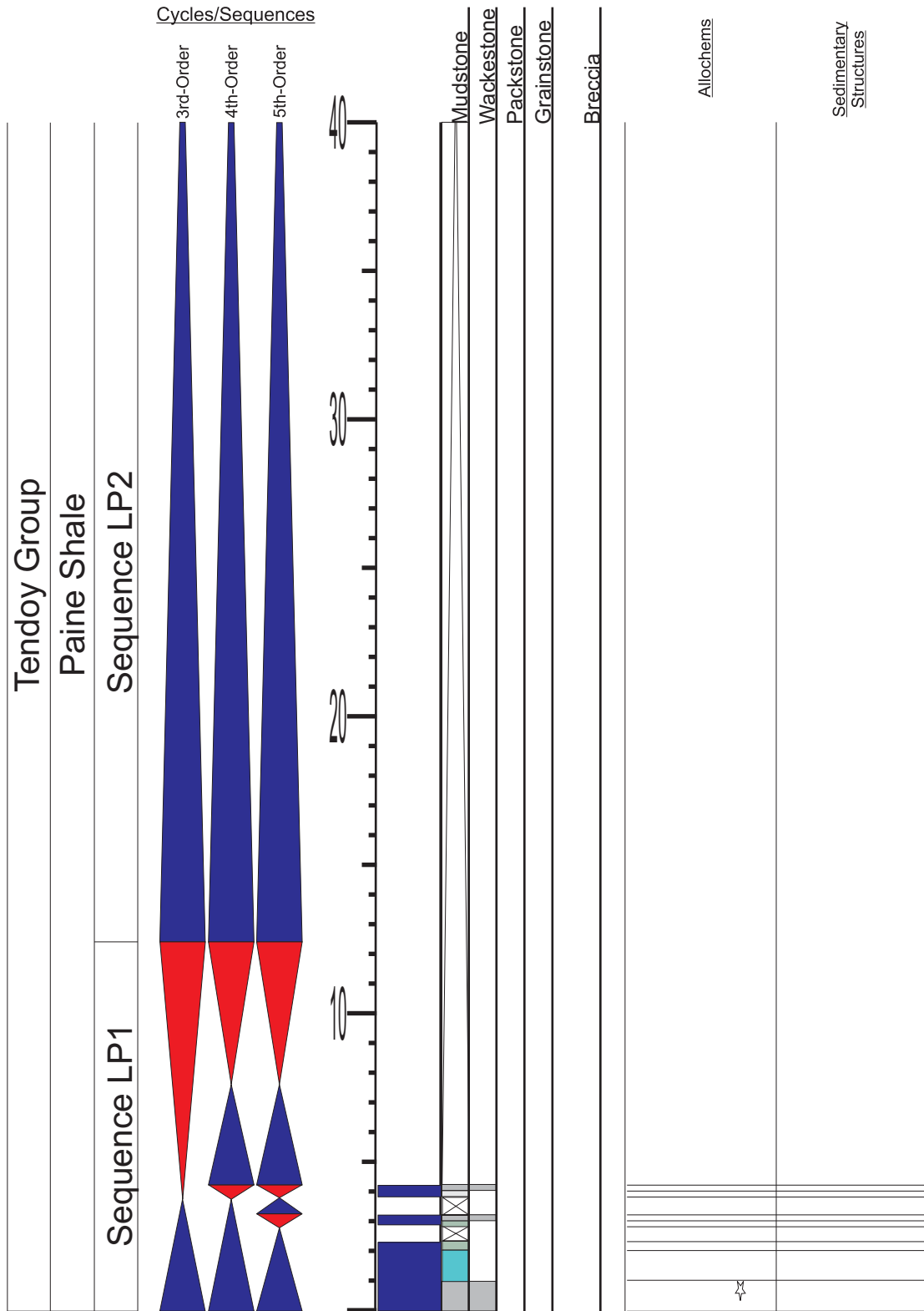
Appendix 7.8: Sedimentary section log for section Ashbough Canyon (Continued). Refer to Appendix 1 for symbols and Figure 3.6 for location.

APPENDIX 7.9



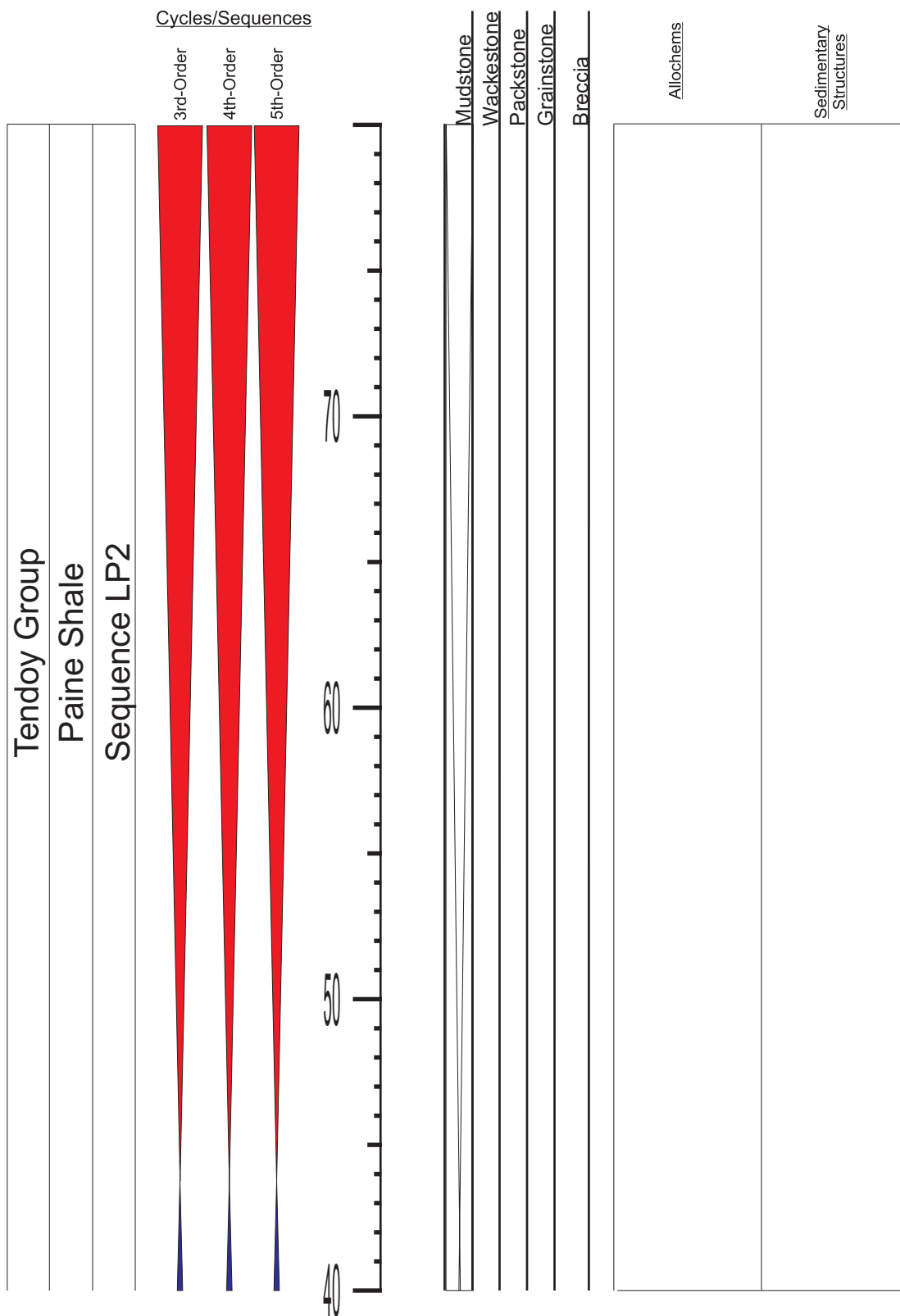
Appendix 7.9: Sedimentary section log for section Ashbough Canyon (Continued). Refer to Appendix 1 for symbols and Figure 3.6 for location.

APPENDIX 8.1



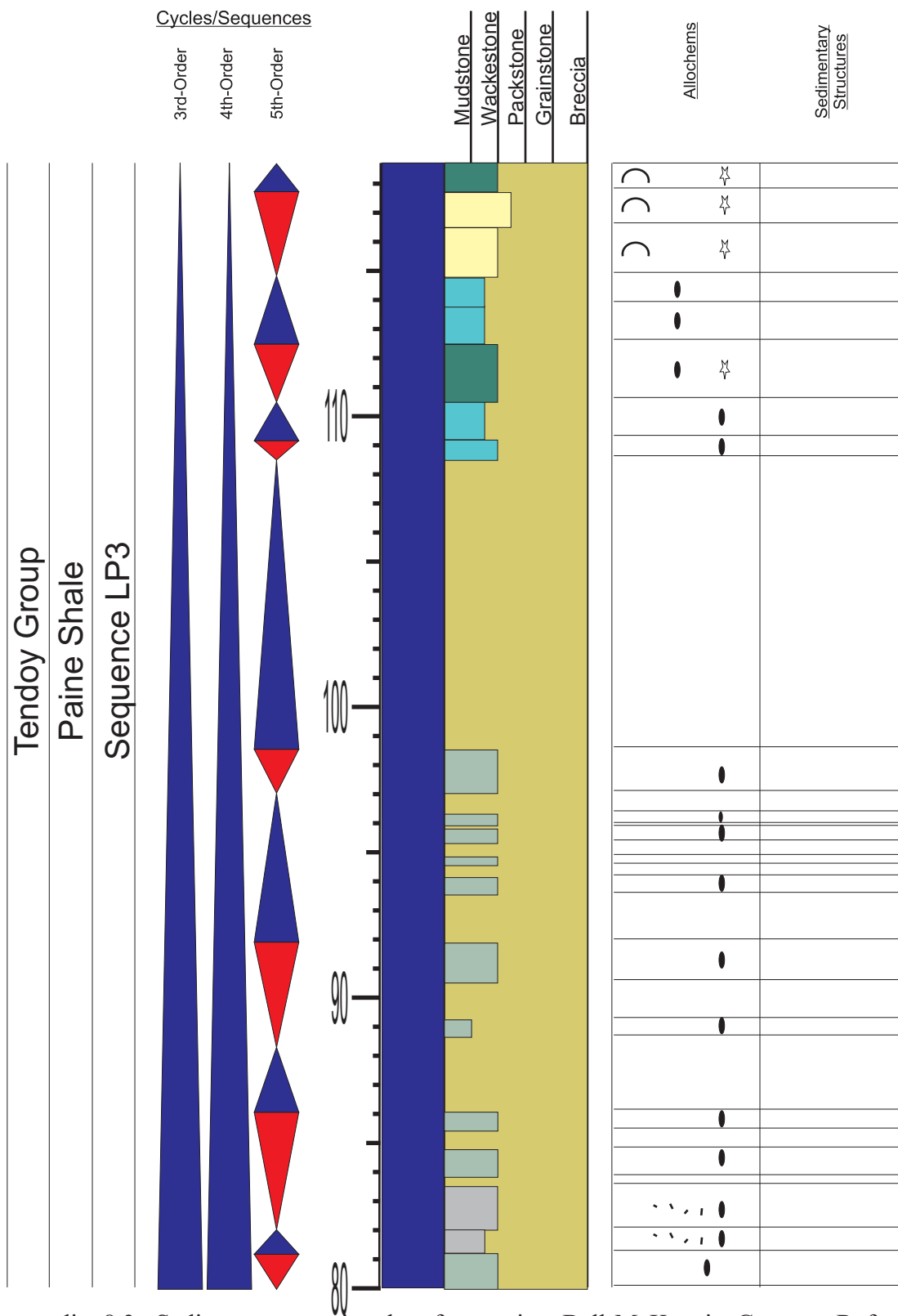
Appendix 8.1: Sedimentary section log for section Bell-McKenzie Canyon. Refer to Appendix 1 for symbols and Figure 3.6 for location.

APPENDIX 8.2



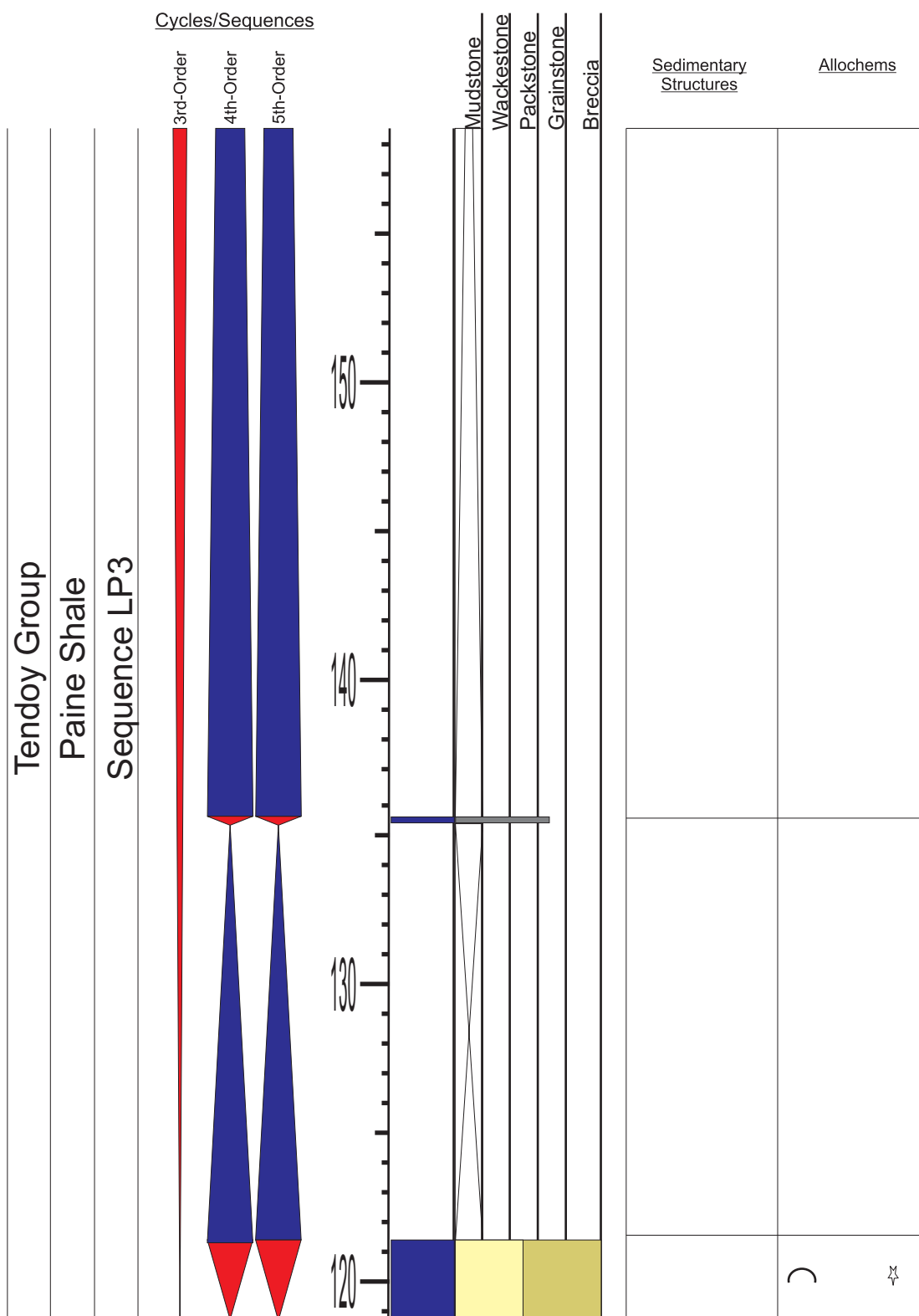
Appendix 8.2: Sedimentary section log for section Bell-McKenzie Canyon. Refer to Appendix 1 for symbols and Figure 3.6 for location.

APPENDIX 8.3



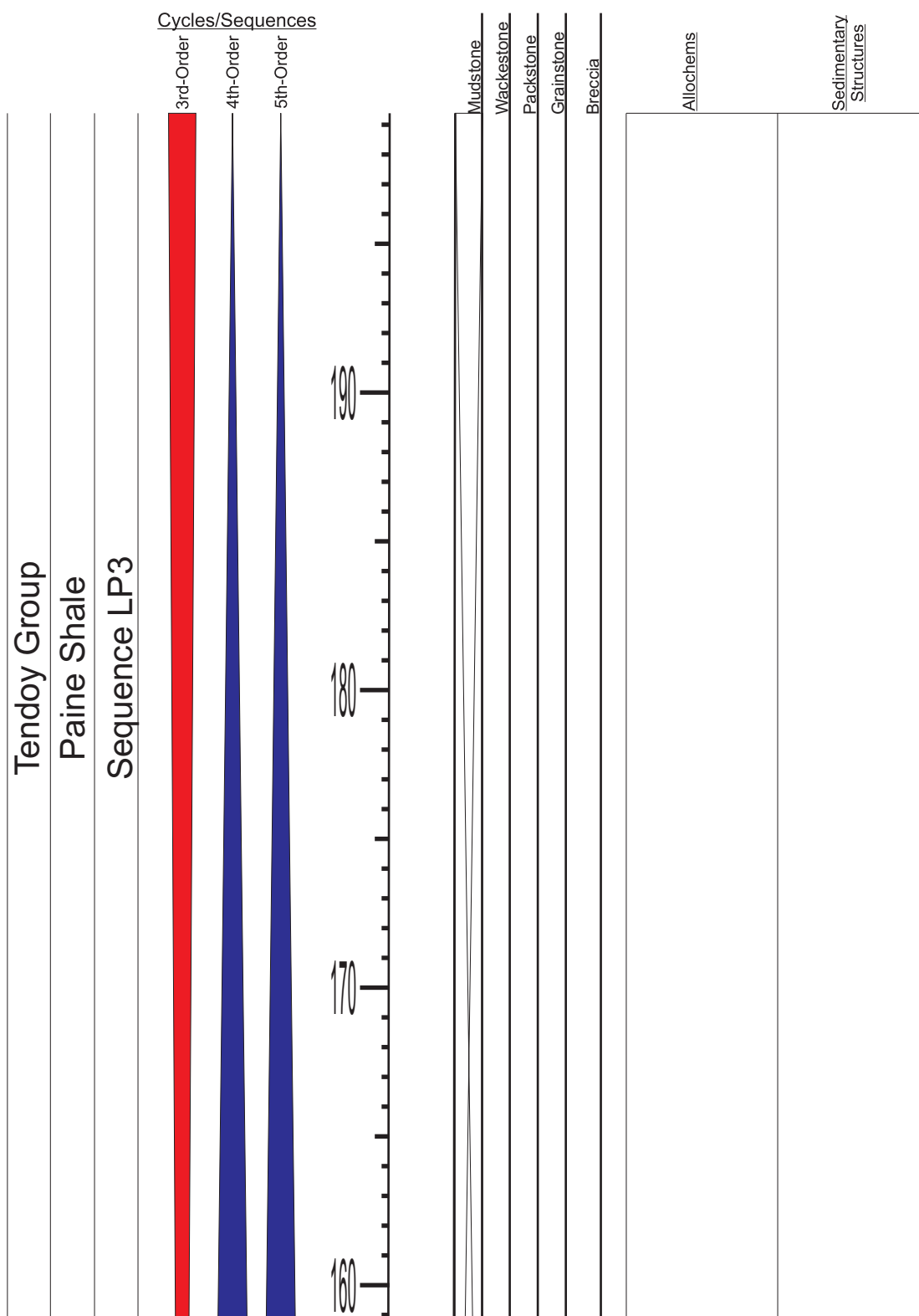
Appendix 8.3: Sedimentary section log for section Bell-McKenzie Canyon. Refer to Appendix 1 for symbols and Figure 3.6 for location.

APPENDIX 8.4



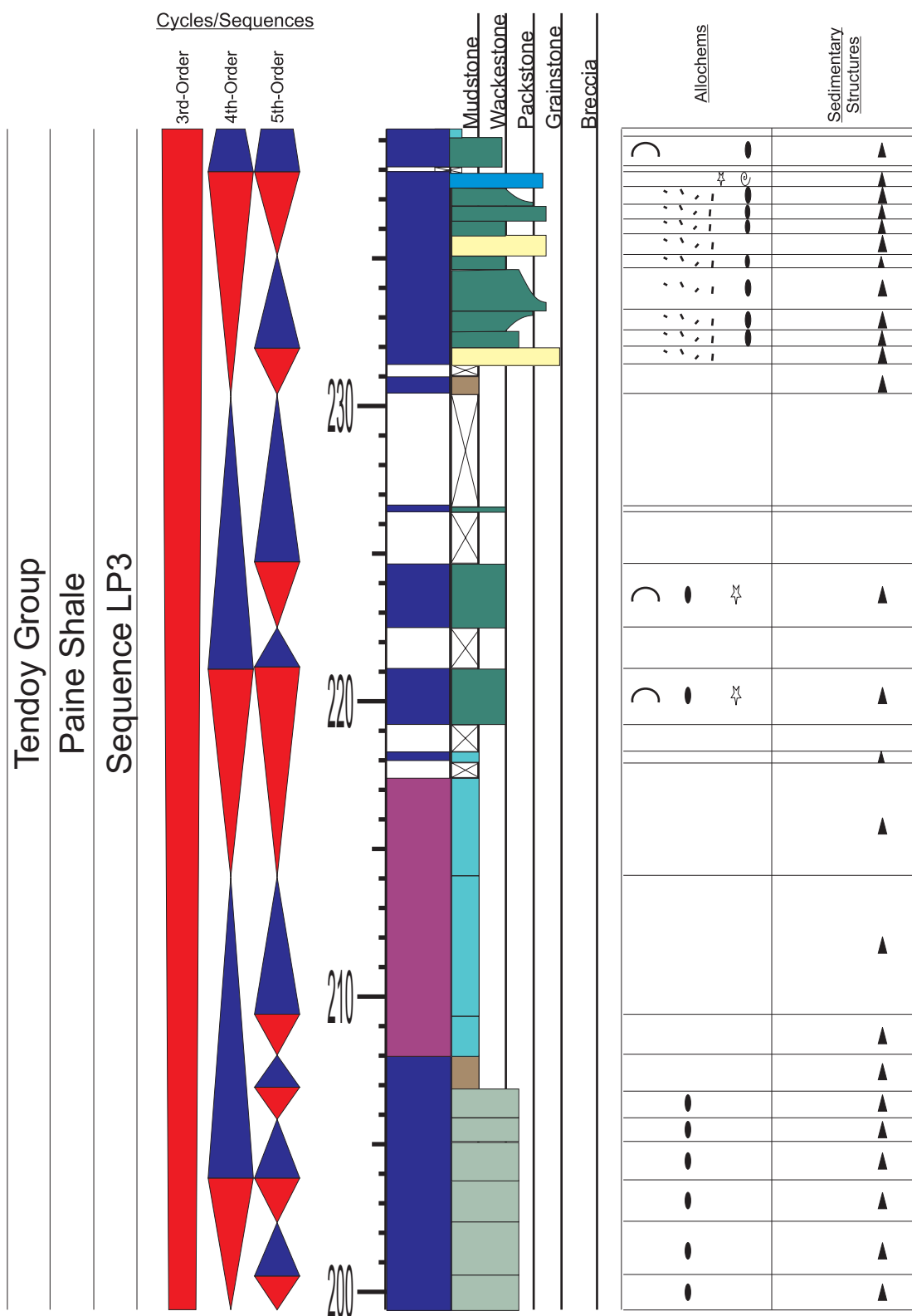
Appendix 8.4: Sedimentary section log for section Bell-McKenzie Canyon. Refer to Appendix 1 for symbols and Figure 3.6 for location.

APPENDIX 8.5



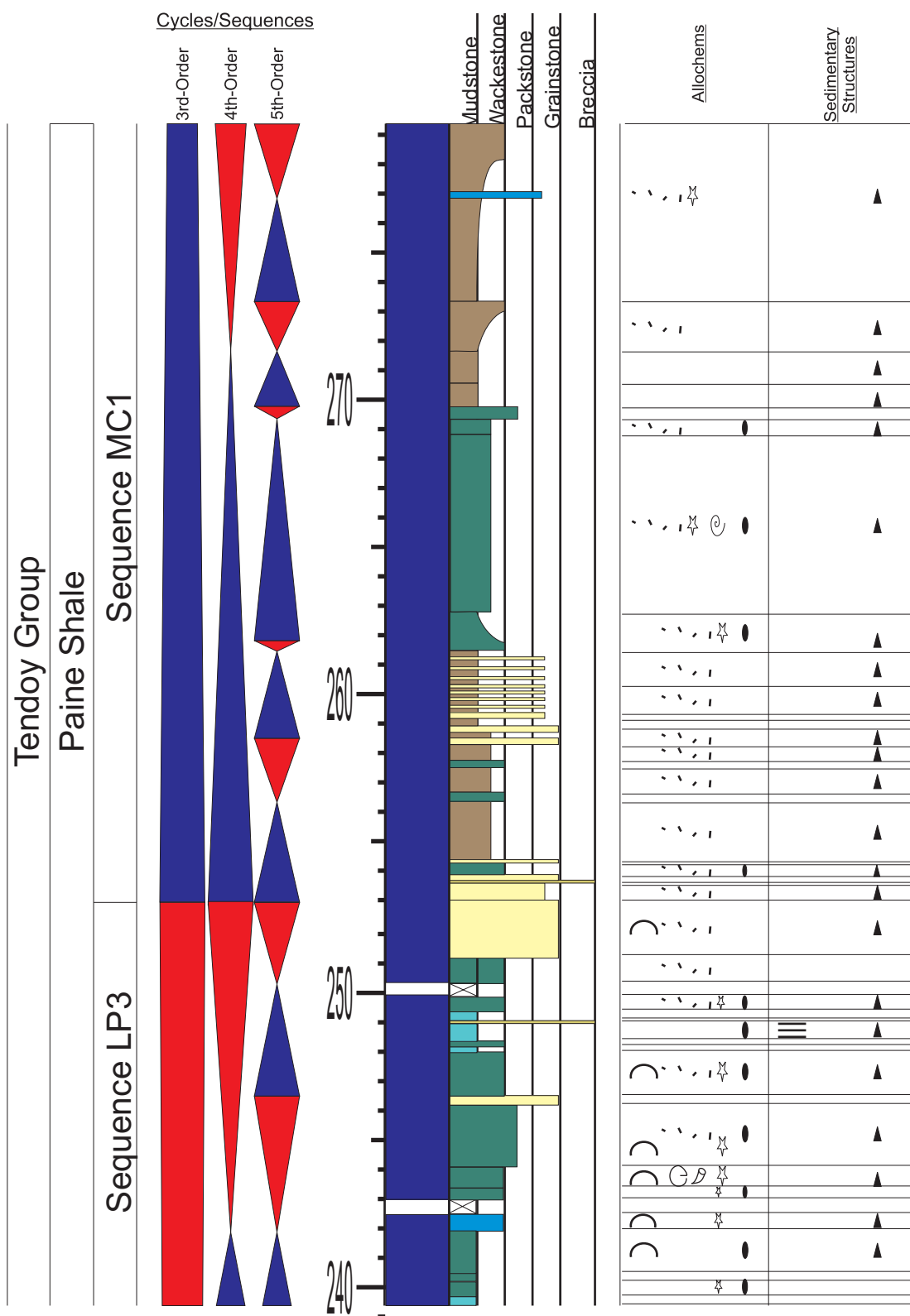
Appendix 8.5: Sedimentary section log for section Bell-McKenzie Canyon. Refer to Appendix 1 for symbols and Figure 3.6 for location.

APPENDIX 8.6



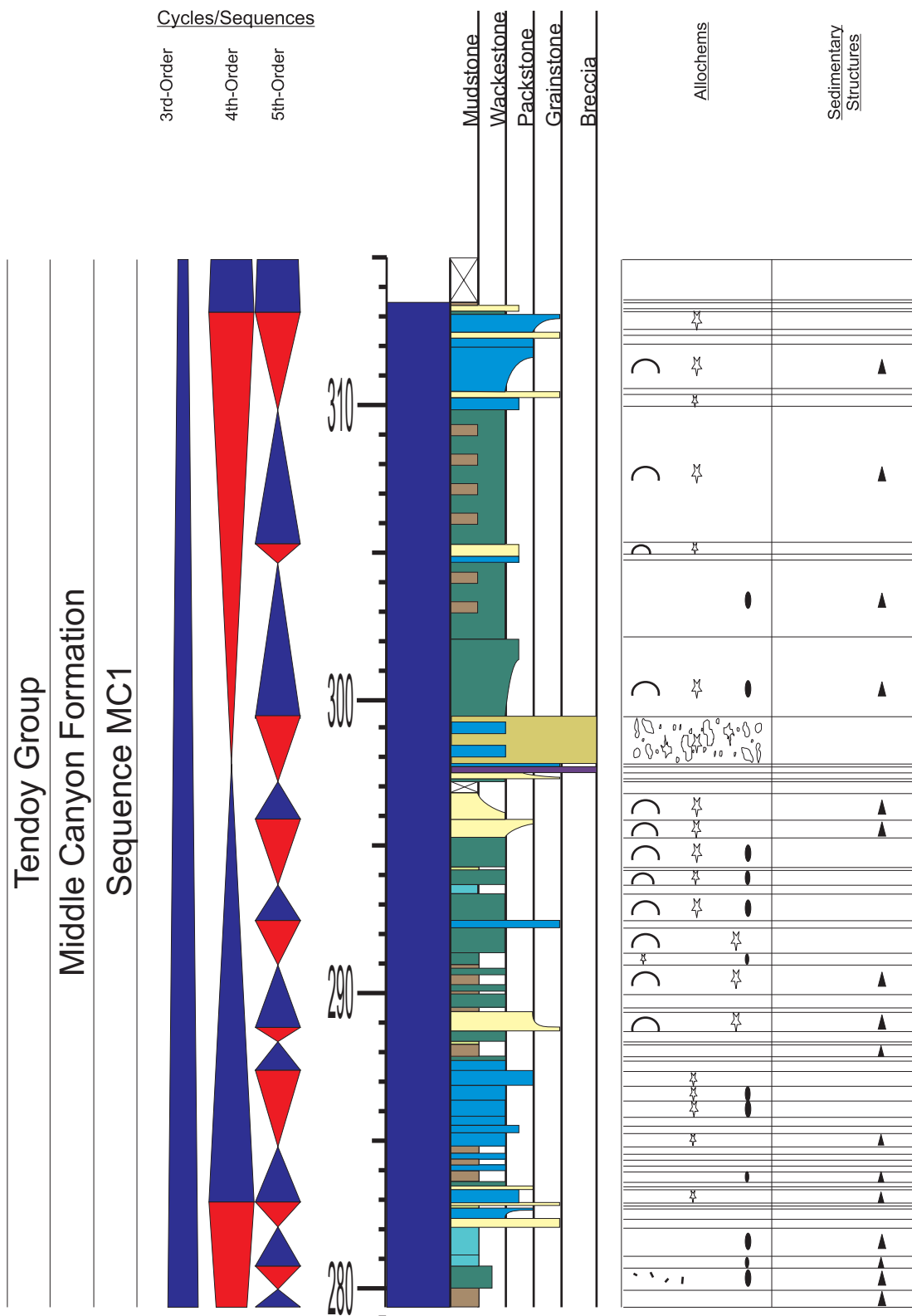
Appendix 8.6: Sedimentary section log for section Bell-McKenzie Canyon. Refer to Appendix 1 for symbols and Figure 3.6 for location.

APPENDIX 8.7



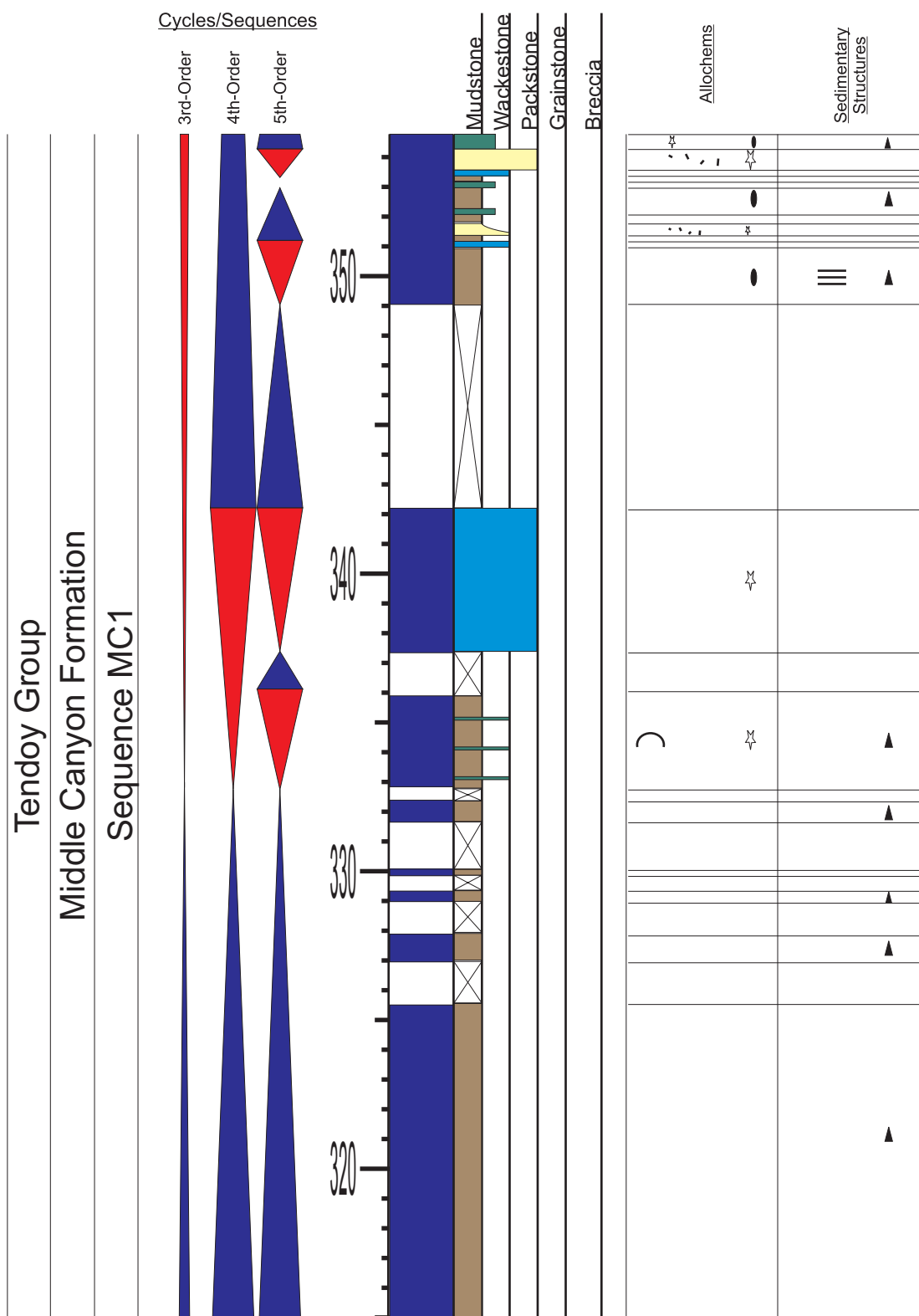
Appendix 8.7: Sedimentary section log for section Bell-McKenzie Canyon. Refer to Appendix 1 for symbols and Figure 3.6 for location.

APPENDIX 8.8



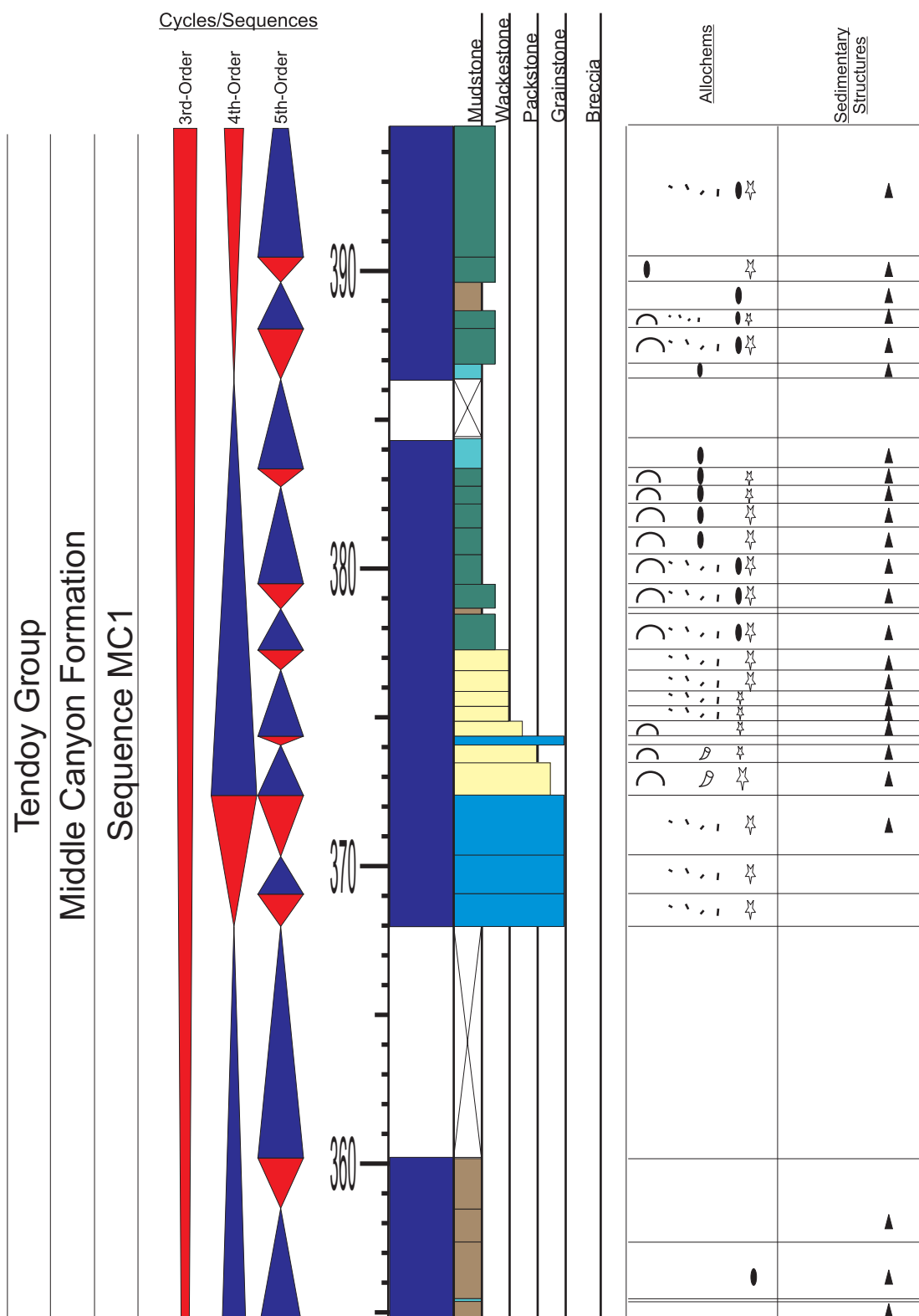
Appendix 8.8: Sedimentary section log for section Bell-McKenzie Canyon. Refer to Appendix 1 for symbols and Figure 3.6 for location.

APPENDIX 8.9



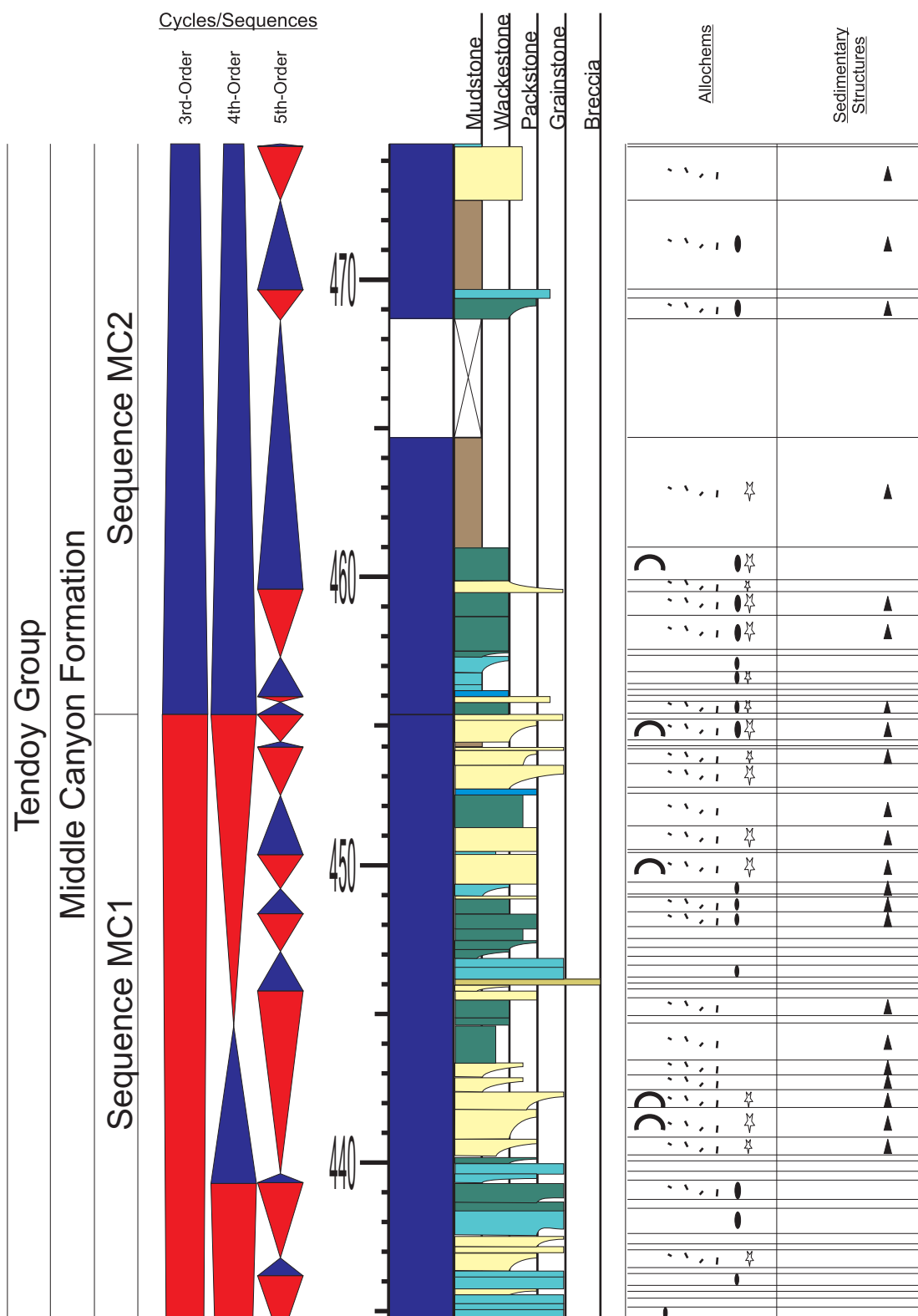
Appendix 8.9: Sedimentary section log for section Bell-McKenzie Canyon. Refer to Appendix 1 for symbols and Figure 3.6 for location.

APPENDIX 8.10



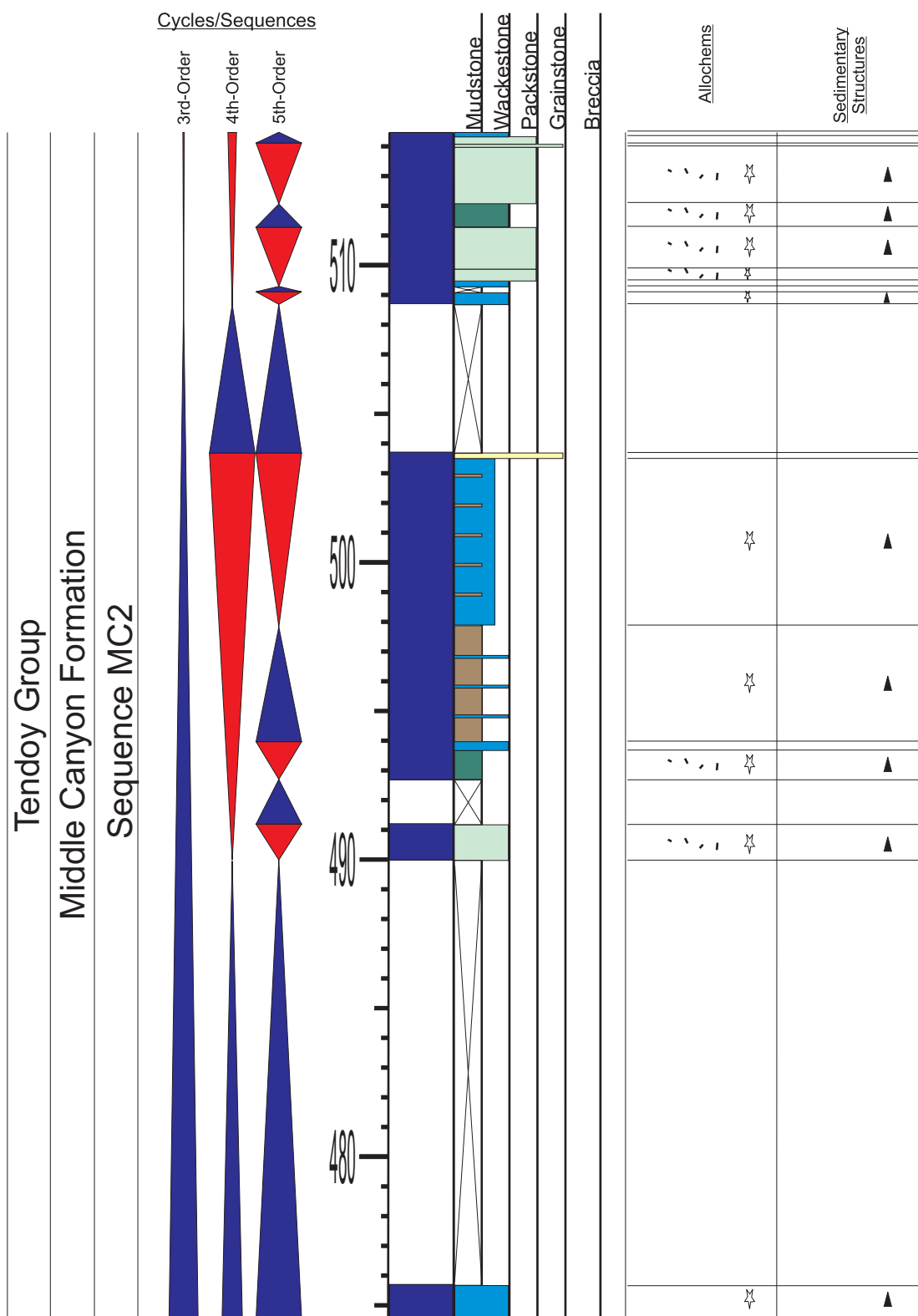
Appendix 8.10: Sedimentary section log for section Bell-McKenzie Canyon. Refer to Appendix 1 for symbols and Figure 3.6 for location.

APPENDIX 8.12



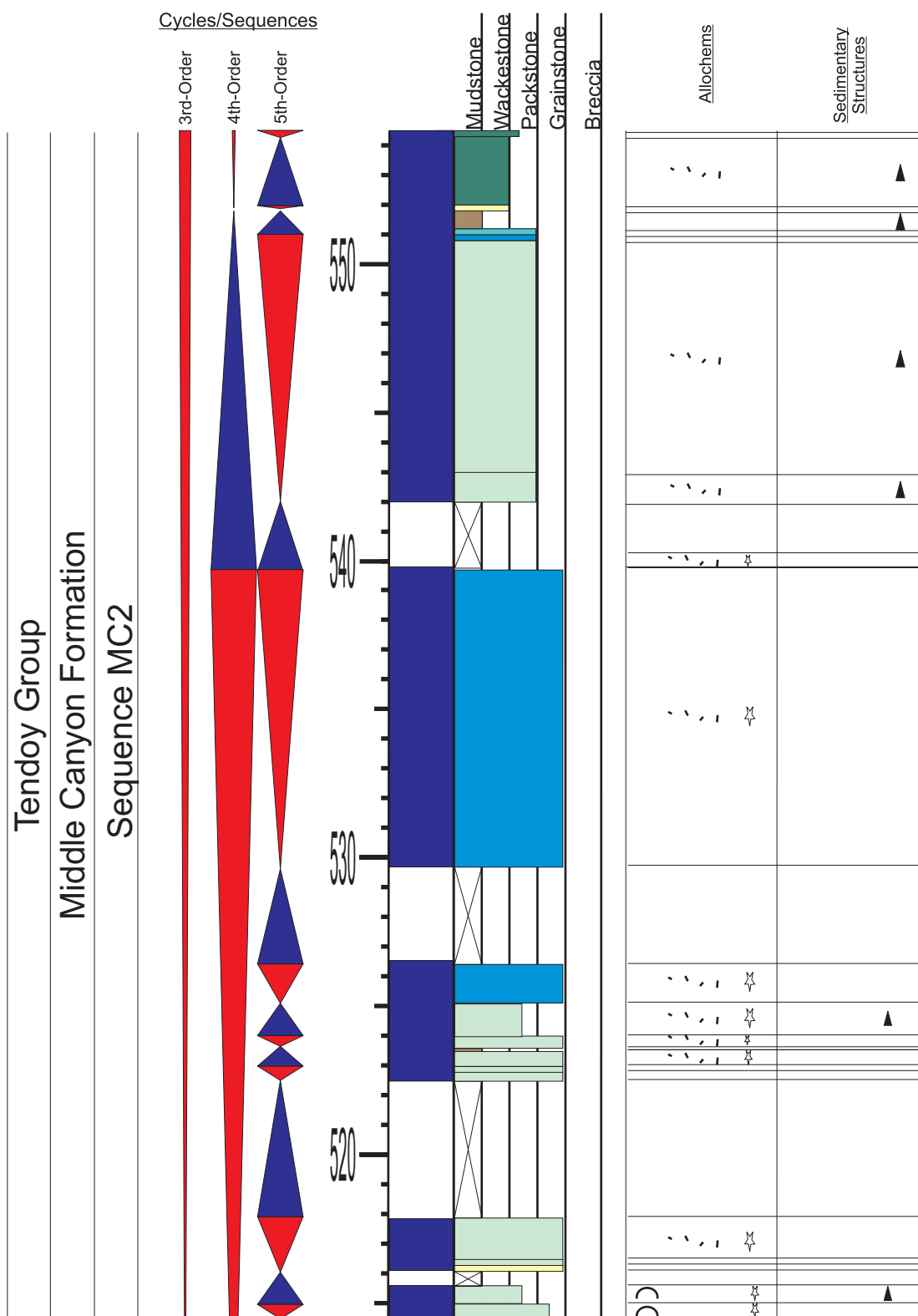
Appendix 8.12: Sedimentary section log for section Bell-McKenzie Canyon. Refer to Appendix 1 for symbols and Figure 3.6 for location.

APPENDIX 8.13



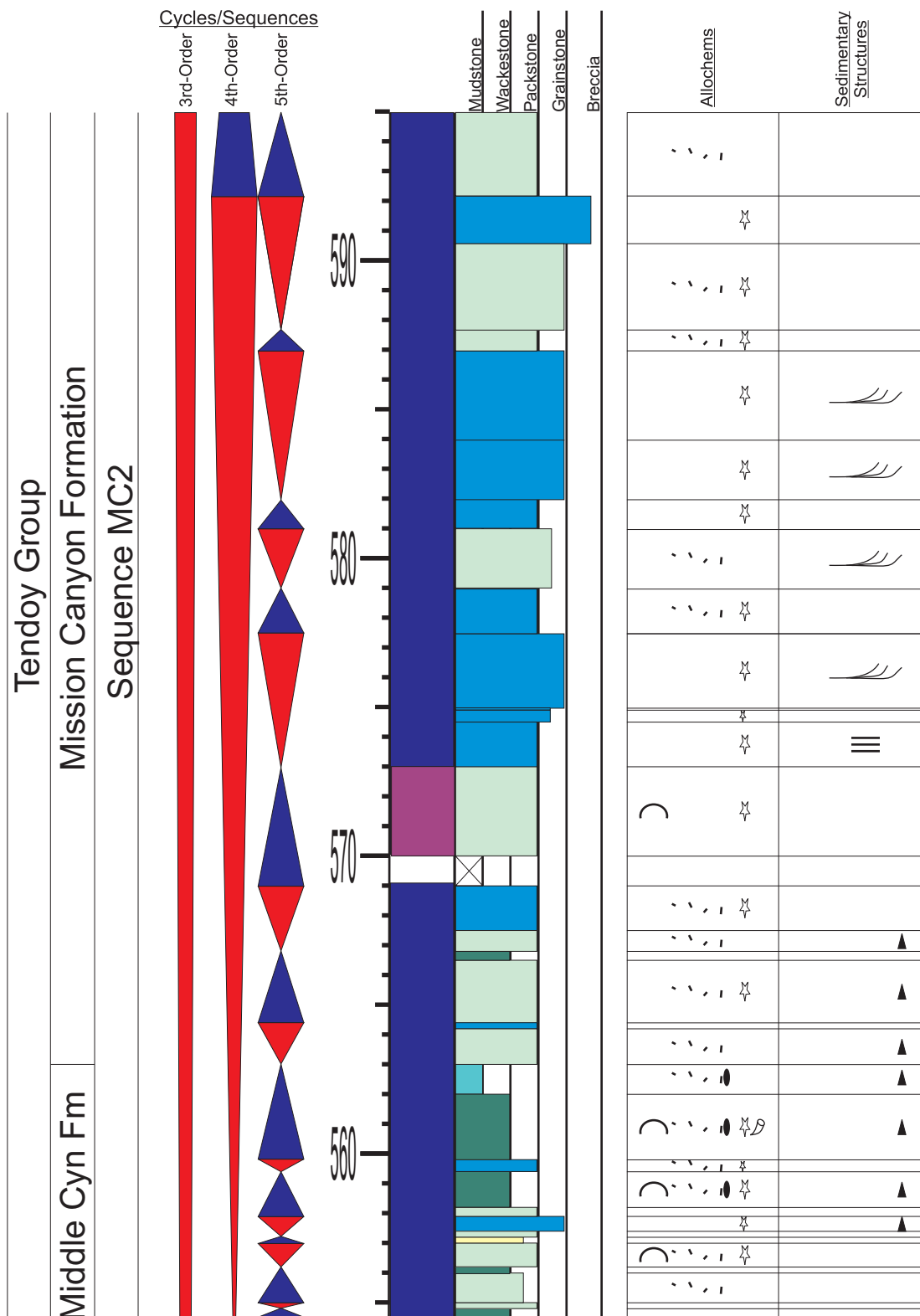
Appendix 8.13: Sedimentary section log for section Bell-McKenzie Canyon. Refer to Appendix 1 for symbols and Figure 3.6 for location.

APPENDIX 8.14



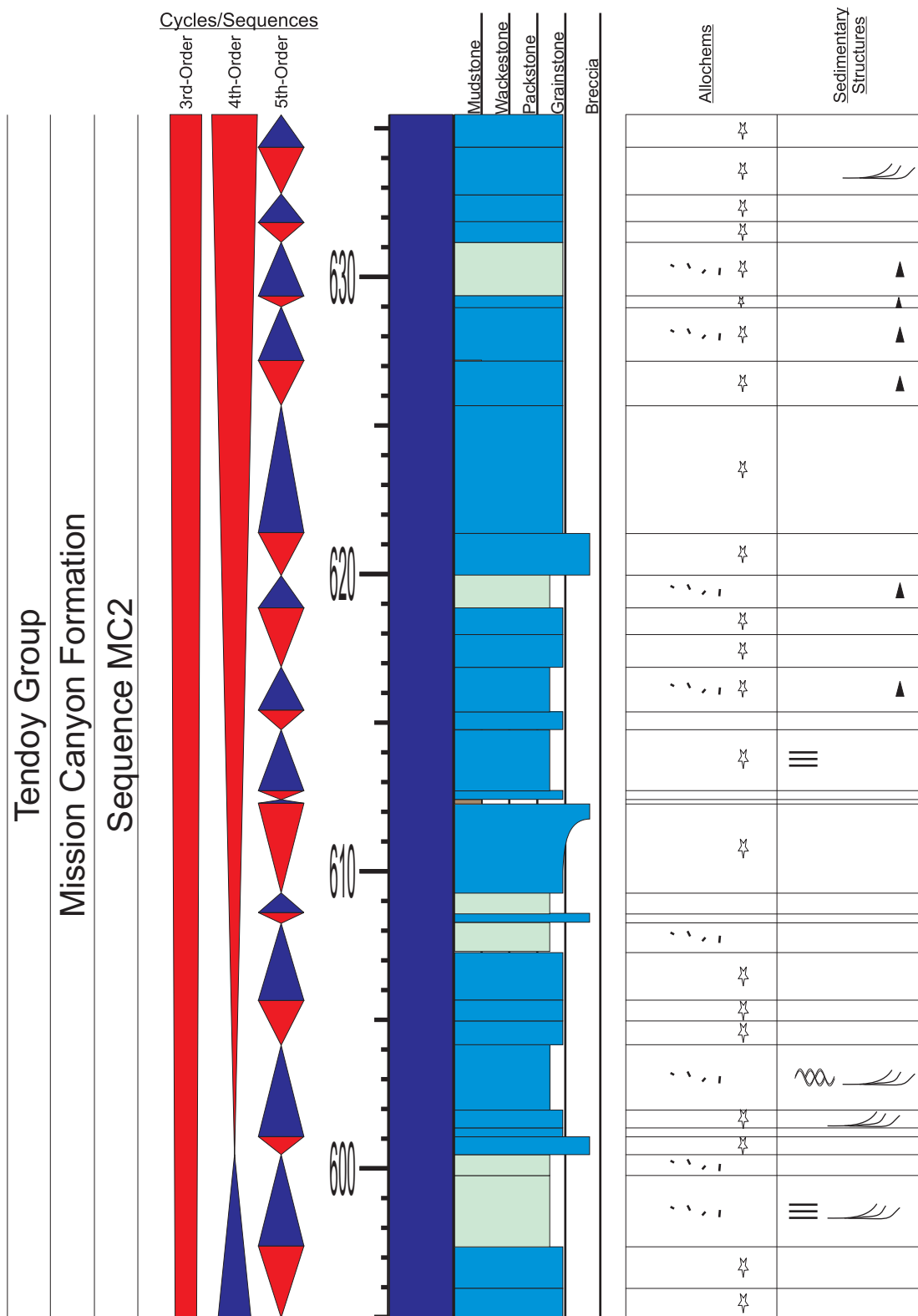
Appendix 8.14: Sedimentary section log for section Bell-McKenzie Canyon. Refer to Appendix 1 for symbols and Figure 3.6 for location.

APPENDIX 8.15



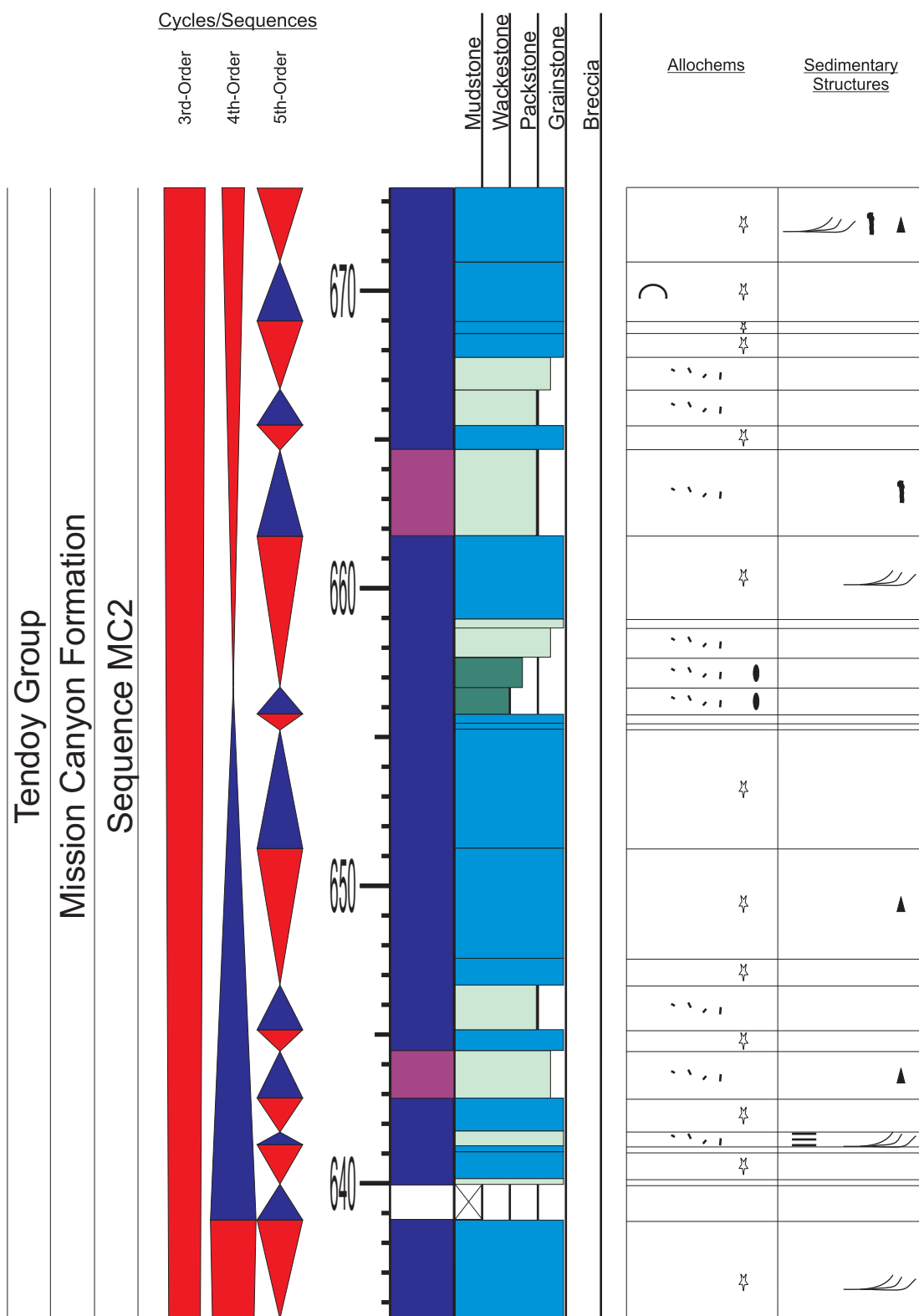
Appendix 8.15: Sedimentary section log for section Bell-McKenzie Canyon. Refer to Appendix 1 for symbols and Figure 3.6 for location.

APPENDIX 8.16



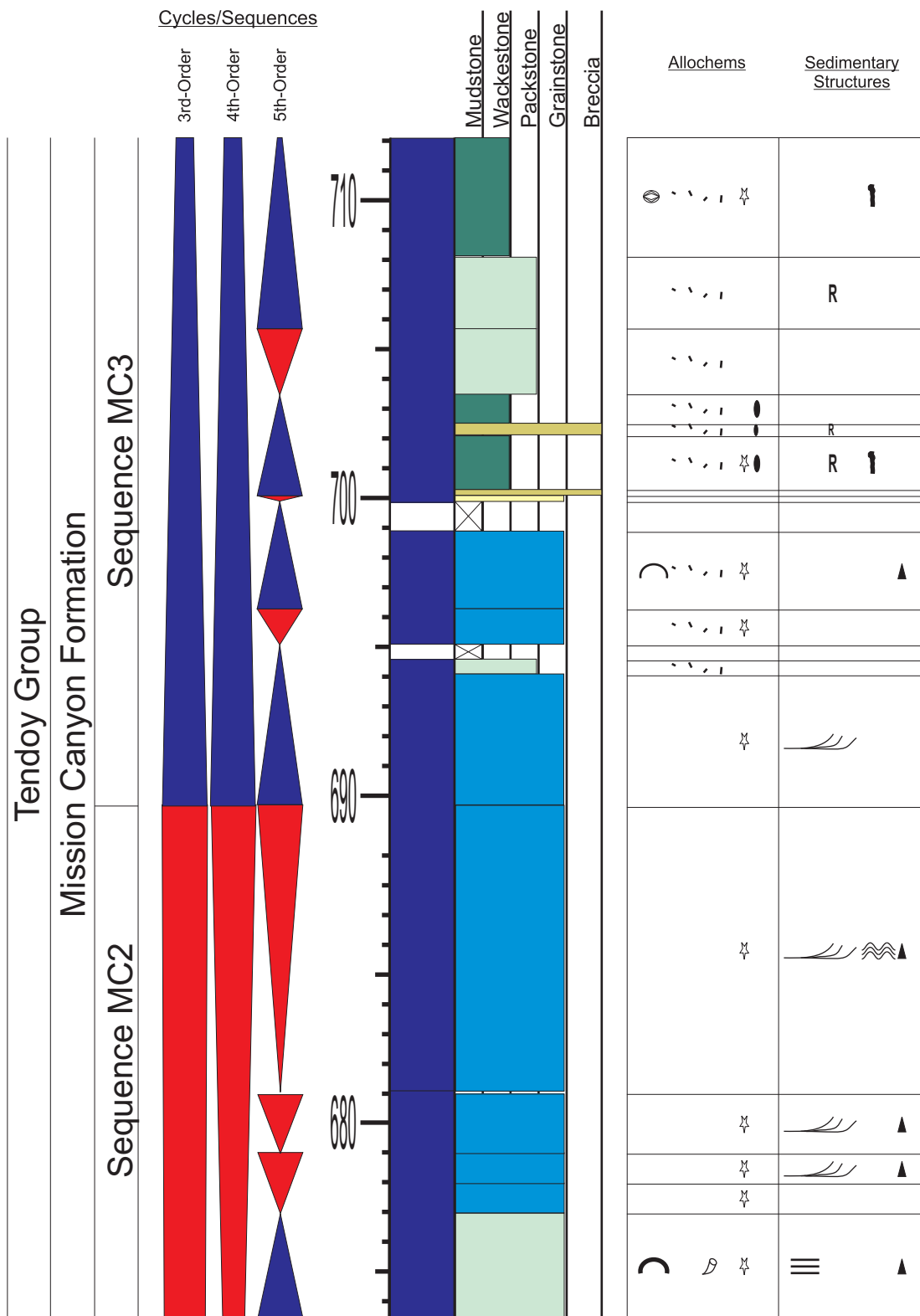
Appendix 8.16: Sedimentary section log for section Bell-McKenzie Canyon. Refer to Appendix 1 for symbols and Figure 3.6 for location.

APPENDIX 8.17



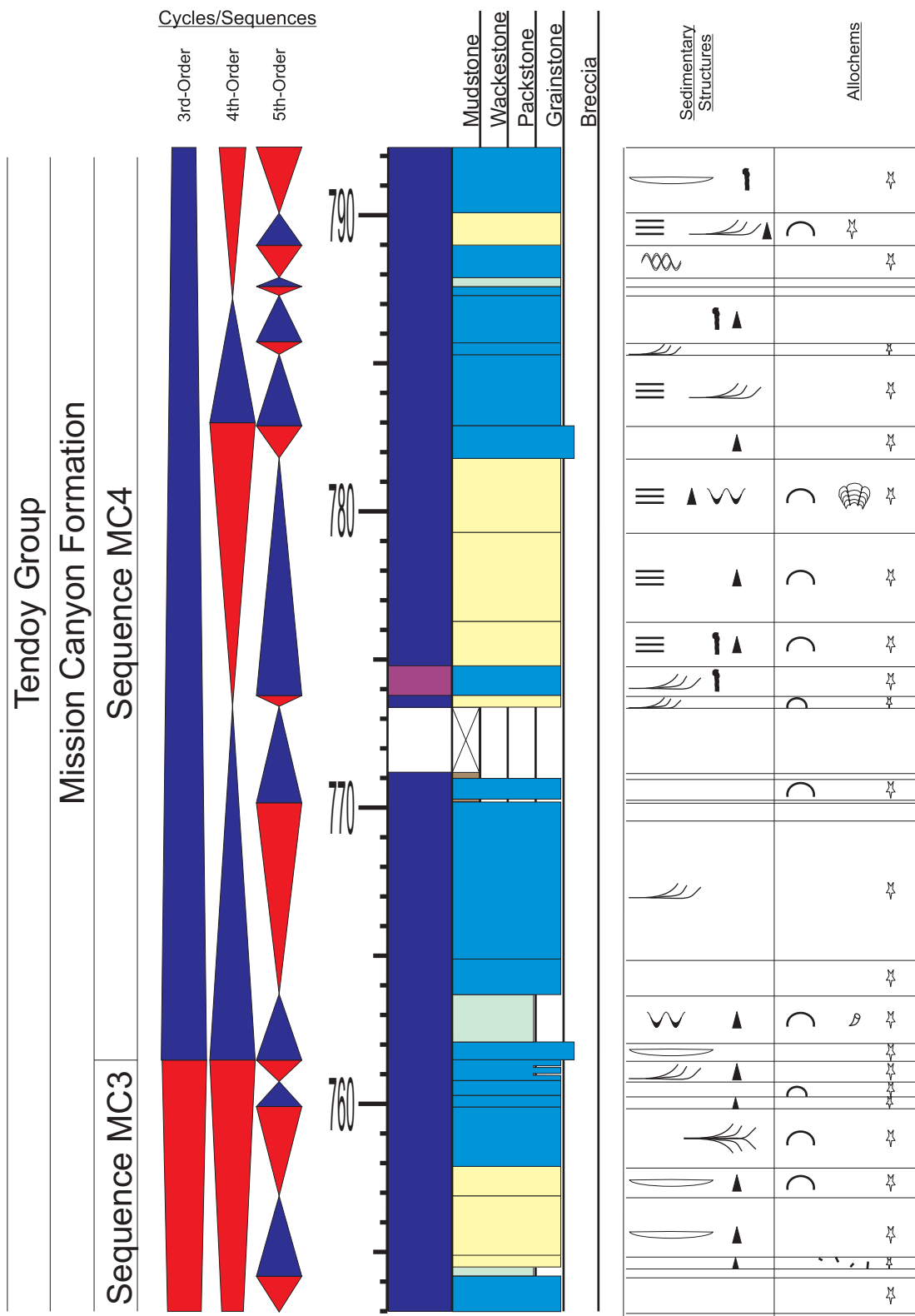
Appendix 8.17: Sedimentary section log for section Bell-McKenzie Canyon. Refer to Appendix 1 for symbols and Figure 3.6 for location.

APPENDIX 8.18



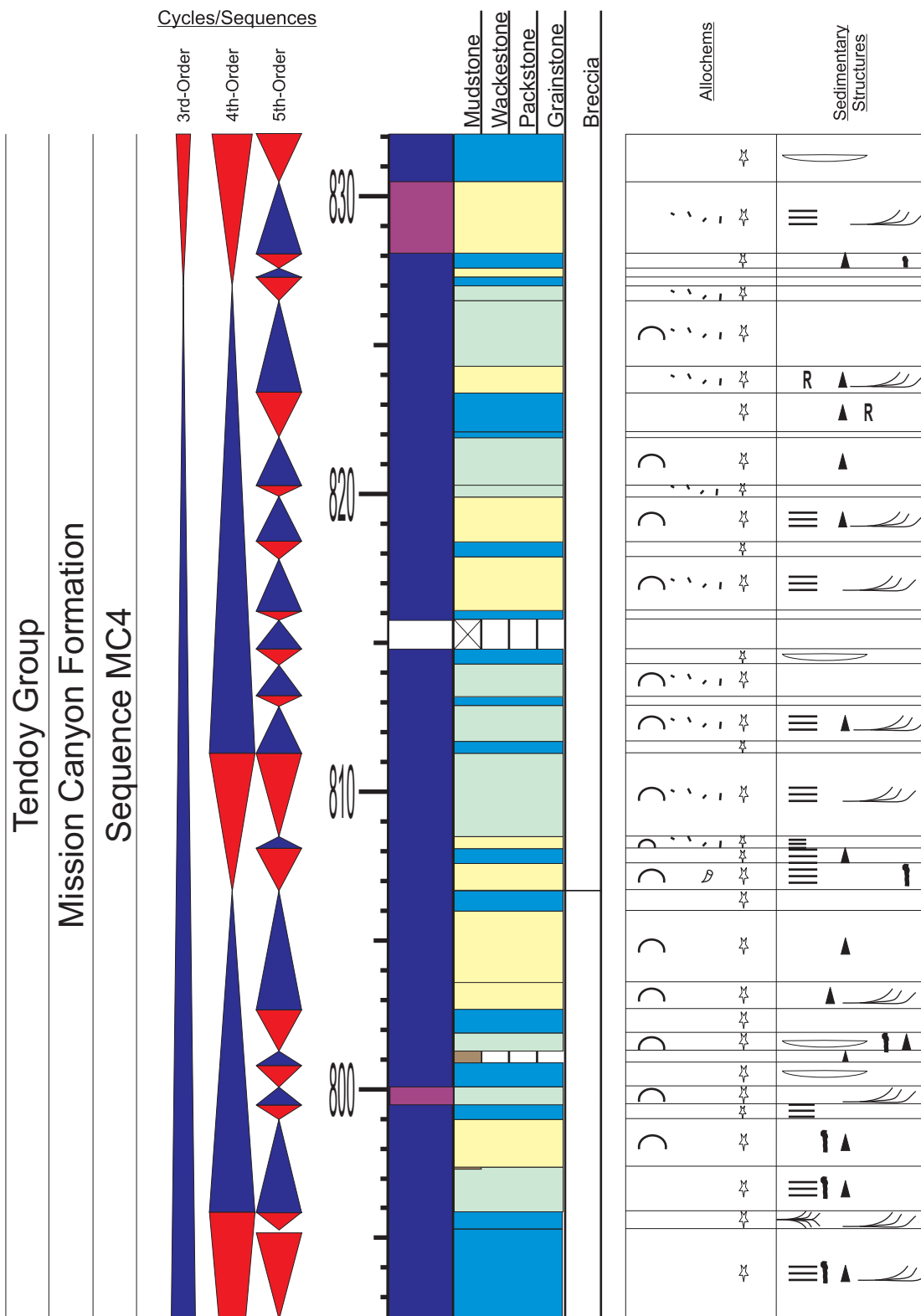
Appendix 8.18: Sedimentary section log for section Bell-McKenzie Canyon. Refer to Appendix 1 for symbols and Figure 3.6 for location.

APPENDIX 8.20



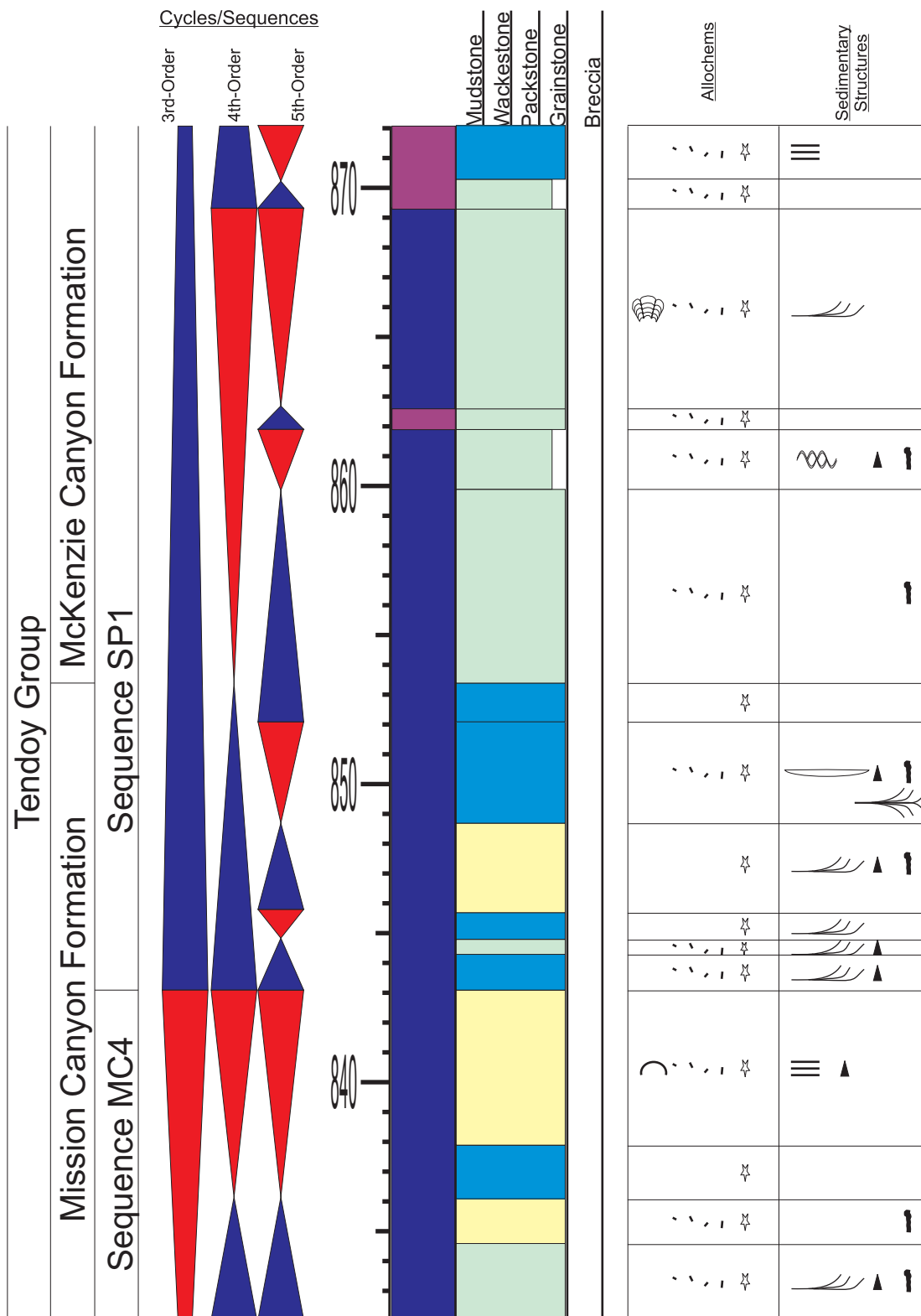
Appendix 8.20: Sedimentary section log for section Bell-McKenzie Canyon. Refer to Appendix 1 for symbols and Figure 3.6 for location.

APPENDIX 8.21



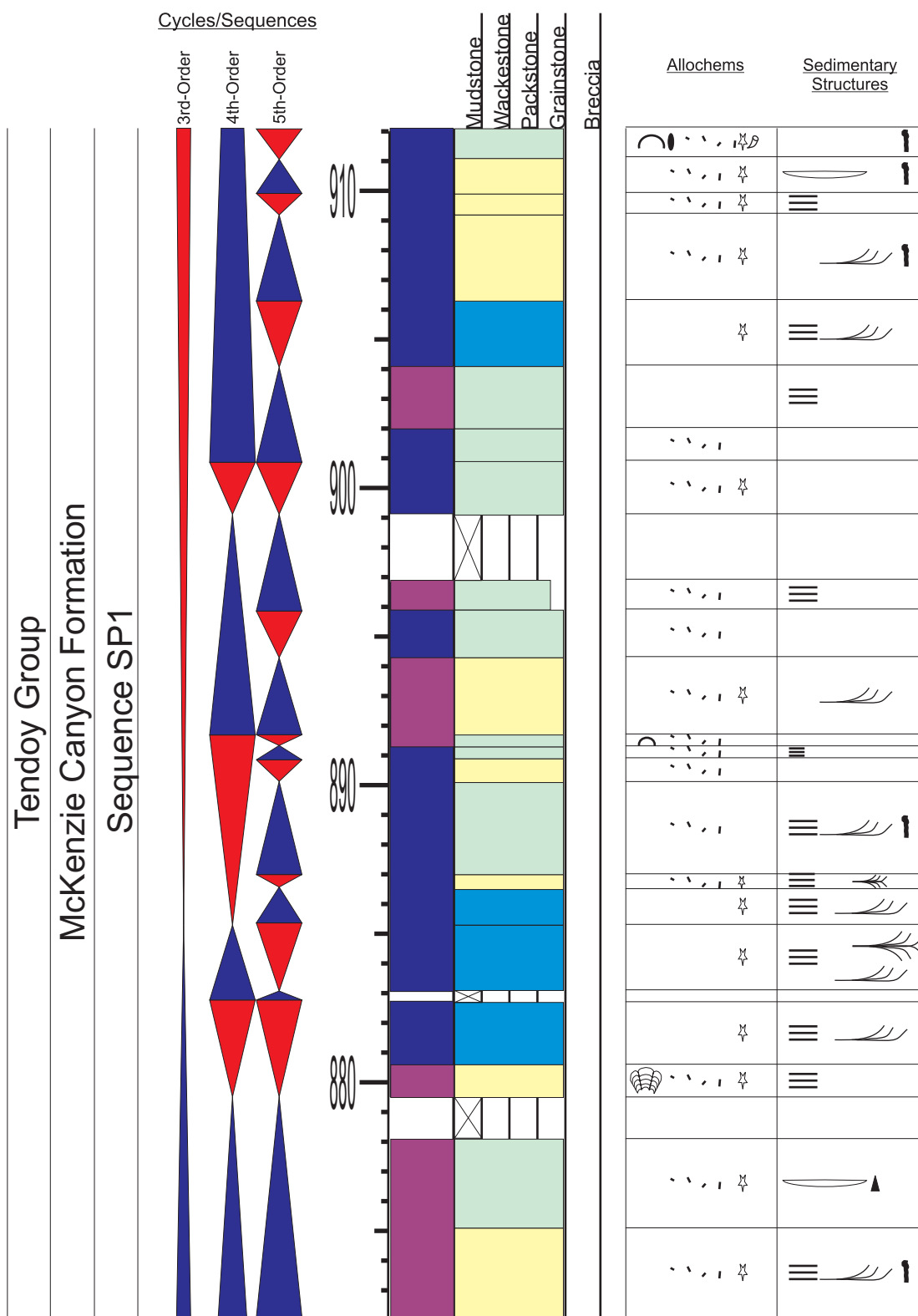
Appendix 8.21: Sedimentary section log for section Bell-McKenzie Canyon. Refer to Appendix 1 for symbols and Figure 3.6 for location.

APPENDIX 8.22



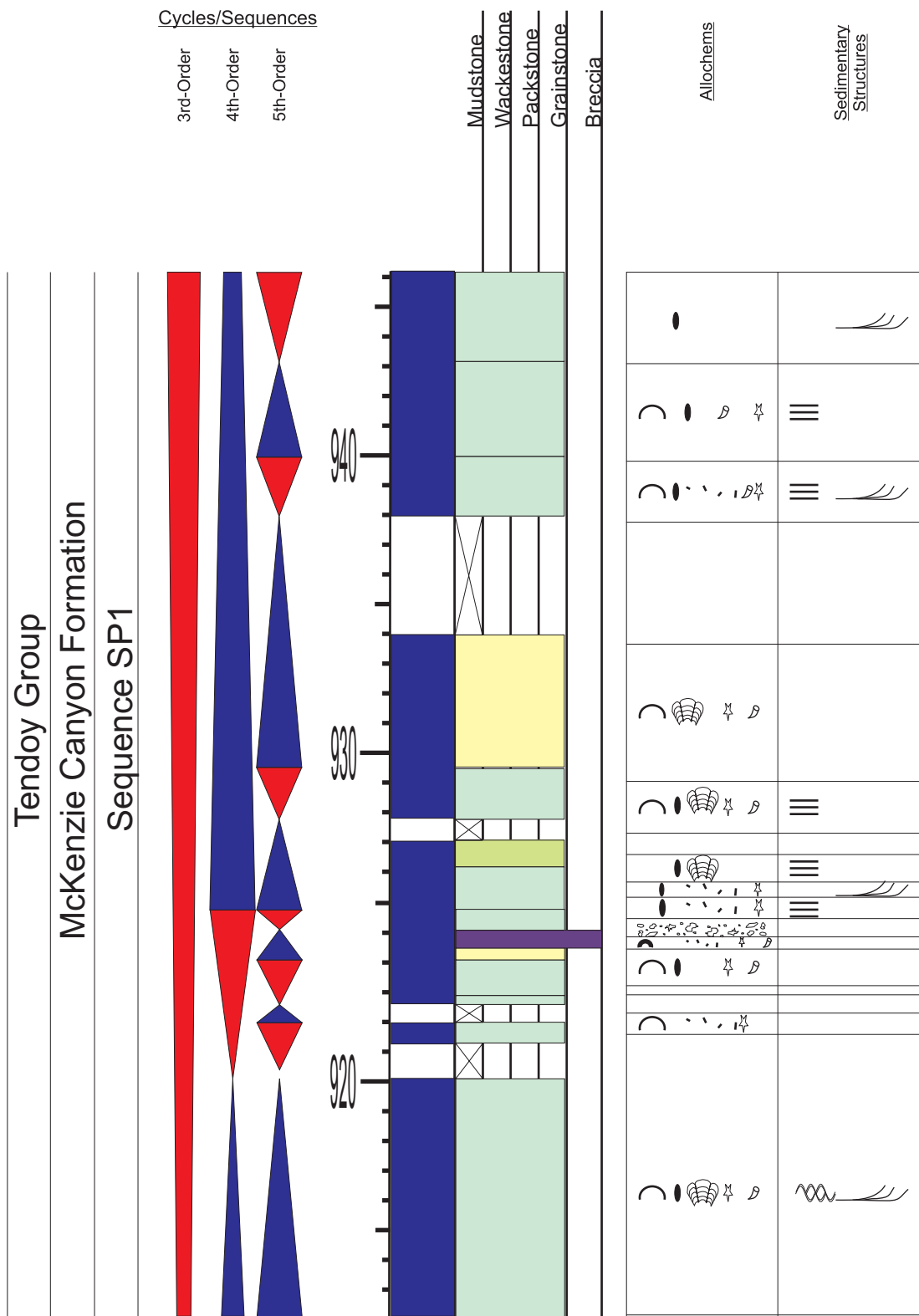
Appendix 8.22: Sedimentary section log for section Bell-McKenzie Canyon. Refer to Appendix 1 for symbols and Figure 3.6 for location.

APPENDIX 8.23



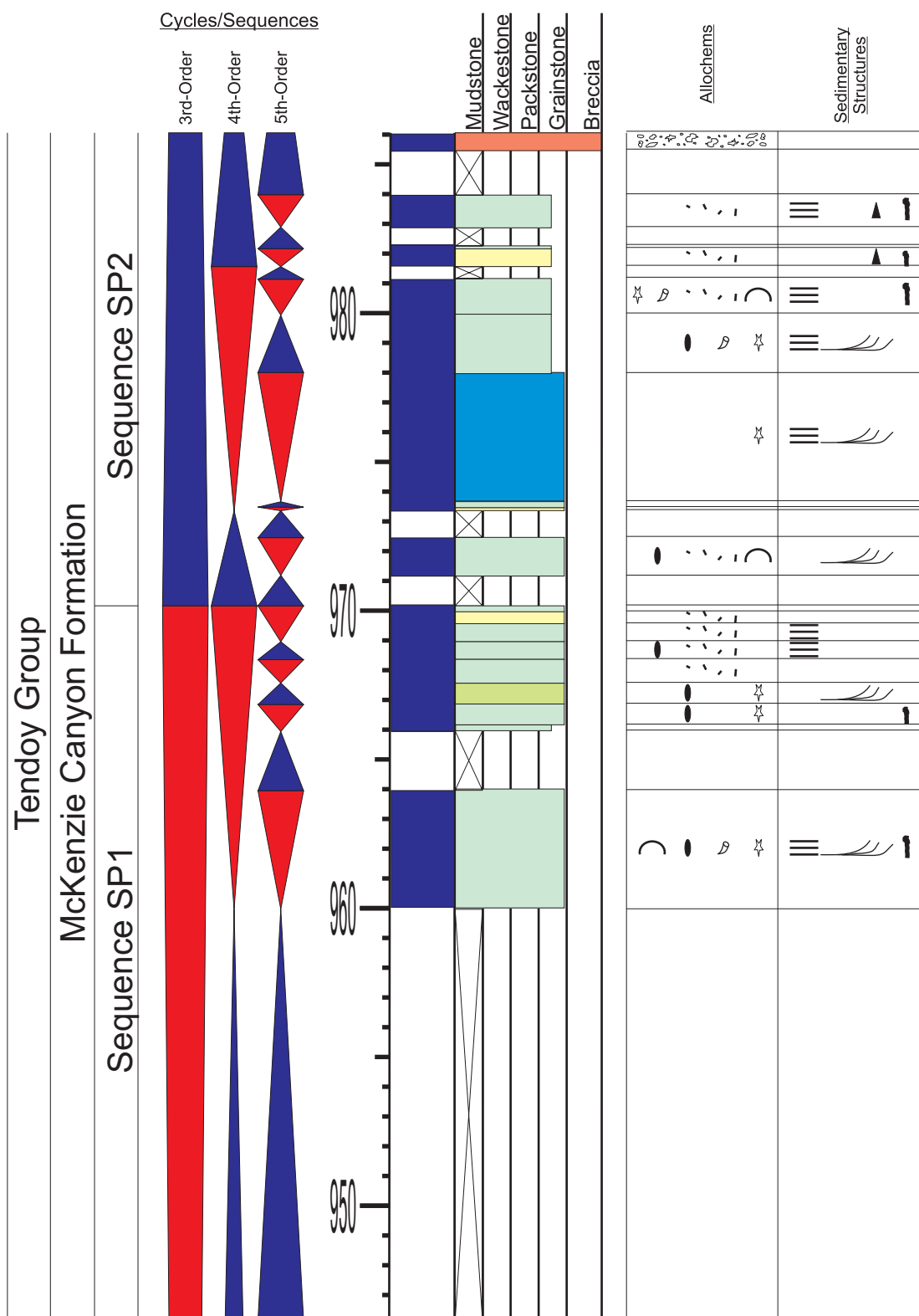
Appendix 8.23: Sedimentary section log for section Bell-McKenzie Canyon. Refer to Appendix 1 for symbols and Figure 3.6 for location.

APPENDIX 8.24



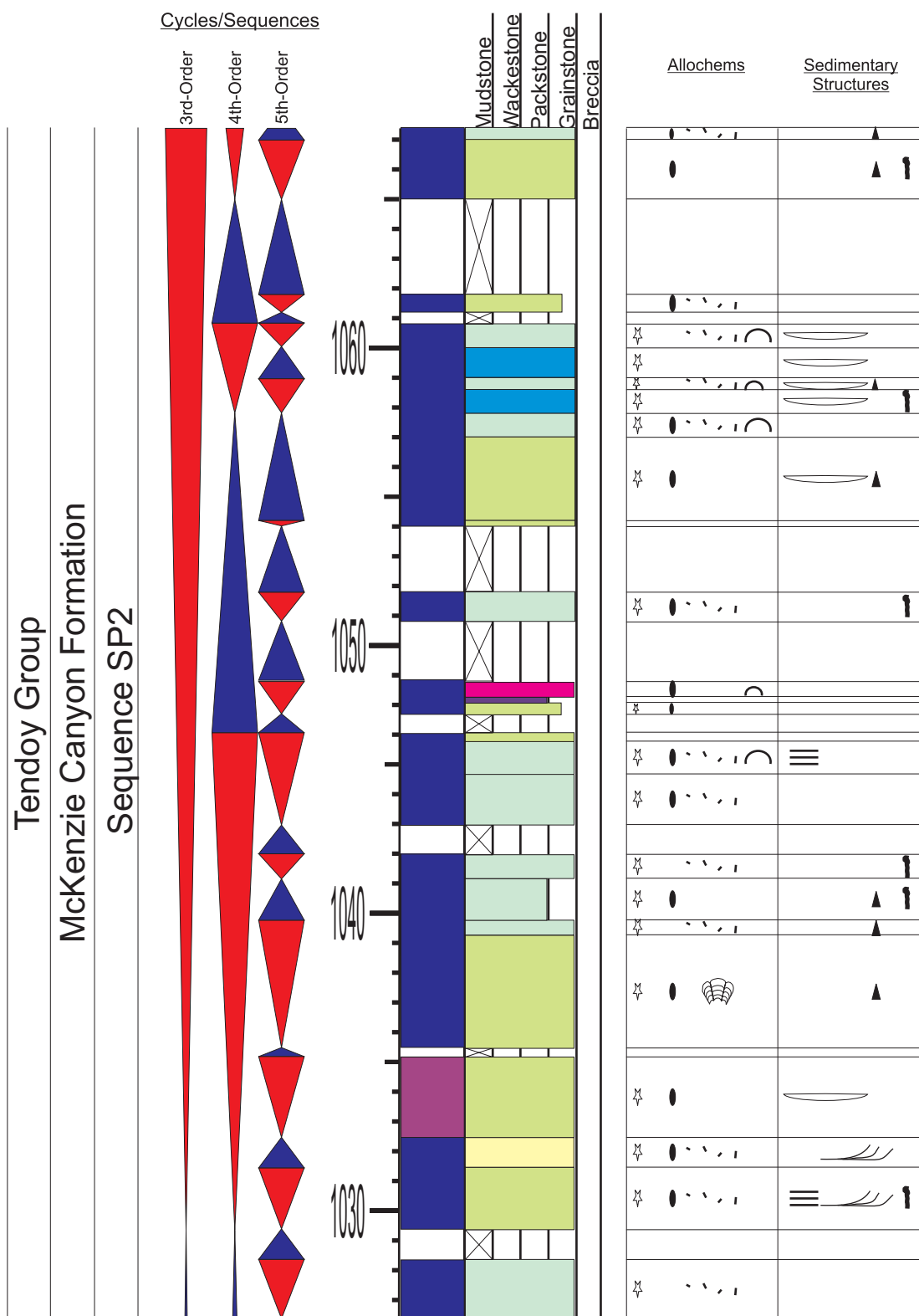
Appendix 8.24: Sedimentary section log for section Bell-McKenzie Canyon. Refer to Appendix 1 for symbols and Figure 3.6 for location.

APPENDIX 8.25



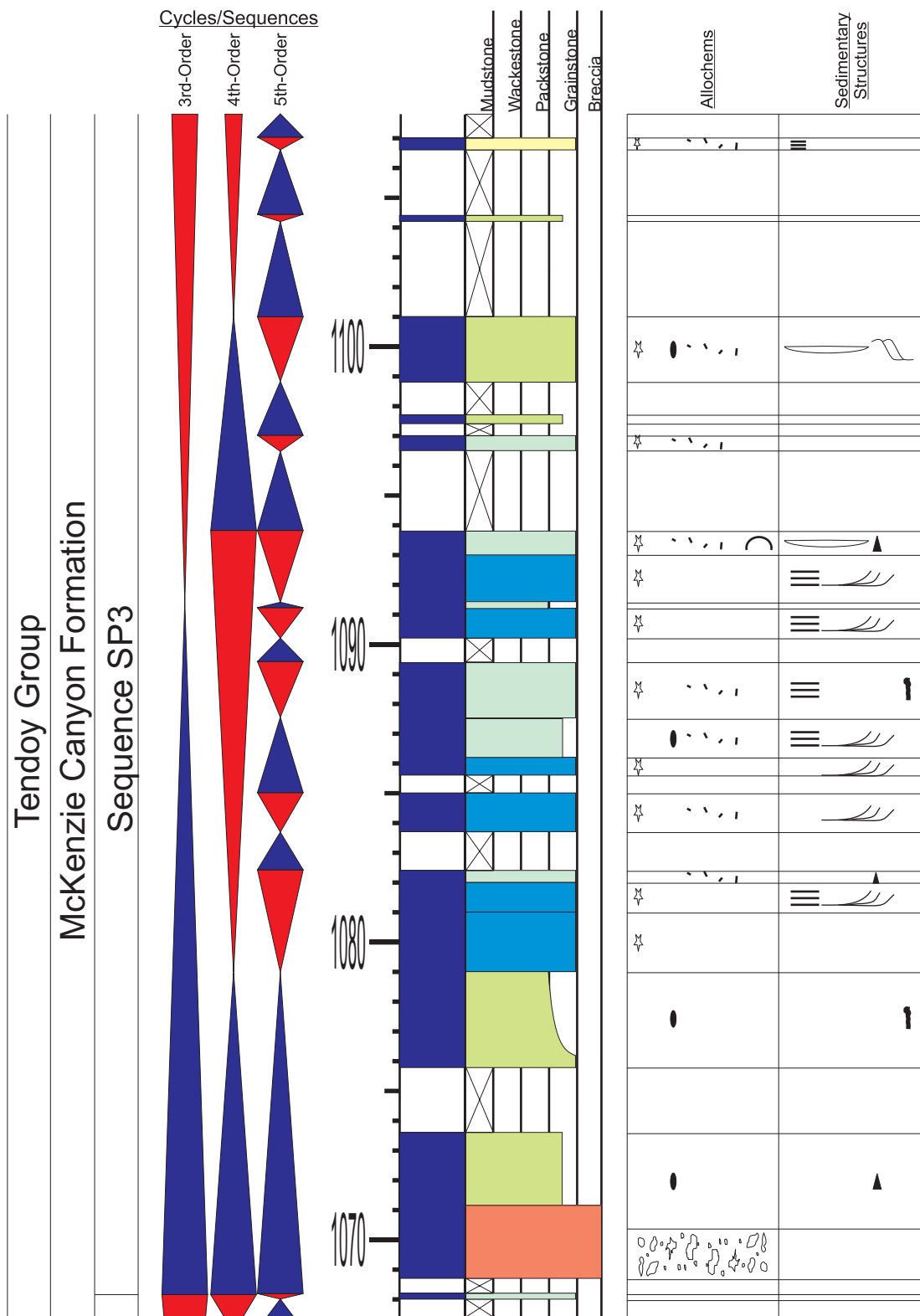
Appendix 8.25: Sedimentary section log for section Bell-McKenzie Canyon. Refer to Appendix 1 for symbols and Figure 3.6 for location.

APPENDIX 8.27



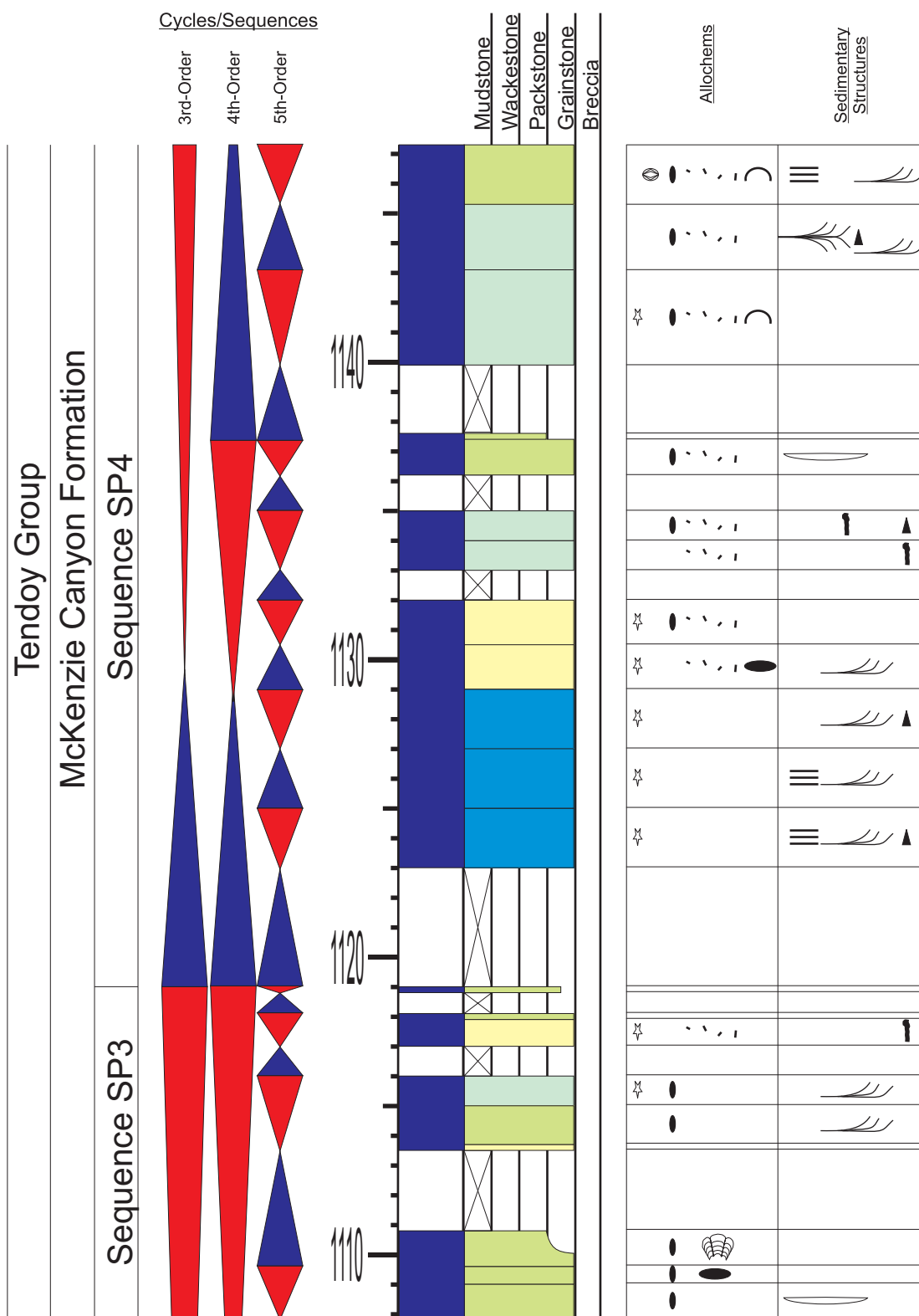
Appendix 8.27: Sedimentary section log for section Bell-McKenzie Canyon. Refer to Appendix 1 for symbols and Figure 3.6 for location.

APPENDIX 8.28



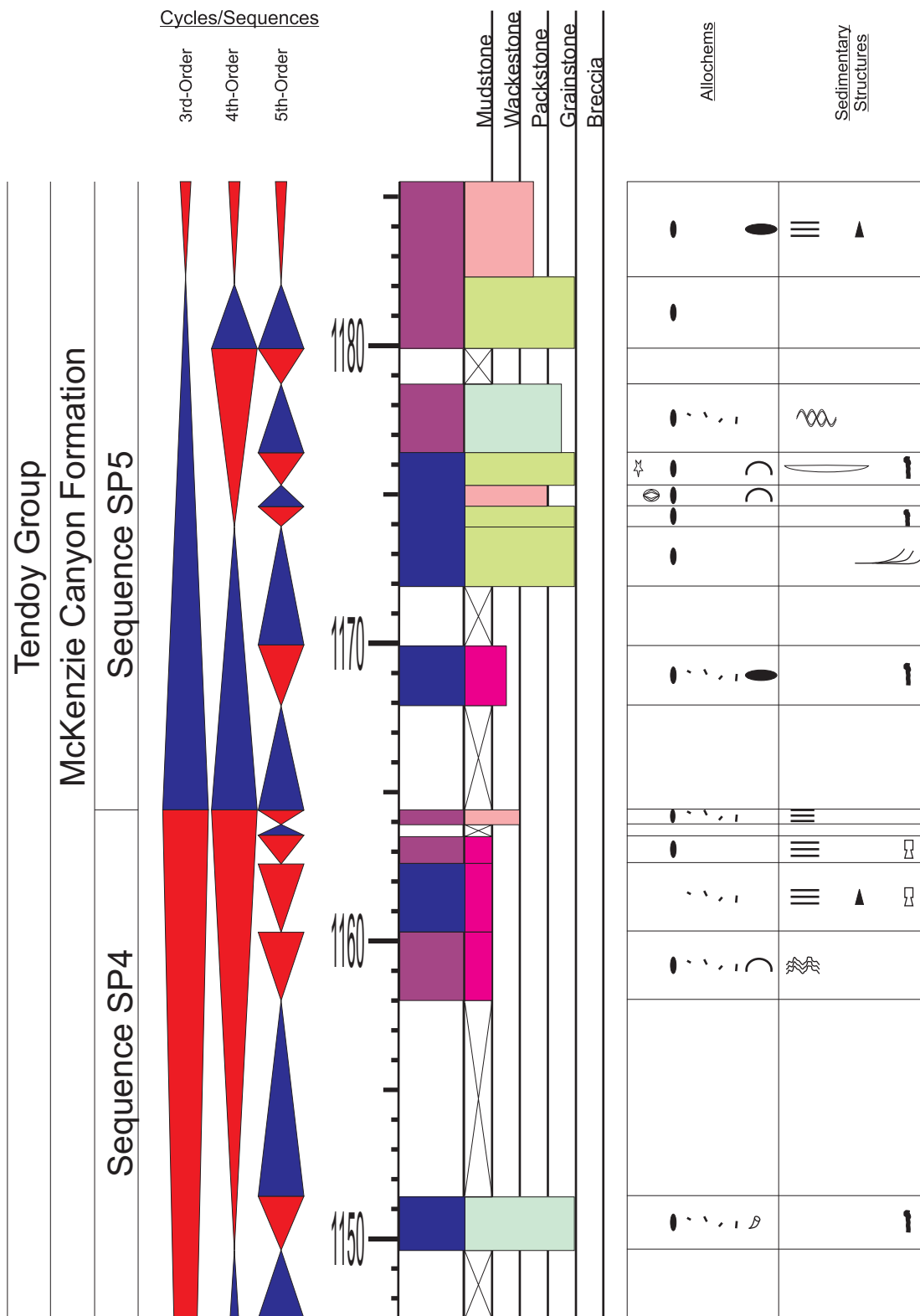
Appendix 8.28: Sedimentary section log for section Bell-McKenzie Canyon. Refer to Appendix 1 for symbols and Figure 3.6 for location.

APPENDIX 8.29



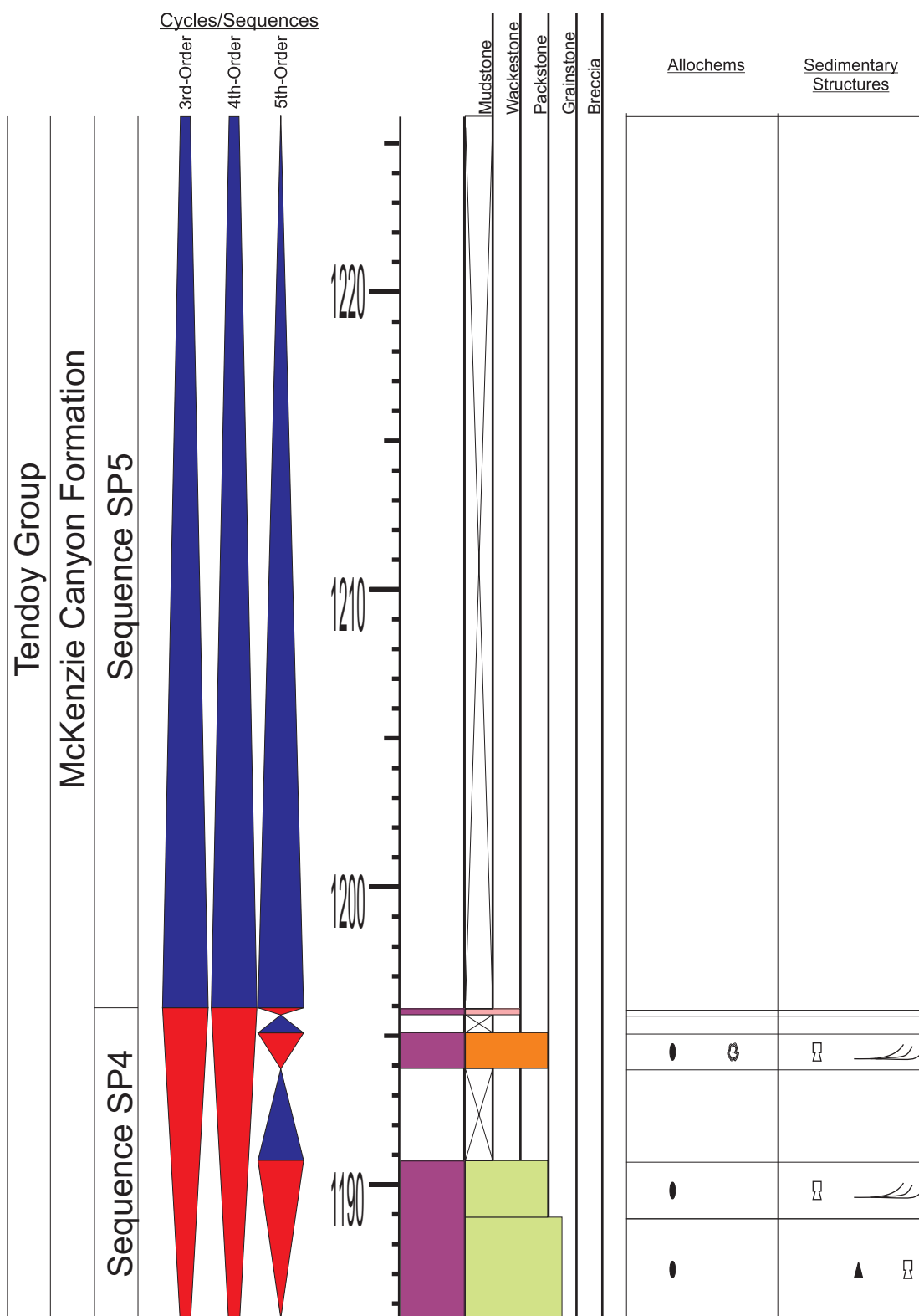
Appendix 8.29: Sedimentary section log for section Bell-McKenzie Canyon. Refer to Appendix 1 for symbols and Figure 3.6 for location.

APPENDIX 8.30



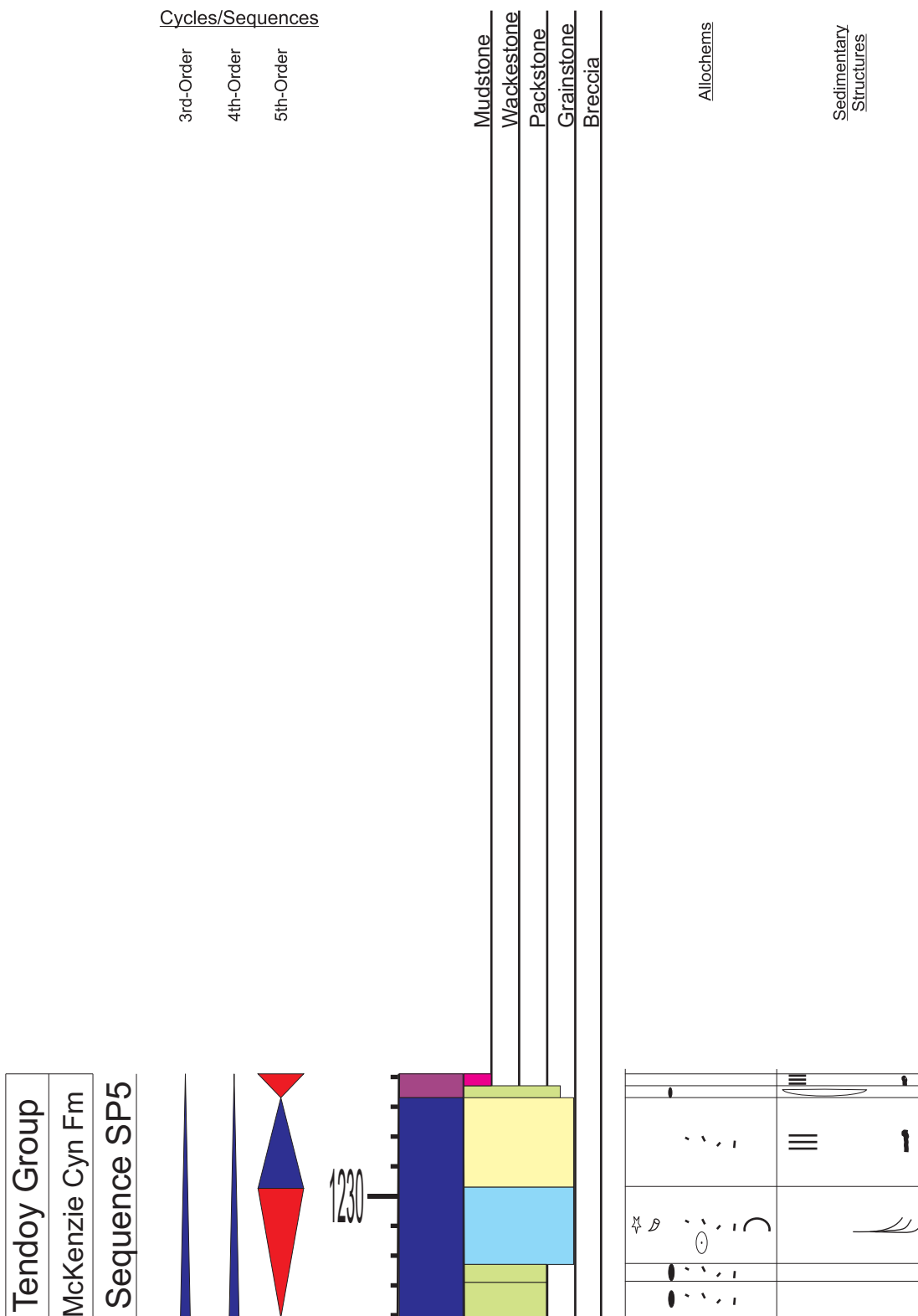
Appendix 8.30: Sedimentary section log for section Bell-McKenzie Canyon. Refer to Appendix 1 for symbols and Figure 3.6 for location.

APPENDIX 8.31



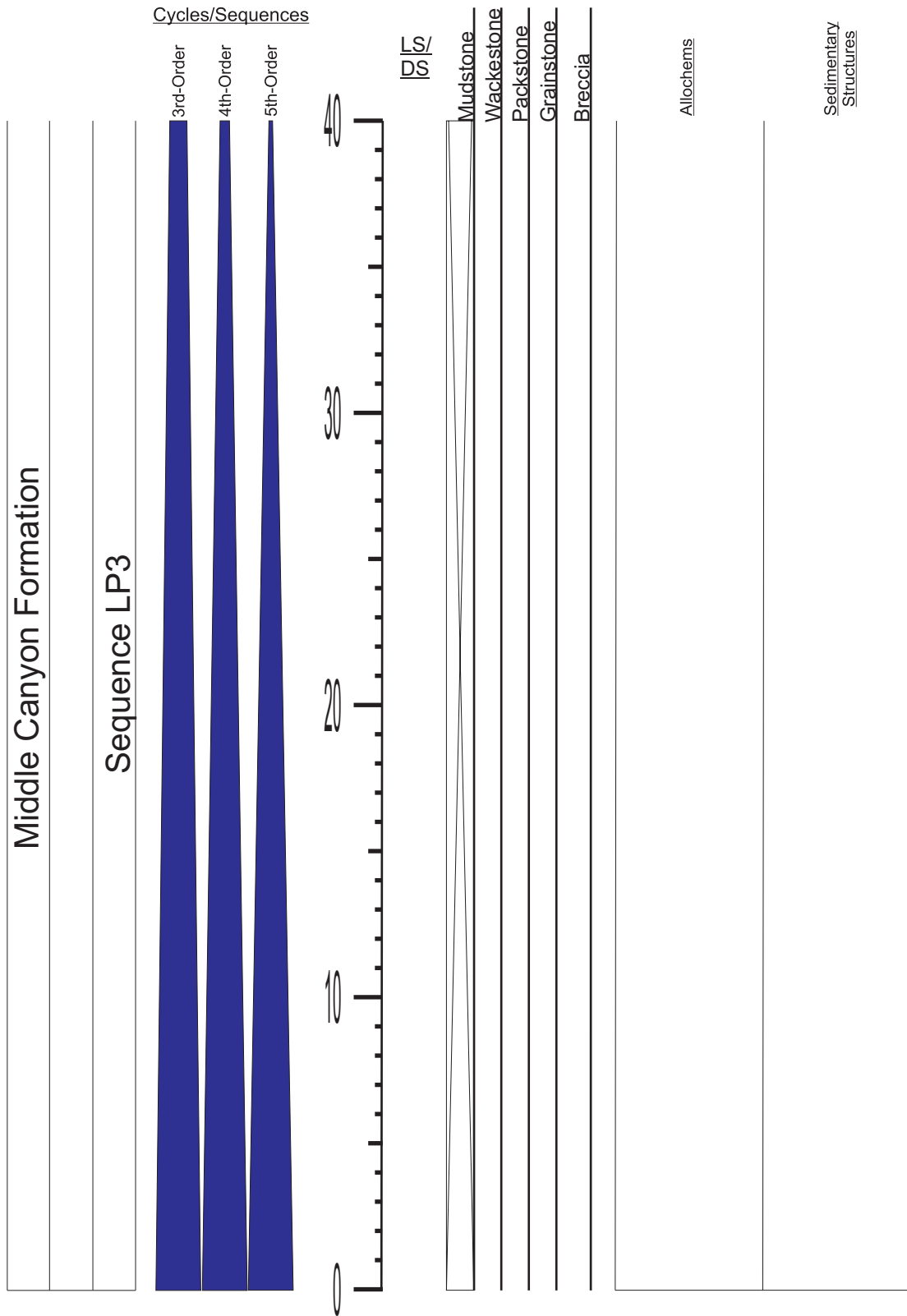
Appendix 8.31: Sedimentary section log for section Bell-McKenzie Canyon. Refer to Appendix 1 for symbols and Figure 3.6 for location.

APPENDIX 8.32



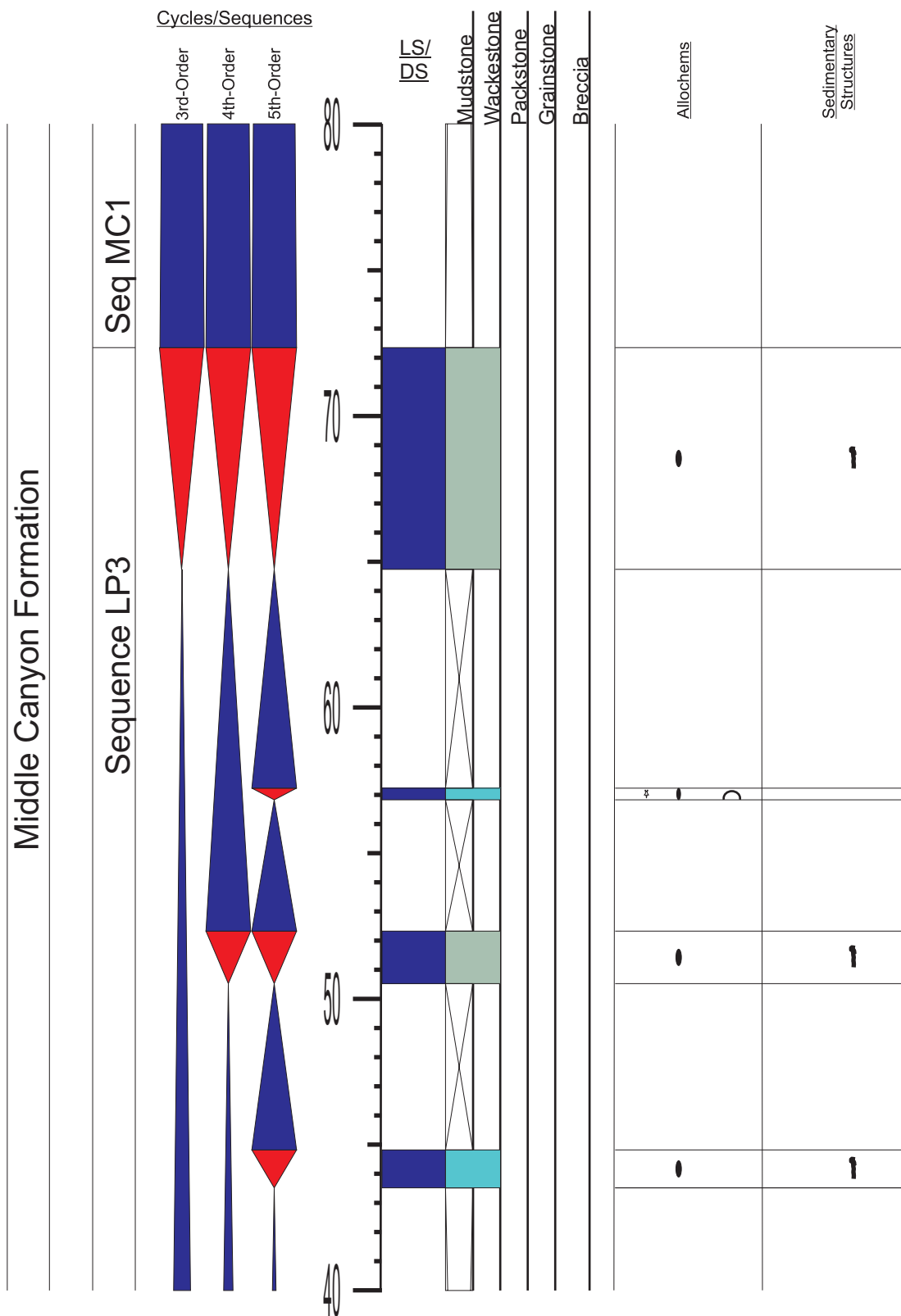
Appendix 8.32: Sedimentary section log for section Bell-McKenzie Canyon. Refer to Appendix 1 for symbols and Figure 3.6 for location.

APPENDIX 9.1



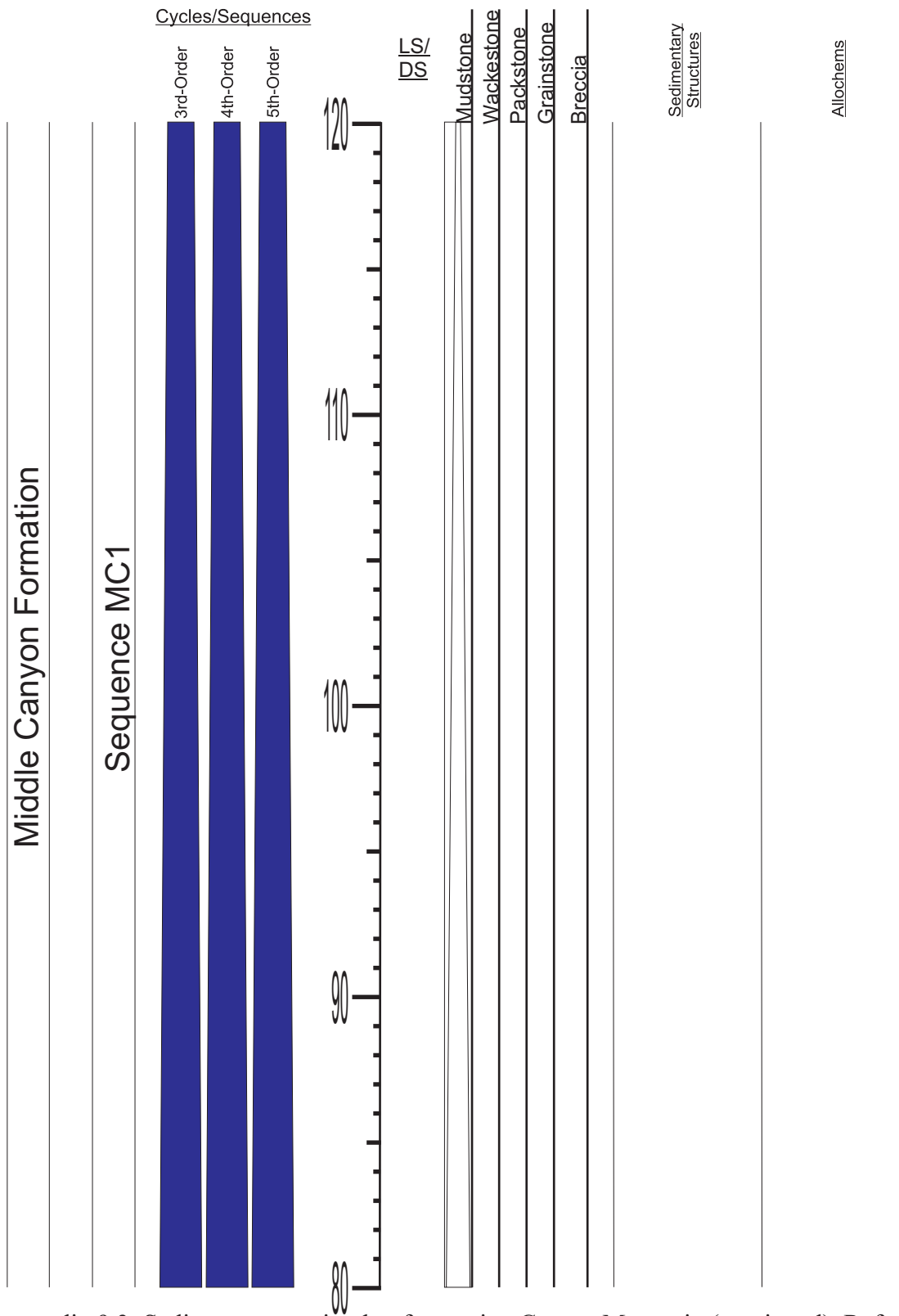
Appendix 9.1: Sedimentary section log for section Copper Mountain. Refer to Appendix 1 for symbols and Figure 3.6 for location.

APPENDIX 9.2



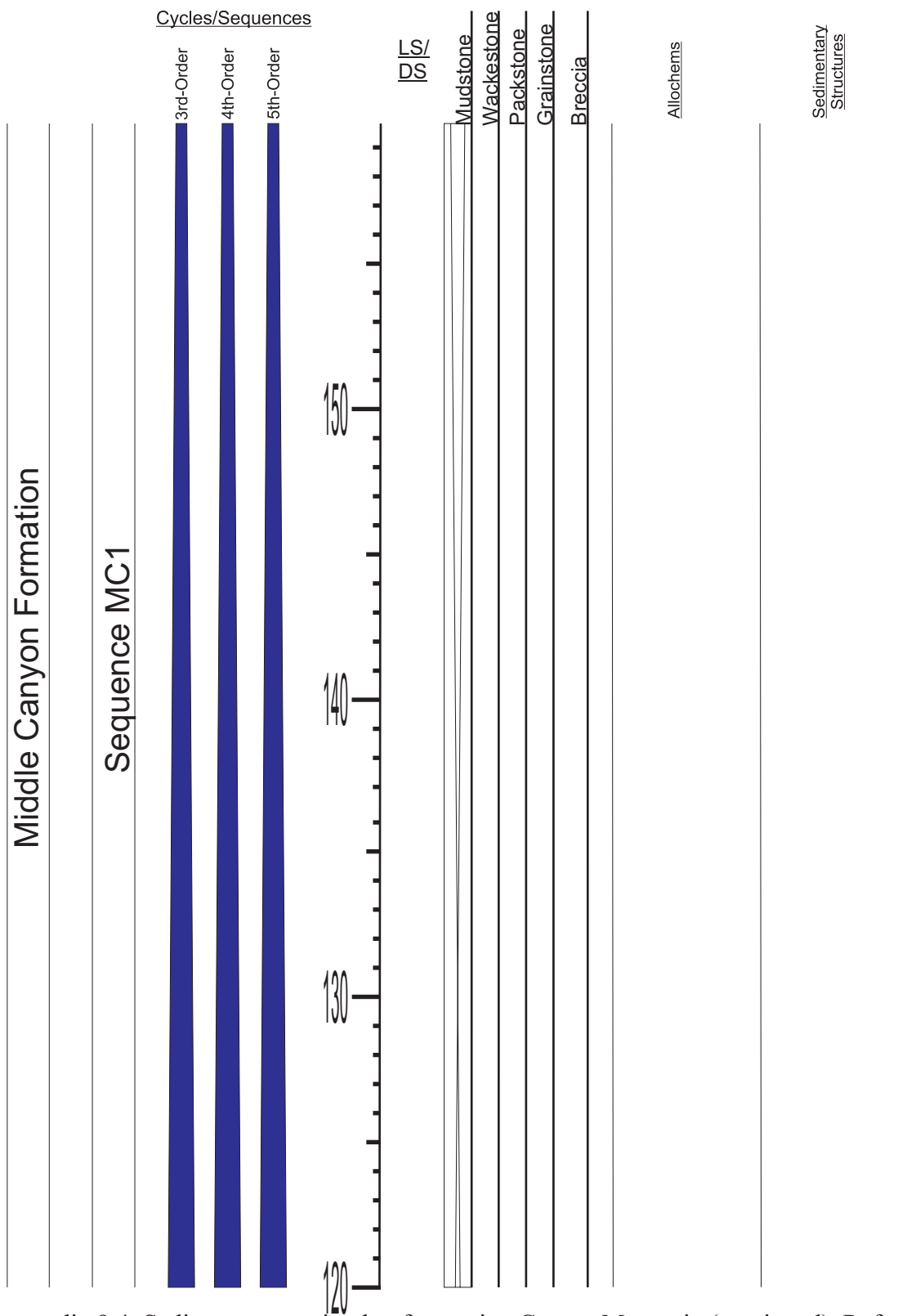
Appendix 9.2: Sedimentary section log for section Copper Mountain (continued). Refer to Appendix 1 for symbols and Figure 3.6 for location.

APPENDIX 9.3



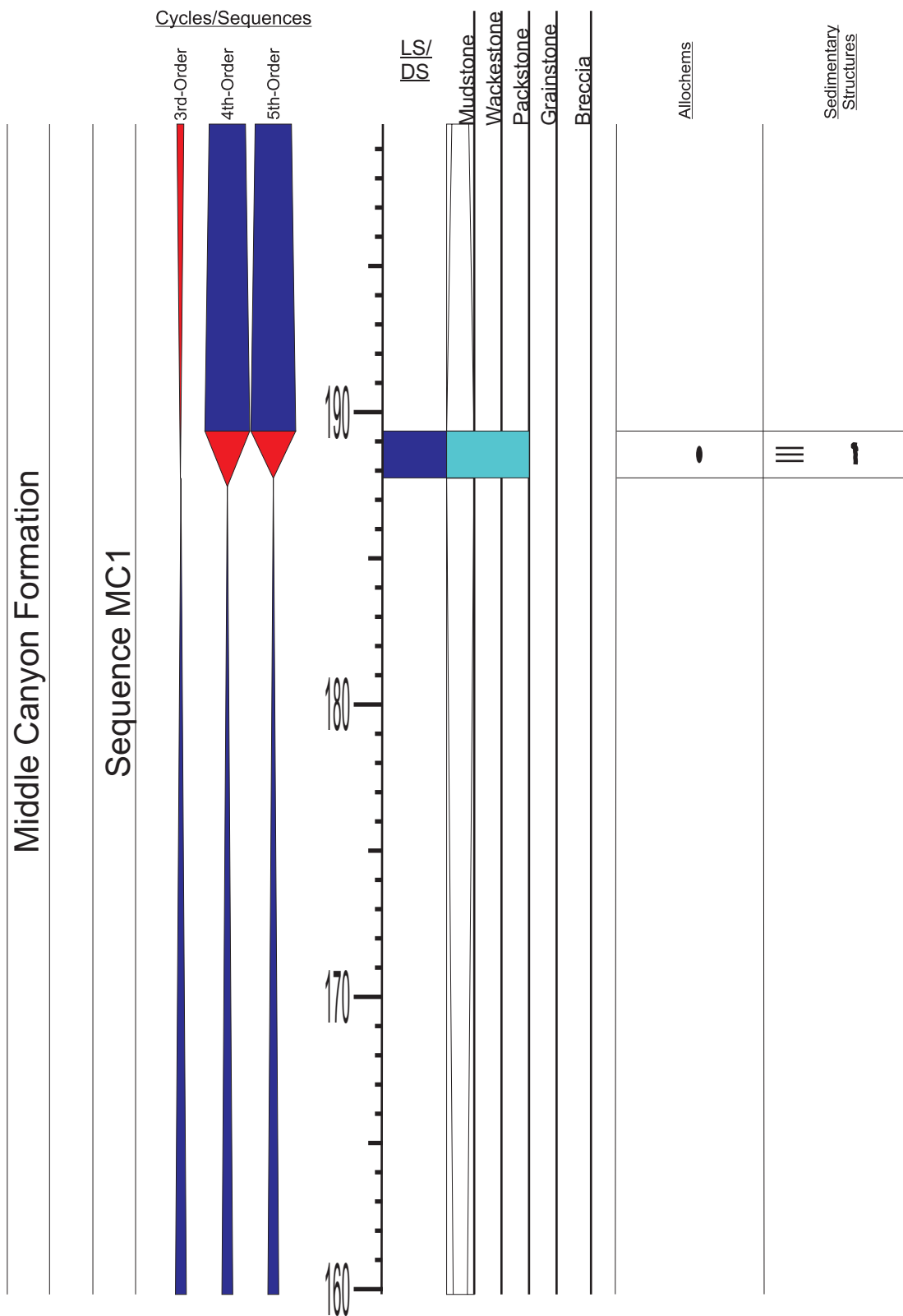
Appendix 9.3: Sedimentary section log for section Copper Mountain (continued). Refer to Appendix 1 for symbols and Figure 3.6 for location.

APPENDIX 9.4



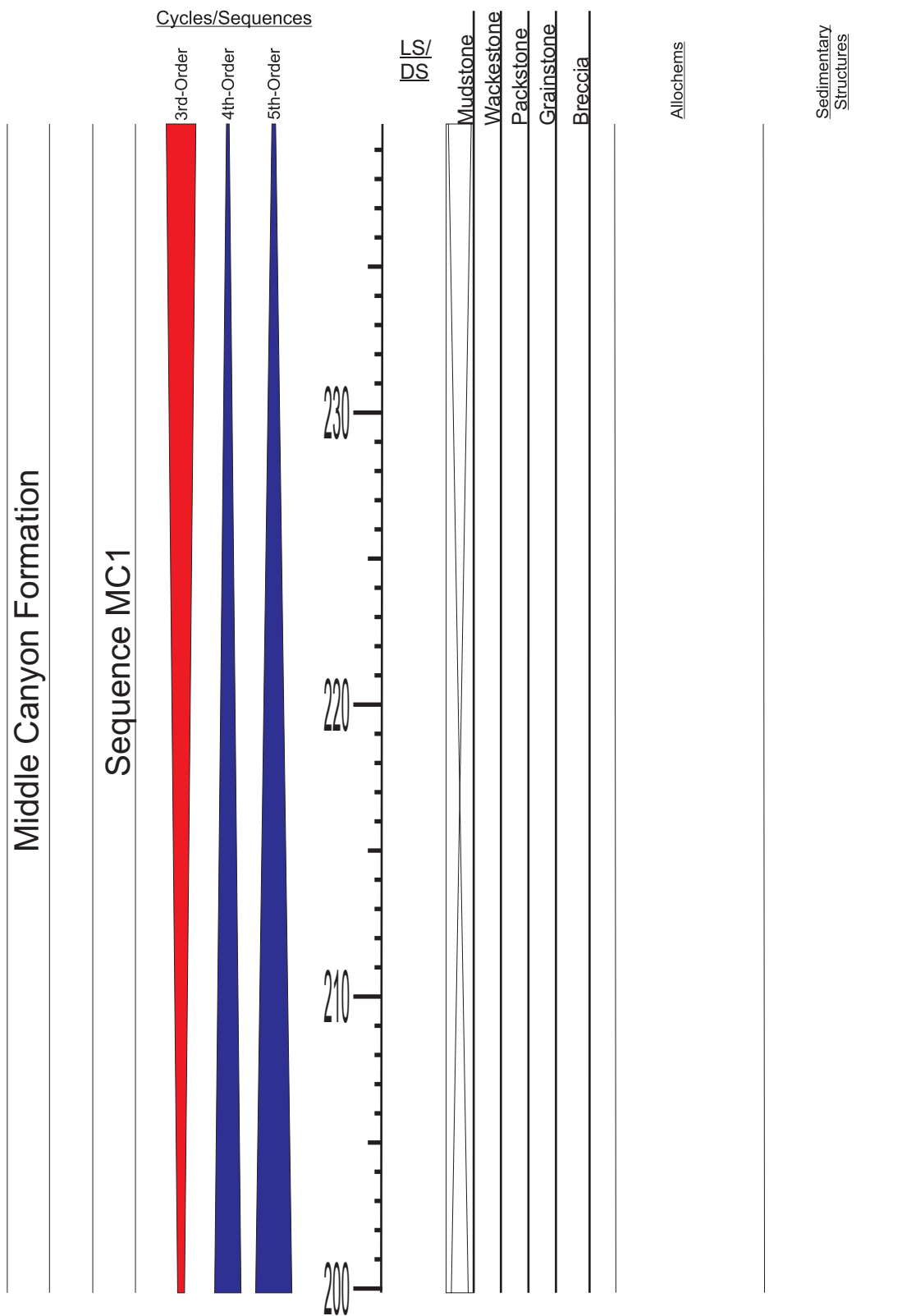
Appendix 9.4: Sedimentary section log for section Copper Mountain (continued). Refer to Appendix 1 for symbols and Figure 3.6 for location.

APPENDIX 9.5



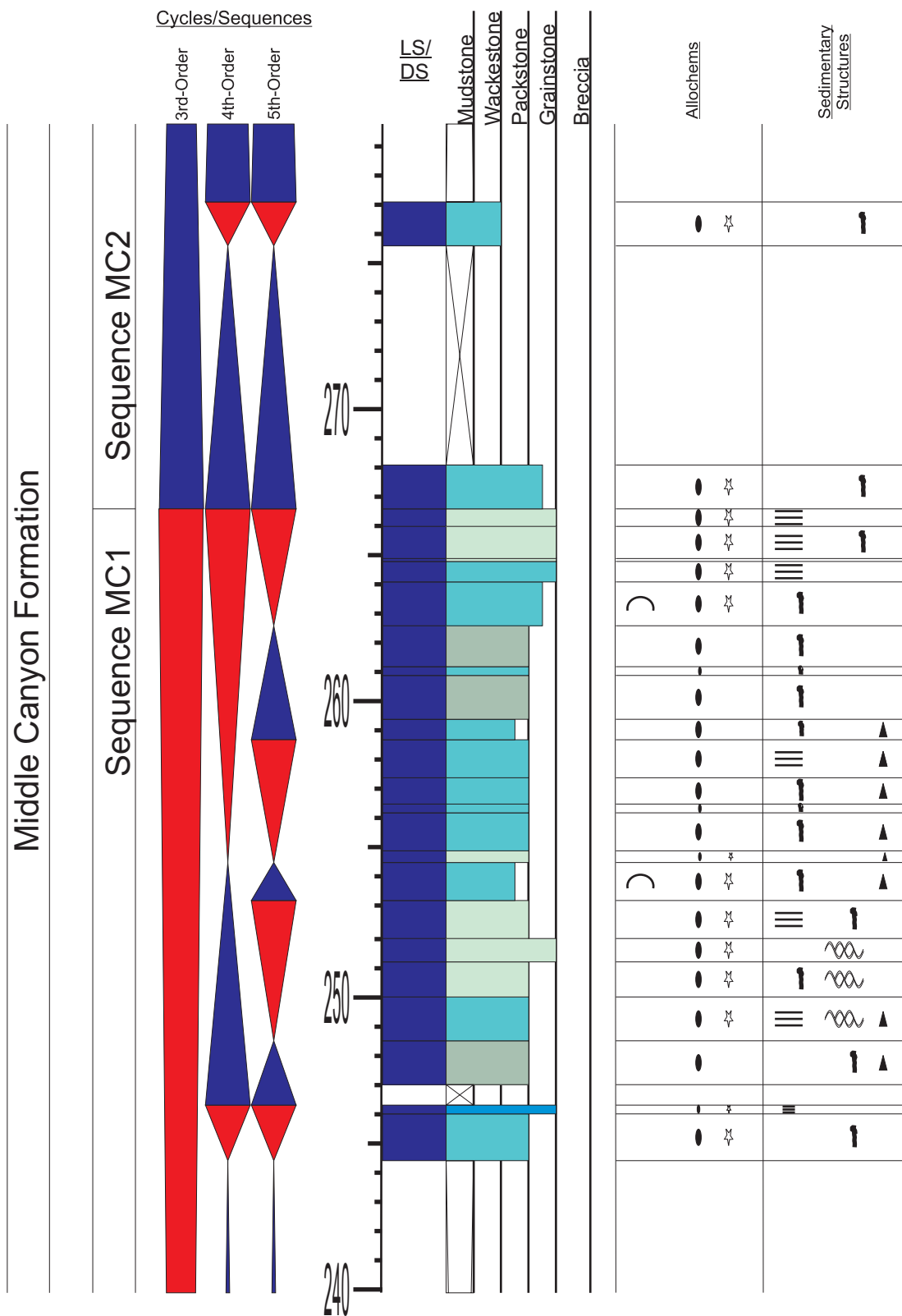
Appendix 9.5: Sedimentary section log for section Copper Mountain (continued). Refer to Appendix 1 for symbols and Figure 3.6 for location.

APPENDIX 9.6



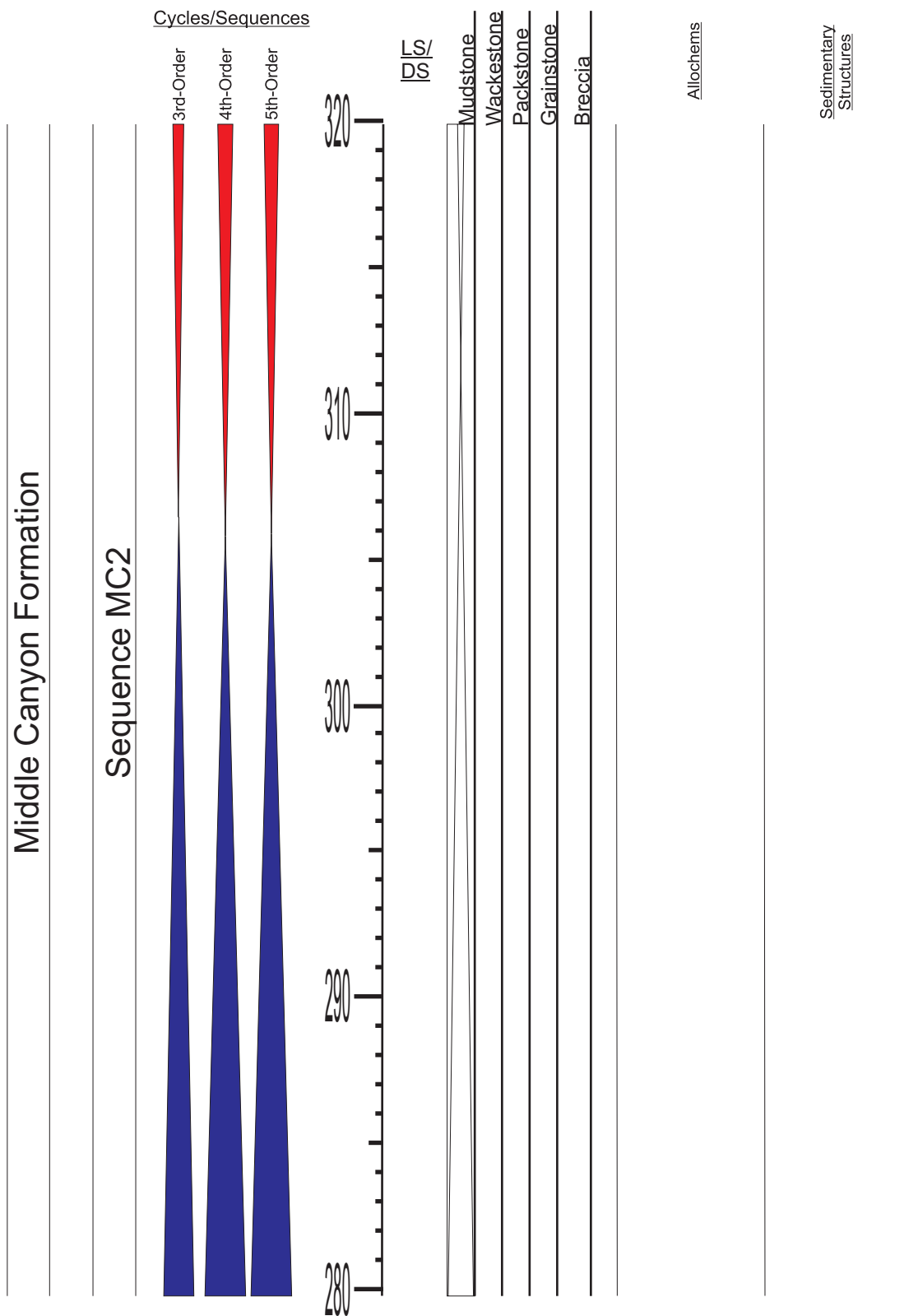
Appendix 9.6: Sedimentary section log for section Copper Mountain (continued). Refer to Appendix 1 for symbols and Figure 3.6 for location.

APPENDIX 9.7



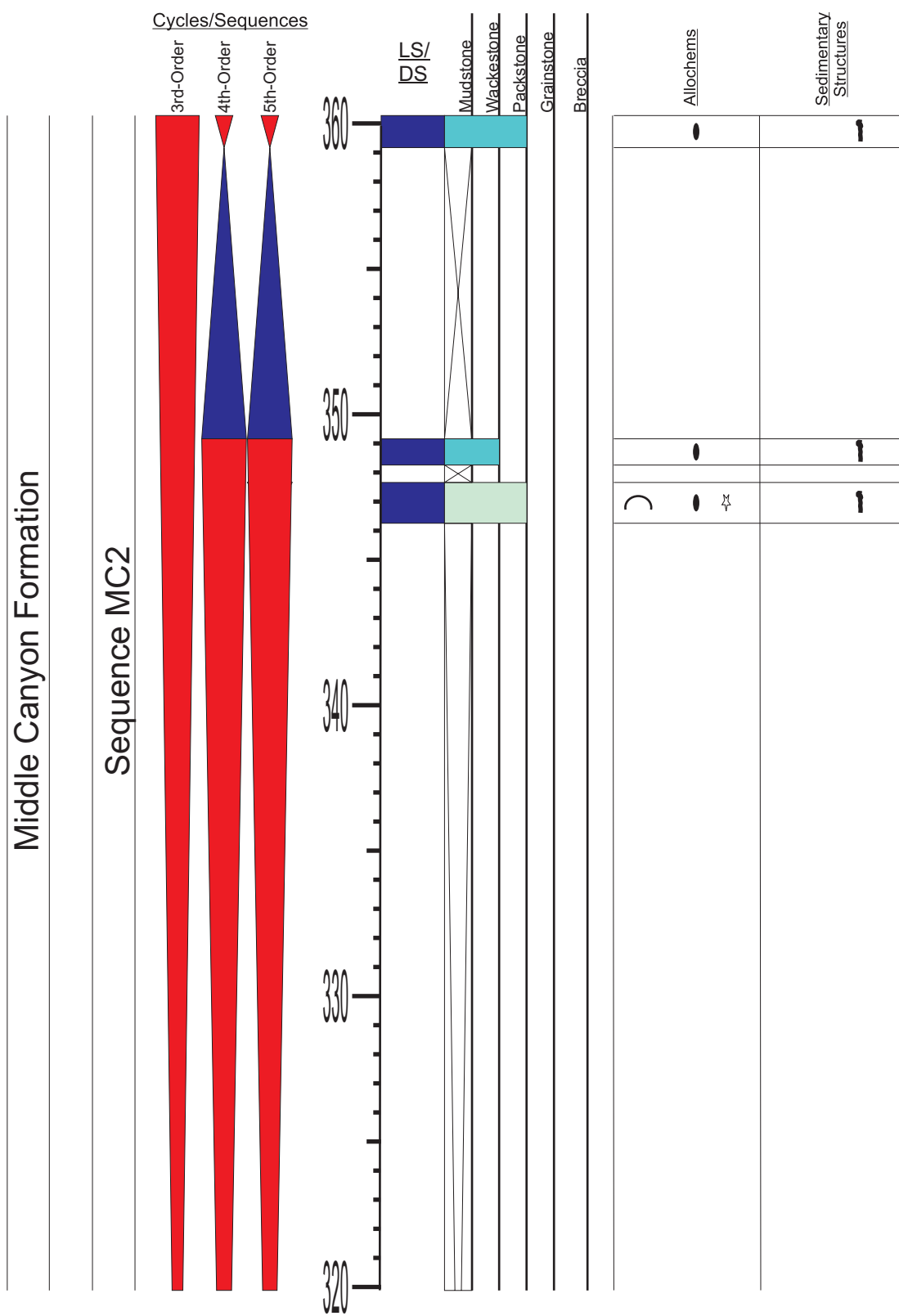
Appendix 9.7: Sedimentary section log for section Copper Mountain (continued). Refer to Appendix 1 for symbols and Figure 3.6 for location.

APPENDIX 9.8



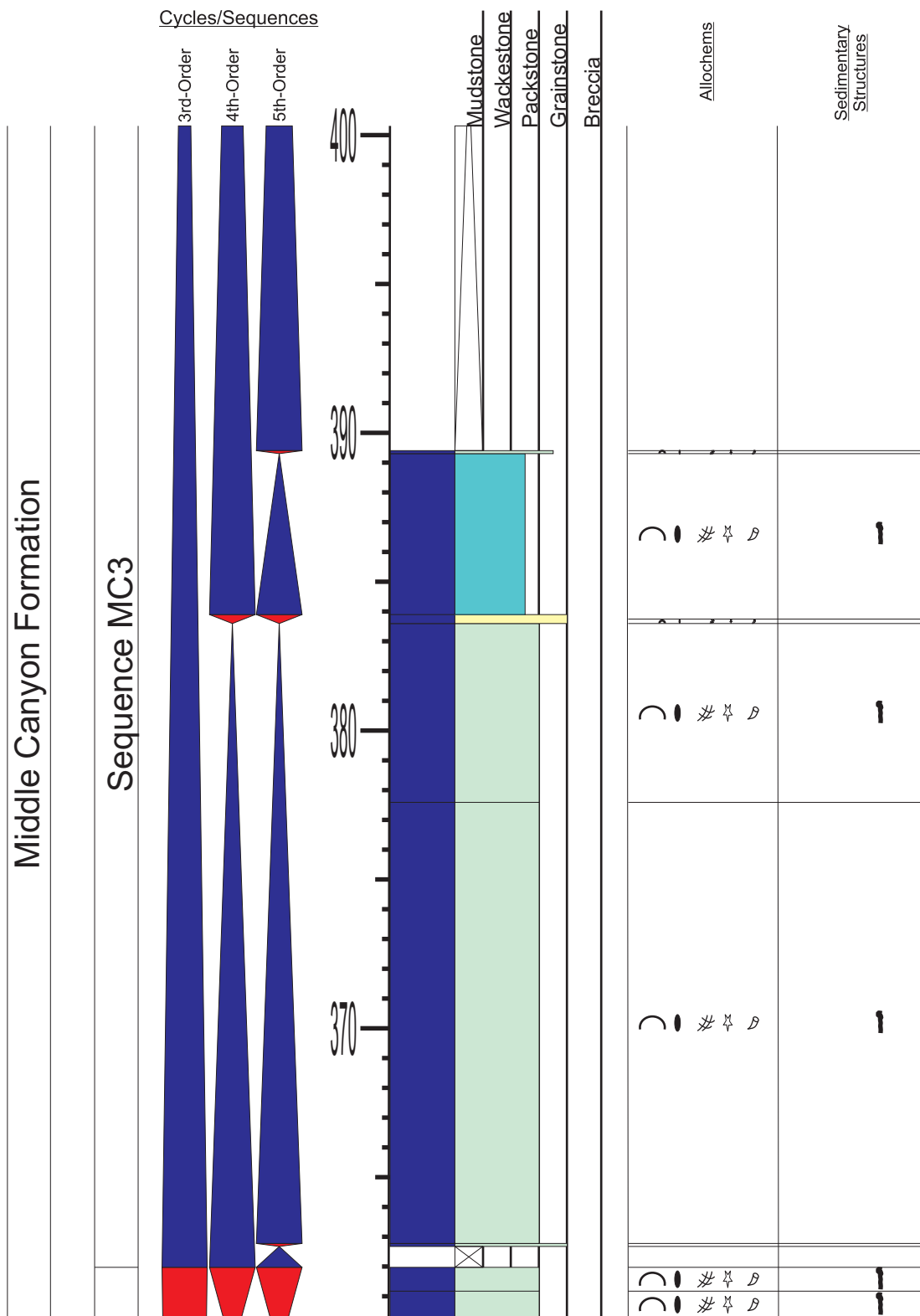
Appendix 9.8: Sedimentary section log for section Copper Mountain (continued). Refer to Appendix 1 for symbols and Figure 3.6 for location.

APPENDIX 9.9



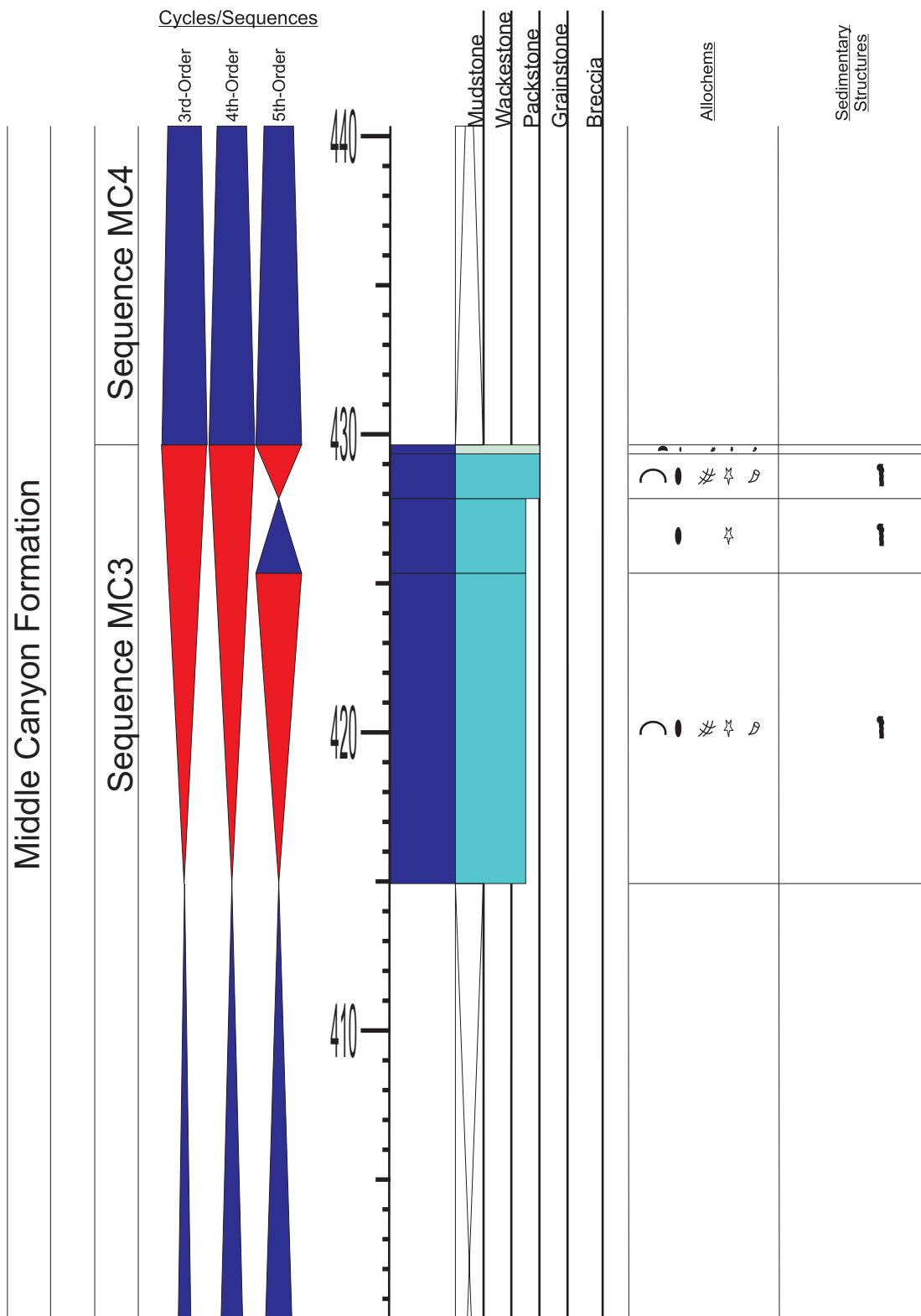
Appendix 9.9: Sedimentary section log for section Copper Mountain (continued). Refer to Appendix 1 for symbols and Figure 3.6 for location.

APPENDIX 9.10



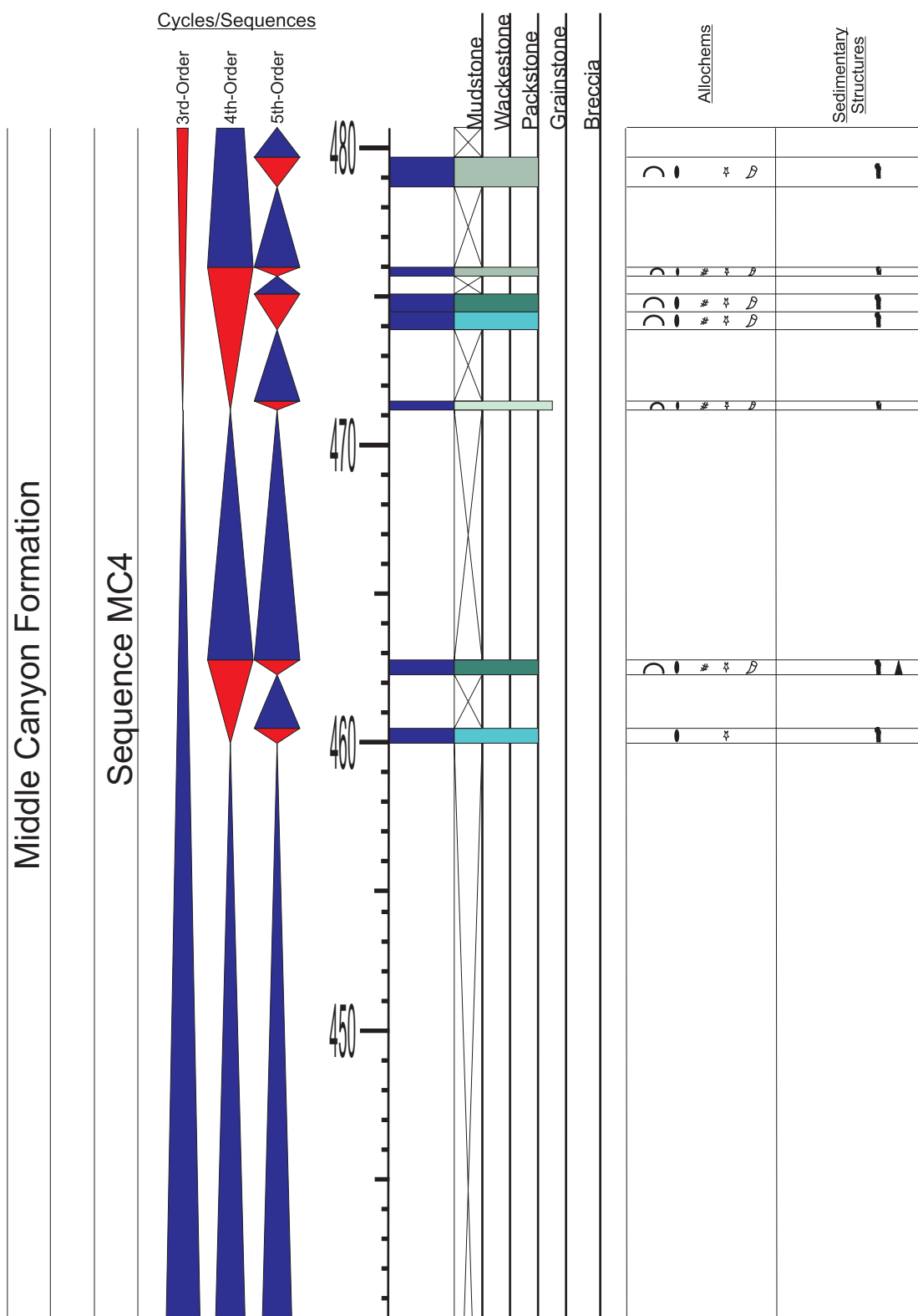
Appendix 9.10: Sedimentary section log for section Copper Mountain (continued). Refer to Appendix 1 for symbols and Figure 3.6 for location.

APPENDIX 9.11



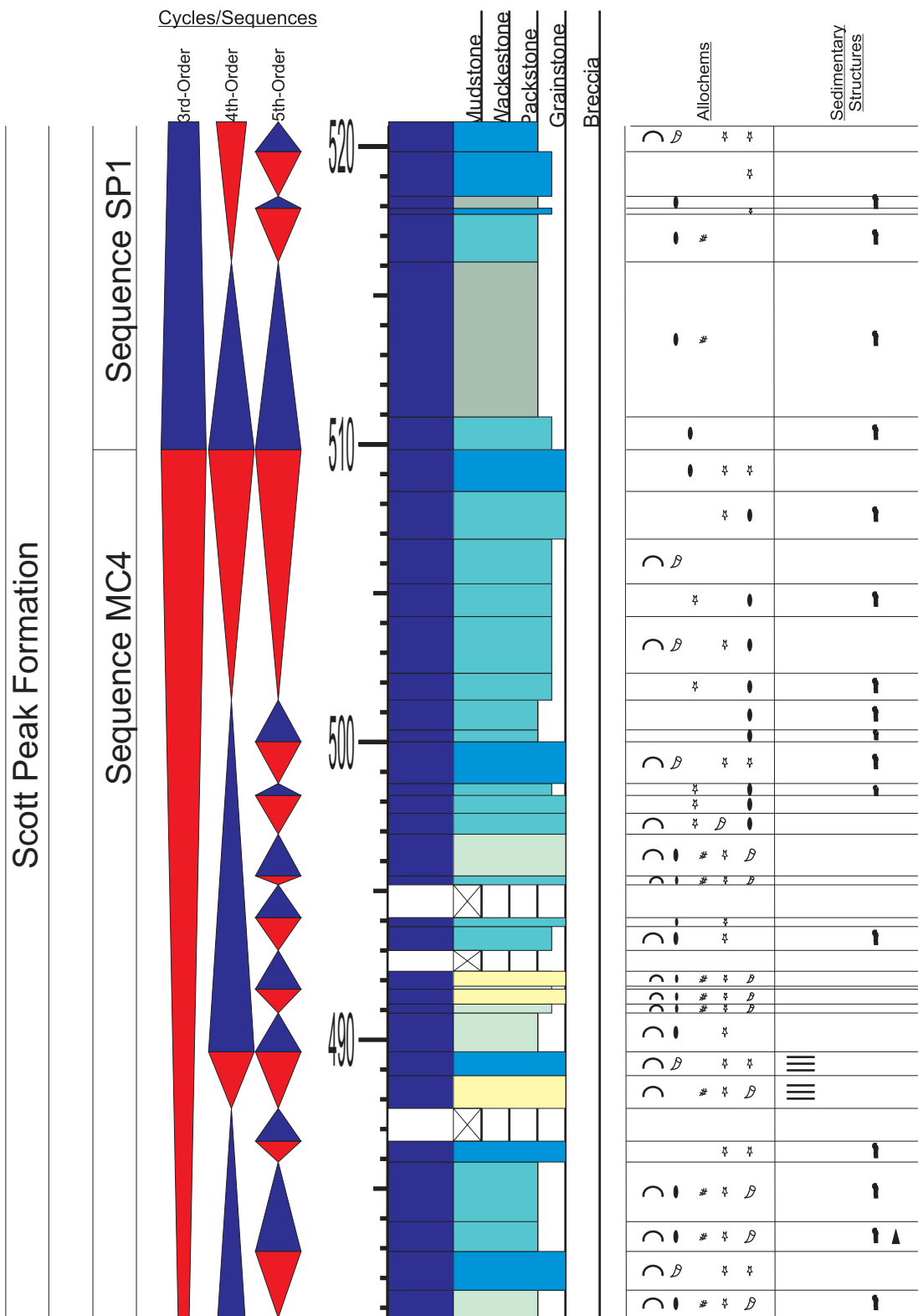
Appendix 9.11: Sedimentary section log for section Copper Mountain (continued). Refer to Appendix 1 for symbols and Figure 3.6 for location.

APPENDIX 9.12



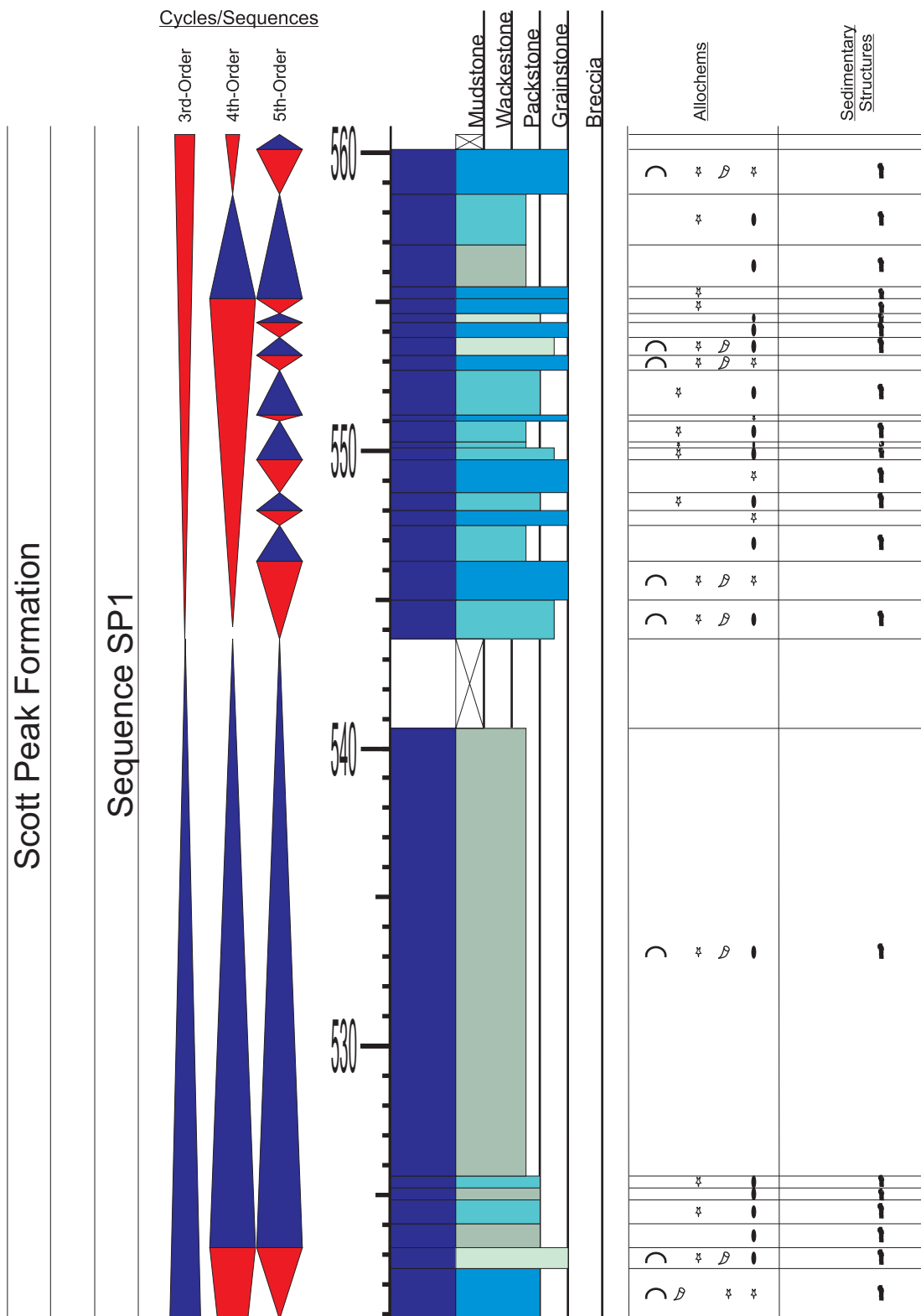
Appendix 9.12: Sedimentary section log for section Copper Mountain (continued). Refer to Appendix 1 for symbols and Figure 3.6 for location.

APPENDIX 9.13



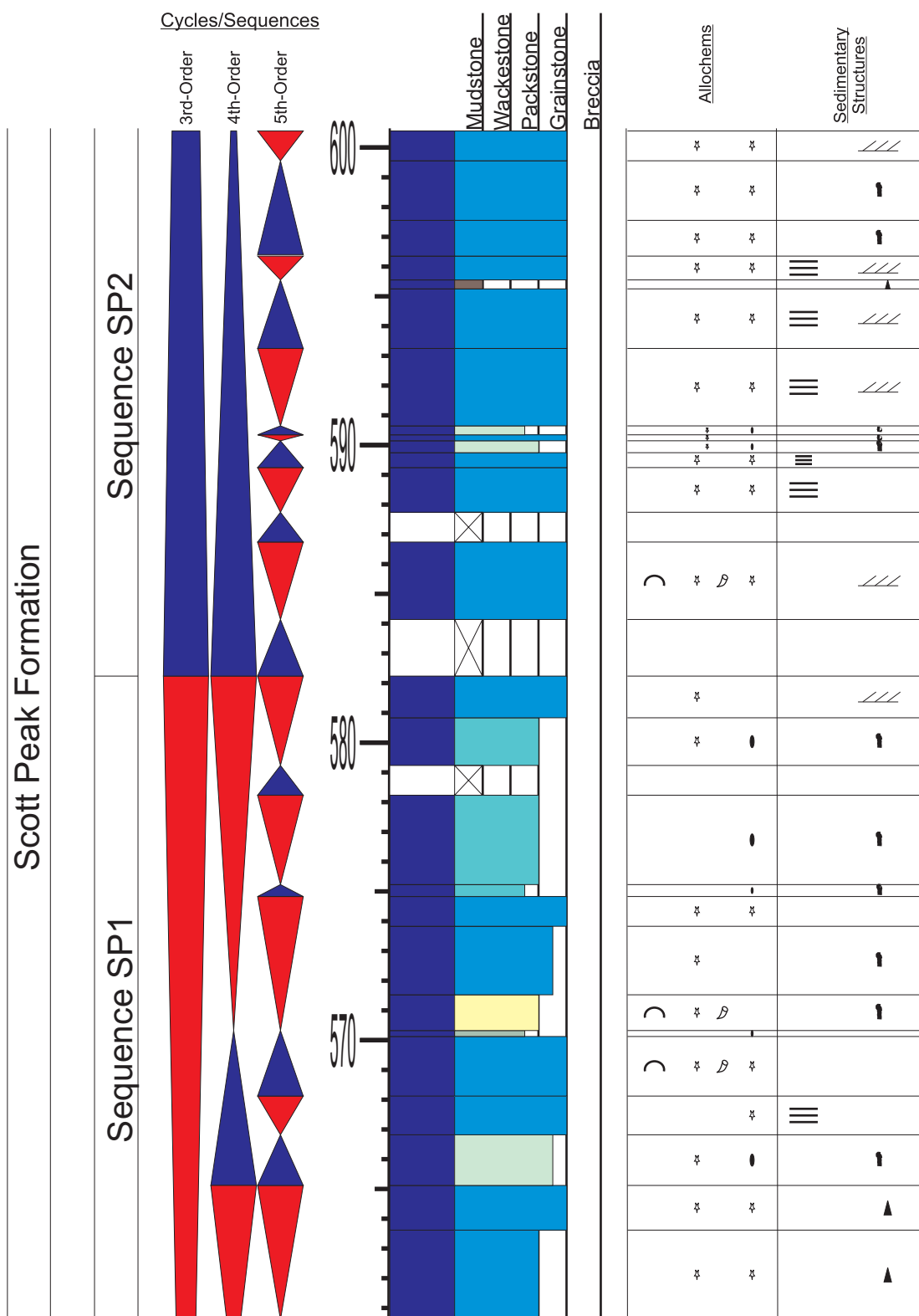
Appendix 9.13: Sedimentary section log for section Copper Mountain (continued). Refer to Appendix 1 for symbols and Figure 3.6 for location.

APPENDIX 9.14



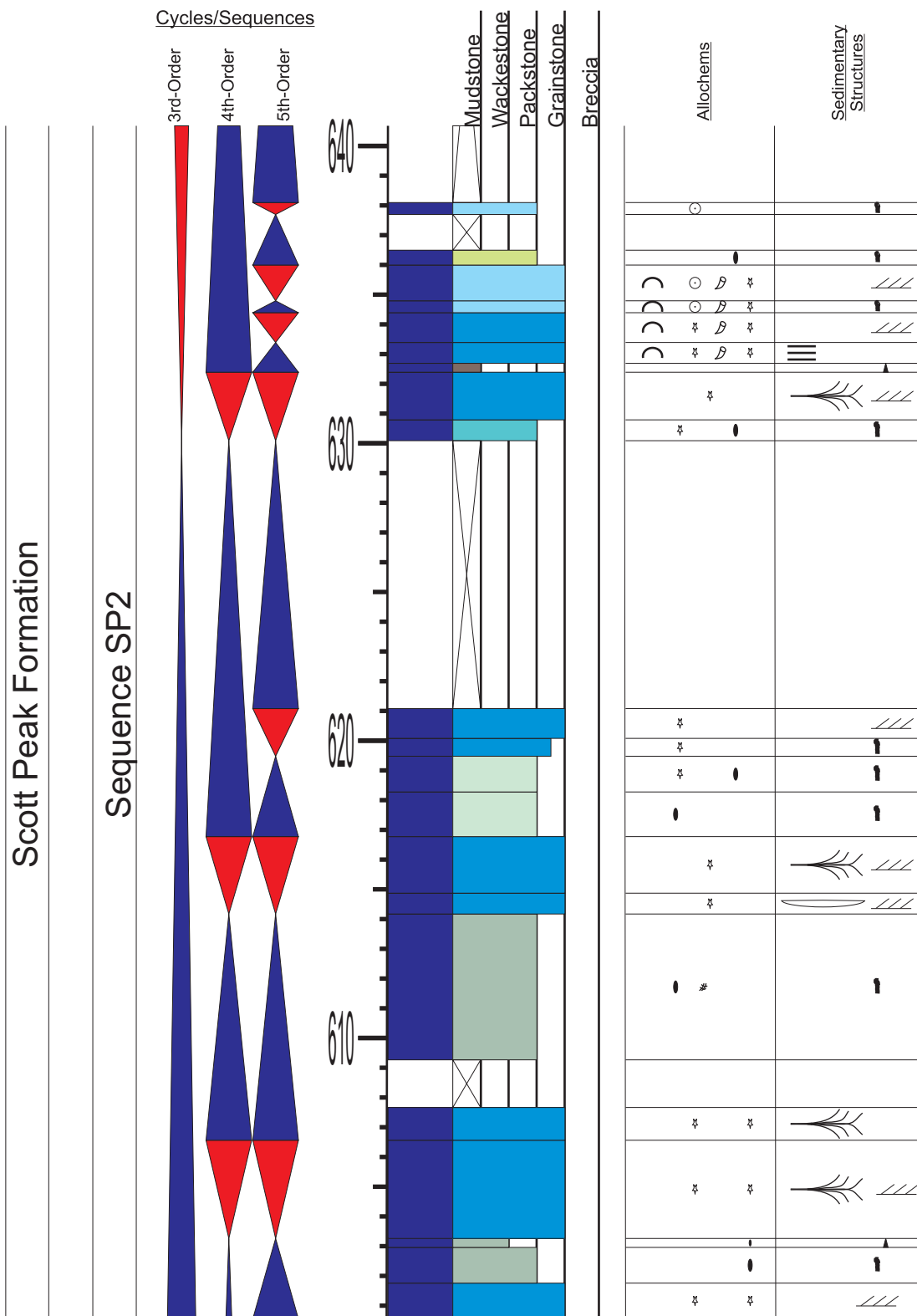
Appendix 9.14: Sedimentary section log for section Copper Mountain (continued). Refer to Appendix 1 for symbols and Figure 3.6 for location.

APPENDIX 9.15



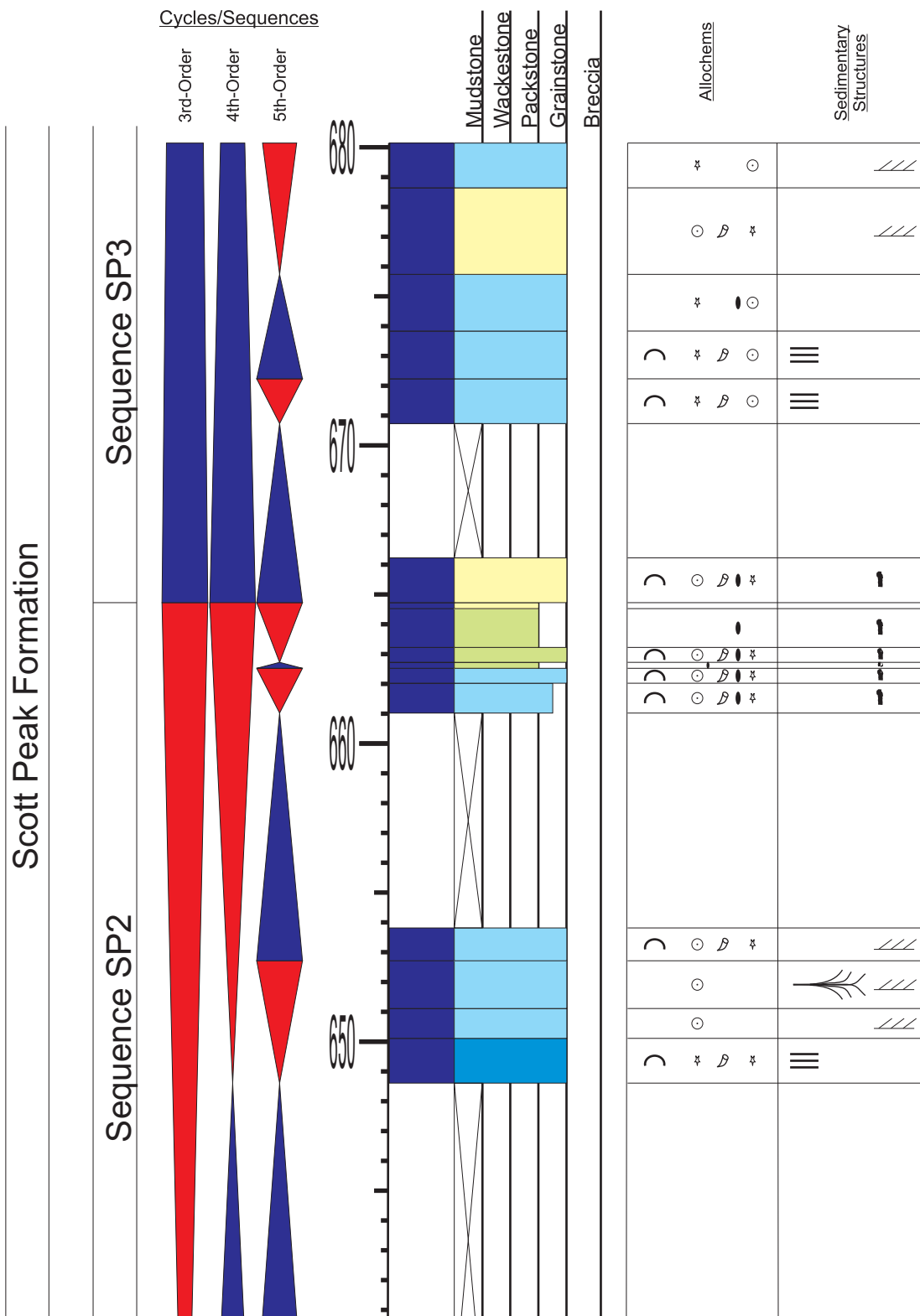
Appendix 9.15: Sedimentary section log for section Copper Mountain (continued). Refer to Appendix 1 for symbols and Figure 3.6 for location.

APPENDIX 9.16



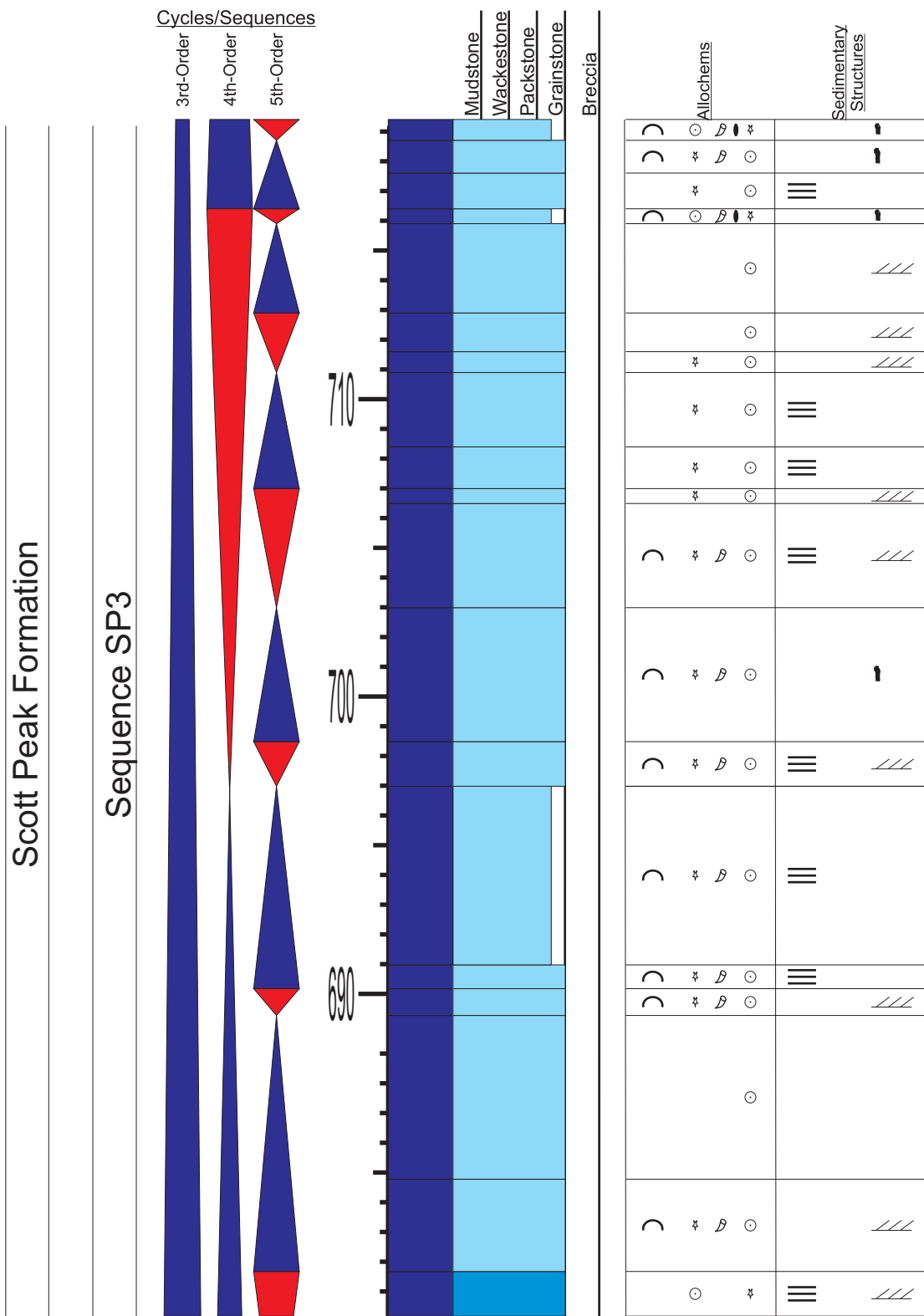
Appendix 9.16: Sedimentary section log for section Copper Mountain (continued). Refer to Appendix 1 for symbols and Figure 3.6 for location.

APPENDIX 9.17



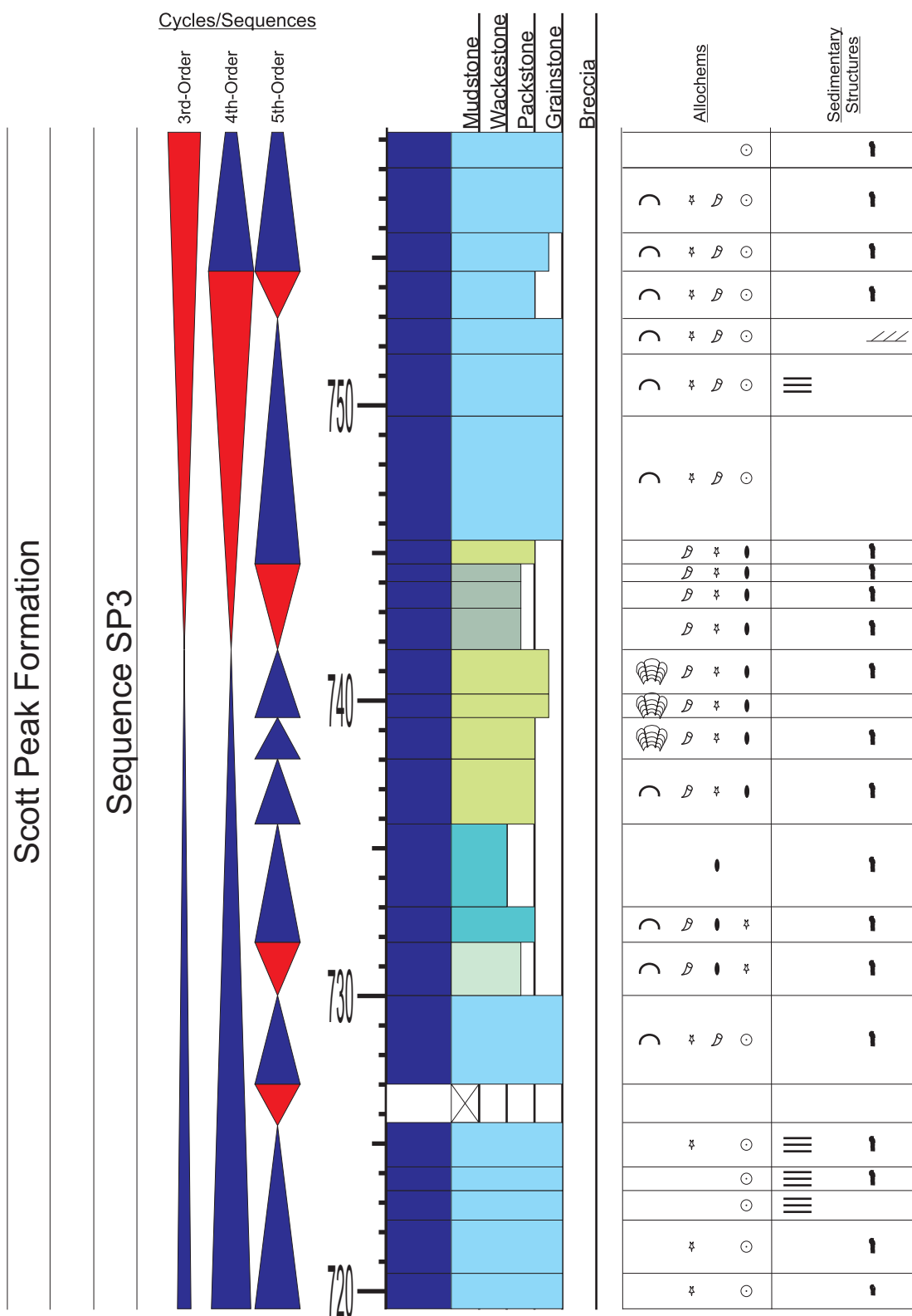
Appendix 9.17: Sedimentary section log for section Copper Mountain (continued). Refer to Appendix 1 for symbols and Figure 3.6 for location.

APPENDIX 9.18



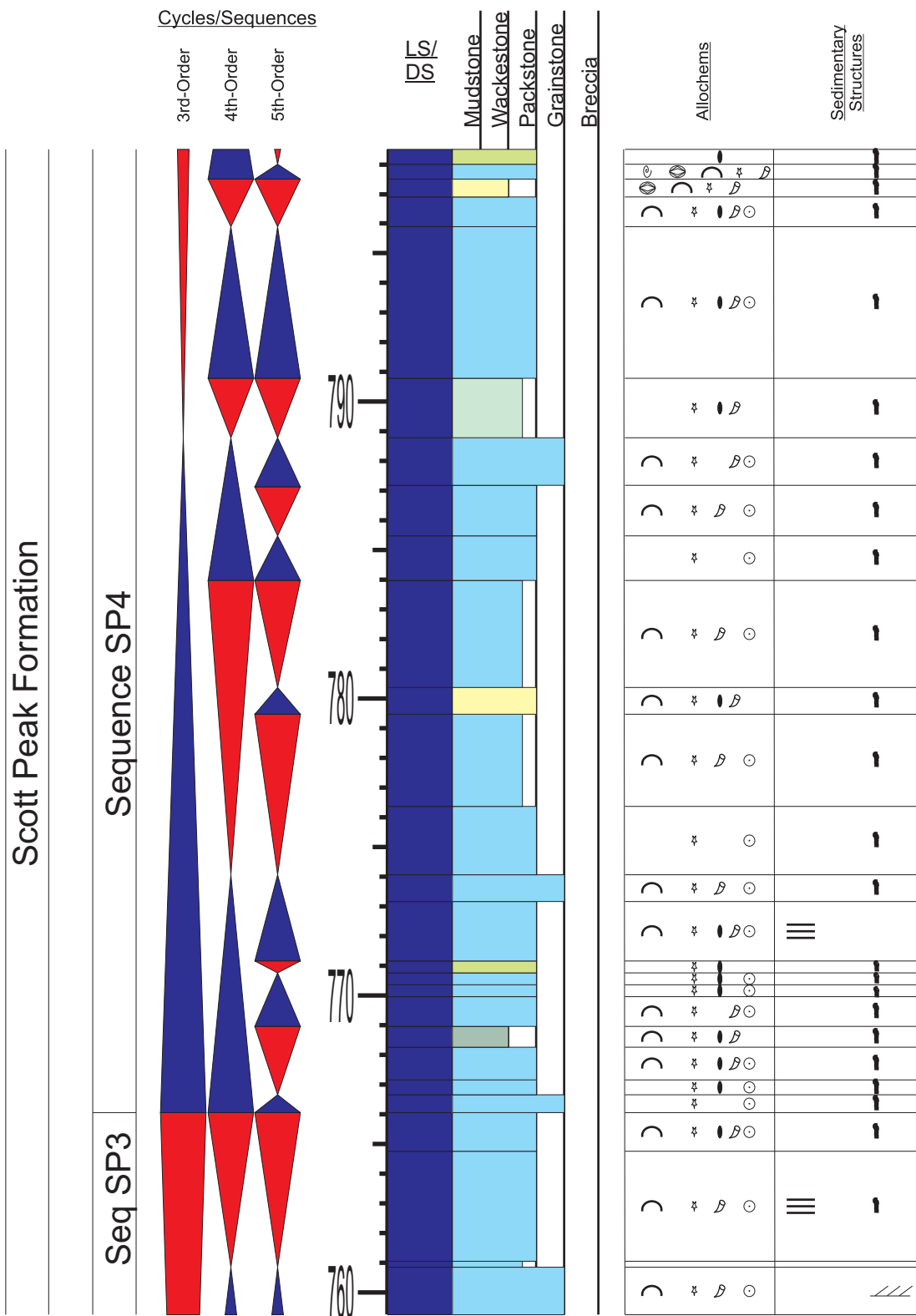
Appendix 9.18: Sedimentary section log for section Copper Mountain (continued). Refer to Appendix 1 for symbols and Figure 3.6 for location.

APPENDIX 9.19



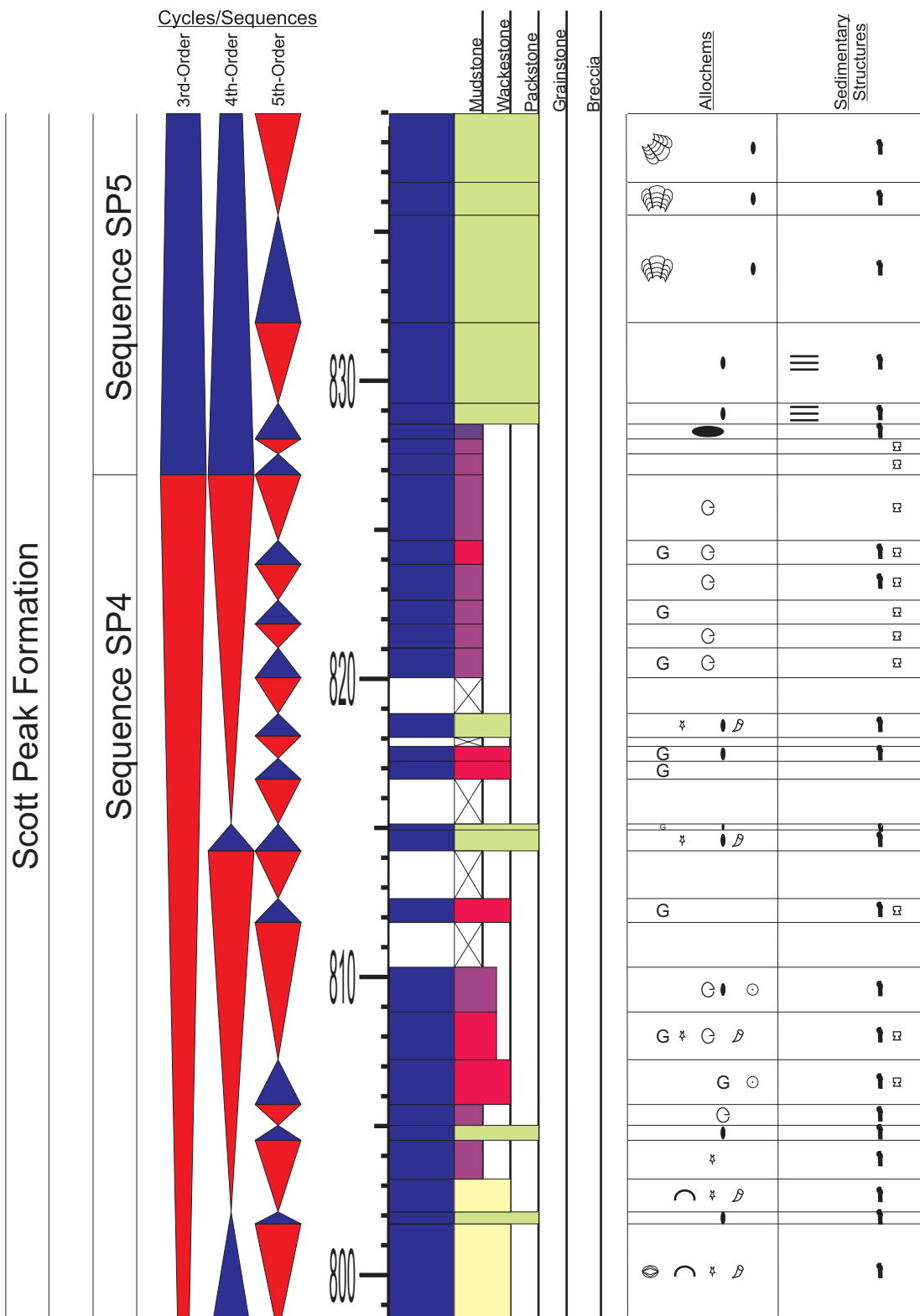
Appendix 9.19: Sedimentary section log for section Copper Mountain (continued). Refer to Appendix 1 for symbols and Figure 3.6 for location.

APPENDIX 9.20



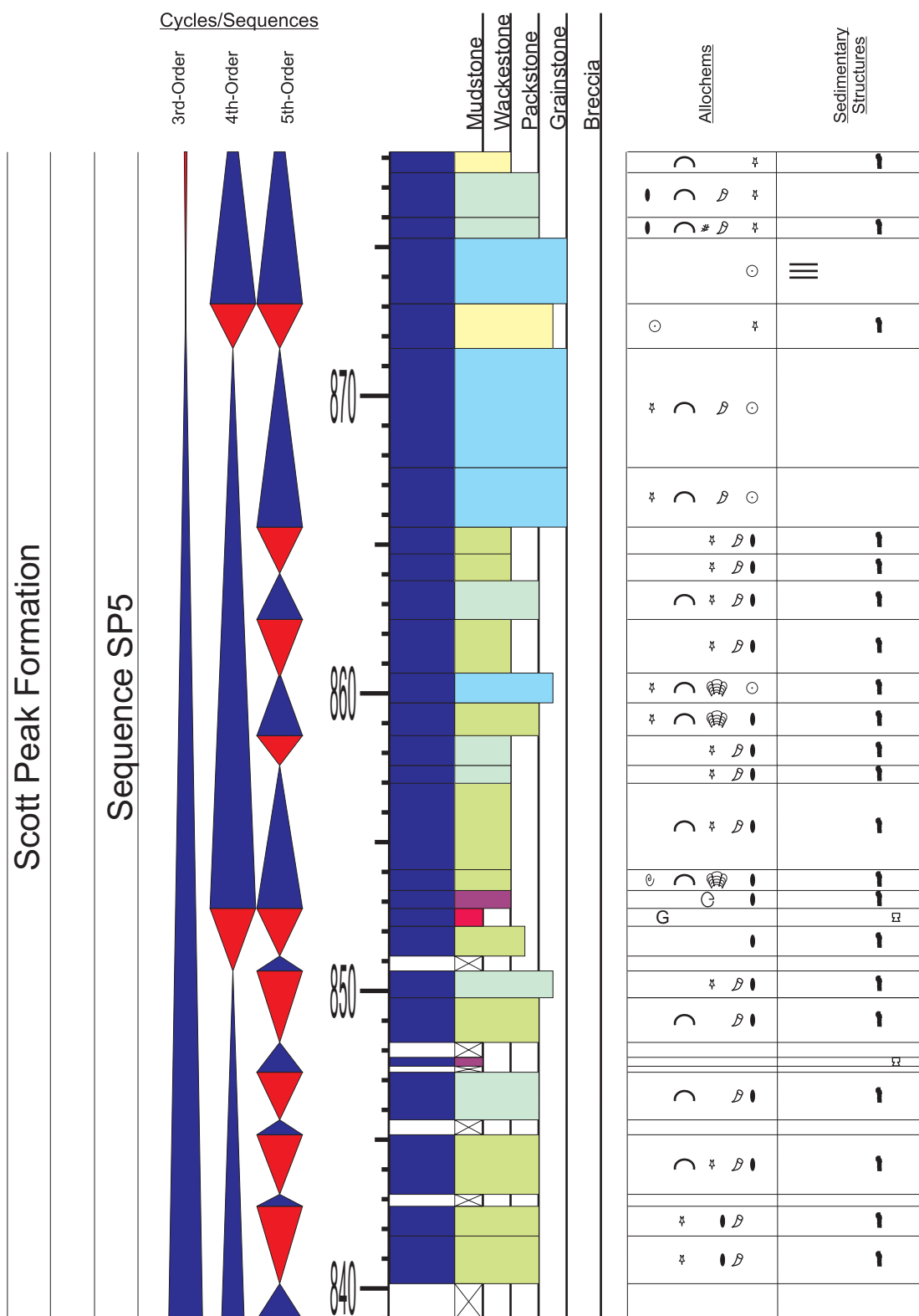
Appendix 9.20: Sedimentary section log for section Copper Mountain (continued). Refer to Appendix 1 for symbols and Figure 3.6 for location.

APPENDIX 9.21



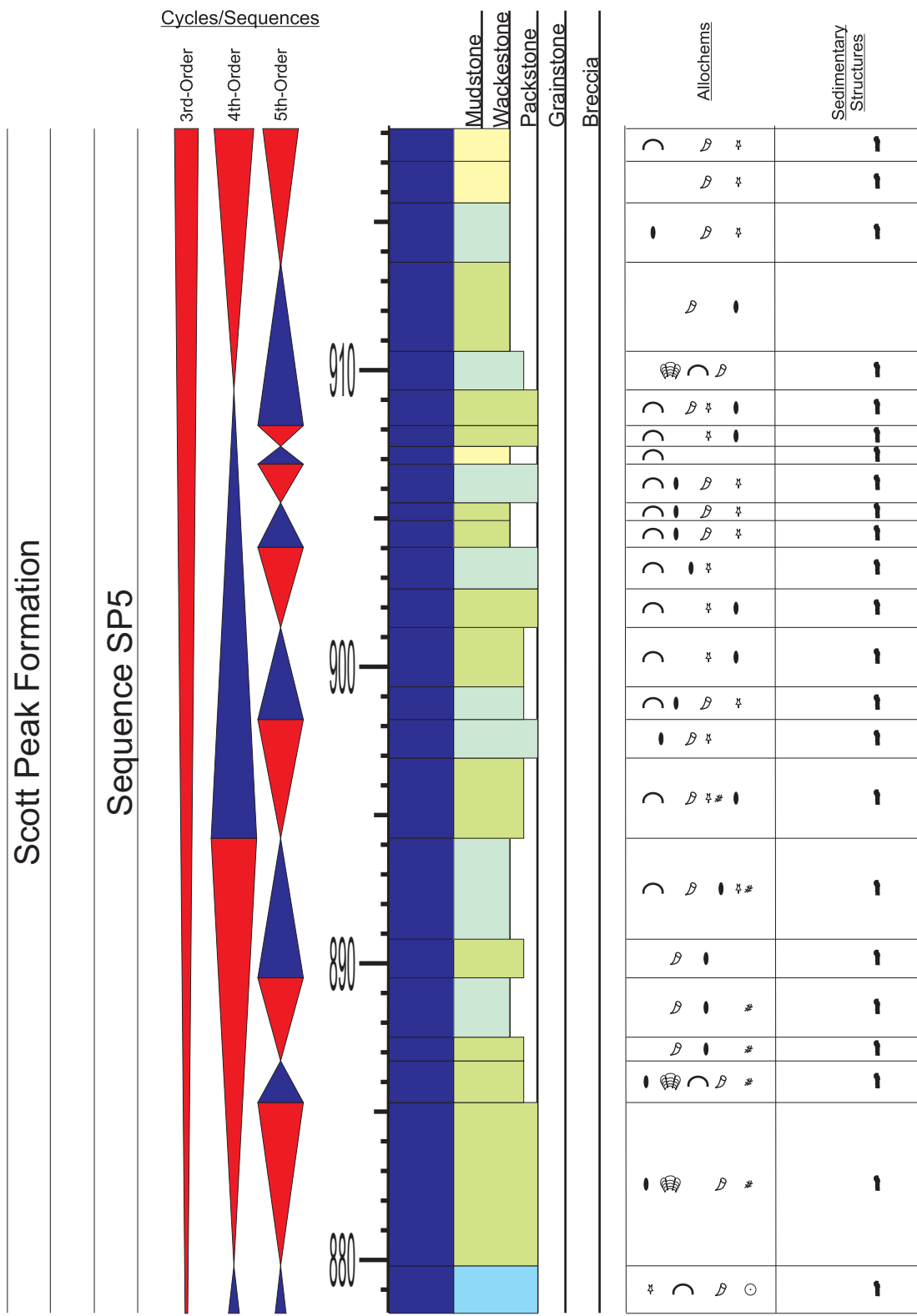
Appendix 9.21: Sedimentary section log for section Copper Mountain (continued). Refer to Appendix 1 for symbols and Figure 3.6 for location.

APPENDIX 9.22



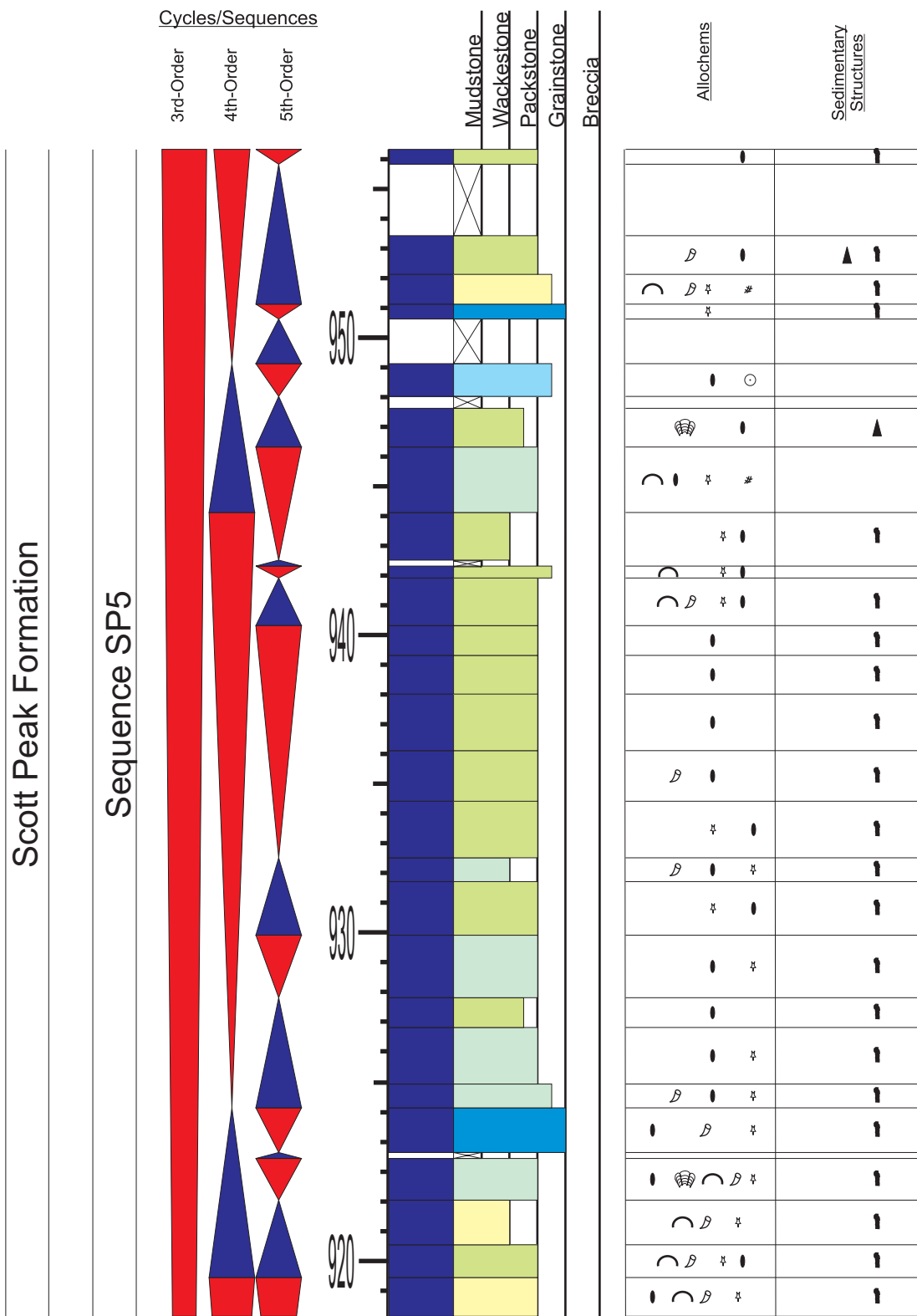
Appendix 9.22: Sedimentary section log for section Copper Mountain (continued). Refer to Appendix 1 for symbols and Figure 3.6 for location.

APPENDIX 9.23



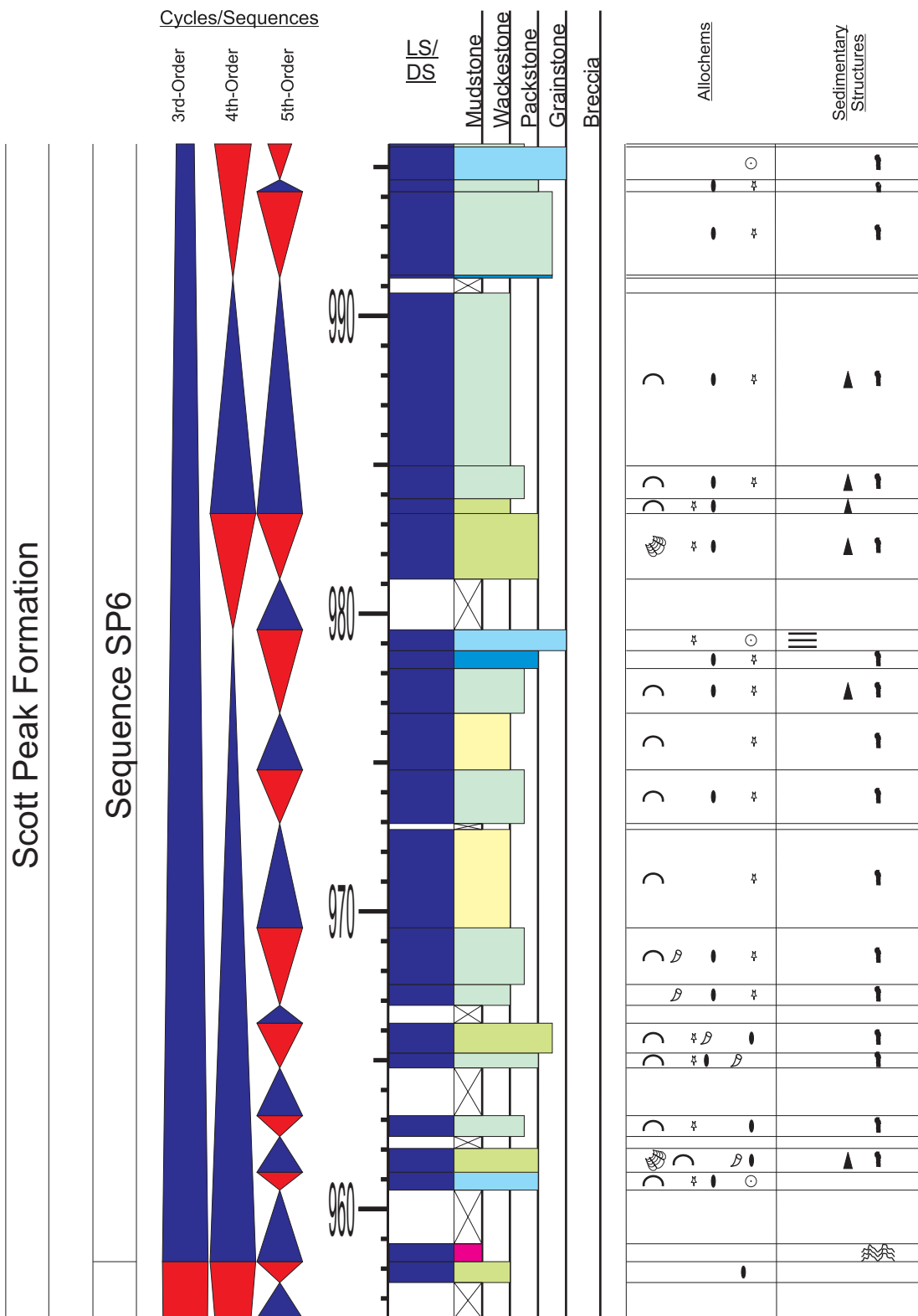
Appendix 9.23: Sedimentary section log for section Copper Mountain (continued). Refer to Appendix 1 for symbols and Figure 3.6 for location.

APPENDIX 9.24



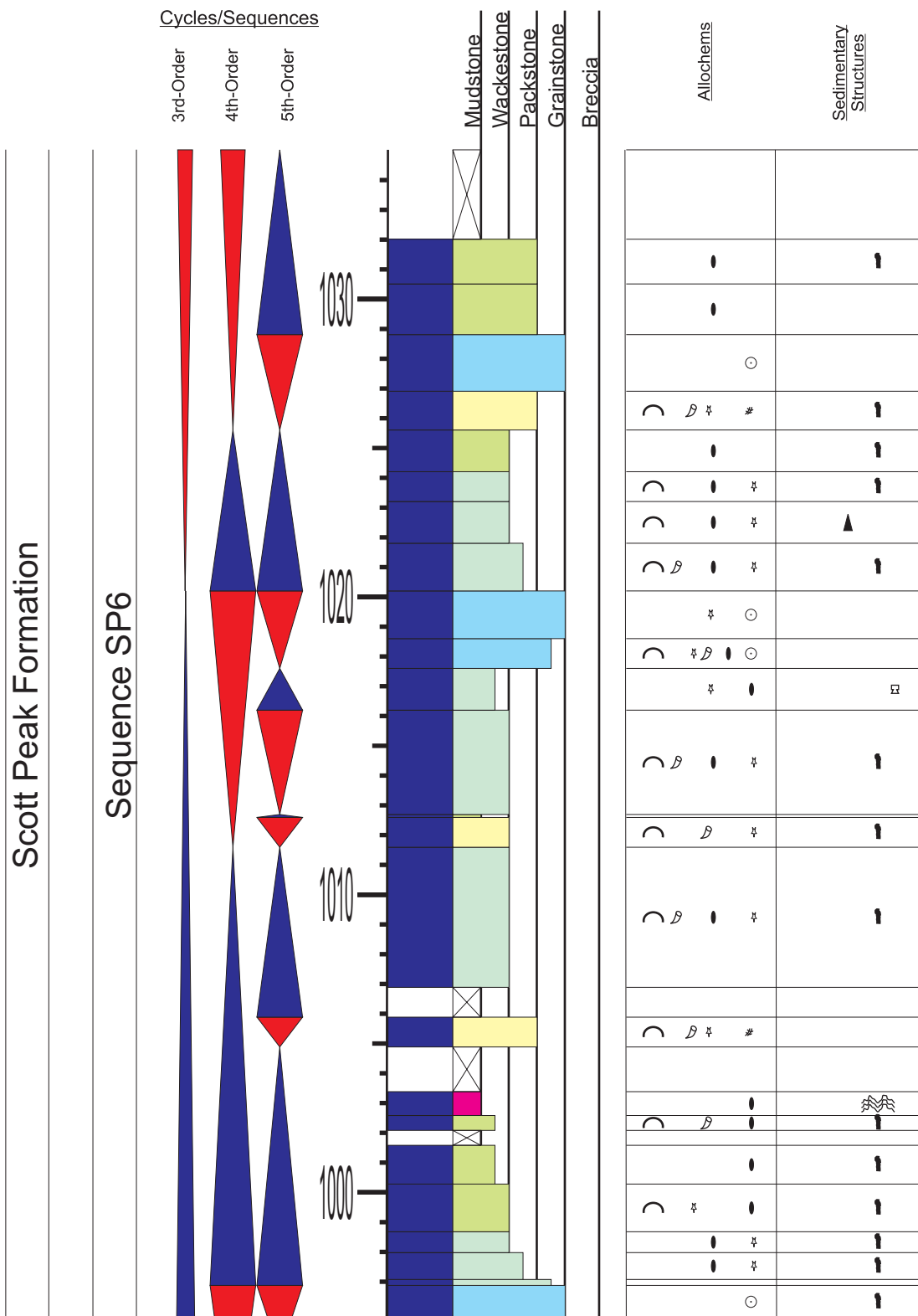
Appendix 9.24: Sedimentary section log for section Copper Mountain (continued). Refer to Appendix 1 for symbols and Figure 3.6 for location.

APPENDIX 9.25



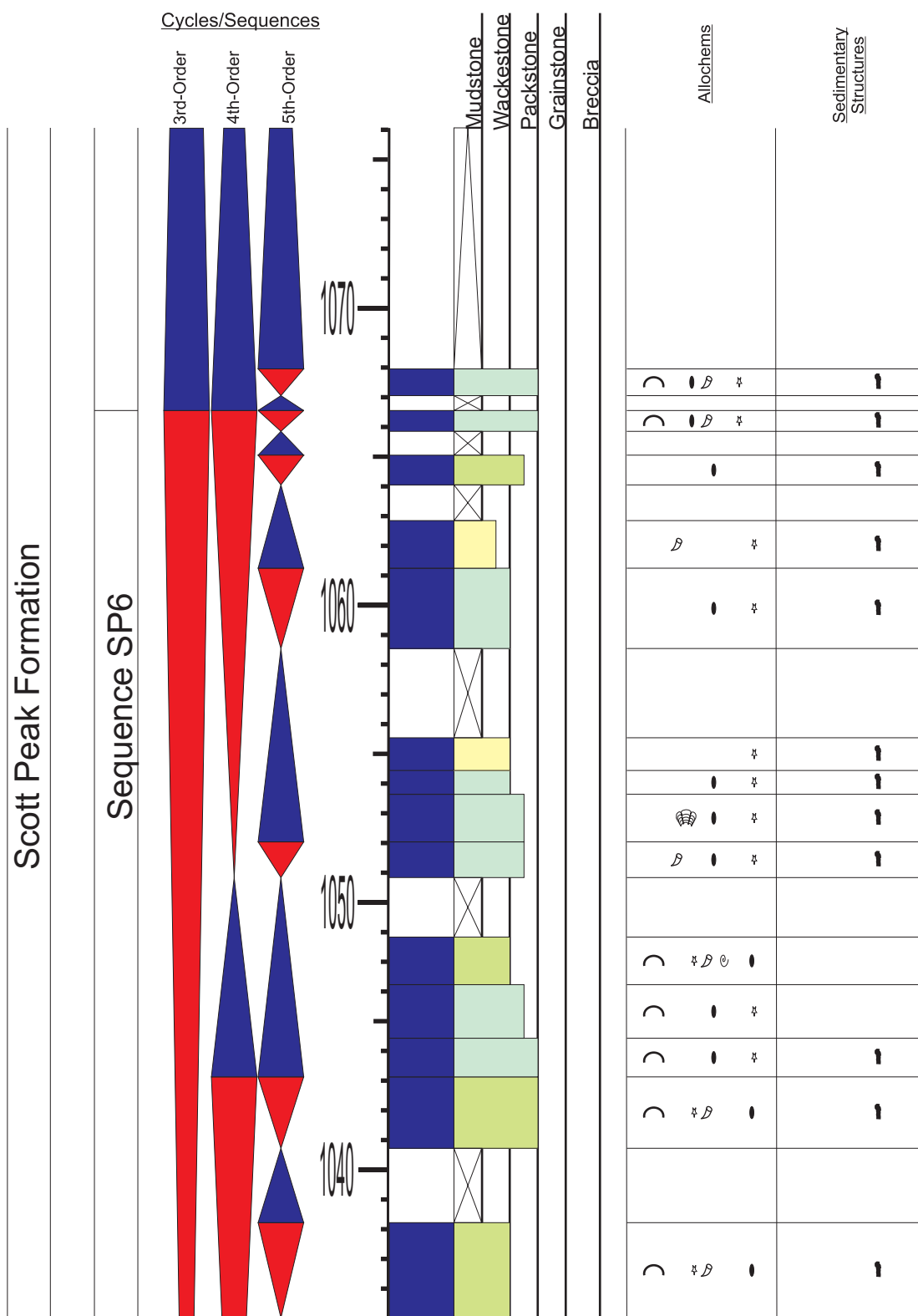
Appendix 9.25: Sedimentary section log for section Copper Mountain (continued). Refer to Appendix 1 for symbols and Figure 3.6 for location.

APPENDIX 9.26



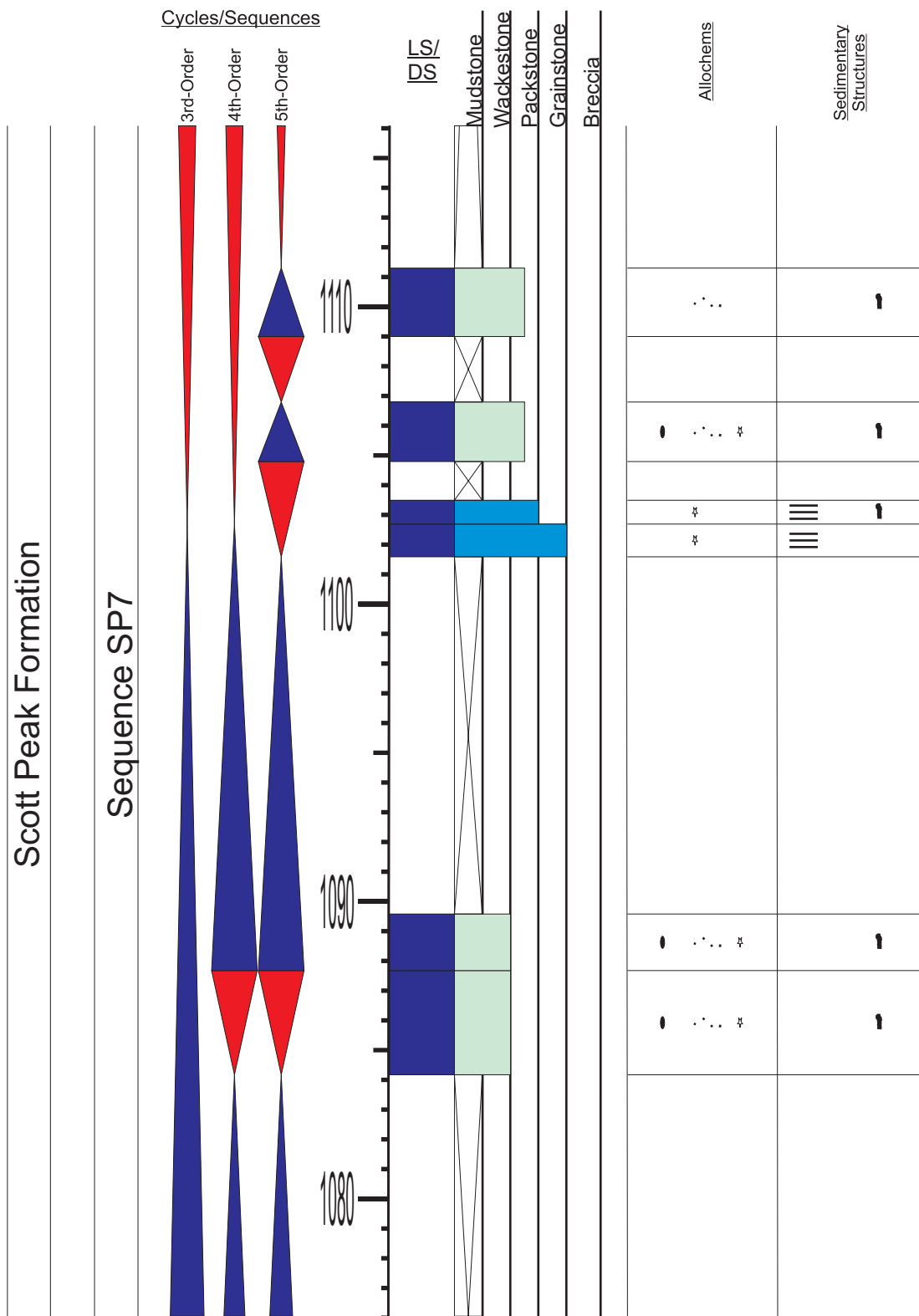
Appendix 9.26: Sedimentary section log for section Copper Mountain (continued). Refer to Appendix 1 for symbols and Figure 3.6 for location.

APPENDIX 9.27



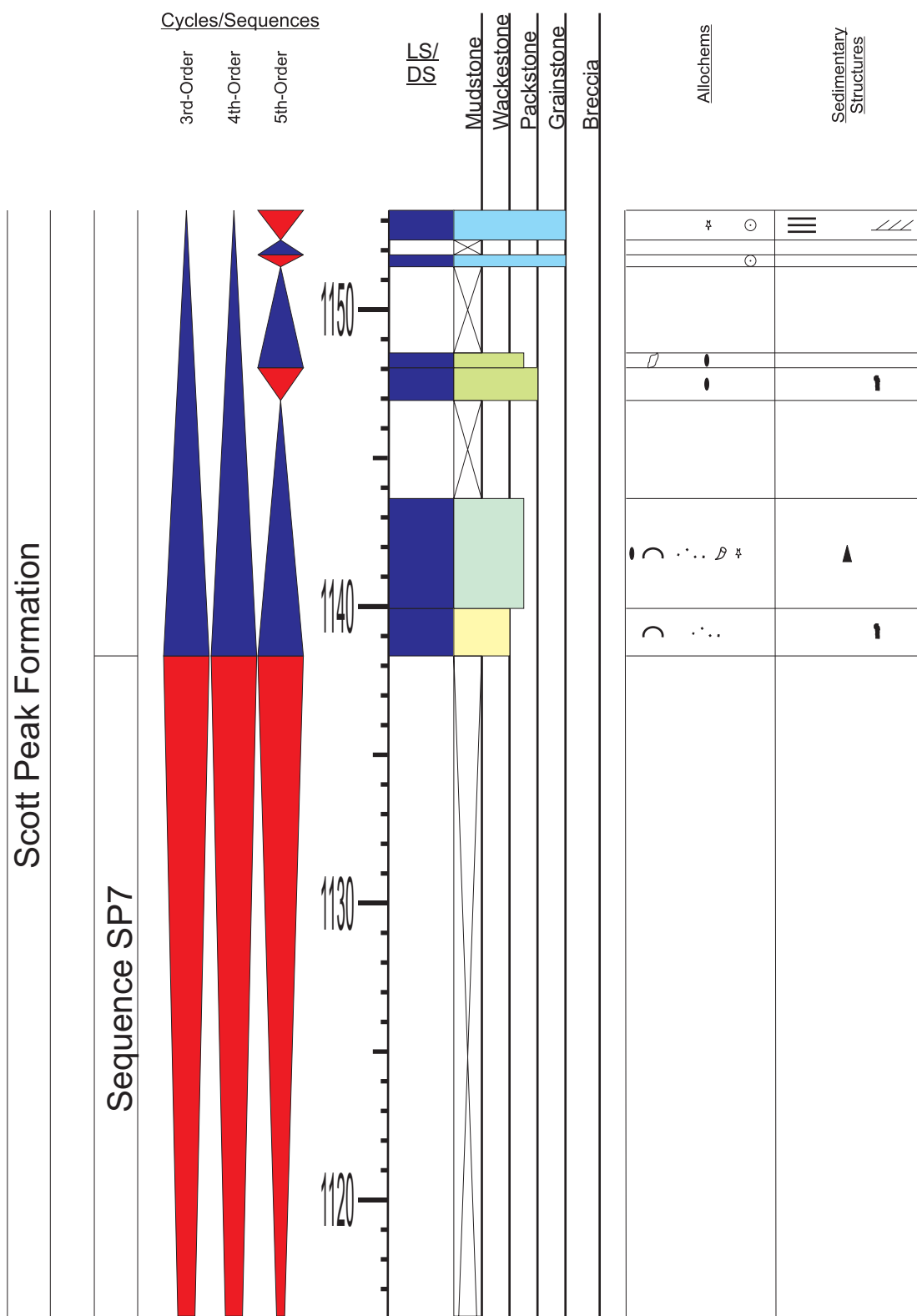
Appendix 9.27: Sedimentary section log for section Copper Mountain (continued). Refer to Appendix 1 for symbols and Figure 3.6 for location.

APPENDIX 9.28



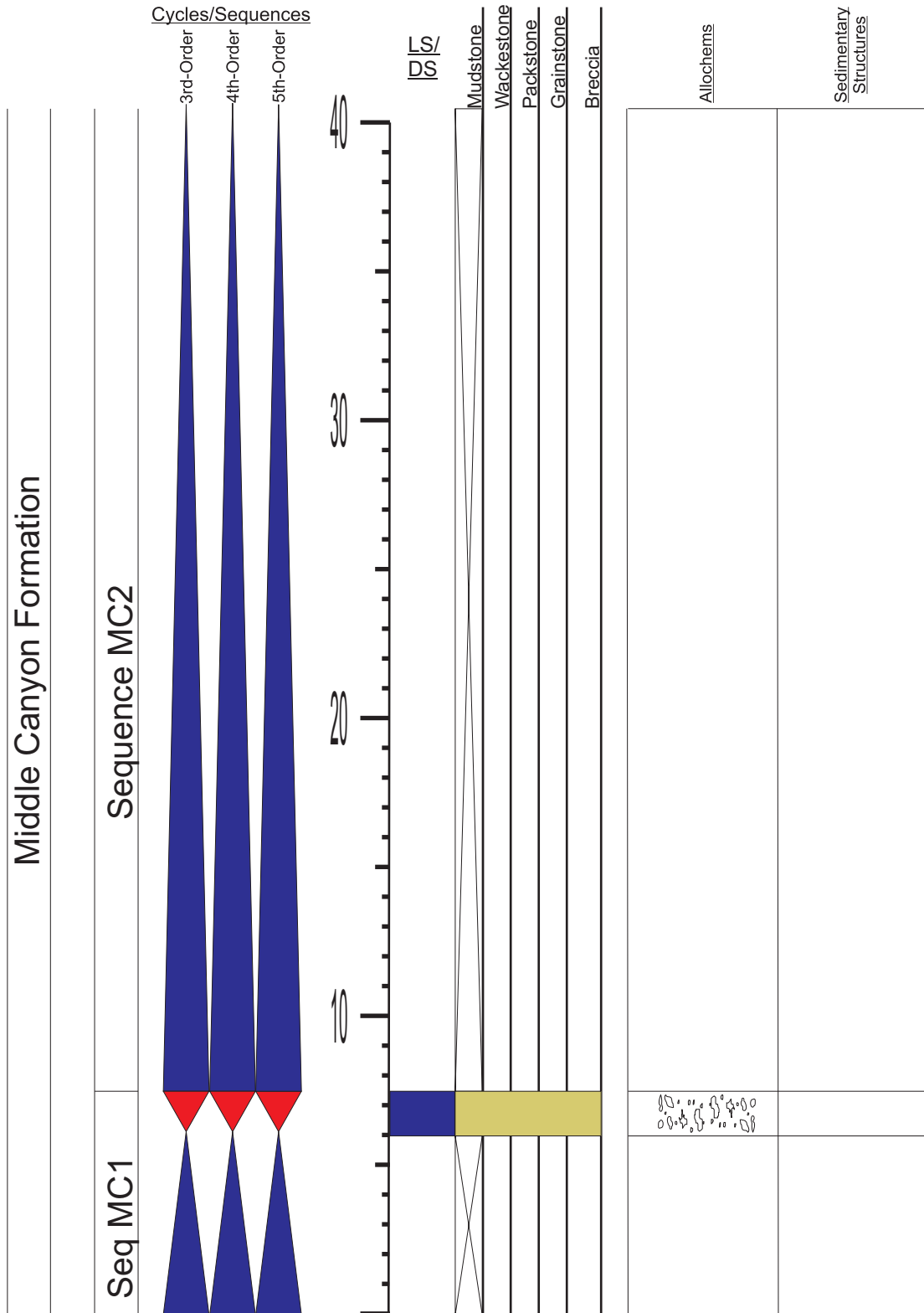
Appendix 9.28: Sedimentary section log for section Copper Mountain (continued). Refer to Appendix 1 for symbols and Figure 3.6 for location.

APPENDIX 9.29



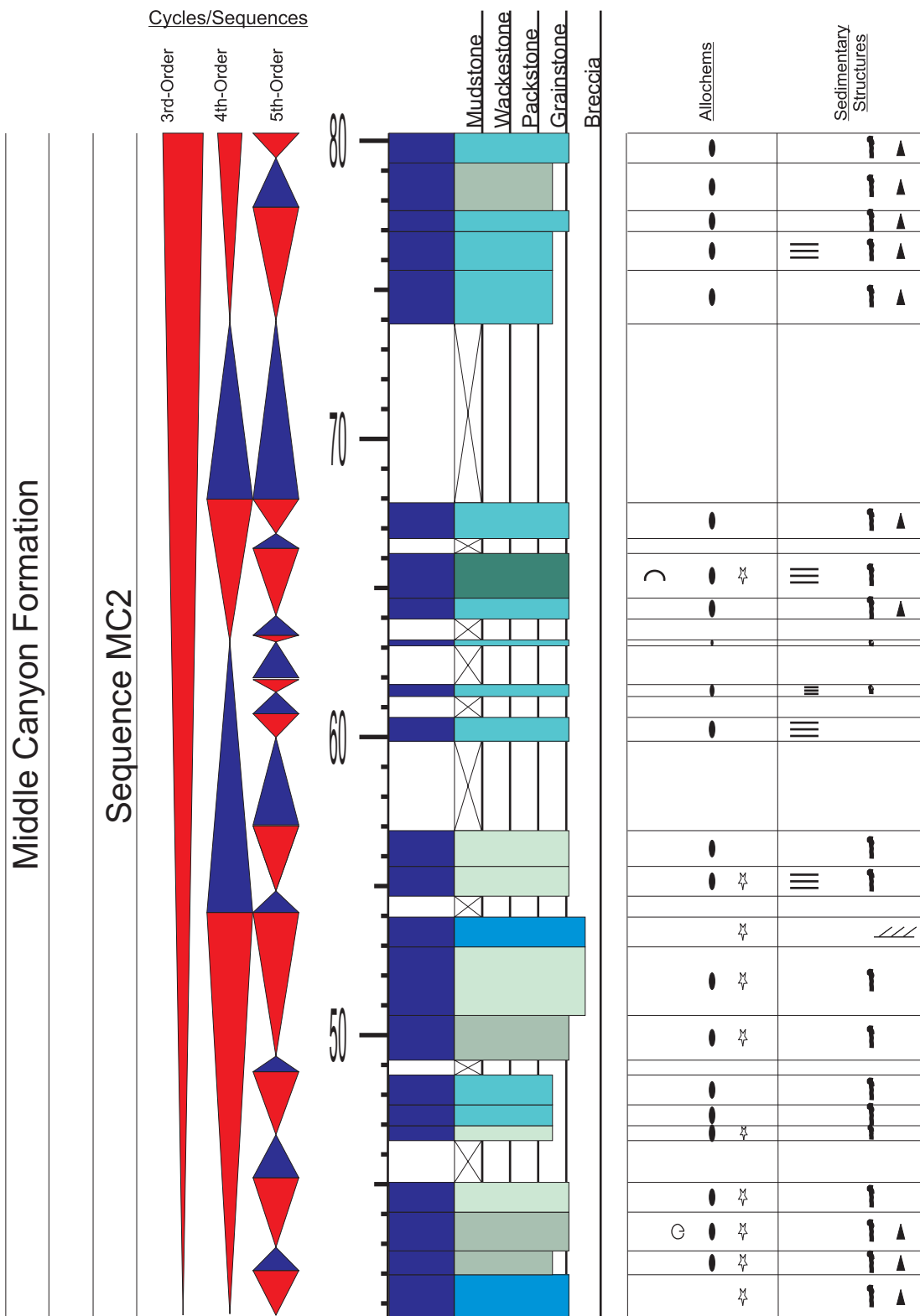
Appendix 9.29: Sedimentary section log for section Copper Mountain (continued). Refer to Appendix 1 for symbols and Figure 3.6 for location.

APPENDIX 10.1



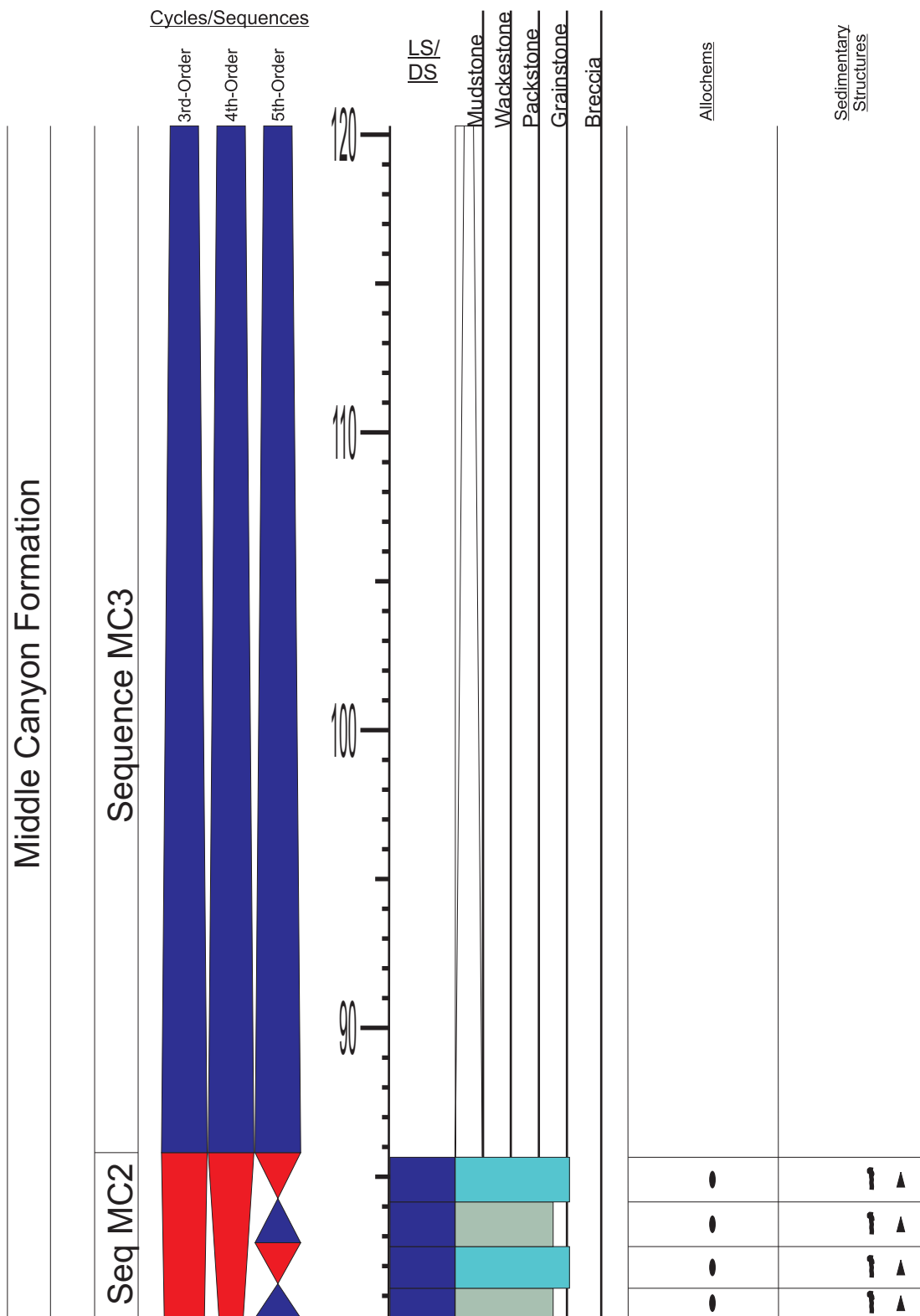
Appendix 10.1: Sedimentary section log for section East Canyon. Refer to Appendix 1 for symbols and Figure 3.6 for location.

APPENDIX 10.2



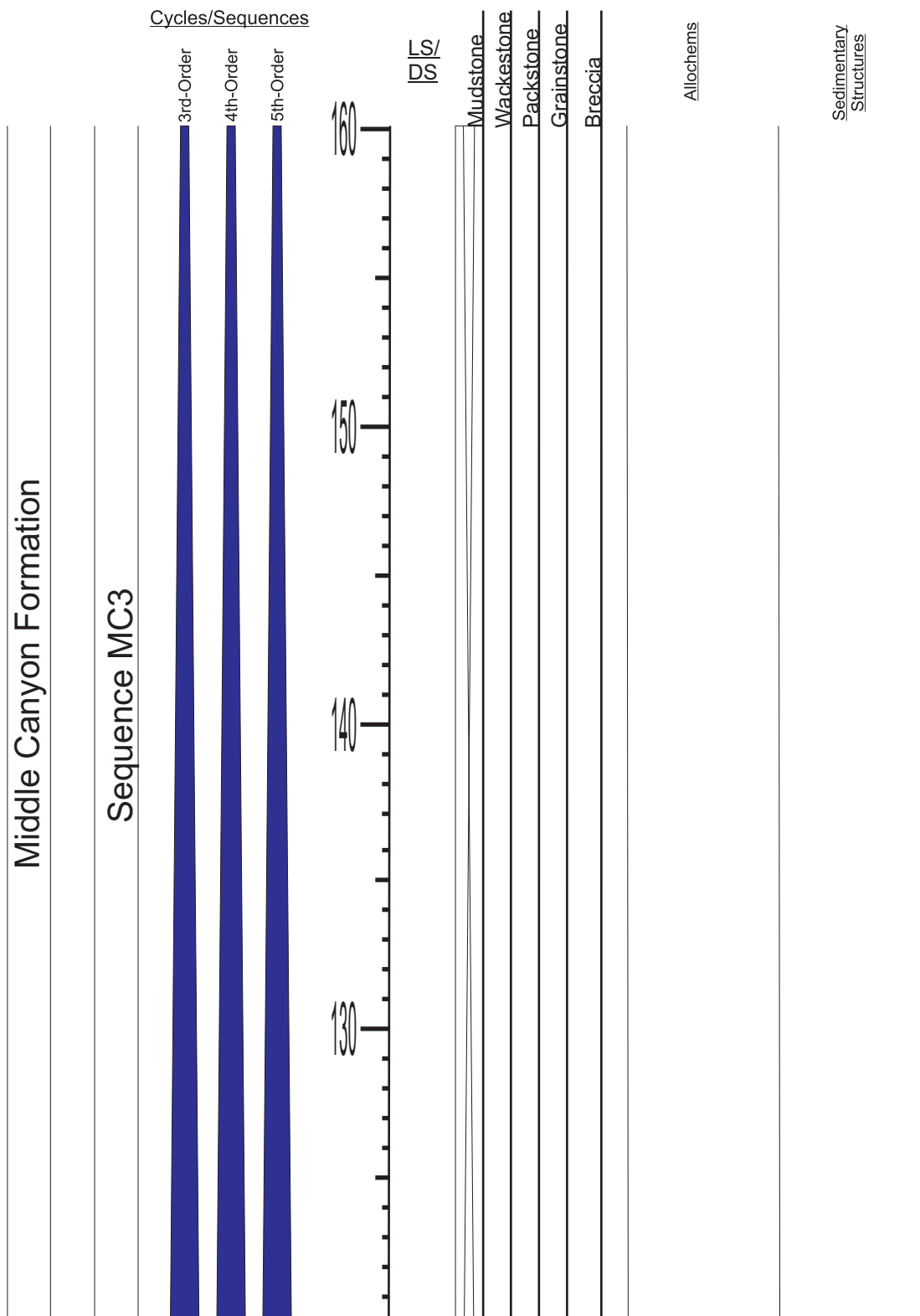
Appendix 10.2: Sedimentary section log for section East Canyon (continued). Refer to Appendix 1 for symbols and Figure 3.6 for location.

APPENDIX 10.3



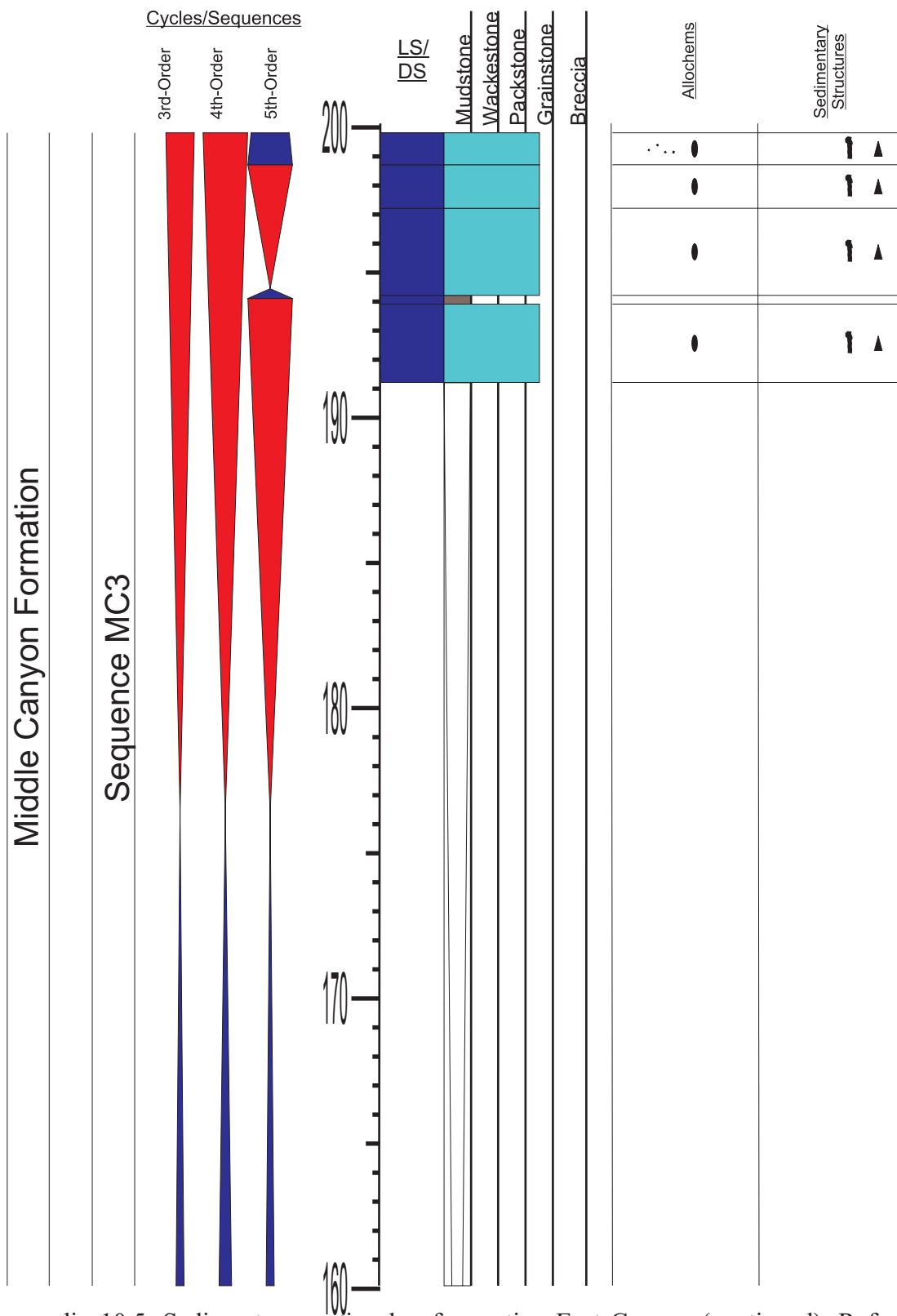
Appendix 10.3: Sedimentary section log for section East Canyon (continued). Refer to Appendix 1 for symbols and Figure 3.6 for location.

APPENDIX 10.4



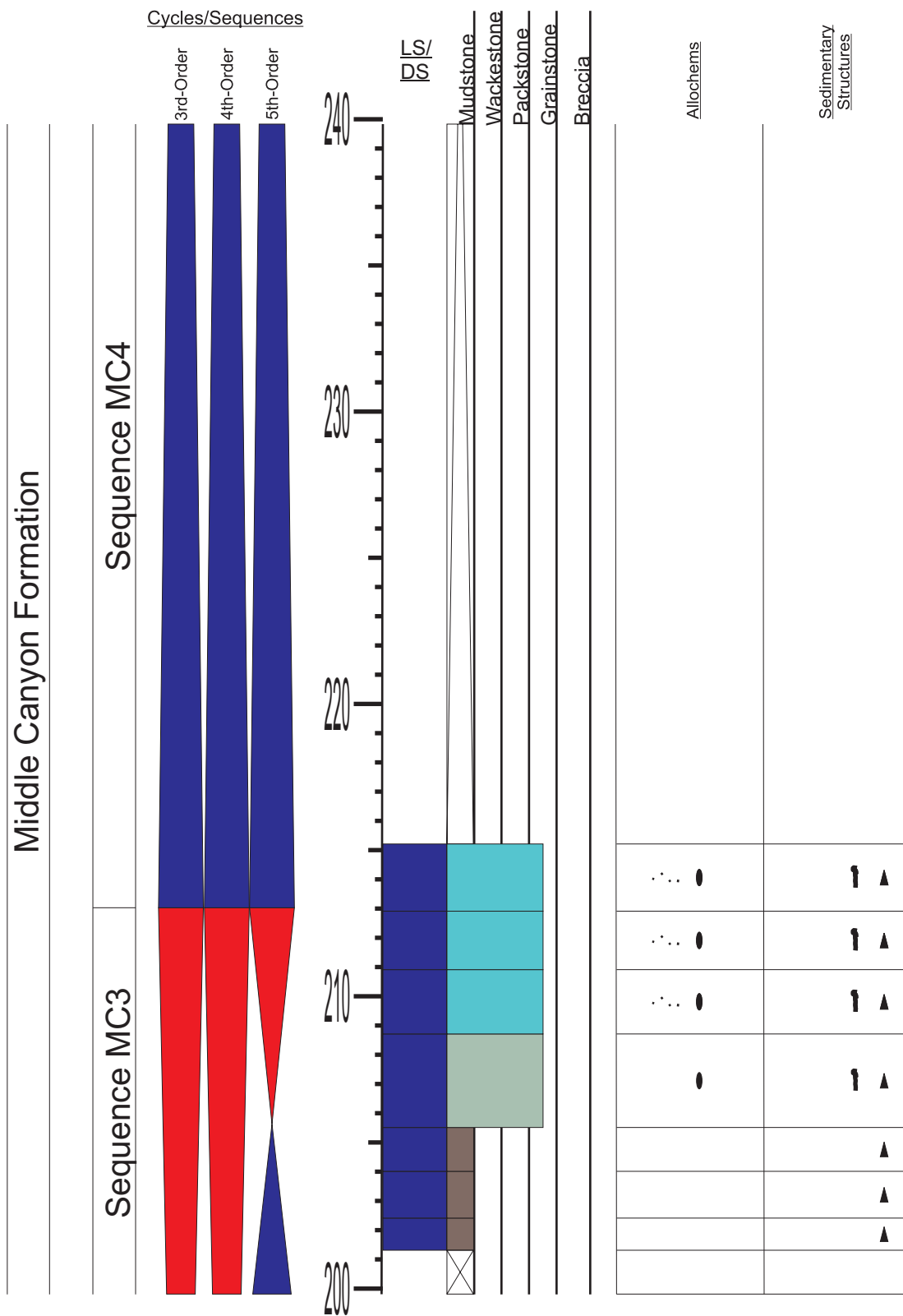
Appendix 10.4: Sedimentary section log for section East Canyon (continued). Refer to Appendix 1 for symbols and Figure 3.6 for location.

APPENDIX 10.5



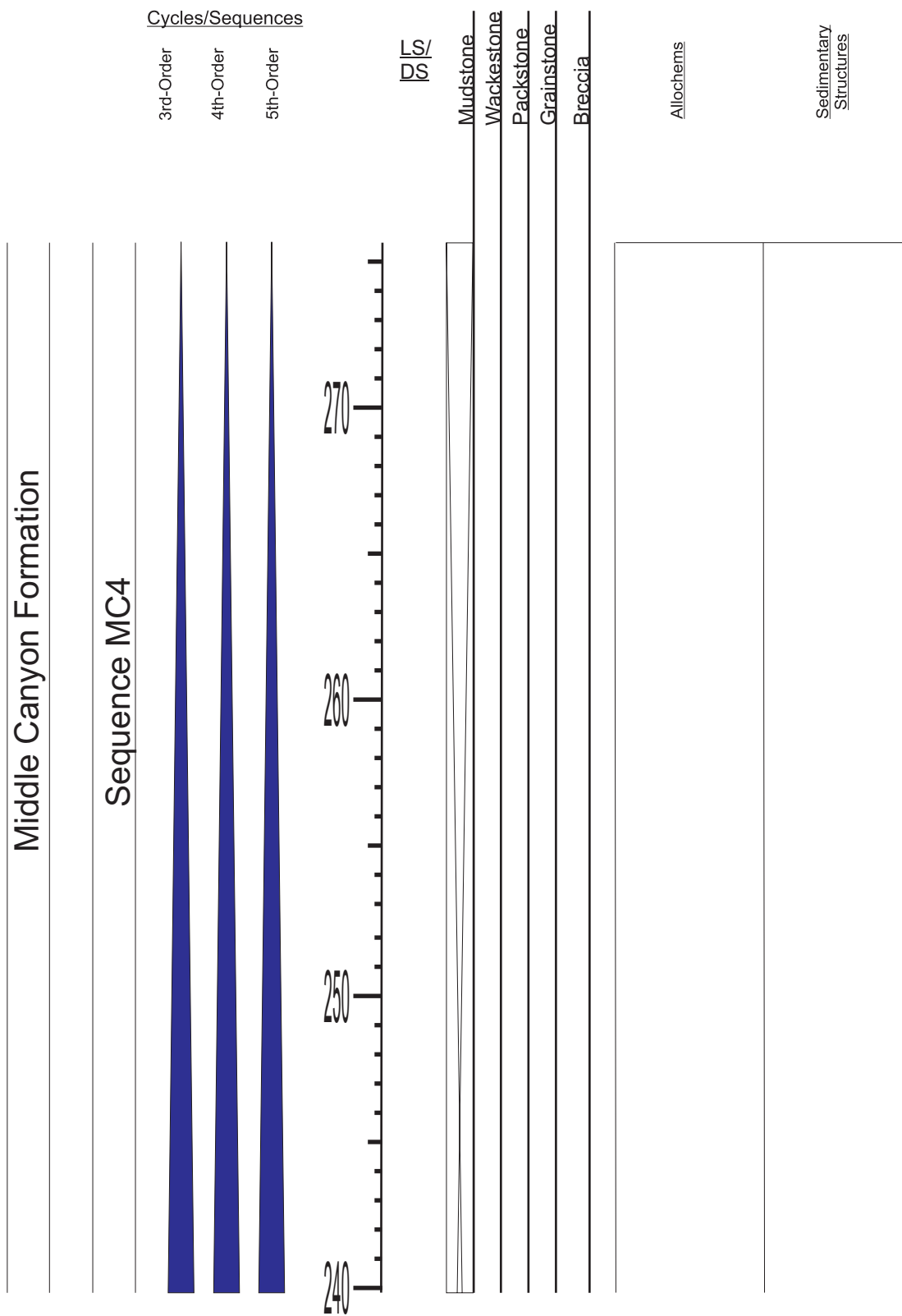
Appendix 10.5: Sedimentary section log for section East Canyon (continued). Refer to Appendix 1 for symbols and Figure 3.6 for location.

APPENDIX 10.6



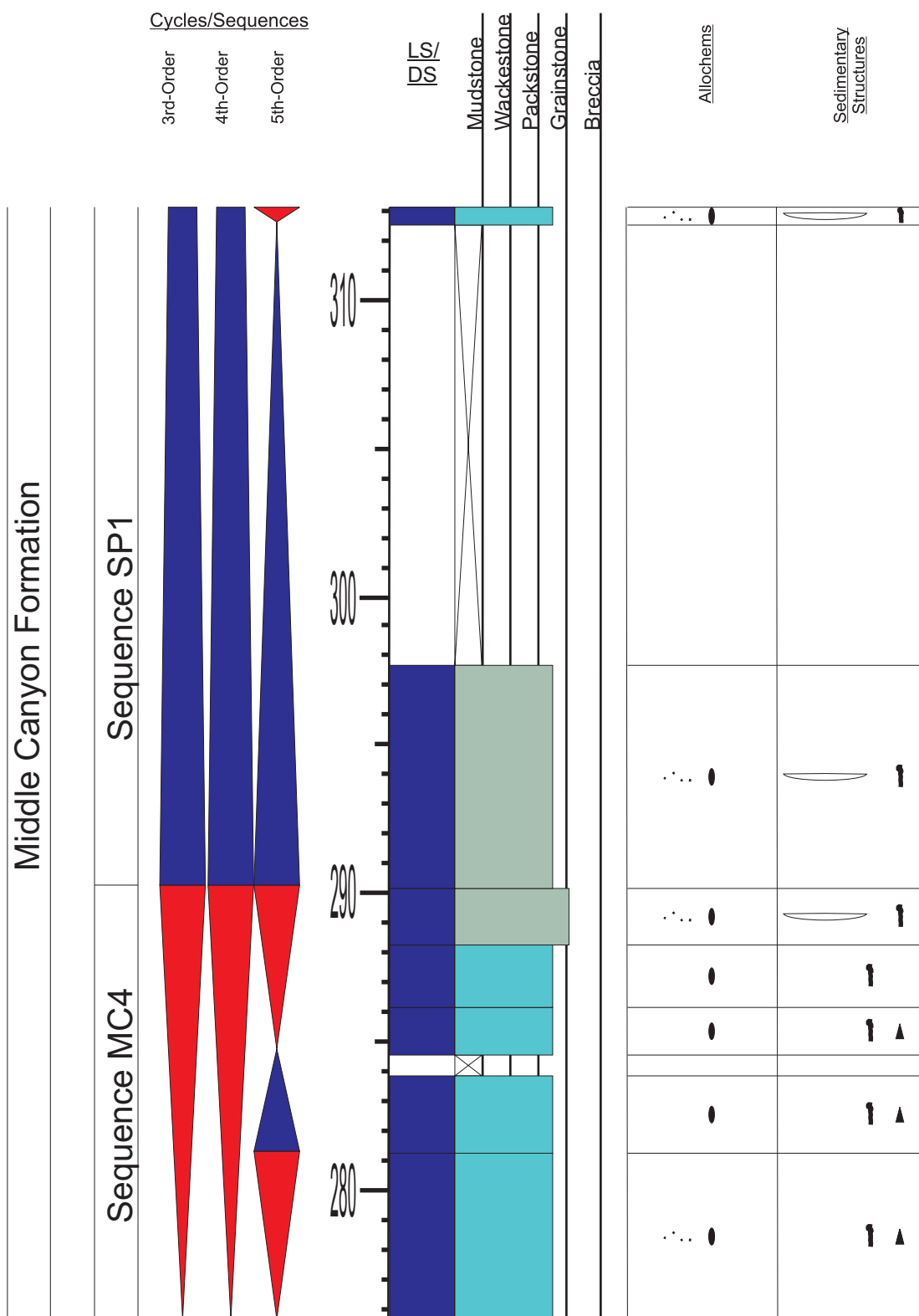
Appendix 10.6: Sedimentary section log for section East Canyon (continued). Refer to Appendix 1 for symbols and Figure 3.6 for location.

APPENDIX 10.7



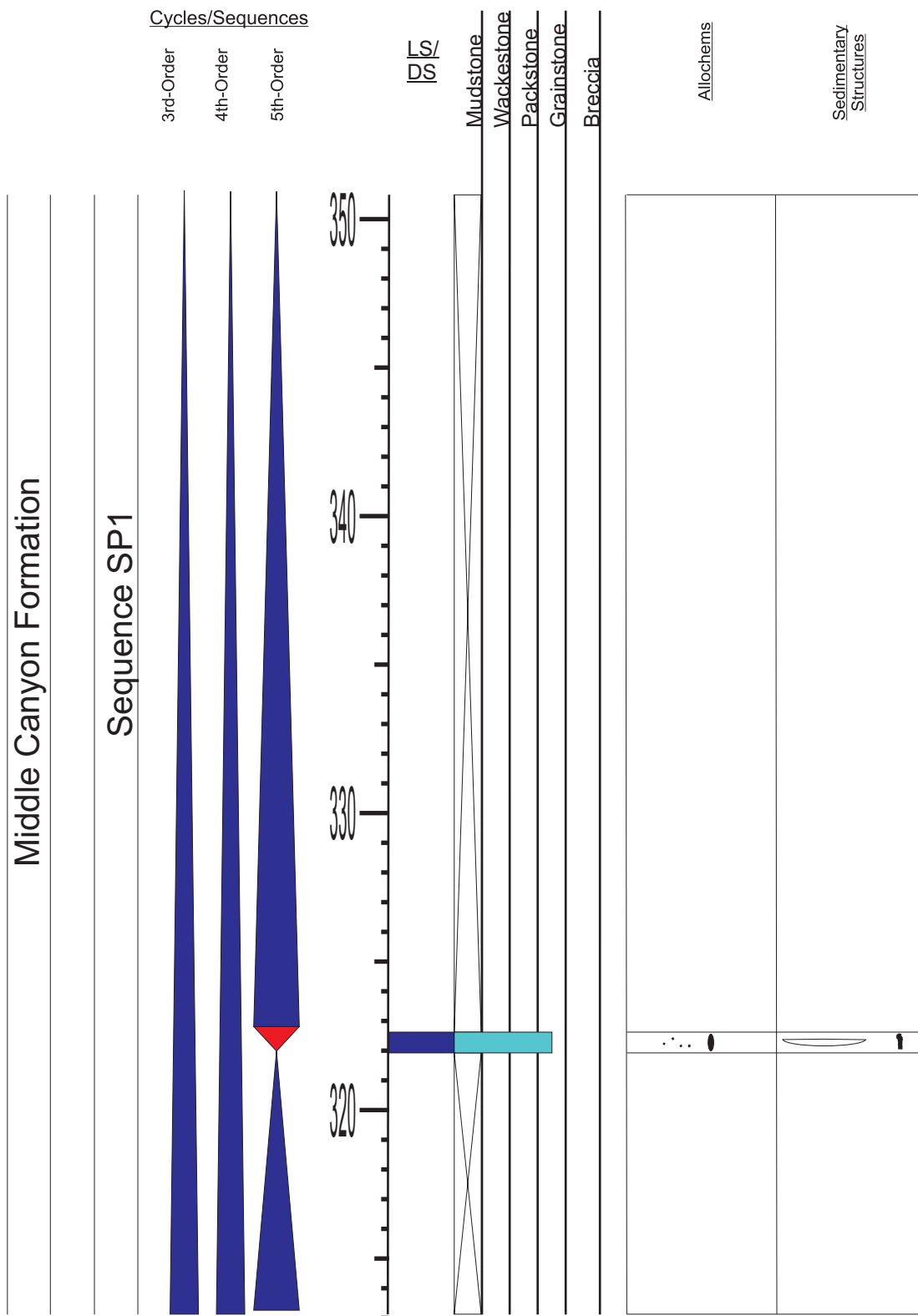
Appendix 10.7: Sedimentary section log for section East Canyon (continued). Refer to Appendix 1 for symbols and Figure 3.6 for location.

APPENDIX 10.8



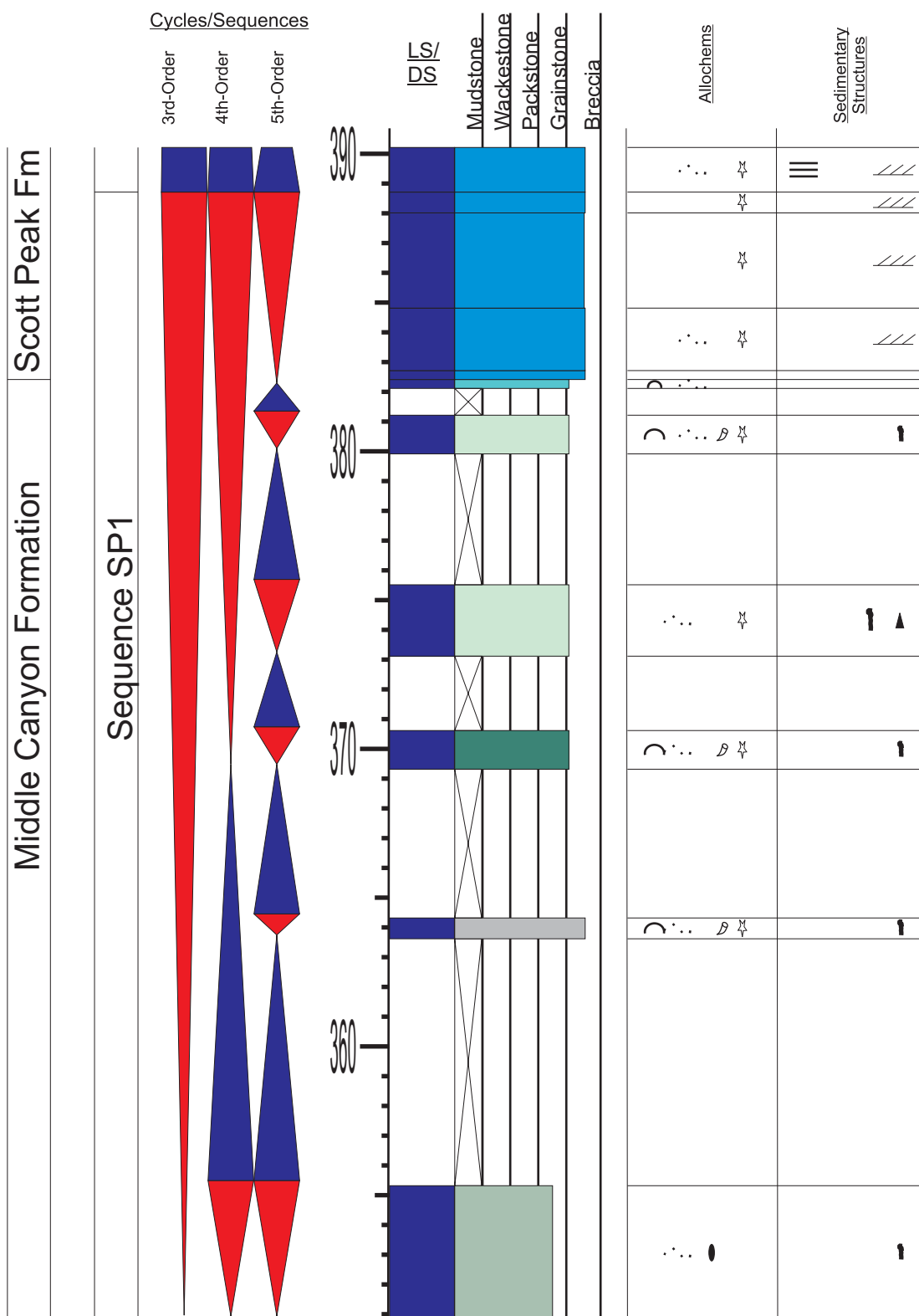
Appendix 10.8: Sedimentary section log for section East Canyon (continued). Refer to Appendix 1 for symbols and Figure 3.6 for location.

APPENDIX 10.9



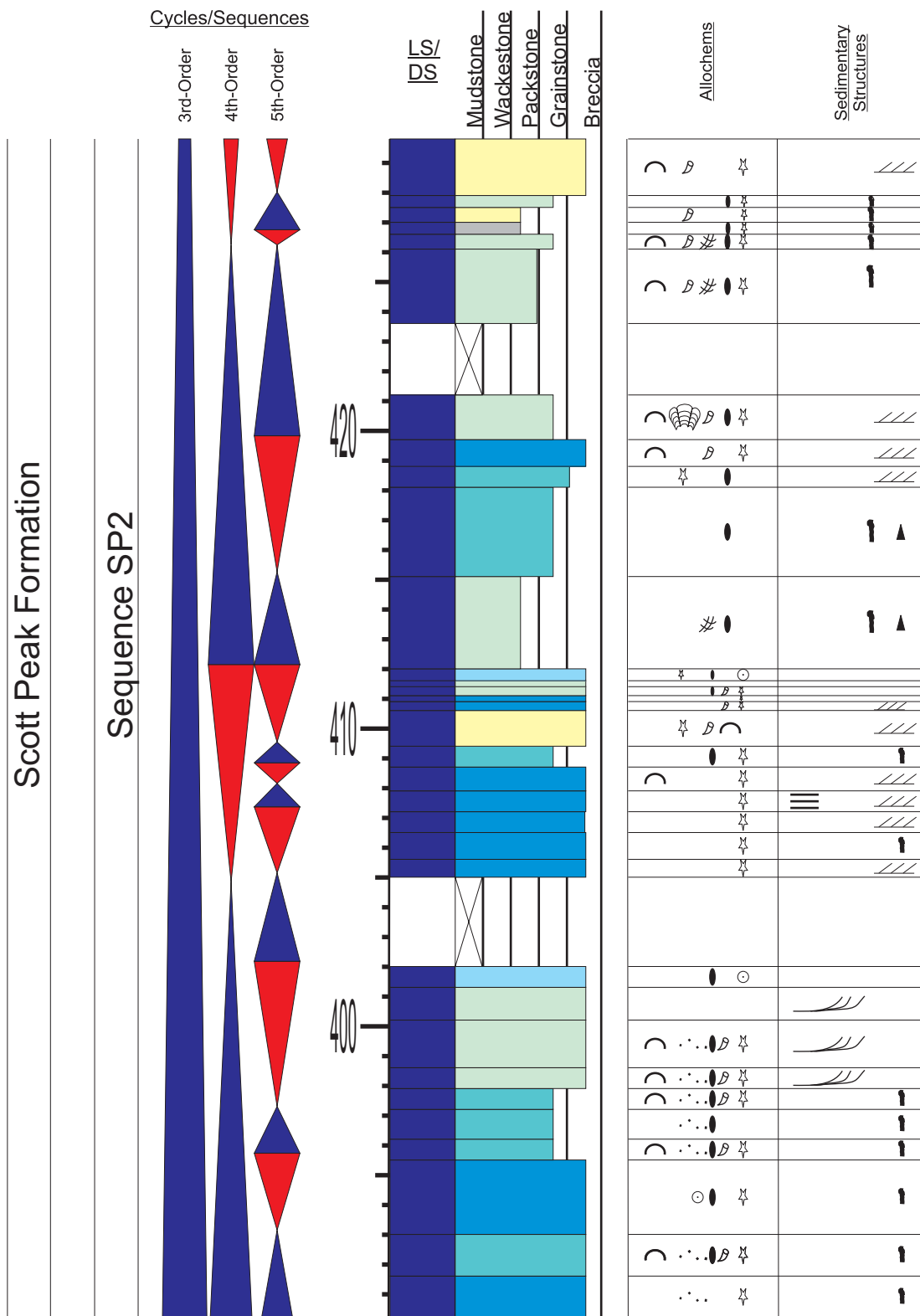
Appendix 10.9: Sedimentary section log for section East Canyon (continued). Refer to Appendix 1 for symbols and Figure 3.6 for location.

APPENDIX 10.10



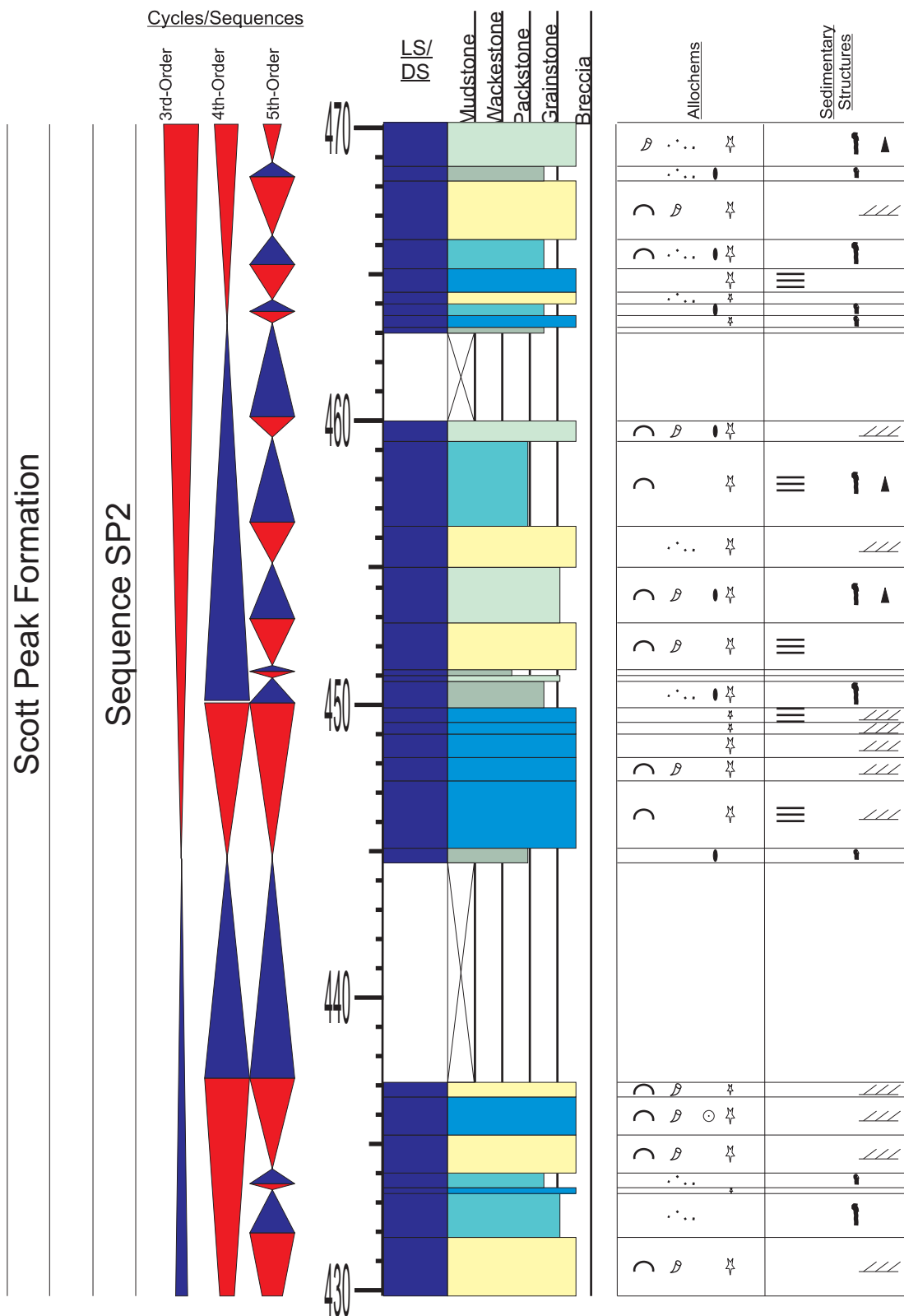
Appendix 10.10: Sedimentary section log for section East Canyon (continued). Refer to Appendix 1 for symbols and Figure 3.6 for location.

APPENDIX 10.11



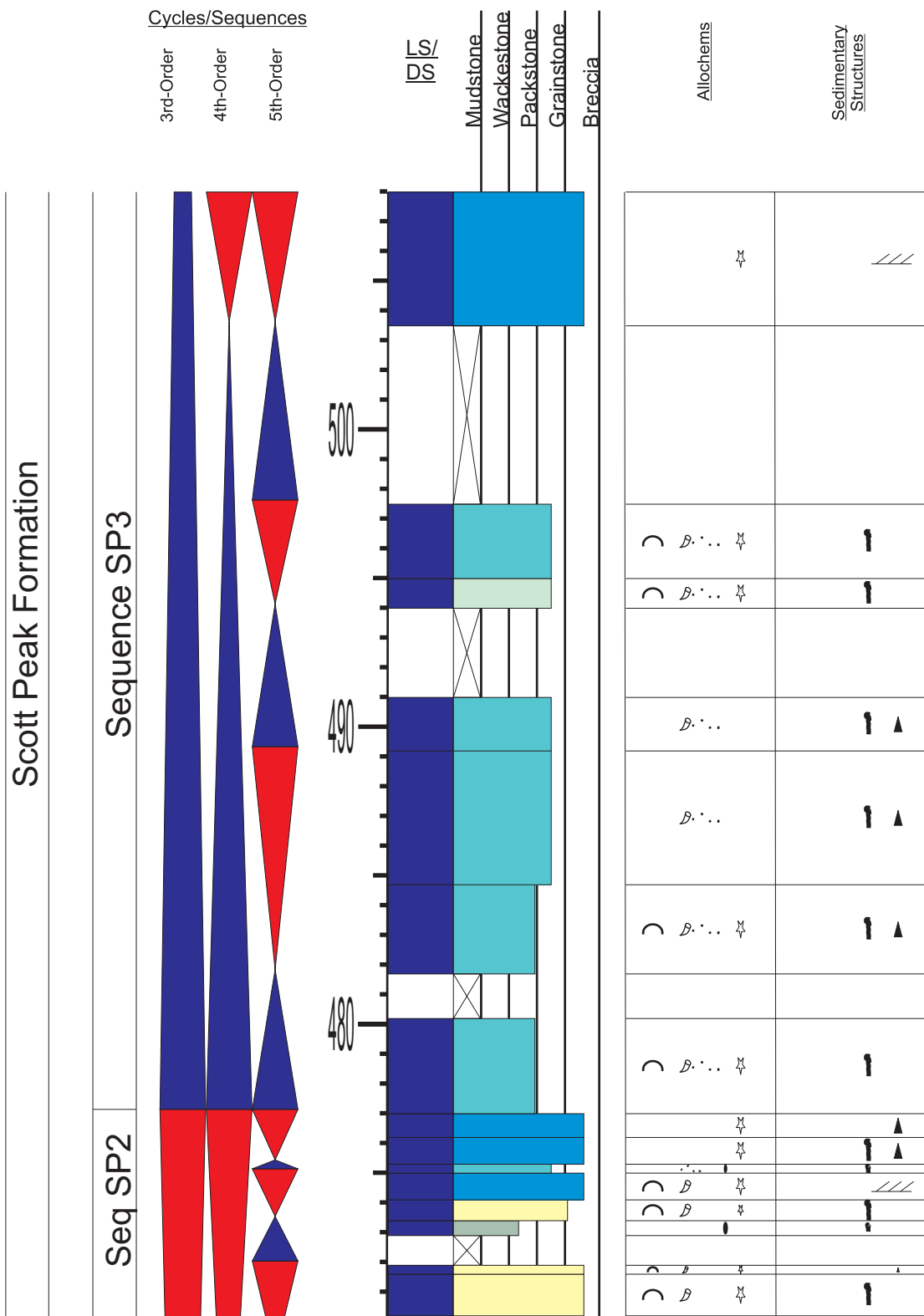
Appendix 10.11: Sedimentary section log for section East Canyon (continued). Refer to Appendix 1 for symbols and Figure 3.6 for location.

APPENDIX 10.12

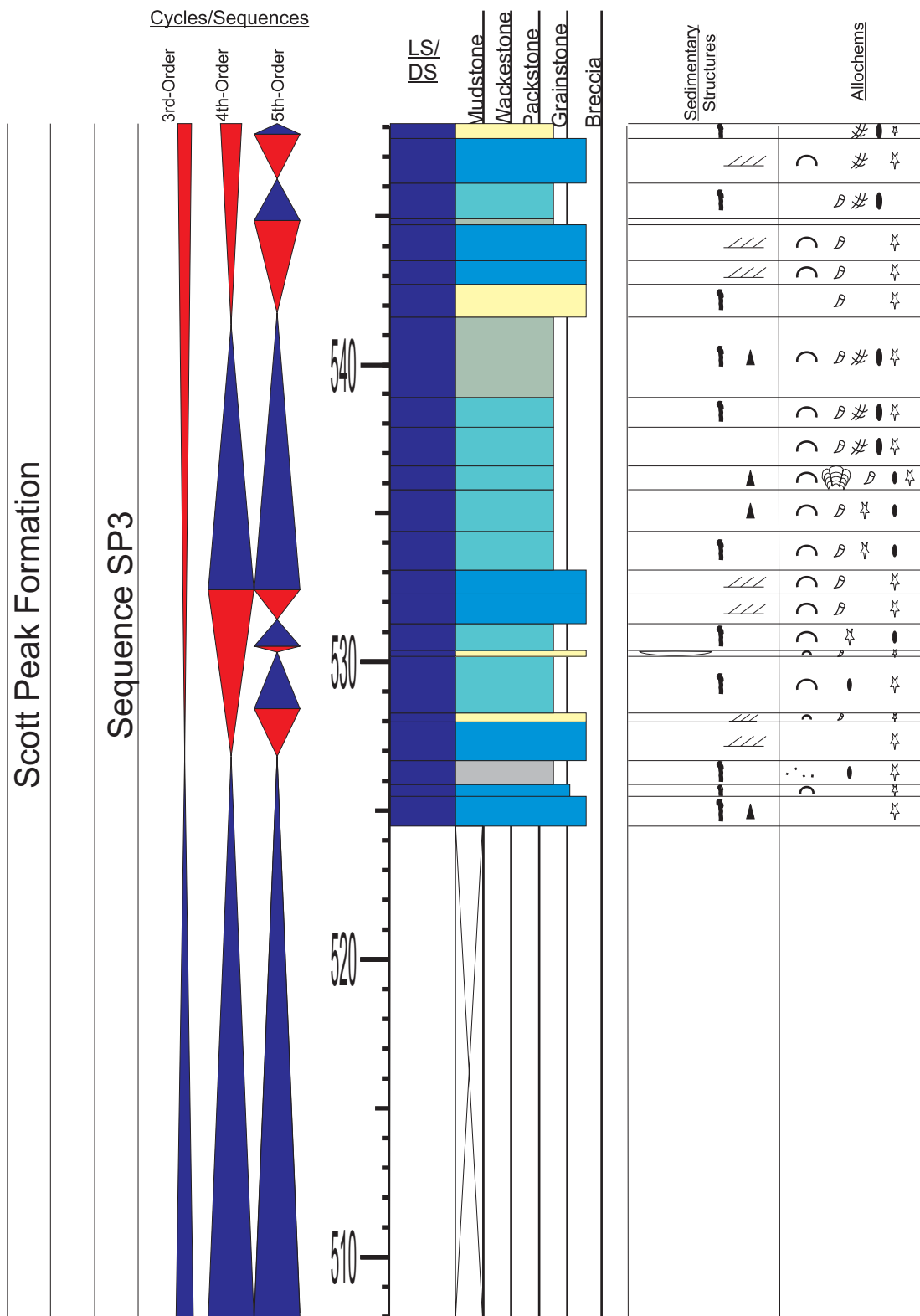


Appendix 10.12: Sedimentary section log for section East Canyon (continued). Refer to Appendix 1 for symbols and Figure 3.6 for location.

APPENDIX 10.13

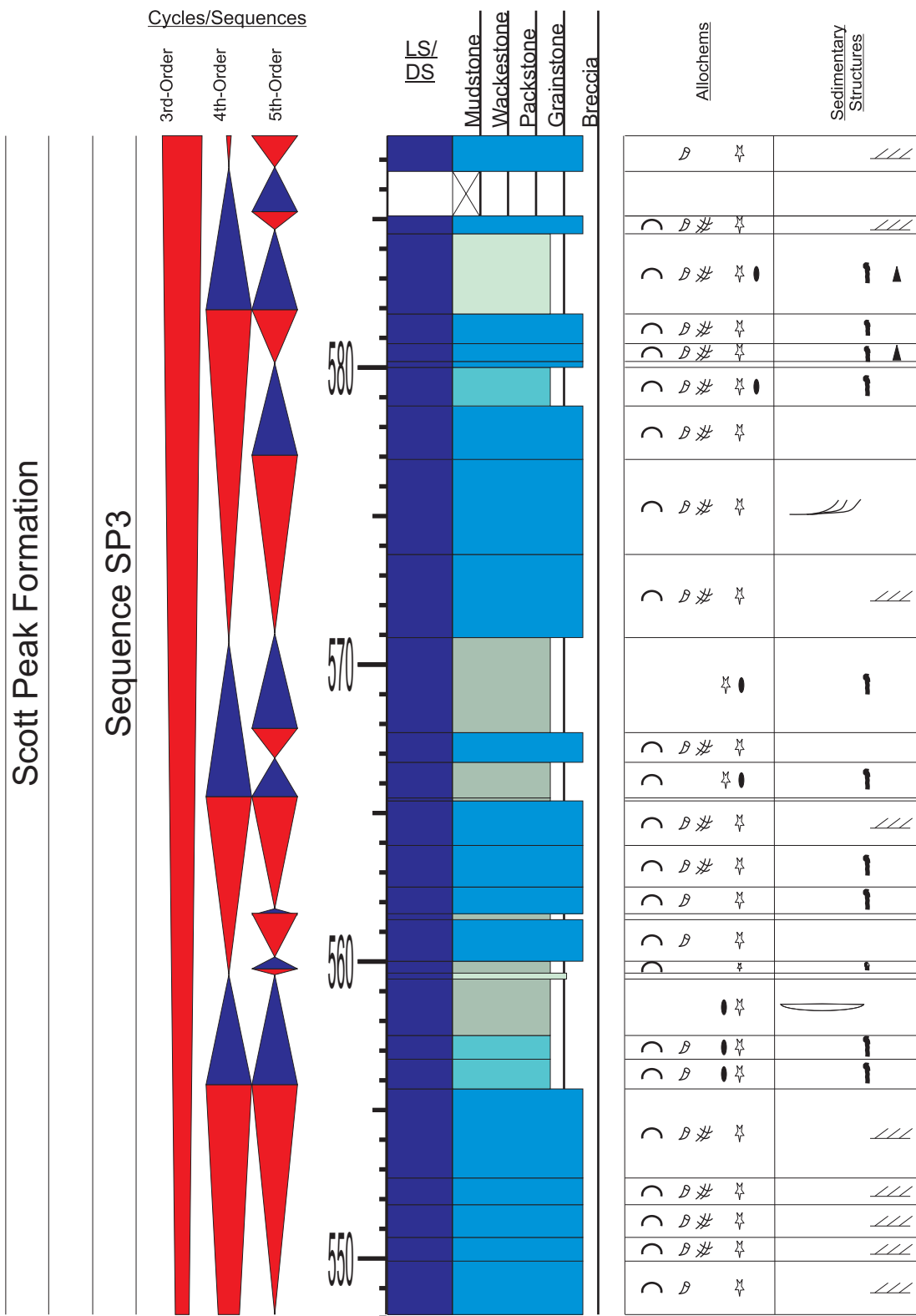


APPENDIX 10.14



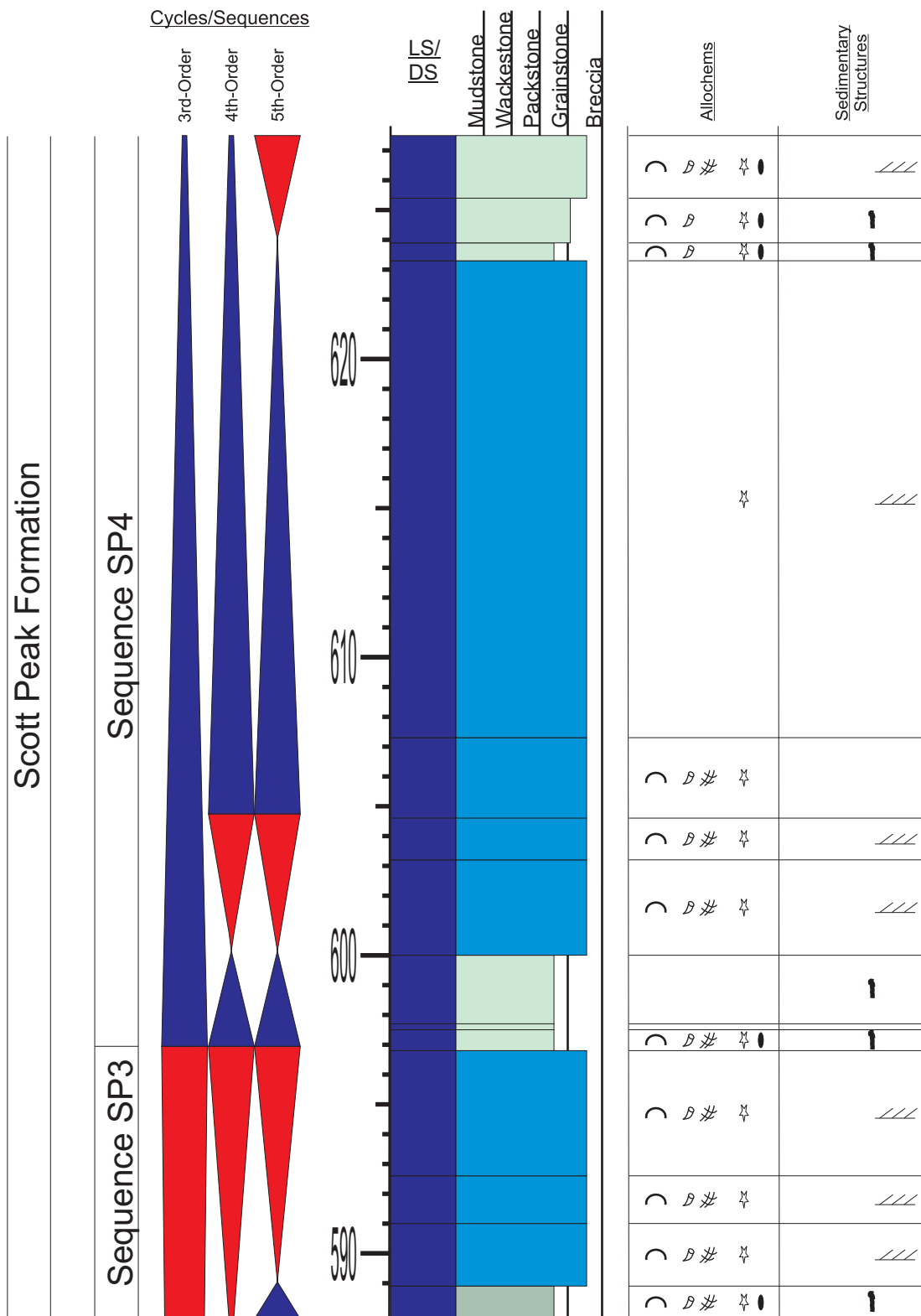
Appendix 10.14: Sedimentary section log for section East Canyon (continued). Refer to Appendix 1 for symbols and Figure 3.6 for location.

APPENDIX 10.15



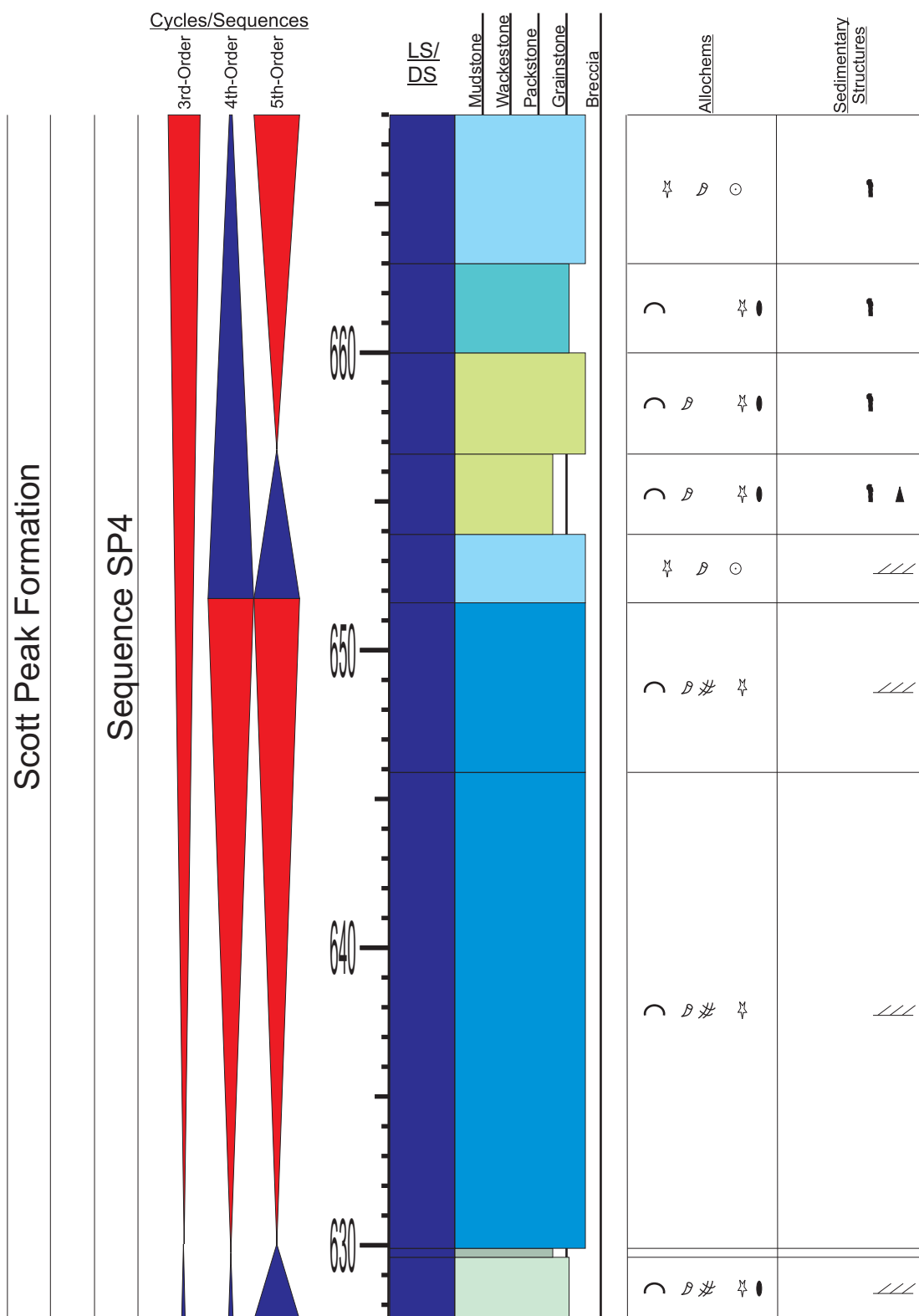
Appendix 10.15: Sedimentary section log for section East Canyon (continued). Refer to Appendix 1 for symbols and Figure 3.6 for location.

APPENDIX 10.16



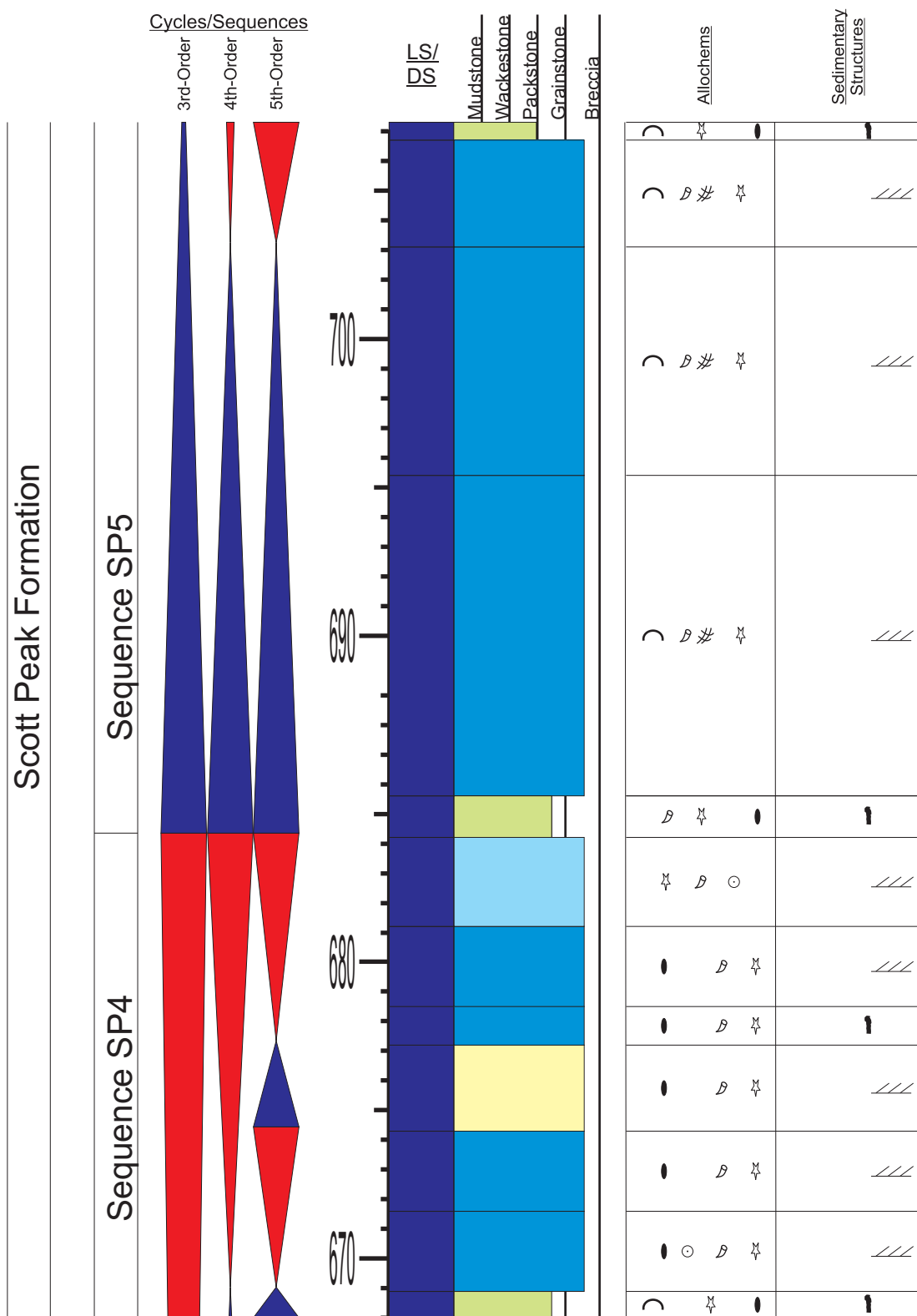
Appendix 10.16: Sedimentary section log for section East Canyon (continued). Refer to Appendix 1 for symbols and Figure 3.6 for location.

APPENDIX 10.17



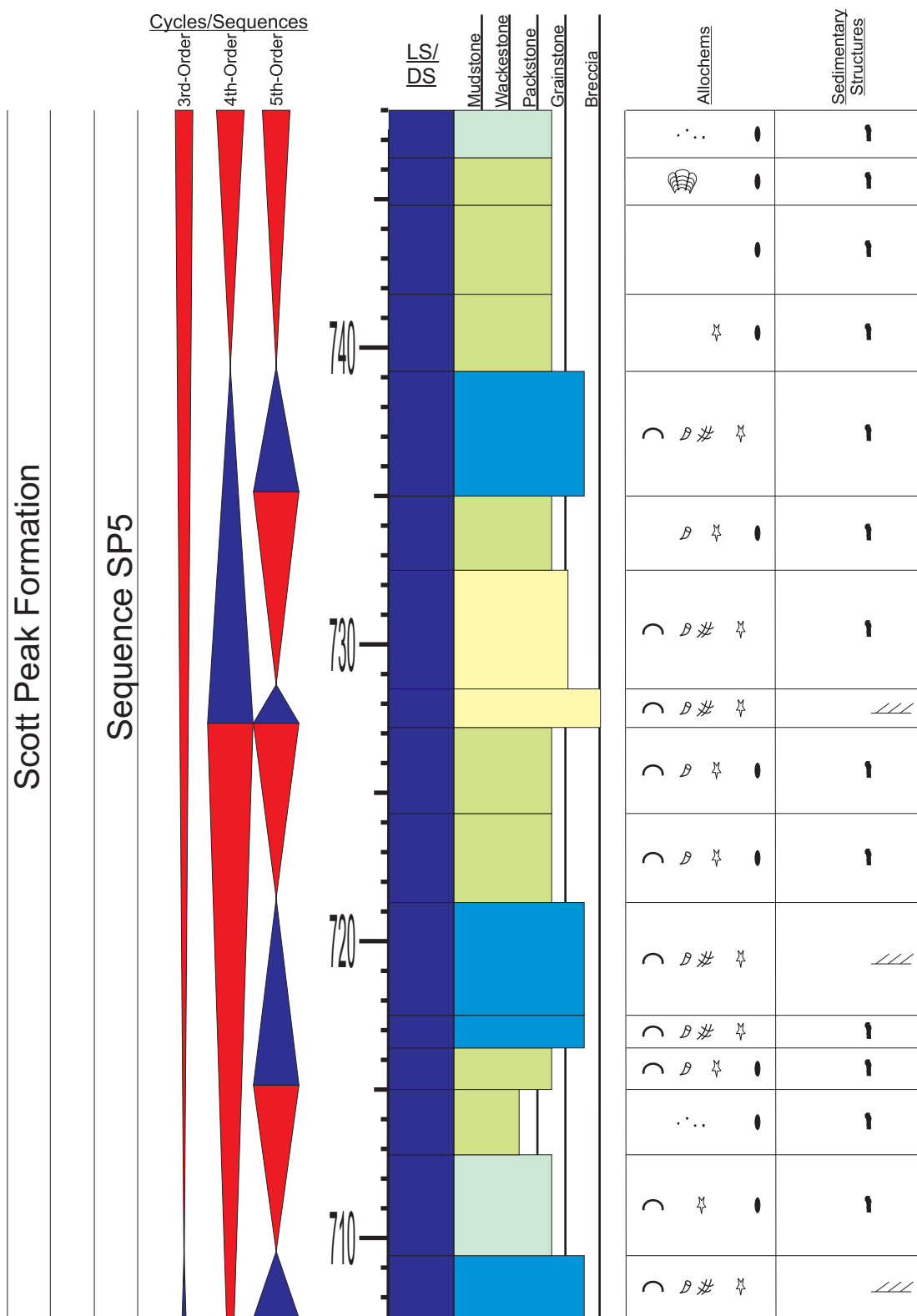
Appendix 10.17: Sedimentary section log for section East Canyon (continued). Refer to Appendix 1 for symbols and Figure 3.6 for location.

APPENDIX 10.18



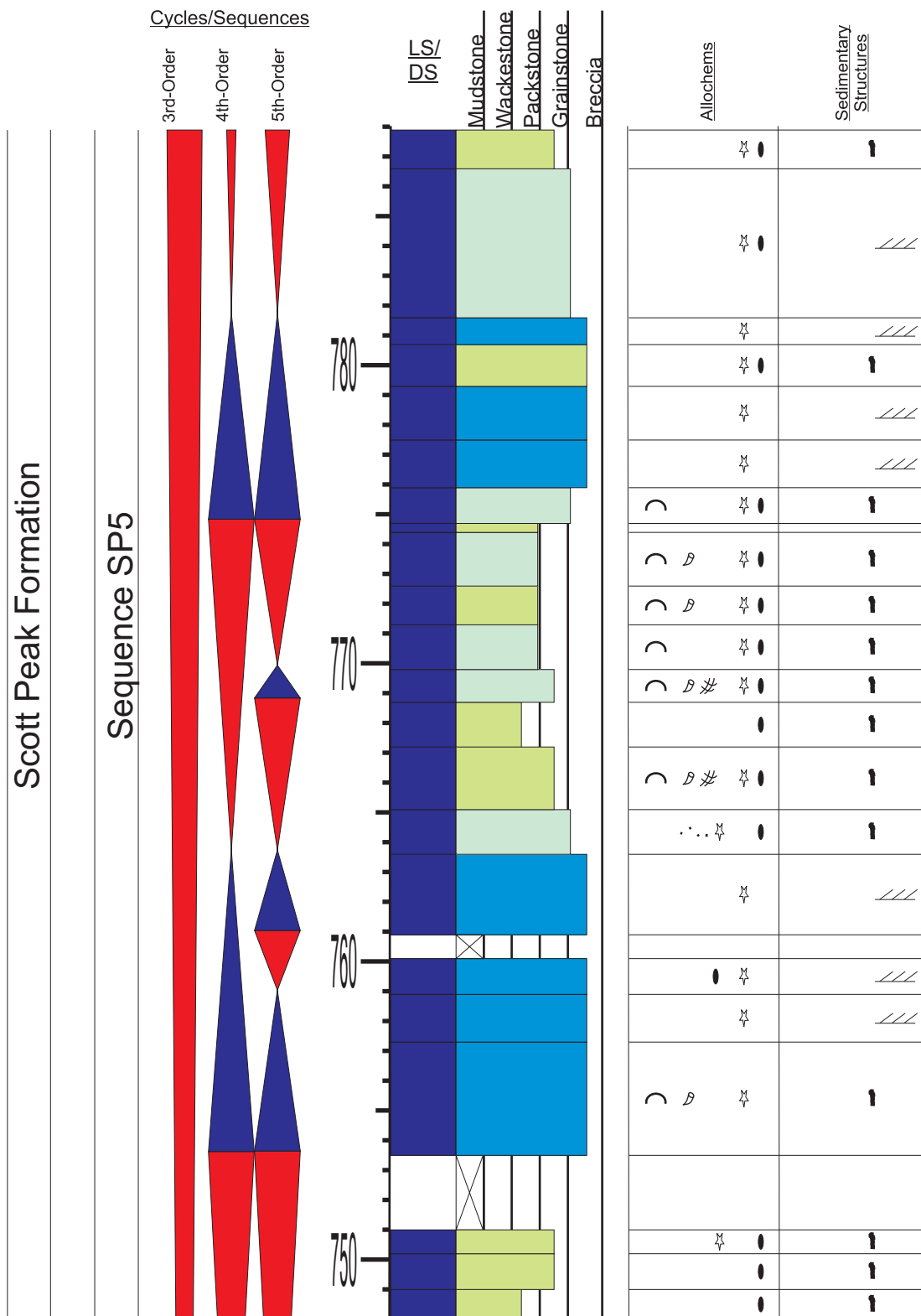
Appendix 10.18: Sedimentary section log for section East Canyon (continued). Refer to Appendix 1 for symbols and Figure 3.6 for location.

APPENDIX 10.19



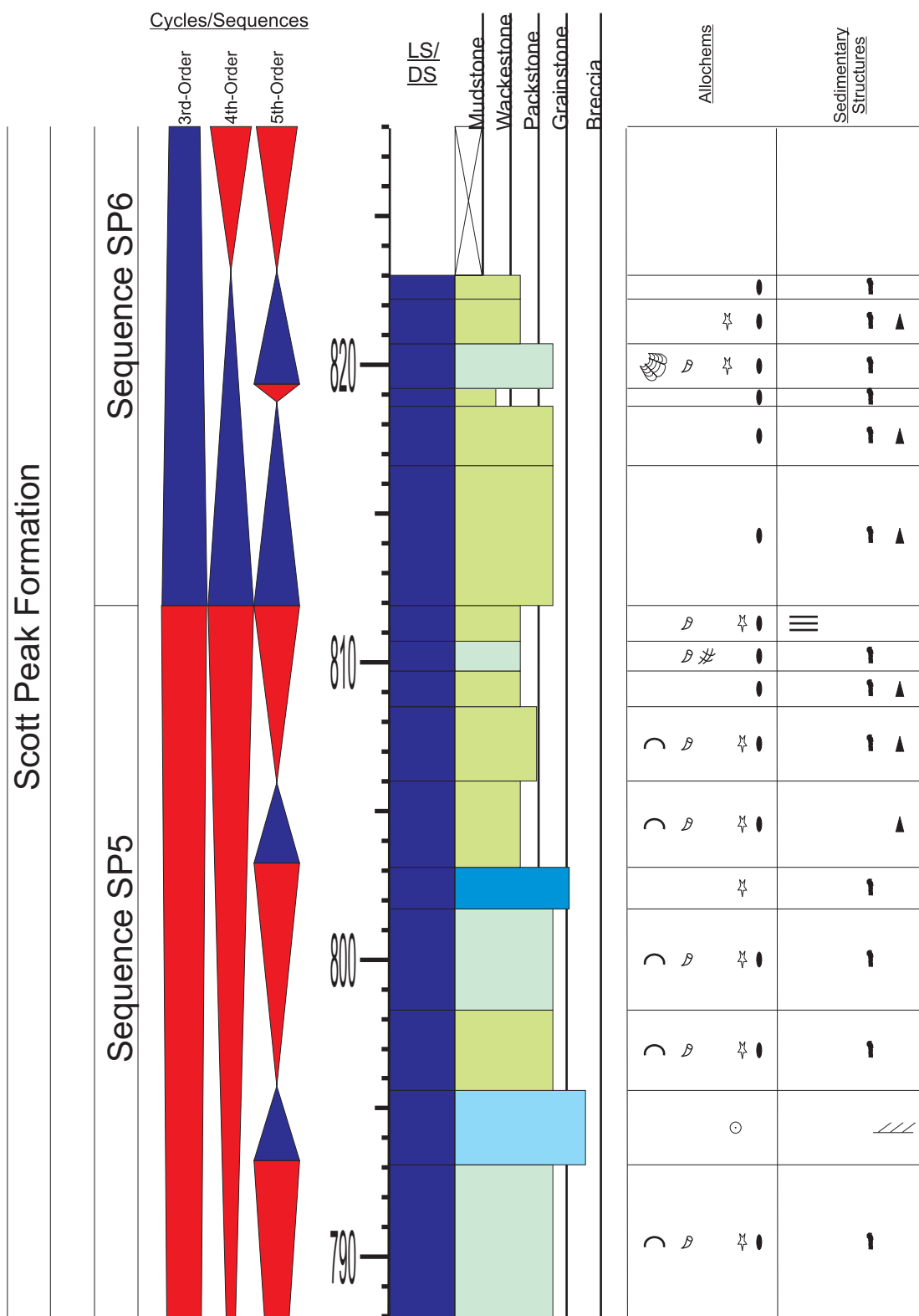
Appendix 10.19: Sedimentary section log for section East Canyon (continued). Refer to Appendix 1 for symbols and Figure 3.6 for location.

APPENDIX 10.20



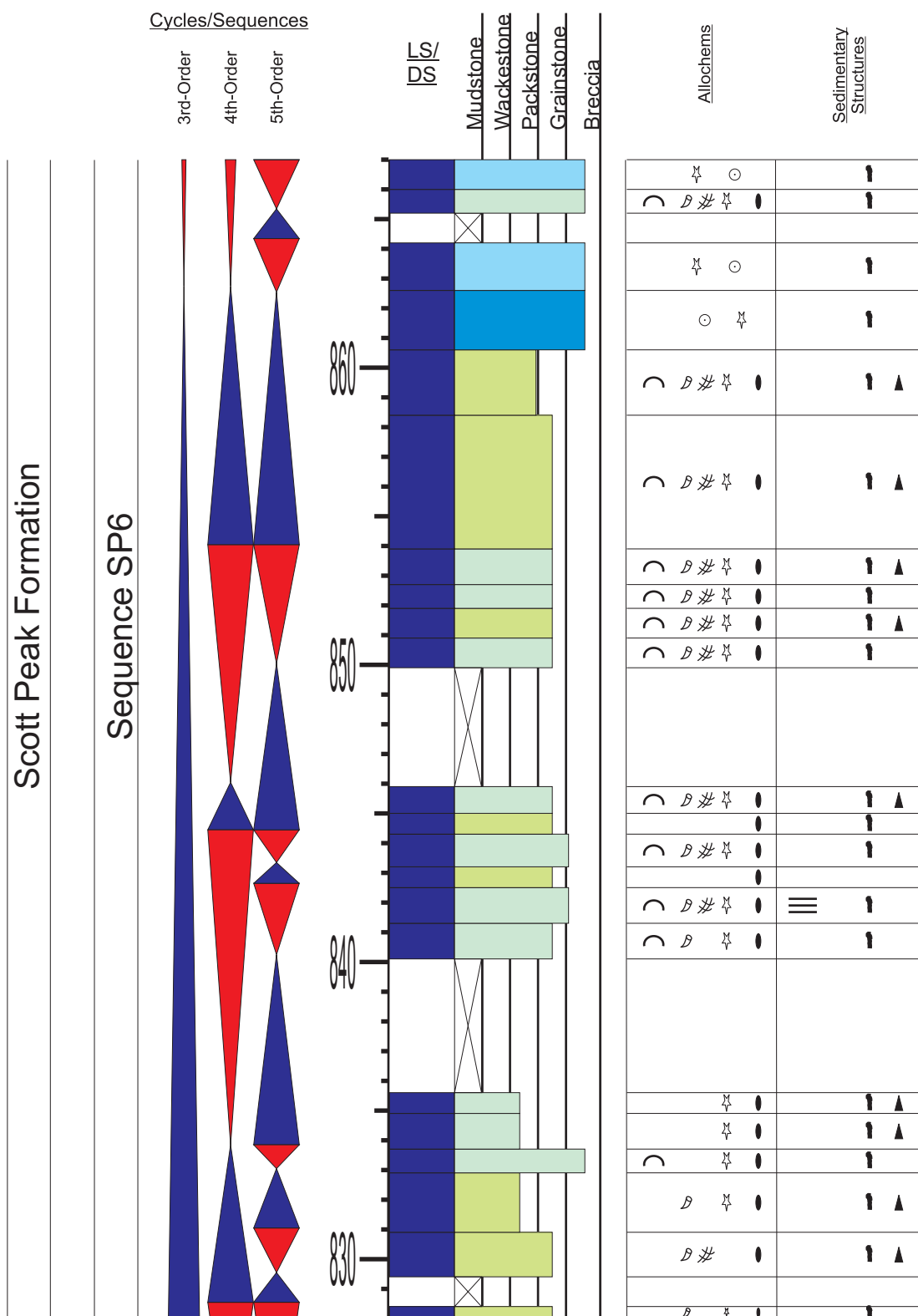
Appendix 10.20: Sedimentary section log for section East Canyon (continued). Refer to Appendix 1 for symbols and Figure 3.6 for location.

APPENDIX 10.21



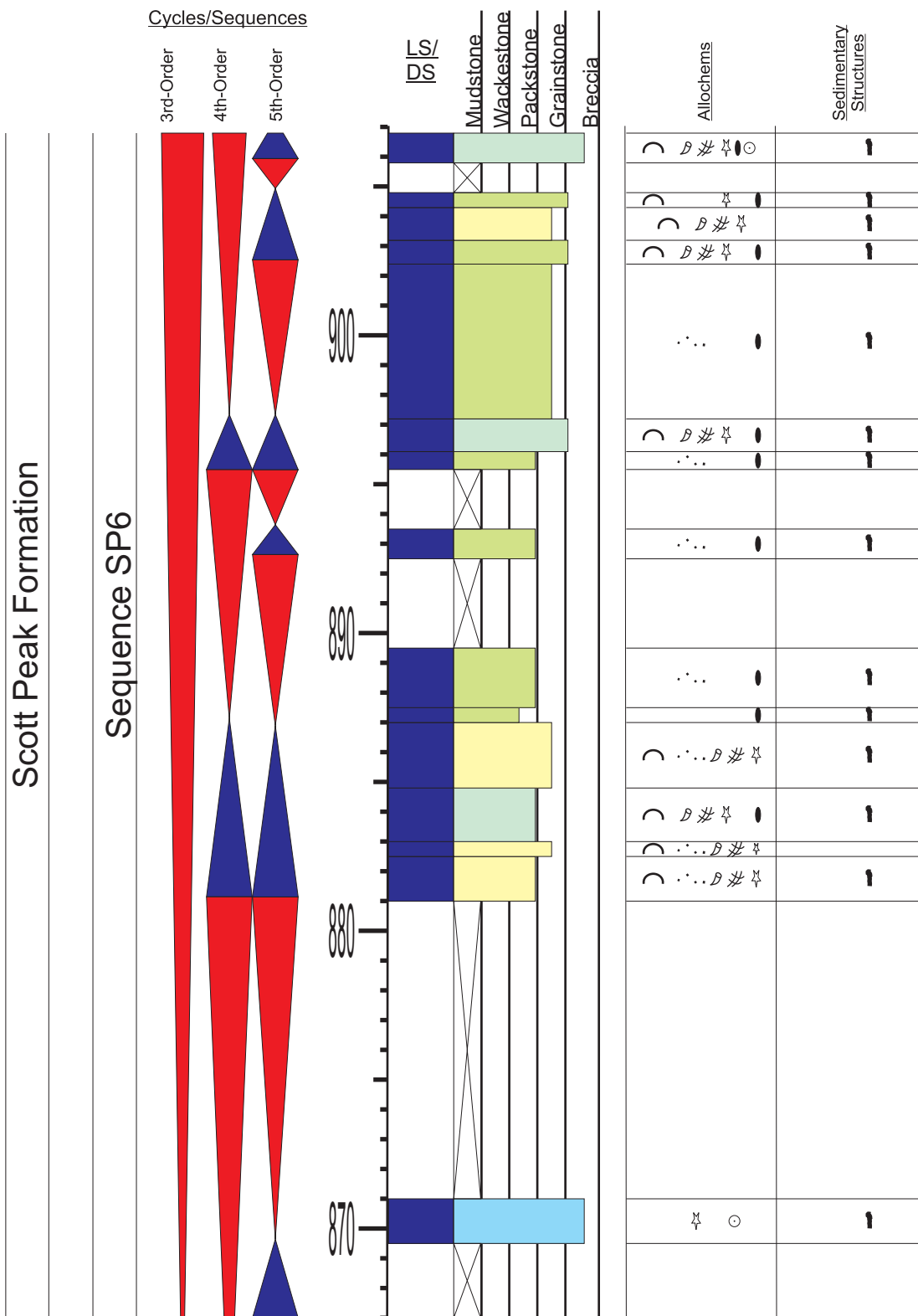
Appendix 10.21: Sedimentary section log for section East Canyon (continued). Refer to Appendix 1 for symbols and Figure 3.6 for location.

APPENDIX 10.22



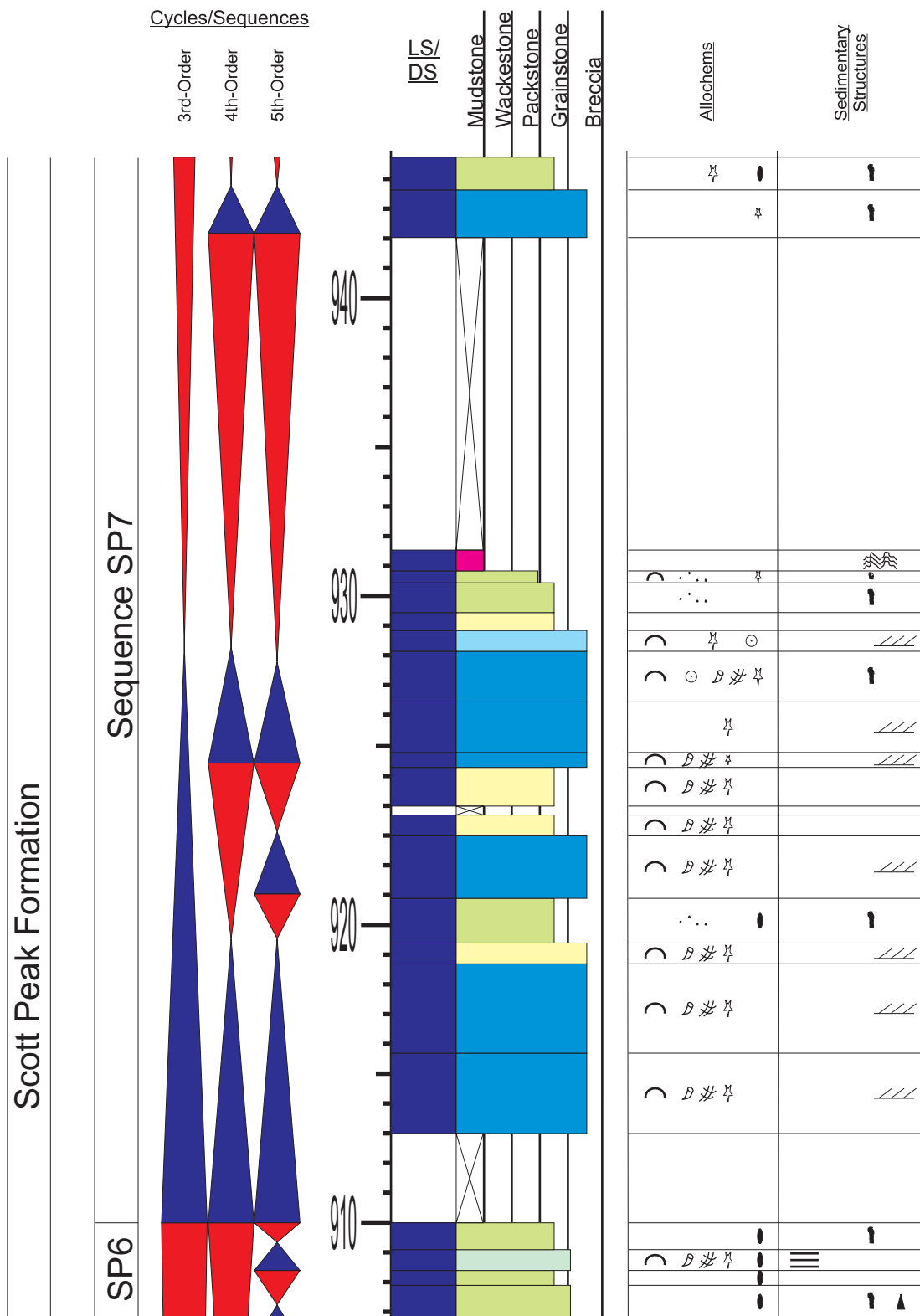
Appendix 10.22: Sedimentary section log for section East Canyon (continued). Refer to Appendix 1 for symbols and Figure 3.6 for location.

APPENDIX 10.23



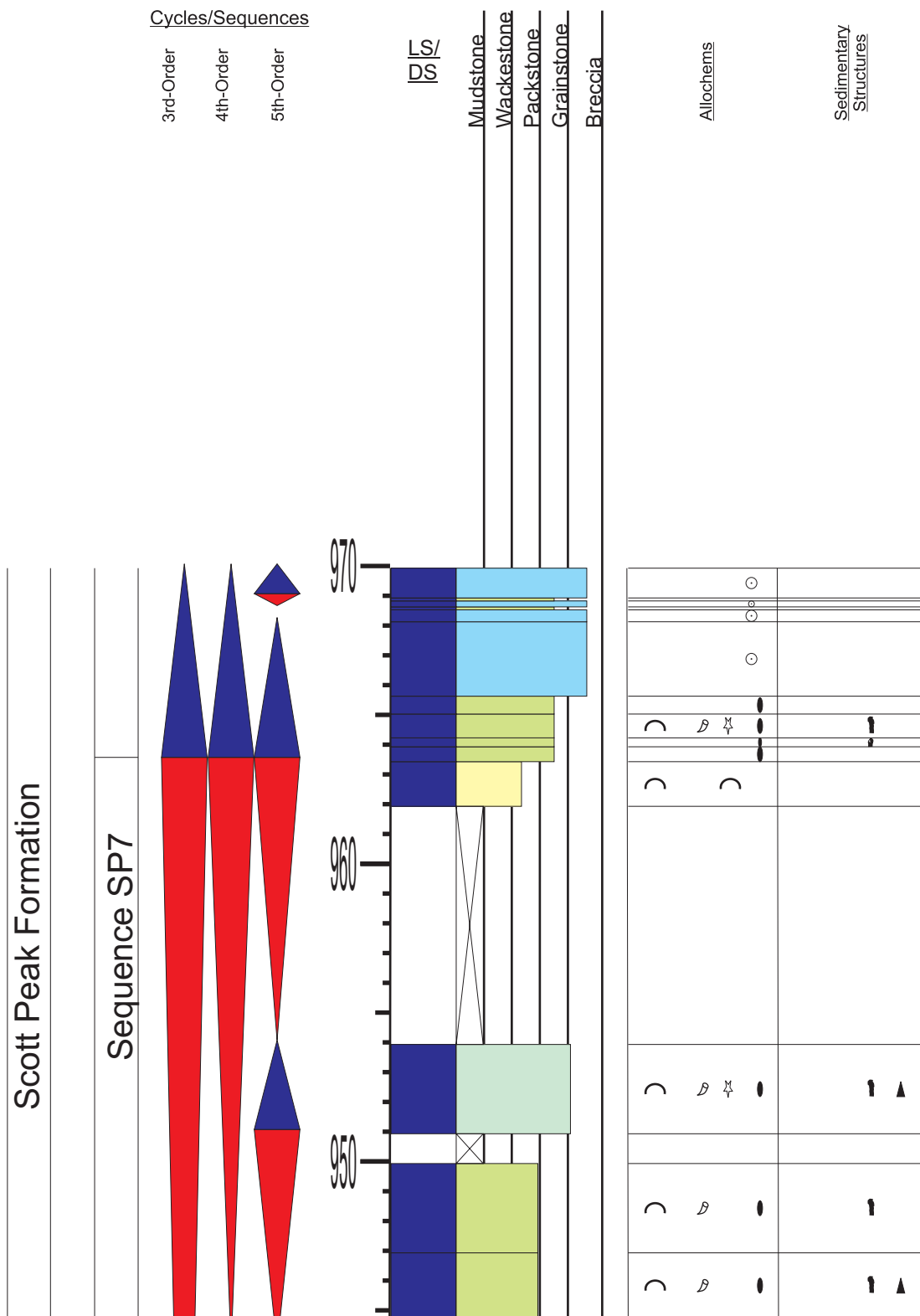
Appendix 10.23: Sedimentary section log for section East Canyon (continued). Refer to Appendix 1 for symbols and Figure 3.6 for location.

APPENDIX 10.24



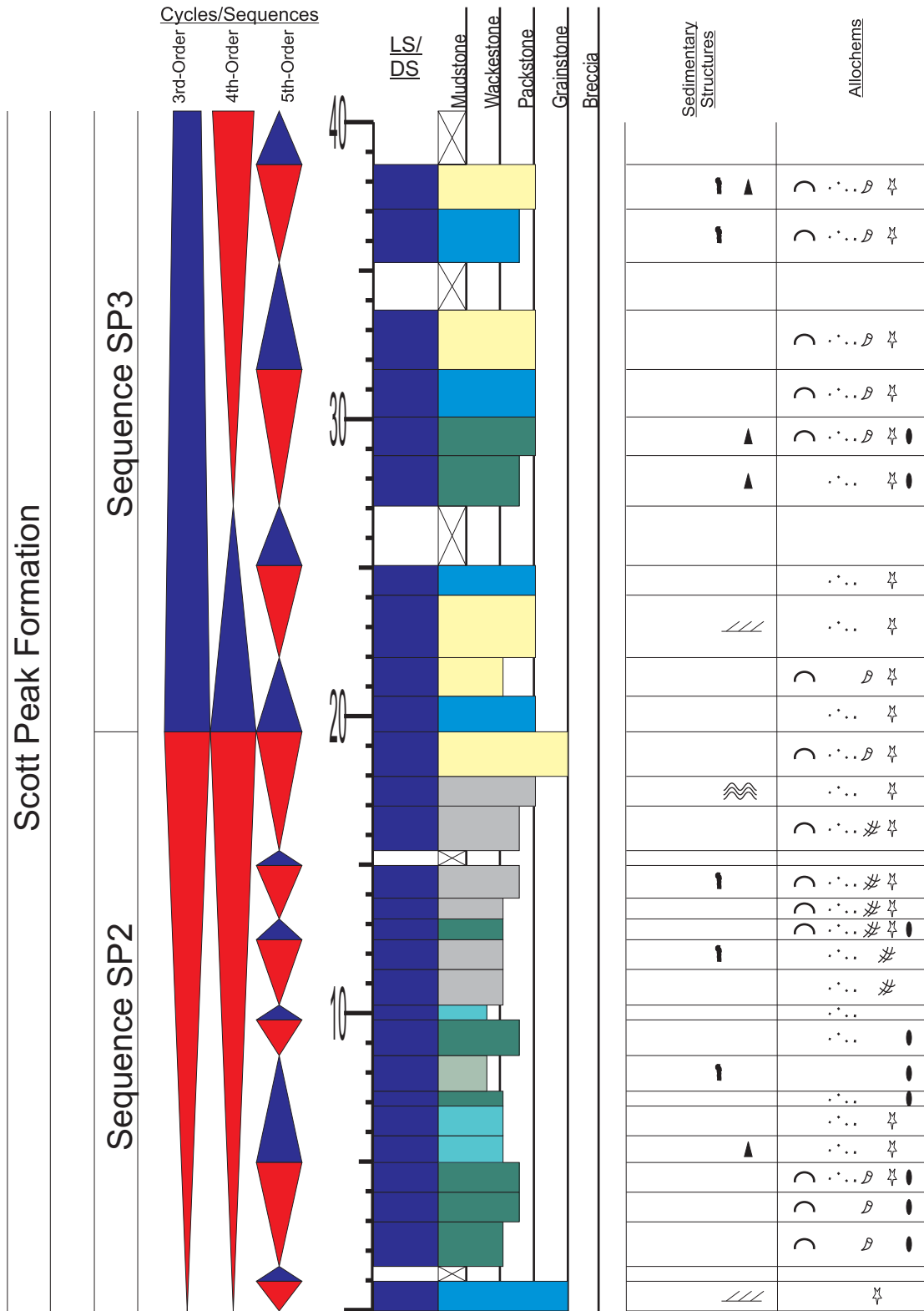
Appendix 10.24: Sedimentary section log for section East Canyon (continued). Refer to Appendix 1 for symbols and Figure 3.6 for location.

APPENDIX 10.25



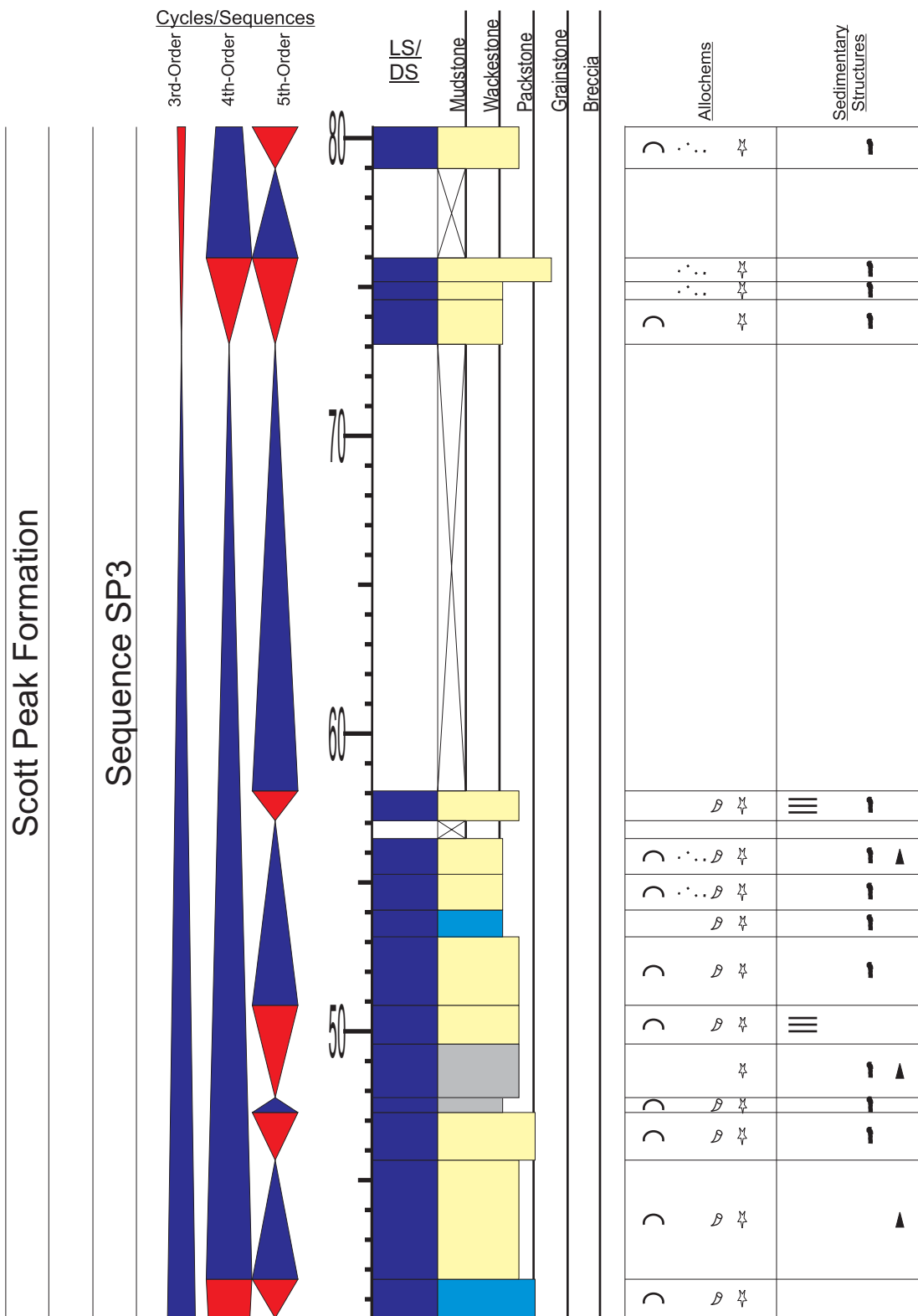
Appendix 10.25: Sedimentary section log for section East Canyon (continued). Refer to Appendix 1 for symbols and Figure 3.6 for location.

APPENDIX 11.1



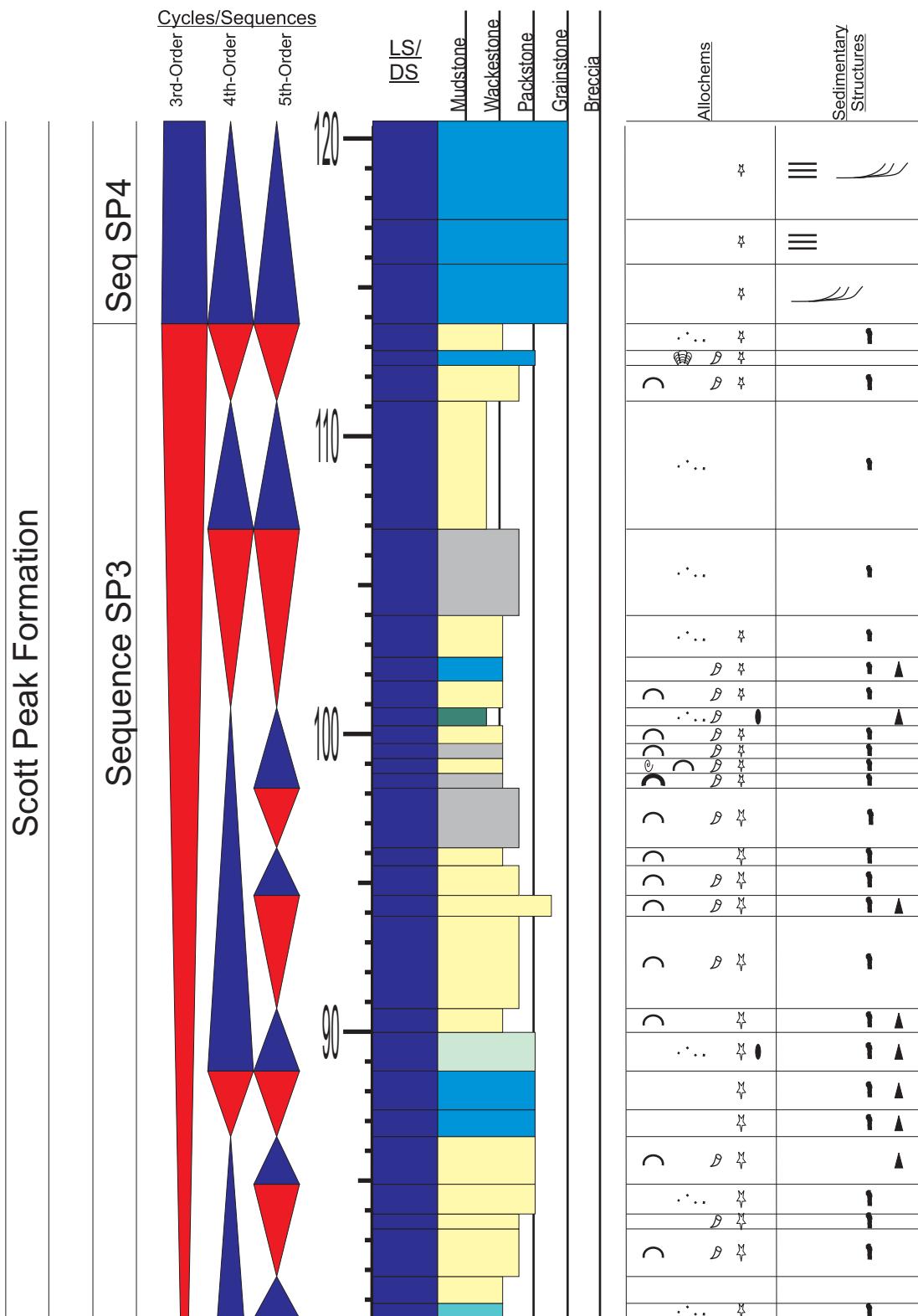
Appendix 11.1: Sedimentary section log for section Upper Pahsimeroi. Refer to Appendix 1 for symbols and Figure 3.6 for location.

APPENDIX 11.2



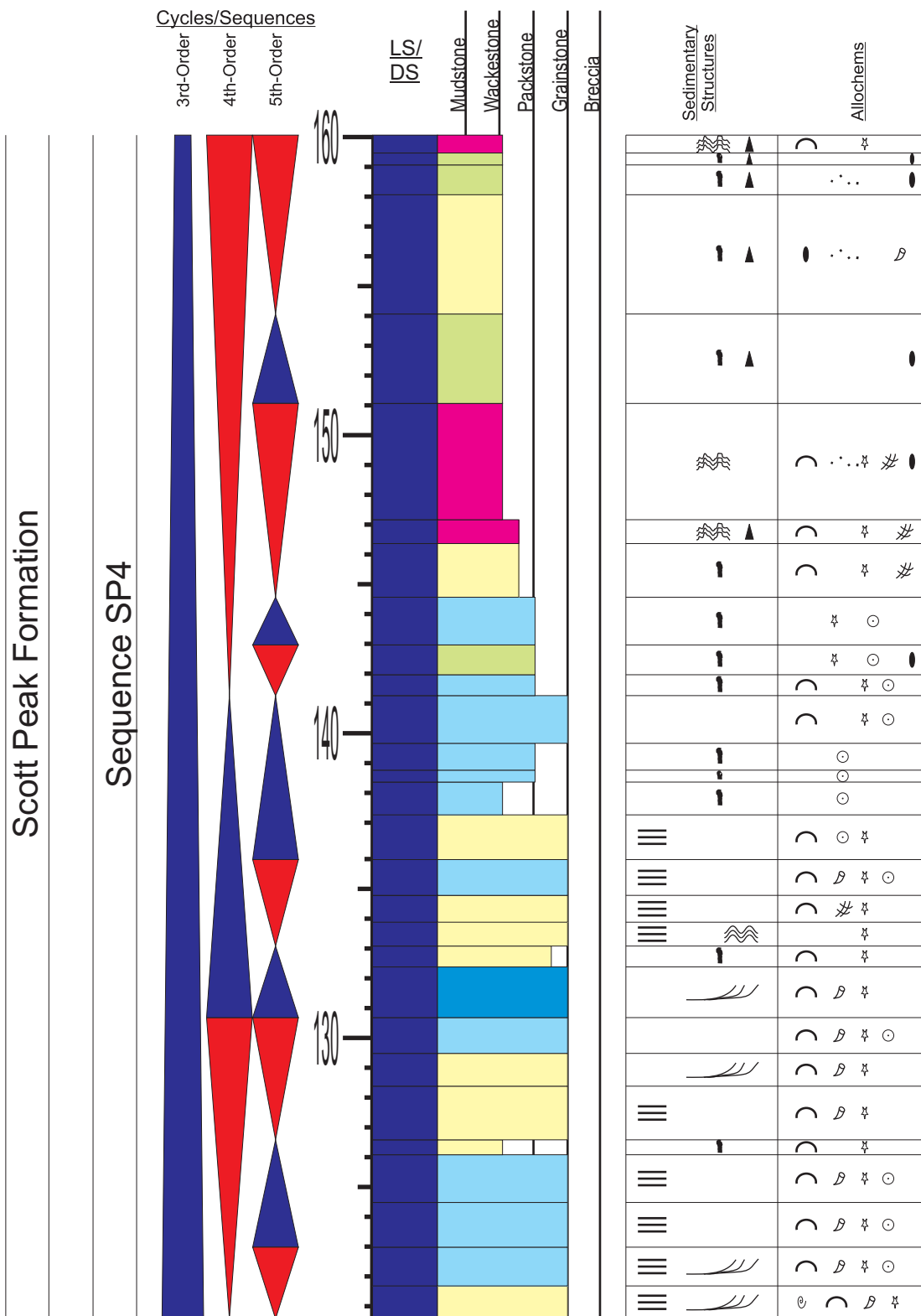
Appendix 11.2: Sedimentary section log for section Upper Pahsimeroi (continued). Refer to Appendix 1 for symbols and Figure 3.6 for location.

APPENDIX 11.3



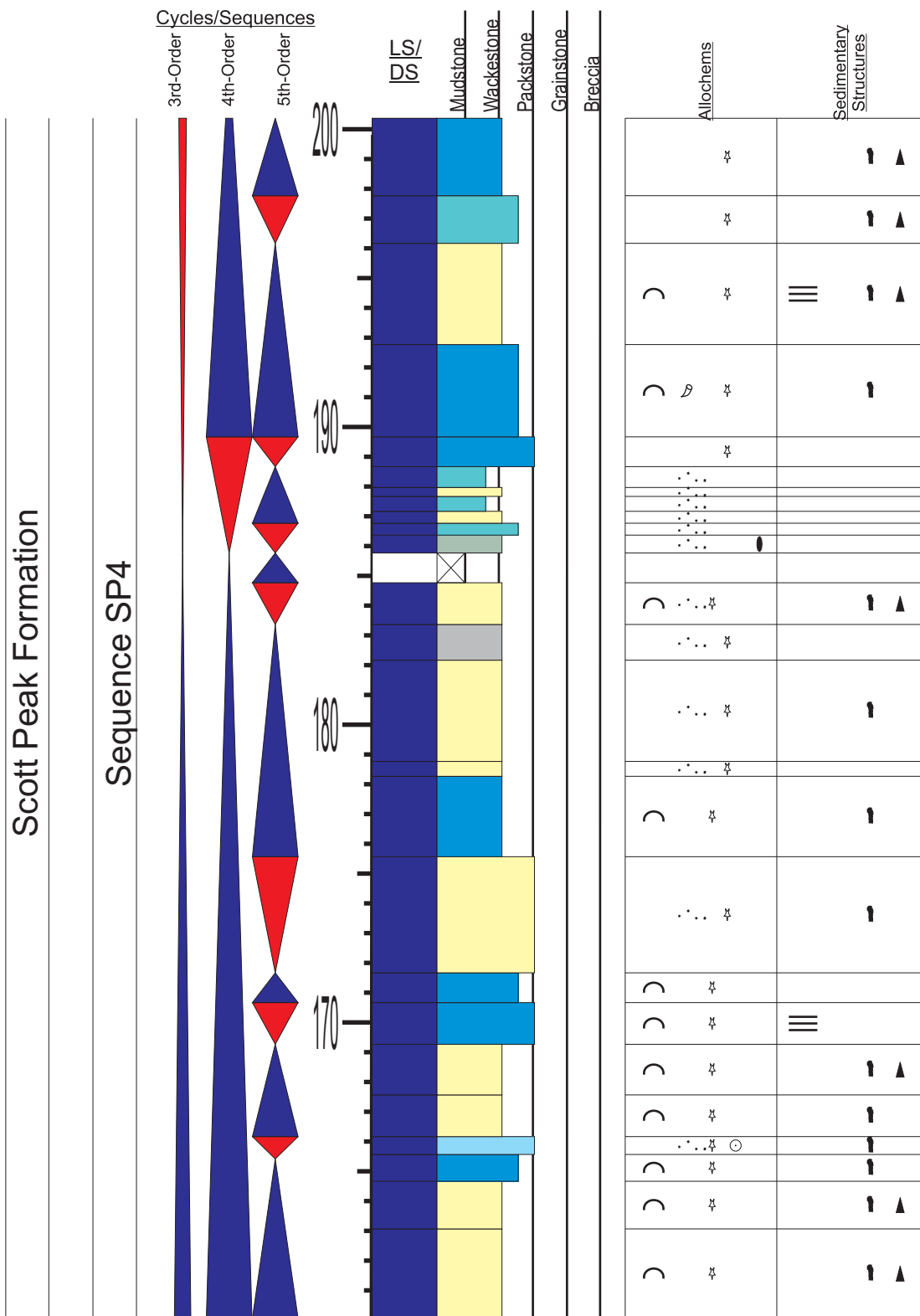
Appendix 11.3: Sedimentary section log for section Upper Pahsimeroi (continued). Refer to Appendix 1 for symbols and Figure 3.6 for location.

APPENDIX 11.4



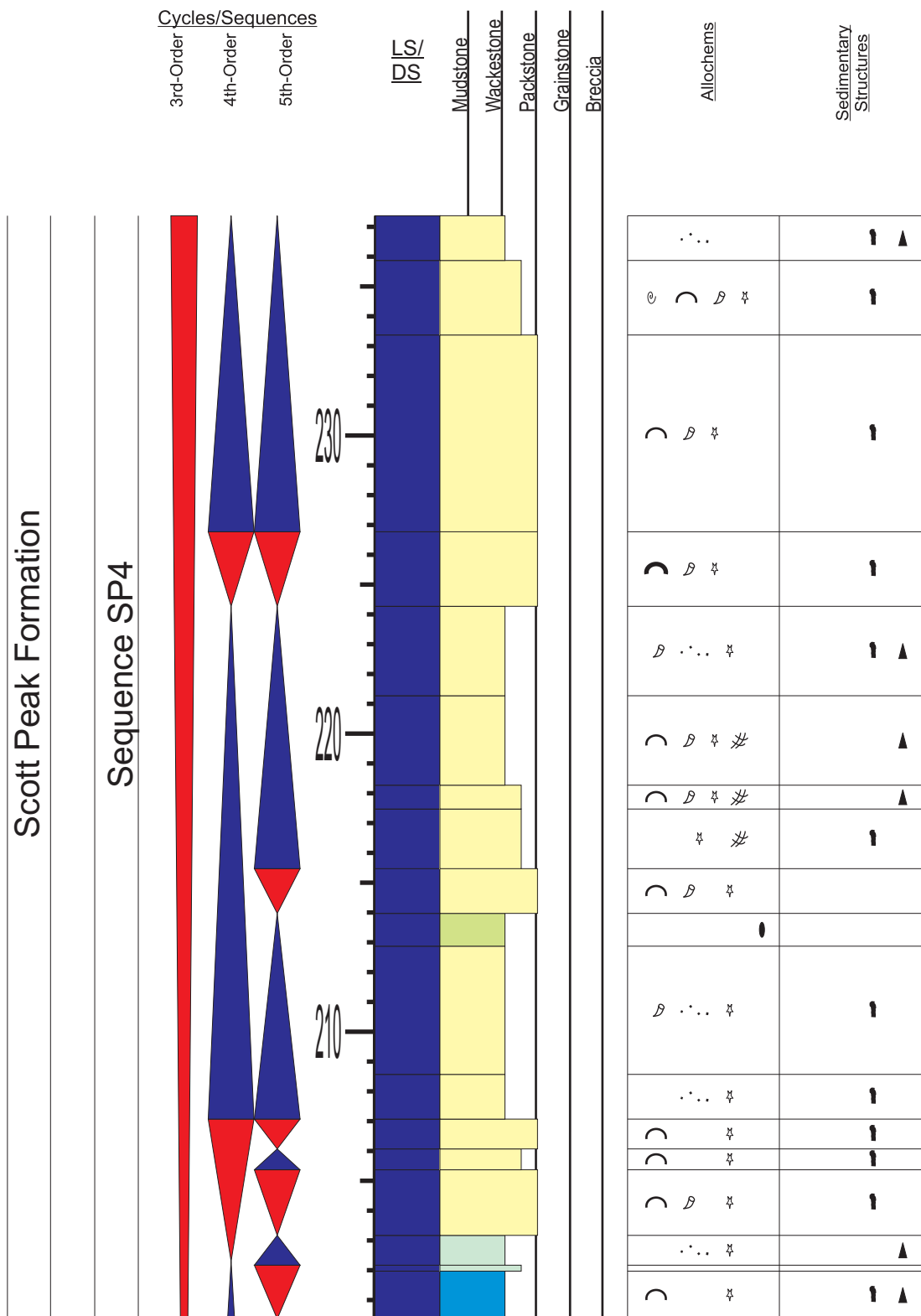
Appendix 11.4: Sedimentary section log for section Upper Pahsimeroi (continued). Refer to Appendix 1 for symbols and Figure 3.6 for location.

APPENDIX 11.5



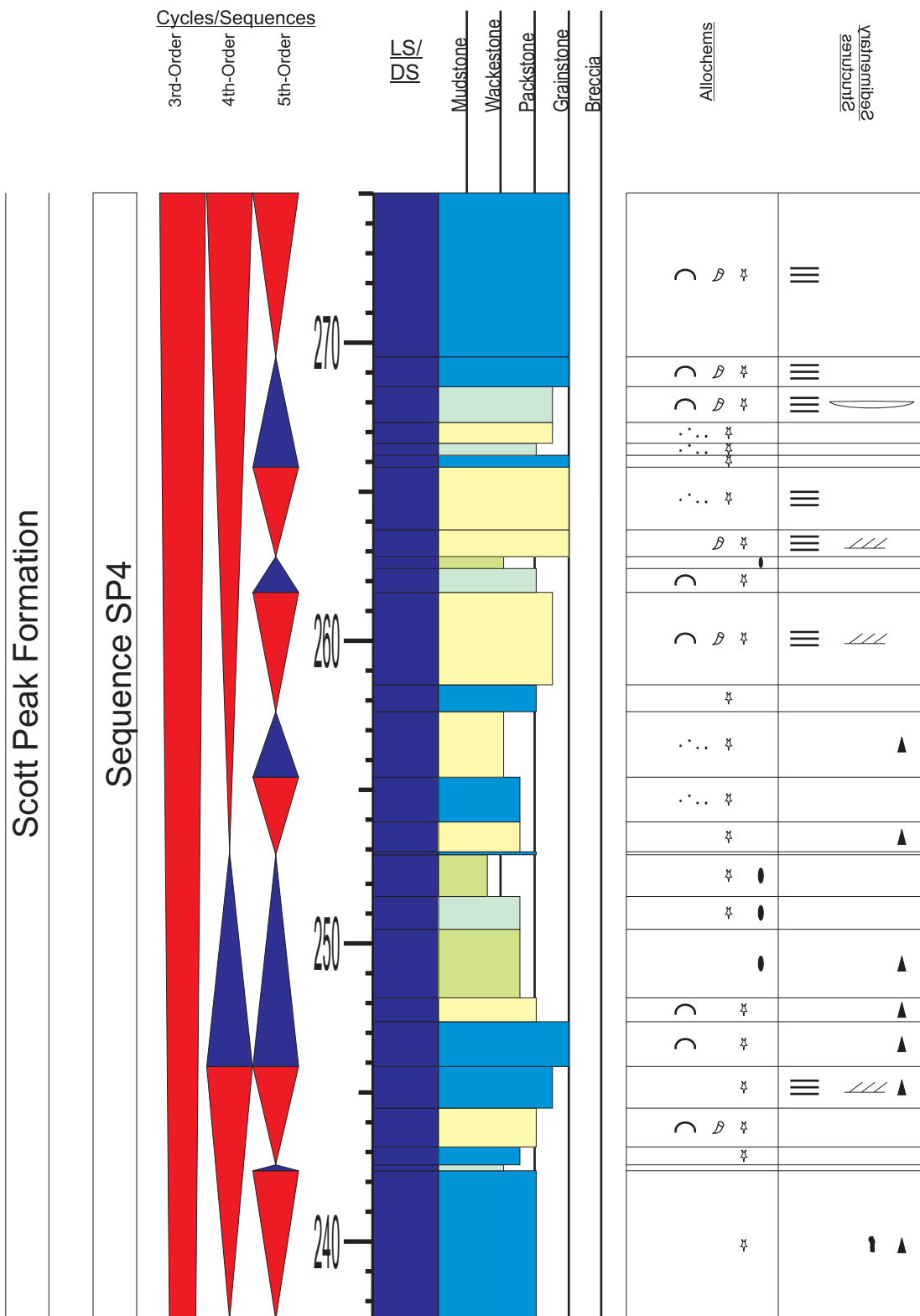
Appendix 11.5: Sedimentary section log for section Upper Pahsimeroi (continued). Refer to Appendix 1 for symbols and Figure 3.6 for location.

APPENDIX 11.6



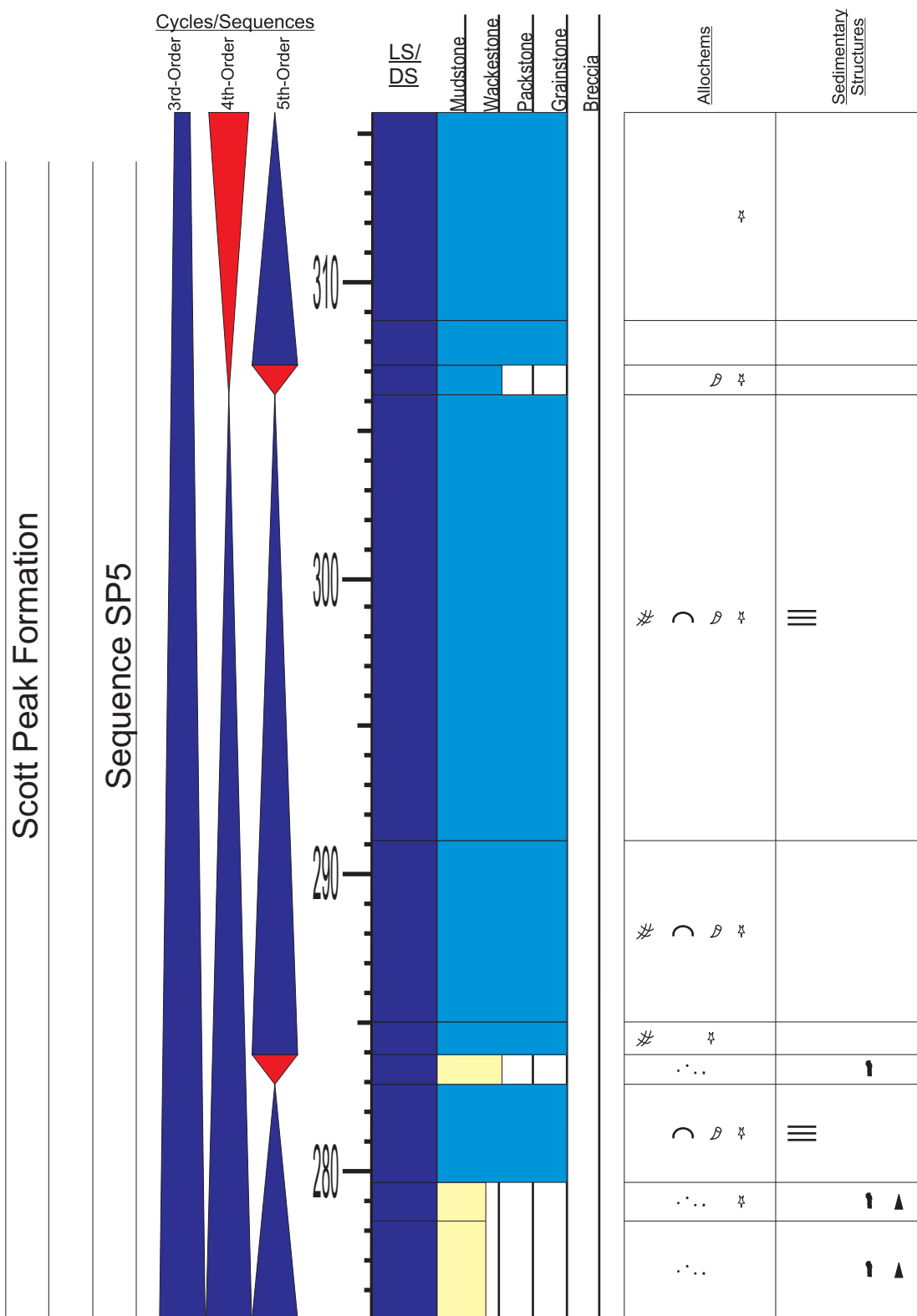
Appendix 11.6: Sedimentary section log for section Upper Pahsimeroi (continued). Refer to Appendix 1 for symbols and Figure 3.6 for location.

APPENDIX 11.7



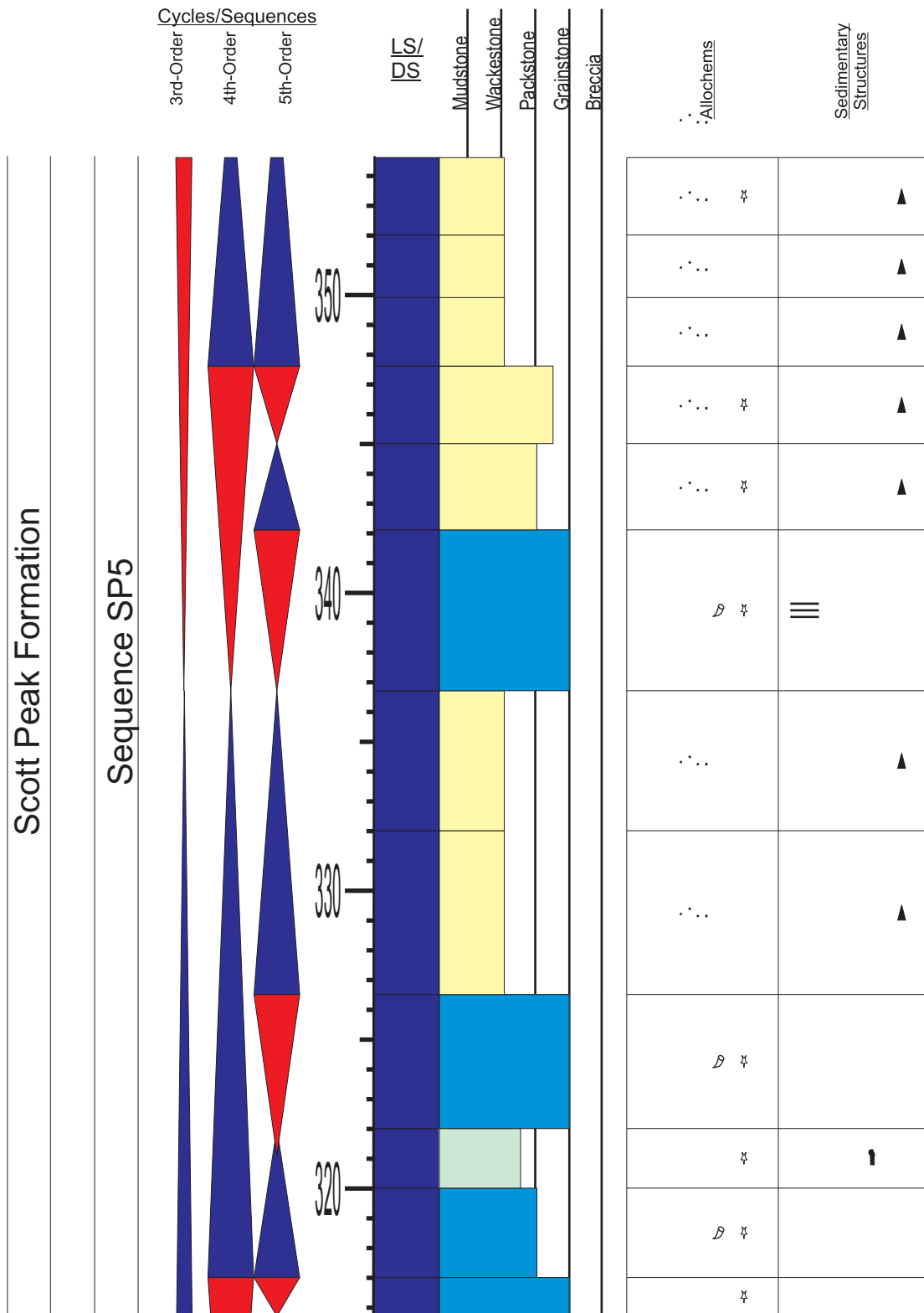
Appendix 11.7: Sedimentary section log for section Upper Pahsimeroi (continued). Refer to Appendix 1 for symbols and Figure 3.6 for location.

APPENDIX 11.8



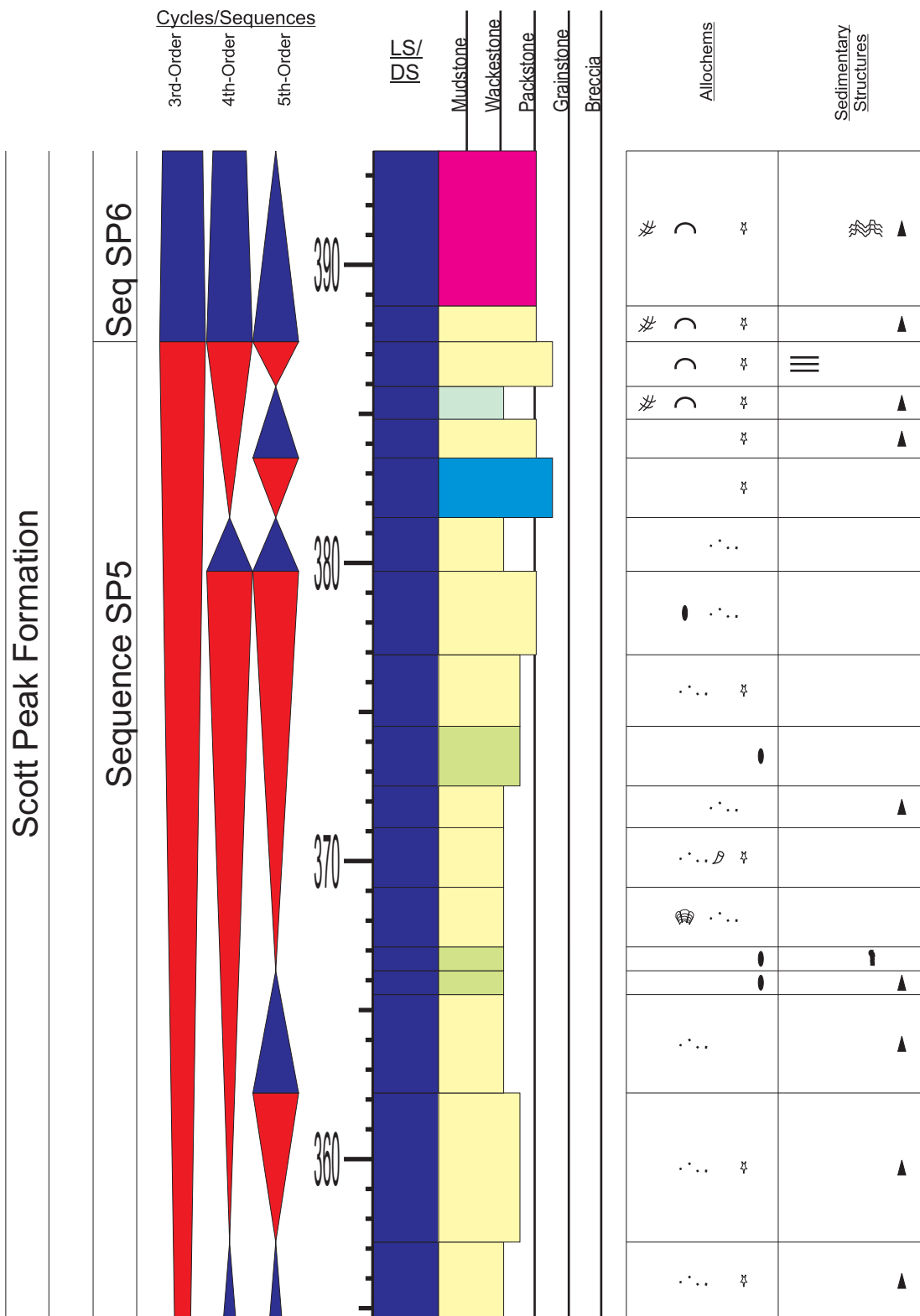
Appendix 11.8: Sedimentary section log for section Upper Pahsimeroi (continued). Refer to Appendix 1 for symbols and Figure 3.6 for location.

APPENDIX 11.9



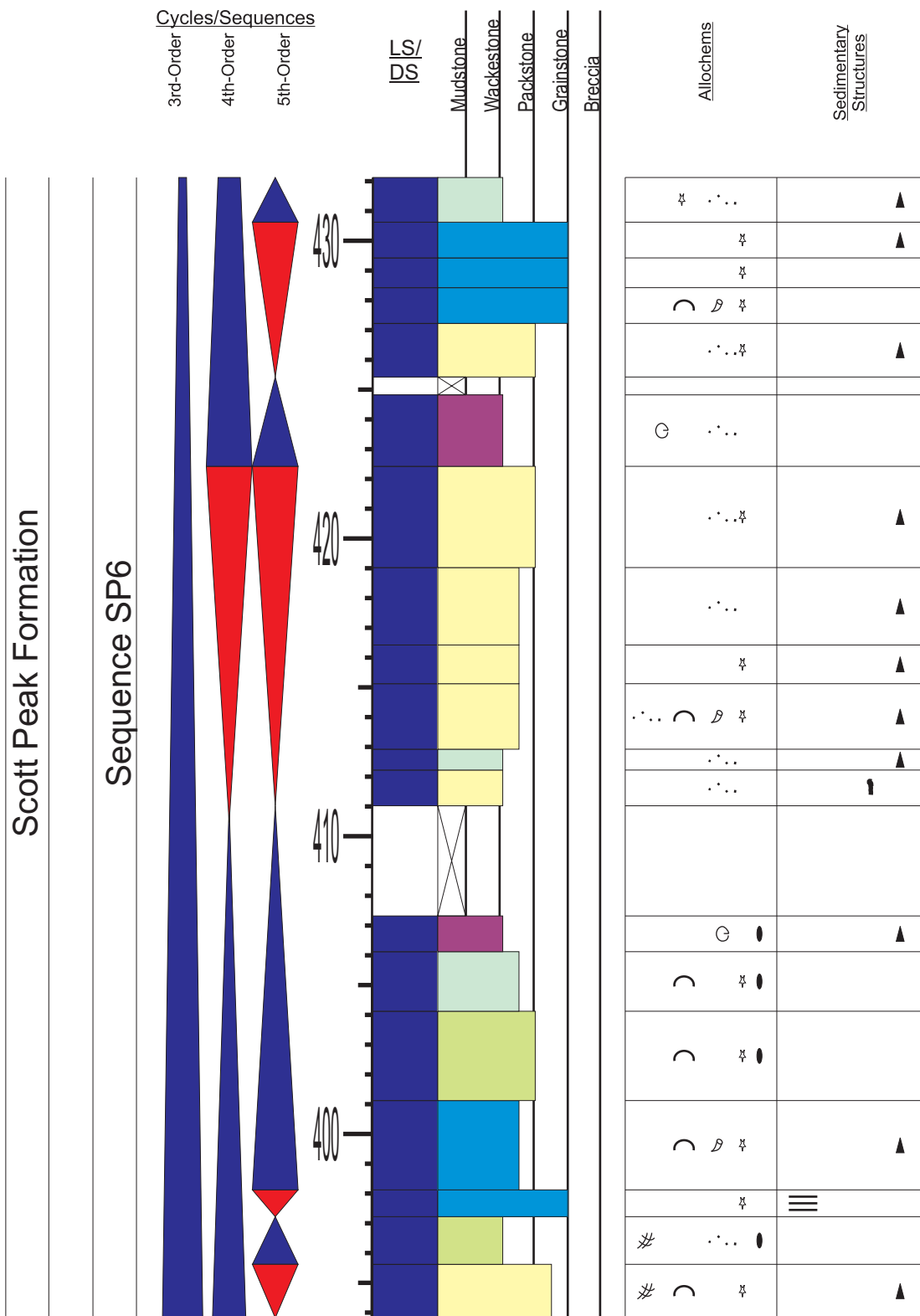
Appendix 11.9: Sedimentary section log for section Upper Pahsimeroi (continued). Refer to Appendix 1 for symbols and Figure 3.6 for location.

APPENDIX 11.10



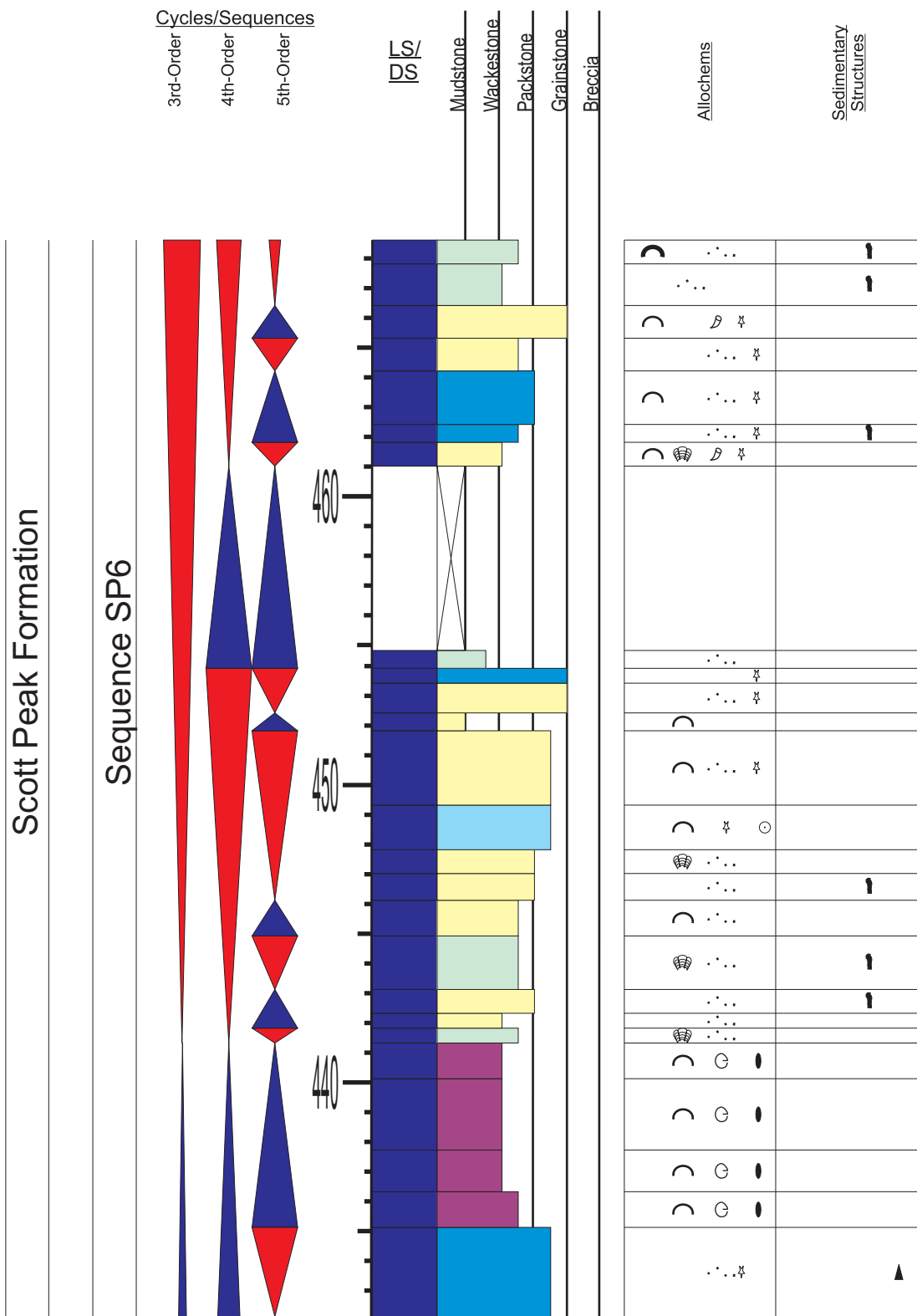
Appendix 11.10: Sedimentary section log for section Upper Pahsimeroi (continued). Refer to Appendix 1 for symbols and Figure 3.6 for location.

APPENDIX 11.11



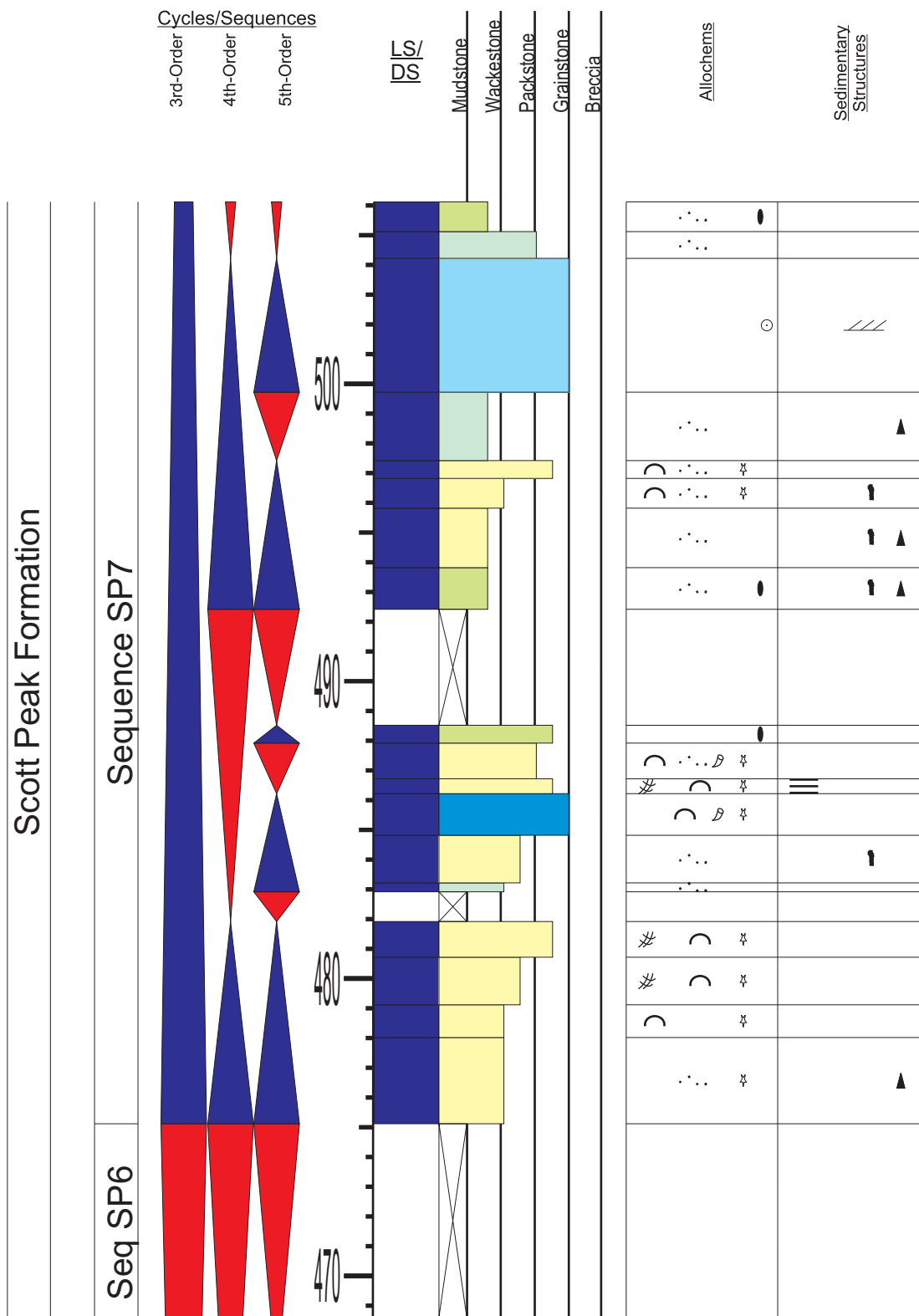
Appendix 11.11: Sedimentary section log for section Upper Pahsimeroi (continued). Refer to Appendix 1 for symbols and Figure 3.6 for location.

APPENDIX 11.12



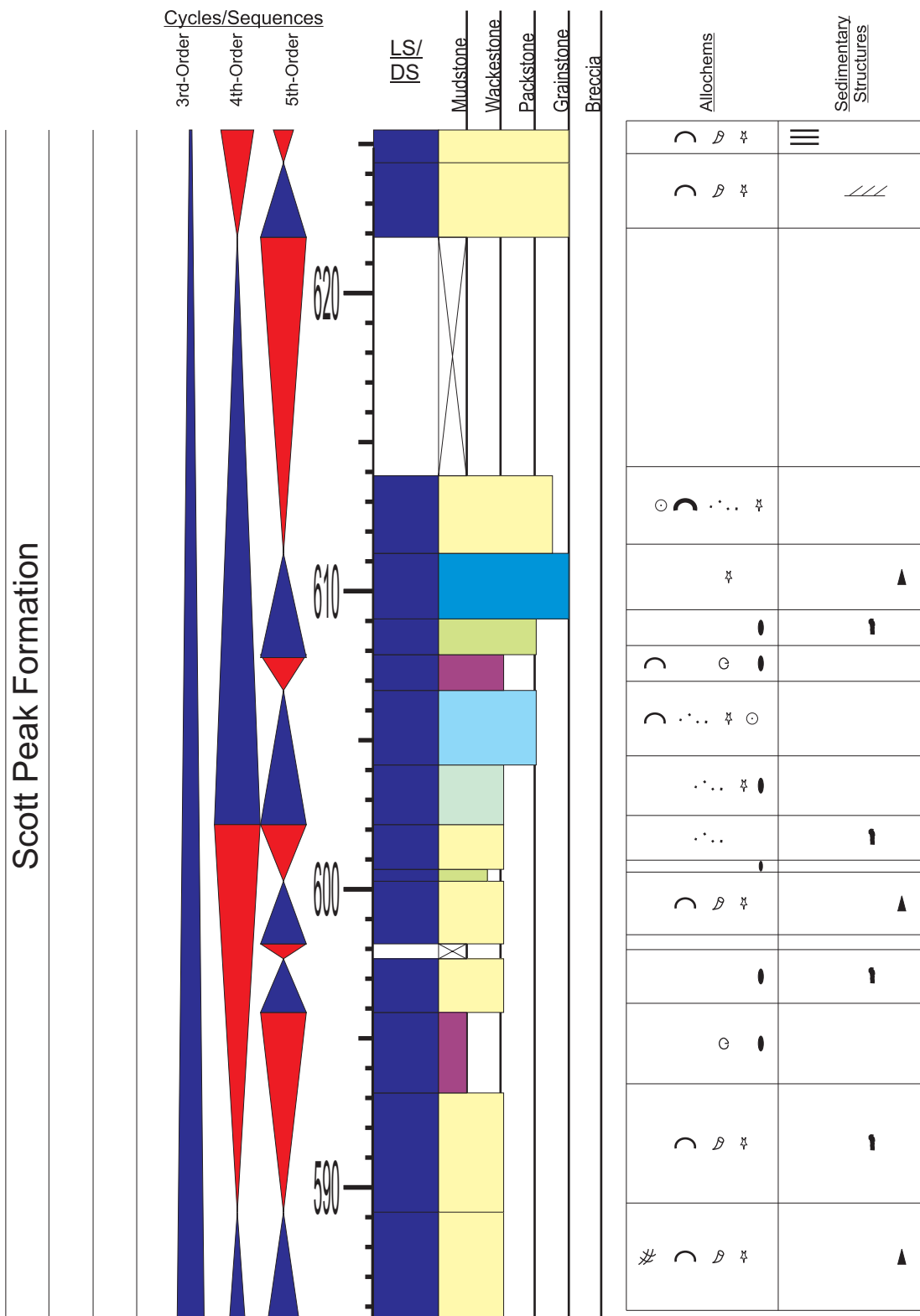
Appendix 11.12: Sedimentary section log for section Upper Pahsimeroi (continued). Refer to Appendix 1 for symbols and Figure 3.6 for location.

APPENDIX 11.13



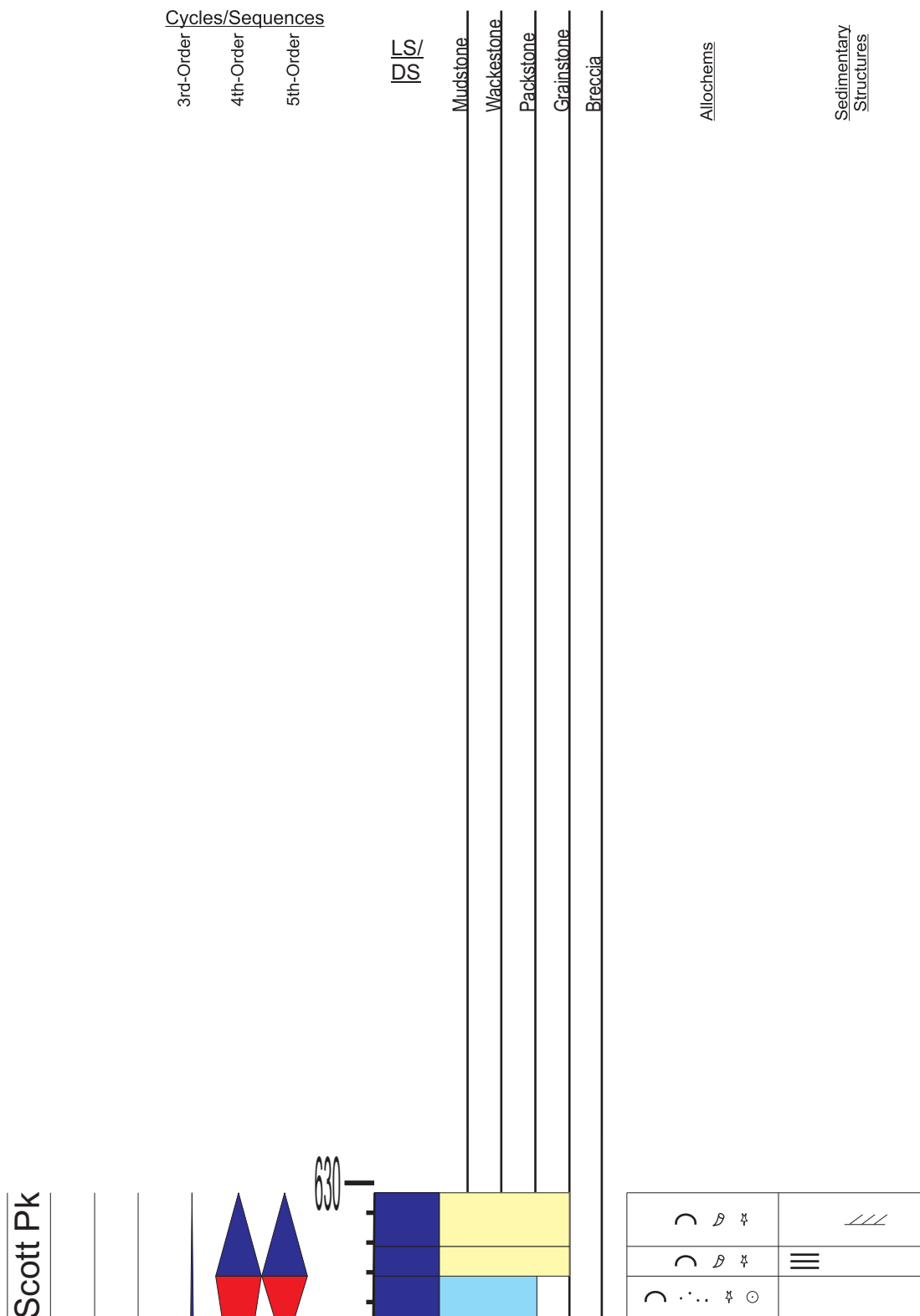
Appendix 11.13: Sedimentary section log for section Upper Pahsimeroi (continued). Refer to Appendix 1 for symbols and Figure 3.6 for location.

APPENDIX 11.16



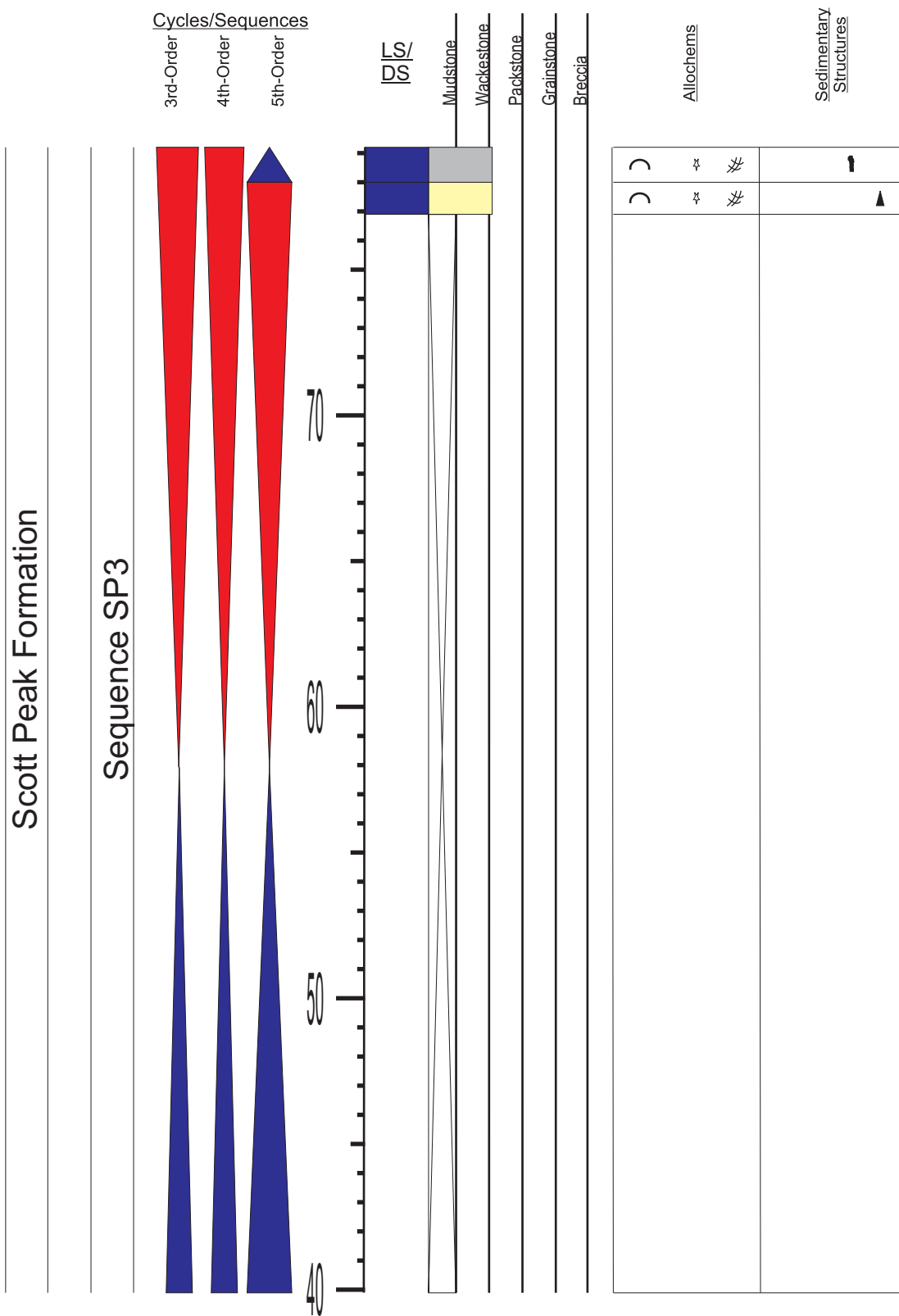
Appendix 11.16: Sedimentary section log for section Upper Pahsimeroi (continued). Refer to Appendix 1 for symbols and Figure 3.6 for location.

APPENDIX 11.17



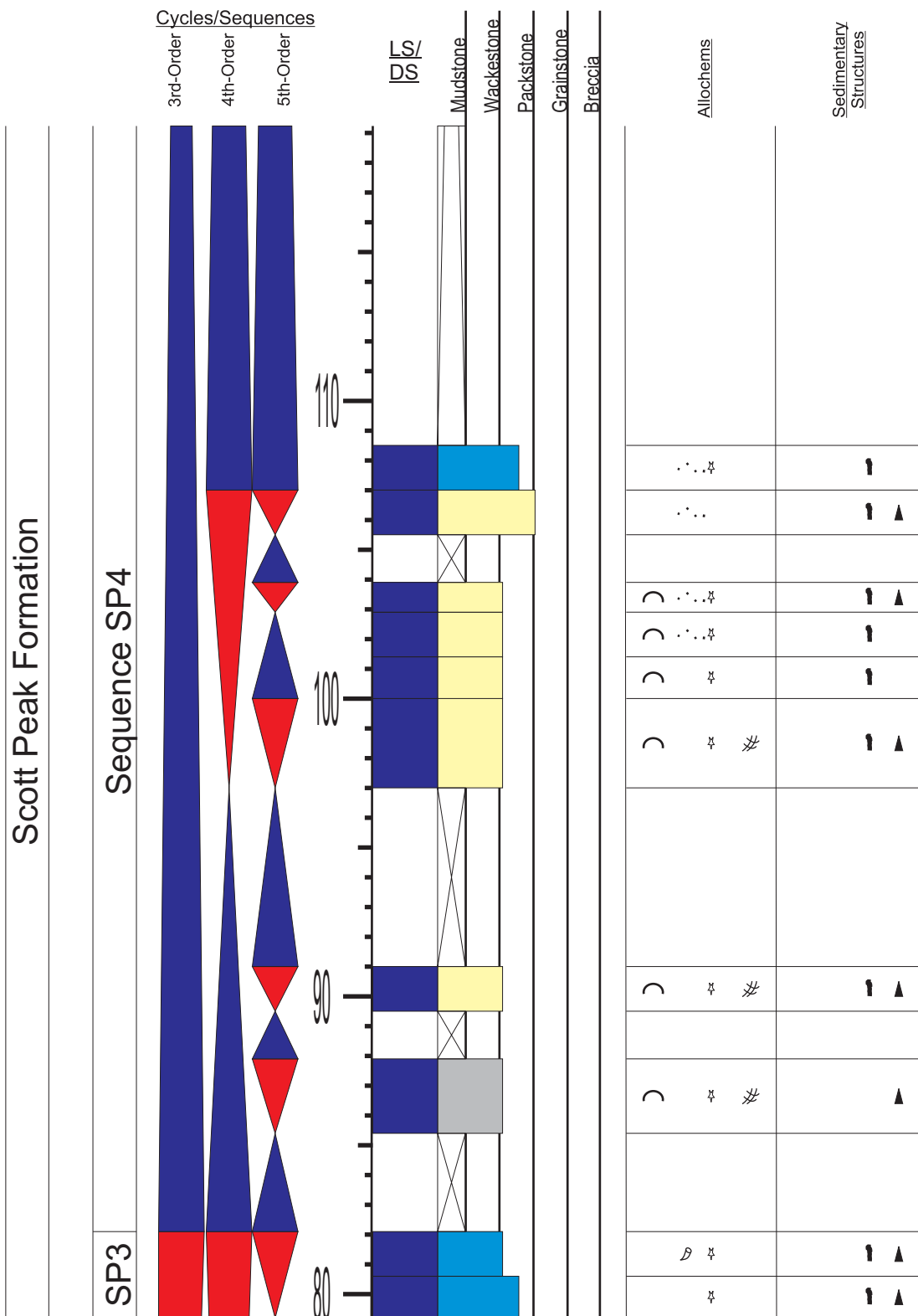
Appendix 11.17: Sedimentary section log for section Upper Pahsimeroi (continued). Refer to Appendix 1 for symbols and Figure 3.6 for location.

APPENDIX 12.2



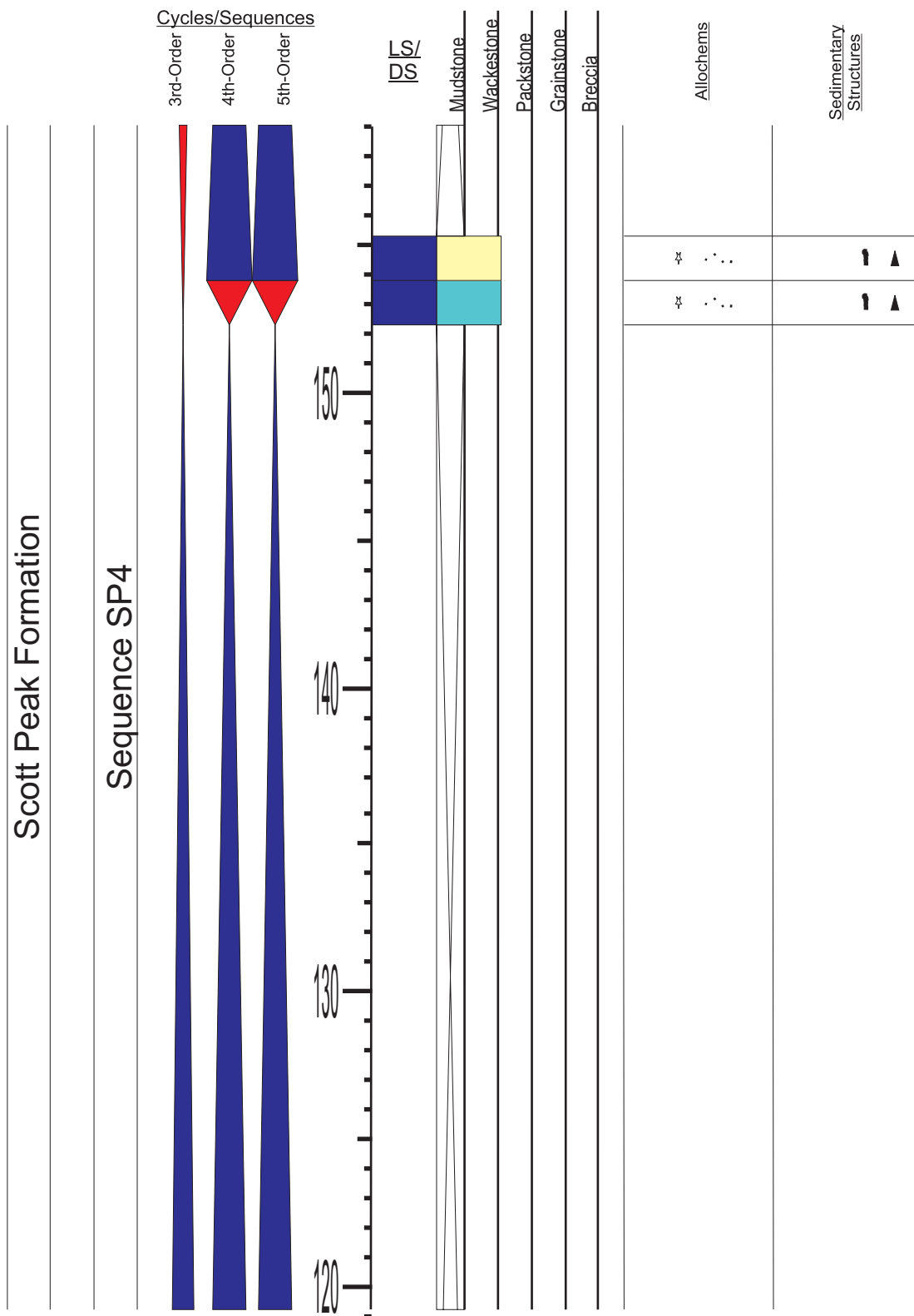
Appendix 12.2: Sedimentary section log for section Antelope Creek (continued). Refer to Appendix 1 for symbols and Figure 3.6 for location.

APPENDIX 12.3



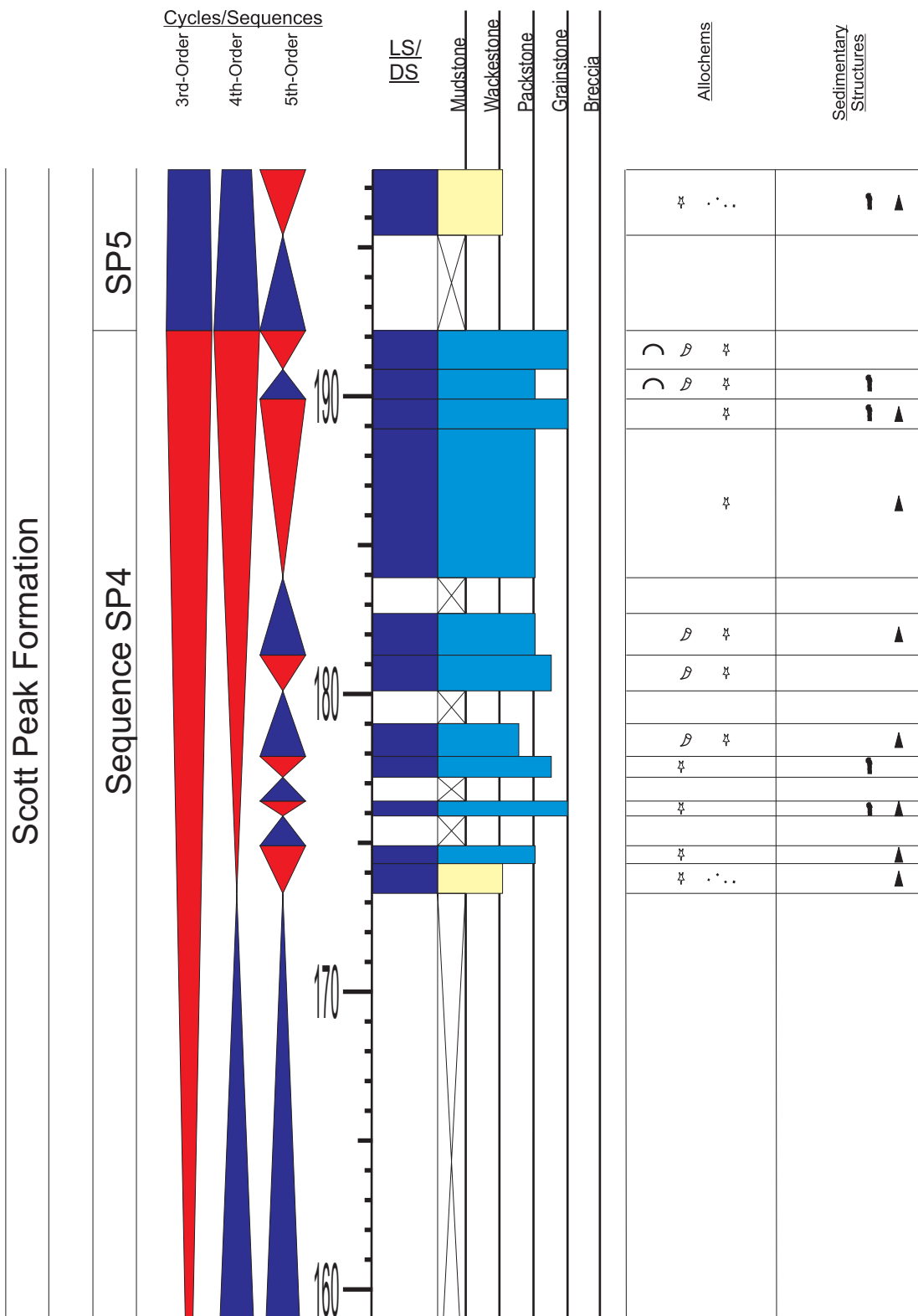
Appendix 12.3: Sedimentary section log for section Antelope Creek (continued). Refer to Appendix 1 for symbols and Figure 3.6 for location.

APPENDIX 12.4



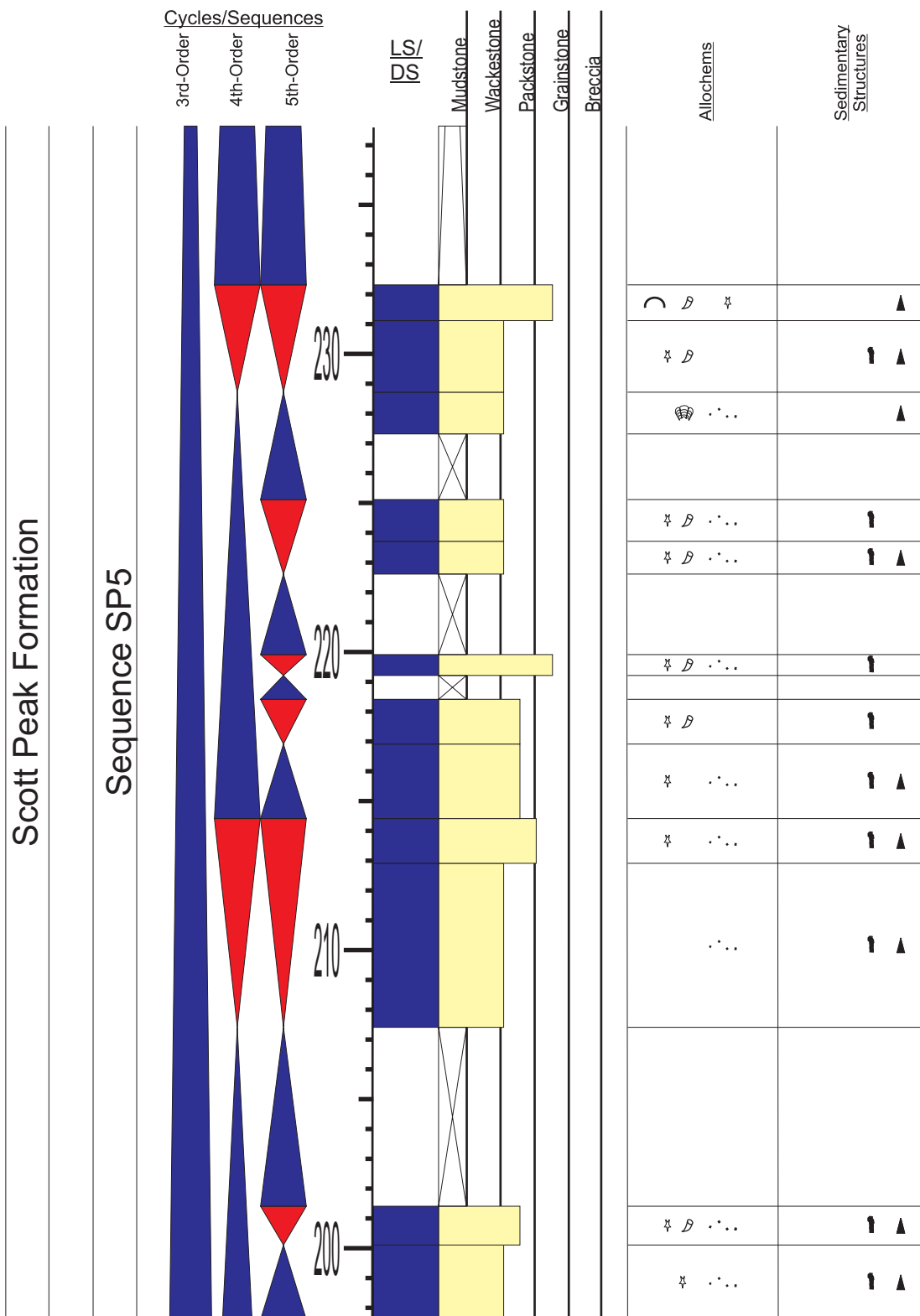
Appendix 12.4: Sedimentary section log for section Antelope Creek (continued). Refer to Appendix 1 for symbols and Figure 3.6 for location.

APPENDIX 12.5



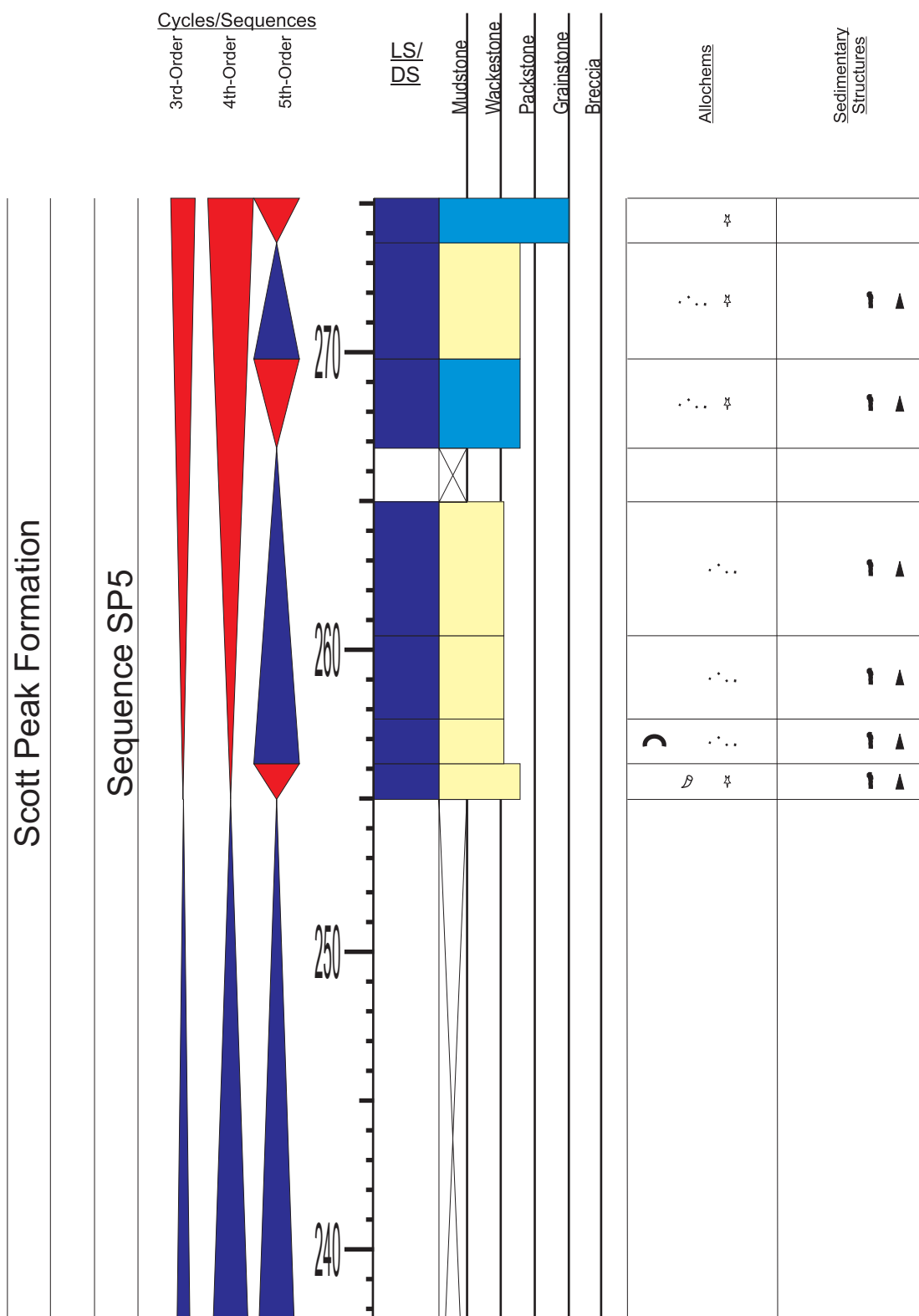
Appendix 12.5: Sedimentary section log for section Antelope Creek (continued). Refer to Appendix 1 for symbols and Figure 3.6 for location.

APPENDIX 12.6



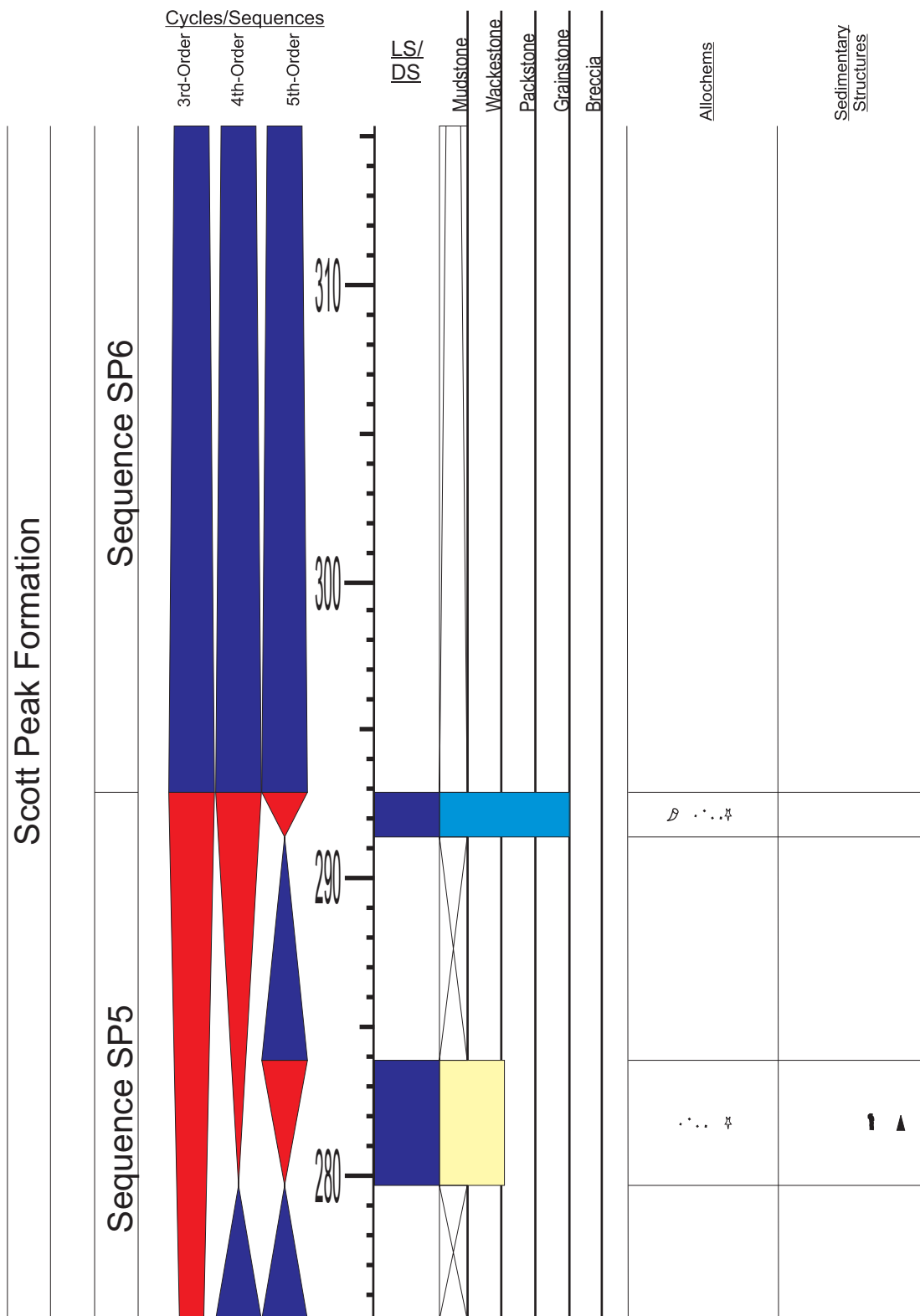
Appendix 12.6: Sedimentary section log for section Antelope Creek (continued). Refer to Appendix 1 for symbols and Figure 3.6 for location.

APPENDIX 12.7



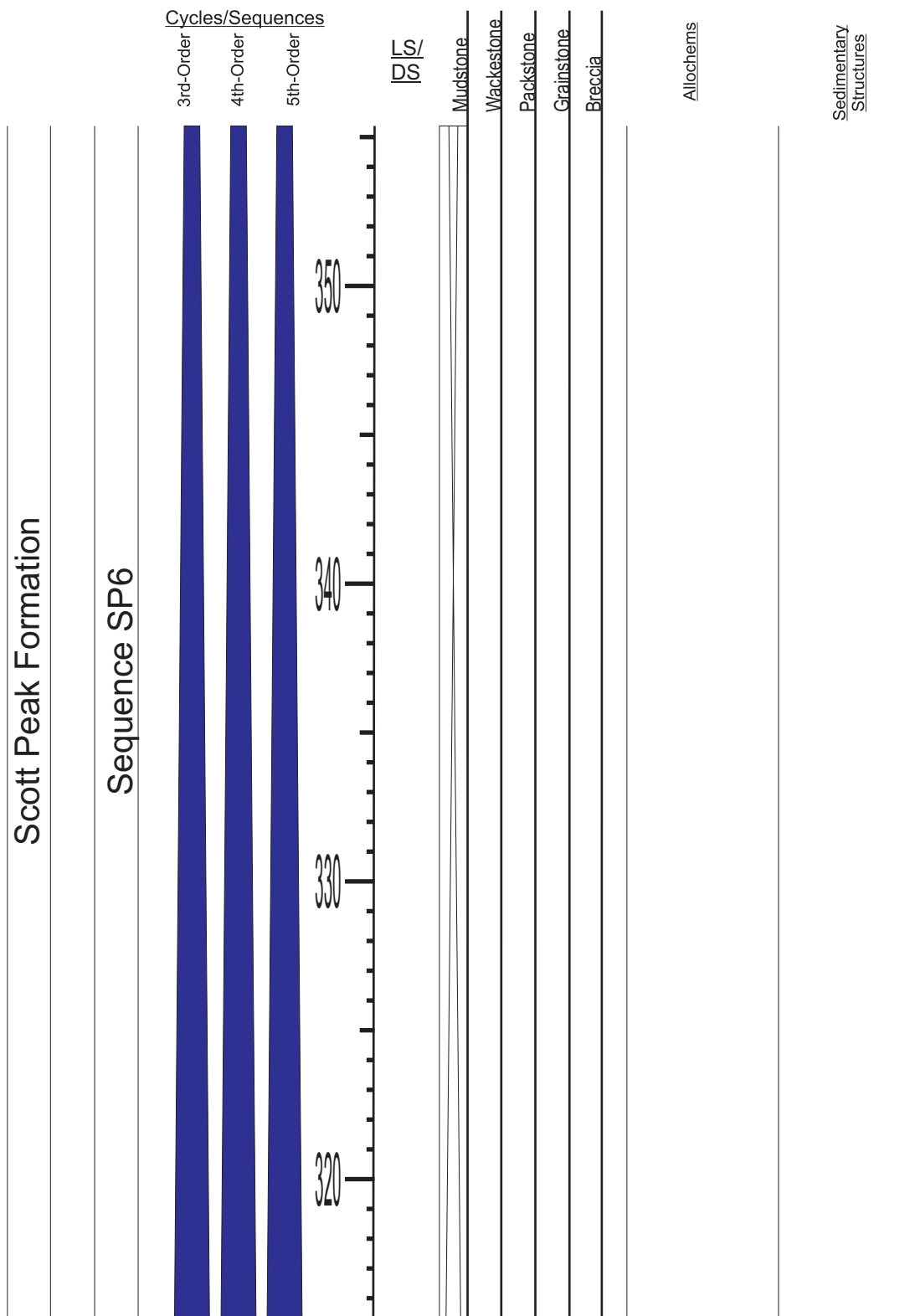
Appendix 12.7: Sedimentary section log for section Antelope Creek (continued). Refer to Appendix 1 for symbols and Figure 3.6 for location.

APPENDIX 12.8



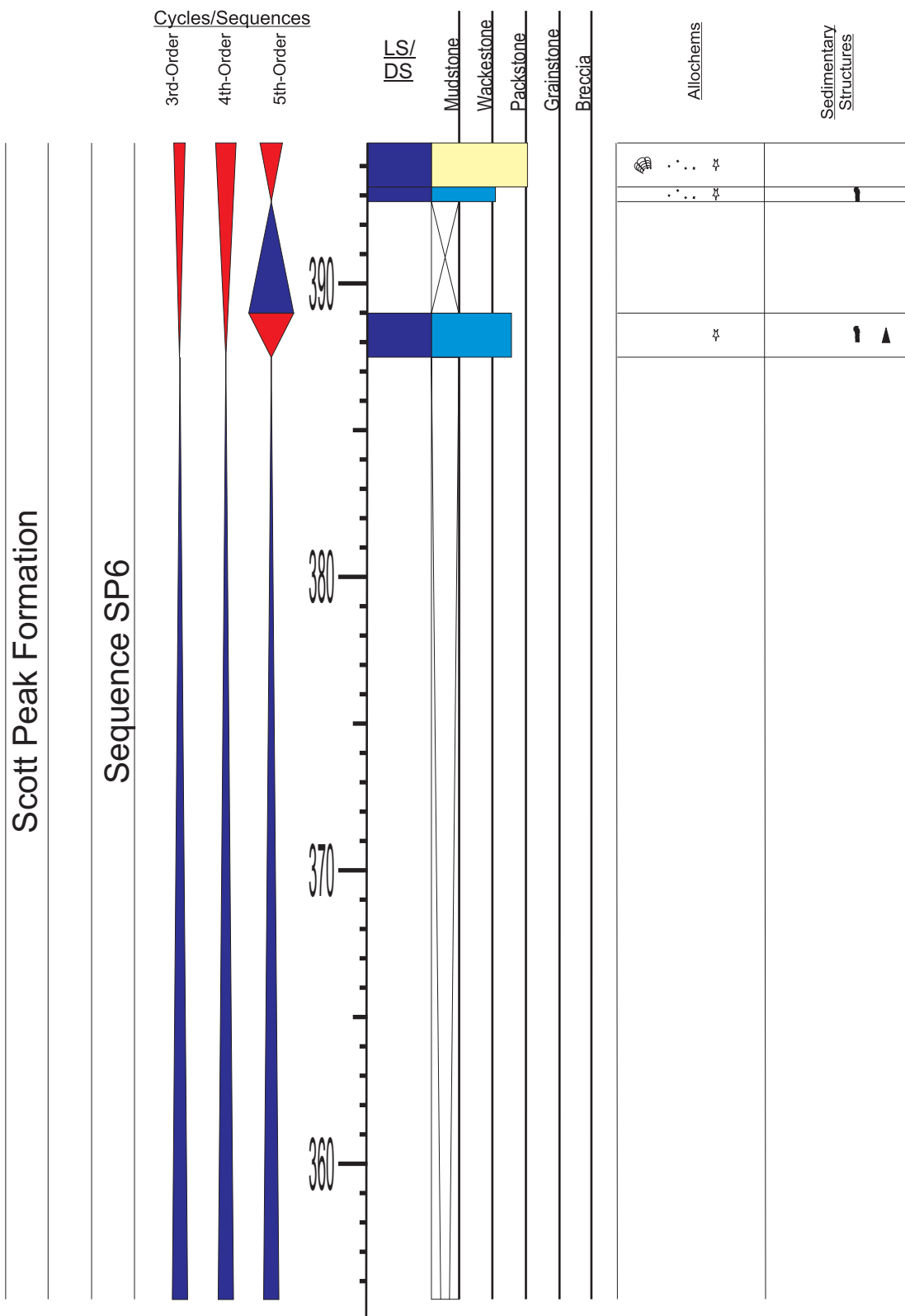
Appendix 12.8: Sedimentary section log for section Antelope Creek (continued). Refer to Appendix 1 for symbols and Figure 3.6 for location.

APPENDIX 12.9



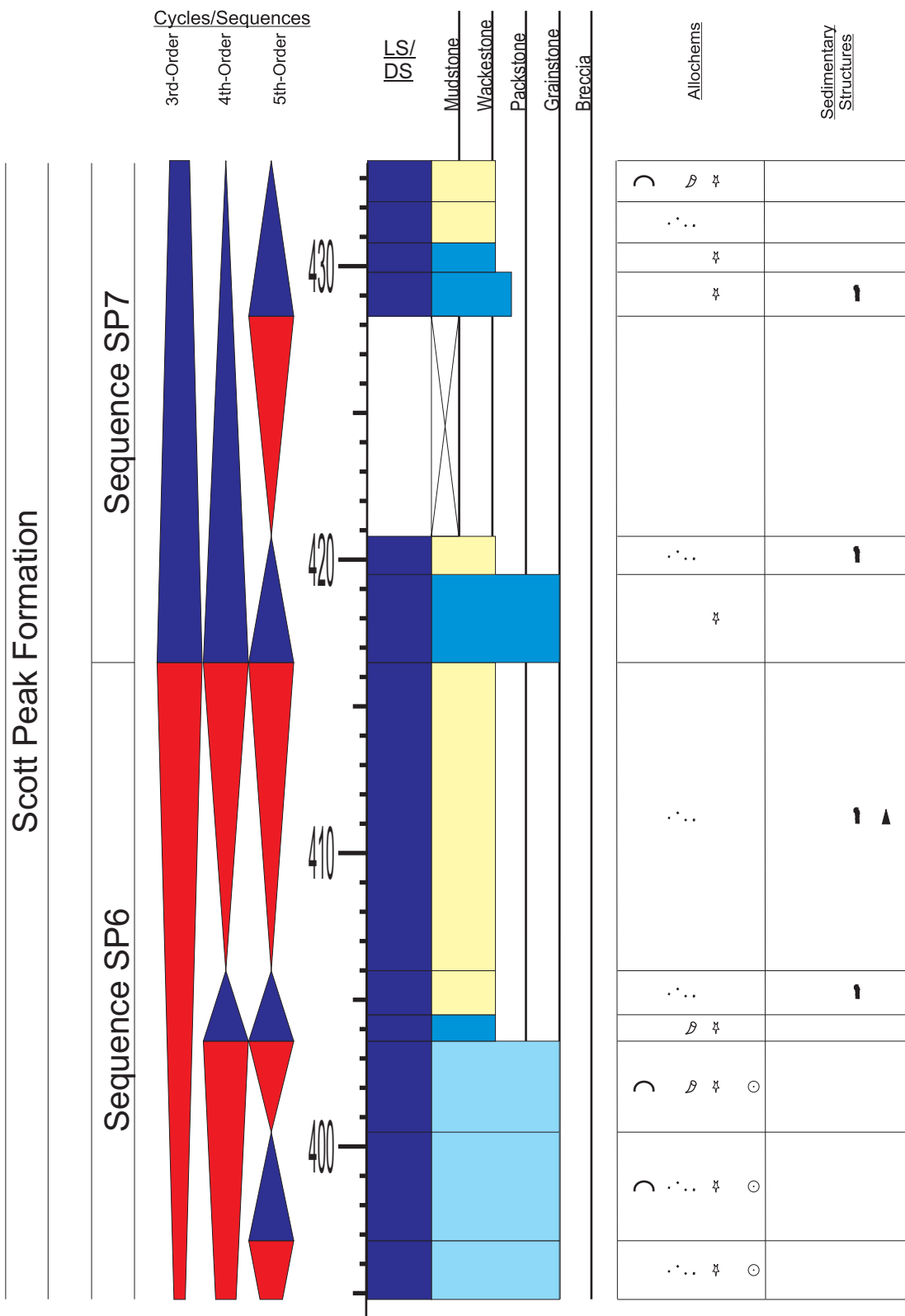
Appendix 12.9: Sedimentary section log for section Antelope Creek (continued). Refer to Appendix 1 for symbols and Figure 3.6 for location.

APPENDIX 12.10



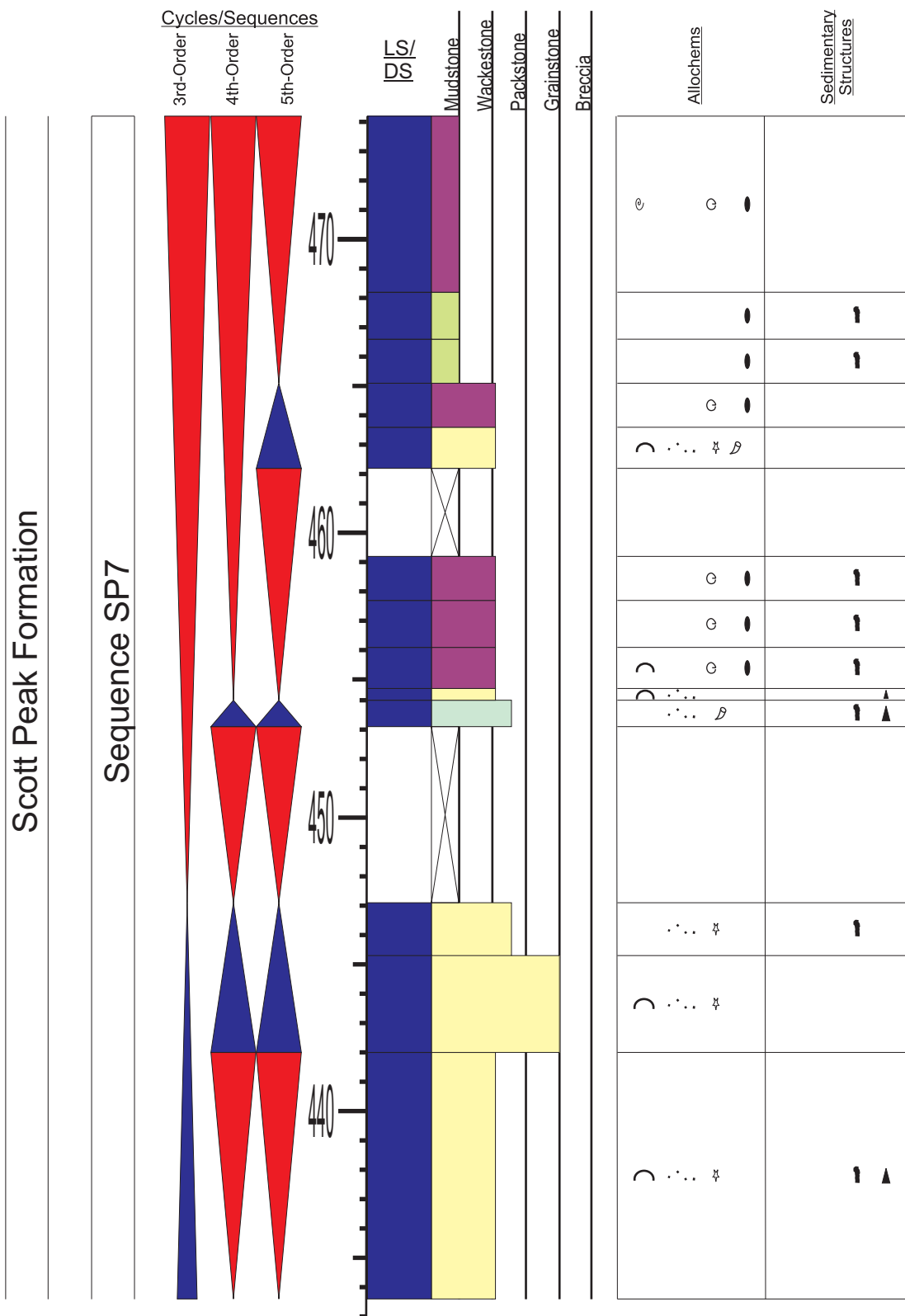
Appendix 12.10: Sedimentary section log for section Antelope Creek (continued). Refer to Appendix 1 for symbols and Figure 3.6 for location.

APPENDIX 12.11



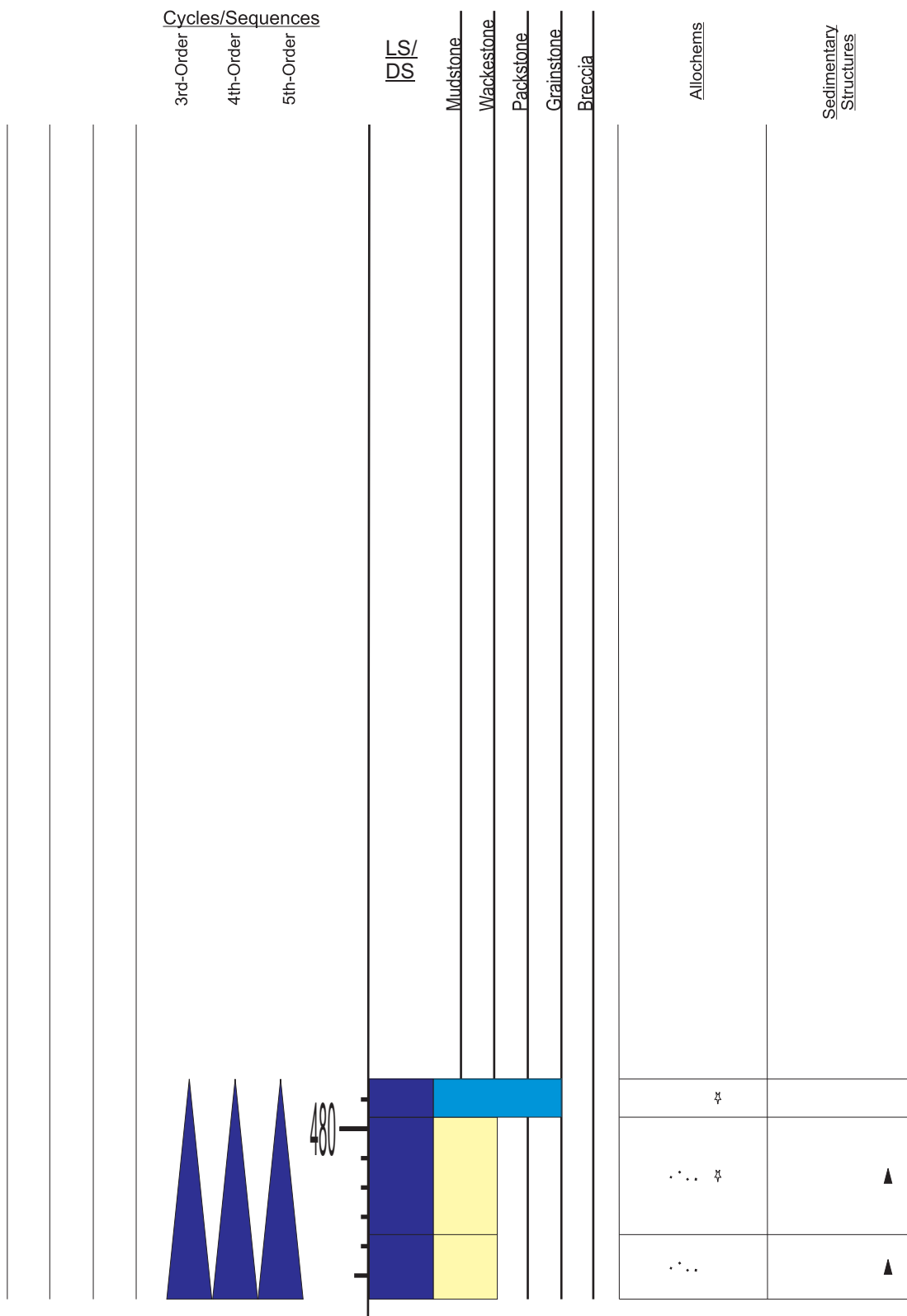
Appendix 12.11: Sedimentary section log for section Antelope Creek (continued). Refer to Appendix 1 for symbols and Figure 3.6 for location.

APPENDIX 12.12



Appendix 12.12: Sedimentary section log for section Antelope Creek (continued). Refer to Appendix 1 for symbols and Figure 3.6 for location.

APPENDIX 12.13



Appendix 12.12: Sedimentary section log for section Antelope Creek (continued). Refer to Appendix 1 for symbols and Figure 3.6 for location.

